Rotating Magnetic Field Separation of Minerals

Neil Robert Allen
BSc, Grad Dip Sc (Hons)

A thesis submitted in fulfilment of the requirements for the degree of Doctor of Philosophy

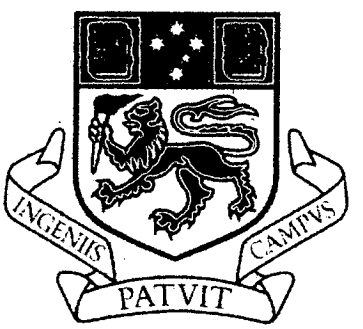

UNIVERSITY OF TASMANIA

School of Earth Sciences

Declaration

This thesis contains no material which has been accepted for the award of any other higher degree or graduate diploma in any university, and to the best of my knowledge and belief contains no material previously published or written by another person, except where due reference is made in the text of this thesis.

Signed .....N. R. Allen.....

N. R. Allen
University of Tasmania
18th March 1999

Authority of Access

This thesis is not to be made available for loan or copying for two years following the date this statement was signed. Following that time the thesis may be made available for loan and limited copying in accordance with the Copyright Act 1968.

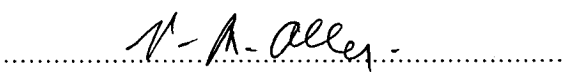

N. R. Allen
University of Tasmania
18th March 1999

Some Constants (SI units)

and Conversion Factors

Mass of electron	9.109×10^{-31} kg
Charge of electron	1.602×10^{-19} coul
Electron magnetic moment magnitude	1.62×10^{-23} J/T
Electron magnetic moment parallel to field	9.3×10^{-24} J/T
Mass of proton	1.672×10^{-27} kg
Magnetic moment of proton parallel to field	1.410×10^{-26} J/T
Bohr magneton	9.27×10^{-24} A.m^2 (or J/T)
Avogadro's number	6.023×10^{23} /mole
μ_0 (permeability of free space)	$4\pi \times 10^{-7}$ Wb/Am
Planck's constant h	6.626×10^{-34} J.s
$\hbar$ $(=\frac{h}{2\pi})$	1.054×10^{-34} J.s
g (gyromagnetic ratio)	1 for orbital motion
	2 for electron spin

1T = 10 000 G

1 Oe = $\frac{10^3}{4\pi}$ A/m (=79.6 A/m)

k_g (mass susceptibility in SI units: m^3kg^{-1}) = k_g (cgs units: $Gcm^3g^{-1}Oe^{-1}$) $\times 4\pi \times 10^{-3}$

Abstract

The behaviour of particles in a rotating magnetic field can be used as a basis for a new mineral separation method, where particles are separated on the basis of their relative ability to rotate in a rotating magnetic field. Both particle attraction and particle rotation separations may be combined in a single separation process, to offer previously impossible magnetic mineral separations, such as the separation of high-Mg ilmenites (picro-ilmenites) from other ilmenites of the same magnetic susceptibility, or to produce separations which are more precise than those currently available, such as the low-entrapment separation of magnetite or monoclinic pyrrhotite.

Whereas mineral separation by particle attraction involves the use of material properties such as the number of unpaired electron spins and their relative orientations, separation by particle rotation adds the properties of magnetic anisotropy and such dynamic magnetisation processes as domain wall velocity in ordered magnetic compounds. The use of a continuously rotating magnetic field also generates eddy currents in particles, in proportion to particle electrical conductivity, which allow conductive particles to be rotated by eddy current effects, and extends the same separation process into the practical separation of small particles of non-magnetic metallic compounds.

Particle rotational characteristics may be estimated using similar equipment to that used for practical rotating field mineral separations, so that these characteristics may be readily applied to practical separations. These estimations are presented in the form of a "rotation index", which relates the actual particle rotation strength to the maximum possible rotation strength indicated by particle magnetisation. Although the measurement of particle rotational characteristics by these methods is only approximate, it is accurate enough to demonstrate the presence of, and estimate the magnitude of, such dynamic magnetisation processes as domain wall velocities in small particles of natural ordered magnetic compounds.

Particle rotation by magnetisation is also shown as being able to cause particle rotations for which the particle rotation axis is at right angles to the field rotation axis, and which are of sufficient strength to play a part in a rotating magnetic field mineral separation process.

Acknowledgments

Many people have helped in the preparation of this thesis, but special thanks must go to the following:

Dr. J. C. van Moort, who was the principal supervisor. Jan spent numerous days reading, discussing and helping with problems. Jan's encouragement was greatly appreciated.

Dr. D. Clark, of the CSIRO Magnetics Laboratory in Sydney, who was co-supervisor. David had the main task of pulling the theory back down to earth, preventing me from making embarrassing mistakes, and making sure I was working with the correct concepts.

Dr. R. F. Berry, of the University of Tasmania geology department. Ron gave a lot of assistance with mineralogy in general and chromites in particular.

Rio Tinto Exploration, (formerly CRA Exploration) in Belmont, W.A., who financially supported the investigation from its commencement in 1994. To a large extent it was the success achieved with Rio Tinto's application which provide the encouragement to continue. Discussions with Hans Lucas, Liz Bullock and Dr. David Richards at Rio Tinto were particularly helpful and encouraging, and Dr. David Richards read and commented on the thesis.

Eriez Magnetics (Aust.), who provided magnets for the construction of separators and test equipment. Continual prompting from Mr. Ron Poole, manager at Eriez Magnetics, helped me to see the full width of possible applications for the separation method, and to keep in mind the reality of practical mineral separation.

Mr. Wieslaw Jablonski, of the central Science Laboratory at the University of Tasmania, who spent many hours making sure the electron microprobe did what we wanted it to do, and that I understood what it was doing.

Contents

List of Tables

List of Figures

Preface

Mineral separation methods can be divided into four main groups. These are:

(a) Specific gravity methods.
(b) Chemical methods.
(c) Electrostatic methods.
(d) Magnetic methods.

This thesis deals with the last of these methods, magnetic separation.

Nearly all magnetic separation, at present, is based on the attraction of magnetic particles in a magnetic field gradient, and therefore the magnetic susceptibility is the main determinant of whether or not a particle can be magnetically separated. However, many magnetic particles, and especially those that are magnetically ordered, are able to rotate to remain aligned with a magnetic field which changes direction. The rotation property of the magnetically ordered particles can therefore be used as a basis for mineral separation.

Mineral separation based on the "rotatability" or "rollability" of particles is the main theme of this thesis. Two secondary themes, which presented themselves as the thesis work progressed, are the use of particle magnetic rotation measurements as a method for determining mineral magnetisation characteristics (e.g. domain wall motion), and the use of rotation measurements as a tool in petrogenesis studies. The relationship between particle magnetic moment and magnetic anisotropy can indicate conditions of mineral genesis. These secondary themes were not able to be examined in detail, but are indicated as areas for further investigation with more accurate measurement techniques.

The primary aim of the thesis is to establish rotating magnetic field mineral separation as an economic and practical method which can solve some current problems in magnetic mineral processing. In achieving this aim it has been necessary to examine the basis for magnetic particle rotation, develop equipment and methods for measuring and quantitatively describing magnetic particle rotations, and develop and test some prototype rotating magnetic field separators.

If a rotating magnetic field is used for mineral separation, particles are being separated on the basis of their magnetic anisotropy (which depends on factors such as exchange forces and crystalline electric fields), and also (in the case of ordered magnetic materials) on the basis of their dynamic magnetisation response to a rotating magnetic field. Therefore much more attention now needs to be given to the dynamics of magnetisation, the crystalline structure of minerals and to the arrangement of magnetic and non-magnetic ions within this structure than is necessary for discussion of mineral separation by particle attraction. Quantum mechanical phenomena such as the Pauli exclusion principle and orbital quenching control magnetic anisotropy, and need to be at least introduced in outline. Precessions as a result of spin reversals (the Einsein-de-Haas effect of rotation by magnetisation) also need to be considered.

The first two chapters of this thesis summarise the basic theory of magnetism and mineral magnetism respectively. This theory forms the background for the rest of the thesis,

and will frequently be referred to. The theory is a little more extensive than that which would normally be necessary for attractive magnetic separation, because of the need to include aspects of quantum mechanics that are relevant to magnetic anisotropy in minerals.

Chapter 3 summarises present magnetic separation methods, which will also frequently be referred to for comparison. The difficulties and limitations of the present methods are also examined here, and these are the problems which rotating field magnetic separation either minimises or overcomes. Later chapters compare rotating field separation results with results which may be achieved by the separations described in chapter 3.

Chapters 4 to 6 extend the basic magnetism theory of chapters 1 and 2 to produce expressions and relationships which either predict particle rotational behaviour or provide a basis for its description. The idea of a particle "rotation index" is introduced here, and is later used throughout the experimental section of the thesis to quantify particle rotational behaviour.

The design and construction of new measurement and trial separation equipment has been an important and necessary part of this thesis. Rather than describe the equipment components separately and individually later on, the equipment descriptions, and the methods used, have all been placed together as chapters 7 to 9.

Chapters 10 to 17 describe experimental results, but wherever the detailed rotational characteristics of a particular mineral have been examined, the mineral structure is first introduced as the basis within which the results must be interpreted. Most of the detailed experimental work was carried out around the three main diamond indicator minerals (picro-ilmenite, kimberlitic chromite and pyrope garnet), because the separation or concentration of these minerals was seen as an important economic application of the method. Some large-scale applications, such as the low-entrapment separation of magnetite and pyrrhotite, are also seen as important applications of the method, and have been examined. The eddy current separation of small conductive particles (down to the tens of microns range) is also seen as a possible future application, and has been experimentally investigated.

The final chapters summarise the theoretical and experimental results, and emphasise that rotating field separation is a method that has a wide range of practical applications. The further development of particle rotation measurements is also presented as an area for future theoretical development.

Many of the figures reproduced in this thesis (and particularly those in chapters 1 and 2) will be familiar to readers, as they have been reproduced in many texts (quite often with no reference to previous appearances), almost unchanged since their first appearance. In these cases the earliest reference known to the author has been given.

Section 1
Theoretical Considerations in Magnetic Mineral Separation and Past and Current Magnetic Separation Methods

Chapter One

The Basis of Mineral Magnetism

Introduction

Maxwell (1873), in "A Treatise on Electricity and Magnetism" gives some interesting background to modern magnetic theory. A theory still common at the time he was writing was that electricity and magnetism were each due to two different (but opposite) types of fluids (four fluids in all). Maxwell describes the reasoning of Poisson who, in order to explain why such fluids could not be isolated by simply breaking a magnet, concluded that such fluids would need to be restricted to individual molecules (which were considered indestructible). Under Poisson's revised theory (which Maxwell describes as "too large for the facts"), magnetising a molecule entailed "polarising" the two types fluids at opposite ends of the molecule. Maxwell reports that Weber, in contrast to Poisson's ideas, assumed that each molecule was already magnetised. Magnetisation of the bulk specimen then only entailed aligning the magnetisation of the individual molecules. Weber went further than just this assumption, probably following Ampere's magnetic theory of 1825 (which hypothesised that all magnetism is due to electric currents), and concluded that the magnetism of the individual molecules was due to electric currents circulating within the molecules. He thus reduced the number of liquids from four (two for electricity and two for magnetism) to two. This was in some conflict with the observation that all electric currents meet with resistance and produce heat, but, as Maxwell describes the situation, "By confining the circuits to the molecules, within which nothing is known about resistance, we may assert, without fear of contradiction, that the current, in circulating within the molecule, meets with no resistance." In order to explain both the magnetisation of iron and the existence of diamagnetism, Weber appears to have recognised the existence of two different types of molecular currents, one of which was caused by an induction effect from other magnets or an external magnetic field, while the other was an "intrinsic" current. The former of these was used in his theory of diamagnetism.

It should be noted that in Maxwell's time the terminology of "molecule" and "atom" was not settled, and Maxwell would often use "molecule" when we would refer to an "atom".

By about 1870, all the essential ideas of modern magnetic theory had been well examined and mathematically developed. They awaited the discovery of atomic structure and quantum mechanics before they could be placed on a firmer footing than the logical assumption of fluid-like molecular (or atomic) currents with no resistance.

Classical Equations of Magnetism

Much of this section has been summarised and modified from Chikazumi and Charap (1978) and Chikazumi (1997), who provide a well organised introduction to classical magnetism.

The basic and perhaps the oldest equation of magnetism, developed experimentally by Coulomb in 1785 and later mathematically by Poisson, describes the force which exists between two magnetic poles.

$$F = \frac{p_1 p_2}{4\pi\mu_0 r^2} \qquad \text{(N)} \qquad 1.1$$

Where:- p_1 and p_2 are the two pole strengths (in Wb)
F is the force exerted (in N)
r is the distance between the poles (in m)
μ_0 is the permeability of free space (= $4\pi \times 10^{-7}$ Wb/Am)

A magnetic field is said to exist anywhere an isolated magnetic pole experiences a force due to its magnetism. Because a magnetic pole experiences a force when placed near any conductor carrying an electric current, an electric current produces a magnetic field. In particular a very uniform magnetic field is produced by a long solenoid. This field is defined by:

$$H = ni \qquad \text{(A/m)} \qquad 1.2$$

Where:- H is the magnetic field intensity (in A/m)
n is the number of turns/metre of the solenoid
i is the current (in A)
(Note:- 1 Oersted = $10^3/4\pi$ A/m, or 1 A/m = $4\pi \times 10^{-3}$ Oe)

The force experienced by an isolated pole placed in a magnetic field H(A/m) is given by:

$$F = pH \qquad \text{(N)} \qquad 1.3$$

Where p is the pole strength (in Wb)
H is the magnetic field intensity (A/m)

Magnetic poles do not exist in a solitary state (although they may often be considered sufficiently isolated for theoretical purposes) and a real magnet has equal and opposite poles, separated by some distance (l). If such a dipole is placed in a uniform magnetic field, the forces exerted on the poles are equal, but opposite ($+pH$ and $-pH$). These forces may act to rotate the magnet, but if they are of the same magnitude they can not provide a nett translational force. However if the field is not uniform, but has a field gradient in some direction (say the "x" direction), then the force on the two poles will be different and a resultant translational force will be applied to the magnet.

$$F = pl_x \frac{\partial H_x}{\partial x} \qquad \text{(N)} \qquad 1.4$$

Where l_x is the length of the magnet (in the x direction)

The product pl is referred to as the magnetic moment.

$$m = pl \qquad 1.5$$

Where m is the magnetic moment (Wb m)

In the presence of magnetised matter it is convenient to introduce a second vector field $\tilde{B}$, called the magnetic flux density or magnetic induction. The magnitude of $\tilde{B}$ is related to the magnetic field (H) by the relationship:

$$B = \mu_0(H + M) \qquad \text{(T)} \qquad 1.6$$

Where;- M is the magnetisation (A/m)
B is the magnetic induction (Wb/m^2 or T). The unit Tesla (T) is normally used instead of the Wb/m^2.

(Note that the terms $\mu_0 H$ and $\mu_0 M$ also have dimensions of Wb/m^2 or T)

$\mu_0 M$ is the magnetic moment per unit volume ($\mu_0 M = \frac{m}{V}$)

The magnetisation (M) depends on the magnetising field H. For many materials (e.g. the paramagnetic materials described in chapter 2) and for sufficiently weak fields M is proportional to H. In this case we can write M as:

$$M = k_v H \qquad \text{(T)} \qquad 1.7$$

Where k_v is a magnetisation constant called the magnetic susceptibility (per unit volume)

Equations 1.6 and 1.7 can be combined to give:

$$B = \mu_0 H(1+k_v) \qquad \text{(T)} \qquad 1.8$$

Equation 1.7 can be written interms of magnetic moment as:

$$m = \mu_0 k_v V H \qquad \text{or} \qquad k_v = \frac{m}{\mu_0 V H} \qquad 1.9$$

The constant k_v (the volume magnetic susceptibility) is a characteristic of the substance being magnetised. Because $\mu_0 M$ is the magnetic moment per unit volume, equation 1.4 can be written to give the magnetic translational force on a particle of volume V and volume susceptibility k_v in a magnetic field H which has a field gradient.

$$F = \mu_0 k_v H V \frac{\partial H}{\partial x} \qquad \text{(N)} \qquad 1.10$$

For a given volume of a particle which satisfies equation 1.7, placed in a particular magnetic field strength and field gradient, the attractive force on the particle is dependent only on the volume magnetic susceptibility k_v, which therefore can be considered as a measure of

the magnetic "attractability" of a particle. As such, it is of great importance in magnetic mineral processing. Its value determines whether a mineral can be magnetically separated or not. In order to magnetically lift a particle the magnetic attraction must be greater than or equal to the force of gravity on the particle:

$$\mu_0 k_v H V \frac{\partial H}{\partial x} = DVa$$

or the product of the field and its gradient must satisfy the equation:

$$H\frac{\partial H}{\partial x} = \frac{Da}{\mu_0 k_v} \qquad 1.11$$

Where:- D is the density of the particle (kg/m^3)
a is the acceleration due to gravity (m/s^2)
k_v is the magnetic volume susceptibility or relative susceptibility.

In mineral processing applications the mass magnetic susceptibility is normally used instead of the volume magnetic susceptibility. The relationship between these two quantities is given by $k_v=k_gD$. Equation 1.11 then becomes:

$$H\frac{\partial H}{\partial x} = \frac{a}{\mu_0 k_g} \qquad 1.12$$

Where k_g is the magnetic mass susceptibility and now has the dimensions m^3/kg (k_gD remains dimensionless)

Equation 1.12 can be written so that the field and gradient needed to lift a particle can be used to measure the particle's magnetic mass susceptibility.

$$k_g = \frac{a}{\mu_0 H \frac{\partial H}{\partial x}} \qquad 1.13$$

This formula has been used extensively in the experimental work in this thesis to provide an estimate of the magnetic susceptibilities of individual small particles.

Equations 1.10 and 1.11 describe the translational force applied to a hypothetical "point particle". For a real mineral particle or sample, the field and gradient will differ from one side of the particle to the other. An accurate equation for the force on such a particle will depend on the geometries of both the particle and the field.

For the traditional Gouy method of magnetic susceptibility measurement a cylindrical specimen is used, with the vertical specimen extending upwards from directly between two pole pieces into a region where the field is comparatively weak (less than 0.01 of the maximum field). The total translational force on the cylindrical specimen is then found by considering the force exerted on a small length of the specimen (using equation 1.10) and integrating over the specimen length. The resulting expression, assuming the force on the upper end of the specimen is negligible, then allows the magnetic susceptibility to be calculated from the measured attractive force on the specimen (see Cullity, 1972).

$$F = \frac{\mu_0 k_v A H^2}{2} \qquad \text{(N)} \qquad 1.14$$

Where:- A is the cross-sectional area of the cylindrical sample
k_v is the volume magnetic susceptibility
H is the field between the magnet pole pieces

The only field measurement required for this method is the field strength between the two electromagnet pole pieces.

This thesis is concerned with the rotation of magnetised particles in a rotating magnetic field, and therefore the torque which can be placed on a magnetised particle by an external magnetic field is of great importance. Torque is a vector quantity, which has its direction along the axis of implied rotation. The torque applied to a particle of magnetic moment m in a field H is given by the cross product, or vector product, of these two quantities ($\vec{m} \times \vec{H}$). The magnitude of this torque is:

$$\tau = mH \sin\theta \qquad \text{(N.m)} \qquad 1.15$$

Or, in terms of particle magnetisation (M):

$$\tau = \mu_0 MVH \sin\theta$$

Where θ is the angle between the magnetic moment m and the field H

While it is sufficient to consider only the magnitude of the torque for most of the applications in this thesis, the direction of the torque vector is of importance when examining the effects of precession in chapter 5. The direction of the vector is along the axis of rotation, in the direction that a right-handed screw would advance if turned from the direction of m to the direction of H (or, if the fingers of the right hand are curled in the direction from m to H, the thumb points in the direction of the torque vector).

Conversions between magnetic susceptibility SI and cgs units

Many magnetic susceptibilities are measured and quoted in the cgs system. This is especially so for mineral susceptibilities, although rock susceptibilities seem to be more often published in the literature in SI units. The situation is made even more confusing with respect to rock susceptibilities because it is often not indicated whether the mass or volume susceptibilities are being given.

Before using cgs susceptibilities in the above equations they need to be converted. To convert the cgs volume susceptibility to SI units, the cgs value needs to be multiplied by 4π. The cgs mass susceptibility needs to be multiplied by $4\pi \times 10^{-3}$ to convert it to SI units.

Magnetism and the Atom

Much of the following theory has been adapted from Turnbull (1979), Chikazumi and Charap (1978), Chikazumi (1997) and Eisberg and Resnick (1985).

The electron

As Maxwell and Weber suspected, the explanation of magnetism lies in small electric currents within the atom. We now associate these electric currents with the motions and properties of charged particles, of which the electron is the most significant. Although we normally think of the electron as a particle, the probabilities and wave functions of quantum mechanics, especially as they apply to the electrons around atoms, bring us back towards the more nebulous electric "fluids" of Ampere and Poisson. Nevertheless, the concept of the electron as a small solid particle is retained here.

The electrons around the atom behave, to some approximation, as though they are actually travelling around the atom in discrete "orbits". Therefore we may consider these orbits as circular or eliptical current elements which produce a magnetic field directed perpendicular to the plane of the orbit.

Moreover, the electrons themselves behave as if they are spinning. That is, they behave as though they have an angular momentum. Because they are charged particles, this spinning amounts to a circulating electric charge, which produces a magnetic field directed along the axis of spin. The spinning electrons then behave like small magnetic dipoles.

Any attempt to deflect the electron spin orientations or the orbital orientations (perhaps using a rotating magnetic field) interacts with the angular momenta of the spins and the orbits, and precessions occur. This response is considered further in chapter 5.

An atom also contains positively charged protons in the nucleus, and these also have spins, but the effect of these particles on the magnetic properties of the atom is several orders of magnitude smaller than for the electrons. Nuclear spins will not be considered here.

The quantum electronic structure of the atom

Within the crystalline structure of a mineral, direct interaction between the magnetic fields associated with the spinning electrons and their orbits is generally far too small to account for the ordered arrangements of electron spins. These ordered arrangements (electron spins arranged parallel or anti-parallel to each other), which are responsible for the response of a mineral particle to a rotating magnetic field, are determined by the rules of quantum mechanics. Therefore it is necessary to examine some of the quantum mechanical rules which determine the electron and orbital configurations of atoms.

The electronic structure of the atom is often compared to the structure of the solar system, in that there is a central and very massive nucleus surrounded by orbiting electrons. This turns out to be an idea which is far too simple for anything but a preliminary concept. The electrons behave as though they are both waves and particles. While it is easy to imagine a solid particle going around in any orbit you please, it is more difficult to imagine a wave in an

orbit, unless perhaps the size of the orbit coincides with an integral number of electron wavelengths. The latter was the concept developed by De Broglie in 1924. It is a concept which provides some intuitive picture of why electrons are restricted to discrete orbits. The electron orbits may be considered to be arranged so that electron waves are able to fit exactly around the orbit and to produce standing waves.

The orbital "size" is described by the principal quantum number n. Quantum mechanics states that angular momentum must come in multiples of Planck's Constant ($\hbar$). Because orbital motion involves angular momentum, the orbits must come in sizes to fit.

$$\textit{Angular momentum} = n\hbar$$

or $$m_e\omega r^2 = n\hbar$$

ie. $$r^2 = \frac{n\hbar}{m_e\omega} \quad \text{(m)} \qquad 1.16$$

Where:- n is an integer
$\hbar$ is Planck's Constant (J sec)
m_e is the mass of the electron (kg)
ω is the angular velocity (sec^{-1})

Therefore we now have an intuitive picture of the electronic structure of the atom (Bohr's theory) as in Figure 1.1.

Figure 1.1
Electronic structure of Bohr's atom

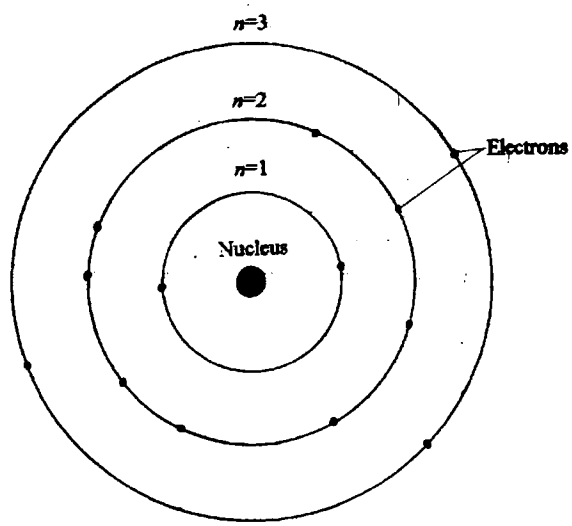

(Not to scale)

Wilson and Sommerfield (1916), in an attempt to account for the number of lines observed in atomic spectra, generalised Bohr's theory to include elliptical orbits and spatial orientation in a magnetic field. Bohr's circular orbits then became special cases of this more general approach. As a result of this generalisation, two other quantum numbers were introduced. One of these, l (Wilson and Sommerfield originally used k (= $l+1$)), describes the

shape of the orbit, and is known as the *orbital quantum number*. Depending on the value of n, l can take a number of different values;-

$$l = 0, 1, 2, \ldots\ldots, (n - 1)$$

The magnitude of the orbital angular momentum is given by:

$$L = \sqrt{l(l+1)}\,.\hbar \qquad 1.17$$

Figure 1.2 illustrates the significance of the orbital quantum number l.

Figure 1.2

The significance of the orbital quantum number l

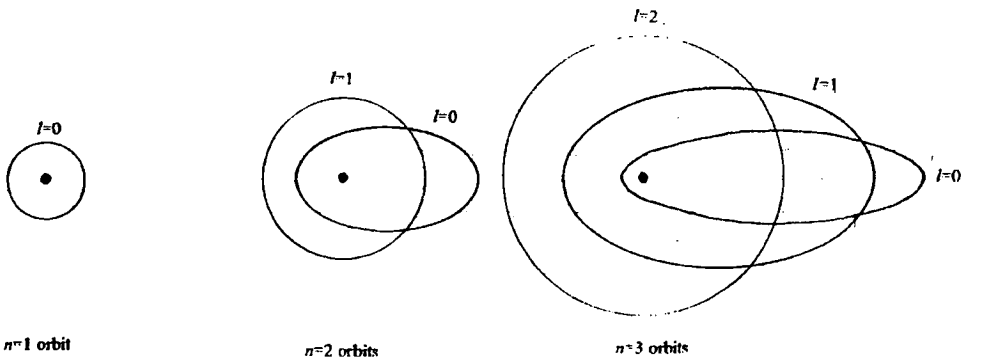

(From Turnbull 1979)

So far we have two quantum numbers:

n describes the size of the orbit.

l describes the ellipticity of the orbit.

The third quantum number m_l (the second new one introduced by Wilson and Sommerfield), becomes important in the presence of a magnetic field and is known as the *magnetic quantum number*. This quantum number describes the orientation of the orbit with respect to a magnetic field. The magnitude of the orbital angular momentum L (equation 1.17) must project onto the direction of the external magnetic field in units of $\hbar$.

$$L_z = m_l\hbar \qquad 1.18$$

As indicated by the subscript ($_l$), the values of m_l depend on l, and m_l can take up values of:

$$m_l = 0, \pm1, \pm2, \ldots\ldots, \pm l$$

Figure 1.3 shows the possible orientations for the case where $l = 3$. In this case the orbit may have one of 7 different orientations to the magnetic field. That is, it may have one of 7 different energies. If l were to equal 1, there would be 3 different orientations and 3 different energies.

Figure 1.3

The significance of the magnetic quantum number m_l

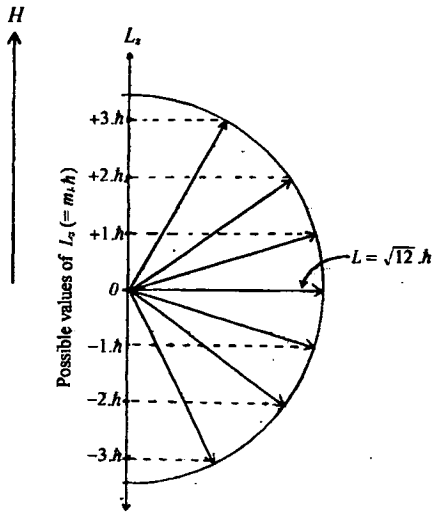

We now have three different quantum numbers which describe the electron orbit (and energy level) around the central nucleus.

n	describes the size of the orbit.
l	describes the ellipticity of the orbit.
m_l	describes the orientation of the orbit with respect to a magnetic field.

The above three quantum numbers allowed Wilson and Sommerfield to correctly predict all the spectral lines observed at the time (which are due to electron transitions between energy levels,- or between quantum numbers). More accurate observations later indicated that each of the Wilson and Sommerfield states could be further split, by the presence of a magnetic field, into two different energy levels. This was explained in 1926 by Uhlenbeck and Goudsmit, who proposed that each electron was a spinning electric charge generating a magnetic moment. The angular momentum S of the spinning electron is then given by:

$$S = s\hbar$$

The only values which can be given to s, and which agree with the doubling of the spectral lines is $\pm\frac{1}{2}$. This means that the difference between the two possibilities or energy levels ($+\frac{1}{2}$ and $-\frac{1}{2}$) is $\hbar$.

The meaning of s is illustrated in figure 1.4. As was the case for the orbits, the electron spin is spatially quantised. The $s\hbar$ value of the angular momentum is really the projection of the actual electron angular momentum onto the direction of the external magnetic field.

Figure 1.4

The significance of the spin quantum number s

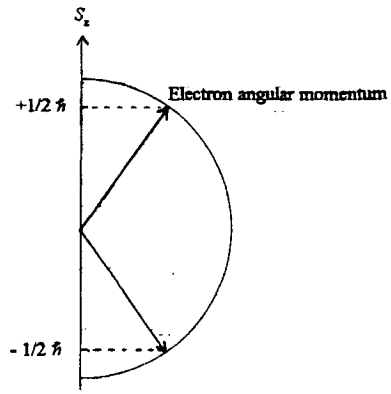

The actual electron angular momentum is given by:

$$S_c = \sqrt{s(s+1)}\,.\hbar$$

$$= \frac{\sqrt{3}}{2}\hbar \qquad (\text{as } s = \tfrac{1}{2}) \qquad 1.19$$

The symbol m_s is usually used instead of just s. Then the angular momentum in the external field direction is:

$$S_z = m_s\hbar \qquad (\text{where } m_s =)$$

m_s is known as the *spin magnetic quantum number*.
An atomic electron is therefore described by four quantum numbers:

n	The principal (orbit) quantum number	(n = 1, 2, ...)
l	Orbital (shape) quantum number	(l = 0, 1, 2, ..., (n -1))
m_l	Orbital magnetic quantum number	(m_l = 0, ±1, ..., ±l)
m_s	Spin magnetic quantum number	(m_s = ±½)

The Pauli exclusion principle states that in an atom no two electrons can have all four quantum numbers the same.

The relationship between electron magnetic moment and electron angular momentum

Consider first the case of the electron travelling in a circular orbit around the nucleus. The electron is a charged particle, so its motion around the nucleus constitutes a circular electric current. This will produce a magnetic field directed parallel to the axis of the orbit. Because we have a rotating mass as well, there must also be an angular momentum associated with it. The magnetic moment and the angular momentum are therefore tied together. The situation is illustrated in Figure 1.5. Note that the magnetic moment and the angular momentum (which are both vector quantities) are in opposite directions.

Figure 1.5

The magnetic moment and the angular momentum produced by an electron travelling around a circular orbit.

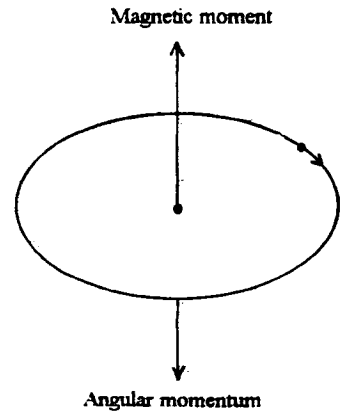

Of course this diagram is a gross over-simplification, but it is at least a picture which can easily be imagined.

The magnetic moment of a current loop is given by electromagnetic theory as:

$$M = \mu_0 niA \qquad \text{(Wb m)} \qquad 1.20$$

Where:- n = No. of turns (No. of coils of wire in a solenoid)
i = current (A)
A = area of loop (m^2)

It is usual to express the magnetic moment in J/T instead of Wb m. (J/T = Wb m/μ_0). Equation 1.20 then becomes:

$$M^1 = niA \qquad \text{(J/T)}$$

If it is assumed that the electron travels around a circular orbit of radius r, with an angular velocity of ω, then this becomes:

$$\mu_l = -\tfrac{1}{2} e\omega r^2 \qquad \text{(J/T)} \qquad 1.21$$

Where: e = electron charge
ω = angular velocity
μ_l = orbital magnetic moment

This may be combined with the relationship for angular momentum ($L = m_e \omega r^2$) to give an equation which contains both the magnetic moment and the angular momentum.

$$\mu_l = -\frac{e}{2m_e} L \qquad \text{(J/T)} \qquad 1.22$$

Where: L is angular momentum
m_e = mass of the electron

Equation 1.22 then gives the relationship between magnetic moment and angular momentum for the orbital motion of the electron.

Quantum mechanics requires that L_z (the component of the angular momentum in the applied field direction, see figure 1.3) must be an integer multiple of $\hbar$ ($L = m_l\hbar$, and $\hbar$ is Planck's constant (h) divided by 2π). Equation 1.22 now becomes:

$$\mu_l = \frac{m_l \hbar e}{2m_e} \qquad \text{(J/T)} \qquad 1.23$$

Where $\hbar$ = (= 1.054 x 10^{-34} J sec)

This indicates that the unit increment for magnetic moment ($\mu_B = \frac{e\hbar}{2m_e}$) is 9.27 x 10^{-24} J/T, which is referred to as the Bohr Magneton. The Bohr magneton is used as a convenient unit of measurement for magnetic moment. Observations of atomic spectra confirm this equation, and also indicate (by the Zeeman effect) that the relation between the magnetic moment and spin angular momentum for the electron itself is given by:

$$\mu_s = -\frac{e}{m_e} S \qquad \text{(J/T)} \qquad 1.24$$

Where:- μ_s is the spin magnetic moment
S is the spin angular momentum

Equation 1.24 is the electron spin equivalent of equation 1.22, and relates the electron spin angular momentum to the electron spin magnetic moment.

In general the magnetic moment can be written as:

$$\mu = -g\frac{e}{2m_e} L \qquad \text{(J/T)} \qquad 1.25$$

or, using the Bohr magneton:

$$\mu = \frac{-g\mu_B}{\hbar} L \qquad \text{(J/T)}$$

Where g is called the gyromagnetic ratio. It equals 1 for orbital motion and 2 for electron spins.

The ratio $g\frac{e}{2m_e}$ is often referred to as the gyromagnetic constant (γ).

The above equations refer to the magnitudes of the magnetic moments and angular momenta as they project on to the direction of an external magnetic field. Because these are the values which are actually detected and measured, they are of great practical importance, but they are not the full orbital or spin values.

The magnitudes parallel to the external field should more correctly be indicated by subscripts as follows:

For orbital motion $\mu_{lz} = -g\mu_B m_l$ (ie $L_z = \hbar m_l$) 1.26

For electron spin $\mu_{sz} = -g\mu_B m_s$ (ie S = $m_s\hbar$, and $m_s = \pm\frac{1}{2}$) 1.27

(Note: μ_{sz} is equal to 9.3×10^{-24} J/T)

The full magnitudes for the orbital and spin magnetic moments are given by using the angular momenta relationships 1.17 and 1.19.

For orbital motion, the magnitude of the total magnetic moment is:

$$\mu_l = -g\mu_B\sqrt{l(l+1)} \qquad (\text{ie } L = \hbar\sqrt{l(l+1)}) \qquad 1.28$$

For the spin magnetic moment, its full magnitude is:

$$\mu_s = -g\mu_B\sqrt{s(s+1)} \text{ or } \quad \mu_s = -g\mu_B\frac{\sqrt{3}}{2} \ (\text{as } s = \tfrac{1}{2}) \qquad 1.29$$

(Note: μ_s is equal to 1.62×10^{-23} J/T)

The values for μ_{sz} and μ_s indicate that the angle between the electron spin axis and the magnetic field is approximately 55^0.

Measured values for g (using gyromagnetic methods) give values only a little less than 2, indicating that almost all of the magnetism of atoms is due to electron spins. If the g value is between 1 and 2 then a proportion of the magnetic moment is provided by orbital motion. Values measured by microwave resonance often give g values slightly more than 2 due to a conserving of momentum when orbital contributions are restricted by the crystal lattice fields (Kittel 1949).

The value of g, measured for Fe^{2+} ions in silicate minerals, can be anisotropic (Coey and Ghose, 1988). That is, it can produce different values depending on the orientation of the mineral during measurements. As an anisotropic g value indicates an anisotropy in the spin-orbit coupling, it is an important point to consider when explaining the particle rotations described later in chapter 13.

Summary

Magnetic induction

$$B = \mu_0(H + M)$$

B = magnetic induction (T)
M = magnetisation (A/m)
H = magnetic field intensity (A/m. 1A/m = $4\pi \times 10^{-3}$ Oe)
μ_0 = permeability of free space ($4\pi \times 10^{-7}$ Wb/Am)

Magnetic moment per unit volume

$$\frac{m}{V} = \mu_0 M = \mu_0 k_v H$$

k_v is the volume magnetic susceptibility (dimensionless)

Magnetic susceptibility

$$k_v = k_g D$$

k_g is the magnetic mass susceptibility (m^3/kg)
D is the density of the magnetic material (kg/m^3)
(k_g in SI units = k_g in cgs units multiplied by $4\pi \times 10^{-3}$)

Measurement of the magnetic mass susceptibility of small particles

$$k_g = \frac{a}{\mu_0 H \frac{\partial H}{\partial x}} \qquad \text{(N)}$$

a is the acceleration due to gravity (m/sec^2)
$\frac{\partial H}{\partial x}$ is the magnetic field gradient (T/m)

Translational force on a particle in a magnetic field

$$F = \mu_0 k_v V H \frac{\partial H}{\partial x} \qquad \text{(N)}$$

V is the particle volume (m^3)

Torque applied to a magnetised particle

Vector product $\qquad \tau = \tilde{m} \times \tilde{H}$

Magnitude of torque $\qquad \tau = mH \sin\theta \,(\text{N.m})$

θ is the angle between the particle magnetisation and the external field

Electron quantum numbers

n is the principal quantum number (main orbit size)
l is the second quantum number and describes the orbit shape, or ellipticity.
(l = 0. 1, 2, ..., n-1)
m_l is the space quantisation number, or orientation of the orbit to the magnetic field.
(m_l = 0. $\pm$ 1, $\pm$2, ... $\pm l$)
m_s is the electron spin quantum number ($\pm\frac{1}{2}$)

Relationship between angular momentum and magnetic moment

$$\mu = \frac{-g\mu_B}{\hbar} L$$

μ is the magnetic moment (J/T)
μ_m is the Bohr magneton (9.27×10^{-24} J/T)
$\hbar$ is Planck's constant (1.054×10^{-34} J sec)
L is the angular momentum (J sec)
g is the gyromagnetic ratio (1 for orbital motion; 2 for electron spin)

Electron orbital magnetic moment

$\mu_l = -g\mu_B\sqrt{l(l+1)}$ (total orbital magnetic moment)

$\mu_{lz} = -g\mu_B m_l$ (component parallel to magnetic field)

Electron spin magnetic moment

$\mu_s = -g\mu_B\frac{\sqrt{3}}{2}$ (total spin magnetic moment)

$\mu_{sz} = -g\mu_B m_s$ (component parallel to magnetic field)

($\mu_s = 1.62 \times 10^{-23}$ J/T)

($\mu_{sz} = 9.3 \times 10^{-24}$ J/T)

Conversions between cgs and SI units for magnetic susceptibility

Mass susceptibility (k_g)

SI units = cgs units x 4π x 10^{-3}

Volume susceptibility (k_v)

SI units = cgs units x 4π

Chapter 2

Mineral Magnetism

Introduction

The previous chapter presented the general equations of magnetism and then examined the basic element of magnetism, the spinning and orbiting atomic electron, and its behaviour in a magnetic field. Unfortunately the macroscopic magnetic properties of a mineral particle can not be deduced simply by adding up the contributions of all the individual electrons.

The ions in a solid are not isolated. They interact with each other to varying degrees through a three-dimensional crystal structure and an electrostatic molecular field. Outer electron orbits become unresponsive to space quantisation, and overlap to a degree determined by the crystal structure and the ion size, forcing electron spin alignments in neighbouring atoms to take account of the Pauli exclusion principle. In addition, all of these interactions are subject to the thermal motions of the ions.

The effect of the crystal lattice is to place restrictions on electron orbit orientations, and in some cases to control electron spin orientations between neighbouring ions that have a magnetic moment. Inner unpaired electrons in an ion (e.g. the rare-earths) may be shielded by the outer electrons from the effects of a crystalline field, and may behave differently to the outer electrons.

The magnetism of an atom

Four quantum numbers n, l, m_l and m_s have been introduced for the atomic electron (see page 13). The principal quantum number n takes the values1, 2, 3, ... In practice these numbers are often referred to by the letters *K, L, M, N,* .... The second quantum number, l, which described the orbit shape, takes the values 0, 1, 2, ..., (n-1). By convention the values of l are referred to as *s, p, d, f, g* (for l = 0, 1, 2, 3, and 4). An electron in the L main orbit (n=2), in an orbit with *s* ellipticity (l=0), is often referred to as a *2s* electron. An electron in the M main orbit (n=3), with *p* ellipticity (l=1), is referred to as a *3p* electron, and so on.

Table 2.1 (from Yarwood, 1973) shows the arrangements of electrons around the atoms of the first 46 elements of the periodic table. The m_l and m_s quantum numbers are not shown in this table, except by the maximum number of electrons possible in any l state. For example the *3p* state can give values for m_l of 0, ±1, and each of these three m_l states can hold two electrons (with $m_s = \pm\frac{1}{2}$). Therefore the *3p* state can accommodate a maximum of 6 electrons.

Table 2.1

Arrangements of electrons in the shells and sub-shells of atoms

Atom	Atomic No. Z	K	L		M			N				O				
		$1s$	$2s$	$2p$	$3s$	$3p$	$3d$	$4s$	$4p$	$4d$	$4f$	$5s$	$5p$	$5d$	$5f$	$5g$
H	1	1														
He	2	2														
Li	3	2	1													
Be	4	2	2													
B	5	2	2	1												
C	6	2	2	2												
N	7	2	2	3												
O	8	2	2	4												
F	9	2	2	5												
Ne	10	2	2	6												
Na	11	Core of 10 electrons as in neon.			1											
Mg	12				2											
Al	13				2	1										
Si	14				2	2										
P	15				2	3										
S	16				2	4										
Cl	17				2	5										
A	18				2	6										
K	19	Core of 18 electrons as in argon						1								
Ca	20							2								
Sc	21						1	2								
Ti	22						2	2								
V	23						3	2								
Cr	24						5	1								
Mn	25						5	2								
Fe	26						6	2								
Co	27						7	2								
Ni	28						8	2								
Cu	29						10	1								
Zn	30						10	2								
Ga	31						10	2	1							
Ge	32						10	2	2							
As	33						10	2	3							
Se	34						10	2	4							
Br	35						10	2	6							
Kr	36						10	2	6							
Rb	37	Core of 36 electrons as in krypton.										1				
Sr	38											2				
Y	39									1		2				
Zr	40									2		2				
Nb	41									4		1				
Mo	42									5		1				
Te	43									6		1				
Ru	44									7		1				
Rh	45									8		1				
Pd	46									10						

(From Yarwood, 1973)

The magnetism of atoms is related to the m_l (space quantised) states. Each of these can hold 2 electrons, one with spin $+\frac{1}{2}$ and one with spin $-\frac{1}{2}$. If both are present (the electrons are paired), their magnetic moments and angular momenta cancel each other, leaving no nett magnetic moment or angular momentum. If only one electron is present (the electron is unpaired), then there is a resultant magnetic moment and an angular momentum for that orbital.

Atomic magnetism is associated with unpaired electrons. Although not all unpaired states may be suggested by table 2.1 (due to no information on the m_l states), any atom (not ion) in the table containing a sub-shell with an odd number of electrons will have a magnetic moment. Unpaired electrons in an atom will all tend to align with spins parallel.

Effects of crystal structure on the magnetic moment of a crystal

The quenching of orbital motion

In chapter 1 the gyromagnetic ratio was introduced (equation 1.24), and it was noted that its value is 2 for electron spins and 1 for orbital motion. Measurement of the gyromagnetic ratio for crystalline substances provide a measurement of the relative importance of the spin and orbital contributions to the magnetic moment of a crystal. The value of g for most crystalline substances is very close to 2, indicating that the magnetic moment is produced almost entirely by electron spins, with orbital motion contributing very little.

The reason for the lack of contribution from orbital motion is that the outer orbits have become fixed relative to the surrounding ions by the large inhomogeneous electrostatic fields associated with the crystal formation and its structure. For most magnetic ions it is the outer electron orbits which contain the unpaired electrons. The orbital motion is said to have been quenched. That is, the orbits are not free to orient themselves in an applied magnetic field and the space quantisation mentioned in chapter 1 does not occur.

To a first approximation, the magnetic moment of a crystal or particle may be considered as due only to electron spin.

Parallel ordering of spins due to electrostatic interactions

Blakemore (1985) gives some interesting information on the development of ferromagnetic theory, which illustrates both the magnitude of the molecular electrostatic interaction and its effect on the ordering of electron spins. Early calculations by Weiss in 1907 showed that while the available magnetic field from neighbouring atoms in iron was about 10^6 A/m, the effective magnetic field strength required to cause the ferromagnetism in iron would need to be about 10^{10} A/m. Magnetic interaction between neighbouring atoms could not therefore account for the ferromagnetism of iron. It was not until 1928 that Heisenberg showed that the ferromagnetism of iron could be explained in terms of a quantum mechanical theory of electrostatic interaction between neighbouring iron atoms. The interaction is explained in terms of an exchange integral (J_e), which is an expression of the electrostatic potential energy between neighbouring spins. This varies according to the ratio r_a/r_{3d}, where r_a is the atomic radius and r_{3d} is the radius of the *3d* electron shell. The resulting curve, known as the Bethe-Slater curve, is illustrated in figure 2.1. The variation of the curve, from negative to positive, is due to quantum mechanical considerations (Pauli exclusion principle) as the atoms come closer together and their outer orbits begin to overlap.

Figure 2.1

Variation of the exchange integral with separation between magnetic atoms
The Bethe-Slater curve

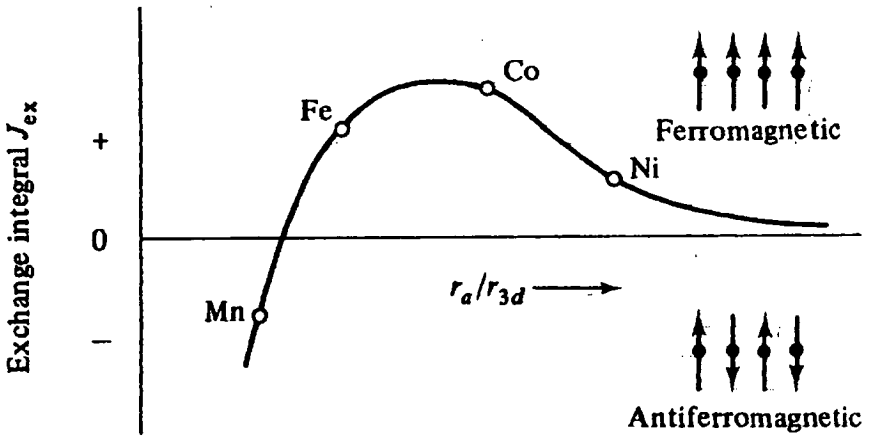

(From Cullity 1972)

If the exchange integral is positive then parallel spin arrangement is favoured between adjacent atoms. The spacing of atoms in iron places the exchange integral in the positive region. If the atomic distances are too small (as in the case of Mn) or too large an anti-parallel arrangement of spins is favoured.

Where a material contains adjacent magnetic atoms, a parallel spin arrangement will result if the atomic spacing is within a narrow range which gives a positive exchange integral for the electrostatic interaction. Atomic spacings for iron, cobalt and nickel fall within this range.

Superexchange effects across intervening ions

The superexchange principle is similar to electrostatic exchange discussed above, but in this case the exchange occurs through an intervening atom such as oxygen or sulphur. Perhaps it is much easier to consider superexchange in a more pictorial way, in terms of a sharing of outer electrons between the overlapping orbits of the magnetic and non-magnetic ions, as illustrated in figure 2.2.

In figure 2.2 the outer orbits of the O^{2-} and Mn^{2+} ions overlap, and the outer (*2p*) electrons of the oxygen ion spend some time in the manganese ions. The Mn^{2+} ion has 5 electrons in the *3d* sub-shell (which can contain 10. See table 2.1). Each of these is in an unpaired state and all five electrons have spins parallel to each other. Therefore the Mn^{2+} ion carries a spin moment of 5 μ_B . If an electron from the O^{2-} ion is to spend any time in the Mn^{2+} ion, it must have a spin which is anti-parallel to the Mn^{2+} moment, because there are no other available parallel spin states. The Mn^{2+} on the other side of the O^{2-} ion must then share the other *2p* oxygen electron, which has the opposite spin. The two Mn^{2+} ions therefore have anti-parallel spins.

Figure 2.2

The relationship between Mn spins as a result of superexchange across an intervening oxygen ion

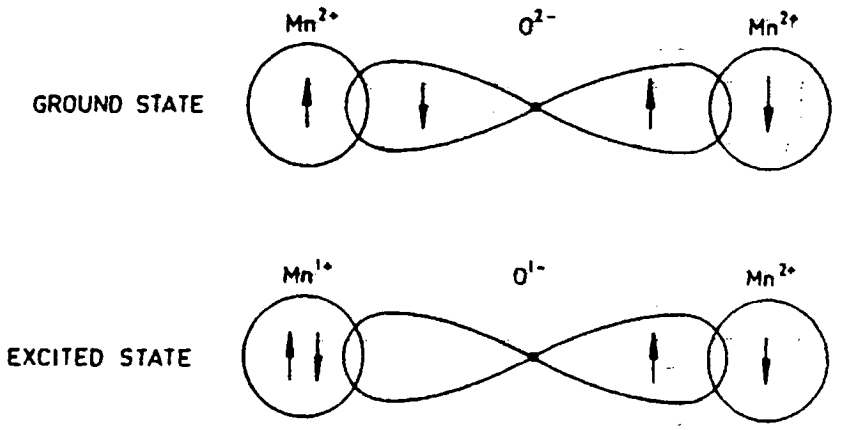

(From Banerjee, 1991)

In figure 2.2 the Mn^{2+} ions are shown directly opposed across the O^{2-} ion. Under these conditions the exchange is the strongest, but more generally the angle formed by the metal ions and the centre of the oxygen ion will be less than 180^0, as shown in figure 2.3.

Figure 2.3

Orientation of metal ions with respect to the *2p* orbit of the oxygen ion.

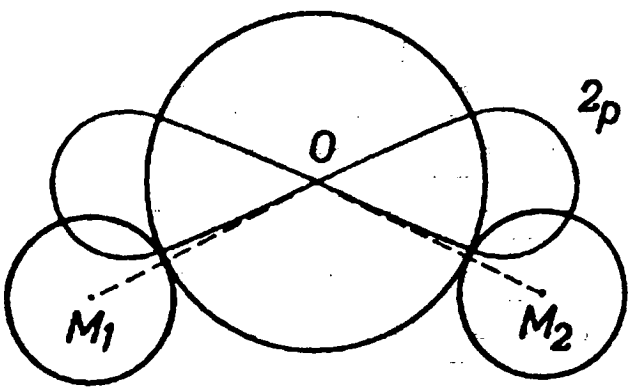

(From Smit and Wijn, 1959)

If the angle M_1 - O - M_2 in figure 3 is between 180 and 90^0, electrons from the oxygen ion are less likely to be found with the metal ions and the resulting superexchange is correspondingly weaker. Therefore it is not only the distance between metal and oxygen (or sulphur) ions which must be considered, but also the position of the metal ions with respect to the anion.

Magnetocrystalline anisotropy

The exchange and superexchange forces discussed above may fix the relative direction of neighbouring atomic moments, through electron spin alignments, but a fixed direction of magnetisation with respect to crystal axes remains to be explained. While the orbitals may be quenched (fixed relative to the crystal structure), and the orientation of electron spins relative to each other may become fixed, so far no reason has been given for any preferred orientation of the electron spins with respect to the crystal lattice.

Cullity (1972) provides a very clear qualitative explanation for a coupling of the electron spins to the crystal lattice, through a magnetocrystalline anisotropy. In a free atom there exists a coupling of the moments from electron spin and orbital motion. This is referred to as spin-orbit coupling. The unpaired electrons responsible for magnetic moment are in the outer atomic orbitals (with the exception of the rare-earths). It is precisely these outer orbitals which become quenched to some degree by the electrostatic crystalline field. Any quenching of the orbital motion will, through the agent of spin-orbit coupling, place a preferred direction of magnetisation on the electron spins. Electron spin moments which are aligned with the orbital moments will be in the lowest energy state. A rotation of the electron spins away from the orbital orientations will require an input of energy to overcome the spin-orbit coupling energy. The amount of energy needed to rotate the electron spins is the same as the spin-orbit coupling energy. Magnetocrystalline anisotropy is very dependent on temperature, decreasing very rapidly with increasing temperature, and vanishing at the Curie temperature (Cullity, 1972).

Therefore spin-orbit coupling is the main cause of magnetocrystalline anisotropy, where crystalline materials show a preferred direction of magnetisation.

An important consideration, especially for this thesis, is that magnetocrystalline anisotropy also appears in cubic crystals. Figure 2.4 shows the magnetisation curves for cubic iron crystals and indicates the directions of easy (low energy state) and hard (high energy state) magnetisation.

Figure 2.4

Magnetisation curves for a single crystal of iron

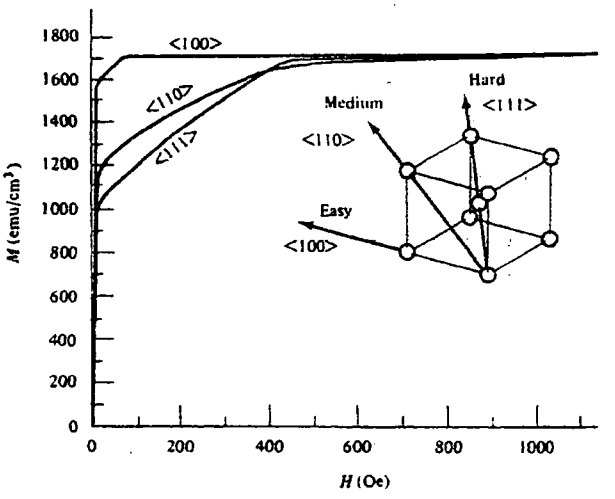

(From Cullity, 1972)

Figure 2.5 shows the distribution of ions around the octahedral sites in the spinel structure. In such a structure the direction of easy magnetisation is along the trigonal axis, as shown.

Figure 2.5

The direction of easy magnetisation in the cubic spinel structure where both sub-lattices contain magnetic ions. (open circles represent oxygen ions and solid ones represent cations)

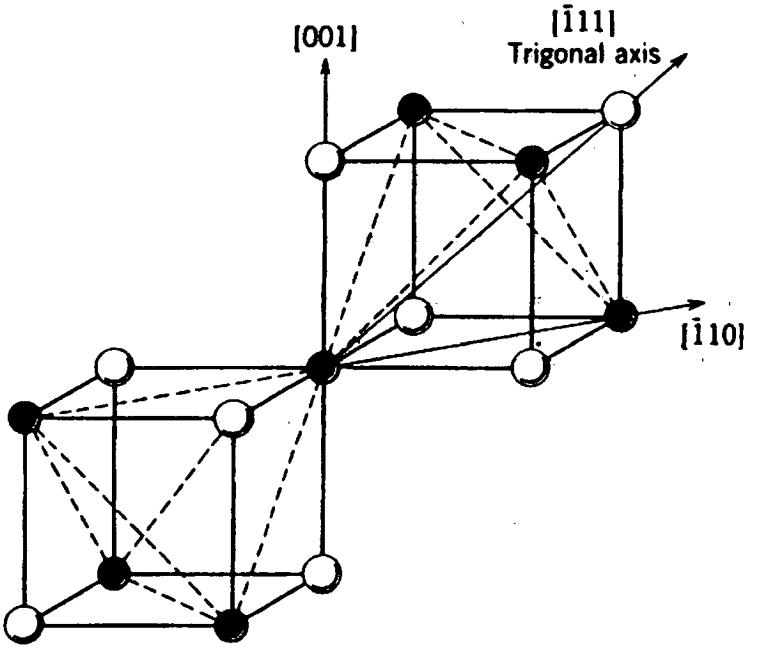

(From Chikazumi and Charap, 1978)

The magnetocrystalline anisotropy of a crystal is usually expressed in terms of anisotropy constants, which describe the maximum energy required to rotate the particle magnetisation away from the directions of easy magnetisation. A general expression, which relates the energy to all the crystal axes, involves a series expansion of even cosine powers (eg. Anderson, 1968), but by restricting the consideration to uniaxial and biaxial anisotropy (such as a plane containing two of the directions of easy magnetisation in a cubic crystal), the expressions are greatly simplified.

For uniaxial anisotropy (eg. hexagonal system), the anisotropy energy density is:

$$E = K_1 \sin^2\theta + K_2 \sin^4\theta + \ldots\ldots \qquad (\text{J/m}^3) \qquad 2.1$$

For a biaxial anisotropy (eg. 001 plane of a cubic iron crystal)

$$E = \tfrac{K_1}{4} \sin^2 2\theta \qquad (\text{with no } K_2 \text{ term}) \qquad (\text{J/m}^3) \qquad 2.2$$

The angle θ is the angle between the spotaneous magnetisation and the direction of easy magnetisation in the crystal, and K_1 and K_2 are the anisotropy constants, which have units of J/m^3. In many cases the K_2 term is small enough to be ignored.

Some values for K_1 are:

For iron:	$K_1 = 4.8 \times 10^4$	J/m^3
For magnetite:	$K_1 = -1.35 \times 10^4$	J/m^3
For nickel:	$K_1 = -5 \times 10^3$	J/m^3

The anisotropy constants decrease with increasing temperature, reaching zero at the Curie temperature.

For a particle of volume V, if the particle magnetisation is rotated to an angle θ from an easy magnetisation direction, a torque is exerted on the crystal. As the energy varies with the angle θ, this torque is consequently given by the derivative of the energy.

$$\tau = \frac{\partial E}{\partial \theta} = -K_1 V \sin 2\theta \quad \text{(N.m)} \quad \text{(for a uniaxial anisotropy)} \qquad 2.3$$

$$\tau = \frac{\partial E}{\partial \theta} = -\frac{K_1}{2} V \sin 4\theta \quad \text{(N.m)} \quad \text{(for a cubic anisotropy, in 001 plane)} \qquad 2.4$$

Where V is the particle volume (m^3)

Anisotropy constants are frequently measured using a torque magnetometer. For this method an external field sufficient to magnetically saturate the specimen is used. The particle magnetisation then remains substantially aligned with the external field as either the specimen or the magnetic field is rotated slowly. The torque which is applied to the particle is measured while the particle is slowly rotated relative to the external field, and equations 2.3 and 2.4 then allow calculation of the anisotropy constant K_1 (K_2 remains undetermined).

The maximum torque magnitude occurs at θ = 22.5^0 (and subsequently at 45^0 intervals) for rotation in the (001) plane of a cubic crystal, and at θ = 45^0 (and subsequently at 90^0 intervals) for a uniaxial crystal (Cullity, 1972).

Sometimes the anisotropy forces are expressed as an anisotropy field (H_A). This is evaluated, for small θ, by equating the torque in equations 2.3 and 2.4 with the torque ($H_A m_s \sin\theta$) due to an anisotropy field, and gives: $H_A = \frac{2K_1 V}{m_s}$ for both uniaxial and cubic ((001) easy axes) anisotropies, and $H_A = \frac{-4K_1 V}{3m_s}$ for a cubic crystal with (111) easy axes (e.g. magnetite).

If the particle magnetisation is being held at an angle θ from the direction of easy magnetisation, the above torques (equations 2.3 and 2.4) must be balanced by an opposite torque applied to the magnetisation, by an external field H at an angle ϕ to the magnetisation. Therefore we can equate the magnitudes of these two torques:

$$mH \sin\phi = K_1 V \sin 2\theta \quad \text{or} \quad \mu_0 MH \sin\phi = K_1 \sin 2\theta$$

i.e.

$$\sin\phi = \frac{K_1 V \sin 2\theta}{mH} = \frac{K_1 \sin 2\theta}{\mu_0 MH} \quad \text{(for a uniaxial anisotropy)} \qquad 2.5$$

$$\sin\phi = \frac{K_1 V \sin 4\theta}{2mH} = \frac{K_1 \sin 4\theta}{2\mu_0 MH} \quad \text{(for a biaxial anisotropy)} \qquad 2.6$$

Where m is the magnetic moment of the particle, and M is the particle magnetisation.

The angle ϕ in equations 2.5 and 2.6 (angle between particle magnetisation and the external field) has been referred to in chapter 4 as the rotation index.

Shape anisotropy

Particles which are long and thin (without considering any magnetocrystalline anisotropy) may be more easily magnetised along their long axis. This is referred to as shape anisotropy, and may be explained in terms of demagnetising fields. The demagnetising fields arise within a particle because the direction of the field H is always from N to S poles, and consequently is directed opposite to the magnetisation within a magnetised material. The strength of the demagnetising field is proportional to the magnetisation and inversely related to the pole separation between the two ends of the particle. For a long thin particle, the demagnetising field is therefore strong across the particle, but weak along it.

The directional variation of the demagnetising field may be described, with reference to three orthogonal axes (a, b, and c), using the demagnetising factors N_a, N_b, and N_c. The relationship between these three factors is:

$$N_a + N_b + N_c = 1 \qquad \text{(SI units)} \qquad 2.7$$

The effect of shape anisotropy is easier to consider for a long thin particle in the shape of a prolate spheroid, where $N_a = N_b < N_c$. Here the situation is similar to that of a uniaxial magnetocrystalline anisotropy. If the magnetisation is rotated away from the c direction, energy must be added, and consequently a torque may be applied to the particle. For the prolate spheroid Cullity (1972) gives a shape anisotropy energy in a similar form (involving a $\sin^2\theta$ term) to that of the magnetocrystalline anisotropy as:

$$E = K_s \sin^2\theta \qquad 2.8$$

Where $K_s = \frac{\mu_0}{2}(N_a - N_c)M^2$ (shape anisotropy constant)

Equations 2.1 and 2.8 both have an angle-independent first term, in order to describe total energy, but this has been omitted as it is isotropic. The torque applied to the crystal by rotating the magnetisation through an angle θ may be obtained in a similar way to that for magnetocrystalline anisotropy. At a certain value of N_a - N_c the value of the shape anisotropy can equal that of the magnetocrystalline anisotropy. Cullity (1972) points out that this occurs for cobalt for a particle that has a c/a ratio of 3.5.

If both anisotropies are along the same axis, equations 2.1 and 2.2 can be combined with equation 2.8 to give a total anisotropy relationship in terms of the angle ϕ.

$$\sin\phi = \frac{(K_1+K_s)V\sin 2\theta}{mH} = \frac{(K_1+K_s)\sin 2\theta}{\mu_0 MH}$$ (for a uniaxial magnetocrstalline anisotropy)

$$\sin\phi = \frac{\frac{K_1}{2}V\sin 4\theta + K_s V\sin 2\theta}{mH} = \frac{\frac{K_1}{2}\sin 4\theta + K_s \sin 2\theta}{\mu_0 MH}$$ (for a plane containing two of the cubic axes of magnetocrystalline anisotropy)

The above two relationships are combined anisotropy versions of equations 2.5 and 2.6.

Diamagnetism

Diamagnetism is the tendency for materials to oppose a magnetic field, and to be repelled in a magnetic field gradient. All substances show this tendency, but the effect is weak and is usually overcome by other magnetic effects.

The elements that are repelled by a magnetic field, which show measurable diamagnetism, are those that have no unpaired electron spins. They therefore have no resultant magnetic moment due to electron spin or orbital motion. Thus the monatomic gases He, Ne and A are diamagnetic. Where filled electron shells are produced by covalent or ionic bonding, diamagnetism is also evident, such as in the polyatomic gases H_2 and N_2, and in the solids NaCl, diamond and glass. Most organic compounds are diamagnetic.

The diamagnetic effect is associated with changes in the orbital motion of electrons in the presence of an external magnetic field. Both classical physics and quantum mechanics arrive at the same end point when explaining diamagnetism, so a classical picture will be given here.

If an electron in an orbit around an atom is considered as a small circulating electric current, then the application of an external magnetic field will induce a change in this current which is in proportion to the strength of the external field. This is exactly the same process that occurs on a macroscopic scale when a current loop is subjected to a changing magnetic field (as in an electric generator). On the macroscopic scale, unless the magnetic field continues to change, the current quickly dies away due to electrical resistance. On the electron orbit scale (as Maxwell pointed out,- see chapter one) there is no electrical resistance, and the induced current remains while the field is present. It produces a small magnetic moment in opposition to the applied field.

The diamagnetism associated with an atom should therefore be obtained by simply adding up all the contributions from all the electrons in an atom. Such a process does give values reasonably close to those actually measured. For example Cullity (1972) gives the calculated and measured values for carbon as -1.5×10^{-6} and -1.1×10^{-6} (cgs) respectively.

Because diamagnetism opposes an applied magnetic field, the effect within a material is to partially exclude the external field from the material (ie. B is reduced within the material). A perfectly diamagnetic solid would be a superconductor, where all magnetic flux is excluded.

While all materials must exhibit diamagnetism, the presence of a single unpaired electron spin in an atom or ion is enough to completely overwhelm it.

Paramagnetism

Provided the applied field is sufficiently weak, paramagnetic materials become magnetised in proportion to the applied magnetic field, but lose their magnetism almost immediately the magnetic field is removed.

Magnetism in these materials is due to unpaired electron spins that are too weakly tied to neighbouring spins through exchange or superexchange mechanisms for long range ordering of spins to develop. For many paramagnetic substances at room temperature, the

exchange and superexchange energies have merely been overcome by thermal energy. At a lower temperature such materials lose their paramagnetism and take on an ordered spin arrangement when the thermal energy becomes less than the exchange energy.

Some paramagnetic substances follow the Curie law, which states that their magnetic susceptibilities are inversely proportional to the absolute temperature.

$$\chi = \frac{C}{T}$$

Where: χ is the magnetic susceptibility
C is a constant
T is the absolute temperature

This law was reported by Curie in 1895 and was later given a theoretical basis by Langevin in 1905 (see Cullity 1972), which assumed that there was no interaction between electron spins. In fact, many paramagnetic substances follow a modified Curie law, in which a constant value needs to be subtracted from the absolute temperature.

$$\chi = \frac{C}{T-\theta}$$

Where θ is a constant with the dimensions of temperature

This relationship, introduced by Weiss in 1907, is referred to as the Curie-Weiss law. The extra term comes about because of the existence of what Weiss referred to as a "molecular field", which tends to align electron spins. Weiss' "molecular field" is due to the exchange and superexchange forces referred to above. In the paramagnetic state, being considered here, thermal energy may have overcome these forces, but their existence has the effect of changing the temperature decrease of susceptibility, as is illustrated in figure 2.6.

Figure 2.6

Variation of susceptibility with absolute temperature for the Curie law and the Curie-Weiss law

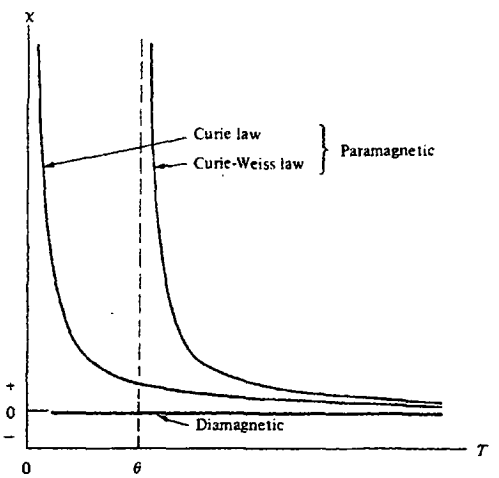

(From Cullity, 1972)

In figure 2.6 the effect of the exchange forces has been to make the susceptibility higher than it would otherwise be (ie. the graph is shifted to the right). This occurs if the exchange forces are positive, favouring a parallel alignment of spins. If the forces are negative then an anti-parallel alignment of spins is favoured, and the graph in figure 2.6 would be shifted to the left, giving a susceptibility lower than it would otherwise be (as it would be for $FeSO_4$ in figure 2.7).

Even though materials that follow the Curie-Weiss law behave magnetically as paramagnetics above the Curie temperature, there is still, except for cubic paramagnetics, an anisotropy in the magnetic susceptibility (Nye, 1957). This arises from spin-orbit coupling forces, as is indicated by anisotropic g values (Calas, 1988), and implies that a weak magnetic anisotropy is present, and that a relatively weak torque may be applied by a change in the external magnetic field direction.

Instead of plotting susceptibility against temperature, it is more usual to plot the inverse of susceptibility. The value of θ is then given from the intercept of the graph with the temperature axis, as shown in figure 2.7 where the $MnCl_2$ gives a positive intercept but the $FeSO_4$ gives a slightly negative intercept.

Figure 2.7

Reciprocal susceptibilities plotted against absolute temperature

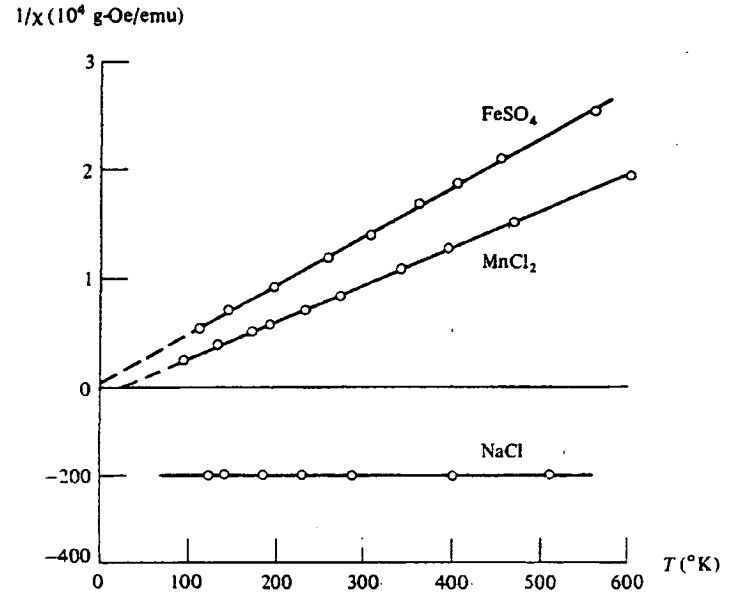

(From Cullity 1972)

Ferromagnetism

Although ferromagnetic materials may sometimes show no resultant magnetisation, within restricted regions, referred to as domains, they exhibit a spontaneous magnetisation, without the need for any external magnetic field. The electron spins are coupled parallel to each other by exchange forces which are of an electrostatic and quantum-mechanical nature.

Kittel (1971) gives the exchange forces as being equivalent to a magnetic field of the order of 10^7 gauss. Dipole-dipole magnetic forces are a factor of almost 10^4 too small, and play little part in the spontaneous magnetisation. Eisberg & Resnick (1985) calculate that, for iron, the dipole-dipole interaction could maintain an ordering of electron spins only to 0.22 K, when thermal agitation would destroy any ordering. In actual fact the ordering is maintained up till 1043 K.

The temperature at which a ferromagnetic condition is destroyed by thermal energy is referred to as the Curie temperature. Below this temperature the material exhibits ferromagnetism, while above it the material closely follows the Curie-Weiss law for paramagnetism. The variation of magnetisation (up to the Curie temperature) and the curves for susceptibility χ and inverse susceptibility (above the Curie temperature) are illustrated in figure 2.8.

Figure 2.8

Ferromagnetic magnetisation and susceptibility curves above and below the Curie temperature. Note that the curve to the left is given in terms of saturation magnetisation σ_s (compared to 0 K temperature magnetisation σ_0) while the curves to the right are in terms of χ or $1/\chi$ (as indicated)

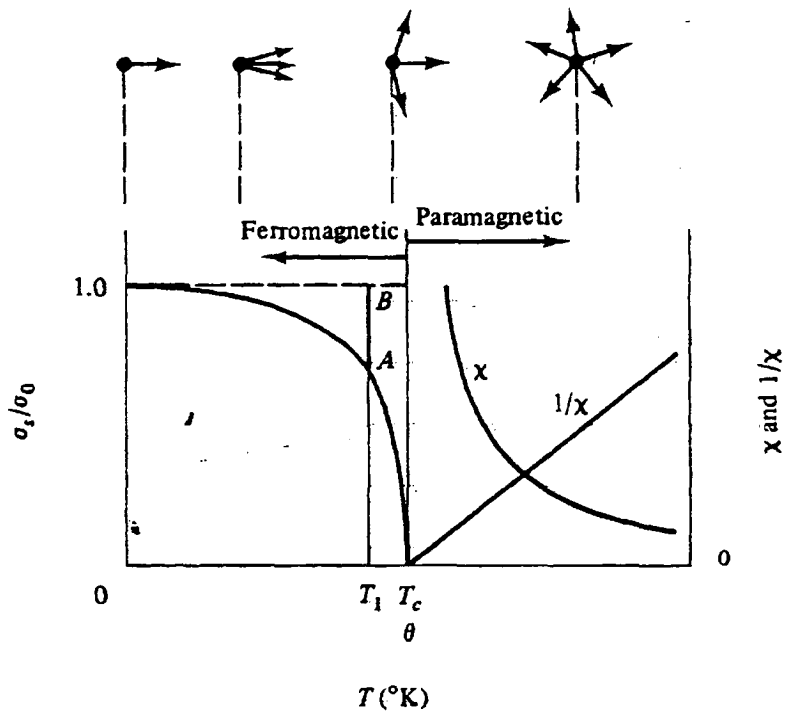

(From Cullity, 1972)

Antiferromagnetism

Antiferromagnetic materials have anti-parallel electron spins in adjacent crystal sub-lattices, usually as a result of superexchange across intervening anions. The ions in each sub-lattice are usually of the same type. The result is that, while being highly magnetically ordered, they appear to be non-magnetic with no external field applied. The classical example

of antiferromagnetism is MnO, represented in figure 2.9. Note that the magnetic cell is twice the dimensions of the chemical unit cell.

Figure 2.9

Structure of MnO. (a) Chemical unit cell. (b) chemical and magnetic unit cells.

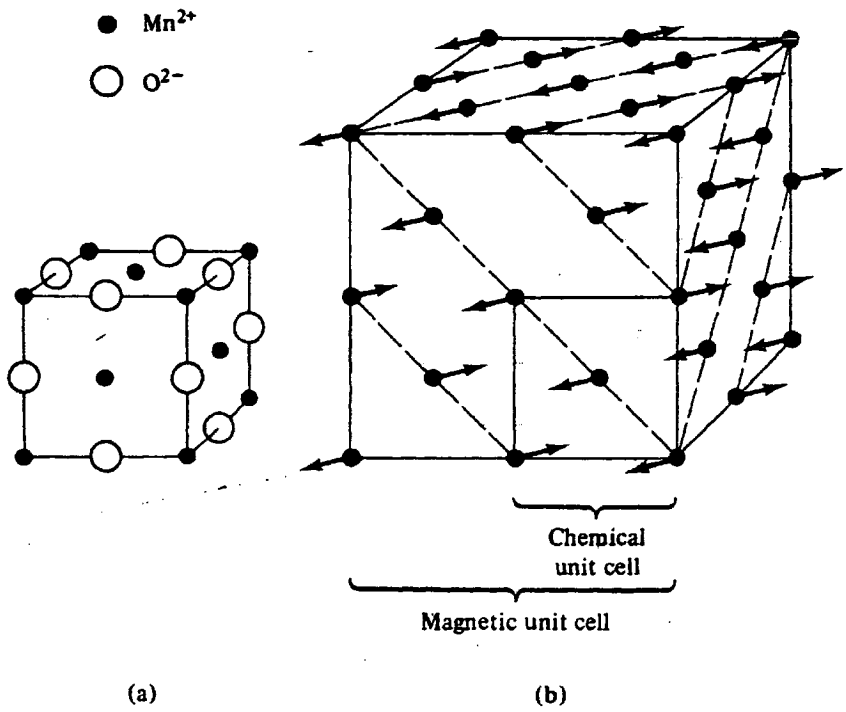

(From Cullity, 1972)

The magnetic susceptibility of antiferromagnetics actually increases with temperature, reaching a maximum at the point where the magnetic ordering breaks down due to thermal energy (see figure 2.10). This temperature is known as the Neel temperature, and is the antiferromagnetic equivalent of the Curie temperature for ferromagnetics.

The increase in susceptibility with increasing temperature below the Neel temperature is caused by a decrease in spin ordering with increasing thermal agitation. As the temperature rises, an external field is therefore able to align more spins in opposition to the molecular field.

Figure 2.10

Temperature variation of the susceptibility and inverse susceptibility for antiferromagnetics

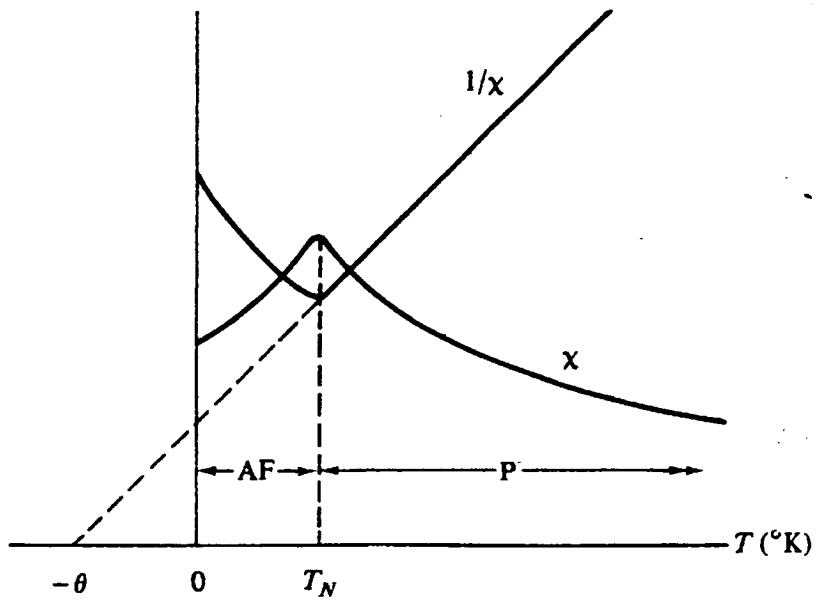

"AF" refers to the antiferromagnetic range, below the Neel temperature.
"P" refers to the paramagnetic range above the Neel temperature.
(From Cullity, 1972)

The $1/\chi$ line, in the paramagnetic region, is a straight line that extrapolates to a negative value of θ because the exchange force is negative, and any attempt to align one moment causes a tendency for the moment on an adjacent ion to point in the other direction.

While antiferromagnetism is common at very low temperatures (more common than ferromagnetism), it usually does not occur at room temperature,- at least for naturally occurring minerals. Some antiferromagnetic minerals are given below in table 2.2.

Table 2.2

Some antiferromagnetic minerals and their Neel temperatures.

Mineral	Composition	Neel temp. (°C)
Ulvospinel	Fe_2TiO_4	-153
Ilmenite	$FeTiO_3$	-205
Wustite	FeO	-87
Goethite	αFeOOH	120
Akaganeite	βFeOOH	-196 to 23
Fayalite	Fe_2SiO_4	-147
Pyroxene	$FeSiO_3$	-233
Troilite	FeS	320
Pyrolusite	MnO_2	-189
Siderite	$FeCO_3$	-233
Rhodochrosite	$MnCO_3$	-243

(Summarised from Carmichael, 1989)

As would be assumed from earlier comments and from figure 2.10, antiferromagnetic materials only show an apparent lack of magnetism if there is no applied magnetic field. As soon as an external magnetic field is applied, the energy balances are upset and a net magnetisation appears.

Applying an external field at right angles to the spin axes causes a canting of the spins of the two sub-lattices until the resultant moment is balanced by the exchange field (molecular field). The situation is described by Cullity (1972) where the degree of rotation (α) is given by:

$$\sin\alpha = \frac{\rho H}{2\gamma M}$$

Where: ρ is the density of the material
H is the applied field
γ is the molecular field constant ($H_m = \gamma M$)
α is the angle of spin rotation
M is the magnetisation of a sub-lattice (which is assumed not to change in response to the applied field for $H << H_m$)

The magnetic susceptibility for an external field at right angles to the spin axes is then:

$$\chi_\perp = \frac{1}{\gamma\rho}$$

This is independent of temperature up to the Neel temperature. It is the parallel susceptibility that increases with temperature below the Neel temperature. The behaviour of these two susceptibilities with increasing temperature is illustrated in figure 2.11.

If a stationary antiferromagnetic particle is placed in a rotating magnetic field, the particle magnetisation will cycle through values which are described by these susceptibilities.

Figure 2.11

Temperature dependence of antiferromagnetic perpendicular and parallel susceptibilities above and below the Neel temperature.

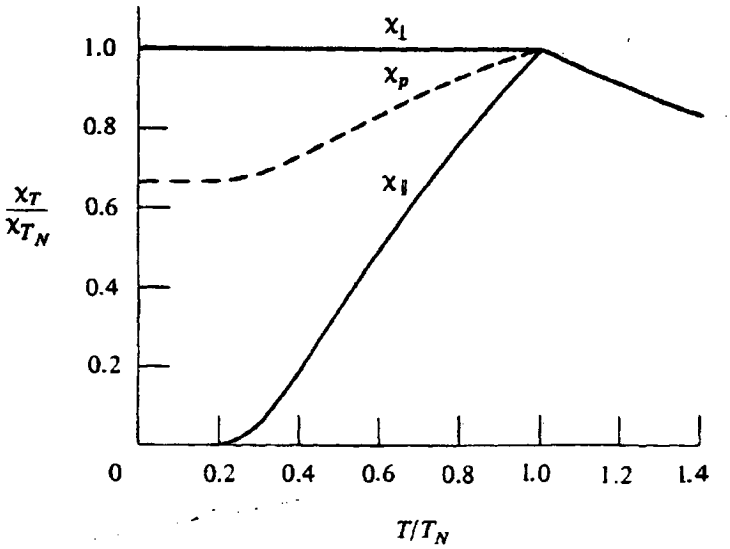

(From Cullity, 1972)

Ferrimagnetism

Ferrimagnetic materials may be considered as unbalanced antiferromagnetics. In an antiferromagnetic material electron spins in adjacent sub-lattices are equal and opposite, while in ferrimagnetic substances they are opposite, but not equal. This leaves the domains in ferrimagnetic materials with a nett spontaneous magnetic moment.

As for ferromagnetic materials, ferrimagnetic materials may show no nett magnetisation unless they are placed in an external field, which causes the preferential growth of magnetic domains aligned closest to the external field. The growth of these domains also follows the velocity relationship mentioned below.

As was the case for antiferromagnetics, the magnetic ordering in ferrimagnetic materials is due to a superexchange across an intervening non-magnetic anion. In antiferromagnetic materials there were equal numbers of magnetic ions and equal numbers of un-paired electron spins in both sub-lattices. In ferrimagnetic materials there are more magnetic ions in one sub-lattice, and the superexchange may involve the interaction of one ion in one sub-lattice with more than one ion in the other sub-lattice. This is illustrated in figure 2.12, where a magnetic ion in the A sub-lattice interacts via a non-magnetic anion with two magnetic ions in the B sub-lattice.

Figure 2.12

Superexchange across a non-magnetic ion in a ferrimagnetic material.

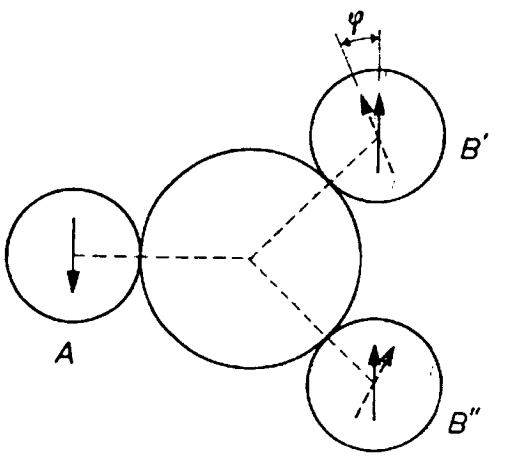

(From Smitt, 1959)

The angle φ depends on the relative magnitudes of the exchange energies between A and B' or B'', and between B' and B''. If $J_{AB} > 2J_{B'B''}$ then $\varphi = 0$. If $J_{AB} < 2J_{B'B''}$ then B' and B'' are no longer parallel.

Unlike antiferromagnetic materials, many ferrimagnetics retain their ferrimagnetism well above room temperature, with ferrimagnetic Curie temperatures as high as 600°C. Above the Curie temperature they become paramagnetic. Some ferrimagnetic materials are listed in table 2.3.

Table 2.3

Some ferrimagnetic materials

Material	Composition	Curie Temp.(^{0}C)
Magnetite	Fe_3O_4	575 to 580
Ilmenohematite	$Fe_{1.25}Ti_{0.75}O_3$	-10
Magnesio-ferrite	$MgFe_2O_4$	310 to 440
Jacobsite	$MnFe_2O_4$	300
Chromite	$FeCr_2O_4$	-185
Trevorite	$NiFe_2O_4$	585
Franklinite	$ZnFe_2O_4$	-264 to -258
Pyrrhotite	$Fe_{1-x}S$	300 to 325

(Summarised from Carmichael, 1989)

For paramagnetic materials and for ferromagnetic and antiferromagnetic materials above their Curie or Neel temperatures, the inverse susceptibility gives a straight line (see figures 2.7, 2.8 and 2.9). This not the case with ferrimagnetic materials, as is illustrated in figure 2.13.

Figure 2.13

The $1/\chi$ vs T curve for ferrimagnetic materials. The dashed line shows the actual inverse susceptibility line, while the solid line is the asymptote.

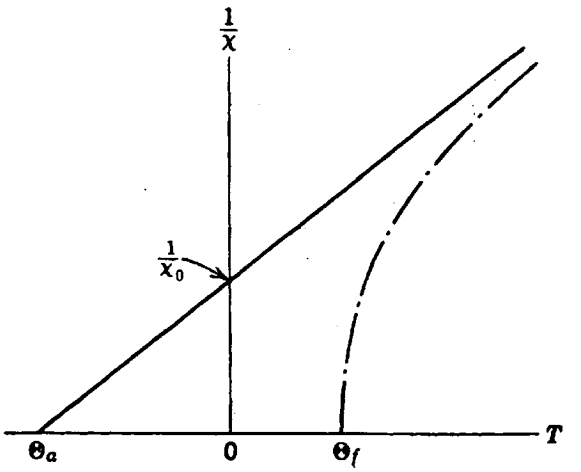

(From Chikazumi, 1978)

The marked deviation of figure 2.13 from the straight line relationship seen for other magnetically ordered materials occurs because of differences between the two sub-lattices in ferrimagnetics. Interactions between the ions in the A sub-lattice are different to the interactions between the ions in the B sub-lattice. Each sub-lattice follows its own Curie law, but at the same time the two sub-lattices are magnetically linked via the intermediate

non-magnetic anions. Although there are also two sub-lattices in antiferromagnetic materials, the ions in each one are the same and in similar crystallographic relationships.

Ferrimagnetics can exhibit a complex behaviour below the Curie temperature. Because the two sub-lattices are different, the magnetisation of each follows a different relationship as temperature increases. These differences are limited by the superexchange forces between the sub-lattices. For some ferrimagnetics (eg. $Li_{0.5}Fe_{1.25}Cr_{1.25}O_4$) a temperature exists where the magnetisations of the two sub-lattices are equal (but opposite in direction). This, when it occurs, is referred to as the "compensation" point. At this point the magnetisation is zero and an antiferromagnetic condition exists, but as the temperature increases further the magnetisation increases again, but with the opposite direction, before decreasing towards zero again at the Curie point.

For most ferrimagnetic minerals, behaviour below the Curie temperature is generally similar to that of ferromagnetics, except that the magnetisation decreases more quickly than for ferromagnetics.

The overall magnetic behaviour of a ferrimagnetic material, with increasing temperature, is shown in figure 2.14.

Figure 2.14

The characteristics of ferrimagnetism.
Note that the left side of the graph describes magnetisation
whilethe right side of the graph describes inverse susceptibility.

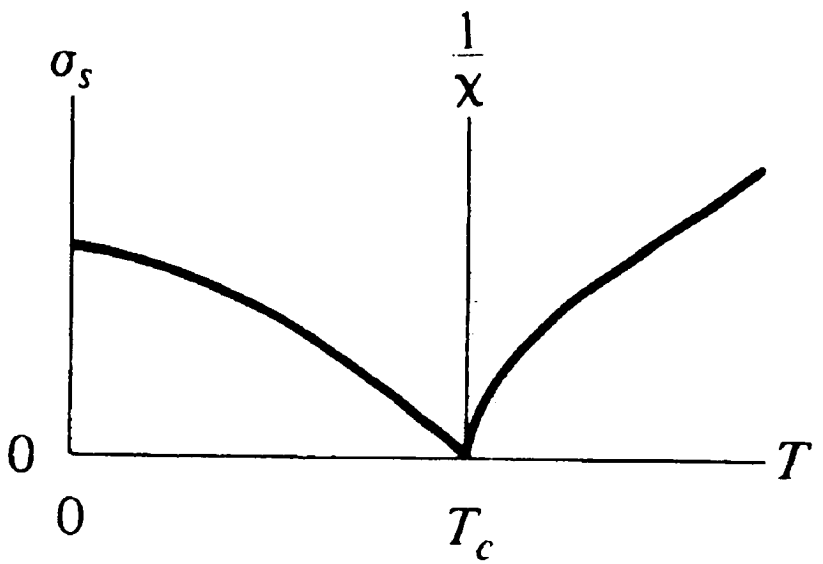

(From Cullity, 1972)

Magnetic Domains

All three of the above ordered magnetic arrangements (ferromagnetism, antiferromagnetism and ferrimagnetism), in the absence of an external field, will organise themselves into small spontaneously magnetised regions called magnetic domains. The appearance of magnetic domains may be seen as a way of reducing the energy of a crystal. In antiferromagnetic materials the domains are anti-phase domains that reduce the free energy of the crystal by increasing disorder. In ferromagnetic and ferrimagnetic materials the domains arise so as to reduce the magnetostatic contribution to the free energy. In particular, ferromagnetic and ferrimagnetic materials may not appear to show any spontaneous magnetisation unless they have first been placed in a magnetic field. The reason is that the above magnetic domains are arranged so that no nett magnetisation results. Placing the material in an external magnetic field causes a change in the domain arrangement so that a nett magnetisation appears.

The behaviour of these magnetic domains in a continuously changing (rotating) magnetic field is of some interest for the process of rotating field magnetic separation.

Domain arrangement

If a large volume of a ferromagnetic material is uniformly magnetised, then a substantial amount of energy is concentrated in an external magnetic field. If the material were to divide itself into two parallel regions, magnetised in opposite directions, then the energy in any external field is approximately halved. The latter is therefore a preferred low-energy situation. The energy of the system could be reduced by further subdivisions, but a point is reached where the energy involved in the walls (or the spin transition regions between domains, referred to as Bloch walls) becomes greater than the energy decrease due to smaller domain formation. It is at this point (less than 10 μm, and usually in the region of 1 μm) that stable domains are formed.

When an apparently unmagnetised ferromagnetic material is placed in an external field, the external field provides an energy bias to the system of domains, such that those domains oriented closest to the direction as the external field now have the lower energy. When this happens the Bloch walls migrate through the material in such a way that the low-energy domains grow at the expense of the higher-energy domains. For an increasing external field strength a point is reached where all the magnetisation is directed in the same direction. This direction will initially be close to the easy magnetisation direction that is closest to the external field orientation. A further increase in the external field overcomes any magnetic anisotropy within the crystal, and the internal field rotates to align itself with the external field. These magnetisation processes are illustrated in figure 2.15.

Figure 2.15

Bloch wall motion and rotation of magnetic moment during magnetisation

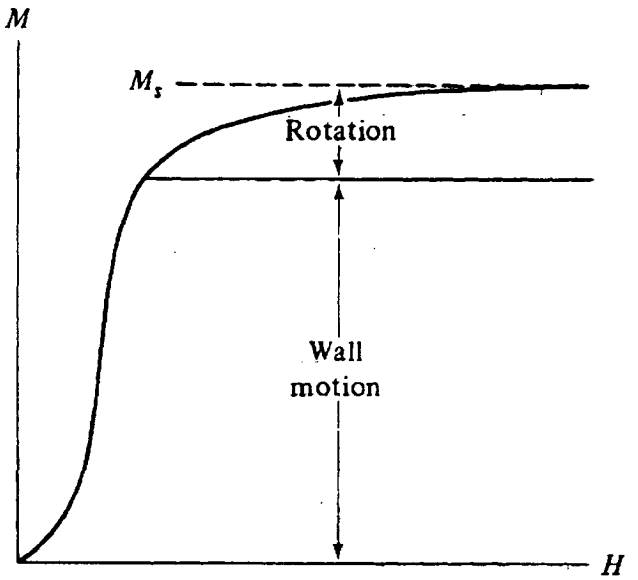

(From Cullity 1972)

It can be seen from figure 2.15 that the final stage of domain rotation requires a relative large increase in field for only a small increase in magnetisation. This reflects the strength of magnetic anisotropy in ferromagnetic materials, and provides the main energy barrier which allows a rotating magnetic field to rotate the particles.

As the size of ferromagnetic particles decreases, they are able to contain fewer domains. Consequently as the particle size decreases there is increasingly imperfect cancellation of equilibrium domain magnetisations, and the nett magnetisation of the particle is not zero. In the case of a single domain particle the nett magnetisation equals the saturation magnetisation, and changing the direction of magnetisation involves overcoming magnetic anisotropy.

Domain wall velocity

The domain growth mentioned above does not occur instantaneously as a field is applied (or changed in direction). Domain walls have a finite velocity, which is limited by damping associated with eddy-current effects and electron-spin rotation effects at the domain walls. The velocity depends on the strength of the applied field and on the material itself. Velocities as high as 14 km/s are reported for long iron whiskers (Dillon, 1963), but velocities in minerals such as natural magnetite are much lower than this. Williams et al. (1950) experimentally examined the factors associated with wall velocities, and, in agreement with previous workers, expressed the velocity as:

$$v = c(H - H_0) \qquad 2.9$$

Where: c is a proportionality factor, referred to as the wall mobility.
H is the external magnetic field
H_0 is the critical field for wall motion (not wall formation)

The value of H_0 depends very much on such factors as shape anisotropy and on crystal imperfections, as well as on the material itself. It is as high as 10^4 A/m for ferromagnetics and as low as 1.4 A/m for some ferrites at low temperatures (Cullity, 1972, and Anderson, 1968). The value of H_0 may be approximately the same as the coercive force H_c, but the concept is a little different. While the coercive force is the field required to reduce remanent particle magnetisation to zero after a magnetising field has been removed, the critical field is the field strength necessary to just maintain domain wall motion. The critical field is usually determined by measuring wall velocities at various fields and extrapolating to zero velocity. Domain wall mobilities vary from as high as 4.5 $m^2/A.s$ to as low as 6×10^{-4} $m^2/A.s$ (Cullity, 1972).

There have been very few attempts to directly measure domain wall velocities in natural crystals. Most direct measurements have been carried out on synthetic crystals of high purity and with minimal imperfections. This was even the case with the early measurements on magnetite, made by Galt (1932). In his 1932 paper Galt refers to unsuccessful attempts to measure wall velocity in natural magnetite, and comments that the difficulties were due to imperfections and impurities which occur in natural compounds. For his pure synthetic magnetite crystal, Galt found the mobility (c, in equation 2.9) for magnetite to be 1900 cm/sec.Oe (0.24 $m^2/A.s$). However Galt's crystal had a saturating field of only 3.5 Oe (278 A/m) and a coercive force of only 0.1 Oe (8 A/m). The latter is a factor of about 10^2 smaller than the expected figure for natural magnetite (see below). Later measurements on individual grains in synthetic polycrystalline manganese-magnesium ferrite (Knowles, 1961) indicated wall mobilities of the order of 500 cm/sec.Oe (0.06 $m^2/A.s$). The latter sample had a coercive force in the vicinity of 0.6 Oe (48 A/m), estimated from domain wall velocity.

While domain wall mobilities may be obtained from ferromagnetic resonance measurements, and may be estimated from magnetisation, anisotropy, and exchange constants (Rado & Suhl, 1963), the obtained values tend to be too high even for pure synthetic crystals.

There is therefore very little information available which could reasonably represent average domain wall velocities across natural magnetite grains of up to 1 mm in diameter.

Domain wall velocity and particle size

Stacey and Banerjee (1974) have described coercivity as "a quantitative measure of the resistance of a domain structure to changes". This serves to illustrate the similarity between coercive force H_c and the critical field H_0, and to justify roughly equating the two quantities below. Coercive force is fairly easily measured, whereas actual domain wall velocity (and hence H_0) is difficult to directly measure on small particles. The comments below assume that variations in the coercive force H_c imply similar variations in the critical field H_0.

Coercive force is very dependent on particle size. Stacey and Banerjee (1974) present this relationship as:

$$H_c \propto d^{-n} \qquad 2.10$$

Where: H_c is the coercive force
d is the particle size
n is in the range $0.25 \leq n \leq 1$

Parry (1965) obtained a value of 0.4 for n, for magnetite grains between 1.5 and 80 μm. Figure 2.16 shows the relationship between magnetite grains and particle size.

Figure 2.16

The relationship between coercive force and particle size
For titanomagnetite particles

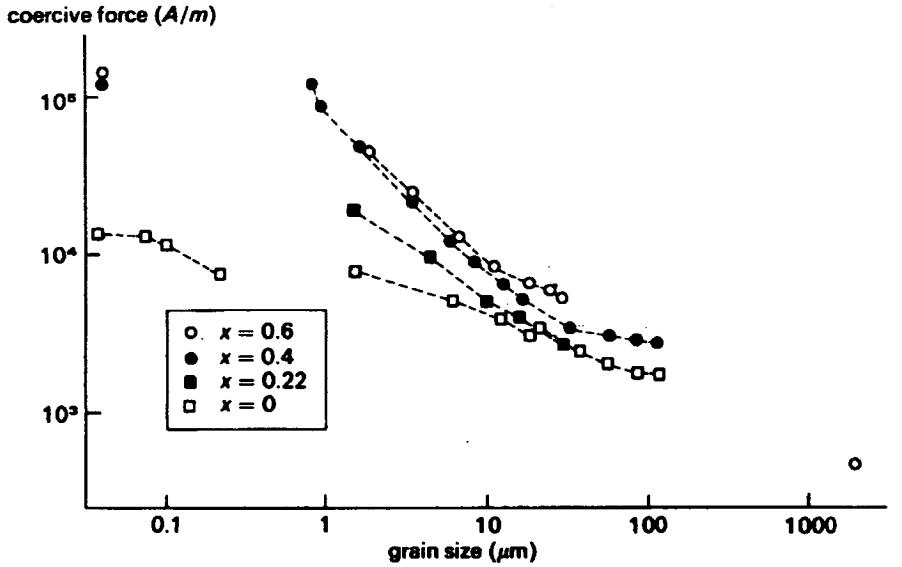

(From O'Reilley, 1984)

The x values given in the lower left of figure 2.16 refer to the grain chemical composition $Fe_{3-x}Ti_xO_4$.

Because domain wall velocities are proportional to the difference between the critical field (indicated here by the coercive force) and the external field, then at any given external field they will be higher for the larger particles than for the smaller particles. This is provided that the domain wall mobility (c in equation 2.9) is not a strong function of grain size.

Domain wall velocity and temperature

As was the case for particle size effects above, variations in coercivity are used here to indicate similar variations in critical field, and therefore to indicate changes of domain wall velocity with temperature.

The coercive force of a particle also falls with increasing temperature, with the relationship being given by O'Reilly (1984) as:

$$H_c = A(T_c - T)^{1-m} + B(T_c - T)^{7m} \qquad 2.11$$

Where the values of A, B, and m are determined empirically for each grain

The variation of coercive force with temperature for a 2 mm titanomagnetite grain, of composition $Fe_{2.4}Ti_{0.6}O_4$, is illustrated by O'Reilly (1984) in figure 2.17. This is the same 2 mm grain shown in the lower right of figure 2.16.

Figure 2.17

The temperature variation of coercive force for a 2 mm titanomagnetite grain of composition $Fe_{2.4}Ti_{0.6}O_4$

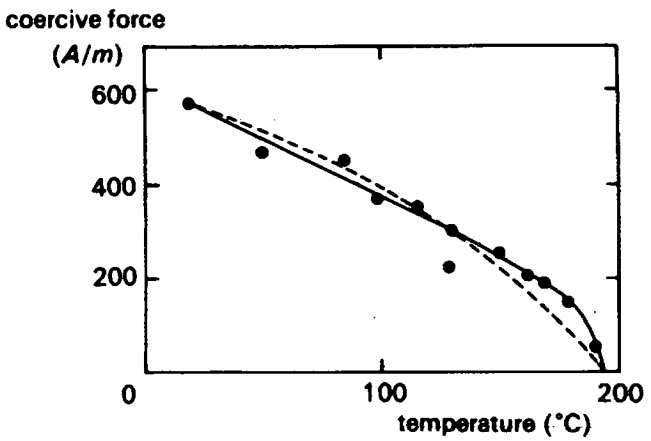

The temperature variation of coercive force in large grain (2 mm) $x = 0.60$. The dashed line is a power law of the form $H_c \propto (T_c - T)^q$ and the solid line $H_c = A(T_c - T)^{1-m} + B(T_c - T)^{7m}$

(From O'Reilly, 1984)

Ignoring any temperature dependence of the damping constant, for a given external field, domain wall velocity, which is proportional to the difference between the external field and the critical field (indicated here by the coercive force), will therefore increase with increasing temperature.

Superparamagnetism

The magnetocrystalline anisotropy energy of a uniaxial particle may be given approximately (from equations 2.1 and 2.2) as:

$$E = K_1 V \sin^2\theta$$

and for a biaxial particle as:

$$E = \frac{K_1 V}{4} \sin^2 2\theta$$

Similar expressions may be written for shape anisotropy (see equation 2.8).

These expressions give the "height" of the energy barrier which must be overcome in order to rotate the particle magnetisation to another direction of easy magnetisation. The expressions also indicate that as the particle size decreases (i.e. as V becomes smaller), the energy barrier also decreases. For a given temperature there is a particle size below which the energy available from thermal agitation is greater than the anisotropy energy. For iron this situation begins to occur below about 0.012 μm at room temperature (Bean and Jacobs, 1956). For such small particles the magnetisation changes randomly, and usually coherently, between directions of easy magnetisation, as a result of thermal agitation.

SPM (superparamagnetic) particles behave in a similar way to individual electron spins in a paramagnetic material, except that very large magnetic moments are now involved compared to that of a single electron.

An SPM particle has the magnetic properties of a paramagnet. Although the particle magnetic moment may be high, no hysteresis occurs, and within the time scale of the measurement process, there is no remanent magnetism after an external field is removed. If an external field is applied to an assembly of SPM particles (perhaps held within a paramagnetic material), and then suddenly removed, the nett magnetisation of the assembly decays exponentially. This decay is given by Cullity (1972) as:

$$m_r = m_i e^{-\frac{t}{\tau}} \qquad 2.12$$

Where m_r is the magnetisation remaining after time t
m_i is the initial magnetisation
τ is the relaxation time

This is a similar relaxation phenomena to that encountered in paramagnetic substances, but on a longer time scale. Relaxation times for an assembly of SPM particles depend on temperature (as they do for paramagnetics) and on the particle size, and over a very narrow range of particle sizes the relaxation time changes by a factor of more than 10^{10}. Relaxation times, at room temperature, for several SPM materials in a paramagnetic matrix are:

Material	Particle size μm	Relaxation time sec	Source
Cobalt	0.0068	10^{-1}	Cullity, 1972
"	0.009	3.2×10^{9}	"
Iron	0.0115	10^{-1}	Rado & Suhl, 1963
"	0.015	10^{9}	"
Magnetite	0.04	10^{2}	Dunlop and Ozdemir, 1997
"	0.03	10^{-5}	"
"	0.02	10^{-8}	"

The relaxation time is used to set a division between SPM particles and stable single domain particles, but this division is relative to the time scale of interest. Particles with relaxation times greater than the time scale of interest (usually the time scale of measurement) are called stable single domain particles. Particles with relaxation times of the same order as measurement times are referred to as viscous particles, and those with shorter relaxation times are then referred to as SPM particles.

Shape anisotropy in SPM particles can become greater than the magnetocrystalline anisotropy, and for very elongated grains of magnetite the critical inclusion volume for superparamagnetism at room temperature is reduced by a factor of 50 (Stacey & Banerjee, 1974).

Summary

Atomic magnetism is due to the presence of unpaired electron spins. In most cases (except where orbital orientation is not quenched) there is very little contribution from orbital motions.

Space quantisation of orbital motion is usually quenched by the electrostatic fields associated with crystal formation and structure.

Magnetic ordering in a crystal is due to quantum mechanical limitations on electron spin directions when outer orbitals are in close proximity (or overlapping), and is associated with an exchange or superexchange energy.

Exchange energy influences electron spin orientations between adjacent magnetic ions, while superexchange energy influences spin orientations in magnetic ions across a shared non-magnetic anion.

Magnetocrystalline anisotropy is one of the main factors producing preferred magnetisation directions in a crystal, and occurs because of a coupling between electron spins and quenched orbital motions (spin-orbital coupling). The torque which may be applied to a particle as a result of anisotropy forces is given approximately (in terms of the first constant only) as:

$$\tau = -K_1 \sin 2\theta \qquad \text{(Nm)} \quad \text{(for a uniaxial anisotropy)}$$

$$\tau = -\frac{K_1 \sin 4\theta}{2} \qquad \text{(Nm)} \quad \text{(for a biaxial anisotropy)}$$

Where: K_1 is the first anisotropy constant (J/m^3)
θ is the angle between the particle magnetisation and the easy magnetisation direction

Particle shape also produces a magnetic anisotropy, which can, for elongated particles, exceed the magnetocrystalline anisotropy. This anisotropy is due to demagnetising forces, and is described in terms of demagnetising factors (N_a, N_b, and N_c) for three orthogonal axes.

$$N_a + N_b + N_c = 1$$

For a prolate shere ($N_a = N_b$):

$$E = K_s \sin^2\theta \qquad \text{(=shape anisotropy energy)}$$

$$\text{Where } K_s = \frac{\mu_0}{2}(N_a - N_c)M^2 \qquad \text{(= shape anisotropy constant)}$$

For magnetically ordered minerals, a temperature exists where the thermal energy overcomes exchange energy, and the magnetic ordering breaks down. For ferromagnetics and ferrimagnetics this temperature is known as the Curie temperature, and for anti-ferromagnetics it is known as the Neel temperature.

Ferromagnetic, antiferromagnetic and ferrimagnetic materials are organised into magnetic domains, with sizes of the order of 1 μm. Each domain is magnetically saturated, but the domains are organised, to minimise energy, so that a larger particle appears to be unmagnetised.

Domain wall velocity in ferromagnetic and ferrimagnetic materials is characteristic of the material, and depends also on the strength of the applied field in excess of the critical field required to commence wall motion. It varies widely (depending on the material) from km/sec down to cm/sec, and has a magnitude given by:

$$v = c(H - H_0)$$

Where: c is a proportionality factor referred to as the wall mobility
H is the external field
H_0 is the critical field required to cause domain wall motion

Domain wall velocity increases with particle size and with temperature.

In very small ferromagnetic particles, where thermal energy becomes greater than anisotropy energy, the magnetisation changes direction randomly as a result of thermal agitation. These particles are referred to as superparamagnetic.

Chapter 3

Magnetic Separation Methods

Introduction

Present magnetic separation methods can initially be divided into two distinct groups:

(a) **Attraction Magnetic Separators**:- Methods designed to separate iron and non-conductive magnetic minerals on the basis of particle magnetic attraction.

(b) **Eddy Current Separators**:- Methods designed to separate non-ferrous and highly conductive metallic particles on the basis of generated eddy currents.

A third distinct group of separation methods is being proposed by this thesis:

(c) **Rotation Magnetic Separators**:- Methods designed to separate non-conductive minerals on the basis of particle rotation in a rotating magnetic field.

The particle rotation separations of the third group use a different mineral magnetic property (the ability of a magnetically ordered particle to be rotated by a rotating magnetic field) as the basis for particle separations and particle transportation, and therefore discriminate between particles in a way that is not possible with magnetic attraction alone. Combined particle rotation and attraction separations may also be used to remove some of the problems associated with straight attraction separation (see chapter 14).

The purpose of this chapter is to briefly summarise present magnetic separation theory, methods and performance, so that rotating magnetic field separation may be viewed and evaluated within the overall context of magnetic mineral separation. Later rotating magnetic field trial separations will refer to the conventional methods discussed here for comparison. In some cases, where magnetic particle rotations have been used to overcome problems with conventional methods, practical rotating field separation will need to be commercially competitive with the conventional methods.

There are numerous different types and models of magnetic attraction separators. The only examples given later in this chapter are those which will be compared to rotating magnetic field separators in later chapters. Some very innovative magnetic separator patents were taken out early in this century. Some of these (eg. Koizumi, 1926, and M°Carthy, 1922) are interesting for their attempt to use particle rotations to remove particle entrapment problems. None of these innovative early separators seem to have survived in the market-place.

Theory of magnetic mineral separation by attraction

Magnetic attraction

Almost all current magnetic separators operate by attracting magnetic particles in the direction of increasing magnetic field intensity. The only exception to this is that diamagnetic minerals (when separation is attempted, as it can be, for example with a Frantz separator) are repelled in the direction opposite to the direction of increasing field intensity.

The magnetic force experienced by a paramagnetic particle has been given in equation 1.10 as:

$$F = \mu_0 k_v H V \frac{\partial H}{\partial x} \qquad \text{(N)}$$

The important thing shown by the above equation is that, to obtain any particle attraction, both a magnetic field and a magnetic field gradient are required. It could be said that first the particle must be magnetised (in a magnetic field) and then it can be attracted (in a field gradient). This situation is illustrated in figure 3.1.

Figure 3.1

In figure A there is a magnetic field but no gradient. The particle may be magnetised, but is not attracted. In figure B there is both a magnetic field and a field gradient. The particle is magnetised and attracted.

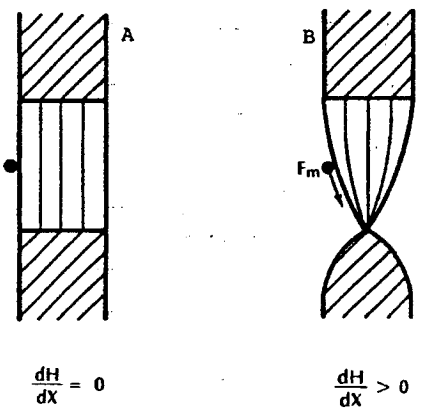

The effect of the competing forces of gravity and hydrodynamic drag

In any separator which uses magnetic attraction, all particles entering the separator are subjected to some non-magnetic force. This force may be gravity, centrifugal force, hydrodynamic drag, flotation, or a combination of these. Magnetic attraction is usually applied in opposition to these forces, and must overcome these forces for a particle to be separated.

If the opposing force is gravity, then the magnetic attraction must overcome the gravitational force on the particle. Because the magnetic field must have a field gradient, the magnetic field must inevitably tend towards zero as the distance from any separating surface increases. This rather obvious fact places a limit on the size of the particles which may be lifted against the force of gravity. While the gravitational force on the particle increases steadily as the cube of the particle radius, the magnetic force, must tend towards a maximum value.

If the opposing force is provided by fluid flow, then the magnetic force must retain or attract the particle against hydrodynamic drag. These drag forces may be calculated approximately using Stokes law. Stokes law becomes less accurate as the particle size increases above about 75 μm but, as can be seen below, it only affects magnetic separation for small particle sizes less than about 100 μm.

For example, in the case of the rare-earth magnet drum described in chapter 7, the magnetic, drag and gravitational forces on a particle with a magnetic susceptibility of k_g = 6.3 x 10^{-7} SI units (50 x 10^{-6} in cgs), in *contact* with the drum surface and immersed in water flowing at 5 cm/sec, are approximately as shown in figure 3.2.

Figure 3.2

Forces Acting on a Particle in a Magnetic Separator

For a particle in contact with the rare-earth drum described in chapter 7. Almandine garnet particle in water. Water velocity 5 cm/sec

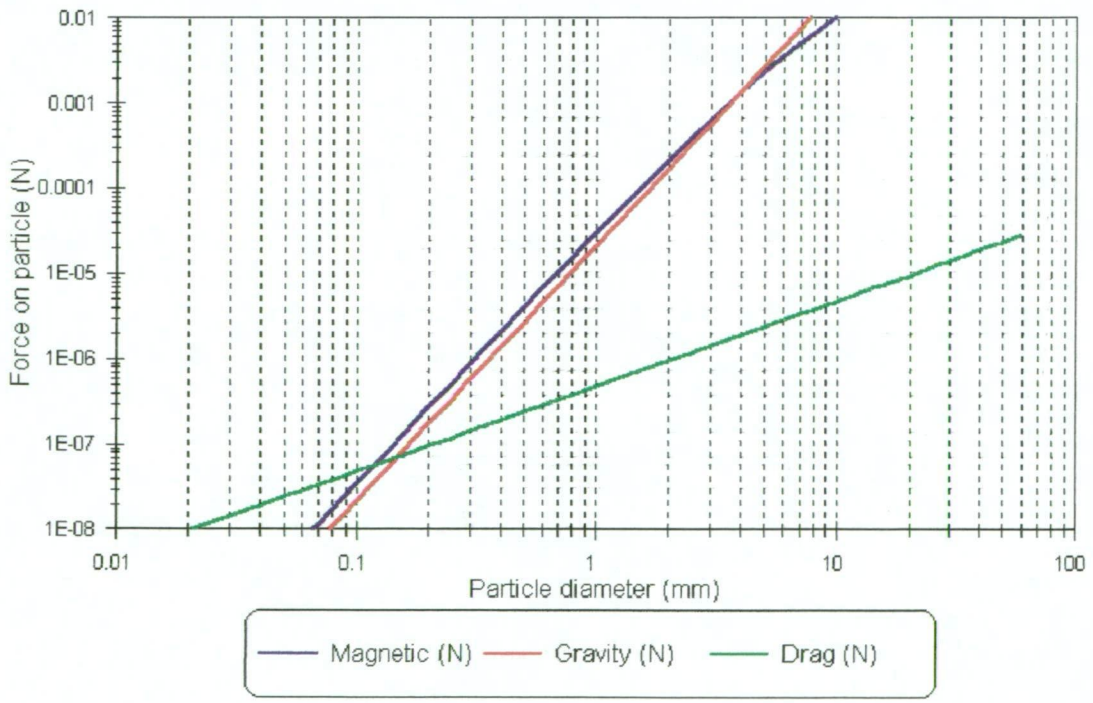

The mass of the particles in figure 3.2 has been assumed to be concentrated at the centre of the particle. While this assumption does not affect the gravitational force, it does mean that the magnetic force is only a close approximation.

It can be seen that, for particles immersed in water, the magnetic force is greater than the gravitational force for particles less than about 4 mm in diameter (if the particles were in air, then only particles less than about 0.7 mm could be magnetically lifted). Meanwhile, hydrodynamic drag forces are greater than magnetic forces (and gravitational forces) for particles less than about 0.1 mm. Therefore, while gravitational forces limit the maximum particle size that can be separated in any attractive separator, hydrodynamic forces limit the smallest particle sizes that can be separated.

If gravitational and hydrodynamic forces act together against magnetic forces, which is usually the case in any wet separator, the particle sizes that may be separated are limited. Figure 3.3 shows that the optimum particle separation size for the particles considered in figure 3.2 is about 0.7 mm.

Figure 3.3

Best Particle Size for Magnetic Separation

For a particle in contact with the rare-earth magnet drum described in chapter 7
Almandine garnet particle in water. Water velocity 5 cm/sec.

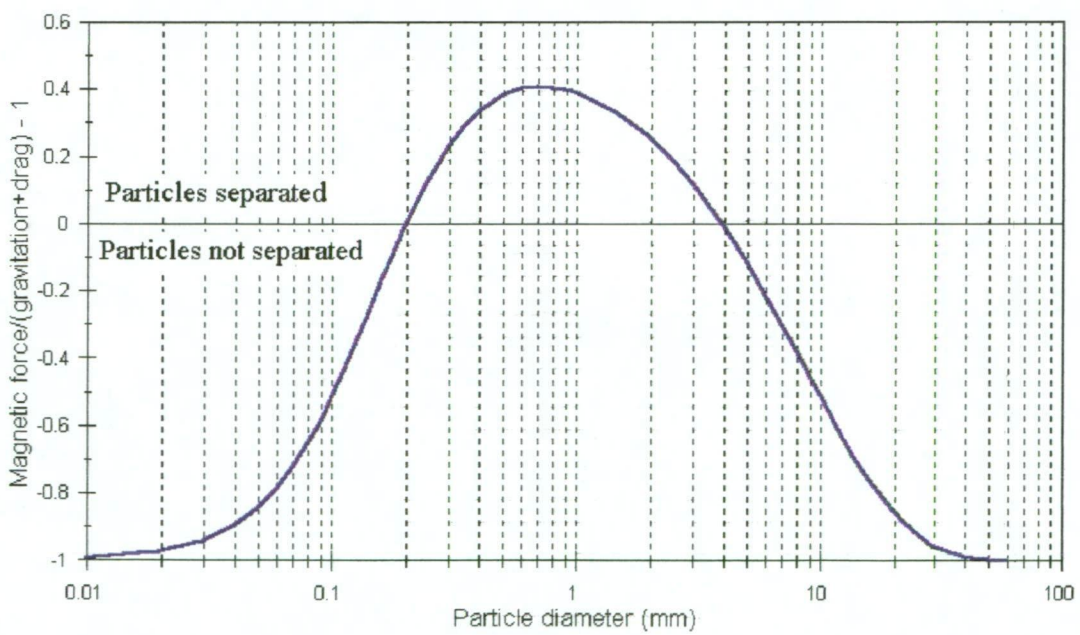

In figure 3.3 the ratio of the magnetic force to the sum of the drag and gravitational forces has been plotted against particle size. If this ratio is greater than 1 then magnetic separation can occur. The graph has been adjusted to show this by subtracting 1 from the ratio, so that a positive value indicates a magnetic separation is possible.

Figures 3.2 and 3.3 refer to a large magnet drum where the field gradient is relatively low. In a real separator using this magnet drum, the actual separation surface will be at some distance (maybe 5 mm) from the drum surface, resulting an even lower field strength and field gradient. The practical rare-earth drum *separator* described in chapter 7 could not retain such garnet particles. The optimal particle size is still about 0.7 mm, but the mass magnetic susceptibility of the particle would have to be around 1.2×10^{-6} SI units (100×10^{-6} cgs units).

High gradient separators such as the WHIMS and HGMS develop high fields and field gradients around strands of thin magnetised wire (or finely corrugated surfaces). This wire forms a matrix within the separator, and is used to trap the magnetic particles. The magnetic field decreases very rapidly away from the wire surface. This leads to a high magnetic gradient, and a strong attraction force close to the wire, but it also means that gravity overcomes the magnetic force at quite a small particle size. Oberteuffer (1974) has shown that the optimal particle size for such separators is about 0.1 mm. The results of his calculations are shown graphically in figure 3.4.

Figure 3.4

Particle magnetic, drag and gravitational forces in a WHIMS and HGMS separator

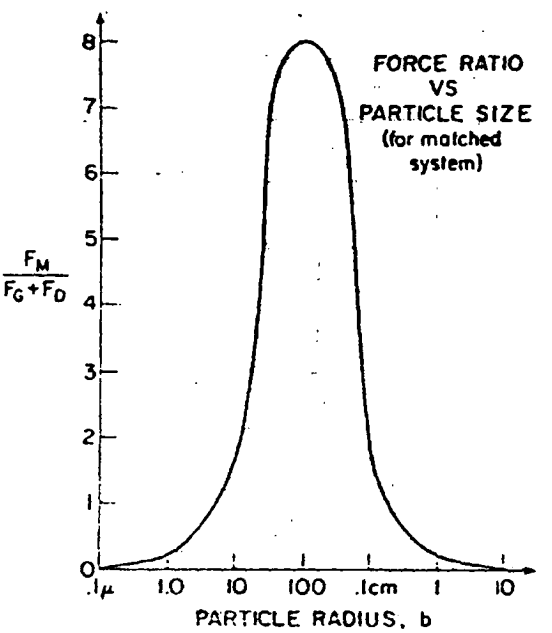

(From Oberteuffer, 1974)

Some general conclusions can be arrived at from the above:

(a) Practical magnetic separation of weakly magnetic materials in a magnetic attraction separator is generally limited by competing gravitational and hydrodynamic forces to particle sizes between about 50 μm and 1.5 mm.

(b) The separation of small particles (less than about 50 μm) should preferably be done dry, so as to remove the competing drag forces in wet separation, but this creates other problems with inter-particle forces.

(c) The separation of larger weakly magnetic particles (greater than about 1 mm) requires a lower field gradient, and therefore a much higher field strength so as to maintain the attractive force on the particle. This is generally incompatible with a practical magnetic attraction separator.

The entrapment of non-magnetic particles within the separating magnetics

Entrapment refers to the trapping of non-magnetic or less magnetic particles within the magnetically separated fraction. Entrapped particles would not normally be magnetically separated. Two entrapment causes need to be considered here.

The first of these is only of significance in ferromagnetic and ferrimagnetic separations where magnetic forces between particles are so strong that long chains and clumps of magnetic particles form, trapping non-magnetic particles. The effect can be seen by dipping any magnet into a mixture of magnetite and sand. In fact just trying this *very quickly* on a 50/50 sand/magnetite mixture (by weight) of 0.1 to 0.8 mm particles can produce a product which still contains up to 40% by weight of sand! In practice such high levels of entrapment rarely occur, but entrapment can still be quite significant. Most separators that deal with strongly magnetic materials such as magnetite attempt to overcome this entrapment by periodically rotating the magnetic field (and the magnetic flocs) as they pass alternate magnetic poles (N-S) on their way through the separator. This releases most of the entrapped non-magnetics, but with such high levels of entrapment possible, it is normal to use several stages of magnetic separation in series, in order to reduce it. An example of this is shown in figure 3.5, where three Eriez Magnetics wet-drum separators are used in series, with demagnetising coils between each stage, to separate magnetite from "black-sands" gold concentrate.

Figure 3.5

A 3-stage Eriez Magnetics wet-drum separator for separating magnetite from black-sands gold concentrate. Between each separation stage there is a demagnetisation coil to facilitate the release of non-magnetics. The schematic on the right identifies the main components of the 3-stage separator.

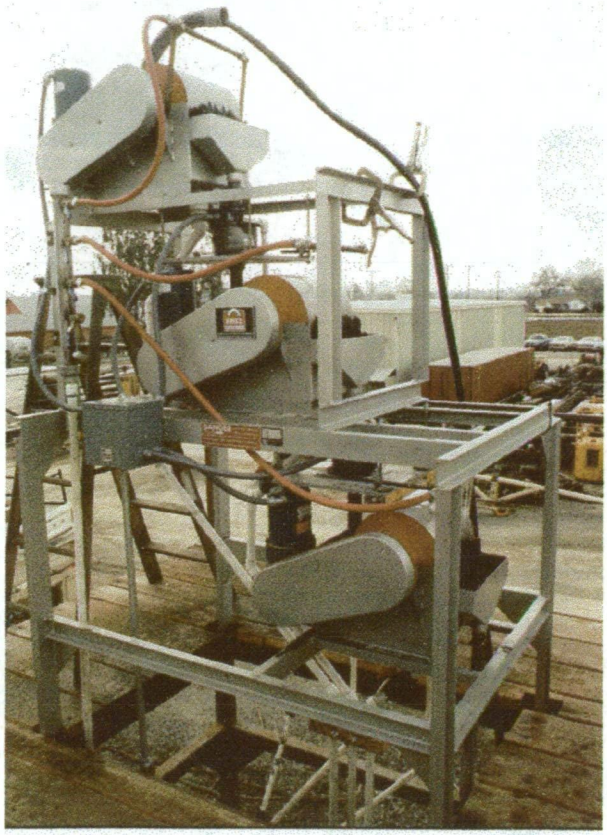

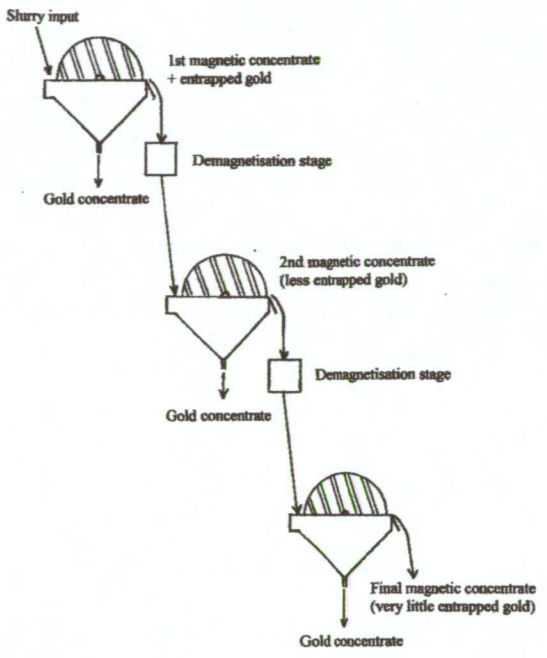

(From Thompson, 1992)

The second cause of particle entrapment is more general, in that it affects all types of magnetic separation, and is due mainly to electrostatic attraction between particles. This attraction is not due only to the surface charging of particles which causes problems with the dry separation of small particles, but is caused by surface charge distributions associated with the molecular structure of the minerals being separated. Therefore it does not disappear for wet separations. The situation is represented in figure 3.6.

Figure 3.6

Inter-particle forces which cause the entrapment of non-magnetic particles

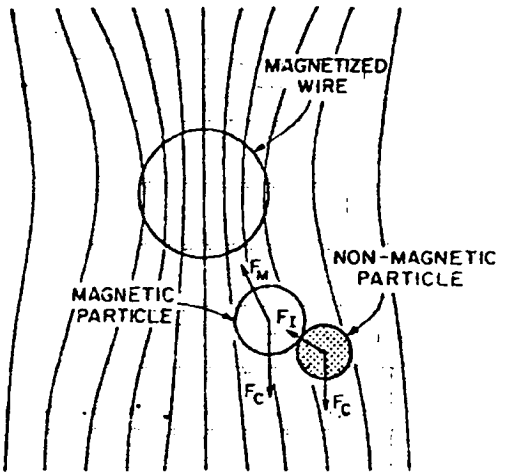

MAGNETIC, INTERPARTICLE AND COMPETING FORCES ON PARTICLES NEAR A MAGNETIZED WIRE

F_M = magnetic force; F_C = competing forces (drag); F_I = inter-particle forces

(From Oberteuffer, 1974)

The inter-particle forces also have the effect of increasing the hydrodynamic drag forces on the magnetic particles, and increasing the minimum particle size that is separated.

A decrease in entrapment requires that the forces between the particles be overcome. This can be done in part by increasing the drag force on the non-magnetic particle. This also increases the drag on the magnetic particle, and to compensate for this it would be necessary to also increase the magnetic force to retain the magnetic particle. The latter can be a very expensive option where high field strengths are already used in the separation of weak magnetic materials.

One method, which is described in more detail later, is to pulse the water flow as it passes through the separator.

Separators that use Magnetic Attraction

Wet drum separators

Low-intensity wet drum magnetic separators are the best-known of all the magnetic separators. They are easy to understand, simple to operate, and very tolerant of operator abuse. Even when operated well outside manufacturer's recommendations, they can give high recovery rates.

They are low-intensity separators, using magnetic fields normally around 1,000 gauss (or 0.1 T). Their use is restricted to the separation of ferromagnetics and the stronger ferrimagnetics, such as iron, magnetite and the more magnetic (monoclinic) pyrrhotite. The basic design of a wet-drum separator is shown in fugure 3.7. This is a co-current separator, which means that the magnetics are transported in the same direction as the slurry flow.

Figure 3.7

The structure of a co-current wet-drum separator

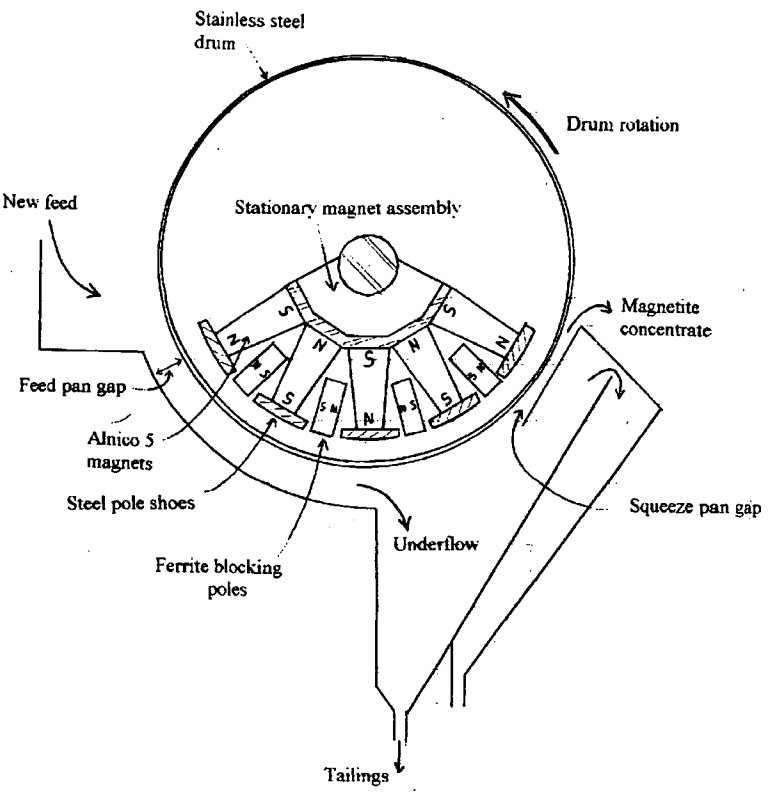

(Adapted from Moskowitz, 1976, and Beros, 1991)

The magnet structure shown in figure 3.7 is an old design (alnico magnets are no longer used), but has the advantage of showing the use of blocking poles (also referred to as bucking poles) in an arrangement very similar to that used in the rotating field separator illustrated in chapter 7.

A stainless steel drum (non-magnetic) rotates slowly around fixed internal magnets. The magnets in figure 3.7 are fitted around an arc of only 120^0. The magnet system is made up of alternating outwardly-facing N and S magnetic poles. The purpose of the blocking magnets is to limit flux leakage from the sides of the main magnets. As the slurry enters the separator it passes through the feed-pan gap, which keeps the feed within the magnetic field for as long as possible. Most of the magnetic material is attracted to the rotating drum surface and separated within a very short distance. The magnetic materials are carried through the separator by the rotation of the drum. After passing through the squeeze-pan gap they are carried past the magnet zone, where they fall away from the drum. The latter is usually assisted in some way either by some form of a brush or scraper or by a water spray.

Because the material being separated is highly magnetic, the particles tend to form long magnetic chains and clumps (magnetic flocs) against the drum surface. Non-magnetic particle entrapment is therefore a problem, as has been discussed above. This is reduced by the rotation of the particle chains (magnetic flocs) as they are carried beneath the alternate N-S magnetic poles.

One important use for these separators has been the recovery of fine magnetite used for heavy-medium washing of coal. In applications such as these, magnetite recovery rates are generally above 95%, and usually above 99% (up to 99.8%). Feed rates for these separators are usually given as cubic metres per hour per unit length of separator drum (per ft. or m), and have been indicated by Rayner (1995) to vary between users from 50 to as high as 100 m^3/hour/m, with a solids content, by weight, up to 40%. Some processing plants have reported using a feed solids percentage as high as 80%, and much to the surprise of the manufacturer have stated that the separator appears to be working well (pers. com., Ron Poole, manager, Eriez Magnetics, 1997).

Eriez Magnetics reports the capacity of their 914 mm diameter wet drum separator as having a feed capacity of 90 m^3/hour/m of slurry, with 20% solids by weight, and a maximum of 11% of total slurry as magnetics. The magnetic separation capacity is given as 11 tonnes/hour/m, at 99.8% recovery of magnetics

Unfortunately most applications, including the application above, are not very concerned about particle entrapment, and figures for entrapment under practical operating conditions are not generally available.

High intensity, high gradient separators

These types of separators include those referred to as WHIMS (Wet High Intensity Magnetic Separator) and HGMS (High Gradient Magnetic Separator). The basic idea behind these separators is illustrated in figure 3.8. The feed slurry is passed through a cell which is located in a strong magnetic field. The cell contains a matrix of some kind which is magnetised only when the magnetic field is applied. The purpose of the matrix is to produce high magnetic gradients in the vicinity of the matrix elements. In this case the matrix is shown as steel wool.

Figure 3.8
Structure of a Kolm type separator

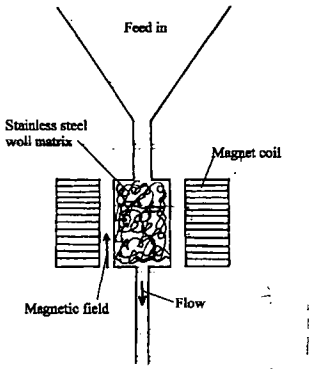

(From Oberteuffer, 1974)

The diameter of the matrix elements is chosen to suit the particle sizes being separated. In general the matrix element diameter should be three times the expected magnetic particle size. These separators are suitable for weak (paramagnetic) materials with particle sizes less than 200 μm.

In operation the slurry is first fed through the cell until the matrix has become saturated with magnetic particles. The feed is then stopped, the external field is removed, and the matrix is flushed out to remove the magnetic particles. This cycling operation takes time and severely limits the throughput of such separators. In order to increase throughput, a carousel arrangement of separation cells is often used. Figure 3.9 shows the structure of a Jones separator which operates on this principle.

The upper diagram shows the magnetic circuit of the Jones separator. The rotor disc forms a part of this circuit. The centre diagram gives a plan view of the carousel arrangement and shows the commencement points for the various cyclic operations. The lower diagram shows the grooved plate arrangement within each feed box (instead of the steel wool used in the Kolm type separator above). As the magnetic field direction is radial through the feed boxes, high field gradients are formed on the ridges of the grooved plates.

The feed boxes are arranged around the outside circumference of a slowly rotating large ferromagnetic disc. Slurry is fed to the feed boxes while they are between the magnetic poles. As the feed boxes move out of the magnetic field, and the field strength begins to decrease, they are flushed initially to remove a middling product. At this point those particles with a weaker magnetism are flushed out. As the feed boxes move completely out of the magnetic field and the grooved plates lose all their magnetism, the stronger magnetics are washed out.

Figure 3.9

The Jones high intensity magnetic separator

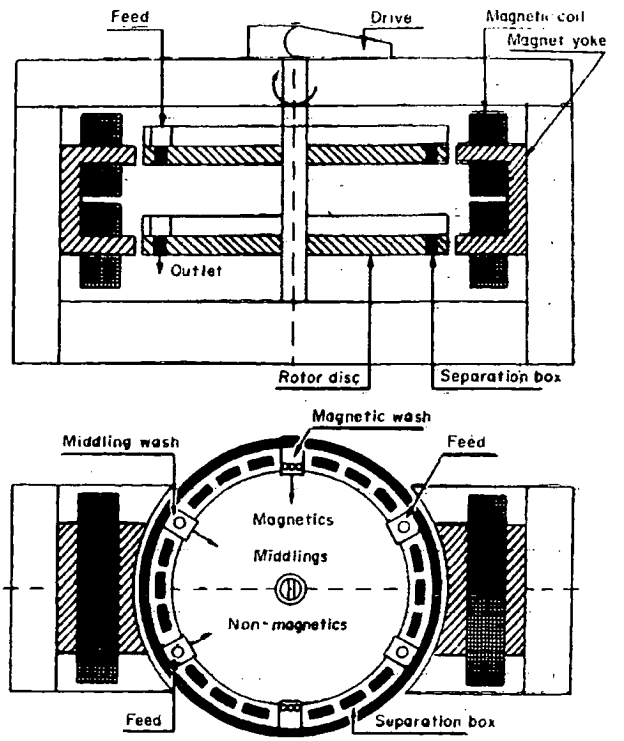

Operating principle of the Jones high-intensity wet magnetic separator.

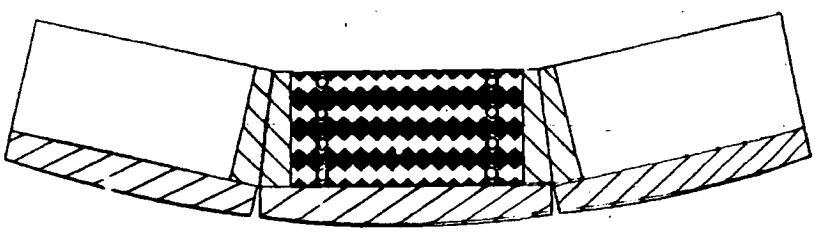

Plan of Jones plate box showing grooved plates and spacer bars.

(From Moskowitz, 1976)

The Magstream Separator

The Magstream separator is a recent development, which has been evaluated in Australia by the Julius Kruttschnitt Minerals Research Centre in Queensland. It is essentially a magnetically controlled heavy media centrifuge. The heavy medium is a ferromagnetic fluid formed by the colloidal suspension of 100 angstrom ferrite particles in a ligno-sulphonate dispersant. The density gradient of the heavy liquid is controlled by a combination of centrifugal force and external magnetic field. Figure 3.10 shows the internal structure of a Magstream separator. The outer casing of the separator remains stationary, while an internal cylinder rotates. The separation takes place in the inner rotating cylinder.

Figure 3.10

Internal structure of a Magstream separator

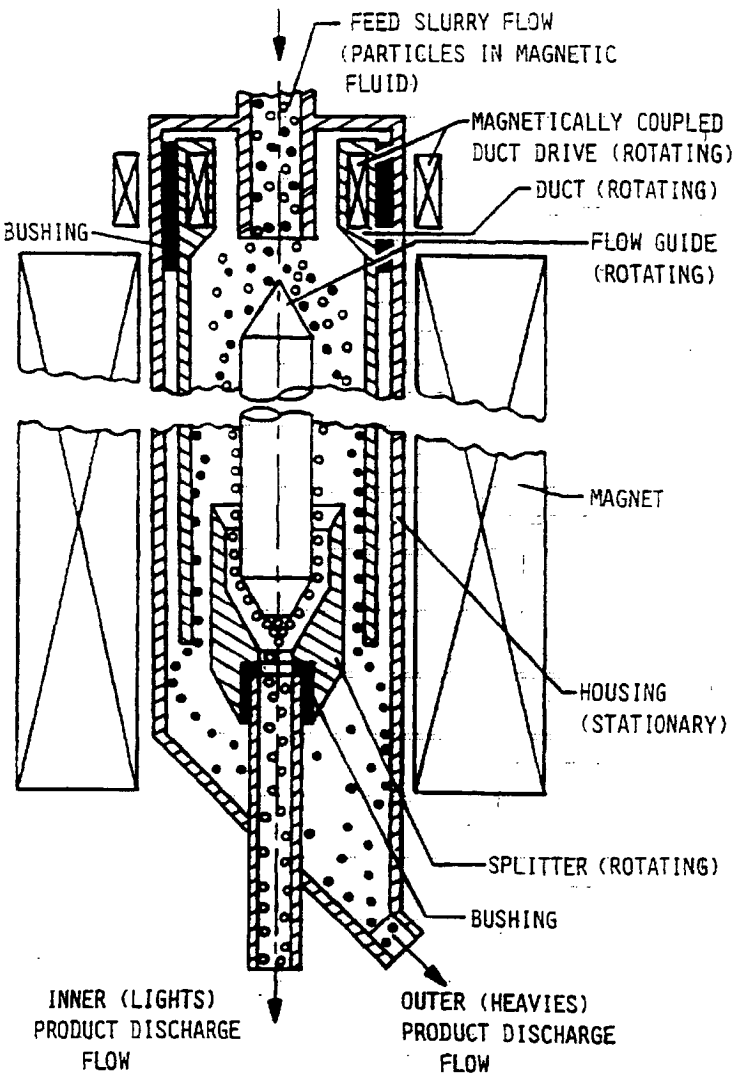

(From Walker, Magstream Company, internal paper, undated, 1990 or 1991)

All particles are bouyed towards the centre of the separator by the outwardly attracted magnetic fluid. The slurry, duct, flowguide and splitter all rotate at the same rate within the outer housing. Particles of higher specific gravity move radially outwards under the influence of centrifugal force (and magnetic attraction if they are magnetic), until a bouyancy point is reached in the density gradient of the fluid or the particles encounter the sides of the duct or inner cylinder. Figure 3.10 shows only a single splitter, but multiple splitters may be fitted to allow the separation of multiple density fractions.

If any magnetic particles are present, they are attracted further into the magnetic fluid than would be the case without the magnetic field. Separation therefore depends on both the density and magnetism of the particles. Particular separations are accomplished by carefully balancing the magnetic field strength and the duct rotation speed. After separation the magnetic fluid is recovered by filtration, and the products are washed with water.

Theoretical Ideas Behind the Magnetic Separation of Non-Ferrous, Non-Magnetic Conductive Particles

This type of separation is usually referred to as eddy-current separation. The basic idea of eddy-current separation is to induce electric cuurents in a conductive particle by placing the particle in a rapidly changing magnetic field. The induced currents then generate their own magnetic fields which are in the opposite direction to the external field. This leads to a repulsive force between the particle and the separator. If the repulsive force can be made large enough, the particle is either "thrown" from the separator or deflected to one side.

It is important to realise that the only force of interest in such a separator has been the magnitude of the repulsive force in the desired direction. This focussing of interest in one direction (literally) has probably been the main factor in restricting the development of eddy-current separators to the separation of larger metallic particles, generally greater than several mm. This has been in spite of some of the theory indicating other particle motions (such as particle rotation) which may be used for separation.

Basic theory of electromagnetic induction

Although eddy-current separation deals with metallic particles which may be solid and have all sorts of geometrical shapes, the principle is the same as the repulsion of a single wire loop in a changing magnetic field. If a wire loop is placed in a changing magnetic field, an induced emf (voltage) will be induced in the loop (Faraday's law of induction), given by:

$$\varepsilon = -\frac{d\Phi}{dt} \qquad \text{(volts)} \qquad 3.1$$

Where Φ is the magnetic flux through the loop.

Note that the voltage is the negative time derivative of the magnetic flux. The negative sign indicates that the induced voltage opposes the effect that caused it. The voltage causes a current to flow, whose magnitude is determined by the electrical resistance in the loop:

$$i = \frac{\varepsilon}{R} \qquad \text{(A)} \qquad 3.2$$

Where R is the resistance (ohms) of the loop.

An electrical current flowing in a closed loop generates a magnetic field. At a point x m from the centre of the loop, on the loop axis, this field is:

$$B = \frac{\mu_0 i A}{2\pi x^3} \qquad \text{(T)} \qquad 3.3$$

Where;- A is the area of the loop (m^2)

μ_0 is the permeability of the vacuum (Wb/Am)

The product iA in equation 3.4 is the magnetic dipole moment of the loop. The force that is applied to the single current loop as a result of the interaction of the loop magnetic moment with the external field is given (from equations 1.10, and 3.1 to 3.2) as:

$$F = -\frac{A\left(\frac{dH}{dt}\right)\left(\frac{dH}{dx}\right)}{R} \qquad \text{(N)} \qquad 3.4$$

The negative sign here indicates that the force is a repulsive one.

This equation relates to a single current loop,but a solid piece of metal can be thought of as being made up of many current loops. At least in theory the force on a real piece of metal could be obtained by integrating this expression over the volume of the metal fragment. In practice such a process is not very easy, especially for larger metal fragments where the field gradient changes significantly across the fragment. However the expression does say something of the requirements for eddy-current separation.

The magnitude of the applied force is proportional to the cross-sectional area of the metal fragment, the rate of change of the external magnetic field (at the metal fragment), and the gradient of the external field (at the metal fragment). It is inversely proportional to the electrical resistance of the metal.

The high rate of change of the external magnetic field is obtained in eddy-current separators by repeatedly changing the direction of the field. This is achieved by either passing the metallic fragments over alternating N-S magnetic poles, or by rapidly moving alternate N-S magnetic poles past the metallic fragments.

Non-repulsion eddy-current effects

It has been known for many years that the arrangements of alternate N-S magnetic poles used to produce rapid field direction changes also produce particle rotations in small particles. For example Schloemann (1980) describes these rotations, but without giving any detailed analysis of them. Figure 3.11 is Schloemann's diagram of such rotations.

Figure 3.11

Eddy-current rotation of small particles on a ramp-type separator

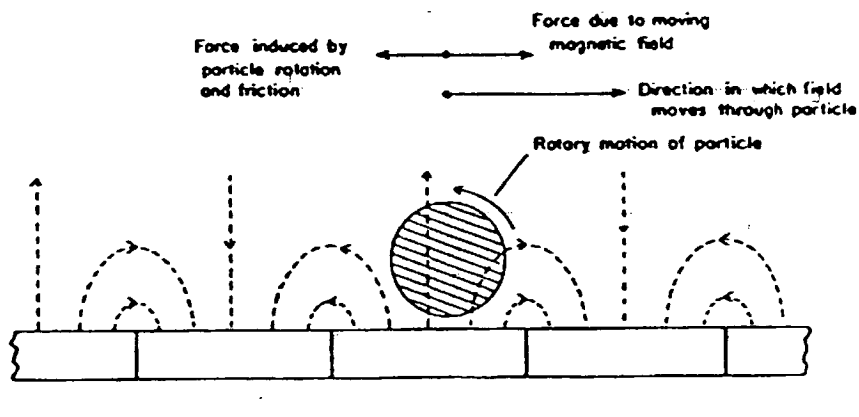

(From Schloemann, 1980)

Schloemann presents the above as a degrading factor in the performance of the ramp separator. He suggests that either the particles be flattened before they reach the separator, in order to reduce the effect, or that separators be designed to reduce the rotation effect.

The rotation effect has also been found to be a nuisance and a limiting factor in the separation of small metallic particles on a rotating drum type separator (pers. com. Eriez Magnetics Australia). As soon as the small particles enter the magnetic field of the rotating drum, they begin a reverse rotation which keeps them stationary on the feed belt. This can cause serious separator problems because the particles become very hot from an eddy-current heating effect, and can burn their way through the feed belt and the cover over the rotating magnet drum (which rotates at up to 3,000 rpm).

It is this rotation effect which is introduced in chapter 6 as the basis of a small-particle eddy-current separation method, for particle sizes down to less than 50 μm.

Types of Eddy Current Separators

Ramp eddy current separators (RECS)

In RECS the metallic particles slide down a ramp of inclined magnet strips of alternate polarity, such as is illustrated in figure 3.12.

Figure 3.12

Schematic of a sliding ramp metal separator, in frontal view (left) and side view (right).

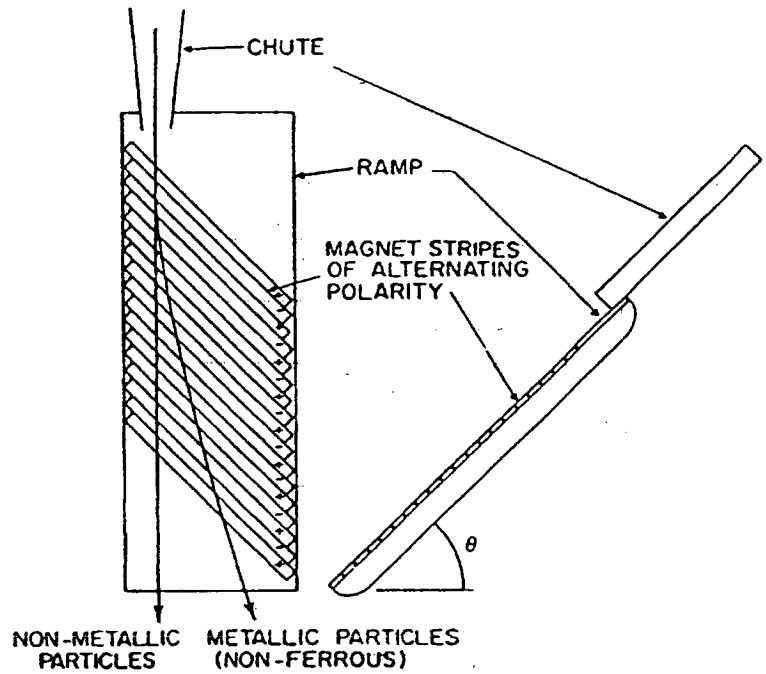

(From Schloemann, 1982)

This type of separator is designed to separate non-ferrous fragments from shredded waste materials. The shredded waste is fed to the top of the separator via the chute. As the metal fragments fall down the ramp they pass over alternate N and S magnetic pole strips, and experience a changing magnetic field. Consequently they experience a deflecting force, described by equation 3.4, which is perpendicular to the magnet strips. the metal fragments are therefore deflected towards the right in the diagram, while the non-metallic fragments fall straight down the ramp.

Schloemann (1982) claims that such separators can achieve a 70% recovery of metallic particles (mostly aluminium) with a 90% metallic purity of the product. He gives a waste feed rate to a practical RECS as about 0.4 tonnes per hour. The feed rate to these separators is quite low due to the necessity for a very narrow feed point at the top of the ramp.

Particle sizes from 4 mm upwards can be separated by these separators. Municipal solid waste and automotive scrap is generally +5 cm, while shredded plastic (P.E.T.) bottles (containing shredded aluminium bottle caps) is usually about 4 mm. The best separation occurs when the width of the magnet strips is roughly the same size as the particles to be separated.

In order to overcome the feed limitations of the RECS separator, Schloemann and Facinaelli (1981) introduced the corrugated ramp separator illustrated in figure 3.13.

Figure 3.13

The corrugated ramp eddy current separator

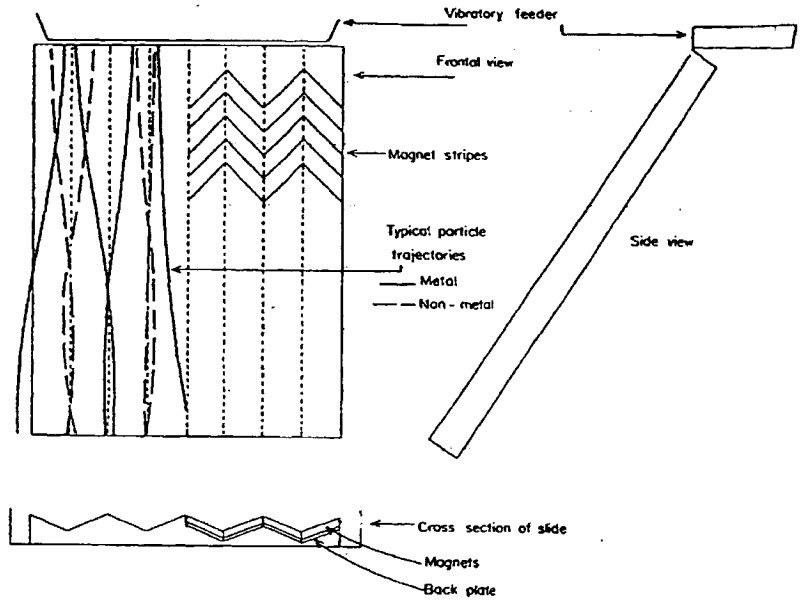

High capacity nonferrous metal separator (corrugated ramp separator).

(From Schloemann, 1982)

Instead of the very narrow feed point for the original ramp separator, this design can be fed across the entire width of the separator (typically about 1.3m), giving a feed rate of about 3

tonnes per hour per metre width. Metallic particles are deflected up the sides of the corrugations so that they travel down the ridges, while non-metallic particles travel down the channels.

Rotating drum eddy current separators

These eddy current separators appear to be becoming the industry standard method.

Figure 3.14 shows the structure of the separator, while the magnet arrangement around the rotating drum is shown in figure 3.15. Feed material is carried over the magnet drum on a conveyor belt. The magnet drum rotates in a counter-clockwise direction (in figure 3.14) inside the end conveyor belt drum. As the metallic particles enter the "alternating" field caused by the rapidly rotating magnet drum they experience a repulsive force which throws them forward and upwards from the end of the separator, into bins set at a suitable distance from the separator. The non-metallic particles are carried down over the end of the separator and deposited in a separate bin.

Figure 3.14

Structure of a rotating drum eddy current separator

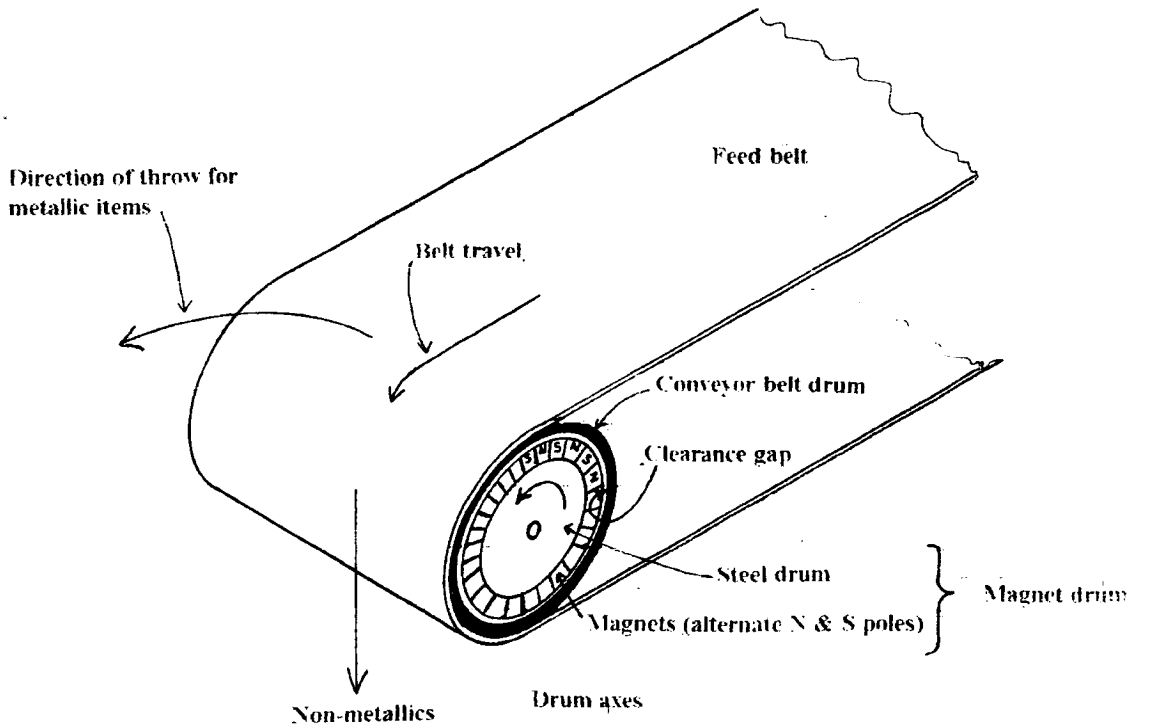

Figure 3.15

Magnetic arrangement around the magnet drum

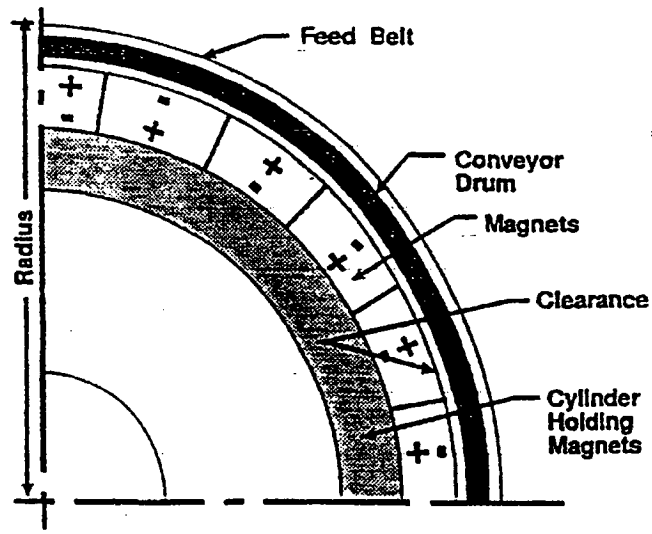

(From Mathieu et. al., 1990)

A separator such as is illustrated above, with a 50 to 60 cm wide conveyor belt, has a feed rate for spent potlining of about 20 tonnes per hour, with the recovery of aluminium better than 85% (Mathieu et. al., 1990).

Eriez Magnetics have related metal conductivity and density to the "throw" distance for their rotating drum eddy current separators (which are similar in construction to figures 3.14 and 3.15). These figures are given in table 3.1, where the throw distances are given relative to aluminium. Actual throw distances will depend on the rotation speed and magnetic field strength of the magnet drum, but for aluminium cans it will normally be in excess of 1 m.

Table 3.1

Conductivity/density ratios related to "throw" distances.
The throw distances are given relative to aluminium.

Metal	100 x Conductivity/density	Relative throw
Al	13.1	100
Cu	6.33	48
Ag	5.99	46
Zn	2.41	18
Au	2.12	16
$Cu_{65}Zn_{35}$	1.66	13
Cd	1.53	12
Ni	1.44	11
Fe	1.28	9.8
Sn	1.19	9.1
Pb	0.4	3.1
Manganese steel	0.19	1.4

(Data provided by Eriez Magnetics)

With increasing emphasis being placed on recycling, more attention is now being given to the separation of smaller metallic particles. In 1991 Eriez Magnetics in the USA were reporting on test separations of small metallic particles (Internal company memo. Pers. com. R. Poole, Eriez Magnetics Aust.). In these tests the same apparatus as illustrated in figure 3.13 was used, but the magnet rotor was run in the reverse direction. While this method overcomes some of the difficulties associated with small particle rotation, bulk particle repulsion is still the main separating criterion.

Summary

There are two main magnetic separation methods in use at the present:

(a) **Magnetic attraction separation**:- particle separation and transport are accomplished mainly by particle attraction in a magnetic field gradient.

(b) **Eddy current separation**:- non-magnetic metallic particle separation is accomplished by bulk repulsion forces from magnetically generated eddy currents

Magnetic attraction separation depends on the attractive force which can be applied to a magnetic particle. This is given by:-

$$F = m\frac{\partial H}{\partial x} \qquad \text{or} \qquad F = \mu_0 k_v H V \frac{\partial H}{\partial x}$$

Where:- m is the magnetic moment of the particle (Wb.m)
μ_0 equals $4\pi \times 10^{-7}$
H is the external field around the particle
V is the particle volume
k_v is the volume magnetic susceptibility (dimensionless)

Attractive separation therefore requires a magnetic field to magnetise the particle and a field gradient to attract it.

There exists an optimum particle size range for attractive separation, where the upper limit is determined by competing gravitational forces, and the lower limit is determined by competing fluid drag forces. This optimum size is around 100 μm for high gradient separators and a little less than 1 mm for drum-type separators.

Particle entrapment problems may be reduced by magnetic floc rotation (low intensity separators) or by some means of fluid pulsing (for high intensity separators).

Eddy current separation depends on an eddy current repulsive force which bodily propells metallic particles in a desired direction. The theoretical repulsive force on a particle can be determined from the basic relationship:-

$$F = \frac{-A\frac{\partial H}{\partial t}\frac{\partial H}{\partial x}}{R}$$

Where:- A represents the particle cross-section
H is the applied magnetic field
R is the particle resistance

Eddy current forces are therefore dependent on the particle size and resistivity and on the the time rate of change of magnetic field and its gradient.

Present eddy current separators cannot effectively separate particles less than 2 mm.

Eddy current particle rolling effects are considered to be a nuisance, which may be overcome by modifying particle shapes and by separator design.

Chapter 4

A Phenomenological Basis for Magnetic Mineral Separation by Particle Rotation in a Rotating Magnetic Field

Introduction

Separation by particle rotation occurs when the rotation of the magnetic particles is the *primary* method for moving the magnetic particles away from the non-magnetic (or less rotationally susceptible) particles, and to the separator outlet.

Particle attraction in a magnetic field gradient may be employed to assist the rotation separation, as has been done with most of the separators described in chapter 8. Conversely, particle rotation may be employed to assist an attraction separation. Particle rotation is used in this way, for example, in a conventional wet drum separator, where periodic particle or magnetic floc rotation is used to release entrapped non-magnetic particles (see chapter 3). In the latter case the separation is not considered as a particle rotation separation, as the magnetic particles are transported through and out of the separator on a moving drum surface: particle rotation is not used for particle transport.

If a magnetic particle is placed in a magnetic field, it will tend to assume a nett magnetisation as close to the direction of the external magnetic field as allowed by the particle anisotropy. This is true for all the types of particle magnetisation described in chapter 2, except for diamagnetic particles where the magnetisation is in the opposite direction to the external magnetic field. If the magnetic field then changes direction, most of these particles will experience some torque which will attempt to keep the original magnetisation direction aligned with the field. For some particles this torque will be small (for example paramagnetic particles) or even zero , while for others it will be strong. The strength of the torque, and its behaviour as the magnetic field continues to rotate, depends on the magnetocrystalline anisotropy.

This chapter describes particle rotation where the rotation axis is parallel to the external field rotation axis. Chapter 5 will examine possible particle rotations perpendicular to the field rotation.

The rotation indices that are described here relate the strength of the particle rotations to either the indicated particle magnetic susceptibility or the indicated particle magnetic moment. The rotation index is not intended as a direct measurement of particle anisotropy forces or as indicating the type of particle anisotropy, although it may later be quantitatively related to these factors, or interpreted in the light of these factors. It is intended primarily as a measurement that has practical significance for particle separation.

The considerations described below may be general in their basic concept, but have been made *equipment specific* in order to make use of them with the available equipment. This equipment is also used to carry out practical mineral separations, so the measurement of particle rotation characteristics reflects the needs and operation of the practical rotating field separation method.

General comments on the rotation of magnetised particles

Ferromagnetic particles

In ferromagnetic particles the electron spins are spontaneously aligned parallel to each other within small regions or domains. The effect of an external field is to initially cause an increase in the size of those domains aligned closest to parallel to the external field, with only a small deflection of domain magnetisation, and then, *if the particle is held stationary*, to cause a re-orientation of the domain magnetisations towards the direction of the external field (see chapter 2). If the particle is free to move, then at some stage during domain growth it will physically re-orient itself so that one of its easy magnetisation directions is aligned with the external field. If the external magnetic field rotates, and the particle is also free to rotate, the particle will attempt to keep its easy magnetisation direction aligned with the external field, and will rotate with the field. To become magnetised in any intermediate direction would be to enter a higher energy state. There is an energy barrier (anisotropy energy) to any *continuous* rotation of the particle magnetisation within the particle, but the magnetisation may jump relatively quickly (by domain re-growth) between directions of easy magnetisation as the external field rotates with reference to the particle. The extent to which the particle magnetisation can follow the rotating applied field by domain rearrangement depends on the strength of the applied field. In strong applied fields the domain structure is largely removed and the particle (now magnetically saturated) acts like a giant single-domain grain, for which the magnetisation must rotate against the torque arising from anisotropy.

If the rotation of the particle is subject to a retarding torque as the rotation frequency increases (e.g. by fluid drag) then the angle between the particle magnetisation and the external field will increase (torque will also increase) until the point is reached when either the magnetostatic energy difference associated with the angle between the particle magnetisation and the external field direction is equal to the anisotropy energy, or the magnetisation direction switches past the external field direction to the next closest direction of easy magnetisation. In the former case a steady state rotation is achieved, and in the latter case the particle rotation slows down and possibly ceases.

If a stationary ferromagnetic particle, resting on a surface, is subjected to a rotating magnetic field that is increasing in field strength, a field strength will be reached when the magnetic torque becomes greater than the retarding torque resulting from gravitational forces. The particle will then commence rotation. For iron particles this generally occurs at field strengths of about 40 gauss. At this point the anisotropy torque is equal to the torque needed to overcome the gravitational forces. If the field rotation frequency is increased, the external field strength and anisotropy energy need to be higher just to overcome particle inertia before the external field rotates on towards the next easy magnetisation direction.

Domain wall velocities were discussed in chapter 2. They could vary from km/sec to mm/sec, depending on the wall mobility, the external field strength relative to the critical field and crystal impurities and defects. A more "normal" wall velocity of 200 m/s would mean that for a 1 mm particle, domain growth in a new direction would take somewhere less than 10^{-5} seconds, and that the average lag in domain growth would be less than half a degree behind the external field rotation at a field rotation frequency of 100 Hz. Such small increases in the angle between the external field and the particle magnetisation are not going to have a significant effect on particle rotations at external field rotation frequencies to be used here.

(generally below 100 Hz), but may assist it. On the other hand, low domain wall velocities of less than 100 cm/sec could produce significant angles of lag. Such increases in lag angle could considerably increase the torque that can be applied to a particle by rotation of the external field.

Chapter 6 examines the effects of eddy currents in highly conductive metallic particles, and indicates that the low magnetic field strengths and field rotation frequencies used for ferromagnetic separation (between 1000 and 2000 gauss, and less than 100 Hz respectively) could only rotate iron particles greater than about 3 to 4 mm. Therefore eddy current effects, or at least those not associated with domain wall motion, can not be the prime cause of any particle rotation, but may assist it.

Ferrimagnetic and antiferromagnetic particles

In ferrimagnetic particles the magnetic moments in adjacent sub-lattices are aligned anti-parallel, and are unequal. The sub-lattices also contain different magnetic ions in different crystallographic sites. As for ferromagnetic particles, ferrimagnetic particles have high magnetic anisotropy energies, and rotate with an external rotating magnetic field.

In antiferromagnetic particles the electron spins in adjacent sub-lattices are antiparallel and equal. The two sub-lattices contain similar ions in similar crystallographic sites. In an external magnetic field the equal magnetisations between sub-lattices become unbalanced (see chapter 2), and the particles show some magnetisation. As very few minerals are antiferromagnetic at room temperatures, antiferromagnetics will not be discussed separately here.

As was mentioned for ferromagnetic particles above, domain wall velocities can vary widely, and it is possible that in low to moderate fields, for field rotations of 50 to 100 Hz, slow domain wall velocities could allow a higher torque to act on a ceramic particle than would be expected from quasistatic field realignment of magnetisation through domain readjustment.

If a ferrimagnetic particle is rotating against some resistance (eg. water drag and surface interaction) in a rotating magnetic field that is increasing in rotation frequency, it will behave as has been described above for a ferromagnetic particle.

If a ferrimagnetic particle is stationary and resting on a surface, in a rotating magnetic field which is increasing in magnitude, particle rotation may commence much earlier than would be expected from the particle magnetisation measured in a stationary magnetic field, due to a slow domain wall velocity.

Paramagnetic particles

The electron spin directions in a paramagnetic material are disordered, thermal energy having overcome any ordering (due to exchange energies) which may have been present at lower temperatures.

In spite of this disorder of spin directions, non-cubic paramagnetic crystals show an anisotropy in their magnetic susceptibilities. The differences are generally quite small; for example Nye (1957) gives the *volume* susceptibility values for hexagonal beryl as 1.29×10^{-5} (SI) for the c axis, and 2.76×10^{-5} for both other axes. While thermal energy may have overcome any magnetic ordering, an anisotropy in the measured g values (Hawthorne, 1988) indicates that the origin of the above susceptibility anisotropy lies in some partial orbital quenching. Cubic paramagnetic crystals do not show any anisotropy of the g values, and have isotropic susceptibility (Nye, 1957).

Therefore, even though a particle may be paramagnetic, if it is not cubic (i.e. not isotropic) a torque, as described by the anisotropy constants introduced in chapter 2, may be placed on the particle by a rotating magnetic field. This torque will generally be very much smaller than for ferromagnetic and ferrimagnetic particles, as is indicated above by the size of the susceptibility anisotropy, but within this limitation the particles should behave in a rotating magnetic field in a similar way to the ferromagnetic particles, with the exception that cubic particles will no longer show any rotation.

A Method for Describing Particle Rotation Parallel to the Field Rotation
The rotation index

Introduction

For a particle to rotate in a rotating magnetic field, there needs to be some angle between the particle magnetisation and the external field. If the maximum attainable angle can be measured, it can be used as a measure of particle "rotatability". Such a measurement would indicate how readily a particle could be rotated, relative to its magnetisation.

In order to measure the above angle it would be necessary to hold a particle stationary while the external field rotated, and then to note the angle where the maximum torque was applied to the particle. Holding a very small particle stationary presents no problems, but quickly and routinely measuring the torque applied to particles as small as 50 μm can not be easily accomplished with simple equipment. Measurements of the torque placed on particles by a magnetic field may already be made very accurately, using such instruments as torque magnetometers, and are used to calculate particle anisotropy (e.g. the values for K_1 and K_2 in chapter 2), but these measurements are not practical on a routine basis for very small particles. In addition to this, the measurements are not made in a dynamic situation where the magnetic field is rotating relatively quickly. While these accurate anisotropy measurements may be used to indicate particle rotation in a continuously rotating magnetic field, they do not take into account such dynamic factors as domain wall velocities, which, for ferrites, can be quite low.

One way to easily obtain a practical and meaningful (but perhaps approximate) measurement would be to try to rotate the particle against the force of gravity holding it down on a surface. If the magnetic field and its gradient are increased to the point where the particle just begins to rotate with the external field, then a measurement of the maximum magnetic torque can be obtained by equating it with the torque needed to physically roll the particle. Because the particle weight against a surface will be affected by any field gradient, it will be necessary to know the field strength and gradient at which the particle commences rotation,

and this further indicates that the particle magnetisation must also be known. For a paramagnetic particle the latter can be calculated from a measurement of the (higher) field and gradient necessary to lift the particle, but for a ferromagnetic or ferrimagnetic particle, where the magnetisation will not be proportional to the external field, it is not so easy. The simplest approximation is to assume that the magnetisation is the same at both lift and rotation (i.e. assume magnetic saturation).

Therefore it should be possible to arrive at a value for the angle between particle magnetisation and the external field by measuring the fields and gradients required for particle lifting and rotation. In practice, notwithstanding the ferromagnetic saturation assumption, any routine particle measurements based on the above method will be approximate, mainly due to the need to make some assumptions about the shape of the particle.

It is actually the *sine* of the above angle of lag between particle magnetisation and external field that has been used throughout this thesis. This can only truly represent the sine of the lag angle if other effects such as particle inertia are taken into account, and more is said about this later in the chapter. The measured quantity has been referred to as the *rotation index* rather than as an indication of lag angle.

The rotation index

The magnet drums used for rotating magnetic field separations are described in chapter 7. The magnetic fields and gradients for these drums can be easily calculated at any distance from the drum surface. Therefore, by balancing particle attraction against gravity (i.e. determining the field and gradient required to lift the particle), a reasonable estimate of particle magnetic susceptibility or particle magnetic moment can be arrived at for small particles. Methods used in this thesis for the estimation of magnetic mass susceptibility and magnetic moment are detailed in chapter 7. The magnetic field and gradient at which a particle commences rotation in a rotating magnetic field can also be readily determined.

Assuming that the particle is paramagnetic, the magnetic susceptibility, measured at the higher (lifting) field strength, can be used to determine the particle magnetic moment for the lower field strength at which rotation occurs.

Assuming that the particle is ferromagnetic, and saturated, the magnetic moment (or, in practice, the moment/mass), measured at the higher (lifting) field strength, can be assumed to be the same as the magnetic moment at the lower field strength where rotation occurs.

Therefore two rotation indices can be calculated, one for each of the above assumptions.

Assuming that the particle is roughly cubic in shape (this is probably close to an average "shape factor", and works out well in practice), the torque needed to rotate the particle against the force of gravity can be estimated. Using the method described in chapter 7, this needs to take into account the magnetic attraction and the buoyancy due to immersion in a fluid.

Therefore, at the point where particle rotation commences, we can say that:

Torque applied by the magnetic field = torque required to rotate the particle against gravity

or:

Particle magnetic moment × *magnetic field* × $sin\phi$ = *torque required to rotate particle against gravity*

then:

$$R = sin\phi = \frac{\text{torque required to rotate particle against gravity}}{\text{Particle magnetic moment} \times \text{magnetic field}}$$

Two values can be calculated for R:

(i) R_p, assuming the particle is paramagnetic, and

(ii) R_f, assuming the particle is ferromagnetic and magnetically saturated.

The values of R_p and R_f can be calculated from measurements of lift and rotation field strengths, using the methods described in chapter 7 This can be done at any field rotation frequency. However, because the field is rotating and the particle is initially stationary, the particle must accelerate until its angular velocity matches that of the external field. This makes the measured rotation index frequency dependent, and this is discussed later.

Calculation of paramagnetic rotation index, R_p

The magnetic susceptibility can be estimated from the field and gradient needed to lift the particle against the force of gravity. In practice the particle is usually immersed in a liquid (normally water). In chapter 1 (equation 1.13) it was shown that the mass magnetic susceptibility could be calculated using:

$$k_g = \frac{a}{\mu_0 H \frac{\partial H}{\partial x}} \qquad \text{(SI units)} \qquad 4.1$$

Magnetic induction (B) is more commonly measured than H. Equation 4.1 can be re-written as follows, to take account of these units and also to make provision for immersion of the particle in a fluid.

$$k_g = \frac{\mu_0 a\left(1-\frac{D_f}{D_p}\right)}{B_l \frac{\partial B_l}{\partial x}} \qquad 4.2$$

Where: k_g is the magnetic mass suceptibility (SI units)
μ_0 equals $4\pi \times 10^{-7}$ (Wb/Am)
a is the acceleration due to gravity (9.8 m/sec^2)
D_f is the density of the immersion fluid. (kg/m^3)
D_p is the density of the particle (kg/m^3)
B_l is the magnetic induction outside the particle, at the lifting field (Tesla)
$\frac{\partial B_l}{\partial x}$ is the magnetic field gradient, at the lifting field (Tesla/m)

Note: If k_g is desired in cgs units (some American data is in cgs units), the right hand of equation 4.2 must be divided by $4\pi \times 10^{-3}$.

If the magnetic mass susceptibility is known, then it is possible to calculate the magnetic torque that could be applied to the particle by the external field, at the lower particle rotation field strength:

$$Torque\ applied = \frac{k_g m_p B_r^2}{\mu_0} \sin(\phi) \quad \text{(N.m)} \qquad 4.3$$

Where: m_p is the mass of the particle (kg)
B_r is the rotation field strength (T)
K_g is the mass magnetic susceptibility (SI units)

The value of R_p can now be obtained by using equation 4.3 with the value of the magnetic field at the point where the particle commences to roll. This assumes that the particle is paramagnetic, and that the particle magnetisation is proportional to the applied field.

$$R_p = \sin(\phi) = \frac{\mu_0 \times RotationTorque}{k_g m_p B^2} \quad \text{(dimensionless)} \qquad 4.4$$

The rotation torque is the torque actually needed to start the particle rolling. This torque can be calculated easily if the particle has a cubic shape. Taking account of the reduced weight of the particle due to its possible immersion in a fluid and to its attraction in a magnetic field gradient, the torque is:

$$Rotation\ Torque = \frac{d}{2}\left(\left(m_p - m_p \frac{D_f}{D_p}\right)a - \frac{k_g m B_r \frac{\partial B_r}{\partial x}}{\mu_0}\right) \quad \text{(N.m)} \quad 4.5$$

Where d is the particle diameter (or side length) (m)

The second term in the above expression represents the decrease in the weight of the particle due to the lifting effect of the magnetic field gradient.

If equation 4.5 is substituted into equation 4.4 an expression is obtained where all the quantities can be measured, or at least reasonably estimated, for individual particles down to about 50 μm.

$$R_p = \frac{d\left(\mu_0 a\left(1 - \frac{D_f}{D_p}\right) - k_g B_r \frac{\partial B_r}{\partial x}\right)}{2 k_g B_r^2} \quad \text{(dimensionless)} \quad 4.6$$

The value of k_g for the particle is calculated at the point where the particle is lifted, but the values for B_r and $\frac{\partial B_r}{\partial x}$ (field and field gradient) in equation 4.6 are measured at the point where the particle begins to rotate (using the relationship described in chapter 7). D_f and D_p are usually known, and d can be reasonably estimated (or measured) through the microscope used to observe the rotation. If reasonable care is taken in choosing particles that are as close as possible to a cubic shape, the values of R_p calculated in practice should be within a factor of 2 of what they should be for paramagnetic particles.

The rotation index has been set up such that the value obtained should represent the sine of the angle between the external field and the particle magnetisation, but this will only be

the case if the measured magnetic moment is really proportional to the external field, as in equation 1.7, i.e. if the particle is paramagnetic.

If the particle is paramagnetic, then anisotropy forces are very small, and the value of R_p is probably less than 0.05 (which represents an angle of about 2.9^0 between particle magnetisation and the external field), but more likely it is near zero. For a cubic paramagnetic particle it is zero. Any paramagnetic particle rotation should be easily overtaken by particle inertia effects as the field rotation frequency increases.

If the particle is ferromagnetic or ferrimagnetic then the use of a magnetic susceptibility (magnetisation proportional to the external field) is incorrect. The particle magnetisation at the rotating field is greatly under-estimated. The calculated ratio is therefore too large, and can even be greater than 1. In this case the value of R_p does not represent the actual angle between the particle magnetisation and the external field.

Calculation of ferromagnetic rotation index, R_f

If the particle is ferromagnetic, and is close to (or at) magnetic saturation at the point where rolling commences, then the magnetic moment of the particle is similar at both the point where it is lifted and the point where it commences rotation. If the magnetic moment calculated from the field and gradient needed to lift the particle is applied at the point where the particle starts to rotate, then, following similar reasoning to above, a value for R_f can be calculated.

The magnetic moment of a particle, indicated by the field gradient at which it is lifted, is given by:

$$m = \frac{m_p a}{\frac{\partial H}{\partial x}} \qquad \text{(Wb.m)}$$

At least the magnetic moment per unit mass;

$$m_m = \frac{m}{m_p} = \frac{\mu_0 a}{\frac{\partial B_l}{\partial x}} \qquad \text{(Wb.m/kg)} \qquad 4.7$$

can easily be determined, as it only requires the field gradient to be known. The torque required to roll the particle is:

$$Torque = \frac{m_m m_p B_r}{\mu_0} \sin(\phi) \qquad \text{(N.m)} \qquad 4.8$$

Where m_m is the measured magnetic moment per unit mass (measured at the lift point)
B_r is the magnetic induction (measured field) at the rotation field strength.

Equation 4.4 can now be written as:

$$R_f = \frac{\mu_0 \times RotationTorque}{m_m m_p B_r} \qquad 4.9$$

and equation 4.6 becomes:

$$R_f = \frac{\mu_0 d\left(a\left(1-\frac{D_f}{D_p}\right)-\frac{mm}{\mu_0}\frac{\partial B_r}{\partial x}\right)}{2m_m B_r} \text{ (dimensionless)} \qquad 4.10$$

If the particle is indeed ferromagnetic, the calculated R_f should be less than 1.

If the particle is cubic, and if the applied field is sufficiently high that the particle is single-domain and the magnetisation follows the field direction as it rotates in a plane containing two of the easy axes, the maximum torque occurs at $\theta = 22.5^0$ (Cullity,1972), where θ is the angle between the nearest direction of easy magnetisation and the particle magnetisation. If the particle is uniaxial, the maximum torque occurs at $\theta = 45^0$. If the applied field is weak and particle magnetisation can not rotate significantly from the direction of easy magnetisation, then the maximum torque occurs at a ϕ (angle between particle magnetisation and applied field) that depends on the coercive force of the particle and the particle magnetic anisotropy. However domain wall velocities may considerably increase this angle, as described below.

If the ferromagnetic index is used, and the particle is paramagnetic, then the magnetic lifting effect in equation 4.10 is greatly over-estimated and the value of R_f can be negative.

The Relationship Between Particle Magnetic Moment (lifting fields) and Rotation Indices

The rotation indices are functions of the lift and rotation fields and gradients. Two particles can have the same rotation indices because the ratio of the lift and rotation fields are the same, but one particle may really be considerably more magnetic than the other. The rotation indices do not predict how easily a particle can be rotated, they just describe how well it rotates relative to its magnetic susceptibility or magnetic moment.

The susceptibility and magnetic moment are determined from the field and gradient at which a particle is lifted. The lifting field is therefore an indication of how magnetic the particle is. Therefore to examine particle rotation trends it is sufficient to consider the lifting field strengths and the rotation index. Figure 4.1 illustrates the expected relationship between lift fields for different ferromagnetic rotation indices. All particles with the same rotation index plot along a vertical R_f line, even though the particles may have widely differing magnetic moments. An inverse scale is used for the y axis in figure 4.1 so as to present the more magnetic particles at the top of the graph. A plot such as figure 4.1, which is more "equipment-related", gives similar information to a plot of magnetic susceptibility against rotation index, and has been used in several places in this thesis.

Figure 4.1

Comparison of Inverse Lifting field to Ferromagnetic Rotation Index

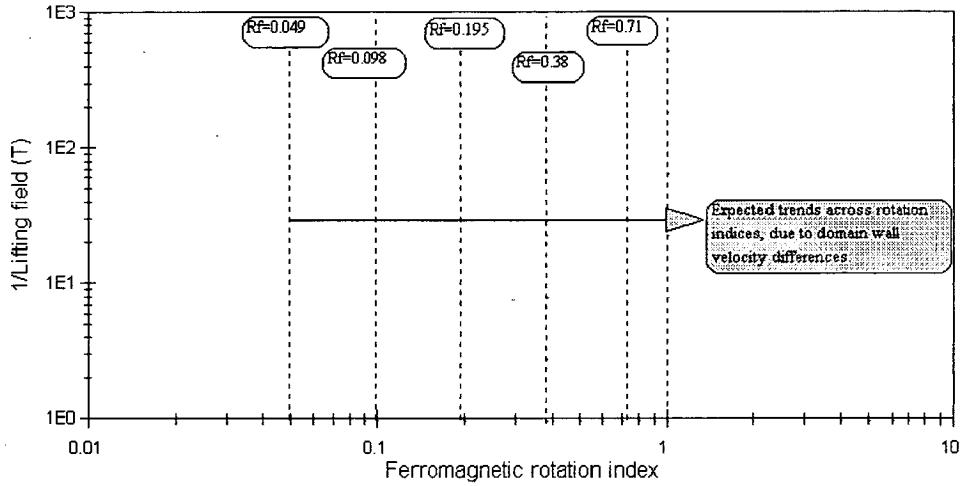

It would normally be expected that all particles of a particular mineral, with the same chemical composition, would plot as a group approximately along one rotation index line, with scatter in the rotation indices arising from variations in grain shape and coercivity.

The Relationship between Rotation Indices and Anisotropy Constants

In chapter 2 relationships were derived (equations 2.5 and 2.6), which gave the expected rotation index ($\sin\phi$) in terms of the anisotropy constant K_1 and the angle between the particle magnetisation and the easy axis of magnetisation.

$$\sin\phi = \frac{K_1 V \sin 2\theta}{mH} \qquad \text{(for uniaxial anisotropy)}$$

and

$$\sin\phi = \frac{K_1 V \sin 4\theta}{2mH} \qquad \text{(for a biaxial anisotropy)}$$

If shape anisotropy is along the same axis as the magnetocrystalline anisotropy, it adds to the particle anisotropy, and the total rotation index can be given as:

$$\sin\phi = \frac{(K_1+K_s)V \sin 2\theta}{mH} \qquad \text{(for a uniaxial anisotropy)}$$

$$\sin\phi = V\frac{\frac{K_1}{2}\sin 4\theta + K_s \sin 2\theta}{mH} \qquad \text{(for a plane containing two of the cubic axes of magnetocrystalline anisotropy)}$$

These relationships are expressed for the special case where the external field rotates in the plane containing the axes of easy magnetisation, as occurs in practice for particles that are relatively free to orient themselves in the field. In practice $\sin\phi$ may not be equal to the rotation index, for reasons that are outlined below. The measured rotation index contains information on the anisotropy constants K_1 and K_s and the angle between the particle magnetisation and the easy magnetisation direction, but it may also contain information on domain wall velocity and particle inertia. The measured rotation index could be written in terms of a number of different factors (assuming that the particle magnetisation at the rotation field is known):

$$R = \frac{\sin(\phi + D_v)}{I} \qquad 4.11$$

Where: D_v is the particle magnetisation lag due to domain wall motion
I is a term that describes the inertia effect

It is interesting to use the anisotropy constant K_1 to estimate the expected maximum values for θ in a ferromagnetic particle *if the external field can be applied at 90° to the particle magnetisation*, and assuming no shape anisotropy. For an iron particle, which has a cubic anisotropy, with $K_1 = 4.8 \times 10^4$ J/m^3, the expected value of θ in a field of 0.01 Tesla is about 11°. For magnetite the angle is about 15°. The field required to begin rotation of iron and magnetite particles (chapter 7) varies between 0.001 and 0.002 T. For these fields the expected value of θ is between 3° and 6°.

The Effect of Coercive Force Magnitude and Anisotropy on the Rotation Indices

Coercive force effects only occur in magnetically ordered materials, and are not applicable to paramagnetic substances. The coercivity of remanence of a crystalline material is the reverse magnetic field needed to reduce the remanent magnetisation to zero after applying a saturating magnetic field. It is a measure of the *average* field needed to move a domain wall through the material, overcoming energy barriers largely due to crystal imperfections.

Two measures of coercivity may be considered. These are illustrated in figure 4.2, which shows a typical hysteresis loop for ferromagnetic and ferrimagnetic materials. At the coercive force point the revrese field H_c is required to reduce the magnetisation to zero. However, if this reverse field is removed, the magnetisation reverts to its remanent value M_r. A larger reverse field H_{cr} is required to leave the material unmagnetised after the reverse field is removed. The ratio $\frac{H_{cr}}{H_c}$ is often quoted in the literature (it depends on grain size and shape, increasing with grain size), and its value can vary from just greater than 1 to as high as 10 (O'Reilly, 1984).

In chapter 2 it was pointed out that coercive force is between 10^3 and 10^5 A/m for magnetite, depending on the particle size and temperature (O'Reilly, 1984). Coercive forces of 10^3 A/m are similar to the fields needed to rotate magnetite particles of about 500 μm in size (typically measured at between 0.001-0.002 T in chapter 10).

Figure 4.2

The magnetic hysteresis loop for ferromagnets and ferrimagnets. The form of the loop, and the numerical values of the ratios M_{rs}/M_s and H_{cr}/H_c depend on microstructure, principally grain size and shape.

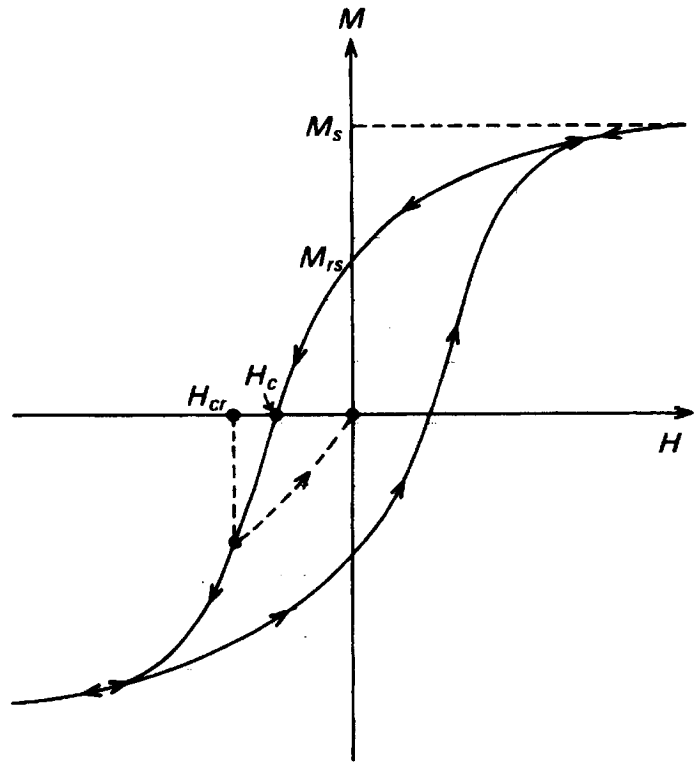

(From O'Reilly, 1984)

If a multidomain ferromagnetic particle is subjected to a rotating magnetic field less than the coercive force, only minor domain re-alignment can take place as the field rotates. If the particle was originally unmagnetised, it is not able to rotate. If it was previously magnetised, then it will experience a torque but little domain movement will occur. For magnetised ferromagnetic particles with a high coercive force, the torque may be high enough to rotate the particle. This of course occurs with permanent magnets.

For such a particle the field required to rotate the particle is lower than the coercive force H_c, and the maximum torque occurs for $\phi = 90^0$ (i.e. magnetisation perpendicular to the external field). For this to occur the relationship between coercive force and external field must be

$$\frac{H_c}{H} > 1$$

In this case the torque on the particle arises from the remanent moment of the grain.

As the field required to rotate the particle becomes greater than the coercive force H_c, it is no longer possible to achieve lag angles between magnetisation and field of 90^0 because $H.sin\phi > H_c$ for some ϕ, and domain growth in other directions is commenced. Domain rotation from easy directions (θ) is only minor at these low fields, where $H << H_A$ (H_A is the

anisotropy field). Domain wall motion in a rotating applied field becomes important when H and ϕ have values such that $H.sin\phi \geq H_{cr}$. That is:

$$\frac{H_{cr}}{H} \leq \sin\phi \qquad (H > H_c) \qquad 4.12$$

For H greater than, but close to H_{cr}, the rotation index could have a value less than 1, depending on the ratio between the external field needed to rotate the particle and the coercive force.

Once the component of the applied field (H) along an easy magnetisation direction becomes greater than H_{cr}, the nett particle magnetisation is able to follow the applied field direction relatively freely. The torque on a particle due to a rotating field is then due to a non-equilibrium domain structure, which can originate from either H_c or from a finite domain wall velocity (discussed below).

However, for a sufficiently high H ($H_A > H > H_{cr}$, where H_A is the anisotropy field), $H.sin\phi$ reaches a value where further reduction in the H_{cr}/H ratio has no effect and the anisotropy constants determine rotation.

Domain rotation, through an angle θ against the anisotropy field, increases with H (see chapter 2). The extent of this rotation (and the energy involved) is determined, for a given field strength, by the angles between the applied field and the easy axes. Until the applied field reaches midway between two easy axes, magnetisation deviation from one of the axes involves a higher energy than the other, and is therefore less favoured for domain growth.

The angle (ϕ) between applied field and magnetisation, determines the torque applied to the magnetisation, but this torque is equalled by the torque between the magnetisation and the anisotropy field. The total angle between applied field and easy axis is now ($\phi + \theta$). When the applied field components along two of the easy magnetisation directions are equal, magnetisation along each of the easy directions is equally energy efficient. The crystal energy is then at a maximum, and torque (the derivative of the energy) drops to zero. For a field rotation between easy axes at 90^0, this occurs at $(\phi + \theta) = 45^0$, and for uniaxial grains, it occurs at $(\phi + \theta) = 90^0$. The maximum torque occurs at 22.5^0 and 45^0 respectively, and the angle ϕ (which determines the rotation index) is smaller again. Rotation indices would be expected to be about 0.4 for cubic and about 0.7 for uniaxial crystals, but decreasing with higher H due to an increased θ. For minerals such as magnetite, the expected value of θ, even if H could be placed perpendicular to magnetisation ($\phi = 90^0$), is about 15^0 at the fields needed to lift the grains (see chapter 2), but is only a few degrees at the fields required to rotate the grains against gravity. It is between 1^0 and 2^0 at $\phi = 22.5^0$.

If $H > H_A$ the magnetisation closely follows the applied field direction, and torque arises because of the angle θ between the magnetisation and the anisotropy field (which is along an easy axis). The angle ϕ, on which the rotation index is based, is very small. Therefore, as H increases above H_A, the ferromagnetic rotation index decreases (it is based on ϕ), but the torque applied to the particle remains constant.

A very small rotation index indicates that the field needed to rotate the particle is greater than the anisotropy field. In practice this means that the anisotropy field is very small.

The above effects are summarised in figure 4.3, for a uniaxial ferromagnetic grain.

Figure 4.3

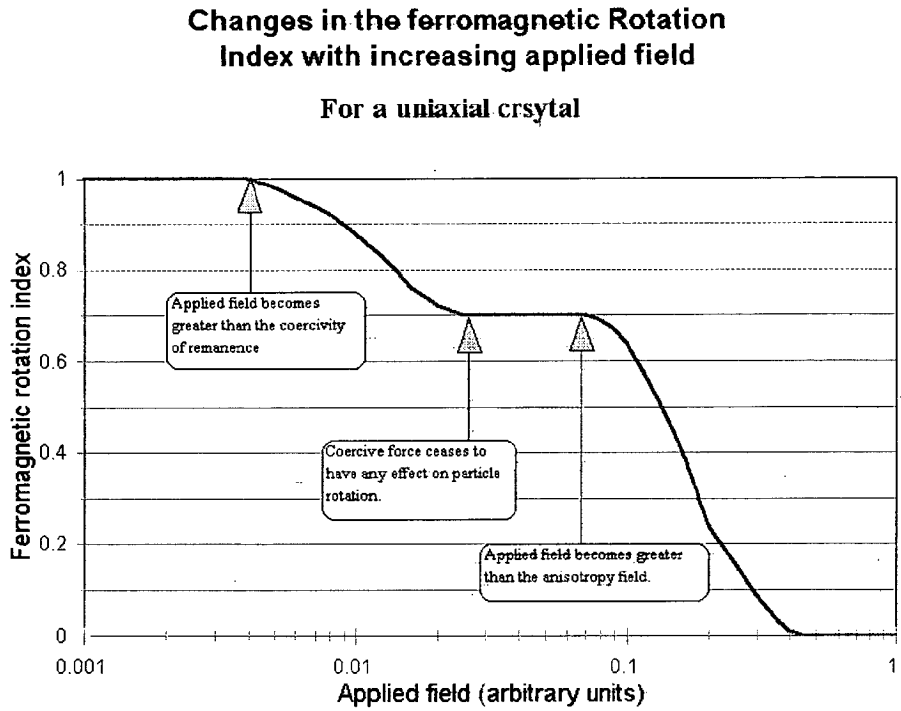

In figure 4.3, the applied field refers to the external field required to rotate the particle.

The Effect of Domain Wall Velocity on the Rotation Index

Domain wall velocity affects the speed at which the magnetisation in a ferromagnetic (or ferrimagnetic) particle is able to change direction.

The resultant magnetisation in an unsaturated ferromagnetic particle is the vector sum of the domain magnetisations, which are directed approximately along the easy directions of magnetisation in the particle. Applying a magnetic field greater than H_c causes domain walls to migrate through the particle such that the domains most closely aligned with the external field grow at the expense of others. In a magnetically saturated ferromagnetic particle there is only one domain, and its magnetisation (in low enough fields) is close to the nearest direction of easy magnetisation to the external field, but deflected somewhat towards the applied field direction. If the external field is rotating, and the particle is not free to follow the field, there is a finite time before the particle magnetisation can re-align itself (by domain re-growth) along a new direction of easy magnetisation, and this leads to larger angles of lag (i.e. the angle ϕ) between the external field and the particle magnetisation than would normally be expected for a stationary external field. As the field rotation frequency increases, the angle of lag (ϕ) is expected to increase, with a consequent increase in the torque applied to the particle.

The maximum torque is applied to a particle if the angle ϕ is 90^0. Even if the ratio H_c/H (above) is less than 1, an angle for ϕ of 90^0 could be achieved in a dynamic system if the

domain wall velocity were sufficiently sluggish. If the field rotation frequency were to be increased further, so that domain growth lagged even further, and ϕ increased past 90^0, then torque would decrease.

Chapter 2, equation 2.9, gave an expression for domain wall velocity as:

$$v = c(H - H_0)$$

Where c was referred to as the wall mobility, H the external field, and H_0 as the critical field.

There is, unfortunately, little information available which could reasonably represent average domain wall velocities across natural magnetite grains of up to 1 mm in diameter.

For domain wall velocities to affect rotation index values, at the field rotation frequencies used here (around 50 Hz), they would need to be in the vicinity of 0.2 to 0.6 m/sec. This is about a factor of about 10^2 smaller than the value obtained by Galt (see chapter 2) for his pure synthetic magnetite crystal, but is not unreasonable considering the dislocations and impurities which may be found in natural crystals. The extent of the latter may be judged by comparing Galt's low coercive force figures for his pure synthetic magnetite with the very much larger figures for natural magnetite (3.5 A/m compared to 800-1600 A/m).

Domain wall velocity effects only affect the commencement of particle rotation (against an opposing torque) when the external field is higher than the critical field (H_0 in equation 2.9 repeated above), which may be approximated by the coercive force H_c.

The minimum time for a domain wall to travel across a particle is given by:

$$t = \frac{d}{c(H-H_0)} \qquad 4.13$$

Where d = particle diameter (m)

This assumes that the wall velocity is constant (at its maximum value). However the wall velocity is lower at small ϕ because the component of H in the new direction is lower. Consequently the travel timeincreases. Nevertheless the above expression serves as an approximation of the travel time.

While the domain walls are travelling through the particle, the external field rotates through an angle α, given by:

$$a = 360^o \times ft = \frac{360^o \times fd}{c(H-H_0)} \qquad 4.14$$

Where f is the field rotation frequency

This angle can be used to approximate the domain wall velocity term (D_v) in equation 4.11, so that the rotation index could be written as:

$$R_f = \frac{\sin\left(\phi + \frac{360fd}{\alpha(H-H_0)}\right)}{I} \qquad 4.15$$

Where I is a term that describes the inertia effect

This is a considerable simplification, because the effects of particle size and temperature on the critical field have not been included. Domain wall velocity will also vary considerably between particles due to compositional differences, crystal imperfections and the number of domain walls. However it does illustrate that the measured rotation index contains information on domain wall velocity.

The Effects of Particle Inertia on the Rotation Index

The rotation index has been defined as a dimensionless ratio of two torques:

$$\frac{\text{Torque required to rotate particle against surface interaction (due to gravity)}}{\text{Particle magnetic moment} \times \text{applied magnetc field}}$$

Because the field is rotating at a constant angular velocity, and a stationary particle must first accelerate to match the field angular velocity, the measured rotation index must include an inertia effect. The field required to commence particle rotation is higher than the field required to maintain particle rotation, and it is the field required to commence particle rotation that is actually measured. The applied magnetic field in the above ratio, if determined by the method described in chapter 7, consists of two components:

$$\frac{\text{Torque required to rotate particle against surface interaction (due to gravity)}}{\text{Particle magnetic moment} \times (\text{acceleration field} + \text{rotation field})}$$

or:

$$\frac{\tau_g}{\tau_a + \tau_m}$$

Where τ_g is the torque to rotate particle against surface interaction
τ_a is the torque to accelerate the particle
τ_m is the torque to maintain particle rotation

This could be written as:

$$\frac{\frac{\tau_g}{\tau_m}}{1+\frac{\tau_a}{\tau_m}} \qquad 4.16$$

Equation 4.18 now becomes:

$$R_f = \frac{\sin\left(\phi + \frac{360fd}{\alpha(H-H_0)}\right)}{1+\frac{\tau_a}{\tau_m}}$$

(Note that the inertia term in the denominator, and the whole expression, remain dimensionless)

The torque required to accelerate a spherical particle to the field rotation frequency is equal to the moment of inertia times the angular acceleration. This implies:

$$\tau_a = \frac{\pi^2 D d^5 f^2}{30A} \qquad 4.17$$

Where D is the particle density (kg/m^3)
d is the particle diameter (m)
f is the field rotation frequency (Hz)
A is the fraction of a cycle available for the particle to accelerate to field rotation frequency, assuming a constant angular acceleration.

and the magnetic torque for a ferromagnetic particle (field at 90^0 to magnetisation) is:

$$\tau_m = \frac{\pi d^3 m_m H D}{6} \qquad 4.18$$

Where m_m is the particle mass magnetic moment (Wb.m/kg)
H is the applied field (A/m)

The measured ferromagnetic rotation index can then be written as:

$$R_f = \frac{\sin\left(\phi + \frac{360fd}{c(H-H_0)}\right)}{1+\frac{\pi d^2 f^2}{5Am_m H}} \qquad \text{(dimensionless)} \qquad 4.19$$

The domain wall velocity term and the inertia term in equation 4.19 have been treated above as though they are independent of each other, but this is not really the case because the time available for particle angular acceleration is also affected by domain wall velocity and by viscous drag. The quantity A in equation 4.19 is complicated and frequency dependent.

Equation 4.19 implies that the value of the rotation index, as originally defined, can be obtained by extrapolating the measured rotation index to a zero field rotation frequency. It also implies that the frequency dependence of the measured rotation index could in principle provide information on domain wall velocity in a ferromagnetic particle.

By similar reasoning, the measured paramagnetic rotation index can be written as:

$$R_p = \frac{\sin\phi}{1+\frac{\pi d^2 f^2}{5Ak_g H^2}}$$

Where k_g is the mass magnetic susceptibility

Summary

Magnetic separation by particle rotation in a rotating magnetic field is a separation method based primarily on particle crystalline structure and magnetic exchange forces. It is a method that depends on magnetic anisotropies.

The rotation characteristics of a particle can be described using by finding the value of R (= $sin\phi$) from the relationship:

Particle magnetisation × *rotation field* × R = *Torque to rotate particle against gravity*

The value of R is referred to here as the rotation index, and can be calculated from measurements of particle lift and particle rotation field strengths. Two rotation indices can be calculated:

(a) The paramagnetic rotation index:

$$R_p = \frac{d\left(\mu_0 a\left(1-\frac{D_f}{D_p}\right)-k_g B_r \frac{\partial B_r}{\partial x}\right)}{2k_g B_r^2}$$

(b) The ferromagnetic index:

$$R_f = \frac{\mu_0 d\left(a\left(1-\frac{D_f}{D_p}\right)-m_m \frac{\partial B_r}{\partial x}\right)}{2m_m B_r}$$

Where: $\frac{\partial B_r}{\partial x}$ is the magnetic field gradient at first rotation (T/m)
B_l is the magnetic induction outside of the particle at first rotation (T)
d is the particle length (m)
μ_0 equals $4\pi \times 10^{-7}$
D_f is the density of any immersion fluid (kg/m^3)
D_p is the density of the particle (kg/m^3)
a is the acceleration due to gravity (m/sec^2)
k_g is the particle mass susceptibility (SI units)
m_m is the magnetic mass moment at saturation (Wb.m/Kg)

The relationship between the rotation index R, the magnetocrystalline and shape anisotropy anisotropy constants k_1 and k_s respectively, and the angle θ between the particle magnetisation and the direction of easy magnetisation is:

$$R = \sin\phi = \frac{(K_1+K_s)\sin 2\theta}{mH} \qquad \text{(for a uniaxial anisotropy)}$$

and

$$R = \sin\phi = \frac{\frac{K_1}{2}\sin 4\theta + K_s \sin 2\theta}{2mH} \qquad \text{(for a cubic ferromagnetic)}$$

(provided that domain wall velocity, and external field at particle rotation, are sufficiently high, and both anisotropies are along a common axis)

If the external rotating field is smaller than the coercive force of a ferromagnetic particle, at rotation, then the rotation index approaches 1.

If the applied rotating field is greater than the remanent coercivity of a ferromagnetic particle but less than the anisotropy field, the ferromagnetic rotation index should be approximately 0.4 or 0.7 for cubic and uniaxial anisotropies respectively.

If the applied rotating field is greater than the anisotropy field, the rotation index decreases towards zero as the applied field increases.

The ferromagnetic rotation index measured by the methods described later (chapter 7) is influenced by domain wall velocity and particle inertia, and contains information on these factors. The measured ferromagnetic rotation index can be written (approximately) as:

$$R_f = \frac{\sin\left(\phi + \frac{360fd}{c(H-H_0)}\right)}{1+\frac{\pi d^2 f^2}{5Am_m H}}$$

Where f is the field rotation frequency (Hz)
d is the particle diameter (m)
c is the domain wall mobility (m^2/A.s)
H is the applied field (A/m)
H_0 is the critical field for domain wall motion (A/m)
A is the fraction of a cycle available for particle acceleration
m_m is the particle mass magnetic moment (Wb.m/kg)
ϕ is the angle between particle magnetisation and applied field

The measured paramagnetic rotation index is similar to the above, but without a domain wall velocity term.

Chapter 5

Spin Precession Effects Produced by a Rotating Magnetic Field

Introduction

If an attempt is made to tilt a spinning top, it precesses around an axis which is at right angles to the axis of the tilting torque.

Each electron has an angular momentum, as if it were spinning on its axis. In an external magnetic field this angular momentum has a component either parallel or anti-parallel to the external field (it actually precesses around the external field direction). If the external field now begins to rotate, there will be a precession of the electron angular momentum which will have its axis at right angles to the external field rotation axis. The effect is illustrated in figure 5.1, and is described well by Chikazumi and Charap (1978).

Figure 5.1

Sideways precession of an electron in a rotating external magnetic field

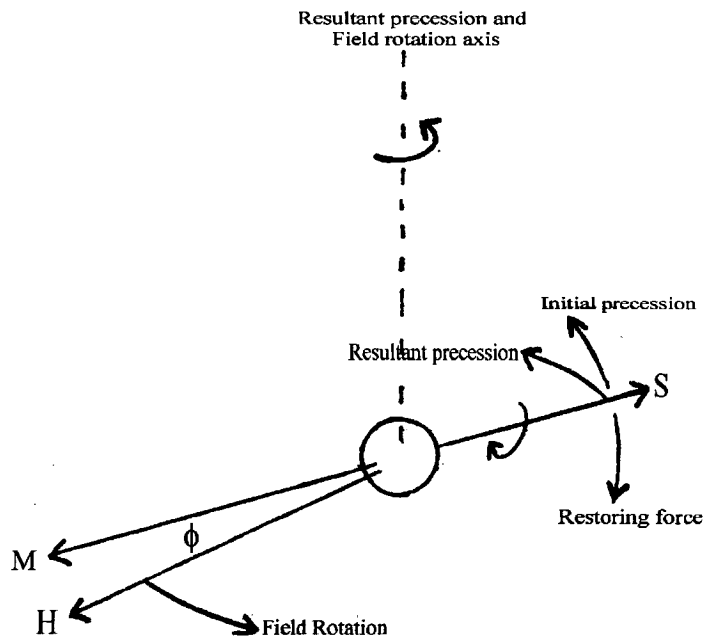

If H rotates as shown in figure 5.1 then the electron spin axis (shown as S in figure 5.1) must rotate to remain aligned with H. This action produces an upwards (in figure 5.1) precession of the spin axis, which is opposed by the magnetic field H or by crystal field energies. The torque that opposes the initial precession causes a resultant precession which is in the same direction as the original field rotation, and has a precessional angular velocity equal to the external field rotation velocity.

If the grain is perfectly free to rotate, the torque acting between the spins and the lattice causes the grain to follow the spin precession, producing a "perpendicular rotation". The axis of this rotation is in the plane of the field rotation, and except for a slight lag (ϕ in figure 5.1), follows at right angles to the field. From a fixed viewpoint in the rotation plane of H, the sense of the rotation would appear to change from clockwise to anti-clockwise every half-cycle of the field rotation.

It is the aim of this chapter to examine whether such precessions could cause observable "perpendicular" particle rotations.

The Torque Required to Rotate a Particle Against Gravity

Consider a particle with mass m_p, density D_p and magnetic mass susceptibility of k_g, which is immersed in a liquid of density D_f. The weight of the particle is reduced by attraction in a magnetic field gradient. Let the diameter of the particle be d. The torque needed to rotate the particle against the surface it rests on is given from equation 4.5 as:

$$Torque = \tfrac{1}{2} dm_p \left(a\left(1 - \frac{D_f}{D_p}\right) - \frac{k_g B \frac{\partial B}{\partial x}}{\mu_0} \right) \quad \text{(N.m)}$$

Where m_p is the mass of the particle

The factor ½ in this equation is really a "shape factor", which refers to the length of the moment arm in comparison to the particle diameter (or particle length in equation 4.5). It can be replaced by a fraction $C_p/2$, where $0 < C_p < 1$. The equation can now be written as:

$$Torque = \frac{C_p}{2} dm_p \left(a\left(1 - \frac{D_f}{D_p}\right) - \frac{k_g B \frac{\partial B}{\partial x}}{\mu_0} \right) \quad \text{(N.m)}$$

Applying this relationship to cubic-shaped 0.5 mm particles of magnetic susceptibility about 50×10^{-6}, in a field of about 0.3 Tesla, gives required torques of the order of 10^{-11} Nm.

Estimation of the "Precession Torque" that Could be Applied to a Particle as a Result of a Continuously Rotating External Magnetic Field

The description of the precessions caused by the rotation of the external field given in the introduction is really a very much simplified picture. In reality the detailed precessional motion will be more complicated, but can be represented as shown in figure 5.1 for simplicity.

All the unpaired electrons in a paramagnetic particle will undergo the above precessions, but some of them have their magnetic moments anti-parallel to the field, and will experience a restoring torque in the opposite direction to the others. Only the excess number of electrons aligned parallel to the external field will contribute to any resultant torque, and this number of electrons is indicated by the magnetic susceptibility of the particle.

Estimation based on an assumption of constant resultant precession at the field rotation rate

The following examination of the problem is based on a calculation of the "restoring torque" magnitude needed to cause the final precession at the field rotation rate.

The resultant precessional angular velocity around the axis of the external field rotation is described by the classical angular momentum equation 5.1. This is the final, rather slow, resultant precession caused by the "restoring force" in figure 5.1.

$$\omega_p = \frac{\tau_p}{L_s} \qquad 5.1$$

Where: τ_p is the torque attempting to re-align the electron with the field
L_s is the angular momentum of the electron spin.

But $\omega_p = 2\pi f$ (where f is the rotation frequency for the external magnetic field), and $L_s = \frac{m_e \mu_s}{e}$ by equation 1.23, where m_e is the electron mass, μ_s is the electron magnetic moment, and e is the electron charge. Therefore an expression for the torque applied to a system of n electrons, in order to keep them precessing in the direction of the external field rotations is:

$$\tau_p = \frac{2n\pi f m_e \mu_s}{e} \qquad \text{(N.m)} \qquad 5.2$$

The value of $n\mu_s$ in equation 5.2 is really the total magnetic dipole moment of the particle (in A.m^2).

The magnetic moment (in Wb.m) associated with n electrons is:

$$m = n\mu_0\mu_s \qquad \text{(Wb.m)} \qquad 5.3$$

Where; $\mu_0 = 4\pi \times 10^{-7}$ (Wb/A.m)
n is the excess number of electrons aligned with the external field.
μ_s is the spin magnetic moment (9.27×10^{-24} A.m^2 = μ_B).

The magnetic moment per unit volume ($\mu_0 M$) for the particle is therefore:

$$\mu_0 M = \frac{n\mu_0\mu_s}{V} \qquad \text{(Wb/m}^2\text{)} \qquad 5.4$$

Where V is the particle volume.

From the relationship for magnetic susceptibility (equation 1.7), using the mass magnetic susceptibility:

$$M = k_g D H \qquad \text{(A/m)} \qquad 5.5$$

Where D is the particle density (kg/m^3).
H is the magnetic field (A/m).
k_g is the mass magnetic susceptibility (note that $k_g D$ is dimensionless)

The total dipole moment (in $A.m^2$) may be expressed in terms of magnetic mass susceptibility by combining equations 5.4 and 5.5:

$$n\mu_s = k_g m_p H \qquad (A.m^2) \qquad 5.6$$

This can now be used in equation 5.2 to obtain:

$$\tau_p = \frac{2\pi f k_g m_p m_e H}{e} \quad (N.m) \qquad 5.7$$

Where m_p and m_e are the masses of the particle and electron respectively.

In terms of the magnetic induction B, equation 5.7 becomes:

$$\tau_p = \frac{2\pi f k_g m_p m_e B}{\mu_0 e} \quad (N.m) \qquad 5.8$$

This is exactly the same equation as is obtained by applying the relationships for the Barnett and Einstein de-Haas effects to calculate the axial magnetic field developed by a rotating specimen, and then calculating the torque which would be applied by interaction of this axial field with the external field. The relationships for the Barnet and Einstein de-Haas effects would more normally be used to estimate g values, and are described by Chikazumi (1997) but are perhaps more completely given (for the purposes here) by Chikazumi and Charap (1978).

For a 0.5 mm particle of magnetic mass susceptibility around 50 x 10^{-6} (cgs), in magnetic fields of about 0.3 Tesla which rotate at about 30 Hz, the above equation gives "perpendicular" torques, due to electron precession effects, of the order of 10^{-17} Nm. Clearly a constant electron precessional mechanism, as envisaged above, can not produce easily observable "perpendicular" particle rotations. The available torque is 6 orders of magnitude too small, and implies an effective (virtual) axial field of the order of 10^{-11} Tesla

Torque produced by precession effects from sudden spin reversals or direction changes

Stephenson (1980) examined the remanent rotational magnetisation produced in a rock that rotates in an alternating magnetic field. Previously, gyromagnetic factors, based on roughly similar reasoning to that given above, were considered to be insignificantly small, and unable to explain such magnetisations. Stephenson's advance was to consider the precessions that occur during sudden spin direction changes as a result of a pulsed magnetic field during rotation of the sample (or rotation of the external field). Under these conditions the spins changed direction in times of the order of 10^{-8} to 10^{-7} sec. as they re-align with the external field. This gives effective spin rotation rates around 10^7 Hz, rather than the 10 to 10^2 Hz of the actual sample or external field rotation rate. Stephenson calculated that an effective ("virtual") axial field of about 10^{-3} Tesla would be implied, rather than the previously estimated field of about 10^{-11} Tesla.

Stephenson's estimated axial field of approximately 10^{-3} Tesla can be used to calculate a "perpendicular" torque that could be applied to a particle. The calculation assumes that the particle is ferromagnetic.

$$\tau_{\perp} = \widetilde{m} \times \widetilde{H_{gyr}}$$

$$\tau_{\perp} = mH_{gyr} \quad \text{(Nm)} \qquad 5.9$$

For a 0.5 mm particle with a magnetic moment of 6.6×10^{-14} Wb.m. equation 5.9 gives a "perpendicular" torque of 5.3×10^{-11} Nm, and this, if it acted continuously, would be sufficient to cause particle rotation perpendicular to the external field rotations.

Figure 5.2 assumes that the above precessional torque is continuous, and illustrates the relative magnitudes of this precessional torque and the torque required to roll an almandine garnet particle while it is contained in a glass tube as illustrated in chapter 7.

Figure 5.2

Comparison of available precessional torque and the torque required to roll a particle

For a roughly spherical 0.5 mm particle with a mass magnetic susceptibility of 60E-6 cgs, and with 20% of particle diameter in contact with a surface. Field rotation frequency at 30 Hz.

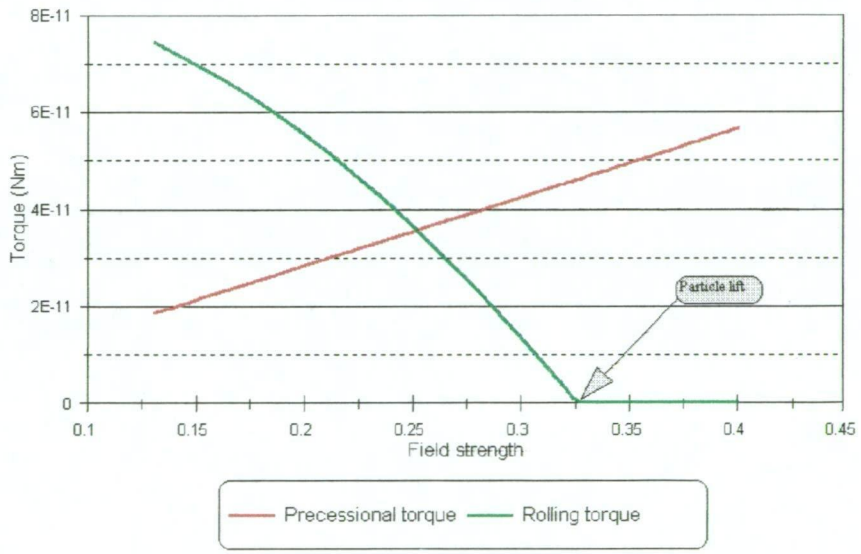

Figure 5.2 illustrates that above an external field of about 0.25 Tesla , the *magnitude* of the precessional torque is greater than the torque reqired to roll particles with a magnetic mass susceptibility of 7.5 x 10^{-7} (SI).

The above calculations have assumed that the axial field described by Stephenson (1980) acts continuously. In fact it only acts for the duration of the spin reversal, which is only 10^{-8} secs. The precessional torque will really consist of a series of 10^{-8} sec. pulses (60 pulses per second, given a 30 Hz field rotation frequency). The *average* applied torque is actually the same as would be applied by a constant electron precession at 30 Hz, that has been calculated using equation 5.8 above.

Particle precessional rotations (perpendicular to the external field rotations) should be easily prevented by even the smallest fluid drag forces or surface interactions. Even if the magnitude of the precessional torque were to be sufficient to cause precessional rotations (e.g.

if continuous spin reversals could occur), it is not immediately obvious how "perpendicular" particle rotation around a given axis could be produced.

Requirements for a continuous precessional rotation

Even if the "perpendicular" torque is firmly coupled to the crystalline structure of the particle, a rotating magnetic field of constant magnitude, rotating at a constant angular velocity, should not cause a continuous particle rotation. At best it could cause a "wobbling" of the particle at the field rotation frequency. There should be no continuous "perpendicular" rotation because the precessional rotation axis would rotate to remain perpendicular to the external field.

Figure 5.3 illustrates the relationship which is required to exist between rotations for a continuous perpendicular particle rotation.

Figure 5.3

The relationship between continuous particle rotation and external field rotation

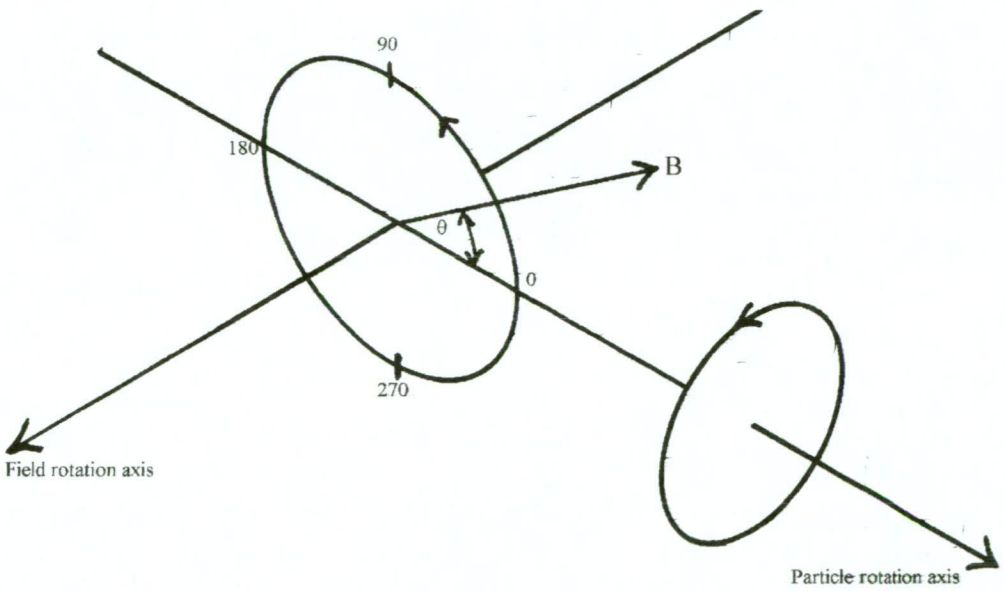

Changing the magnitude of the external field throughout a complete field rotation could generate a resultant torque. For example, if the external field was greater for θ from 0^0 to 180^0, with reference to some arbitrary direction (eg. horizontal where $\theta = 0^0$), the particle would then have a resultant torque, and it could rotate on average in one sense. This bias on the magnetic field did actually exist (by accident of construction) in the field produced by the original magnet drum with which these observations were made. If this effect is taken into account, and if only the component of torque attempting to turn the particle around a horizontal axis is considered, equation 5.9 now becomes:

$$\tau_{\perp} = MH_{gyr}(1 + y\sin\theta)\sin\theta \qquad \text{(N.m)} \qquad 5.10$$

or, assuming paramagnetism:

$$\tau_{\perp} = 4\pi\mu_0 k_g m_p H_{gyr} H_{ext}(1 + y\sin\theta)\sin\theta \qquad \text{(N.m)} \quad 5.11$$

Where y is the fractional ($\pm$) variation of H_{ext}.

Conclusions

Continuous particle rotation with the rotation axis perpendicular to the field rotation axis ("perpendicular" rotation), on the basis of torque *magnitudes* alone, appears to be a possibility, and should be able to be enhanced by increasing a directional bias on the rotating magnetic field strength.

Calculations based on a constant precession of spins, such as is envisaged for the Einstein de Haas effect, show that this effect can not provide sufficient torque to cause "perpendicular" particle rotations. Estimations of the torque provided by sudden magnetisation jumps, as envisioned by Stephenson (1980), show that sufficient torque *magnitude* is available, but that its duration (10^{-8} secs) is too short. The *average* torque produced by Stephenson's effect is the same as that produced by the Einstein de Haas effect.

Chapter 6

Eddy Current Rotation of Small Non-Ferrous Metallic Particles

Introduction

Eddy current separation has not previously been considered to be a *mineral* separation method. The method has been developed with the recycling industry in mind, and has been used to separate much larger particles (usually greater than 4 mm) than are encountered in most mineral processing situations. The eddy current separation of small gold particles (less than 1 mm) has not been considered as practical, or even possible.

Nevertheless eddy current separation is a magnetic separation, and the results presented in this thesis (chapter 17) indicate that it should be considered as a mineral separation method. The particles being separated may be non-magnetic, but the repulsion or rotation is due to a reaction between the external magnetic field and the magnetic field generated by induced current elements within the particle. The indication here and in chapter 17 that gold particles down less than 50 μm in diameter may be able to be separated by rotating magnetic field eddy current methods, places rotating field eddy current separation into the mineral separation area.

It was mentioned in chapter 3 that eddy current rolling of particles has been known for some years, but has been considered as an effect to be minimised rather than used. As particle sizes become much less than the width of the magnet strips used in most eddy current separators, the particles increasingly respond to the field changes by rotation rather than by repulsion. For particles below about 4 mm it becomes increasingly difficult to design a machine with narrow enough magnet strips and an acceptable depth of field to repell the particles. Therefore at the smaller particle sizes it becomes logical to switch from a repulsion separation to a rotation separation, and as the minimum particle size decreases, the eddy current separation of gold particles becomes practical.

The purpose of this chapter is to estimate the minimum metallic particle size that can be rolled by a given magnetic field strength and field rotation frequency. The relationship derived here will be compared with experimental rotating field eddy current separations in chapter 17.

The Torque Experienced by a Conductive Particle in a Rotating Magnetic Field

Placing a conductive particle in a rotating magnetic field is an equivalent situation to rotating a particle in a stationary magnetic field. As the latter is more easily recognised from texts, the rotation of a simple current loop is considered to begin with.

Figure 6.1

Current generation by the rotation of a single conductive loop in a magnetic field

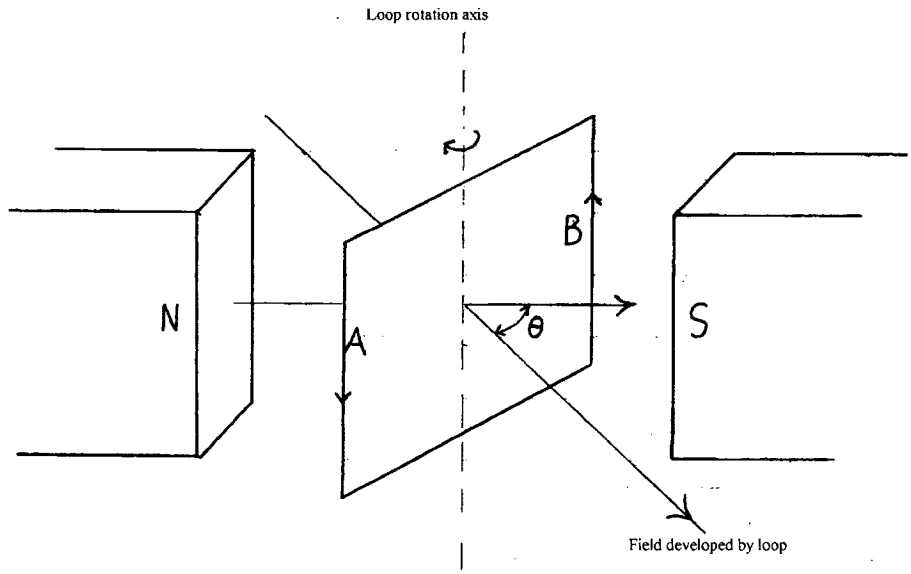

The magnetic flux passing through the square loop in figure 6.1 is given by:

$$\phi = BA\cos\theta = BA\cos(2\pi ft)$$

Where: B is the magnetic field (T)
A is the loop area (m^2)
f is the loop rotation frequency (sec^{-1})

and the induced voltage is given by Faraday's law as:

$$V = -\frac{\partial\phi}{\partial t}$$

Therefore the electric current induced in the wire loop shown is given by:

$$i = \frac{V}{R} \text{ or } \quad i = \frac{2\pi BAf\sin\theta}{R} \quad \text{(A)} \qquad 6.1$$

Where: R is the resistance of the wire in the loop (ohm.m)

Such a current flowing in the loop produces a magnetic moment given by:

$$M' = \frac{2\pi BA^2 f\sin\theta}{R} \quad \text{(J/T or A.m}^2\text{)} \qquad 6.2$$

Due to the angle θ between this moment and the external field direction, there will be a torque on the loop, whose magnitude is given by:

$$\tau = \frac{2\pi B^2 A^2 f \sin^2\theta}{R} \qquad \text{(N.m)}$$

The resistance (R) of the wire loop depends on its perimeter and on the cross-sectional area of the wire. A better quantity, which is characteristic of the loop material is the resistivity (ρ), which is related to the resistance by:

$$R = \frac{4l\rho}{A_w} \qquad \text{or} \qquad R = \frac{4l\rho}{dldz}$$

Where A_w is the cross-sectional area of the wire which can be represented by $dl.dz$.

The torque on the wire loop is then:

$$\tau = \frac{\pi B^2 l^3 f \sin^2\theta}{2\rho} dldz \quad \text{(N.m)} \qquad 6.3$$

A square disc may be considered to be the sum of many such square loops, and the torque on a disc at θ = 90^0 (i.e. sin(θ) = 1) to the field can be obtained by integrating over l.

A cube may be considered as the sum of many such discs and, to a first approximation, assuming the same orientation to the field for all the discs (sin(θ) = 1), the torque on a cube may be obtained by integrating over z. Therefore the torque placed on the cube is approximately:

$$\tau = \frac{\pi B^2 l^5 f}{8\rho} \qquad \text{(N.m)} \qquad 6.4$$

For a sphere of diameter l the torque is given by a similar calculation as:

$$\tau = \frac{\pi B^2 l^5 f}{60\rho}$$

Where ρ is the resistivity of the metal (ohm.m)
l is the particle diameter (m)

For the particle sizes and field rotation frequencies considered here (generally below 0.5 mm and 1000 Hz respectively), the skin depth effects are negligible, being much greater than the particle size (e.g. skin depth approximately 4 mm for Cu at f= 300 Hz).

If such a torque can be placed on a particle by a rotating magnetic field, and the particle is resting on a surface, the particle will be rolled when the torque becomes greater than the gravitational forces holding the particle against the surface. The gravitational torque preventing a cubic-shaped particle from rolling is:

$$\tau_g = \frac{l^4 Da}{2} \qquad \text{(N.m)} \qquad 6.5$$

Where: a is the acceleration due to gravity. (m/sec^2)
D is the particle density

Combining equations 6.4 (for a cubic particle) and 6.5 gives an estimate of the minimum particle size that could be rolled at a given magnetic field strength.

$$l = \frac{4a\rho D}{\pi B^2 f} \quad \text{(m)} \qquad 6.6$$

While equation 6.6 should give an a reasonable estimate of the minimum "rollable" cubic particle size if the rotating magnetic field has its rotation axis at the centre of the particle, it will not give an accurate figure for the more practical situation where the rotating field is produced by a magnet drum such as described in chapter 7. The magnetic structure of this drum is similar to those already used for eddy current separation, and similar to any that are likely to be used for eddy current rotation separation. So far as the particle is concerned, the field is not only rotating, but also moving through the particle. On a rotating particle, this moving field effectively produces a field which rotates in the opposite direction at half the field rotation frequency.

Therefore an *estimate* of the minimum *rollable* cubic particle size is given by 6.7. This may not be a good estimation of *separable* particle size, because particle shapes will vary considerably (e.g. the torque on a spherical particle is smaller, but it also rolls easier), and the effects of physical interference with other surrounding particles have not been considered.

$$d = \frac{8a\rho D}{\pi B^2 f} \quad \text{(m)} \qquad 6.7$$

The Eddy Current Separation of Various Small Metallic Particles

While the reclamation of metals from shredded scrap, or crushed potlining (see chapter 2), usually deals with particle sizes above 4 mm, most mineral processing applications deal with particle sizes from a few mm down to a few μm, and usually less than 0.5 mm. One obvious potential use for eddy current separation is for the recovery of gold particles. The eddy current removal of gold particles above about 20 μm would be quite attractive in some situations, and because the eddy currents are necessarily restricted to the metal particles, the separation works just as well in water.

Equation 6.7 indicates that the metal resistivities and densities are important factors in determining minimum separable particle sizes. Resistivities and densities for some metals are given in Table 6.1.

Table 6.1

Resistivity and density values for some metals

Metal	Resistivity (x 10^{-8} ohm.m)	Density (kg/m^3)
Al	2.82	2.7
Cu	1.77	8.9
Ag	1.59	10.5
Zn	5.8	7.1
Au	2.4	19.3
Cd	7.6	8.6
Pb	22	11.3

With magnet drums similar to the one described in chapter 7, it is possible to employ rotating magnetic fields of 0.4 Tesla or more, and field rotation frequencies of between 500 and 1000 Hz. Consider a separator with a magnetic field at the separation surface of 0.45 Tesla, then the field rotation frequencies required to separate particles of various sizes are shown in figure 6.2.

Figure 6.2

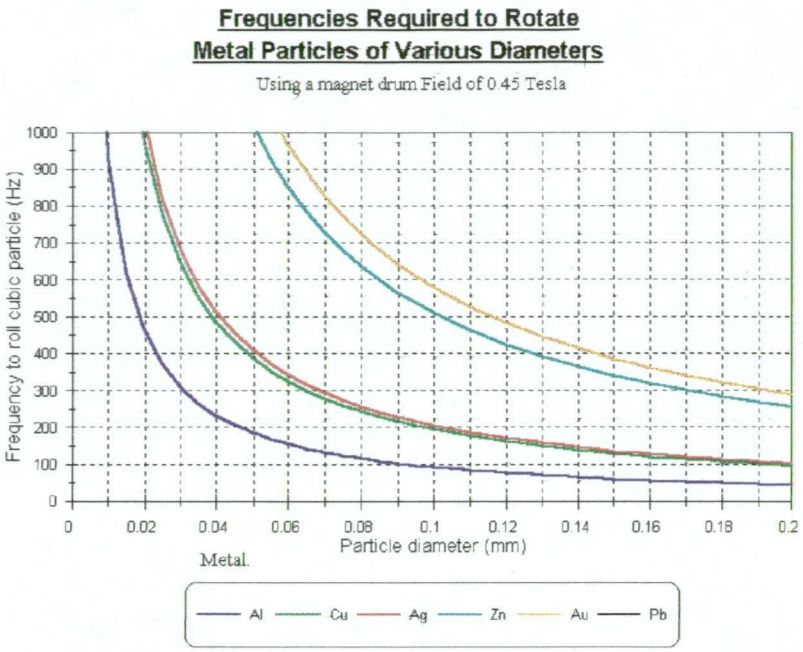

The calculations suggest that separation of gold particles down to 60 μm can be achieved using a field rotation frequency of 1000 Hz. Of the common metals shown, only lead (which does not show in figure 6.2) would present some difficulty for separation by eddy current rolling.

While the above theoretical calculations suggest that particles down to 20 μm can be separated by eddy current rotation in a 0.45 Tesla field rotating at 1000 Hz, the rotations for these small particles would be expected to be very weak, and easily stopped by any interference from non-metallic particles. In spite of this, the results of trial separations (chapter 17) indicate that the induced particle rotations are surprisingly robust.

Summary

Eddy current rotation of metallic particles is theoretically possible down to particle sizes of less than 20μm.

The minimum separable particle size is given approximately by:

$$l = \frac{8a\rho D}{\pi B^2 f} \quad \text{(m)}$$

Where: a is the acceleration due to gravity (m/sec^2)
ρ is the particle resistivity (ohm.m)
D is the particle density (kg/m^3)
B is the magnetic field (T)
f is the field rotation frequency (Hz)

Because the minimum separable particle size is inversely proportional to B^2, a high field strength is the most important factor for an eddy current separator.

Section 2

Experimental Methods and Equipment

Chapter 7

The Rotating Field Magnet Drum and its Field Characteristics

Introduction

A distinction needs to be made between a magnetic field that is *oscillating* and a magnetic field that is *rotating*. An oscillating magnetic field is similar in concept to an alternating electric current in a wire. The field direction is always parallel or anti-parallel to a given direction, and undergoes periodic reversals in direction. For a rotating magnetic field the field direction rotates at a constant angular velocity.

Separation by rotating magnetic field employs a rotating magnetic field rather than an oscillating one. Ideally the field should be of a constant magnitude and its axis of rotation should be through the centre of any separating particle, but in a practical situation, where thousands of particle over an extended area must be rotated at any one time, this can not be maintained. The method used here to generate a rotating magnetic field is practical, but not ideal. The axis of the field rotations is not through the centre of any of the separating particles, and the magnitude of the field varies slightly throughout a field rotation.

Construction of the Rotating Field Magnet Drum

If alternate N-S magnetic poles are moved under a ferromagnetic particle resting on a surface, as shown in figure 7.1, the particle experiences a field that appears to be rotating in an anti-clockwise direction.

Figure 7.1

A rotating field effect caused by moving alternate N-S magnetic poles past a stationary particle

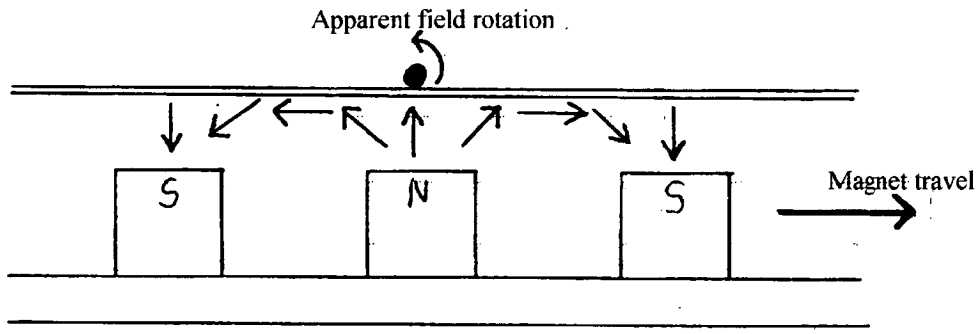

In order to obtain a continuous field rotation, the arrangement shown in figure 7.1 can be "wrapped" around the circumference of a rotating drum, as shown in figure 7.2.

Figure 7.2

The basic rotating field magnet drum, with alternate N-S magnetic pole strips mounted around the circumference of a steel drum

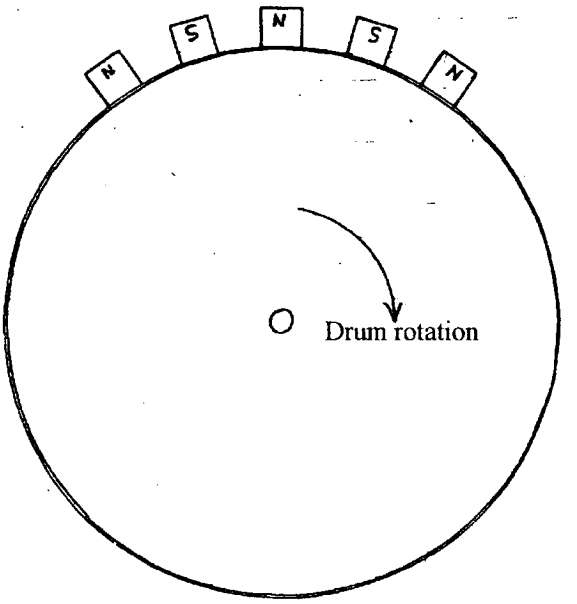

The magnetic arrangement shown in figure 7.2 does produce quite an effective rotating magnetic field, but the field strength between the magnet poles (which is tangential) is very much weaker, for the same radial distance, than the field above the magnetic poles. In order to increase the tangential field between the radial poles, "bucking magnets" are fitted between the radial poles, as shown in figure 7.3.

Figure 7.3

The final magnetic arrangement around the circumference of the 180 mm rotating field magnet drum, showing the location of the "bucking magnets"

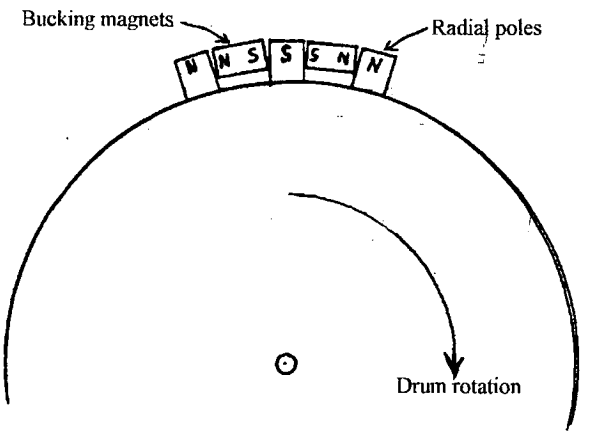

The actual magnet drum used for most of the experimental work for this thesis is shown in figure 7.4, during its construction. The outer surface of the drum is bound with carbon fibre under a fibre-glass outer coating. There are 22 radial magnets, giving 11 field

rotations per drum rotation. The magnetic field *at the drum surface* is 0.425 Tesla (± 10%) for both the radial and tangential fields.

Figure 7.4

The rotating field magnet drum constructed for this thesis.
The magnet drum diameter is 180 mm, and the drum length is 50 mm.

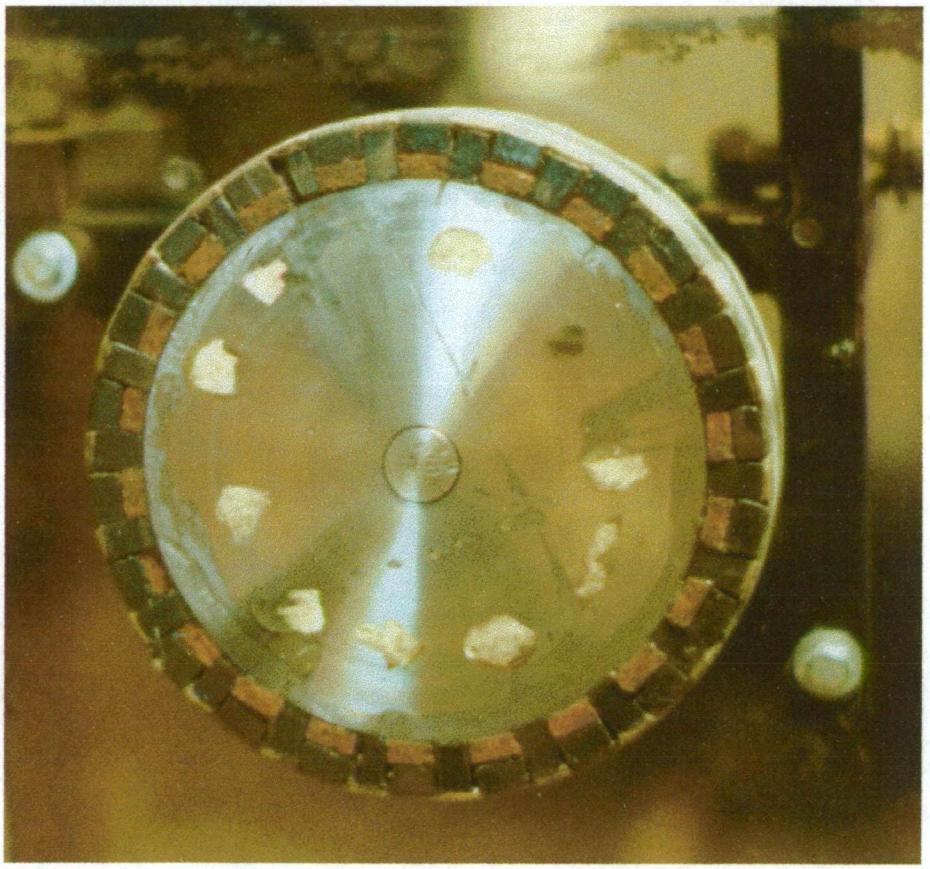

The magnets used for the drum were rare-earth (FeNdB) permanent magnets. These were magnet off-cuts provided by Eriez Magnetics (Aust.) of Melbourne, and were not all exactly the same magnetic strength. The resulting field strength inequalities (±10%) appear to have contributed to the accidental observation of the "perpendicular" particle rotations introduced theoretically in chapter 5 and characterised experimentally in chapter 13.

Magnetic Fields and Gradients Around the Magnet Drum

Magnetic fields and directions radially outwards from the magnet drum surface, above both the radial poles and the bucking magnets, were measured with a Bell hand-held Gauss/Tesla meter (model 4048). The actual probe element has dimensions of approximately 3 mm by 2 mm by 1.5 mm, with the length in the field direction being 1.5 mm. The probe length in the field direction is therefore relatively small in comparison to the magnet dimensions. Figure 7.5 shows the variation in magnitude of the magnetic field between adjacent poles, at 10 mm above the magnet surface. Figure 7.6 shows the angular variation of the field between adjacent poles. Some slight irregularities (deviations from a straight line) occur in figure 7.6. These occur above the edges of the radial and bucking poles.

Figure 7.5

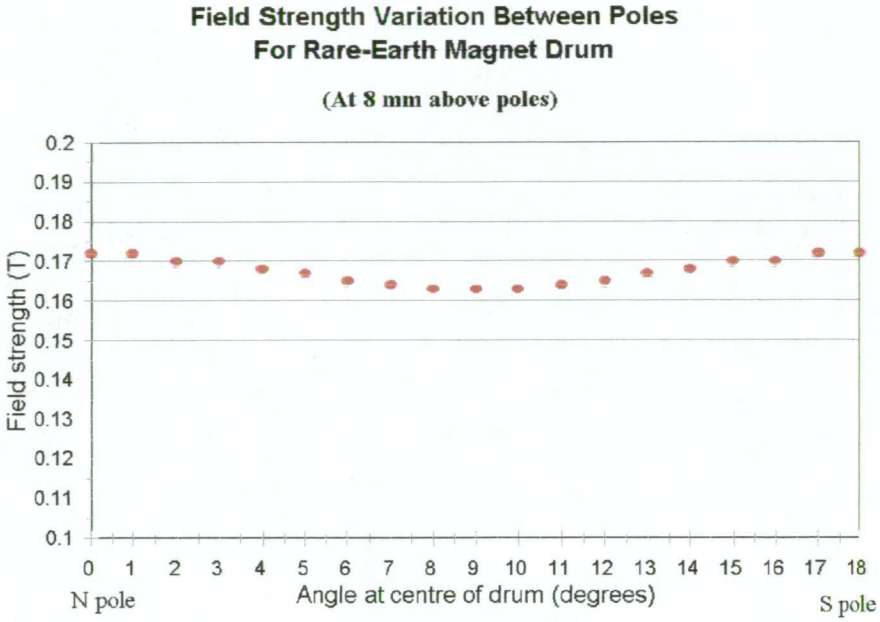

Figure 7.6

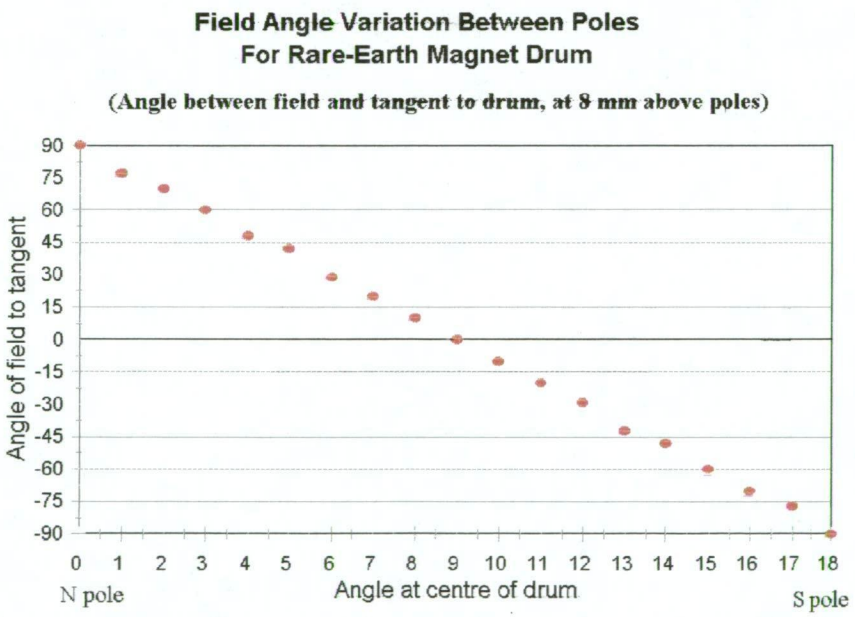

While the field strength is obviously not uniform throughout a field rotation, the variation is generally within +/- 5% of the mean value. In some cases the field above adjacent radial poles varied by up to 7%. Figure 7.6 indicates that the angular velocity of the field direction is reasonably constant.

The variation of the field with distance radially outwards from the drum surface is shown in figure 7.7, where it is compared with a calculated field based on equation 7.1 below. The values plotted in figure 7.7 are for the magnet drum illustrated in figure 7.4, which has been used for measurements and separations throughout this thesis.

Figure 7.7

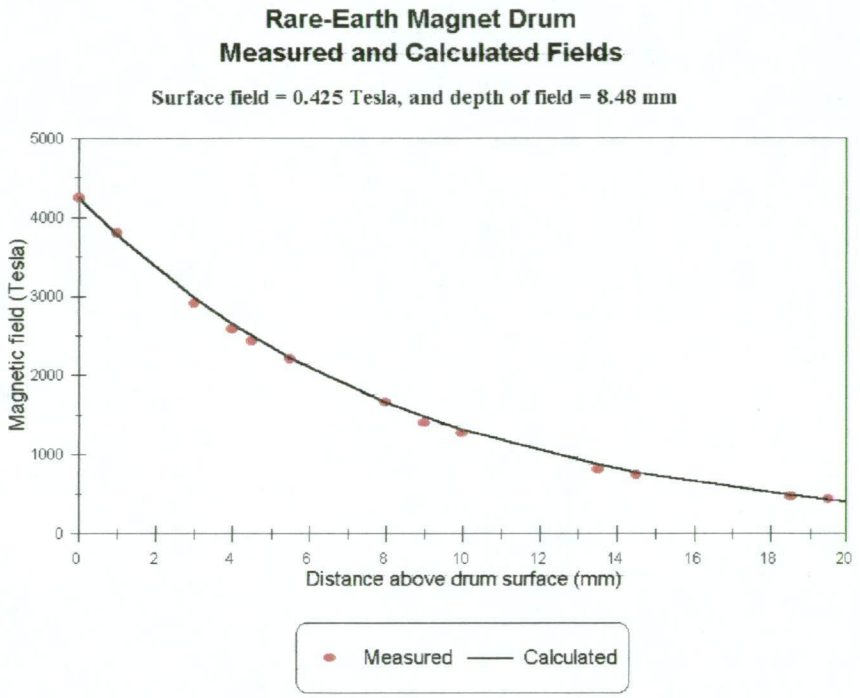

Five rotating field magnet drums, with diameters varying from 120 mm to 300 mm have been constructed so far, and for all of these drums, the magnetic field magnitude radially outwards from the drum surface has been found to be closely approximated by the expression:

$$B = \frac{B_s}{e^{\left(\frac{x}{x_o}\right)}} \qquad \text{(T)} \qquad 7.1$$

Where: B_s is the magnetic field at the drum surface (T)
x is the distance radially out from the drum surface (m)
x_o = is the distance from the drum surface where the field falls to $\frac{1}{e}$ of its value at the drum surface. (m)

The value of x_0 can be used as an indicator of the "depth of field" for a particular magnet drum, and will be referred to as the "depth of field" in later equations.

It can be seen from figure 7.7 that the fit between the calculated values (from equation 7.1) and the measured values is good. For the magnet drum used for the particle measurements in this thesis, the value of x_0 is 8.48 x 10^{-3} (m). Therefore, if the distance from the drum surface is known, the magnetic field can be calculated with reasonable accuracy.

The field gradient is simply the derivative of equation 7.1:

$$\frac{\partial B}{\partial x} = \frac{-B_s}{x_o e^{\left(\frac{x}{x_o}\right)}} \qquad \text{(T/m)} \qquad 7.2$$

Using the Drum to Measure Magnetic Susceptibility, Magnetic Moment and Particle Rotation Indices

Measurement of particle lifting distance

The particles are placed in individual water-filled small-bore glass tubes, as shown in figure 7.8, and held horizontal beneath the magnet drum by a clamp, which can be adjusted vertically and which is fitted with a calibrated vertical scale.

Figure 7.8

Arrangement for measuring particle lifting distances

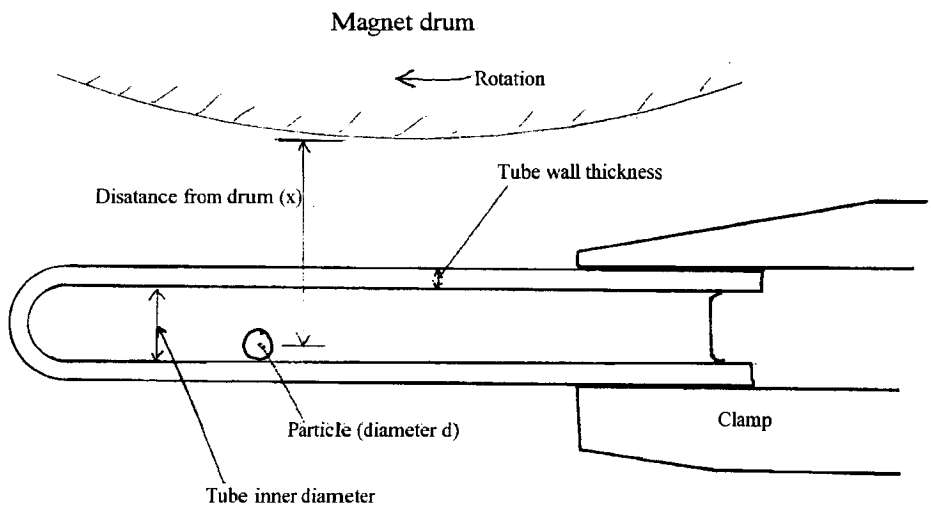

The glass tube is raised towards the magnet drum until the particle lifts, the reading on the vertical scale is noted, and the tube is raised until it just touches the drum so that the scale zero can be checked. The particle diameter can be estimated by observation through a microscope. As the tube dimensions are known (inside diameter 1.5 mm, and wall thickness 0.75 mm for the tubes actually used), the distance to the centre of the particle can be estimated with good accuracy. The vertical scale can be read to an accuracy of $\pm$ 0.25 mm. Distance measurements are therefore given to the nearest 0.5 mm.

The equipment used for these measurements is shown in figure 7.9. The microscope used to observe the particles and their lift and rotation points can be seen (out of focus) in the lower left of figure 7.9.

Figure 7.9

Experimental arrangement for observing particle rotations and for measuring particle lift and rotation distances.

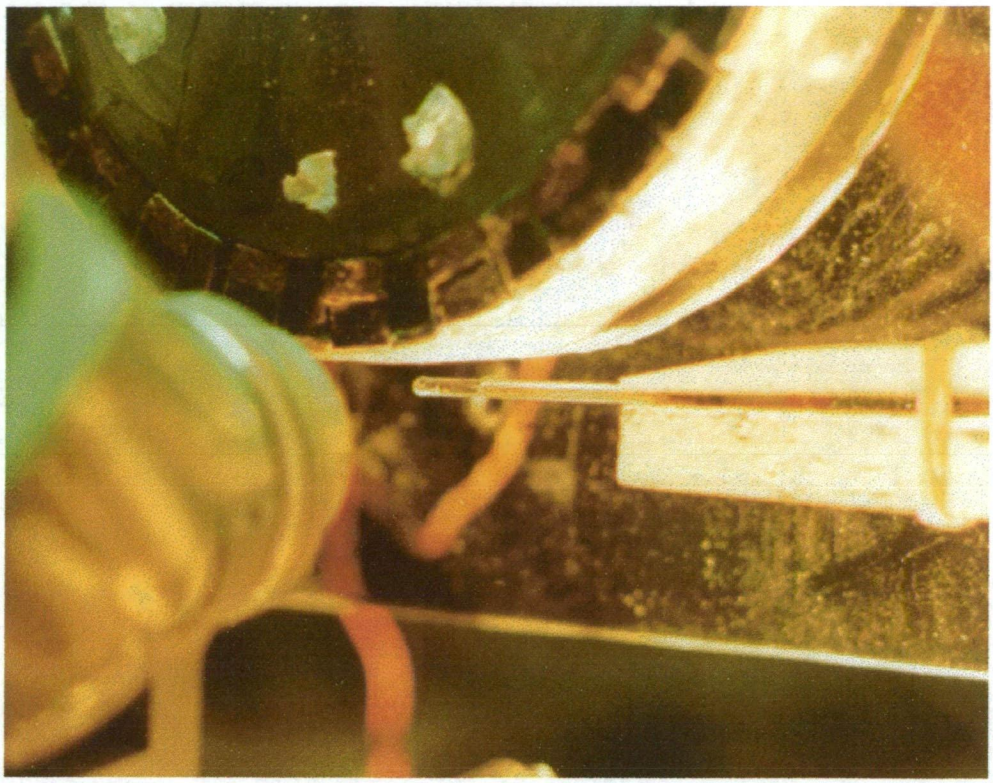

Measurement of particle rotation distance

The same method as described above is used to measure particle rotation distance. In fact the two measurements are normally made at the same time. The distance at which the particle commences rotation is not always easy to determine accurately if it is greater than about 30 mm, because many particles are prone to intermittent wobbles and part-rotations. Therefore the distance at which a *continuous* rotation can be maintained is measured. However, as the distance from the drum surface increases, the field gradient becomes lower. The distance scale can be read to an accuracy of $\pm$ 0.25 mm. At 2 mm from the drum surface this gives (from figure 7.7) a field strength accuracy of approximately $\pm$ 0.015 Tesla. At 30 mm from the drum surface, a measurement error of about $\pm$ 2 mm is required for the same error in field strength.

Using the above methods, the rotation and lift distances can be measured at any field rotation frequency from 10 Hz to the maximum available. The field rotation measurements use a coil pick-up mounted at 3 mm from the drum surface, capable of measuring field rotation frequencies from 10 to 150 Hz. This sensor therefore detects the actual field rotations rather than motor revolutions or drum shaft revolutions. Particle distance from the magnet drum is read from a scale attached to the sample clamp, and can be read to $\pm$0.25 mm.

Calculation of magnetic susceptibility from particle lifting distance below magnet drum

Equation 4.2 showed that the magnetic susceptibility of a small mineral particle could be calculated using the expression:

$$k_g = \frac{\mu_0 a\left(1-\frac{D_f}{D_p}\right)}{B\frac{\partial B}{\partial x}} \qquad \text{(SI units)} \qquad 7.3$$

If the values for the magnetic field and its gradient are inserted into equation 7.3, then the magnetic mass suceptibility may be calculated directly from the distance below the magnet drum where the particle is lifted:

$$k_g = \frac{\mu_0 a\left(1-\frac{D_f}{D_p}\right)x_o e^{\frac{x}{x_0}}}{B_s^2} \qquad \text{(SI units)} \qquad 7.4$$

Where: a is the acceleration due to gravity (m/sec^2)
x_0 is the depth of field for the magnet drum (m)
x is the distance from the magnet drum surface (m)
B_s is the field at the drum surface (T)
μ_0 equals $4\pi \times 10^{-7}$

Calculation of particle magnetic moment

If the value of the magnetic field gradient is inserted into equation 4.7 then the magnetic moment per unit mass can be calculated from the distance at which the particle is lifted. The value calculated here is the magnetic moment only at the point where the particle is lifted. Whether this figure is the same as, or approximately the same as the magnetic moment where the particle rolls, will depend on whether the particle is magnetically saturated at both points.

$$m_m = \frac{\mu_0 a\left(1-\frac{D_f}{D_p}\right)x_o e^{\frac{x}{x_o}}}{B_s} \qquad \text{(Wb.m)} \qquad 7.5$$

Calculation of rotation indices

The particle paramagnetic and/or ferromagnetic rotation indices can be calculated by inserting the values from equations 7.4 and 7.5 into the appropriate equation from chapter 4.

Particle size limitations to rotating field separation

It was mentioned in chapter 4, when discussing the rotation indices, that smaller particles will be rotated more easily than larger particles.

Consider the particle resting on the surface shown in figure 7.1. The magnetic torque that can be applied to this particle, as result of the rotation of the magnetic field, depends on the rotation index (which gives the maximum angle between the particle magnetisation and the external field) and the particle magnetisation. The magnetic moment is proportional to the mass of the particle, or its volume. The magnitude of the magnetic torque can be described by:

$$\tau = mH\sin(\phi) \qquad \text{(Nm)} \qquad 7.6$$

Where: m is the particle magnetic moment (Wb.m)
H is the external magnetic field (T)
ϕ is the angle between the magnetisation and the external field.

Opposing the magnetic rotation is the reaction of the particle with the surface. This is proportional to the force holding the particle against the surface (ie. to the mass, or the volume) multiplied by its radius. The force holding the particle against the surface has two components: the first being the magnetic attraction, and the second being the force of gravity. The force of gravity will be either positive or negative with respect to the magnetic attraction, depending on whether the particle is resting on the upper surface or is being held up underneath the magnet drum. The magnitude of the surface reaction torque is:

$$\tau = \frac{d}{2}(m\frac{\partial H}{\partial x} \pm m_p a) \quad \text{(Nm)}$$

or, writing the gradient in terms of the magnetic field (see relationships 7.1 and 7.2):

$$\tau = \frac{d}{2}(\frac{mB}{\mu_0 x_0} \pm m_p a) \qquad \text{(Nm)} \qquad 7.7$$

Where: d is the particle diameter (m)
m_p is the particle mass (kg)
a is he acceleration due to gravity (m/sec^2)
x_0 is the depth of field for the magnet drum (m) (see equation 7.1)

At the point where particle rotation ceases, these two torques have equal magnitudes (but opposite directions). By equating the two magnitudes an expression for the maximum separable (by particle rotation) particle size can be found.

$$d = \frac{2R_f}{\frac{1}{x_0} \pm \frac{\mu_0 a}{m_m B}} \text{ (m)} \qquad 7.8$$

Where m_m is the particle magnetic moment per unit mass (Wb.m/kg)
The magnetic field is now given in Tesla, which are the units normally measured.

The maximum separable particle size is therefore primarily determined by the particle rotation index and the depth of field for the magnet drum. The particle magnetic moment and the external field strength merely determine the difference between separable particle sizes under the magnet drum and over the top of the magnet drum.

To give the above expression some practical meaning, consider the separation of magnetite particles. If the value of R_f is taken as 0.38, and the magnet drum described in figure 7.7 is used for a separation (in the form shown in chapter 8, figure 8.5), operating at a field strength of 0.1 Tesla, then the maximum separable particle sizes are:

7.2 mm, beneath the magnet drum (and in water);
5.7 mm, on top of the magnet drum (and in air).

The above sizes are for separation using a rare-earth magnet drum with a relatively shallow depth of field ($x_0 = 8.48 \times 10^{-3}$ m). If the sizes are calculated for a larger diameter (600 mm) low-intensity (ceramic magnets) magnet drum that would actually be used for commercial magnetite separation (with a depth of field (x_0) of around 33.8×10^{-3} (m), the maximum separable magnetite particle sizes are greatly increased:

54 mm, beneath the magnet drum;
17 mm, on top of the magnet drum.

While low-intensity rotating field separation is limited by a maximum separable particle size, this limitation is not going to be of much concern in normal mineral processing applications where particle sizes may generally be expected to be less than 1 mm in diameter. In fact, the smaller the particle, the better it will rotate against a surface, or against any interfering particles.

Chapters 2 and 4 did indicate that particle rotation should be affected by domain wall velocities and coercive force effects, which are dependent on particle size. These effects can change the effective rotation index. However most practical *separations* are carried out in a high-field situation, where $H >> H_{cr}$ and domain wall velocities and coercive force effects are insignificant. In this case the rotation index is determined mainly by the particle anisotropy.

The Relationship Between Ferromagnetic and Paramagnetic Rotation Indices

Ferromagnetic and paramagnetic rotation indices can be calculated for each particle, but it may not always be obvious whether the particle being measured is paramagnetic or ferromagnetic. Therefore it may be interesting to know the relationship between the two calculated indices, and to be able to convert between paramagnetic and ferromagnetic rotation indices without having to return to the original field measurements.

For a saturated ferromagnetic, if the magnetic field and its gradient are known at the lift point, the particle magnetic moment can be calculated, and it has the same value at both the lift point and the rotation point. In this case, because the relationship between the field and its gradient is well defined, only the field strength is needed. For the equipment used here (described above), the particle mass magnetic moment and the implied "magnetic susceptibility" can be calculated using:

$$m_m = \frac{\mu_0 a x_0}{B_l} \qquad \text{(from 4.7, 7.1 and 7.2)} \qquad 7.9$$

$$k_g = \frac{\mu_0 a x_0}{B_l^2} \qquad \text{(from 4.1, 7.1 and 7.2)} \qquad 7.10$$

If the particle being considered is a saturated ferromagnetic, the value of m_m in 7.9 is one of two factors that determine the field at which the particle is rotated. The other factor is the angle that can be maintained between the external field and the particle magnetisation, and it is the sine of this angle that is given by the ferromagnetic rotation index R_f.

The field (B_r) at which a cubic-shaped saturated ferromagnetic particle rotates can be obtained using equations 4.9 and 4.10 (leaving out, for the purpose here, the bouyancy term):

$$B_r = \frac{B_l d}{2R_f x_0 + d} \qquad 7.11$$

If the above expressions (from equations 7.10 and 7.11) are then used to find the value of the paramagnetic rotation index from equation 4.6, a relationship between R_p and R_f is obtained:

$$R_p = \frac{2R_f^2 x_0}{d} + 2R_f \qquad 4.14$$

Where R_f and R_p are the rotation indices
x_0 is the depth of field
d is the particle diameter (length of cube in this case)

The relationship is dependent on the particle size and also on the particular magnet drum used (or, more specifically, on its depth of field), but is independent of the particle magnetic moment or magnetic susceptibility. The above relationship between the two relative indices is illustrated graphically in figure 7.10.

Figure 7.10

Relationship Between Ferromagnetic and Paramagnetic Rotation Indices

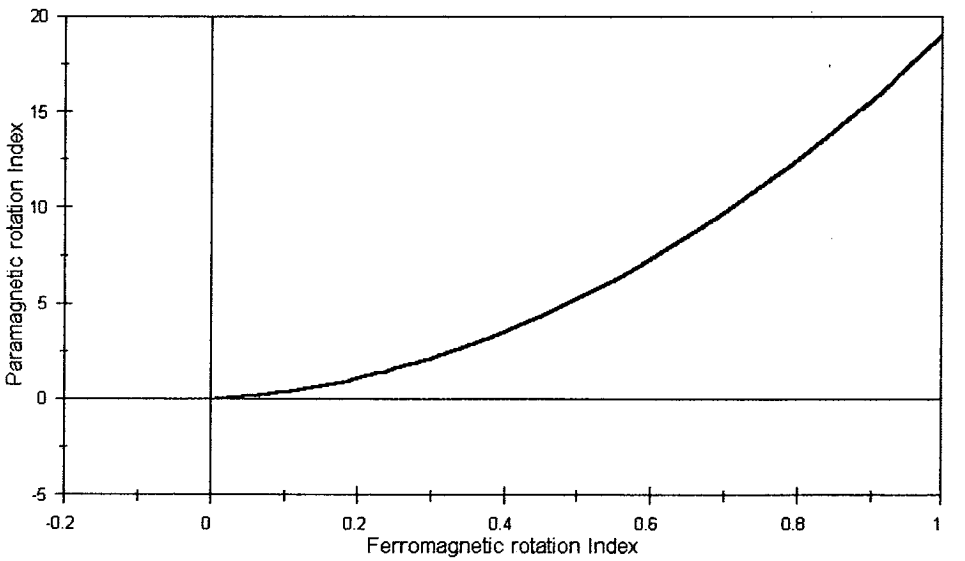

Summary

The magnetic field at a given distance from the magnet drum surface can be calculated from the expression:

$$B = \frac{B_s}{e^{\frac{x}{x_0}}} \qquad \text{(T)}$$

Where: B_s is the field at the drum surface (T)
x_0 is the distance from the drum surface at which the field drops to $\frac{1}{e}$ of its value at the drum surface (m)
x is the distance from the magnet drum surface (m)

The field gradient at any distance from the drum surface can be calculated from the expression:

$$\frac{\partial B}{\partial x} = \frac{B_s}{x_o e^{\frac{x}{x_o}}} \qquad \text{(T/m)}$$

The magnetic mass susceptibility of a particle, calculated from the distance below the drum surface at which it lifted is given by:

$$k_g = \frac{\mu_0 a\left(1-\frac{D_f}{D_p}\right)x_o e^{\frac{2x}{x_o}}}{B_s^2} \qquad \text{(SI units)}$$

Where a is the acceleration due to gravity (m/sec^2)

The magnetic moment per unit mass for a particle, calculated from the distance below the magnet drum at which it is lifted, is given by:

$$m_m = \frac{\mu_0 a\left(1-\frac{D_f}{D_p}\right)x_o e^{\frac{x}{x_o}}}{B_s} \qquad \text{(Wb)}$$

The maximum separable particle size, in any rotating field separation where the particle is held against a surface by magnetic attraction, is given by the relationship:

$$d = \frac{2R_f}{\frac{1}{x_0} \pm \frac{\mu_0 a}{m_m B}} \qquad \text{(m)}$$

Where: R_f is the particle rotation index
x_0 is the depth of field for the magnet rotor
a is the acceleration due to gravity (m/sec^2)
m_m is the mass magnetic moment of the particle (Wb.m/kg)
B is the external magnetic field (T)

The positive sign refers to a particle resting on a surface above the magnet drum, and the negative sign refers to a particle held against gravity to a surface under the magnet drum.

The relationship between the calculated values for the ferromagnetic and paramagnetic rotation indices, measured with equipment similar to that described here, is:

$$R_p = \frac{2R_f^2 x_0}{d} + 2R_f$$

Where: R_p and R_f are the paramagnetic and ferromagnetic rotation indicses
x_0 is the depth of field for the particular magnet drum in use
d is the particle diameter.

Chapter 8

Rotating Magnetic Field Separation Methods and Equipment

Introduction

The field characteristics of magnet drums were discussed in chapter 7. In fact two quite different magnet drums were constructed and used for test work and trial separations. The first of these was the rare-earth magnet drum shown in figure 7.4, which was employed for all particle rotation measurements, for all separation trials in chapters 15 to 17, and for one of the separations in chapter 14. The second was constructed using larger (and considerably cheaper) ceramic magnets. The latter was 240 mm in diameter and 300 mm in length, and was used for low-intensity test separations described in chapter 14. It produced a magnetic field of 0.1 Tesla at 10 mm from the drum surface, and had 7 field rotations per drum rotation. Other than the size and the field strengths, the two drums were constructed in the same way and had similar field characteristics. The rare-earth drum was driven by a variable-speed motor and was fitted with a field rotation frequency read-out, but the ceramic drum had a fixed-speed drive which could only be altered by changing pulley sizes.

The separation launders (vessels enclosing the larger capacity separations) and cells described below are experimental constructions designed either to test theoretical ideas presented in earlier chapters, or to evaluate some rotating magnetic field separation methods for commercial applications. No large metal parts can be used near the magnet drum in the construction of these cells and launders, due to the generation of eddy currents. Fortunately, the field depth above the magnet drums is not great, and at distances greater than about 50 mm the eddy current effects can be ignored.

The larger launders have been constructed from fibre-glass, while the smaller separation cells have generally been constructed from acrylic sheet. Where copper or brass tubing has been used near the magnet drum (e.g. for small cell outlets) it is cooled by water flow.

Basic Magnet Drum Units

Rare-earth magnet drum units (FeNdB magnets)

This unit was constructed as a basic unit for both particle measurements and test separations. It has a 1 cm thick acrylic sheet as a backing plate behind the rotating magnet drum, so that different test and separation units can be easily mounted and removed. Figure 8.1 shows this separation unit set up for observing particle rotation and lift distances.

The variable speed drive motor is almost out of the picture in the top left of the photograph. The field rotation frequency read-out can be seen below the motor. The sensor for the frequency read-out can be seen mounted above the magnet drum in this view, but it can be mounted anywhere around the drum.

Figure 8.1

The rare-earth magnet drum separator unit.
Set up for the measurement of particle lift and rotation distances.

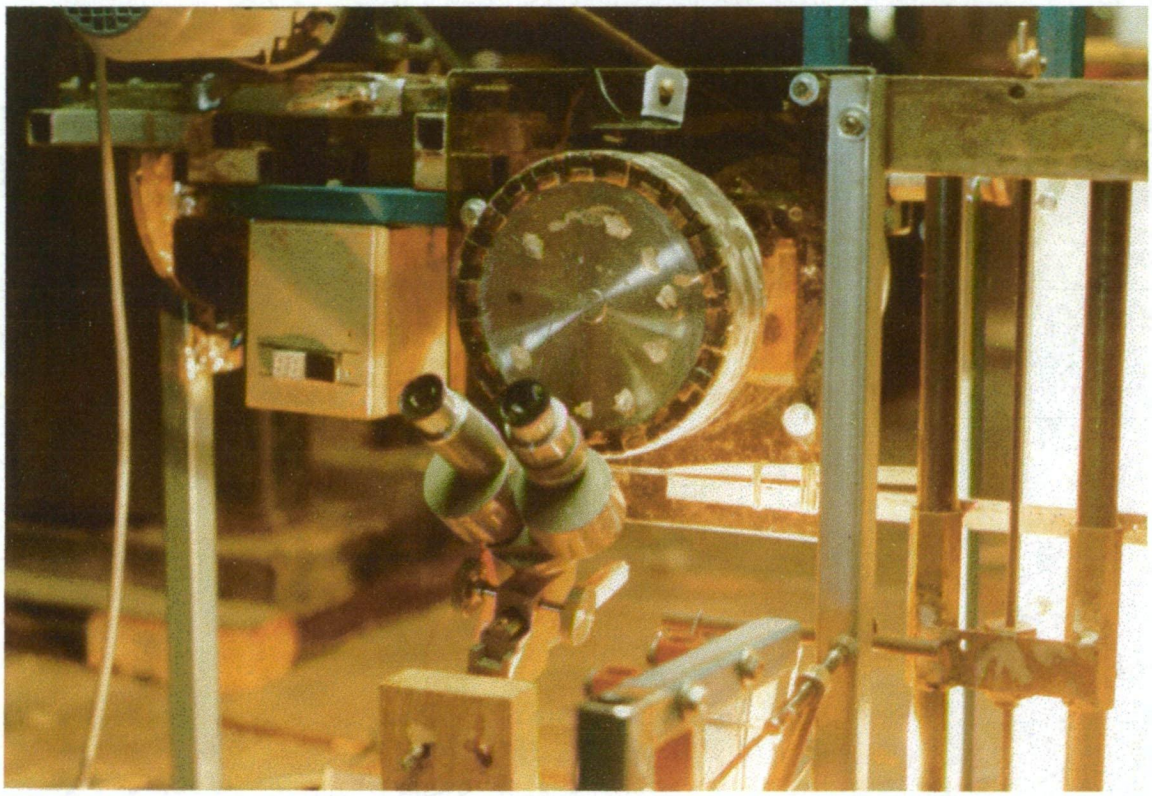

The entire motor, magnet drum and read-out is mounted on a sub-frame which can be rotated around a horizontal axis, setting the drum rotation axis at an inclined angle for some separations when necessary (eg. separations discussed in chapters 15 and 16). The entire separator unit is mounted on rubber feet, so as to cut down any transfer of vibration to other units when the magnet drum is rotating at high speeds (up to 1500 rpm).

The sample holder and the microscope are mounted on a separate frame. Wood has been used in some places on this frame to damp out any vibrations that might make observations difficult or less accurate.

Note: Since the completion of practical work for this thesis, a large 400 mm diameter unit has been constructed commercially as a flexible test unit for the development of specialised particle separations in the mineral exploration industry.

Ceramic magnet drum separator unit

This separation unit was constructed to test various low-intensity rotating field separation methods. Its magnetic field is too low to use it for any particle measurements. The unit is shown in figure 8.2, without any separation launders fitted.

It is of a size which is suitable for meaningful estimations of separator performance for commercial applications.

Figure 8.2

Low intensity separation unit constructed for testing practical applications of low-intensity rotating field separation

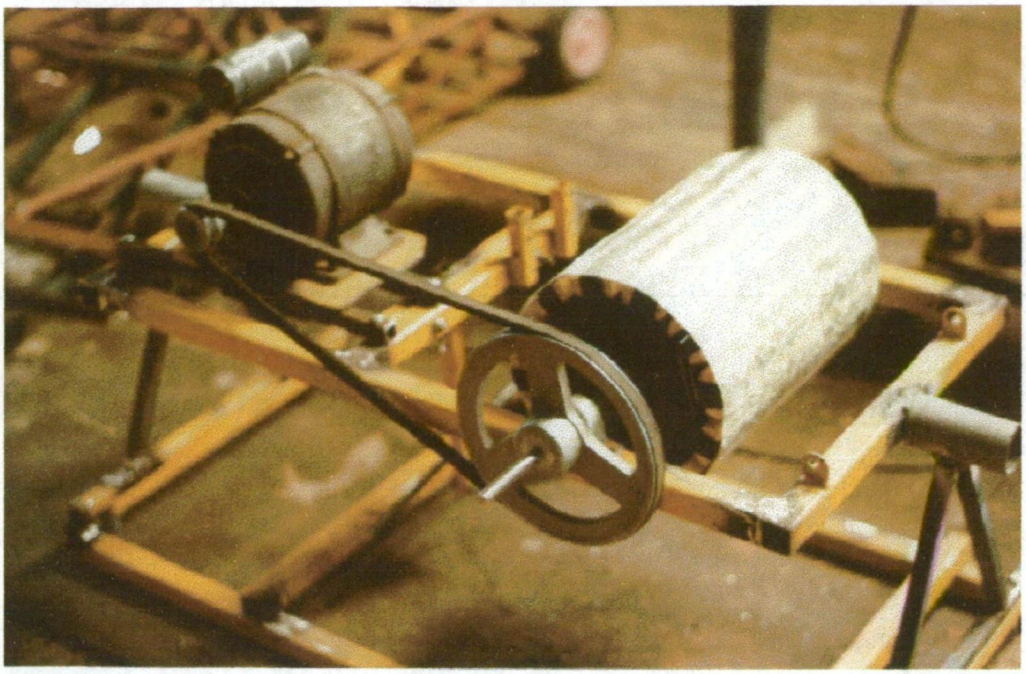

Using the pulley sizes in the diagram, the separator produces a field rotation frequency of 25 Hz, but in actual operation it was normally run at a field rotation of 50 Hz. Similar to the more powerful unit described above, the magnet drum and drive can be rotated about a horizontal axis, but this was not used for any separations reported in this thesis.

Note: Since the completion of practical work for this thesis, the above unit has in fact been used for preliminary assessment of low-intensity, low-entrapment rotating field separation in a real mineral processing situation, and a large 600 mm diameter pilot plant separator unit is under construction.

Launders for Wet Rotating Field Separations

Low-Intensity magnetite/grinding iron separation

Such particles as magnetite, and iron particles from grinding operations, are easy enough to remove by any type of magnetic separation, but when large amounts of magnetic material is being separated it is not so easy to avoid the entrapment of non-magnetic particles within the magnetics. In most applications particle entrapment is not an important consideration, but in some applications, such as the separation of magnetite and iron from gold concentrates, it must be kept to a minimum.

The launders described here represent trial versions of designs that are now being developed for the gold mining industry.

Figure 8.3 is a cross-section through one version of a wet rotating field magnetite separator. This launder is not concerned with producing a magnetic product with a minimum water content, and would be used where the magnetic fraction is run to waste.

Figure 8.3

A cross-section through an enclosed ferromagnetic separator
1st version

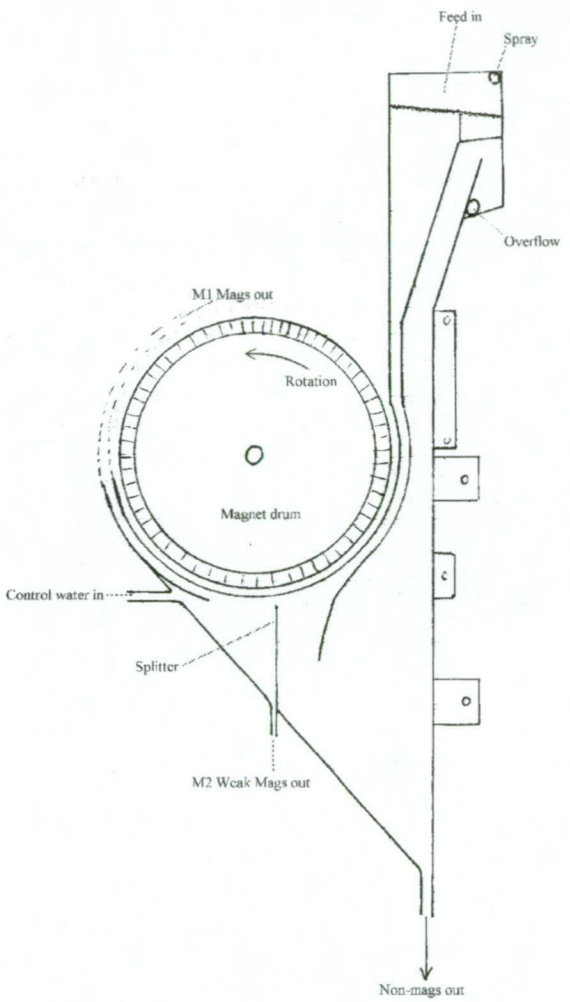

In this separator the slurry is fed in at the top left. As it passes down through the separator the magnetics begin rotating and are attracted towards the inner separation surface which is concentric with the magnet drum. The magnetics roll under the magnet drum and up the other side towards the main magnetics outlet (M1). Any weaker magnetics are not able to roll up towards the main magnetics outlet, and fall off (assisted by water turbulence) under the magnet drum to pass out of the M2 outlet. A control water supply enters just below the main magnetics outlet. The flow rate for this water is set so that water flow past the top of the splitter is close to zero. The movement of the M1 magnetics out of the separator is assisted by water flow through the outlet tube. Slurry (plus any extra water) needs to be fed to the separator so that the water level is maintained at the top of the overflow weir. Figure 8.4 is the actual trial version of this separator. The launder has a width of 100 mm.

Figure 8.4

Trial version of the separator illustrated in figure 8.3

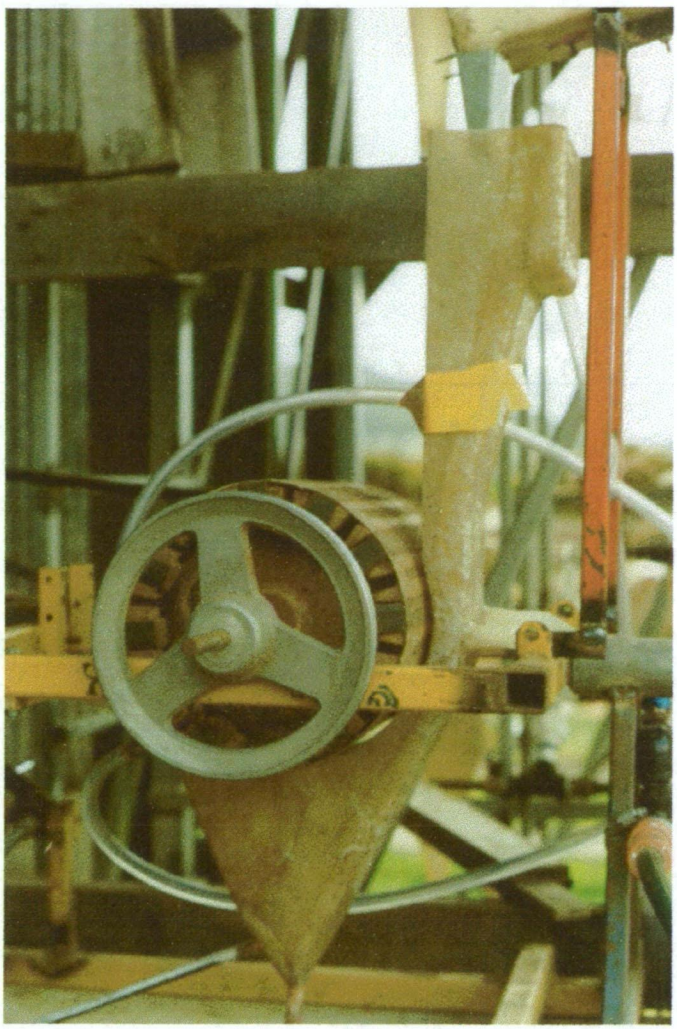

The launder in figures 8.3 and 8.4 produces magnetics products that are very clean, but which are contained in large quantities of water. The launder illustrated in figure 8.5 forces the separating particles to roll themselves out of the water and over the top of the magnet drum. The product therefore contains only that water which is carried by the separating particles, plus the water which may need to be be sprayed onto the upper surface to avoid particle rotation problems associated with water surface tension forces.

Particles enter the separator between the magnet drum and the "down-hill" separation surface. As they pass down through the separator, the magnetic particles commence spinning and are attracted towards the magnet drum. The magnetic particles then roll themselves under the drum, up the other side, and out of the water. As they roll over the top of the magnet drum, the separation surface moves further away from the magnet drum, decreasing the particle attraction and eventually allowing the particles to fall away from the surface. The auxiliary water supply provides clean water around the separating magnetics, preventing the accidental separation of any very small non-magnetics which may become caught in the induced water flow surrounding the magnetic particles. Although no provision has been made in this particular separator for a weaker magnetics fraction, it can be done in a similar way to that shown in figure 8.3.

Figure 8.5

Internal structure of an open wet-to-dry rotating field separator

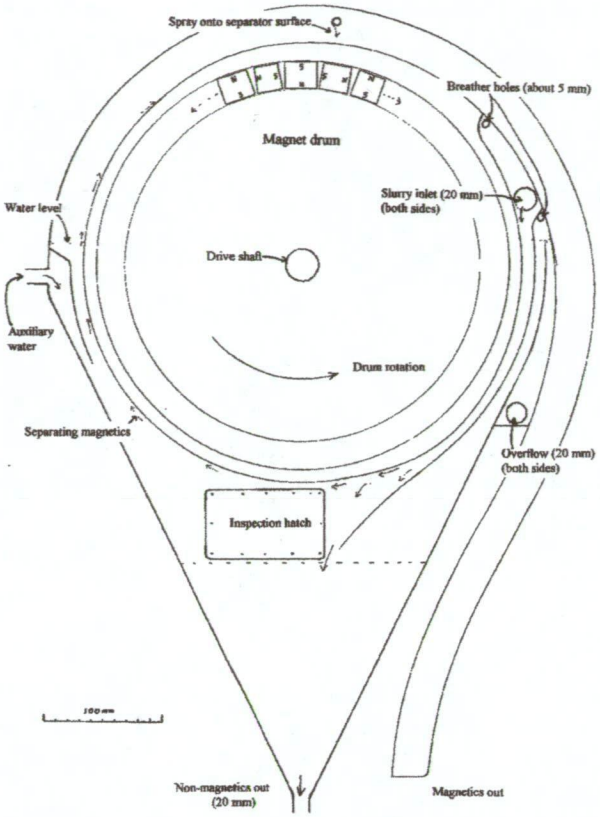

Figure 8.6 shows the trial version of this separator.

Figure 8.6

Trial version of the wet-to-dry rotating field separator shown in figure 8.5.

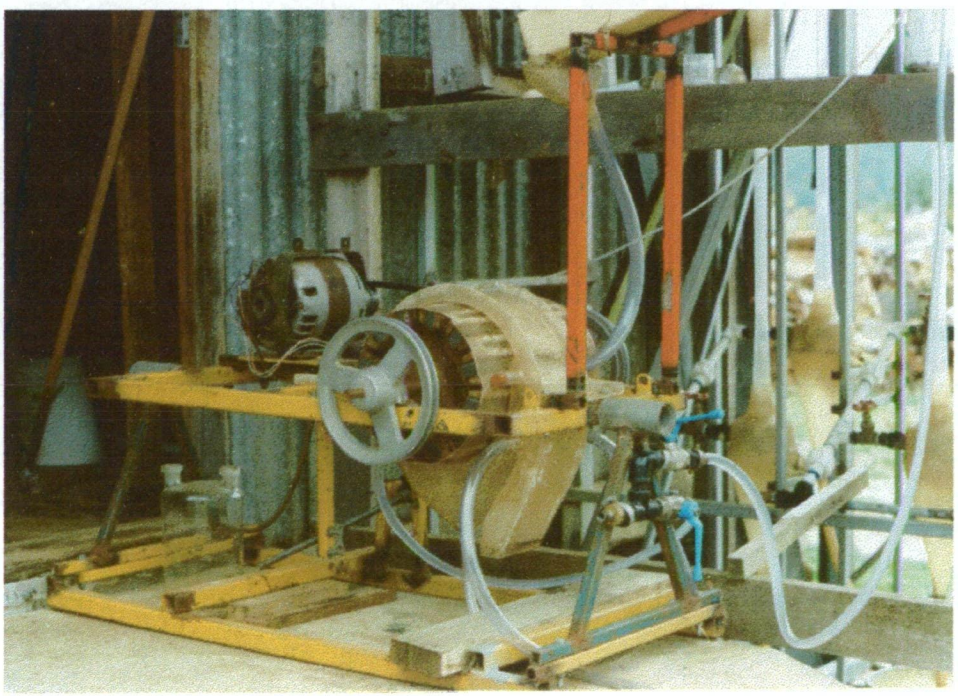

Wet separation of ferromagnetics and stronger paramagnetics

By using rare-earth magnets around a magnet drum, the separation of minerals with magnetic susceptibilities as low as almandine garnet can be accomplished. Testing of such separations was carried out using the separator unit shown in figure 8.1, fitted with the launder illustrated in figures 8.7 and 8.8.

The structure of the separator illustrated in figure 8.7 and 8.8 is similar to the wet ferromagnetic separator shown in figure 8.3, and works in a similar way. The exception is that the magnetic field is now higher at the separation surface (about 0.25 Tesla for the unit above), and two splitters are now employed. In preparation for a separation, the control water is adjusted so that there is zero or very little flow past the top of the splitter above the mag. 3 outlet. Minerals such as almandine garnet (magnetic susceptibility about 60 x 10^{-6} cgs units) are attracted towards the magnet drum, but do not rotate significantly with the magnetic field. They move down the separation surface until they accumulate below the magnet drum and are easily removed by water turbulence from the mag. 2 splitter. Stronger magnetics (such as some ilmenites) usually do show a weak rotation and are carried around past the mag. 2 splitter, but do not have sufficient rolling strength to climb to the mag. 1 outlet or to avoid being detached by the water turbulence near the control water inlet.

This separator therefore produces three grades of magnetics, plus a non-magnetic tail.

Figure 8.7

A cross-section through an enclosed rotation/attraction separator for feromagnetic and stronger paramagnetic particles

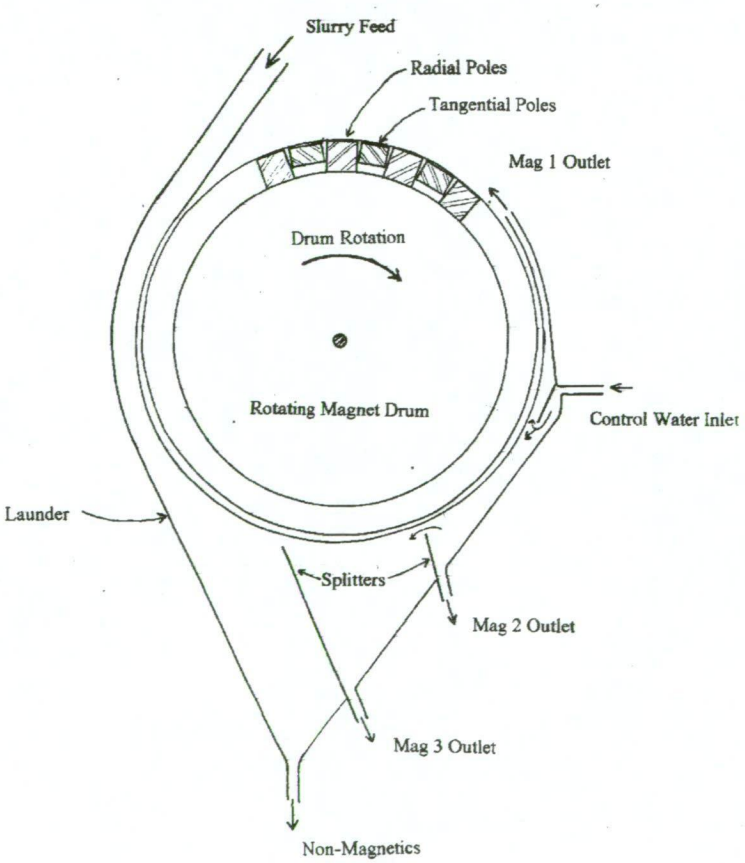

Figure 8.8

The practical version of the experimental enclosed separator shown in figure 8.7

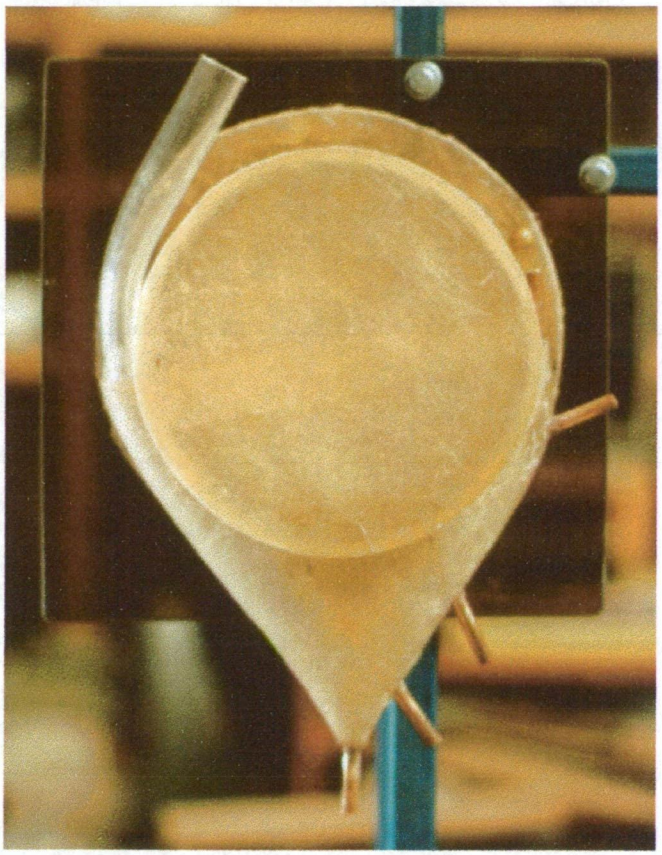

Launders for dry rotating field separations

Dry rotating field separation is most useful for the separation of minerals such as magnetite and grinding iron from very finely ground powders, and the launder below was constructed to test such separations. Magnetic materials are difficult to remove efficiently from such powders without also removing considerable amounts of entrapped non-magnetics, and leaving behind too much trapped magnetic product. The rapid magnetic particle rotations free the magnetic particles from non-magnetic electrostatic flocs and also energetically throw out any entrapped non-magnetics from the magnetic product.

Dry over-drum separation

Figure 8.9 shows the test launder used for this type of separation, mounted on the separation unit shown in figure 8.1.

Figure 8.9

A dry over-drum ferromagnetic separator

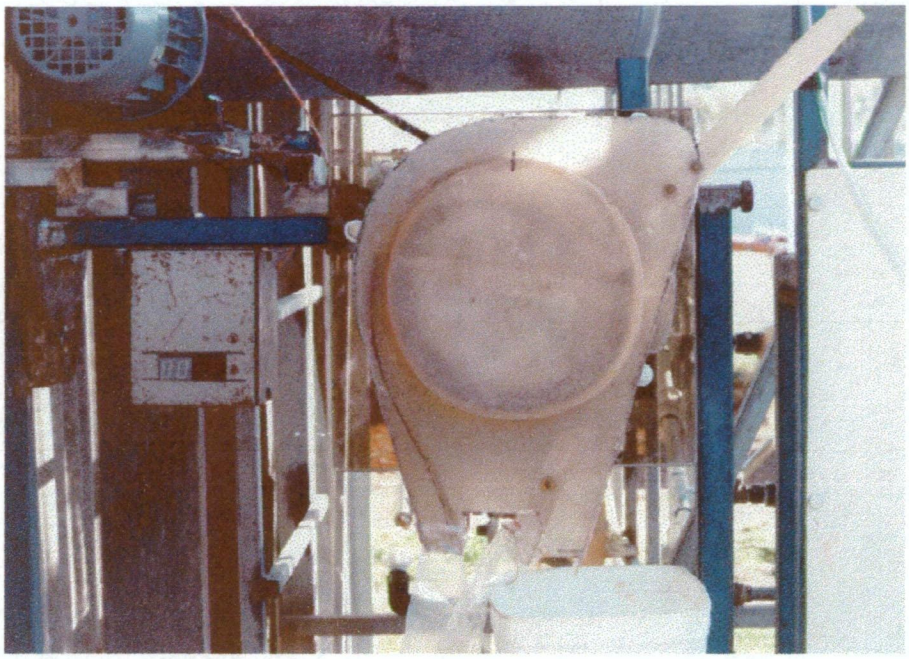

The powder to be separated enters via the chute in the upper right of the photograph. As the material falls down the right side of the separator, towards the non-magnetic outlet (the white bucket), any ferromagnetics commence spinning under the influence of the rotating field, and are attracted towards the magnet drum. At the separating surface the magnetic particles roll themselves up and over the drum. As they roll down the left side of the drum, the separation surface moves further away from the magnet drum surface, until the particles break free from the magnetic field and fall into the magnetics outlet (the left hand plastic bag in this case). Any weaker magnetics that are unable to roll up and over the top of the separator, fall down under the right hand side of the magnet drum, where the separation surface moves further away from the magnet drum and the particles fall to the second magnetics outlet (another plastic bag in this case, just to the left of the non-magnetics outlet).

Separation Cells for Special Applications

A separation cell here refers to small enclosed launders intended for small or very small sample separations.

A cell for the rotating field separation of samples less than 0.5 g

This cell was constructed for the routine separation of diamond indicator minerals, such as kimberlitic chromites and picro-ilmenites, from very small panned concentrates of geochemical soil samples. These two minerals do not rotate with the magnetic field (chapters 11 and 12) and remain unseparated. The structure of the cell is shown in figure 8.10.

Figure 8.10

A cell for the routine rotating field separation of diamond indicator minerals from very small samples

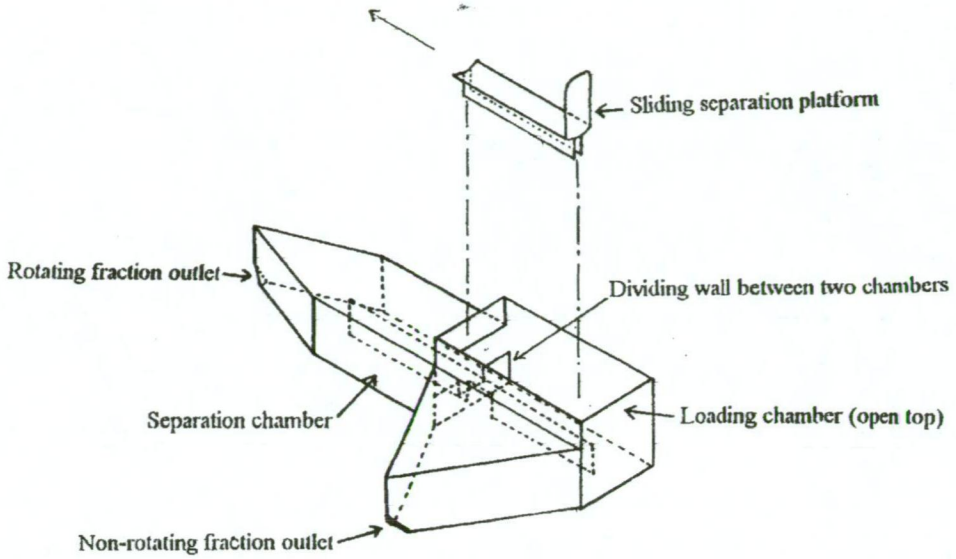

To carry out a separation, the two outlets are first sealed with small pieces of masking tape and the cell is filled with water. With the sliding separation platform slid out into the loading chamber, the small sample is placed, under water, on the separation platform (which is slightly concave) through a small funnel (not shown). Detergent is placed into the loading chamber before loading any samples, so as to avoid any surface-tension floating of particles. The separation platform is then slid forwards into the separation chamber, as it is shown in figure 8.11. The cell is then slid into a holder beneath the magnet drum, as shown in figure 8.11, and slowly wound up towards the rotating magnet drum. As it approaches the magnet drum, the particles that rotate roll themselves off the edge of the separation platform and fall to the bottom of the separation chamber. Particles that do not rotate remain on the separation platform. Occasionally some rotating particles become trapped under non-magnetic particles, and when released they are lifted against the upper surface of the separation chamber, where they roll themselves to one side. To release these, the cell is wound up and down under the magnet drum a few times, and this allows them to fall to the bottom of the chamber past the separation platform.

When all rotating particles have been separated, the cell is wound down away from the magnet drum and removed from the cell holder. The separation platform is then slid out into the loading chamber, lifted slightly to clear the slide, and the non-rotating minerals are tipped into the loading chamber. To remove the two fractions from the separation cell, the cell is held over a container and the tape is removed from one chamber, allowing the water and mineral particles to run out of one chamber. The other fraction is removed in a similar way. The water is then decanted from the containers, and the samples are dried in preparation for examination.

Figure 8.11

The small-sample separation cell in position below the rotating field magnet drum

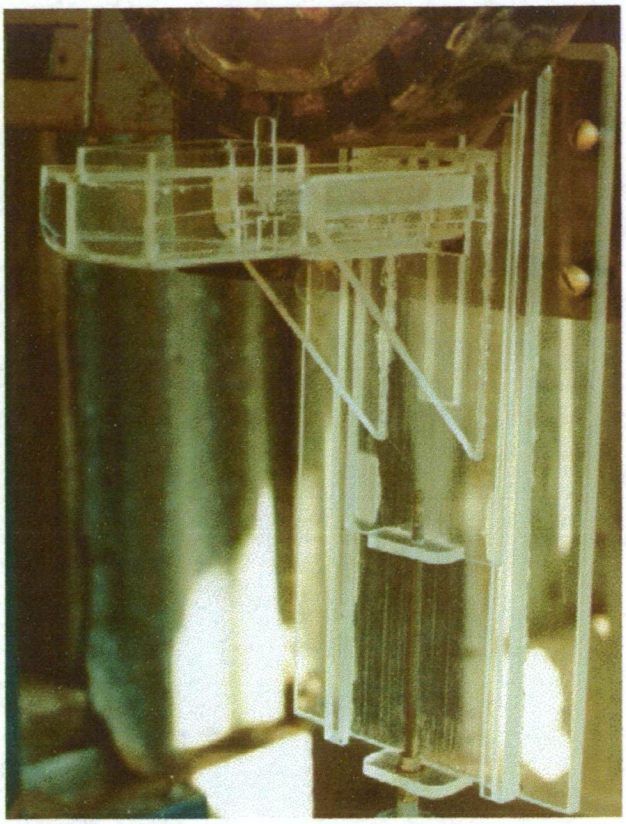

The cell is fairly quick to use, requiring less than 5 minutes per sample, although considerably more time is needed to obtain the concentrate and then to dry and examine the separated products.

A cell for continuous rotating field separation of larger samples

Batch separation of very small samples is the only practical option for small heavy mineral concentrates that may be obtained from small (say 2 kg) samples of soil or clay, but once the concentrate mass is more than about 0.5 g the above cell becomes too inefficient due to particle interference. Then a continuous separation is required.

The cell illustrated below is the continuous (rather than batch) version of the cell shown in figures 8.10 and 8.11. The structure of the cell is illustrated in figure 8.12. It is mounted under the rotating magnet drum, as shown in figure 8.13, so that the separation platform is tilted downwards to allow particles to travel down it. As the particles move down the platform, those particles that rotate are rolled off to one side and pass out the "rotating" outlet. The non-rotating particles continue on to the end chamber and down to the "non-rotating" outlet.

Because it is no longer possible to gradually move the cell nearer to the magnet drum, and therefore to gradually separate the more magnetic particles as the magnetic field increases, the more magnetic particles must be removed (by a ferromagnetic separation) before the rotating field separation is carried out.

Figure 8.12

Rotating field separation cell for continuous separation

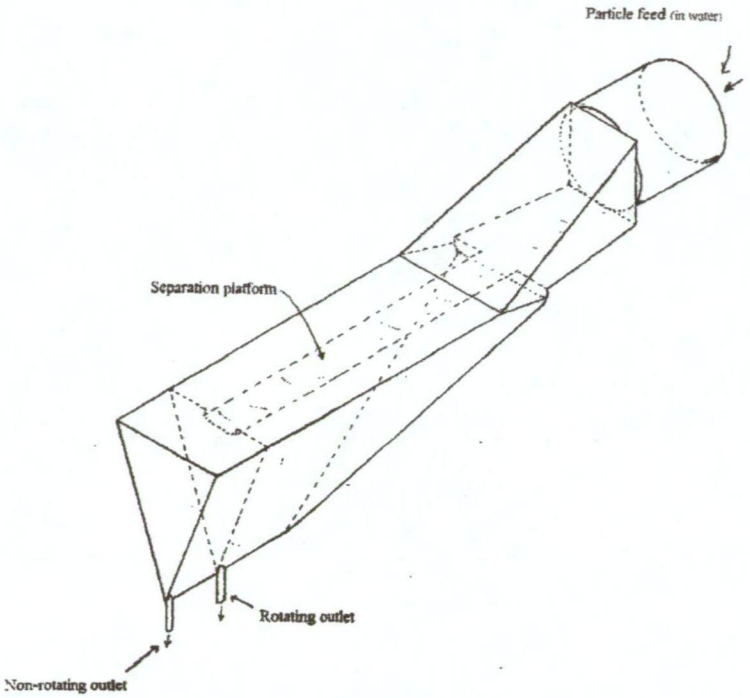

Figure 8.13 shows the cell used for continuous separation, while the collection method for the products is shown in figure 8.14, and the feed control to the separator is shown in figure 8.15.

Figure 8.13

The continuous feed rotating field separation cell, arranged ready for a separation.

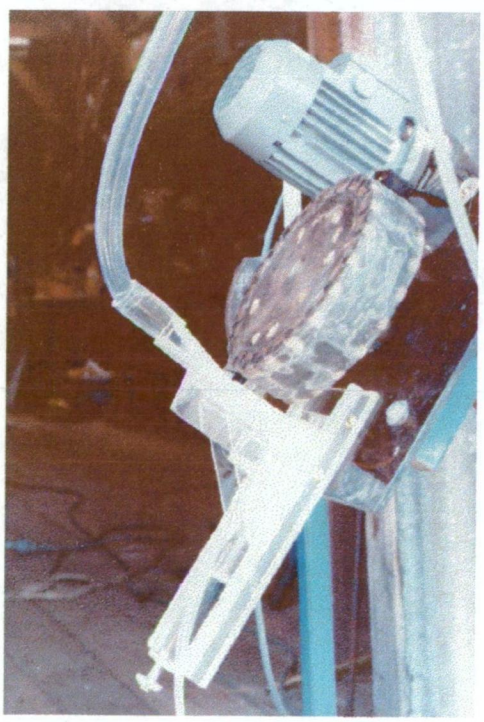

Figure 8.14

Collection bottles used with the continuous feed separation cell.
The water flow through the separator is controlled by clamps
on the overflow from these bottles.

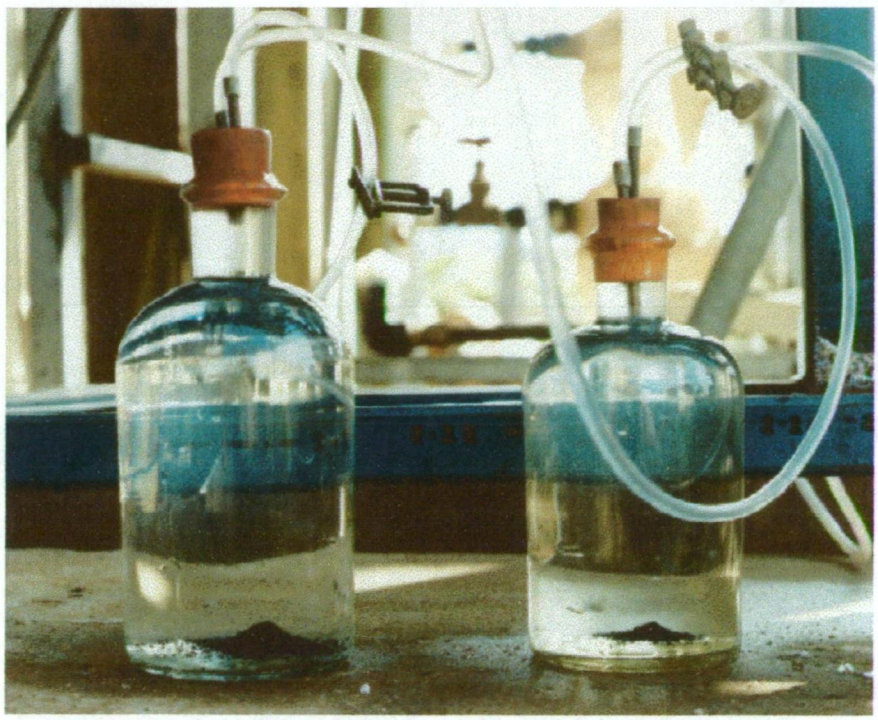

In the above photograph the rotating minerals are collected in the left hand bottle, and the non-rotating particles, which include any picro-ilmenites and kimberlitic chromites, are collected in the right bottle. Clamps can be seen on the overflow lines from each bottle. These are used to control the water flow through the separator.

Figure 8.15

The particle feed rate control for the continuous feed separator cell

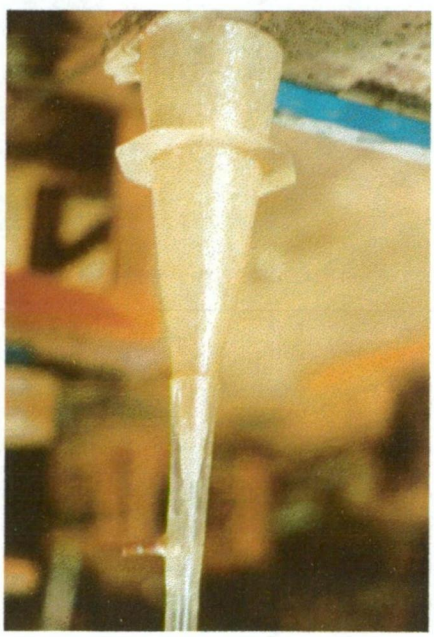

The sample to be separated is placed in the feed cone shown above, which is really a simple reverse-flow elutriator. The lower end of the feed cone is narrow, and is enclosed inside an outer tapered plastic tube. Feed control water is fed into the outer plastic tube through the copper inlet at the lower left. Because the water flow through the separator is controlled separately by the clamps on the collection bottles, feed control water can be adjusted so that there is an upwards flow of water through the narrow lower end of the feed cone. This upwards water flow is adjusted so that particles escape from the feed cone at the desired rate.

A more versatile system for continuous rotating field separation

Once continuous feed is used, it is no longer possible to progressively separate the more magnetic particles by winding the separation cell closer to the magnet drum. As mentioned above, this problem may be overcome by carrying out an initial separation to remove the more magnetic particles that would otherwise clog the separator.

In figure 8.16, two different separation cells have been placed in series. The first cell, concentric to the magnet drum, removes the more magnetic particles. The non-magnetic fraction from this separation is then sent through the separation cell shown in figure 8.12.

Figure 8.16

A two-stage rotating field separation.

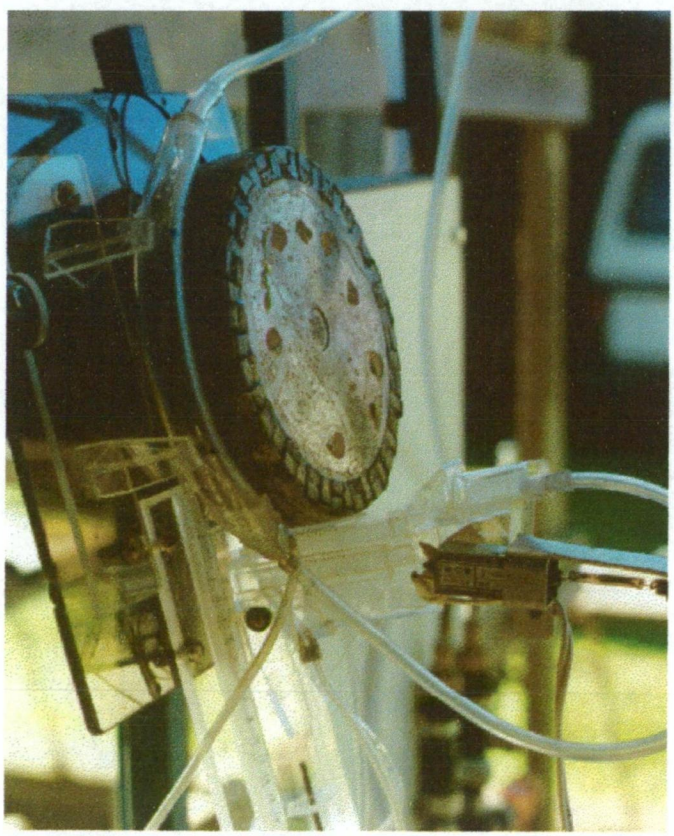

Particle feed enters the top of the concentric separation cell in figure 8.16. This first cell is a simplified version of the separator shown in figure 8.8. The more magnetic particles, and those particles that rotate strongly (in most cases, but not all, stronger rotation implies higher susceptibility), follow the inside surface of the cell beneath the magnet drum, where

they are removed through an upper outlet tube to a collection bottle. The weaker magnetic and non-magnetic particles fall to the outside surface of the concentric cell, and pass out a lower exit, to be carried on to the input of the separation cell shown in figures 8.12 and 8.13. Because the magnet drum axis can now not be inclined as much as shown in figure 8.13, without degrading the concentric separation products, the travel of particles down the separation platform in the second cell now has to be assisted by a vibrator, which can be seen attached below the input to the second cell.

Note: Since completion of experimental work for this thesis, the above special separation process has now been further developed for the mineral exploration industry, around a new commercially-built 400 mm diameter rare-earth magnet drum, and is now capable of producing up to 6 different magnetic fractions based on combinations of particle rotation and attraction.

Eddy Current Metallic Particle Separation Methods

The discussion of metallic particle rotation using eddy currents, in chapter 6, indicated that rotating field separations of metallic particles should be possible down to particle sizes below 20 μm. The separation units described below were constructed to test these predictions, given the limited field strengths and field rotation frequencies available with existing equipment.

Initial experimental eddy current separator for small particles

The initial eddy current trials were carried out by passing the feed material parallel to the drum axis and across the top of the drum. Metallic particles rolled by eddy currents were then rolled to one side, away from the non-metallics. The unit used in these trials is illustrated in figure 8.17, and the complete separator, set up ready for separation is shown in figure 8.18.

Figure 8.17

The separation unit used for initial trials of small-particle eddy current separation

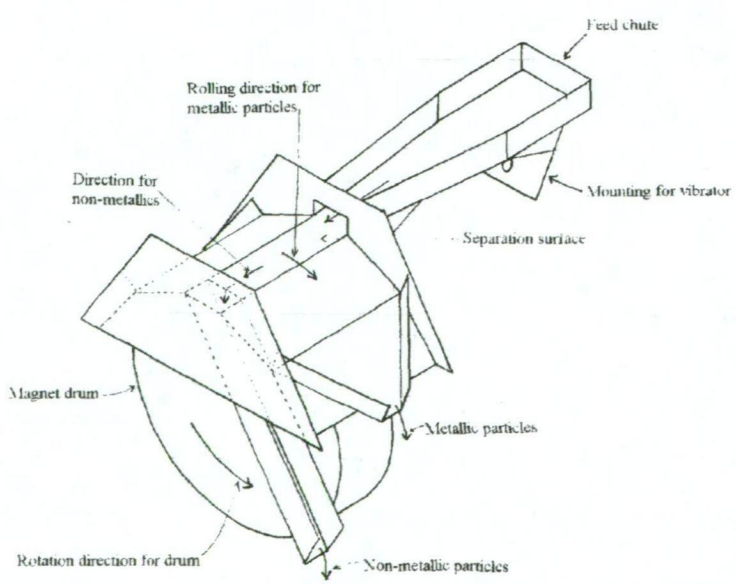

Figure 8.18

Initial small-particle eddy current separator, set up ready for trials

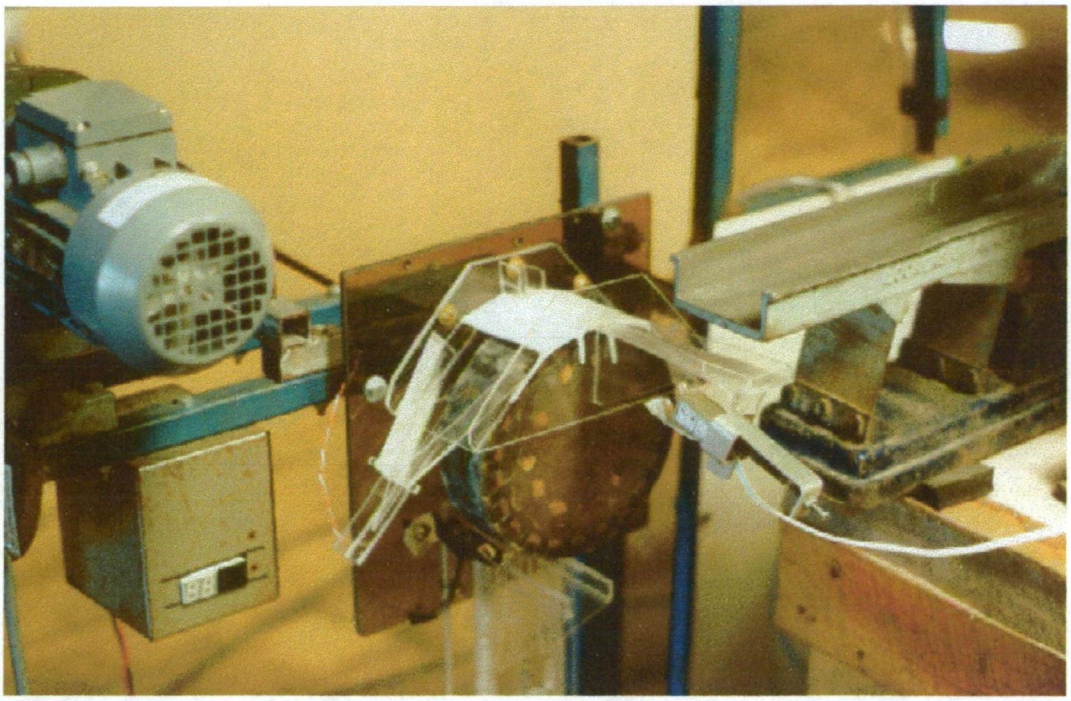

Particles are fed into the separator feed chute by another vibrating tray. The vibrator fixed under the feed chute then moves the particles down across the rotating magnet drum. Metallic particles that react sufficiently to the rotating field are rolled sideways off the separation surface, as shown in figure 8.18, while non-metallic particles travel straight down the separator to the non-metallic outlet behind the magnet drum.

A more practical higher capacity eddy current separation method

The previous separation method required a very slow feed rate. Although it did show that the eddy current separation worked as it should, separation by sideways rolling, from feed passing parallel to the magnet drum axis, did not allow any real increase in separation rates for an increase in magnet drum length. The method shown in figures 8.19 and 8.20 is an experimental version of a method which can be expanded much further, and possibly even to a commercial level.

Figure 8.19

Schematic of a small-particle eddy current separator
with feed across the whole magnet drum length

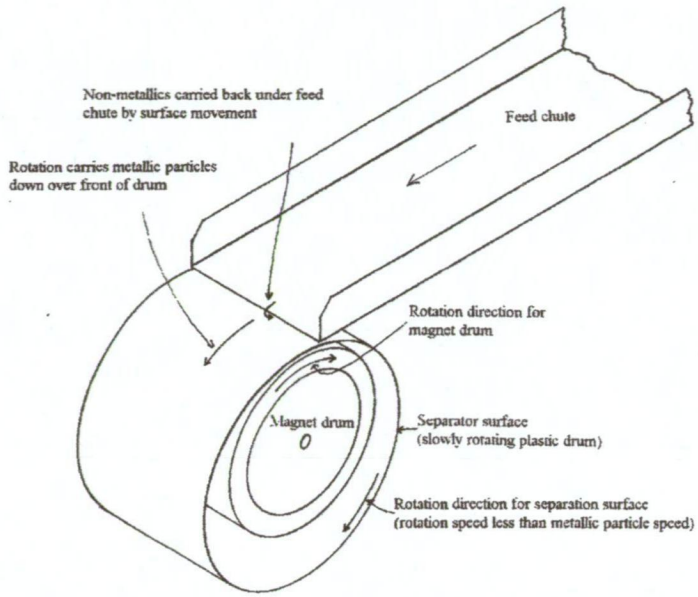

The separator consists of an inner magnet drum rotating at high speed (up to 3,000 rpm) in the direction shown, and an outer, much larger diameter, drum rotating slowly in the same direction as the magnet drum. The rotation axes of the two drums are off-set, as indicated in figure 8.19. As particles are dropped onto the outer drum surface, the metallic particles (plus any magnetite or iron particles) commence rotation and roll themselves very quickly down over the front of the outer drum, against the drum rotation. Non-metallic particles are carried backwards and over the back of the outer drum by the drum rotation.

Figure 8.20 shows the trial unit for this type of eddy current separation.

Figure 8.20

Experimental separator for evaluation of the dual-drum
eddy current separation of small particles

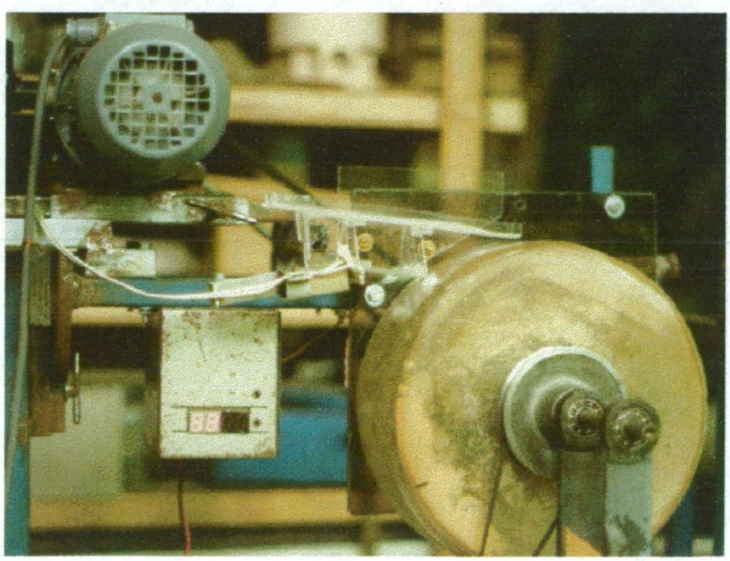

The particle feed in figure 8.20 is from the opposite direction to that indicated in figure 8.19, even though the separating metallic particles move in the same direction (back under the feed chute in figure 8.20). This was altered so that most metallic particles will not have to overcome too much interference from blocking non-metallics before their rotation allows them to escape. Most of the metallic particles will be on the bottom of the feed as it is dropped onto the outer drum.

Note: The above method has also been further developed, with a new 400 mm diameter rare-earth magnet drum. Instead of using rotation of an outer drum to carry away the non-metallics, a slowly-moving conveyor-belt is used.

Chapter 9

Monitoring and Analysis Methods for Separations and Rotation Measurements

Introduction

Wherever possible, the results from particle lift and rotation measurements have been applied to the solution of practical problems in the mineral processing area. The idea has been that mineral rotation characteristics can be used to develop new magnetic processing technology to solve particular problems in the industry. The monitoring and analysis of the results is therefore at two different levels.

The first level concerns the relationship between particle rotation characteristics and the composition and crystalline structure of the mineral. This involves the micro-analysis of every individual particle for which rotation data is available.

The second level concerns the performance of specially-constructed experimental mineral separators designed to make practical use of the particle rotation characteristics.

The Monitoring of Particle Rotation and Lift Results

The measurement of particle lift and rotation, and the calculation of individual particle magnetic susceptibility, magnetic moment and particle rotation indices, have already been described in chapter 7. For particles that rotated in the same direction as the magnetic field rotations, particle lift and rotation distances were measured and entered into a spreadsheet programme (Quattro Pro was used in this case) set up to calculate the susceptibilities and rotation indices, using the equations described in chapter 7. For particles that rotated at right angles to the field rotations (chapter 13) the field rotation frequencies at which the particles commenced and then later ceased rotation were noted. For these particles the maximum field strength allowed by the equipment was used in each case. The right angle ("perpendicular") rotation of several particles was also video-taped through a microscope.

Particles were removed from the glass tubes by inverting the tubes into a small amount of water on a watch glass. After the particles were pushed out of the water with an aluminium probe (non-magnetic), they were picked up by adhesion to the probe and transferred to some double-sided sticky-tape on a glass surface. Once all the particles had been arranged on the tape, and a record had been made of their locations, a cylindrical mold was placed around them and 6 g of epoxy (resin to hardener ratio of 5:1) was poured in. When the epoxy had set, the mold was removed and the lower surface of the grain mount was polished ready for particle analysis by a Cameca SX50 electron microprobe. Completed grain mounts, ready for analysis are shown in figure 9.1.

For most grains, analysis was carried out on a single 10 μm diameter area of the grain, chosen so that it was free of any scratches, fractures or weathering effects, and so that it was in the interior of the grain. If any inclusions could be seen, they were separately analysed.

Particles that had exhibited some unexpected rotational or lift characteristics were frequently analysed at a number of points along a line. Usually the line analysis was done along a 150 μm line across the particle, at 15 μm intervals using a 10 μm spot size.

For some particles (chromite grains that contained platinum), compositional maps, 150 μm by 150 μm and analysed on a 15μm x 15 μm grid, were produced.

Figure 9.1

Grain mounts ready for analysis, after particle rotation and lift measurements

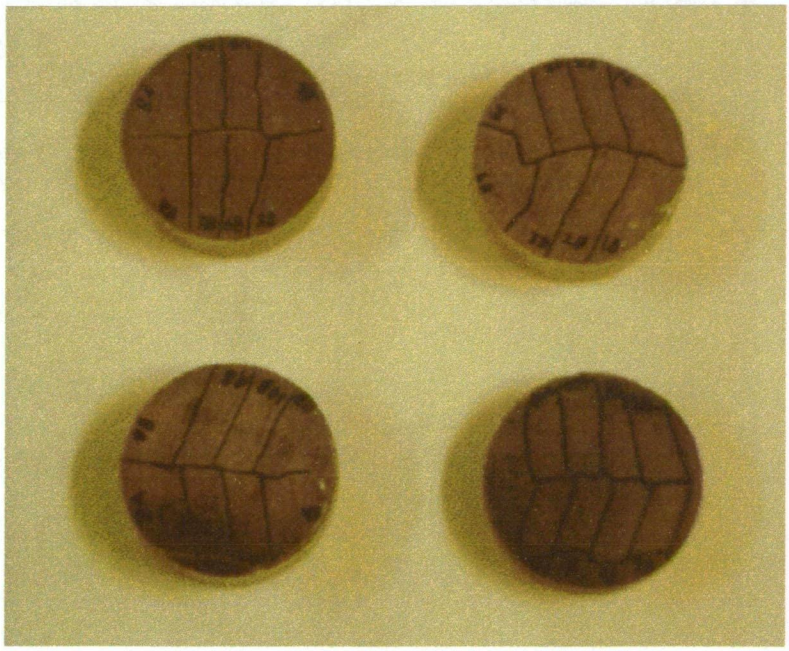

Analysis results (or average analysis figures in the case of line analyses) were then entered into the spreadsheet and compared graphically with rotation and lift characteristics.

Several chromite particles that showed high rotation indices were compositionally mapped, on a 2 μm pixel scale.

Monitoring of Separation Results

Four methods have been used to monitor the results of particle separation experiments.

Low intensity magnetic separations and eddy current separations

These separations produced one or two magnetic fractions and one non-magnetic fraction. They were carried out on mixtures made up for test purposes, where the exact composition of the mixture and its weight were known. The mixtures contained only one magnetic mineral (magnetite), but usually at least two non-magnetic minerals of differing specific gravities, such as quartz and cassiterite. Monitoring of the separation results then

involved the weighing of the dried products, followed by a determination of the purity of each product and the degree of non-magnetic entrapment within the magnetic fractions. The measurement of purity and entrapment was accomplished by repeated dry separations of the products (or representative portions of the products) using hand magnets. The hand-magnet separations were repeated until no further separation occurred, and the separated impurities (non-magnetics in the magnetics, and magnetics in the non-magnetics) were weighed.

In the case of the eddy current separations the mixture contained only one metal (copper) and one non-metal (usually zircon). The copper particles had been obtained from copper filings that had been dropped through an oxy-acetylene flame to round them off. Zircon was normally used as the non-metal for separation tests because its particle shape was similar to that of the rounded copper particles. The product purity after eddy current separation was determined by particle-counting under a microscope. This gave a volume percentage of impurity present, from which the approximate percentage recovery could be calculated.

Small-scale separations, involving sample weights less than 0.5 g

These separations were carried out on very small quantities of heavy mineral concentrates (< 0.5 g) obtained from a geochemical soil sampling programme.

Because the number of particles involved was relatively small, monitoring was done by electron microprobe analysis of representative grains from each fraction. Up to 40 particles (if available) were usually chosen from each fraction, mounted in epoxy, and individually analysed. Analysis in these cases was single point for each particle.

Separations of larger samples of real mineral concentrates

The samples separated here were concentrates obtained from various points within treatment plant cycles, and were provided by a mining company. The original samples contained many different minerals, and the products also contained a wide range of minerals. Three magnetic fractions and a non-magnetic fraction were produced in these separations.

In these cases the separated products were returned to the mining company, who then determined the bulk composition of each fraction, using X-ray fluorescence analysis (XRF) or atomic absorption spectrometry (AAS). Wherever possible the analysis results were compared with results achieved by conventional magnetic separation.

Picro-ilmenite separations

These separations were carried out for Rio Tinto Exploration (formerly CRA Exploration) in Perth, W.A. The samples to be separated had been "salted" (by Rio Tinto) with a number of picro-ilmenite grains, which had been marked by a line across the particle using a laser. Separation results here were evaluated by visually picking out the picro-ilmenites after separation and weighing the concentrate that contained them.

Section 3

Experimental Results
for
Particle Rotation Measurements

Chapter 10

The Response of Iron and Magnetite Particles to Rotating Magnetic Fields

Introduction

Iron (Fe) and magnetite ($Fe^{3+}(Fe^{2+},Fe^{3+})O_4$) are examined here partly because they represent the two main types of ordered magnetic materials encountered at room temperature (ferromagnetic and ferrimagnetic), and partly because magnetite is the mineral most commonly separated by magnetic methods. Both of these materials will be at, or reasonably close to, magnetic domain re-orientation along easy axes at the field strengths employed for the measurement of particle lift.

It is not an aim in this chapter to try to relate iron and magnetite rotational characteristics to chemical composition.

Relationship between the lift and rotation magnetic field strengths and the ferromagnetic rotation indices

The 500 μm (approximately) iron and stainless steel particles were obtained from filings, and tended to be elongated and flattened in shape. While measurements of particle lift could be made with reasonable accuracy, the irregular iron particle shapes made rotation field measurements difficult to acquire accurately. The rotation field values for individual iron particles could be in error by as much as ±30%, and shape errors could reduce the apparent rotation indices by as much as another 30%. The magnetite particles (also approximately 500 μm) were from crushed material. They tended to be roughly cubic in shape. The expected error in rotation field measurements for magnetite particles would be about ±10%, but particle shapes between cubic and spherical could produce higher apparent rotation indices, giving indices up to 50% higher than they should be. The above field measurement errors represent the maximum field strength range over which the commencement of particle rotation may be difficult to recognise.

Particle lift and rotation measurements were made as described in chapter 7, and paramagnetic and ferromagnetic rotation indices were calculated using the equations given in chapters 4 and 7. The lift and rotation fields are given in appendix A, together with the analysis data for some of the measured iron and magnetite particles. Lift and rotation fields were actually measured twice for each particle; once with frequency increasing and once with frequency decreasing. If the measurements appeared to be giving an unusual pattern, then they may have been repeated several more times. In general the two sets of measurements were either very close or exactly the same, particularly for the lift fields, but some irregular-shaped particles gave variable rotation field results depending on the particular face the grain previously came to rest on. Rotation indices for some of the larger and irregular magnetite

grains have a *maximum* error of $\pm$ 20%, but rotation indices for some of the very irregular iron grains could have an error as large as $\pm$ 40%.

Figure 10.1 shows the relationship between the lift and rotation fields for these particles. This type of diagram was introduced in chapter 4 as a way to show the relationship between magnetic moment (or magnetic susceptibility) and rotation index. The more magnetic particles plot towards the top of the graph. Particles of the same type of magnetic anisotropy (eg. uniaxial or cubic) should plot along one of the rotation index lines, irrespective of their magnetic moments. If there are no coercive force or domain wall velocity effects, differences in magnetic moments should only spread the particles vertically along the rotation index line, not horizontally.

Figure 10.1

Comparison of Inverse Lifting field to Ferromagnetic Rotation Index

For steel and magnetite particles at 10 Hz field rotation frequency

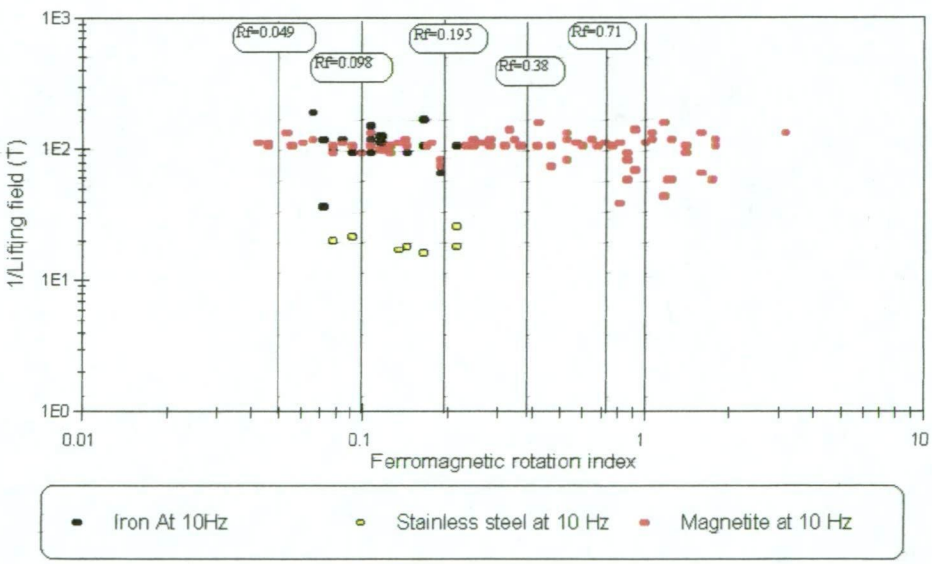

In spite of the difficulty in obtaining accurate rotation field measurements, the iron particles did not show an unreasonable range of ferromagnetic rotation indices. The iron ferromagnetic rotation indices are between about 0.07 and 0.2, with the mean value being about 0.15. This range of values corresponds well to the expected range due to measurement error. The average value of about 0.15 would suggest a maximum attainable angle between particle magnetisation and external field of roughly 9^0. With an angle between the easy magnetisation directions for iron of 90^0 (figure 2.4, page 23), and for an sufficiently greater than H_{cr}, there will be zero torque at an angle of 45^0 between external field and easy magnetisation direction. If the torque curve is not skewed (unlikely at such low fields) the maximum torque should occur at about 22.5^0 (R_f = 0.38). There will be some rotation of particle magnetisation, and the angle attained between particle magnetisation and $\widetilde{H}$ will be slightly less than this. Given the generally flattened particle shapes, the polycrystalline nature

of the iron, the retarding effects of particle inertia, the existence of an angle of medium magnetisation at 45^0, the suggested lag angle between magnetisation and field of 9^0 is very low, but not totally unreasonable.

The stainless steel ferromagnetic rotation indices are also restricted to between 0.09 and 0.2, and give an average value of 0.18, which indicates an average angle between particle magnetisation and the external field of approximately 10^0. Given experimental error, this result is essentially the same as for iron. Even though these particles are less magnetic, the rotation index is roughly the same as for the more magnetic iron. This would be expected for ferromagnetic particles with approximately the same angle between magnetisation directions.

The magnetite particles show a distinct trend across the rotation index lines, and this trend extends past the ferromagnetic index of 1, which represents (for a ferromagnetic particle) an angle between particle magnetisation and external field of 90^0. Standly (1972) reports that the directions of easy magnetisation in magnetite are along the cell body diagonals, and this is also illustrated by Chikazumi (1997) and Ckikazumi and Charap (1978) (see figure 2.5 on page 24). The maximum attainable angle between particle magnetisation and external field should be about 22.5^0, and the measured ferromagnetic rotation indices would be expected to be about 0.38 (as for iron). Considering that magnetite would be expected to be very close to domain alignment along easy magnetisation directions, and even allowing for a possible error towards the higher indices of up to 60% (instead of the estimated maximum of 20%), some magnetite particles are still well outside any reasonable error range, and do appear to be rotating very much better than would be indicated by their anisotropy and their magnetic moments measured at lift, even if they had easy magnetisation directions at 180^0.

The magnetite results may be indicating a high value for the coercivity of remanence (H_{cr}) for some grains, due to the presence of crystal imperfections. If H is only slightly greater than H_{cr} rotation indices close to unity could occur. However, values of R_f greater than unity require some further explanation, such as slow domain wall motion.

Effects of Field Rotation Frequency and Particle Size on Particle Rotation

The overall effect of field rotation frequency on particle rotation index (R_f)

Figure 10.2 shows the average effect of field rotation frequency on the ferromagnetic rotation indices for iron and magnetite. This graph is presented only to illustrate general trends; it has little statistical significance. Figure 10.1 shows the great range of rotation indices for magnetite grains, and the magnetite particles used to construct this graph covered a wide size range, from 180 to 1000 μm in diameter. Therefore indications of possible measurement error would be meaningless here. The rotation index frequency dependence for magnetite is discussed in more detail later

It was mentioned in chapter 4, that a decrease in rotation index with increasing field rotation frequency would be expected from particle inertia effects. As the field rotation frequency increases there is less time available for the particle to reach the field rotation angular velocity before the field moves on to the next direction of easy magnetisation. A consideration of domain wall velocity effects in chapter 4, leading to equation 4.18, also predicts such a decrease in rotation indices at higher field rotation frequencies. Some

magnetite particles, and especially those particles larger than about 500 μm, do show an apparent increase in ferromagnetic rotation index at field rotation frequencies between 20 and 40 Hz, and this is discussed in more detail below. There is no hint in figure 10.2 of a similar peak in iron particle rotation indices.

Eddy current rotation of particles was discussed in chapter 6, but for the field rotation frequencies used here (between 10 and 60 Hz) the torques produced are a factor 10 too small to rotate the iron particles, and are much smaller still for magnetite. Eddy current torque adds to the magnetic torque, but its effect is below the expected measurment errors in this case. Eddy current torque should also increase proportionally with field rotation frequency, but over the frequency range used here the eddy current effect will remain below the error level.

Although the average ferromagnetic rotation index shows a general decrease as the field rotation frequency increases, as illustrated in figure 10.2, the mass magnetic moment of the particles showed no change with increasing field rotation frequency.

Figure 10.2

Dependence of Ferromagnetic Rotation Index on Field Rotation Frequency

For steel and magnetite particles

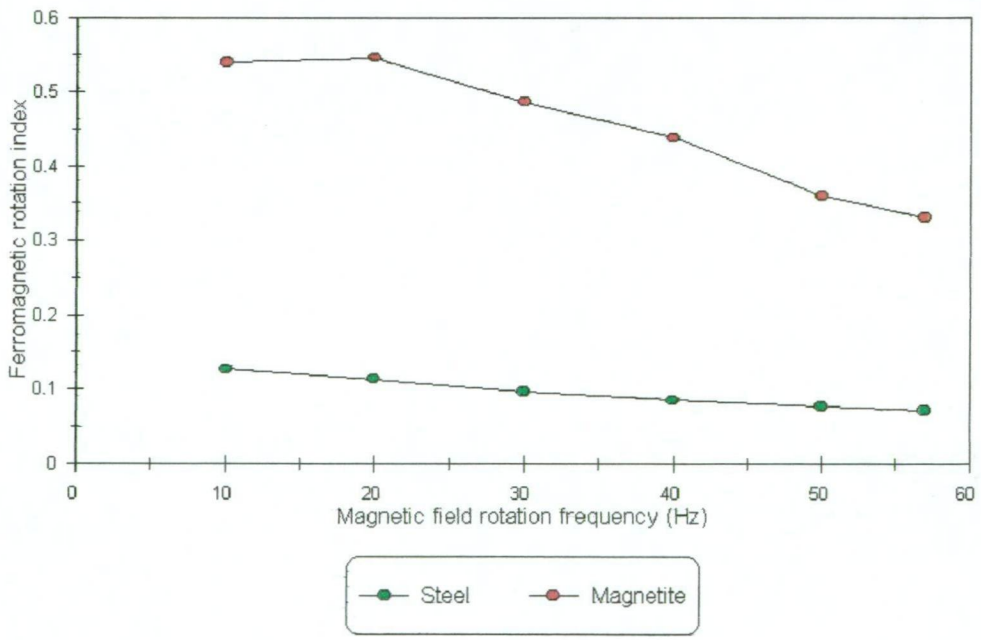

It is interesting to attempt to model the frequency response of the iron and magnetite measured rotation indices, using expression 4.19. For the present exercise, equation 4.19 has been simplified considerably to:

$$R_f = \frac{\sin(\phi + Cf^m)}{1 + Bf^n}$$

Where A, C, m and n are constants
f is the field rotation frequency

This is an adaption of equation 4.19, where $\frac{360df}{c(H-H_0)}$ has been approximated by Cf^m, and $\frac{\pi d^2 f^2}{5Am_m H}$ has been approximated by Bf^n. The fractional indices for f are allowed for because the variation of H has not been separately included here, and the frequency dependence of A in equation 4.19 is not determined. The average values illustrated in figure 10.2 can be used for this exercise. A comparison between the average measured and the fitted values are shown for the hypothetical iron particle in figure 10.3 and for the hypothetical magnetite particle in figure 10.4.

For the iron particle the curve is best fitted if it is assumed that domain wall velocity is too high to have any effect (C set to 0), and if the values of B and n are 0.015 and 1.05 respectively.

Figure 10.3

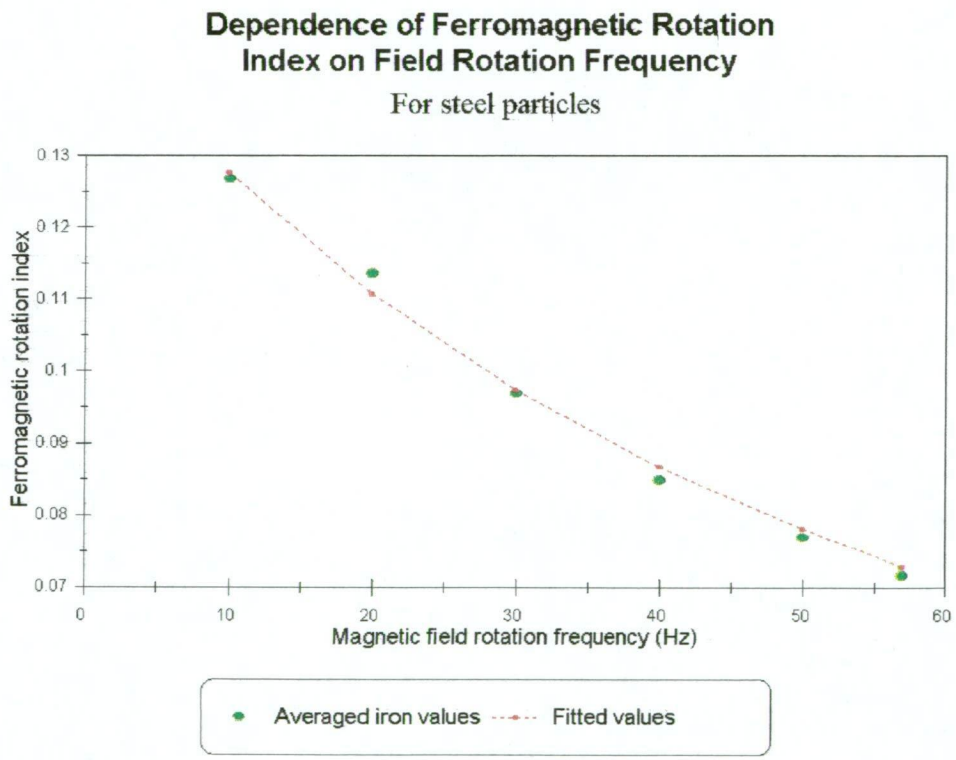

For the magnetite particle it is necessary to include a term for domain wall velocity, with C=3.5 and m=0.81. For the inertia term the fit is best if n=1.05 (as for iron particles) and A=0.026. It is necessary to set ϕ at 22^0.

Figure 10.4

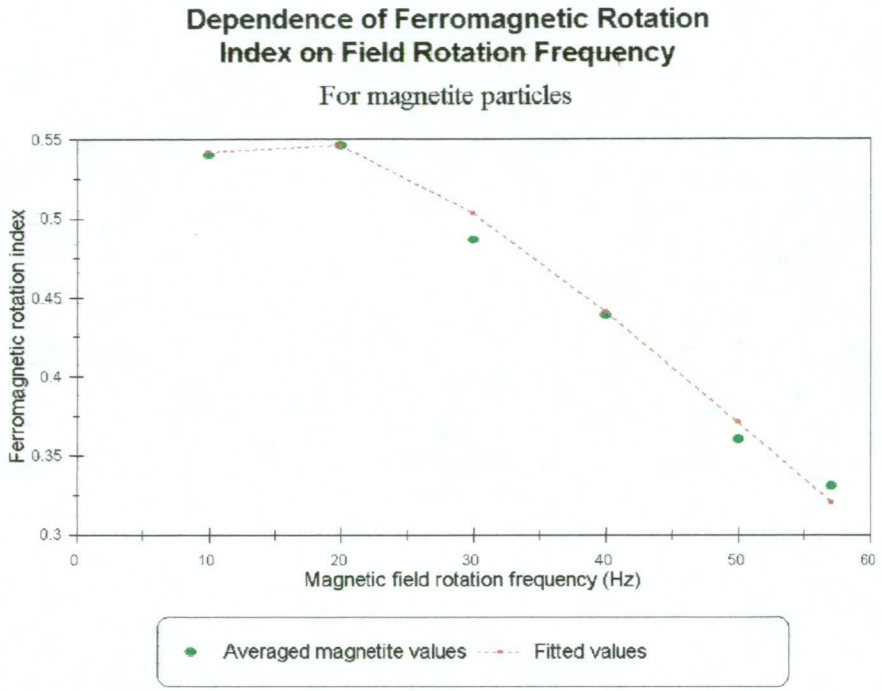

The modelling of the magnetite values indicates that the large rotation indices measured for magnetite could be, in part, due to domain wall velocity effects. The indicated value for ϕ, using the values graphed in figure 10.2, has been reduced now close to the expected value of 22.5^0.

The modelling of rotation index values for real grains, such as those illustrated in figures 10.6a to 10.6d, is a little more uncertain. This is due primarily to particle shape effects which may or may not be raising or lowering the rotation index. However, at least in theory, the response of the rotation index to field rotation frequency could be used to obtain information on average domain wall velocities in individual magnetite grains.

The overall effect of particle size on the magnetite rotation index

A series of lift and rotation measurements was carried out on magnetite particles from 130 μm to 1000 μm in diameter. These measurements are included in appendix A, and have also been included in the data illustrated in figures 10.1, 10.2 and 10.3. As well as the normal measurements required to calculate magnetic moments and rotation indices, these particles were also observed for particle rotation direction.

Because of the difficulties in determining accurate rotation fields for the very irregular iron particles, and because of the difficulty in estimating the true particle size for these particles, no particle size effects were attempted on iron particles.

The magnetite particle size had no significant effect on the mass magnetic moment of particles, but as the particle size increases the *range* of the rotation index values increases.

This is illustrated in figure 10.5. It needs to be emphasised here that this range indicates differences between individual particles. It is not an indication of measurement error. The latter is usually within 10% of the indicated value, and occasionally, for some larger particles (e.g. Grain 1 in figure 10.6a), within 20%. The latter increased measurement uncertainty appears to be due to the particle coming to rest (after each measurement) in different orientations.

Figure 10.5

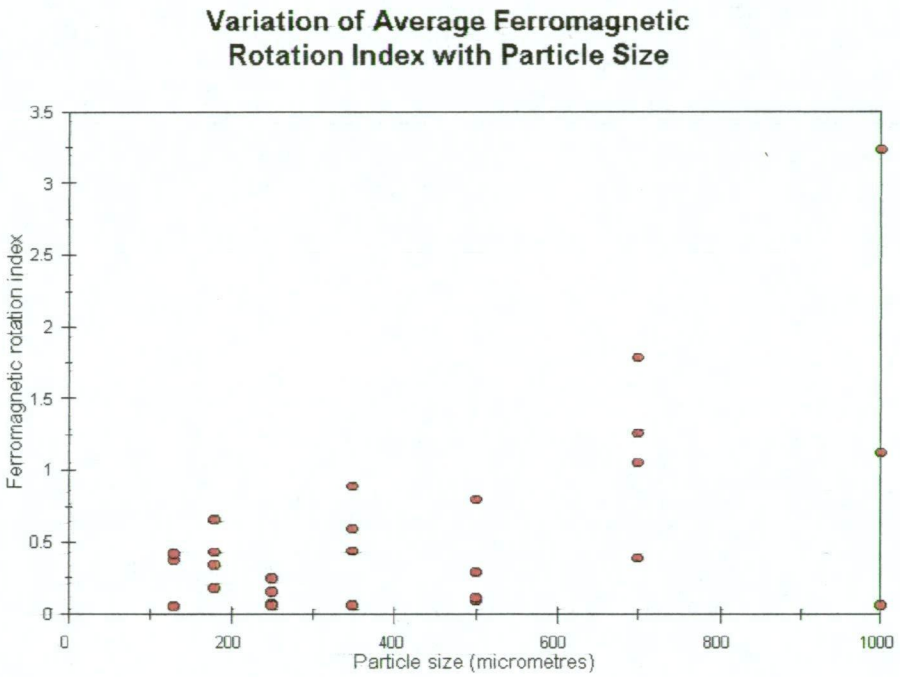

The impossibly high rotation indices (greater than 1) may be partly accounted for by a general domain wall velocity effect, which would be expected for larger particles (see chapters 2 and 4), and partly by the fact that these particles, and particularly the larger ones, had shapes part way between cubic and spherical. Rotation index calculations assumed a cubic shape for all the particles. A more rounded particle will roll at a lower field strength, and will therefore give a higher rotation index.

The more detailed effect of both particle size and field rotation frequency on rotation indices

Figure 10.2 illustrated trends for the frequency dependence of rotation index. When this frequency dependence is broken down by particle size, some particle size differences become apparent. Figures 10.6 shows the frequency response for some individual particles, ranging in size from 1 mm down to 0.18 mm. As was mentioned above, the error in the individual measurements is generally $\pm$ 10%, but for some of the larger grains it can be as high as $\pm$ 20%.

It is very noticeable in figure 10.6 that the larger particles tend to have larger rotation indices. Rotation indices greater than 1 are theoretically impossible, but in practice they may *measure* as greater than 1 if the particle rolls easier than a cubic-shaped particle. The larger magnetite particles actually tended to be closer to spherical than to a cubic shape, and, after each measurement, they tended to come to rest in unpredictable orientations. The smaller particles (< 0.5 mm) usually came to rest in the same orientation after each measurement.

Figure 10.6

(a)

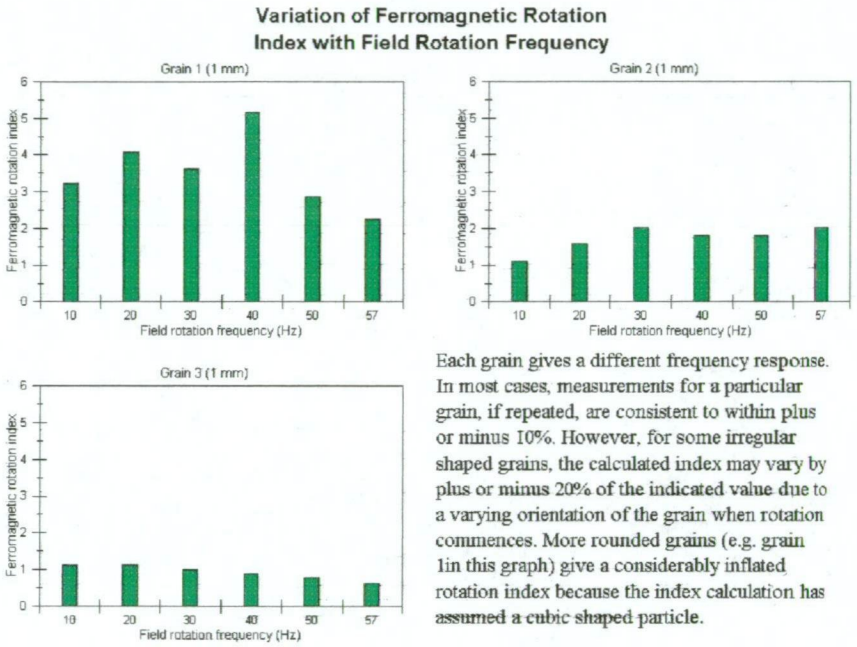

Each grain gives a different frequency response. In most cases, measurements for a particular grain, if repeated, are consistent to within plus or minus 10%. However, for some irregular shaped grains, the calculated index may vary by plus or minus 20% of the indicated value due to a varying orientation of the grain when rotation commences. More rounded grains (e.g. grain 1in this graph) give a considerably inflated rotation index because the index calculation has assumed a cubic shaped particle.

(b)

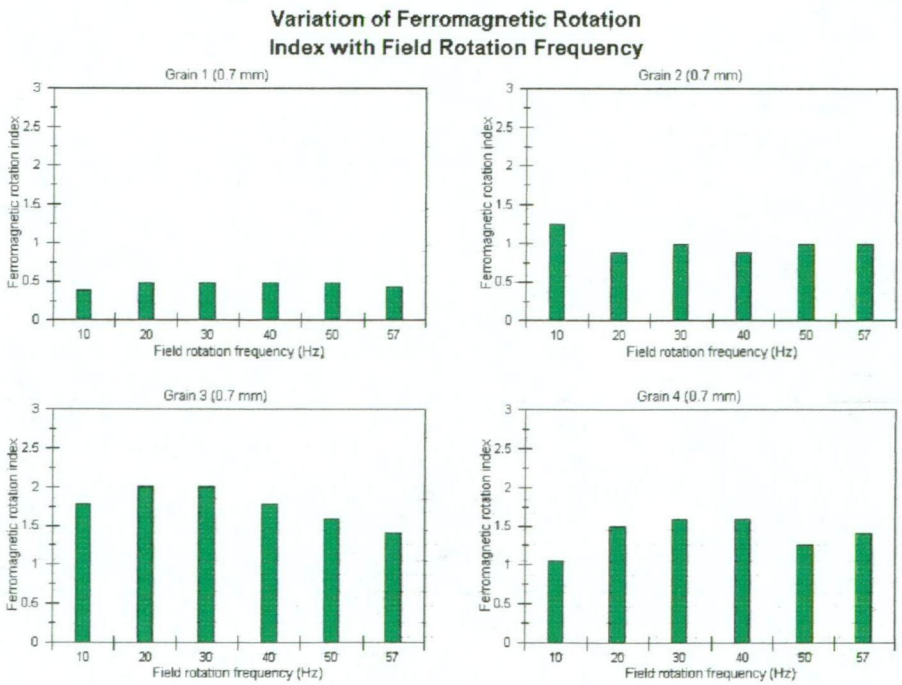

(c)

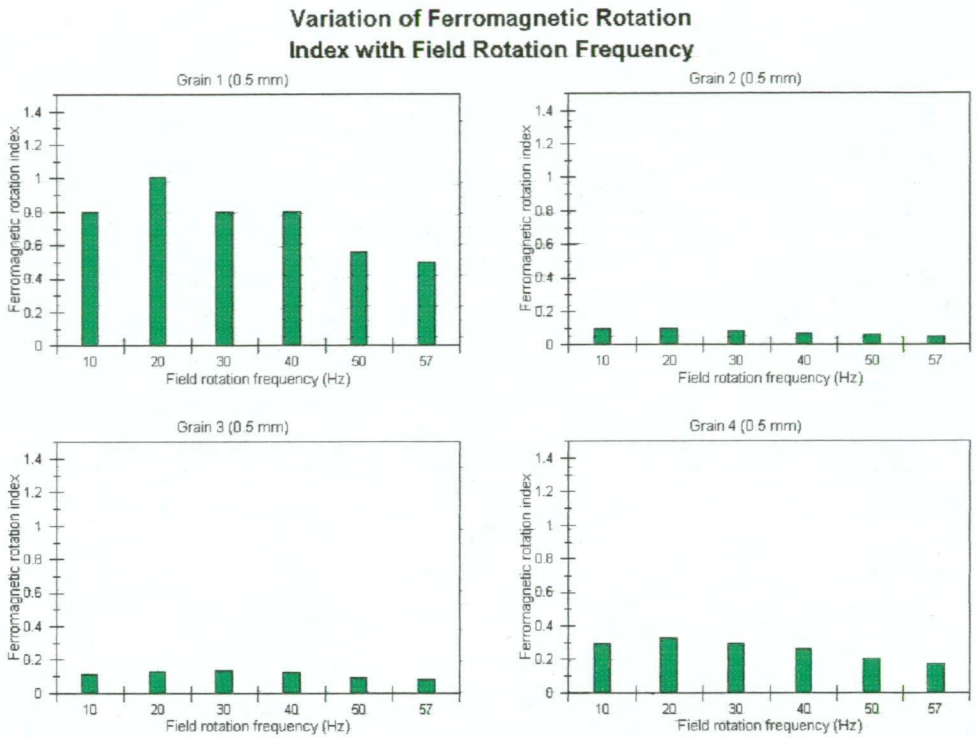
Variation of Ferromagnetic Rotation Index with Field Rotation Frequency
Grain 1 (0.5 mm)
Grain 2 (0.5 mm)
Grain 3 (0.5 mm)
Grain 4 (0.5 mm)
Ferromagnetic rotation index
Field rotation frequency (Hz)
0
0.2
0.4
0.6
0.8
1
1.2
1.4
10
20
30
40
50
57

(d)

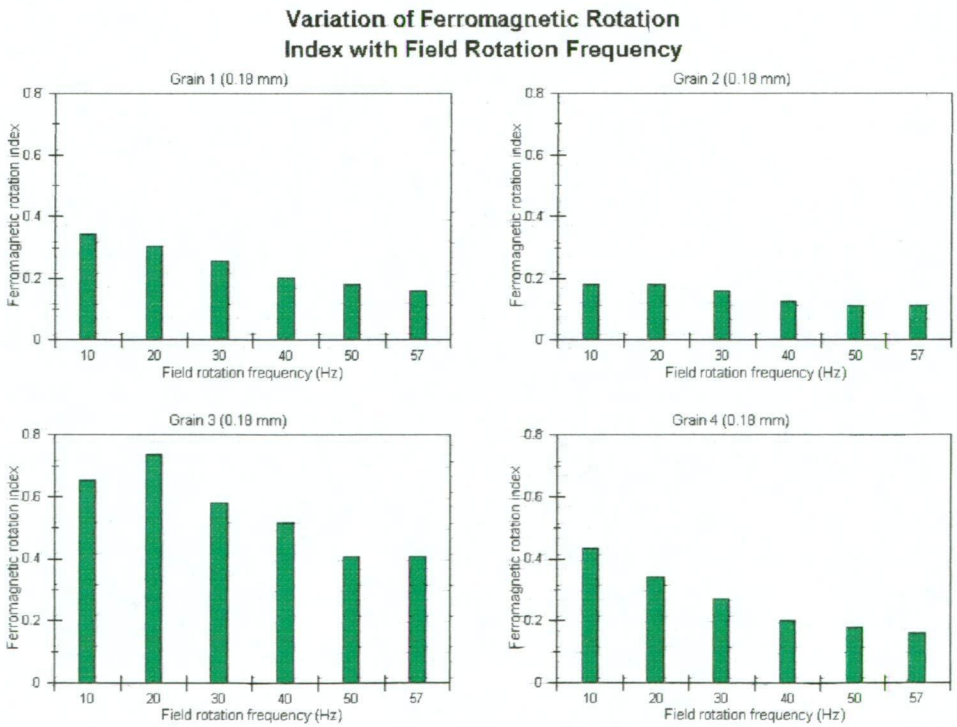
Variation of Ferromagnetic Rotation Index with Field Rotation Frequency
Grain 1 (0.18 mm)
Grain 2 (0.18 mm)
Grain 3 (0.18 mm)
Grain 4 (0.18 mm)
Ferromagnetic rotation index
Field rotation frequency (Hz)
0
0.2
0.4
0.6
0.8
10
20
30
40
50
57

Smaller particles (< 0.5 mm) usually show a steady decrease in rotation index with increasing frequency (grain 3 in figure 10.6d is a fairly rare exception to this). In contrast to this, most of the larger particles (> 0.5 mm) do show a peak in rotation indices, usually between field rotation frequencies of 20 and 40 Hz.

If the peak in rotation indices in figure 10.6 is due to a slow domain wall velocity, then, for 1 mm particles it would imply an average wall velocity of less than 50 cm/sec, for a single domain wall travelling across the crystal. This is quite within reason if the external field strength is very close to the critical field for domain wall motion, as is suggested by the comments on domain wall mobilities in chapter 4. If multiple domain walls are travelling through the crystal, then the travel time quickly becomes too short to cause any effect, and this may explain why some particles showed the peak in rotation indices while others did not.

Evidence for Perpendicular Particle Rotations in Magnetite

The direction of particle perpendicular rotation was not always easy to observe directly, especially at rotation frequencies above about 20 Hz, but the rotation direction can usually be inferred from the particle rolling direction within the glass tube illustrated in figure 7.8. If the particle rolls with the field rotations, it will roll to the left (along the bottom of the glass tube) before it lifts, and to the right (along the top of the glass tube) after it lifts. If the particle rotates around a vertical axis, it will tend to spin without moving significantly one way or the other. If it rotates perpendicular to the field rotations, and around a horizontal axis, it will tend to climb the walls of the glass tube. The presence of very small sand particles (<20 μm) can also be used to detect particle rotation direction by revealing water turbulence patterns.

For particles above about 700 μm, and to a lesser degree for particles between 500 μm and 700μm, a particle rotation occurs which has its axis horizontal and at right angles to the field rotation axis.

As the field strength is increased towards the point where particle rotation begins, the initial particle rotation is usually hesitant, and often around a vertical axis. Further increasing the field strength causes rotations with the field to commence, and these appear to be superimposed on any earlier vertical axis rotations.

As the field strength is further increased, but before particle lift occurs, a particle rotation occurs around a horizontal axis at right angles to the field rotation axis. This is shown by a tendency for the rotating particles to climb the tube wall furthest from the observer, and implies a "perpendicular" particle rotation where the top of the particle is moving away from the observer in figure 7.8.

Increasing the field strength further causes the particle to lift by rolling itself up the rear wall of the glass tube. After the particle is lifted against the upper surface of the glass tube, further increasing the field strength causes the particle to roll part way down the near side of the tube. At field rotation frequencies above about 40 Hz, rotation in the same direction as the field rotation appears to decrease shortly after particle lift, and then to increase again as the field strength is further increased.

For particles less than about 500 μm, perpendicular rotations become less obvious as the particle size decreases. For 130 μm particles, the only evidence of perpendicular rotation is a tendency for particles to travel around the rear wall of the glass tube as they lift.

Using the present equipment it has only been possible to obtain broad relative impressions of the perpendicular rotations. These observations of perpendicular rotations are *qualitatively* summarised in figure 10.7.

Figure 10.7

A qualitative summary of "perpendicular" rotation strength observations in magnetite particles

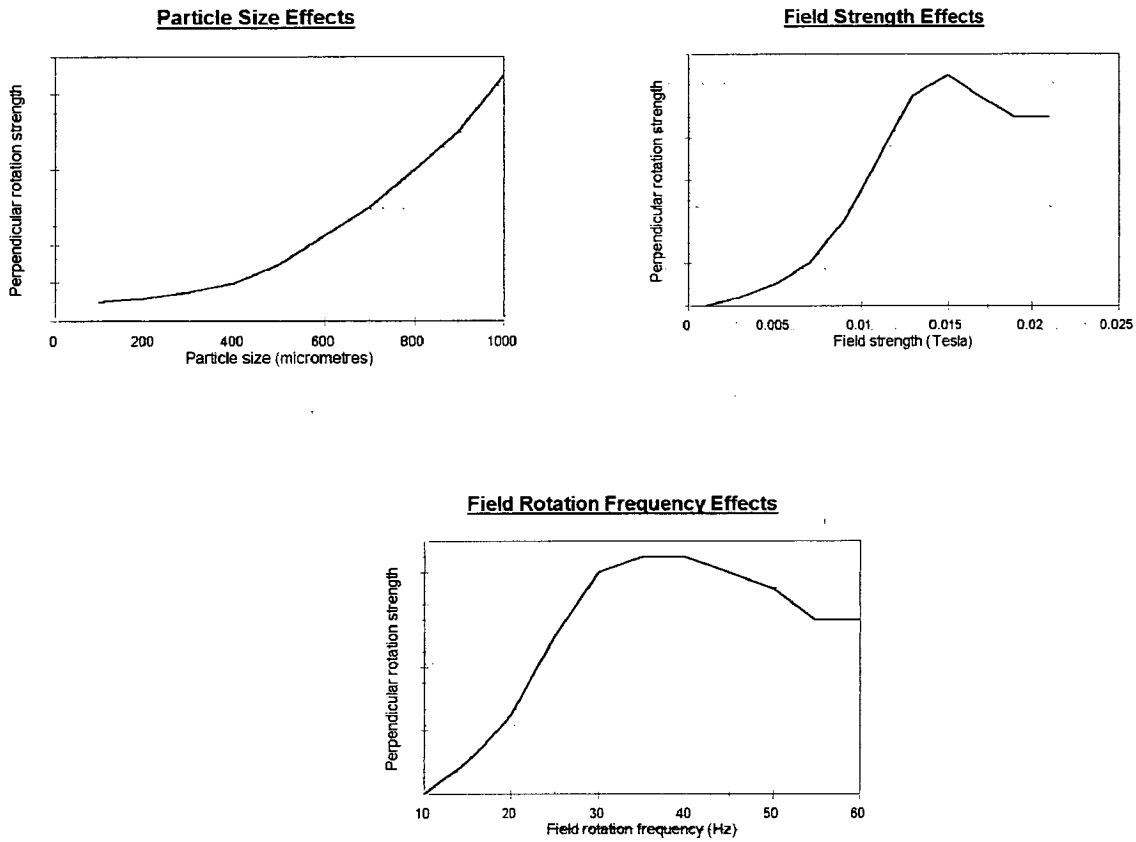

Following the observation of an apparent peak in rotation indices for larger particles rotating in the same sense as the field rotations (see previous section), an attempt was made to produce these particle rotations at lower field strengths, by measuring rotation indices with the particles immersed in di-iodo-methane, of specific gravity about 3.3. The idea was to lower the opposing torque due to gravity and therefore to reduce the field strength required for particle rotation. This would place the applied field much closer to the critical field for domain wall motion and slow down the domain wall velocity. The observed peak in the rotation indices would then be expected to move to a lower field rotation frequency.

In fact it proved almost impossible, with any acceptable accuracy, to determine the commencement of particle rotation in the same direction as the field rotations, due to a greatly enhanced particle rotation perpendicular to the field rotation.

Discussion

The apparent magnetic susceptibility of both the iron and magnetite particles does not change significantly as the field rotation frequency is increased. The ferromagnetic rotation indices decrease consistently with increasing field rotation frequency for the smaller particles, while the rotation indices of the larger magnetite (ferrimagnetic) particles show an increase between about 20 and 40 Hz before they begin to decrease significantly.

When particle magnetic moment is being measured (at the point of lift), the particles are already rotating strongly at the same frequency as the magnetic field, the field strength is more than sufficient to rotate the particles, and the particles are free of interaction with a surface. Therefore the torque needed to keep them rotating must only overcome fluid drag forces, which are relatively small. Consequently the angle between the particle magnetisation and the external field does not need to be large to supply the required torque. Therefore, as is found, no significant change of magnetic moment would be expected with increasing field rotation frequency.

When the rotation field is being measured (at the point of particle rotation), the particle is stationary and interacting significantly (through gravitational forces) with the surface it is resting on. The magnetic field strength is relatively weak, and the torque needed to start the particle rotating against its inertia is much greater than the torque needed to keep it rotating. At the point where the particle commences rotation, the maximum possible angle (maximum torque) exists between the particle magnetisation and the external field, and this angle is related to the particle magnetic anisotropy directions. The maximum torque that can be applied to a particle, against its anisotropy forces, should occur at one quarter of the angle between adjacent directions of easy magnetisation. At angles greater than this domain re-orientation begins to occur, until at half the angle the domain orientations are equally divided between the adjacent easy magnetisation directions, and the torque becomes zero. Therefore the maximum ferromagnetic rotation index which would normally be expected would be 0.71, for easy magnetisation directions at 180^0. For both magnetite and iron, where the easy magnetisation directions are at right angles, the expected maximum value would be 0.38.

As was discussed in chapters 2 and 4, these expected rotation index values could be significantly increased if the rotating field was close to the field required to cause domain wall motion. Low domain wall velocity then increases the rotation index, and if domain wall velocity is slow enough it can add significantly to the rotation index, but will tend to produce peak values for the rotation index at certain field rotation frequencies.

The measured relationship between lifting and rotation fields for the ferromagnetic iron particles give average ferromagnetic rotation indices about 0.15, and suggest a maximum lag angle between particle magnetisation and external field of 9^0. Such a rotation index appears to be well below the expected value of 0.38. The lower rotation indices may be partly explained by a need for a high "shape factor" for the irregular particles used. Another factor in producing the lower rotation indices may be the existence of an intermediate medium magnetisation direction in iron, between the easy directions. The curve-fitting exercise (figure 10.3) indicates that domain wall motion is not a significant factor controlling the measured rotation index for iron. Within these considerations, and the limits of the experimental accuracy, the results achieved for the iron particles are not unreasonable.

The magnetite results show a clear horizontal trend (in figure 10.1) across the rotation index lines, from an R_f of only 0.05 to a value for R_f of more than 2. Some of the particles were more spherical than cubic in shape, and this could have caused errors of much more than 50% in the rotation indices, for the larger particles in particular. Even this large error can at best reduce some of the indicated rotation indices to the maximum possible index of 1. The high rotation index values indicate one of:

a) The appearance of some extra magnetic moment as a result of the field rotation.
b) Uniaxial rather than the expected cubic anisotropy (e.g. a shape anisotropy).
c) A delaying of domain re-orientation, due to slow domain wall velocity and/or a high H_c/H ratio.
d) A particle which is more rounded than a cube.

The first of the above possibilities is ruled out by the magnitude of the exchange energies involved. Spin reversals of the required magnitude in one sub-lattice should not be possible. Even if some spin canting did occur, it could not begin to account for the magnitude of the observed increase in rotation indices.

Uniaxial rather than cubic anisotropy could only increase the expected rotation index to 0.71, which, even after applying the maximum possible errors, is only half the required angle between particle magnetisation and external field for many of the particles. By itself it also leaves unexplained the further increase in rotation indices, for the larger particles, between the field rotation frequencies of 20 and 40 Hz.

The most plausible explanation is that the high rotation indices are the combined result of high H_c/H ratio and slow domain wall velocities, which prevent the particle magnetisation from changing to other easy orientations fast enough to keep up with the field rotations. If the domain wall velocities were in the vicinity of about 25 cm/sec, which would seem allowed by current knowledge, and the H_c/H ratio is greater than about 0.7, then the lag between particle magnetisation and the external field could become very close to 90^0, giving the *impression* of a particle which was not only uniaxial but uni-directional. In the larger particles, it would even be possible to exceed a lag angle of 90^0, but this should show up as an apparent peak in the rotation indices at the field rotation frequency when it occurred. Such a peak is suggested in the observed rotation indices for particles above about 0.7 mm diameter (and may also be present in the smaller particles). Theoretical considerations of domain wall velocity effects (chapters 2 and 4) predict that this peak in rotation indices would probably occur at about the same field rotation frequency for most particle sizes, and this is suggested in the data. The curve-fitting exercise illustrated by figure 10.4 also indicates that slow domain wall velocity has increased the average rotation index by a factor of about 2.

From the considerations in chapter 5, particle rotations that are perpendicular to the field rotations should not occur, even in magnetite. However, for the larger magnetite particles (> about 500 μm) the perpendicular rotations appear to be quite strong. It is possible that the parallel rotations decrease surface interaction to a point where the perpendicular rotations are able to occur.

Decreasing the gravitation forces that oppose particle rotation, and also decreasing the external field strength to a value which would be very close to *or less than* the critical field for domain wall movement, appears to emphasise the perpendicular rotations over the parallel rotations. If the external field is less than the critical field, a particle containing many randomly-oriented domains remains essentially unmagnetised, with minimal domain wall motion. Under these conditions parallel rotations should become very weak, due to opposing

torques from the randomly oriented domains. This suggests that the perpendicular rotations arise from spin reversals during limited domain wall oscillations, possibly assisted by thermal agitation.

Chapter 11

The Response of Ilmenite Particles to Rotating Magnetic Fields

Introduction

The separation of ilmenite ($FeTiO_3$), as an economic mineral, may be accomplished by a combination of conventional specific gravity and magnetic methods. In these cases the aim is simply to separate the ilmenite from other minerals, without paying very much attention to the detailed composition of the ilmenite being separated. Such separations are not of concern in this chapter.

A much more specific use for ilmenite is as an indicator mineral in diamond exploration. This relies on the fact that ilmenite crystals formed under different conditions of temperature and pressure, and in different chemical environments, have characteristic compositions. In particular, those ilmenites formed in an environment suitable for diamond formation and preservation have a high Mg content. The practical problem here is not only to separate ilmenite, but to separate a particular type of ilmenite. At present such detailed separations are carried out very tediously by hand, particle by particle, under a microscope. Such work requires very highly trained observers, capable of maintaining a high level of concentration over extended periods. Observer through-put is measured in kilograms per year, rather than in the tens of tonnes per hour usually associated with commercial mineral separation. Therefore any ability to reduce sample sizes for observation, by concentration of the Mg ilmenites, would considerably benefit diamond exploration activities.

It is the aim of this chapter to examine the response of ilmenite particles to a rotating magnetic field, and to relate this response to the chemical composition of the ilmenite. A more specific objective is to identify the rotational characteristics of high-Mg ilmenite particles (picro-ilmenites) that will allow them to be magnetically separated from other ilmenites.

Samples of ilmenite particles were obtained from:

(a) Dorset Flats, near Pioneer, in NE Tasmania (EL 11/96).

(b) Rio Tinto Exploration (formerly CRA Exploration). A sample of mixed "normal" alluvial ilmenites.

(c) Rio Tinto Exploration (formerly CRA Exploration). Examples of picro-ilmenites from
  (i) Duck Creek (DR 2187).
  (ii) a kimberlite called Skerring.

(d) Rio Tinto Exploration (formerly CRA Exploration). High magnesium ilmenites from NSW.

In all, about 300 ilmenite particles, within the size range 0.4 to 2 mm, were individually measured for rotational characteristics and analysed for composition. The methods used to obtain rotation measurements and analysis data have been described in chapter 9. Some analysis results for picro-ilmenites were also provided by Rio Tinto Exploration, and have been included without rotation measurements.

Ilmenite Structure and Composition

Ilmenite has a structure similar to the trigonal corrundum structure illustrated in figure 11.1. The lower drawing (plan of the lower layer of the corrundum cell) shows the octahedral arrangement of the oxygen ions and the placement of the metal ions, while the upper drawing shows how the layers are stacked above each other.

Figure 11.1

The corrundum structure (which is also shared by ilmenite)

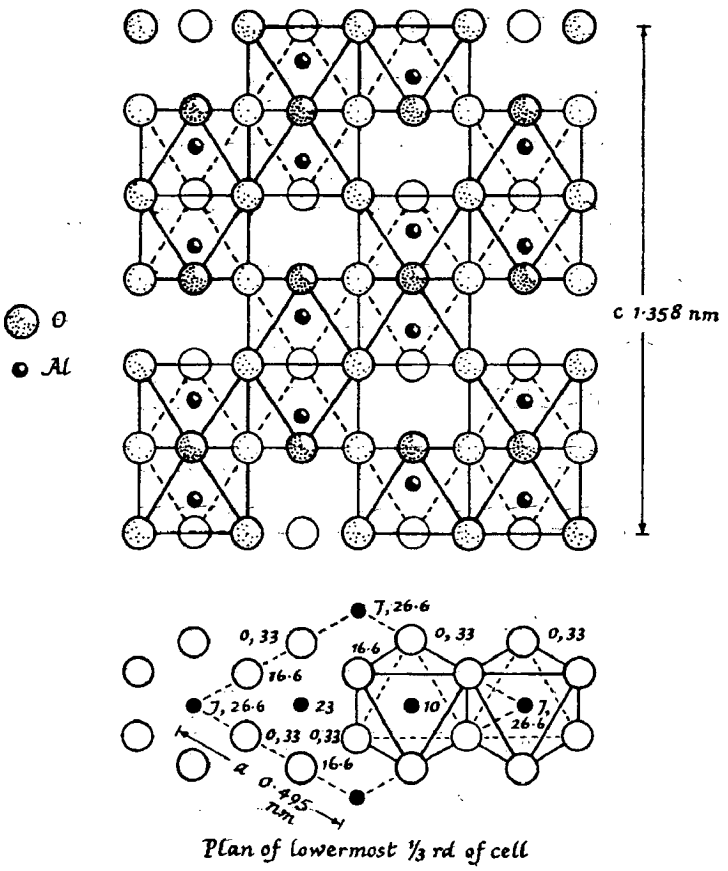

(From Battey, 1981)

In corundum all the metal ions are Al, with the Al ions arranged in layers between layers of O ions. In pure ilmenite ($FeTiO_3$) all the metal ion sites in one layer contain Fe, with the next layer of metal ion sites containing only Ti.

Pure $FeTiO_3$ rarely occurs in nature, with most natural ilmenite falling somewhere along the solid solution series $xFeTiO_3(1\text{-}x)Fe_2O_3$. Other ions can also enter into the basic ilmenite composition, and Suwa et al (1987) writes that the ilmenite formula could be more fully expressed as $(Fe,Mg,Mn,Zn)TiO_3$.

While pure ilmenite, at one end of the above series, is completely ordered with respect to cation location (all Fe in one layer and all Ti in the next), at some point along the ilmenite-hematite series there is a temperature-dependent transition from a cation-ordered phase to a cation-disordered phase. This has been described by Gordon et al (1989), and is illustrated in figure 11.2. In the cation-disordered phase the distribution of Fe and Ti ions becomes random rather than each type of ion being restricted to its own sub-lattice. Gordon et

al also point out that the cation-ordered phase produces strong ferrimagnetic properties while the cation-disordered phase produces only weak ferrimagnetic properties. Figure 11.2 also has the Curie temperature trend superimposed on it. As the composition trends towards Fe_2O_3, the Curie temperature rises towards 680°C. It can be seen from the graph that ilmenite with very little Fe_2O_3 will be above the Curie temperature at room temperature, and consequently will behave as a paramagnetic substance.

Figure 11.2

Phase diagram showing the cation order-disorder transition in ilmenite-hematite and the relationship between Curie temperature and composition

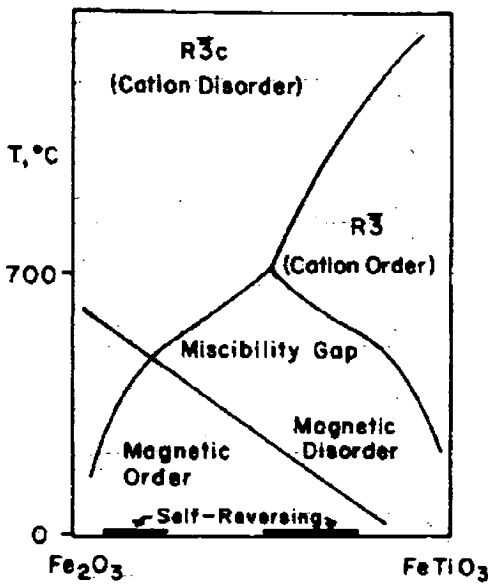

(From Gordon et al, 1989)

Carmichael (1961) examined the magnetic anisotropy of ilmenite-hematite and reported a uniaxial remanence anisotropy in the basal plane, with a very strong magnetic anisotropy between the basal plane and the *c* axis. That is, directions of easy magnetisation lie in the basal plane. That being the case, the ferromagnetic rotation index introduced in chapter 4 should give values of about 0.7, at least for those particles which are ferrimagnetic at room temperature. Carmichael also examined the magnetic contributions of exsolution lamellae (high hematite composition), which tend to lie parallel to the basal plane. He determined that these were responsible for most of the remanent magnetisation, with high coercive forces (about 1500 Oe, or 119400 A/m) being associated with the very small lamellae and low coercive forces (about 200 Oe, or 15900 A/m) being associated with the larger lamellae. The latter were assumed to be multi-domain, while the former were considered single-domain.

Analysis Results for Measured Ilmenite Particles

The full analysis results are given in appendix B, together with the lift and rotation magnetic fields for field rotation frequencies of 10 and 57 Hz.

The analysis results presented in this chapter suggest that ilmenite can contain significant amounts of either Mg or Mn, but apparently not both. This is illustrated in figure

11.3, and immediately divides the ilmenites into two reasonably distinct compositional groups which might be expected to have different magnetic properties.

Note that cation numbers have been used in the presentation of the composition graphs. These numbers refer to the relative numbers of each cation in the basic formula $x(Fe^{2+},Mg,Mn)TiO_3.(1-x)Fe_2O_3$.

Figure 11.3

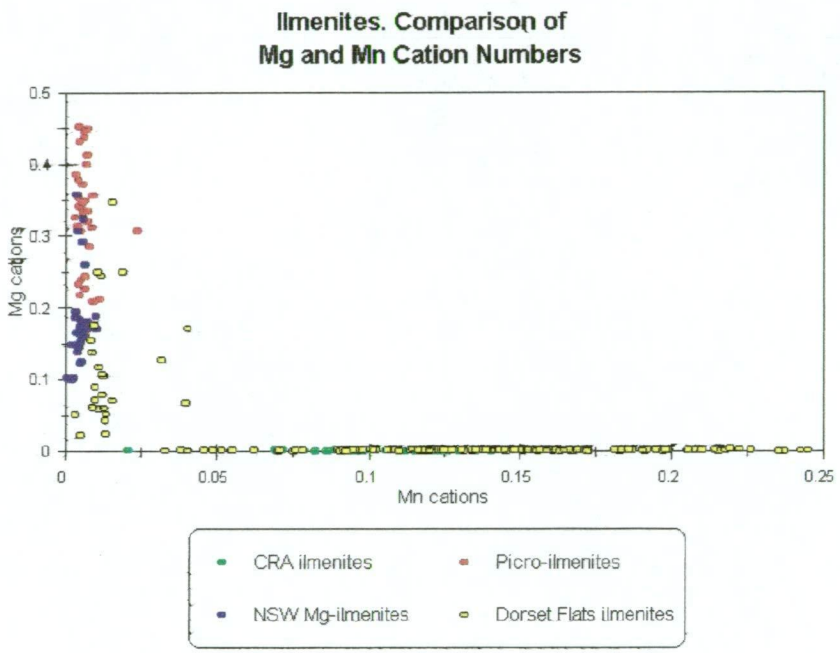

Three distinct substitution series can be identified from the analysis results, which are illustrated by figures 11.4, 11.5, and 11.6.

(a) A picro-ilmenite series (Mg cations > about 0.25), where the substitution is predominantly one of substituting Mg for Fe^{2+}. The Ti and Fe^{3+} remain substantially constant, and Mn is only in trace amounts.

(b) A lower-Mg series (Mg cations < 0.2), where the substution involves the replacement of two Fe^{3+} ions by an Mg/Ti or Fe^{2+}/Ti pair. Mn again is only in trace amounts.

(c) A Mn series, which is the Mn eqivalent of (a), where the substitution is predominantly one of substituting Mn for Fe^{2+}. The Ti and Fe^{3+} remain substantially constant, and Mg is now only in trace amounts.

In figures 11.4, 11.5 and 11.6 the particles have been colour-coded according to source. The picro-ilmenites are a combined sample from the two sources given in the introduction, and the Dorset Flats ilmenites are from a greisen environment above granite in NE Tasmania.

It is interesting that several of of the measured Dorset Flats ilmenites have Mg compositions similar to those of picro-ilmenites. Mg-ilmenites from Dorset Flats in NE Tasmania are examined further in chapter 15.

Figure 11.4

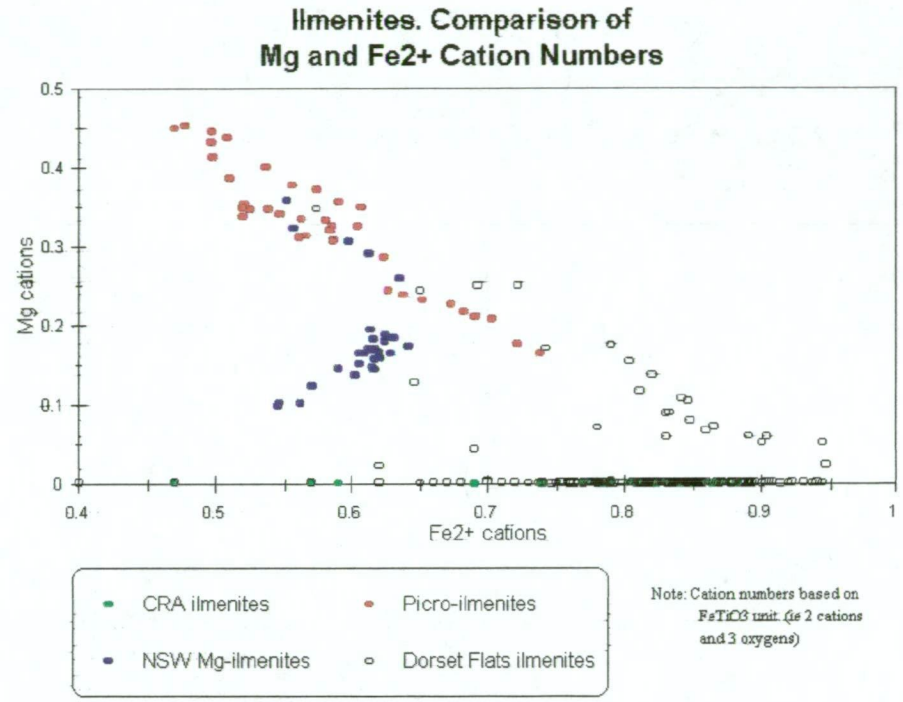

Figure 11.5

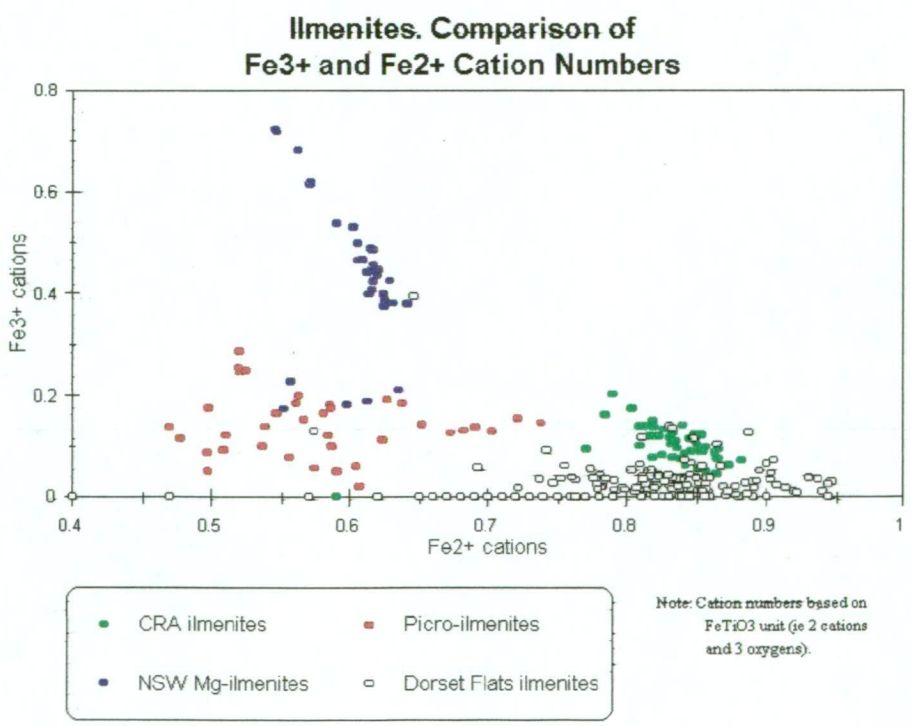

Figure 11.6

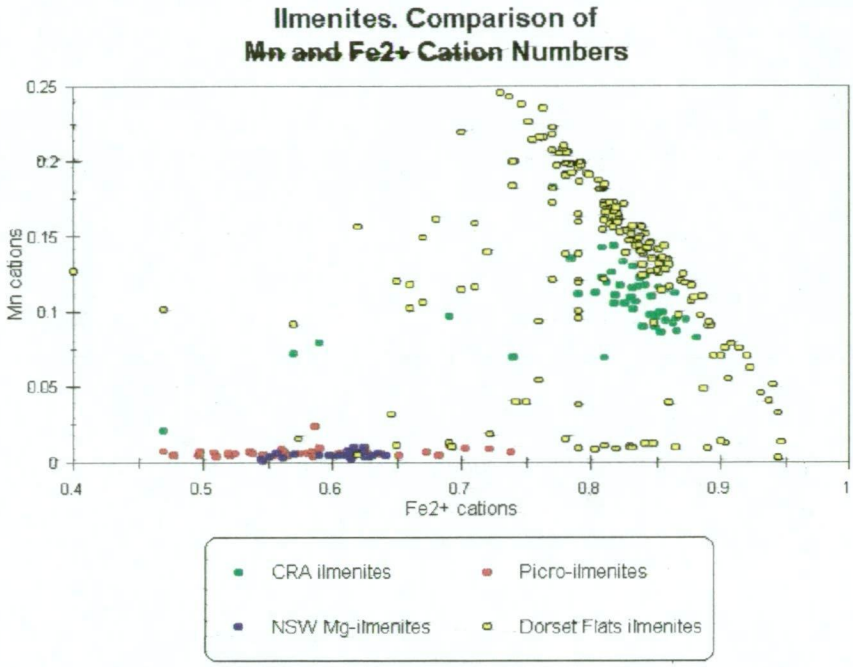

Ilmenite Rotational Characteristics

Figure 11.7 examines the relationship between the lifting magnetic field strengths and the ferromagnetic rotation indices for the measured ilmenites. The ferromagnetic rotation index has been used here because many of the particles have a ferromagnetic rotation index well above 0.15 (which imples a paramagnetic index well above 1). If any magnetic ordering is present in ilmenite-hematite at room temperature it will be ferrimagnetic in nature, with a uniaxial magnetic anisotropy (Carmichael, 1961), so the maximum expected *ferromagnetic* rotation index is about 0.71. Many of the particles will in fact be paramagnetic, and for these particles, a *paramagnetic* rotation index of 0.71 corresponds to a ferromagnetic index (in figure 11.7) of 0.12. The probable existence of predominantly hematite lamellae (Carmichael, 1961), with coercive forces varying from as high as 120 000 A/m down to 16 000 A/m, means that for some of the particles, at least a part of the rotational torque was due to rotational field strengths below the coercive force.

The horizontal trend across the rotation index contours is obvious in figure 11.7, with some of the ilmenites showing more magnetic moment than would normally be expected for a uniaxial ferromagnetic particle magnetised to the point of complete domain orientation along a direction of easy magnetisation. Unlike magnetite, some particles will have rotation indices close to 1 because the external field is below the coercive force for fine hematite-rich lamellae. Many of the rotation indices above 0.7 may also be accounted for within an expected maximum 30% error. Some of the ferrimagnetic particles, with lower coercive forces, may be exhibiting domain wall velocity effects. There are sufficient explanations for the larger rotation indices in the case of ilmenite, and the rotation indices are not as high as was the case for some magnetite particles.

The problem here is to account for some rotation indices which fall well below the ferromagnetic index value of 0.7 and even well below 0.15. Of course many of these particles will be paramagnetic, especially those with little Fe^{3+}. However, in the paramagnetic condition the anisotropy is weak, allowing greater deviation of the particle magnetisation from the easy axes of magnetisation, in response to the field rotation. The maximum attainable lag angle (and consequently the rotation index) between magnetisation and external field will be reduced by the amount of the magnetisation deviation from the easy magnetisation directions. This is in contrast to the case for magnetite, where the deviation of magnetisation from the easy axes was negligible at the rotation field strength, due to high anisotropy forces. For the paramagnetic ilmenite-hematite particles, the maximum attainable lag angles should be very small, probably *much* less than 10^0 (which would imply an anisotropy field as high as 10,000 A/m for many of the particles). This means that the paramagnetic rotation index should be much less than 0.17 (equivalent to a ferromagnetic index in figure 11.7 much less than 0.05). There is therefore a large group of particles in figure 11.7 which have rotation indices too high to be paramagnetic.

Figure 11.7 emphasises the fact that some particles may have a high magnetic moment, but a low rotation index. Those particles which plot towards the top of the graph (NSW high-Mg ilmenites) have a much higher magnetic moment than any of the other ilmenite particles, but at the same time have low rotation indices (0.04 to 0.1)

Figure 11.7

Comparison of Ilmenite Lifting Fields and Ferromagnetic Rotation Indices

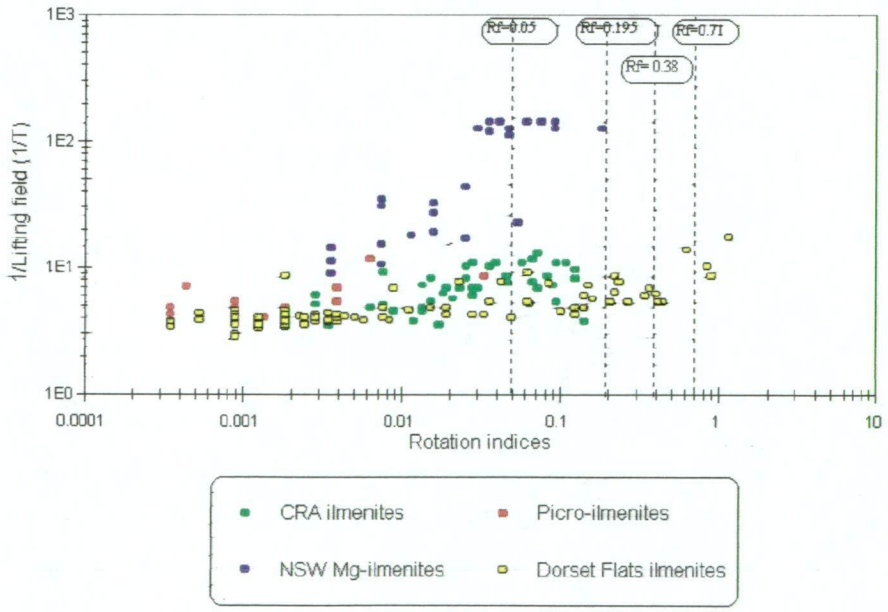

It can be seen that although the picro-ilmenites have generally higher magnetic moments, and are lifted at lower field strengths than for example the Dorset Flats ilmenites, all except one have rotation indices which are lower than most of the other particles.

The product of a rotation index and particle magnetisation can give a reasonable and practical indication of particle "rollability". In figure 11.8, which plots the ilmenites in terms of their Fe^{2+} and Fe^{3+} compositions, the particles have been colour coded in group intervals of the product of paramagnetic rotation index and indicated magnetic susceptibility.

Figure 11.8

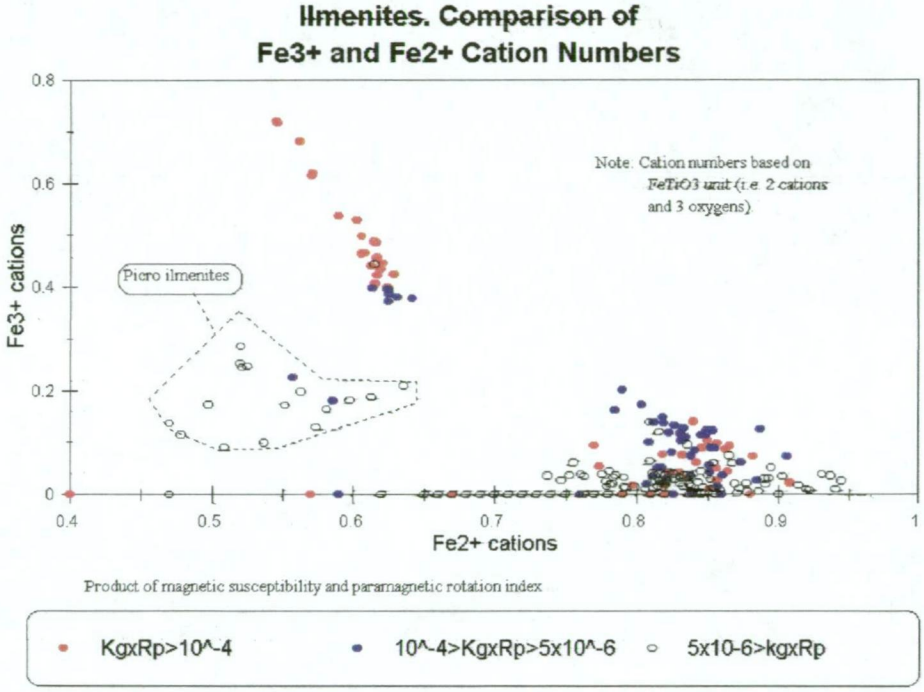

While most ilmenite particles rotated at all measured frequencies from 10 Hz to 57 Hz, the picro-ilmenites and the paramagnetic low-Fe^{3+} Mn ilmenites, if they rotated at all, did not rotate above 30 Hz even when freely suspended by attraction in the field gradient. The picro-ilmenites show up as a group which, along with some paramagnetic Mn ilmenites, should remain unseparated in a practical rotating field magnetic separation. The magnetic concentration of picro-ilmenites is further examined below.

In figure 11.9 the ratio of ferromagnetic rotation index to magnetic susceptibility has been plotted against the Fe^{3+} composition for all measured particles. Note that because many of the ilmenites appear to be paramagnetic rather than ferrimagnetic, and may therefore have negative *ferromagnetic* rotation indices, it has been necessary to add 0.02 to the ferromagnetic index so as to avoid an image effect around the zero ratio value.

Figure 11.9

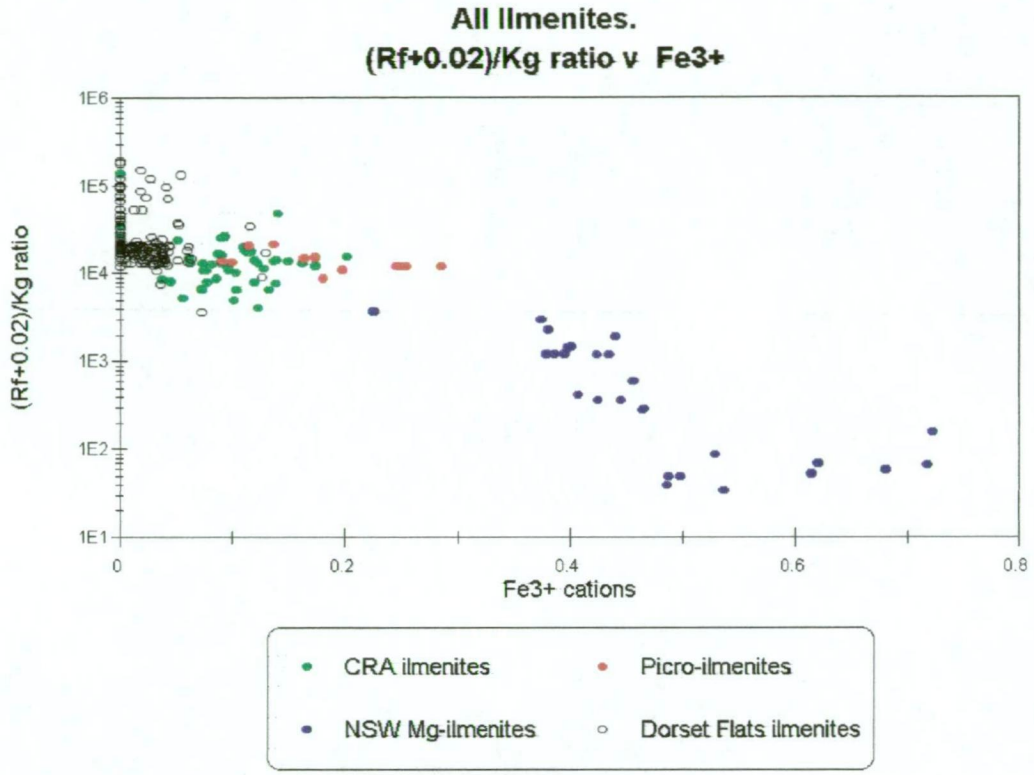

The general trend in figure 11.9 is for a decrease in the R_f/k_g ratio with increasing Fe^{3+}. Particles with a very low Fe^{3+} (Dorset Flats ilmenites) have a high rotation index for their magnetic susceptibility. They tend to rotate better than would be expected. Particles with a high Fe^{3+} have a lower rotation index for their magnetic susceptibility, and tend to rotate much weaker than would be expected.

Figure 11.9 may be compared with figure 11.7. The most magnetic ilmenites in figure 11.7 (the NSW high-Mg ilmenites), which trend across the rotation index contours at the top of the graph, are the "descending" group of ilmenites in figure 11.9 with an Fe^{3+} content between 0.35 and 0.45.

The impression from the above is that the Fe^{3+} content is the main factor determining the relationship between rotation index and magnetic susceptibility. This implies that as the Fe^{3+} content increases, the coupling of the magnetic moment to the crystal structure becomes less effective, in spite of the general increase in magnetic moment. It is also implied that the high Fe^{3+} in the NSW Mg-ilmenites is distributed randomly throughout the crystal, and is not in the form of hematite-rich lamellae.

The Magnetic Concentration of Picro-Ilmenites

Figures 11.10 and 11.11 show the frequency distribution of ilmenite particles across magnetic susceptibility and rotation indices. The picro-ilmenite ranges have been superimposed on these distributions, but are only diagrammatic (rather than accurate histograms).

Figure 11.10

Magnetic Susceptibilty
Frequency Distribution

(All measured ilmenites)

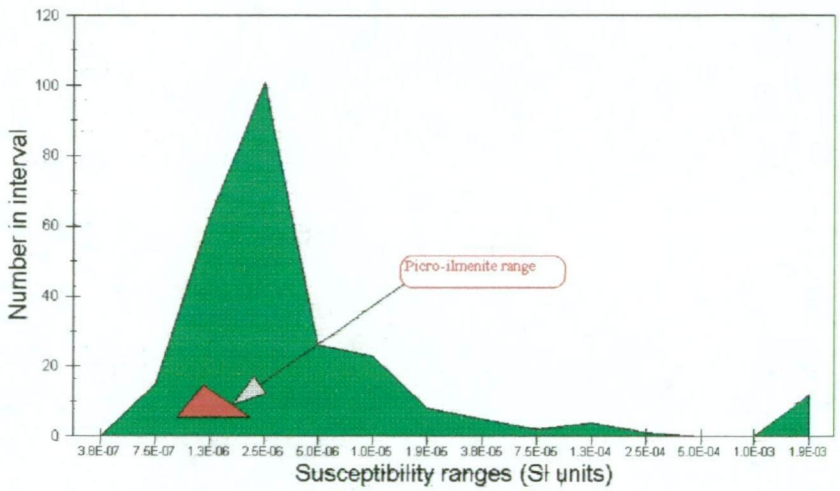

Figure 11.11

Rotation Index
Frequency Distribution

(All measured ilmenites)

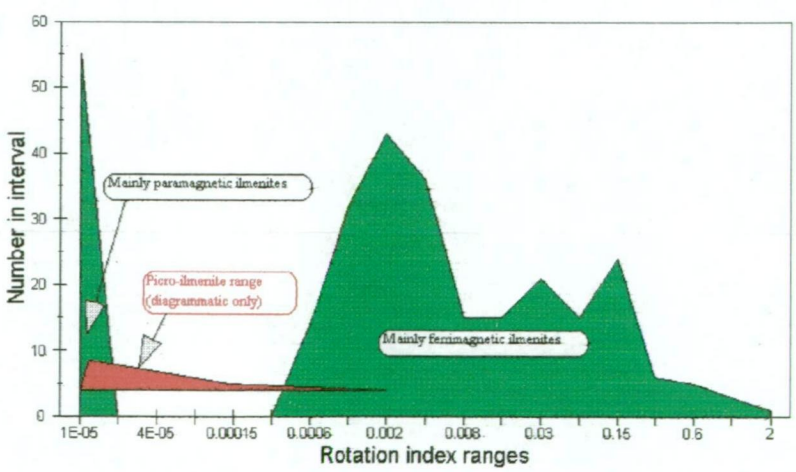

From figure 11.10 it can be seen that any concentration by magnetic attraction will concentrate the picro-ilmenites in about 50% of the total ilmenites. This will make the detection of any picro-ilmenites easier, but not greatly so.

Figure 11.11 indicates that separation by particle rotation will concentrate the picro-ilmenites in about 20% of the total ilmenites. This is a considerable improvement in concentration, but could still leave some ilmenites with higher magnetic susceptibilities but low rotation indices.

The concentration method suggested by these results is to first remove the more magnetically susceptible ilmenites by attractive separation, and then to remove those with a higher rotation index by a rotating field separation. This method was used in test separations, and the results are given in more detail in chapter 16.

Discussion

It has been mentioned above that, for a ferromagnetic material magnetised to the point of complete removal of domain structure, the ferromagnetic rotation index gives the angle between the particle magnetisation and the external field. The statement of the expected rotation indices (at 0.71) has been based on the assumption that the particle magnetisation is not rotated away from its easy magnetisation direction. This was shown to be a valid assumption (well within expected measurement error) in the case of magnetite (see chapter 4), but may not be valid for ferrimagnetic ilmenite and will certainly not be valid for paramagnetic ilmenite.

As anisotropy forces become lower, this assumption becomes less accurate, and particle magnetic moment is able to be rotated further from the directions of easier magnetisation. This gives lower rotation indices than would be expected from known angles between easy magnetisation directions. In the limit of zero anisotropy, there is no angle between the particle magnetisation and the external field. The particle magnetisation follows the external field direction without placing any torque on the particle.

In ilmenite-hematite the strong magnetic anisotropy is generally between the basal plane and the *c* axis. The anisotropy in the basal plane is relatively weak. As the cation ordering decreases, and anisotropy in the basal plane decreases, the particle magnetisation follows the external field with smaller lag angles. Consequently the rotation indices trend towards zero. Therefore the horizontal trend, across the rotation index contours in figure 11.7, to ferromagnetic rotation indices greater than 1, is all the more noticeable. It is possible that measurement error could reduce most of the rotation indices to below a value of 0.71, but not to 0.15 (i.e. not to the maximum ferromagnetic index possible for a paramagnetic). Particles with a ferromagnetic rotation index above 0.15 must actually be ferrimagnetic, or at least contain a ferrimagnetic phase.

The higher rotation indices, above about 0.71, must indicate either a slow domain wall velocity in these highly magnetically ordered particles (as was also indicated for magnetite), or a rotation field which is of the same order as the coercivity. The curve-fitting method used for magnetite in the previous chapter indicates that no domain wall velocity effects are involved, implying that the high rotation indices are caused by high coercivity

The NSW high-Mg ilmenites, although having a high magnetic moment, generally have low rotation indices. The low rotation indices, while mostly indicating ferrimagnetism, imply weak anisotropy. The fact that they also have the highest Fe^{3+} (from about 0.4 to 0.75 cations)

fits well with the data from Gordon et al (1989), which would place them within the cation-disordered region at formation, and also within the self-reversing range.

The highest rotation indices, by a considerable margin, come from some ilmenites with low Fe^{3+} (between 0 and 0.2 cations). This is in spite of their generally low magnetic moment, and a composition that would normally be expected to be paramagnetic. The high rotation indices imply a high magnetic anisotropy and consequently a cation-ordered state. In chapter 4 it was pointed out that the rotation index is independent of the particle magnetic moment, and, if the moment is due to a ferromagnetic inclusion, of the size of the inclusion. The high rotation indices found in these particles could therefore be accounted for by the presence of fine hematite lamellae within a basically paramagnetic grain.

Most of those ilmenites with very little to trace levels of Fe^{3+} show rotation indices around zero, as well as very low magnetic moments (and magnetic susceptibilities). These ilmenites come within the compositional range where they would be expected to be sufficiently above their Curie temperatures to be magnetically disordered (ie paramagnetic) at room temperatures.

One obvious difference between the picro-ilmenites and other more magnetic ilmenites with a similar Fe^{3+} content, is the substitution of a non-magnetic Mg ion for a magnetic Fe^{2+} ion. Between a third to a half of the Fe^{2+} has been replaced by Mg. The suggestion is that such a level of substitution of a non-magnetic ion has greatly reduced both the magnetic anisotropy and the exchange forces to the point where the mineral is effectively paramagnetic, in spite of the higher Fe^{3+} content.

Conclusions

Analysis results indicate that for the analysed ilmenite particles there are three different substitution series:

(a) The picro-ilmenites, where Mg has replaced Fe^{2+}, with the Ti and Fe^{3+} remaining substantially constant.
(b) Mg ilmenites where two Fe^{3+} ions are replaced by an Mg/Ti or Fe^{2+}/Ti pair.
(c) Mn ilmenites, where Mn has replaced Fe^{2+}, with the Ti and Fe^{3+} remaining substantially constant.

The analysed ilmenites suggest that ilmenites often contain significant amounts of either Mg or Mn, but generally not both at the same time.

The Mg ilmenites, with lower Mg than the picro-ilmenites but higher Fe^{3+}, represent a ferrimagnetic group with weak anisotropy. These particles tend to have a high magnetic moment, but low rotation indices.

Some ilmenites with low to very low Fe^{3+} give very high rotation indices, but low magnetic moments. This suggests the presence of fine hematite lamellae within a generally paramagnetic grain.

Most ilmenites with very low Fe^{3+} behave magnetically as though they are paramagnetic.

The picro-ilmenites form a reasonably distinct magnetic and compositional group. The ferrimagnetic ordering that would normally be expected where significant Fe^{3+} is present has been destroyed by the substitution of the non-magnetic Mg ion, leaving the mineral in a paramagnetic or very weak ferrimagnetic state at room temperature. They have lower rotation indices than all other ilmenites except for those Mn ilmenites with very low or only trace Fe^{3+}, but can be distinguished from the latter by their generally higher magnetic susceptibilities.

A rotating magnetic field separation could be used to roll most ilmenite-hematite grains, leaving behind the picro-ilmenites and those Mn ilmenites with only trace or very low Fe^{3+}. In order to make certain that no picro-ilmenites are separated by this method, the magnetic field rotation frequency should be between 30 and 40 Hz. If it is then possible to carry out a precise separation based on magnetic attraction, the picro-ilmenites, with their higher magnetic susceptibility, could be concentrated further by being lifted out of the Mn ilmenites.

Chapter 12

The Response of Chromite Particles to Rotating Magnetic Fields

Introduction

Chromite is a mineral which is perhaps of as much interest as a petrogenetic indicator as it is as an economic mineral. It is also one of the three main minerals (picro-ilmenite, pyrope garnet, and chromite) that are used as indicator minerals in diamond exploration. Because of this, its range of compositions and their properties have received considerable attention. The spinel group in general, which includes magnetite and synthesised ferrites, is also of interest for its magnetic properties as ceramic magnets, magnetic recording media, transformer cores, and (at least in the early days of computers) for magnetic memory units.

As was the case with the identification and separation of picro-ilmenites within the diamond exploration industry, the separation of kimberlitic chromites for diamond exploration is accomplished by the type of tedious hand separation described in the introduction to the previous chapter. While much is known about the magnetism of chromite, the possible magnetic separation of kimberlitic chromites from other chromites appears to have been given little attention.

The finding, by an exploration company in the Ural mountains in Russia, that a significant proportion of their platinum was contained within a chromite concentrate, and apparently within the chromite itself, has also created an interest in the possibility of using magnetic separation to concentrate the platinum-bearing chromite from the largely barren chromite.

The aim of this chapter is to examine the behaviour of chromite particles in a rotating magnetic field, and to relate this behaviour to the compostion of the chromite. Two specific objectives are to determine whether rotating magnetic field separation methods can be used to concentrate kimberlitic chromites for the diamond exploration industry, and to examine the possibility of magnetically concentrating platinum-bearing chromites.

Approximately 270 individual chromite grains, from seven different source areas were measured for lift and rotation, as described in chapter 8, and then analysed for composition.

(a) Kimberlitic chromites from the Mir kimberlite in Russia (CRA Exploration, sample 2).
(b) Kimberlitic chromites from Ellendale in Western Australia (CRA Exploration, sample 1).
(c) Alluvial chromites from the Meander valley, near Exton, northern Tasmania.
(d) Alluvial chromites from Osmiridium Beach in western Tasmania.
(e) Chromites from platinum ore, from 3 different sites in the Ural mountains.

Chromite Structure, Composition and Magnetic Properties

Structure

The spinel structure, to which chromite belongs, can be thought of in terms of stacked layers. Each layer consists of chains of edge-linked octahedra, with the octahedra chains linked to each other by alternately-facing tetrahedra, as illustrated in figure 12.1. Each layer in the stack is rotated 90^0 relative to the layer below it, and is joined to the layer below by the tetrahedra and vertices of the octahedra. Within a unit cell (four layers) 8 of the tetrahedral sites (A sites) and 16 of the octahedral sites (B sites) are occupied by cations. In the normal spinels the A sites are occupied by X^{2+} cations and the B sites are occupied by Y^{3+} cations (giving 8 X^{2+} cations and 16 Y^{3+} cations). In the inverse spinels there are still the same number of X^{2+} and Y^{3+} cations, but now 8 of the 16 Y^{3+} cations occupy the tetrahedral A sites, while the B sites are filled with the remaining 8 Y^{3+} actions and the 8 X^{2+} cations.

Figure 12.1

One of the four layers making up the spinel structure

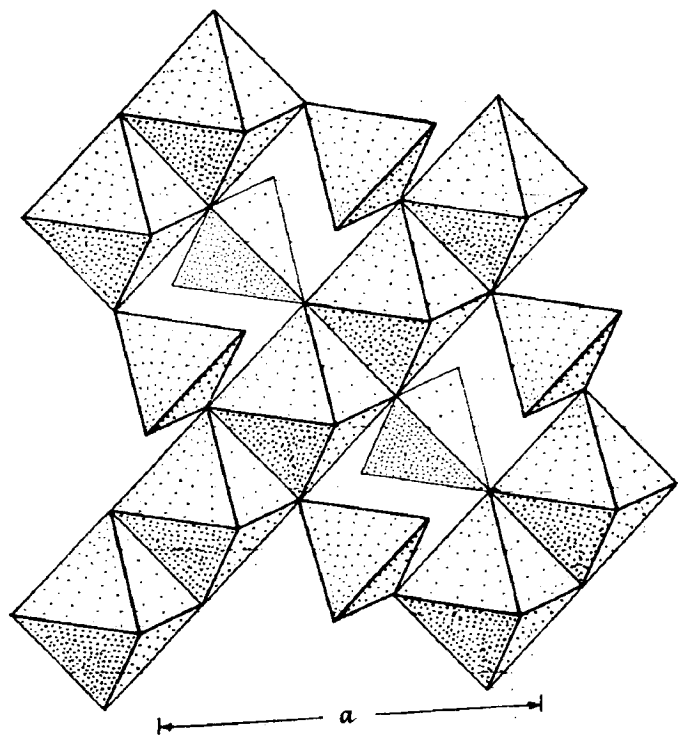

(From Batty, 1972)

Composition

In pure chromite, $8(Fe\ Cr_2O_4)$, the A sites are occupied by Fe^{2+} while the B sites are occupied by Cr^{3+} ions, but most chromites encountered in the field contain other ions such as Al, Fe^{3+}, and Mg. The substitution of these ions for Fe^{2+} and Cr alters the crystal lattice

dimensions and changes the exchange energies in the crystal. Hugh et al (1984) examined the cation distributions in spinels, including the $FeCr_2O_4$ - Fe_3O_4 system, and developed a model to account for cation distributions and thermodynamic properties in oxide spinels. While Mg keeps to the tetrahedral sites and Cr only occupies octahedral sites, the site preference for the Fe^{3+} ion begins to change from octahedral to tetrahedral about one third of the way between $FeCr_2O_4$ and Fe_3O_4 compositions, leading eventually to the full inverse spinel arrangement of cations found in magnetite. The effect of this change in site preference on the crystal lattice is illustrated in figure 12.2, which plots the measured and calculated lattice constants for the system.

Figure 12.2

Measured and calculated lattice constants for the $FeCr_2O_4$ - Fe_3O_4 system

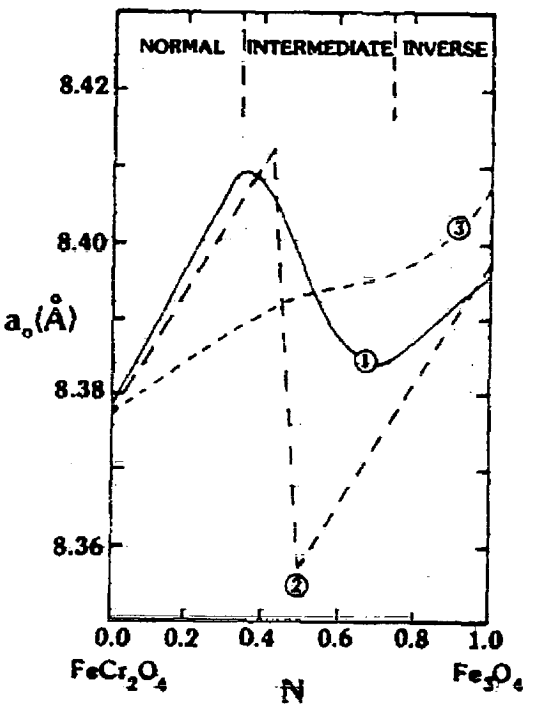

Lattice constant curves for $FeCr_2O_4$ - Fe_3O_4
(1) Experimental data (Robins et. al., 1971): (2) Calculated for equilibrium equilibrium cation distribution at 300 K: Calculated for equilibrium cation distribution at 1000 K.

(From Hugh et al, 1984)

Figure 12.3 shows changes in the cation distribution between the tetrahedral (A) and octahedral (B) sites for the $FeCr_2O_4$ - Fe_3O_4 system. In region 2 (the intermediate region in figure 12.2) the concentration of Fe^{3+} in B sites decreases until most of the A sites are occupied by Fe^{3+}. Above about 0.66 Fe^{3+} cations the chromite moves into the intermediate zone of figure 12.2 or the region 2 of figure 12.3.

Figure 12.3

Distribution of Fe^{2+} and Fe^{3+} between A and B sites for the $FeCr_2O_4$ - Fe_3O_4 solid solutions

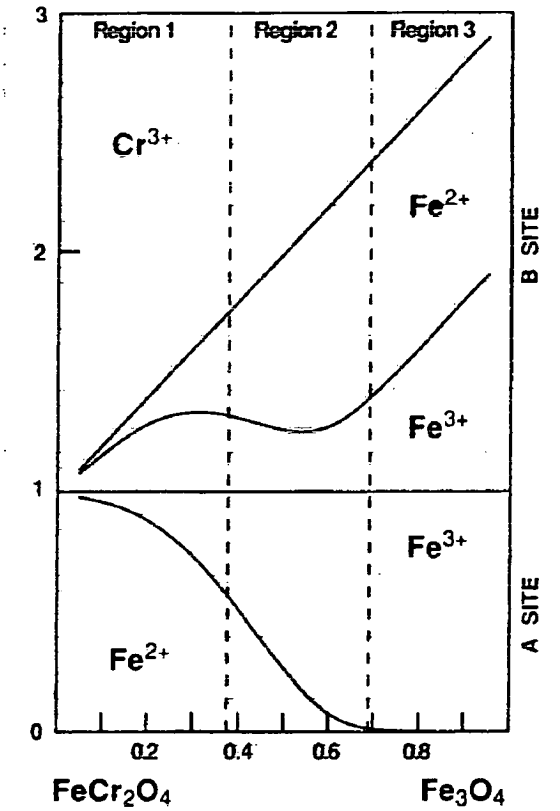

(From Sack and Ghiorso, 1991)

Talkington et al (1983) have identified platinum group mineral inclusions within chromite. These inclusions were less than 20 μm in diameter (often only a few μm), and included the sulphides of Ru, Os, and Ir, and Os/Ir/Ru alloy. Although Pt and Pd were expected neither was found. The chromites also contained silicate and hematite inclusions. Unfortunately Talkington does not give compositions for the host chromite, except to state that all chromites came from the ultramafic zone of a feeder conduit referred to as the Bird River Sill.

Magnetic properties

Krupicka and Novak (1982) have provided a good summary of the magnetic properties of oxide spinels, and most of what follows is summarised from this source.

The A and the B sites may be considered as forming two different sub-lattices. Because the cations in the spinel structure are all separated by oxygen ions, there is little direct exchange between cations and most of the interaction is by indirect exchange (super-exchange) across the oxygen ions. Exchange interactions are strongest between the two sub-lattices, rather than within each sub-lattice. Exchange interactions between magnetic

ions in the A sub-lattice are weak, but significant interaction can occur between ions in the B sub-lattice. If there are magnetic ions in both sub-lattices, the strength of the exchange interaction will, in most cases, be in the order A-B, B-B, A-A.. Most of the exchange integrals are negative, giving an antiferromagnetic ordering. Of course this depends on the particular ions involved, and in some cases a ferromagnetic ordering can result.

If only the A sub-lattice is occupied by magnetic ions, then the magnetic ordering is always antiferromagnetic, but because the A-A interactions are very weak the Neel temperature is very low (e.g.6 K in $MnAl_2O_4$). Therefore such spinels are paramagnetic at room temperatures.

If only the B sub-lattice contains magnetic ions, the magnetic ordering is usually antiferromagnetic. In some cases, involving ions with valencies of +4 and +2, the magnetic ordering is ferromagnetic. Neel temperatures vary from about 15 K to as high as 200 K. These spinels are also paramagnetic at room temperatures.

If both the A and B sub-lattices contain magnetic ions, the exchange interaction can be quite strong, and a collinear ferrimagnetic ordering results. The Neel temperature here can be well above room temperature (e.g. magnetite).

If the exchange interaction between A-B ions becomes roughly equal to the exchange interaction between A-A ions or (more likely) between B-B ions, canted spin arrangements appear. This can occur through the substitution of diamagnetic ions (such as Zn). Such a substitution, if Zn occupies more than about 40% of the A sites, lowers the A-B interactions below the strength of the B-B interactions, and a canted ferrimagnetic ordering is produced. Neel temperatures in this case are well below room temperature.

In chromite, $FeCr_2O_4$, substitution of Mg for Fe^{2+} into the A sites, and Al for Cr into the B sites, can produce 'gaps' in the cation exchange interaction so that regions within a crystal become magnetically isolated from each other. In more general terms, the substitution of non-magnetic ions into both the A and B sub-lattices can produce a type of 'domain' structure within a spinel, where the 'domains' here are regions that are magnetically isolated from each other. Such a magnetic ordering appears to be paramagnetic to most measurements, and is referred to as a spin-glass. Severance et al (1993) have reported on this magnetic ordering in a chromite of the composition $Fe_{0.36}Mg_{0.62}(Cr_{0.62}Al_{0.36})_2O_4$. and presents a diagram (figure 12.4) illustrating the types of magnetic ordering that can occur in normal spinels.

Figure 12.4

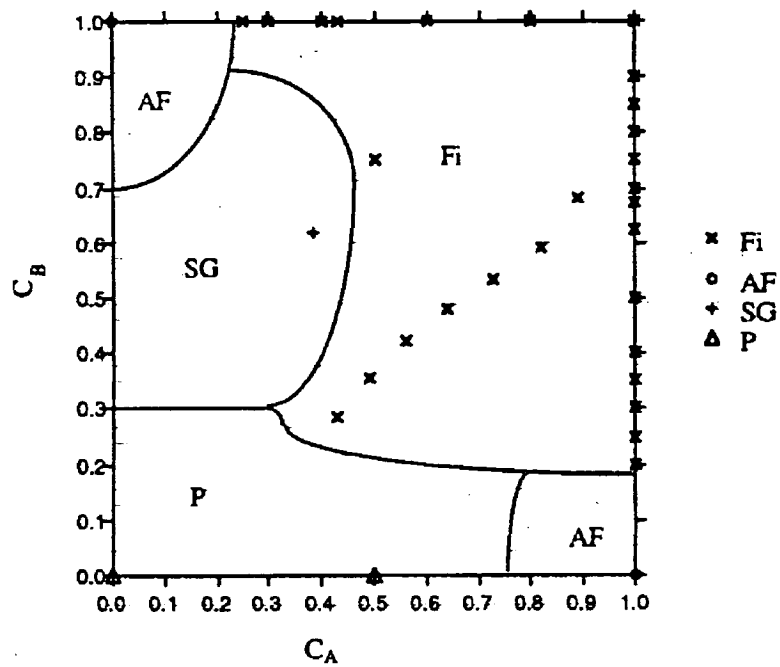

Modified magnetic phase diagram for normal spinels showing the position of the single-crystal chromite in the spin glass region. C_A and C_B are the respective magnetic cation concentrations of the A and the B sites. P = paramagnetic; AF = antiferromagnetic; Fi = ferrimagnetic; and SG = spin glass. The ferrimagnets in the nonborder region are not chromite.

(From Severance et al, 1993)

Most mineral compositions that may be collectively referred to as chromite are paramagnetic at room temperatures, and are magnetically isotropic. They will not respond to a rotating magnetic field. However substitutions of Fe^{3+} for the Cr ions, as indicated above, can lead to phases of intermediate and inverse spinel arrangements with strong ferrimagnetic ordering. The presence of such restricted regions within chromite grains may lead to a resultant magnetic anisotropy of somewhat variable nature.

Analysis Results for Measured Chromite Particles

Most of the chromite particles were analysed from a single 10 μm diameter spot. These analysis results are given in appendix C, together with the lift and rotation magnetic fields. Some of the examples from the Urals were analysed at 10 spots across the grain at 15 μm intervals. These results are given in appendix D. Several of the chromites from the Urals were analysed with a 10μm spot on a 15 x 15 μm grid over an area 150 x 150 μm, and these results are given in appendix E.

Calculations of the Fe^{2+} and Fe^{3+} have been based on the formula described by Finger (1972).

The particles plotted in the following figures are those for which both composition and magnetic measurements have been made. Other chromites have been analysed, in particular from the north-east of Tasmania, but have not been measured for magnetic properties. Analyses for the latter particles are referred to in chapter 15.

Single analyses

The analysis values given here are based on the data in appendix C. In some cases, where the spot analysis differs significantly from the average analysis indicated by line analysis or grid analysis of the same particle, a more representative analysis has been substituted from appendix D or E.

Figure 12.5 plots the Mg cation numbers against the Fe^{2+} cation numbers, and shows that, as expected, Mg has mainly substituted for the Fe^{2+}. This substitution involves the A sites only. There is a group of particles, with between 0.4 and 0.65 Mg cations, that appears to deviate from this trend and, as figure 12.7 illustrates, represent particles with an ulvospinel (Fe_2TiO_4) component. As this group consists entirely of the kimberlitic chromites (CRA Ellendale chromites), it is of some interest.

Figure 12.5

All Measured Chromites. Plot of Mg v Fe2+

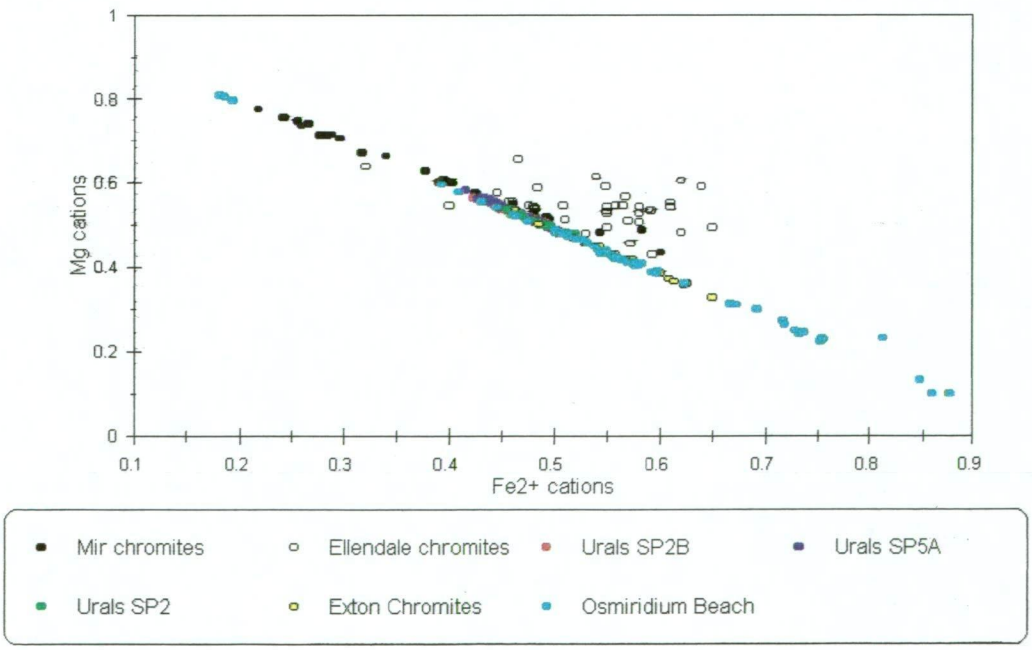

Figure 12.6 plots Fe^{3+} against Cr + Al ions, illustrating the expected trend for Al, Cr and Fe^{3+} ions to substitute for each other in B sites. Once again it is the kimberlitic chromites, and in particular the Ellendale chromites, that deviate from this trend. These chromites appear to have some of their extra Fe^{2+} in the B sites.

Figure 12.6

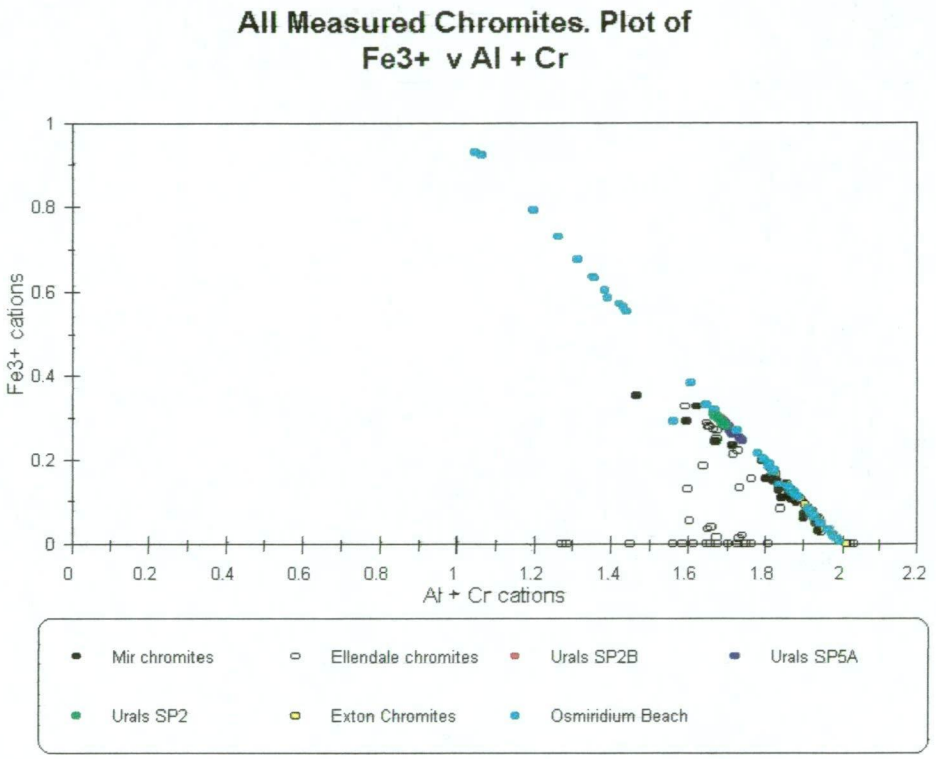

Figure 12.7 below examines the Ti and Si content of the chromites. The deviation of the Ellendale chromites from the trends shown in figures 12.5 and 12.6 now appears to be due to the entry of some Ti and Si into the structure. The field of all the measured kimberlitic chromites (together with the high-Al chromites) now shows up as a high-Mg group (>0.5 cations) which may contain Si and Ti as a trend towards ulvospinel.

The Osmiridium Beach chromites, which have plotted above the CRA kimberlitic chromites in figure 12.7, differ from the kimberlitic chromites by containing high Al.

Figure 12.7

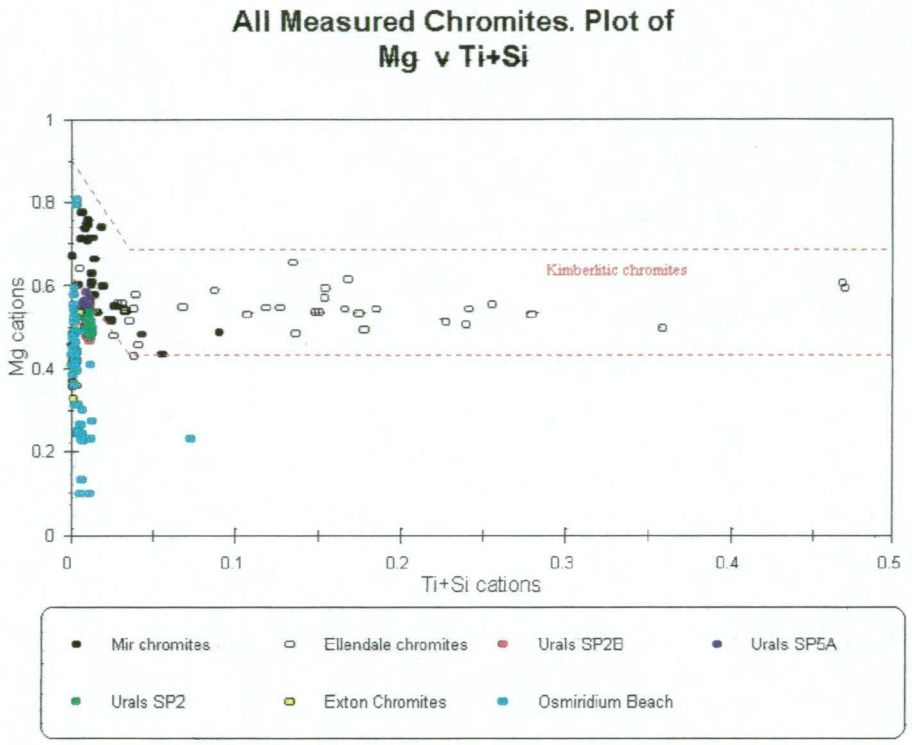

Figure 12.8 plots the compositions of all measured chromites on a conventional Fe/Cr ratio diagram, while figure 12.9 plots the particles according to the approximate number of magnetic ions in each sub-lattice. The number of Cr and Fe^{2+} ions approximate the number of magnetic ions in the B and A sub-lattices respectively, at least for the low Fe^{3+} chromites which make up the majority of those included in this data. The magnetic phase divisions of Severance et al (1993) have been included in figure 12.9. Although the Si, Ti and re-distributed Fe^{2+} ions in the Ellendale chromites, and the tendency to some inversion for the more magnetic chromites, will change site occupancy a little, these changes will not alter many of the predicted magnetic phases.

It is interesting to note that most of the chromites from the second CRA Kimberlitic sample (Mir chromites) fall in the spin glass region (SG), while most of the first CRA sample (Ellendale chromites) plot in the ferrimagnetic region (Fi). Due to the presence of significant Mg, Si and Ti in the Ellendale chromites (which is not considered in figure 12.9) the magnetic divisions, as drawn, may not be applicable. The plotted position of the ferrimagnetic chromites in figure 12.9 can not be used to reliably predict the strength of the particle ferrimagnetism because the diagram does not consider the Fe^{3+} ions or the presence of any Fe^{2+} in B sites.

Figure 12.8

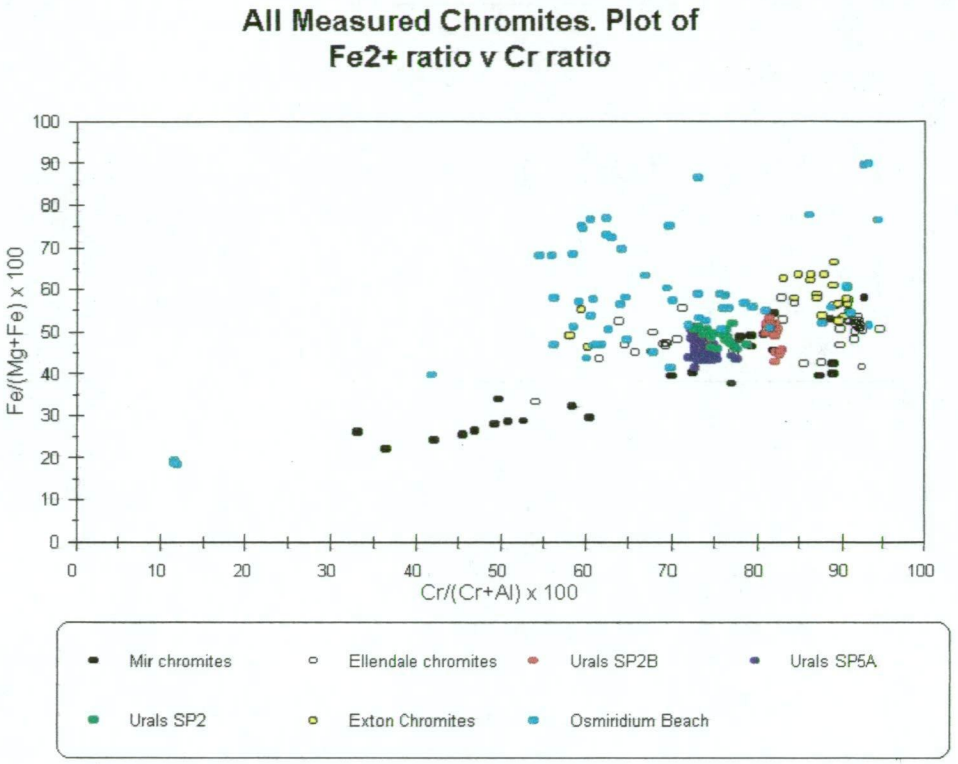

Figure 12.9

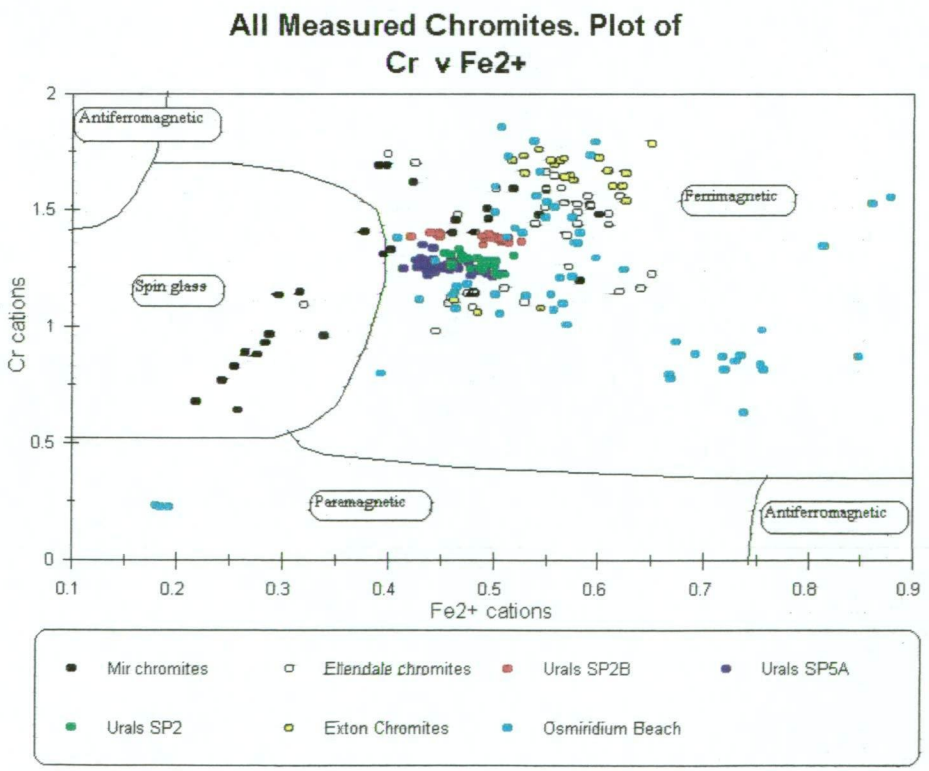

Grain maps

Previous work on the Ural mountains samples (laboratory not known) had involved magnetic separations of the ground rock, and analysis of the magnetic concentrate. The method of magnetic separation used is not known, but analysis of the chromite concentrates for Pt had produced:

SP2 sample, 0.85 ppm Pt
SP2B sample, 0.68 ppm Pt
SP5A sample, 0.2 ppm Pt

Because the average magnetism (attractability) of the chromites from the three samples was in the same order (SP2 chromites were the most magnetic), there was the suspicion that Pt may be contained within the chromites, and the more magnetic chromites may also contain the most Pt. The more magnetic chromites were also very responsive to magnetic field rotation (high rotation indices), and it was thought that this may be caused by Fe/Pt inclusions.

Chromites from the SP2 (most magnetic) and SP5A (least magnetic) samples were chosen to examine this possibility. These grains were measured for magnetic properties and then initially analysed for chromite composition and Pt content at 10 points along a 150 μm line. All Pt analyses used a 10 μm spot size, an electron potential of 20 kV, and a current of 100 nA. The results of the analyses are given in appendix D (magnetic data on these grains is given in appendix C). Pt was detected at isolated points within some chromites, at levels from 100 ppm to 2800 ppm (see appendix D). To give the observed Pt content, any metallic Pt would have been considerably less than 0.5 μm in diameter. Based on the Pt analysis values obtained, the average Pt content of the chromites appeared to be around 10 to 15 ppm. Ignoring the one Pt result of 2800 ppm (grain 74), which may have just been a 'lucky hit', there appeared to be little difference in average Pt between the SP2 and SP5A chromites.

Therefore there remained the problem of why some of the chromite grains were highly magnetic and had high rotation indices, when chromites of an apparently similar composition were very weakly magnetic with rotation indices close to zero.

Grid analysis maps (as described above) were done on two of the chromite grains (grains 60 and 74) from the Urals SP2 sample. Grain 60 was one of the most magnetic of the chromites, while grain 74 was only weakly magnetic, but appeared to contain some Pt in an earlier analysis (see appendix D).

The results of the grid analysis for Pt on grain 74 are shown in figure 12.10, and the Fe^{3+} composition over the same grid are given in figure 12.11. Grain 74 appears to be fairly uniform in composition, except for the measured Pt inclusions. These inclusions do not seem to have significantly affected the magnetic properties of the grain.

Figure 12.10

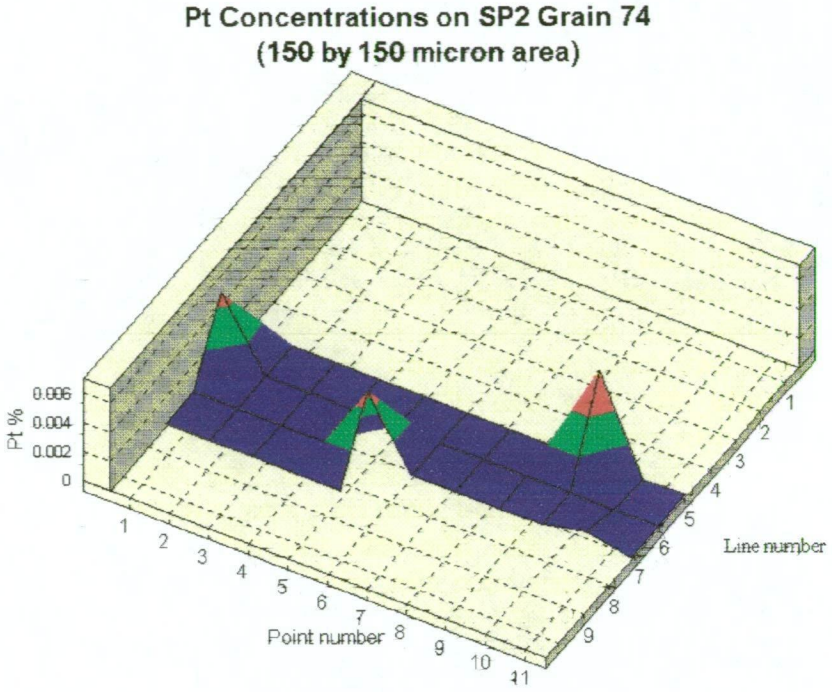

Figure 12.11

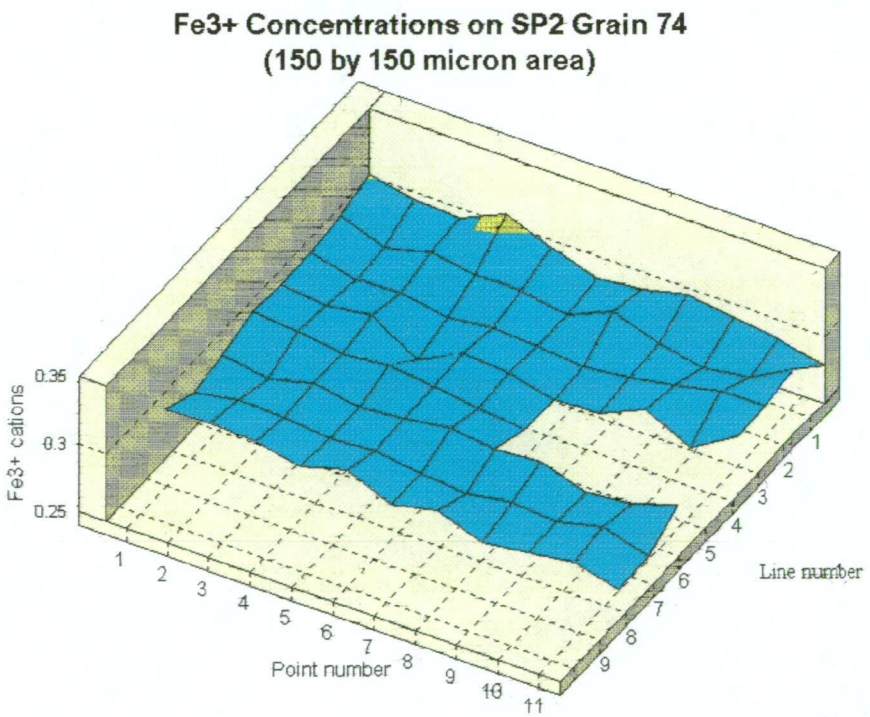

No Pt had been observed in the initial line analysis of grain 60, but the line analysis had revealed considerable variation in Fe content across the particle, and the particle had been measured as one of the most magnetic.

Figure 12.12 shows the variation of Fe^{3+} across the polished surface of grain 60. The red coloured peaks in the map indicate points where the Fe^{3+} content is within the intermediate range between normal and inverse spinel structure, predicted in figures 12.2 and 12.3. Because of this, grain 60 would be expected to contain regions within the crystal that are strongly ferrimagnetic.

Figure 12.12

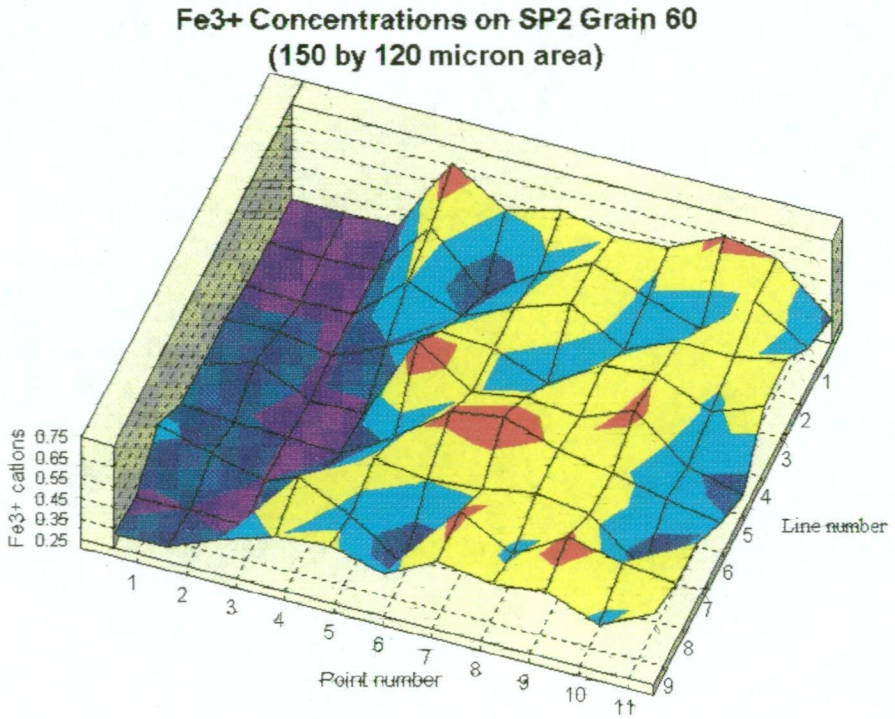

In order to obtain a more complete map of variations in grain composition, a pixel-by-pixel analysis of the grain was carried out, by electron microprobe, for Fe, Cr and Al. The three images were then combined to form an RGB image. Fe formed the red channel, Cr the green, and Al the blue. This type of analysis is qualitative rather than quantitative, but has the advantage of producing a good overall picture of the shapes and sizes of the compostional patterns within the grain. The results of this mapping are shown in figure 12.13.

Figure 12.13

A qualitative compostional map of SP2 grain 60

The approximate area mapped in figure 12.12 by the line analysis method is outlined.
Blue coloured areas are high in Al, Green areas are high in Cr, and Red areas are high in Fe.

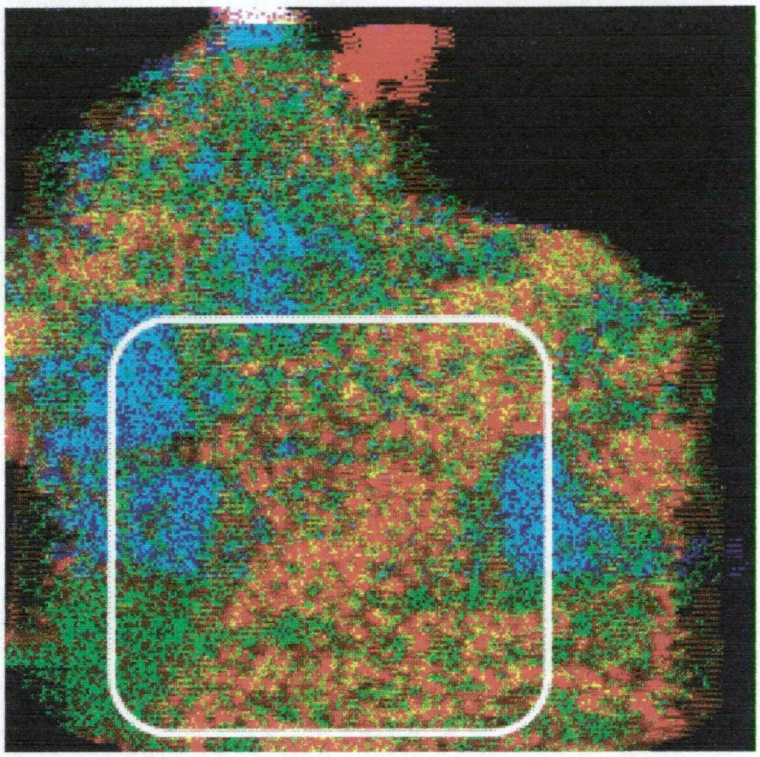

Unfortunately it was not possible to also map the grain for Pt, because of the extended analysis time required at high currents, and its possible effects on later microprobe operation.

There appears to be little evidence that the high magnetic susceptibilities and rotation indices for some of the Urals chromites is due to the presence of Fe/Pt inclusions. It appears to be caused by the presence of regions within the grains which have compositions suggesting an intermediate state between normal and inverse spinel. There is also the interesting suggestion, which has implications for exploration, that rocks which contain this type of chromite may also be more likely to contain platinum.

Results of Lift and Rotation Measurements

Figure 12.14 compares the magnetic susceptibilities and ferromagnetic rotation indices for the measured chromites. These quantities were determined as described in chapters 4 and 8. The two particles examined by analysis on a 15 by 15 μm grid, and described above, are indicated.

Some of the Osmiridium Beach chromites are interesting because of their very high magnetic susceptibilities but quite low ferromagnetic rotation indices. These particles have an Fe^{3+} content of about 0.6 cations or above, and an Fe^{2+} content above 0.65, and are therefore situated just on the borderline of the intermediate range between normal and inverse spinel structure described by Hugh et al (1984).

The SP2 sample from the Urals also contains very magnetic chromites, but these are magnetically distinct from the highly magnetic Osmiridium Beach chromites, due to their higher rotation indices. Two of these particles have apparent ferromagnetic rotation indices greater than 1, which is physically impossible. Values greater than 1, for reasons already discussed with reference to the magnetite and ilmenite results, must be due to measurement error, high coercive force, or domain wall velocity effects. Applying a possible measurement error of 30% places these particles within the range of possible rotation indices, but still too high for the maximum index of 0.71 for the case of a uniaxial anisotropy, and much too high for a cubic anisotropy. As was the case with magnetite, the only reasonable explanations for such high rotation indices are a rotating field close to the domain wall critical field, and slow domain wall velocity.

Figure 12.14

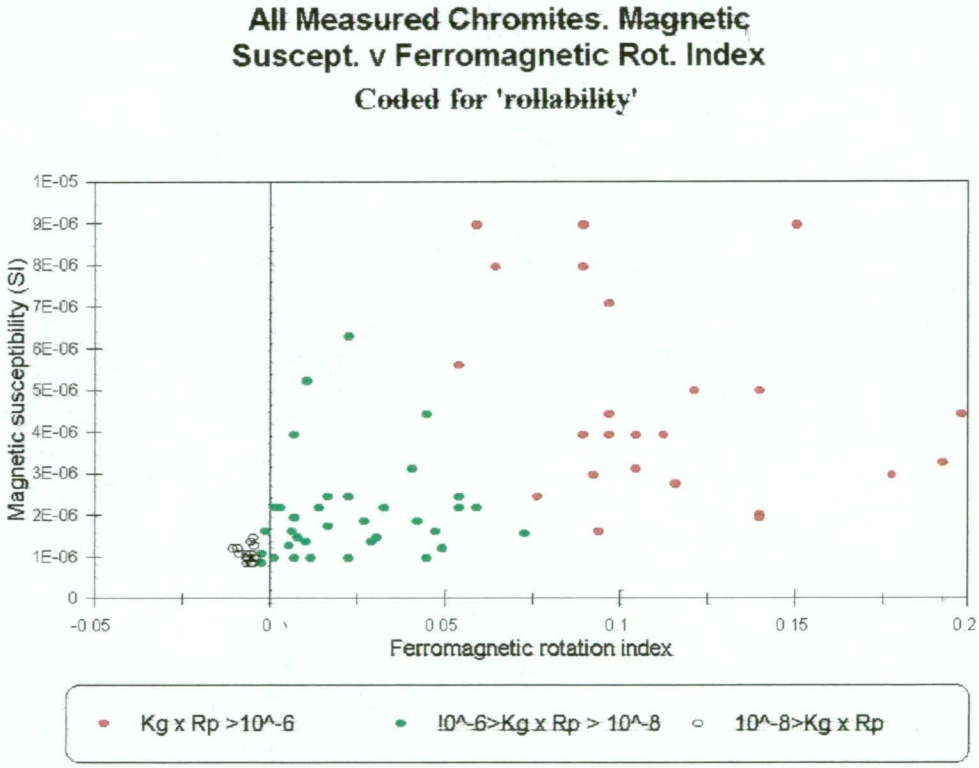

Figure 12.15 plots the inverse lifting fields for the chromites against the ferromagnetic rotation index. This type of diagram was introduced in chapter 4. The particles are colour-coded according to location. The trend across the rotation index lines is obvious. It is important to consider what such a trend could mean. If a particle has an increase in magnetic ions, but the same magnetic anisotropy, then it may lift easier and rotate easier, but it will only plot further up the rotation index line because the ratio of lift to rotation remains constant. Therefore, for example, a quartz particle with a small magnetite inclusion will plot on the same rotation index line, but lower down, as a quartz particle with a larger magnetite inclusion. For particles to plot on different rotation index lines implies that they have different magnetic anisotropies, different coercive forces (as Carmichael, 1961, determined for ilmenite-hematite) or different (slow) domain wall velocities. The maximum attainable rotation index for the strongly rotating chromite particles, if they have a cubic anisotropy similar to magnetite, and if

coercive force and domain wall velocities are not considered, would be expected to be 0.38. However, if the particles contain thin lamellar regions high in Fe, as may be suggested in figure 12.12, they could well show a uniaxial shape anisotropy, with the expected rotation index of approximately 0.7.

In figures 12.14 and 12.15 the particles from some samples can be identified as following slightly different magnetic trends, and can also be identified as having distinct chemical compositions, Because the magnetic characteristics must depend on the detailed cation distributions, more detailed and accurate work may be able to tie the chemical compositions and magnetic properties together to arrive at better petrogenesis models. This has previously been suggested by Severance et. al. (1993).

Figure 12.15

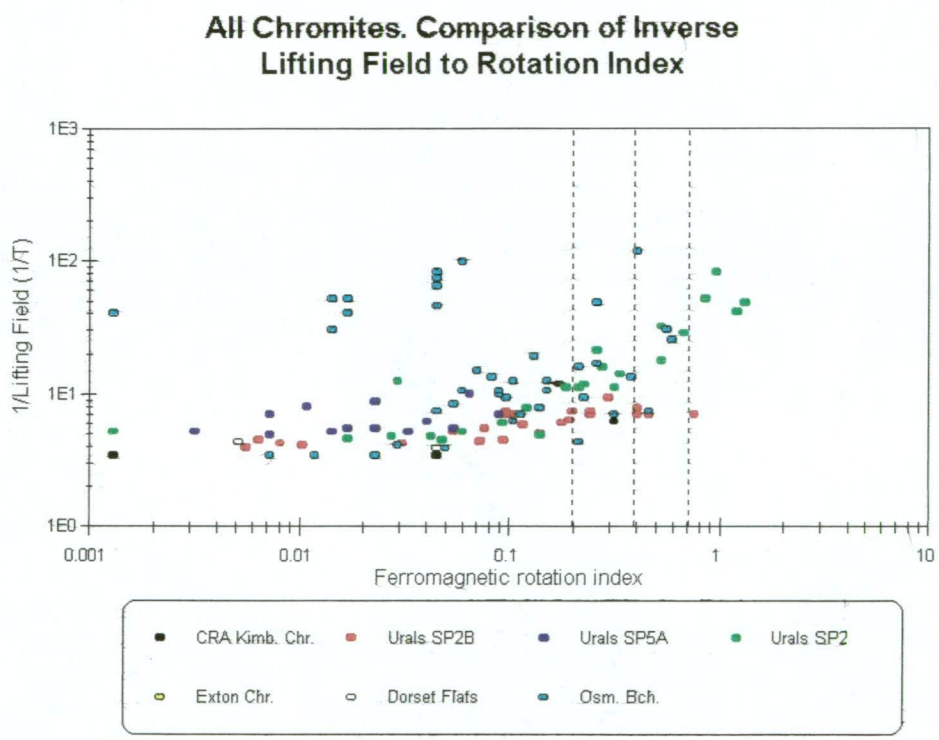

Although most of the kimberlitic chromites plot amongst the "non-rotating" particles (and consequently do not plot at all in figure 12.15), three of them show uncharacteristically high rotation indices. The two most magnetic of these come from the Mir sample, but otherwise they are not able to be recognised as having any composition or physical characteristics different from the other kimberlitic chromites. At the moment it is considered that they must contain some undetected inclusions.

In a practical magnetic mineral separation method using rotating magnetic fields, where the particles are both lifted and rolled, both the magnetic lift on a particle (which reduces interaction with a surface) and the rotational torque that can be placed on the particle

are important. These two factors have been combined in the diagrams below, by using their product. This product is then a measure of the ease with which a particle may be magnetically rolled.

The plot of Cr content against Fe^{2+} content in figure 12.16 (which should be compared with figure 12.9 above), shows that the high Mg members of the Ellendale chromites which fall within the spin-glass region of the magnetic phase diagram of Severance et al (1993) are in the "non-rotating" group. This would be expected of particles with isolated magnetic regions.

Figure 12.16

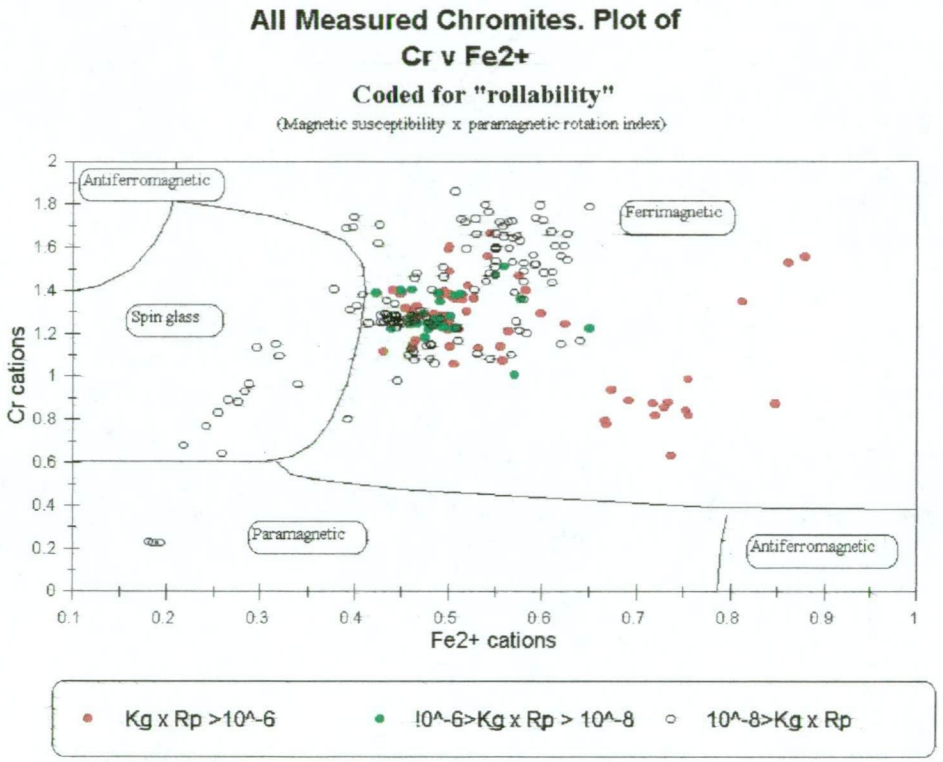

Figure 12.7 shows the present "non-rotating" chromite compositional field on the normal Cr - Fe^{2+} ratio diagram. The field superimposed in figure 12.17 includes all of the kimberlitic chromite field, but also includes those particles that rotated strongly due to the presence of thin inversion lamellae. In particular it includes the diamond inclusion compositions, in which the particles are all indicated as being non-rotating.

Figure 12.17

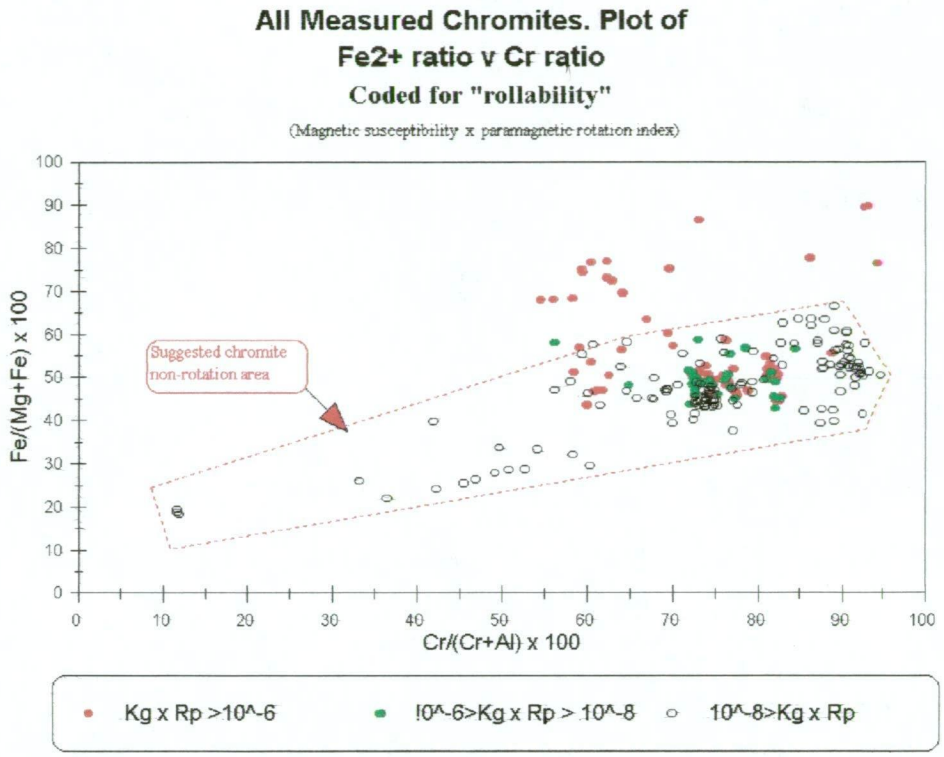

The very magnetic Urals chromites (SP2, SP2B and SP5A), which fall within this non-rotation field, may be seen as forming under different and somewhat varying conditions to those applying to kimberlitic chromites. This is shown by the varying composition across the particle in figure 12.13.

It was mentioned above that some chromites have high magnetic susceptibilities but low rotation indices, while other chromites are the other way around (see figure 12.14). It is interesting then to examine changes in the relationship between magnetic susceptibility and rotation index as the composition of the chromite changes. Such changes are illustrated in figure 12.18, where the relationship between these two quantities are examined as the Fe^{3+} content of the chromite changes. The general trend is for the rotation/susceptibility ratio to decrease as the Fe^{3+} content increases. This is a very similar trend to that seen for the ilmenites in chapter 11. Due to their variable and complex compositional structure, the Urals SP2 and SP2B samples have been excluded from this diagram. It is noteworthy perhaps that the analysis results for the latter chromites places them (and the SP5A chromites) at an Fe^{3+} content in figure 12.18 immediately preceeding the decrease in the rotation/susceptibility ratio.

The relationship between the ferromagnetic rotation index and the magnetic susceptibility appears to be controlled by the Fe^{3+} content of the chromite. Between 0.35 and 0.6 Fe^{3+} cations the magnetic anisotropy of the chromite particles decreases relative to the magnetic susceptibility (which actually increases). This range in Fe^{3+} content fits well with Robbins' data illustrated in figure 12.2 (from Hugh et al, 1984). In fact the shape of the whole graph matches well with the graphed experimental data shown in figure 12.2.

Figure 12.18

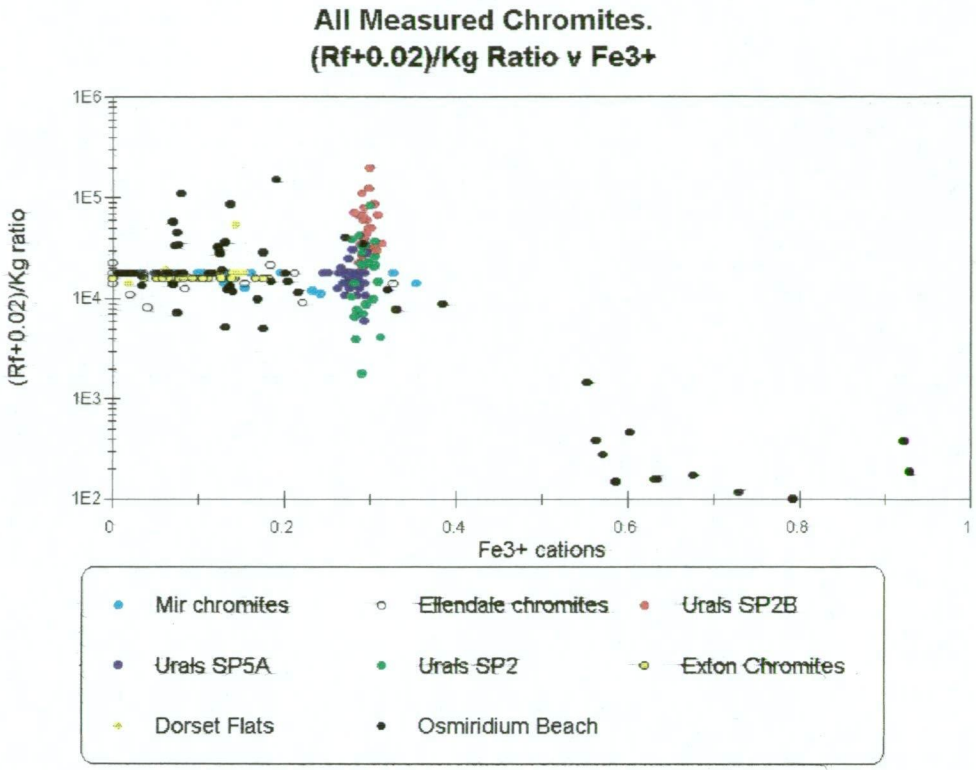

Discussion and Conclusions

Discussion

It is obviously difficult and confusing to try to group chromites (or any other natural mineral) by considering only one particular cation. A two-dimensional discrimination based on two different ions, or two different ratios between ions such as the Fe^{2+} and Cr ratios (figure 12.8), produces a better picture. In the same way it is difficult to try to magnetically group or discriminate between chromites by considering only magnetic susceptibility. Information needs to be included about the type of magnetic ordering or about the relationship between the magnetic moment and the crystal structure. This is done here by using the rotation index.

Compositional control of chromite magnetic properties is obvious in some cases but apparently not in others (e.g. the Urals samples). Cases where chemical composition has clearly determined magnetic properties include:

(a) Chromites with Mg>0.5 cations. These have low magnetic susceptibilities and low rotation indices.

(b) High Fe^{2+}-Fe^{3+} chromites. These have high magnetic susceptibilities, but low rotation indices. Compositionally they contain $Fe^{2+} > 0.65$ and $Fe^{3+} > 0.5$.

(c) Those chromites containing small elongated regions of high Fe^{3+}, which probably represent regions of inversion, or regions that are intermediate between normal and inverse spinel. These have high magnetic susceptibilities, and high rotation indices as well.

Almost all the kimberlitic chromites fall within group (a), which has very low magnetic susceptibilities and very low rotation indices.

Conclusions

Differences in the rotational and susceptibility chracteristics of chromite grains can both be related to chemical composition. Chromites with high Mg have low magnetic susceptibilities and low (or zero) rotation indices. Chromites with high Fe^{3+} are very magnetic, and the amount of Fe^{3+} in the chromite particles determines the relationship between the magnetic susceptibility and the rotation index, with higher Fe^{3+} giving higher magnetic susceptibilities but lower rotation indices.

The Kimberlitic chromites generally have Mg values above 0.5 cations, and therefore have low susceptibilities and low (or zero) rotation indices.

Chromite particles that contain narrow regions or thin lamellae of inverse or intermediate composition tend to have high magnetic susceptibilities and high rotation indices.

The measuring of particle magnetic susceptibility and rotation characteristics can therefore be used to place chromite particles in one of at least three different compositional groups, with one of these groups including the kimberlitic chromites.

Alternatively, a magnetic mineral separation method that employed combinations of magnetic attraction and magnetic rotation could be used to isolate chromites from any one of the three main magnetic groups mentioned above, while a magnetic separation method employing only magnetic attraction could not distinguish between chromites with high Fe^{3+}, and those containing only narrow regions high in Fe^{3+}.

In a rotating field separation designed to concentrate picro-ilmenites, the kimberlitic chromites would remain with the picro-ilmenites, and would themselves be concentrated by the removal of any high Fe^{3+} chromites and chromites with any inversion or intermediate phases.

Chapter 13

The Response of Almandine Garnets to Rotating Magnetic Fields

Introduction

Garnets have been used as gems and in the manufacture of jewelry. Garnets have also been used as a bearing material in watches and other very small machinery. The hardness of garnets, and the sharp and irregular shapes when they are fractured, has made them popular as an abrasive. This is their greatest use at the present. More recently pyrope garnets (Mg-garnets) have been used as one of the three main indicator minerals for diamond exploration, because they form under similar conditions to those required for diamond formation, and are found as inclusions within diamonds.

Most pyrope garnets can be neither lifted nor rotated by the equipment used here to measure the magnetic characteristics of the ilmenites or chromites. In this chapter the main interest is in the more magnetic and commonly occurring almandine (Fe, Al) garnets. Some almandine garnets can be rotated in a similar way to that observed for iron, magnetite, ilmenite and chromite, but many almandine particles exhibit a rotation that is perpendicular to the external magnetic field rotation. This type of individual particle rotation does not seem to have been reported before. It is initially puzzling, and demands an explanation.

This chapter presents the limited data acquired so far. The theoretical consideration in chapter 5 indicates that particle rotations which have their axis perpendicular to the field rotation axis should be possible in almost any ferromagnetic mineral particle in a rotating magnetic field. Such rotations are indicated from observations of magnetite rotations detailed in chapter 10. The difference between the "perpendicular" rotations in almandine and magnetite is that, in almandine, they can be observed without the presence of simultaneous rotations parallel to the field rotations.

The Structure and Composition of Garnets

The general garnet formula can be written as $(Fe^{2+},Ca,Mg,Mn)_3(Al,Ti,Cr,Fe^{3+})_2Si_3O_{12}$. The structure of garnet is illustrated in figure13.1

Figure 13.1

The structure of grossular garnet. Projection on (001)

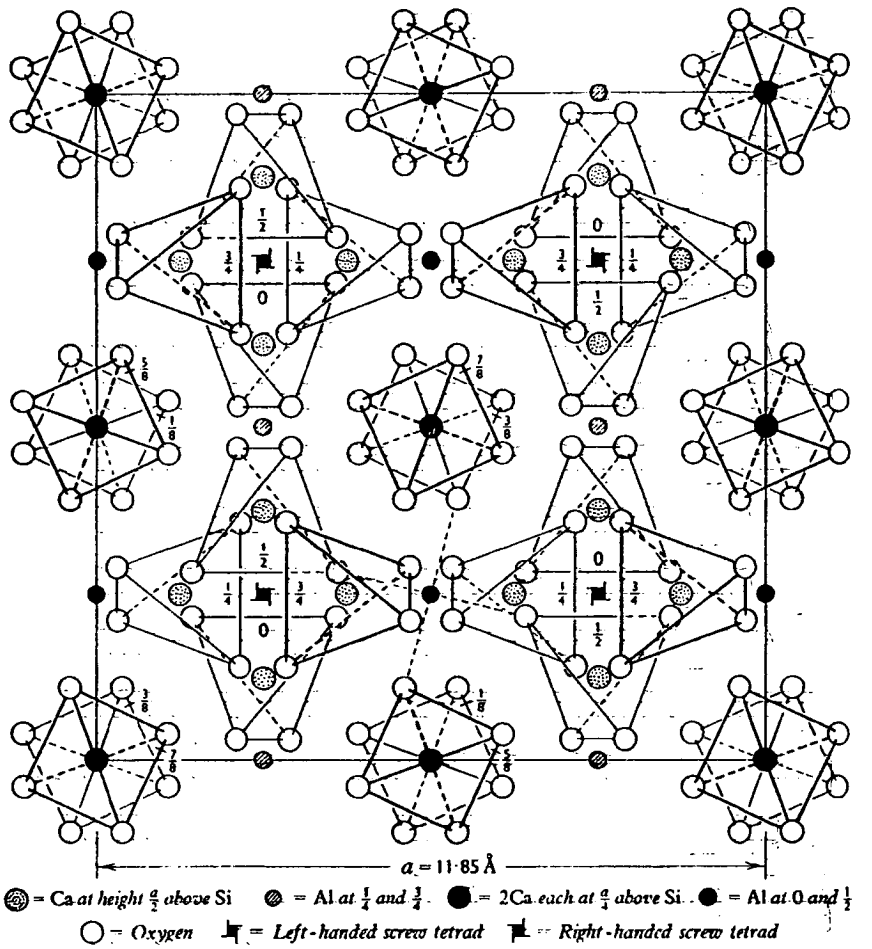

(From Deer et al, 1965)

Only the Si-O tetrahedra are shown in figure 13.1. These are arranged in vertical (i.e. out of the page in figure 13.1) columns and spirals, which could be described as:

(a) a column with two tetrahedra stacked, one above the other, and rotated 45^0 with respect to the one below, with Ca (or Mg or Fe^{2+} or Mn) in between the tetrahedra. In one column the tetrahedra are at heights of a/8 and 5a/8 within the unit cell, and in the adjacent column they are at heights of 3a/8 and 7a/8.

(b) a spiral with tetrahedra arranged at 90^0 intervals at heights of 0, a/4, a/2, 3a/4 within the unit cell. Adjacent spirals are in opposite directions.

The spirals and columns are arranged alternately across the diagonals of the cell base. Al (or Cr or Fe^{3+} or Ti) occupy the centre of octahedral sites which join with the tetrahedra of both the columns and the spirals. The octahedra are not drawn in figure 13.1.

Cations (or Mg etc.), as well as occupying sites between the tetrahedra of the columns, also occupy sites in the spiral a/2 above each Si. The latter sites are in the spaces between the octahedra-tetrahedra network.

Figure 13.2 shows a slice through the garnet structure, about half way up through the plan shown in figure 13.1. This shows the arrangement of the octahedra, and how they join to the spirals and columns of tetrahedra.

Figure 13.2

A section through the garnet structure of figure 13.1
Showing locations of the octahedra

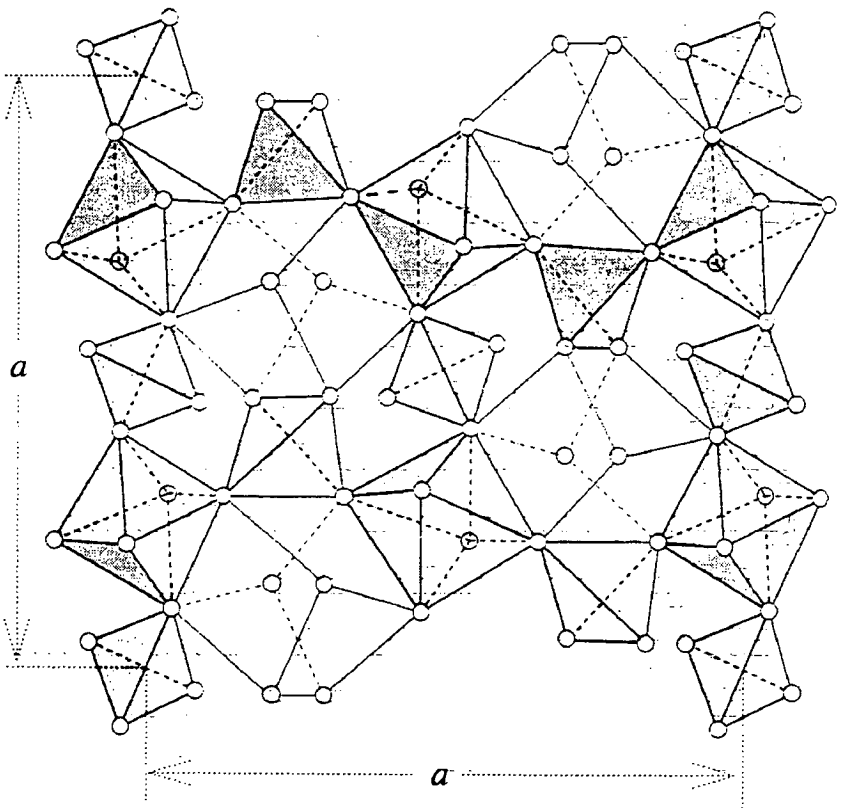

(From Putnis, 1992)

The divalent cations are located in the centre of the distorted cubic spaces, each surrounded by 8 oxygen ions. The distorted cubic cation sites are referred to as the A sites, while the octahedral cation sites are referred to as the B sites.

Garnets are initially classified into two main series:

(a) $(Fe^{2+},Mg,Mn)_3Al_2(SiO_4)_3$

(b) $Ca(Al,Cr,Fe^{3+},Ti)(SiO_4)_3$

Each of these series is then be split up and named according to the dominant A site ion (for group (a)), or the dominant B site ion (for group (b)).

(a) almandine $Fe^{2+}{}_3Al_2(SiO_4)_3$
pyrope $Mg_3Al_2(SiO_4)_3$
spessartine $Mn_3Al_2(SiO_4)_3$
(b) grossular $Ca_3Al_2(SiO_4)_3$
andradite $Ca_3(Fe^{3+},Ti)_2(SiO4)_3$
uvarovite $Ca_3Cr_2(SiO_4)_3$

The groups almandine, pyrope, spessartine, grossular, etc. are named according to the main cation in the A or B sites. Natural almandine garnets, for example, also contain lesser amounts of just about all the other cations. Within each of the two series there is extensive solid solution, but differences in cation size make this very temperature and pressure-dependent. For example the A site is slightly too large for the Mg ion, while some rotation of the silcon tetrahedra is required to make it large enough for the Ca ion. The interplay of high pressure (to fit Mg) and temperature (to fit the Ca) therefore determine the formation of pyrope and the degree of exsolution of Mg and Ca. For reasons such as these, the composition of garnet reflects the conditions under which it was formed.

The Magnetic Properties of Almandine Garnets

Considerable attention has been given to the compositional and structural variations within the garnet group, but compared to the oxides (eg. ilmenites and spinels), little attention has been given to examination of the magnetic ordering in garnets, and even less to the detailed examination of the magnetic ordering in naturally occurring garnets. Most of the work on magnetic ordering in the silicate garnets has been carried out on synthetic end-members.

Coey and Ghose (1988) report that, in all examined cases, iron silicate end-members are found to order antiferromagnetically. This is often in spite of the exchange interactions being of a ferromagnetic nature (positive), and is due to the effects of the crystalline field, which affects Fe^{2+} ions rather than Fe^{3+} or Mn^{2+} ions.

In the Al garnets ((a) series above) nearly all the magnetic ions are in the A sites (distorted cubic or dodecahedral sites), separated from each other not just by O ions but by whole silicon tetrahedra. This makes the ion separation far too great for direct exchange energy to play any part in magnetic ordering, and it would be thought that there would be no superexchange either. In fact some superexchange does occur across the silicon tetrahedra, and almandine garnet is reported as being antiferromagnetically ordered at 4.2 K (Coey and Ghose, 1988). In a more recent experiment Anovitz et al (1993) examined heat capacity changes in synthetic end-member almandine garnet, and from these changes concluded that pure almandine garnet orders antiferromagnetically below 8.7 K, due to the ordering of the Fe^{2+} ions. At room temperature almandine behaves as a paramagnet, and all other naturally occurring members of the Al garnet series are also predicted as being paramagnetic. The susceptibility of paramagnetic garnets with perfect cubic symmetry should be isotropic (Nye, 1957)

Results of Garnet Analysis and Magnetic Rotation Observations

A total of 136 garnets were analysed. Most of these were almandine garnets obtained from garnet samples supplied by Rio Tinto Exploration (formerly CRA Exploration), but 4

were spessartine garnets from a mineral sand sample at the University of Tasmania, 3 were spessartines from Broken Hill, and 6 were pyrope garnets provided by Rio Tinto Exploration.

Fifty four of the particles were observed only for rotations perpendicular to the field rotations. For these particles the observations were carried out using a magnet drum as illustrated in figure 7.4.

Forty nine of the particles were measured for parallel rotations using the magnet drum illustrated in figure 7.4, and were then observed for perpendicular rotations using the "uneven-field" magnet drum illustrated in figure 13.3 below.

The remaining garnets (thirty three) were not measured for rotation at all, and are included here only to produce a better illustration of compositional variation.

The magnet drum shown in figure 13.3 was constructed only for the observation of perpendicular rotations in garnet, and was not described in chapters 7 or 8. It was constructed to produce a rotating magnetic field that is always stronger in one direction than the opposite. The effect is similar to applying a constant direction biasing field. According to the theoretical considerations in chapter 5, such a biased magnetic field should enhance the perpendicular particle rotations.

Figure 13.3

'Uneven-field' magnet drum used for observing particle rotation perpendicular to the external field rotation

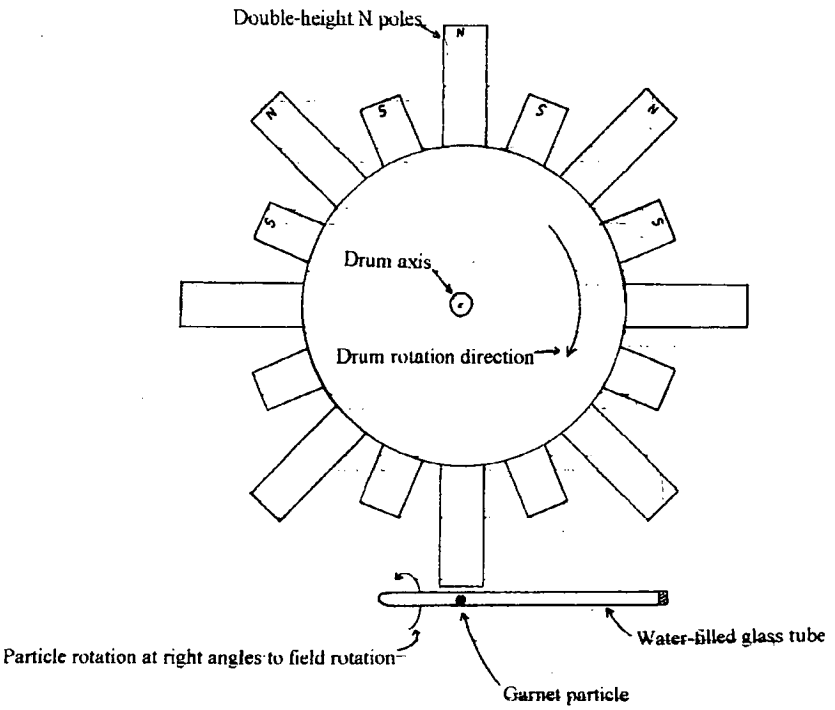

A preliminary set of observations of perpendicular particle rotation was made using a conventional magnet drum as illustrated in figure 7.4 (see appendix F). This drum had a variation between N and S pole strengths of up to 10%. With this earlier drum, only about 4% of the garnets were observed to rotate perpendicular to the magnetic field rotations. The

percentage of particles showing the perpendicular rotation was greatly increased with the 'uneven-field' drum in figure 13.3.

Observations of the strength of the weaker perpendicular rotation, using the equipment in figure 13.3, have involved subjective judgements. The rotations have been assigned a number between 0 and 10, according to the perceived strength of the rotations. A value of 10 is the strongest. While the modified magnet drum does seem to have increased the perpendicular rotations, it also increased the difficulty in observing them by introducing particle vibrations.

Chemical analysis

The full susceptibility, rotation and chemical analysis results are given in appendix G. Figures 13.4 and 13.5 illustrate the Mg, Al, Fe^{2+} and Fe^{3+} composition of the garnets.

Figure 13.4

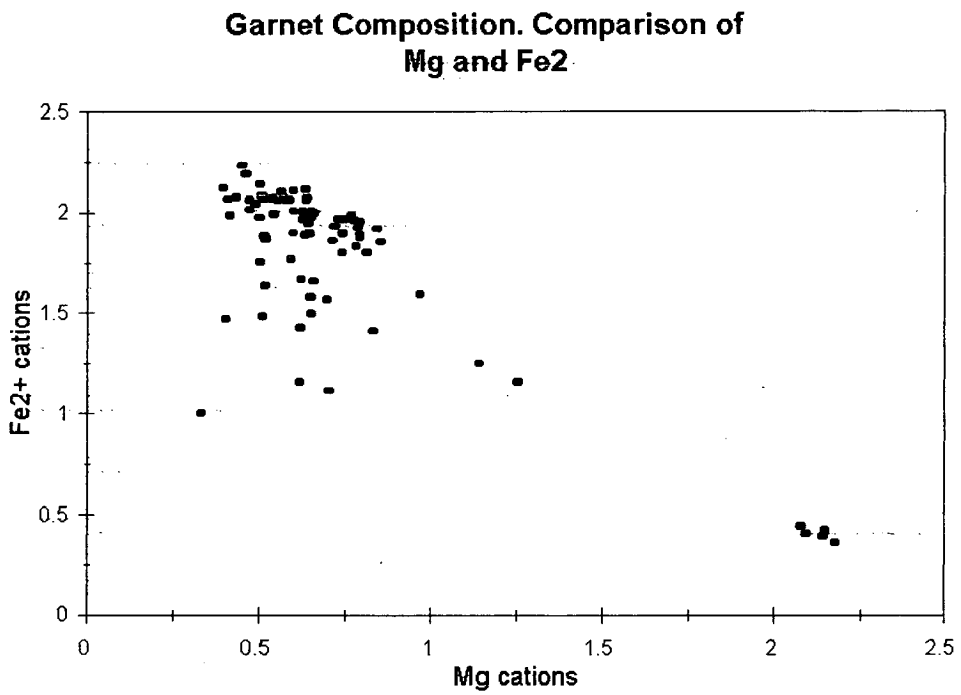

The cation numbers are given relative to a formula of $A_3B_2(SiO_4)_3$, with Fe^{2+}, Mg, Ca, and Mn substituting into the A position and Al, Fe^{3+}, Cr and Ti substituting as B ions. Six of the garnets analysed as pyropes, with the remainder being almandine. The Mn content (not illustrated) varied up to 0.8 cations, with Si between 2.86 and 2.98. From the analysis illustrated above and in appendix F, it can be seen that variations in the Fe^{2+}, Mn, Mg and Ca involved only substitutions in the A sites, while Fe^{3+} (average about 0.2 cations) appears to have gone into all three cation sites (including for Si). Except for the six pyrope garnets, which contain up to 0.27 Cr cations, Cr content is less than 0.02 cations. For most of the garnets about 2/3 of the A sites were occupied by Fe^{2+}.

Figure 13.5

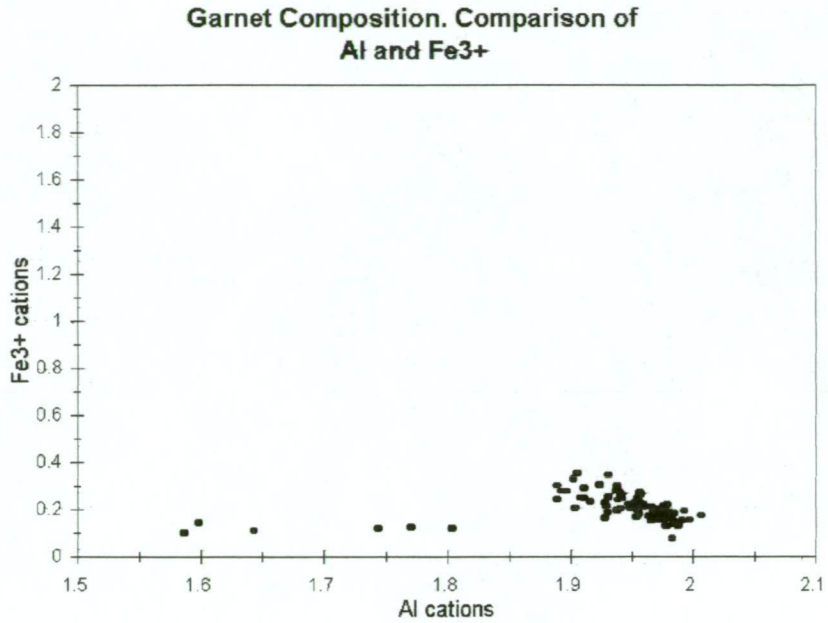

Magnetic susceptibility measurements

Figures 13.6 and 13.7 illustrate the relationship between magnetic susceptibility and composition. The plotted points have been colour-coded according to magnetic susceptibilities, which have been given in cgs units ($\mu G.cm^3/g.Oe$).

Figure 13.6

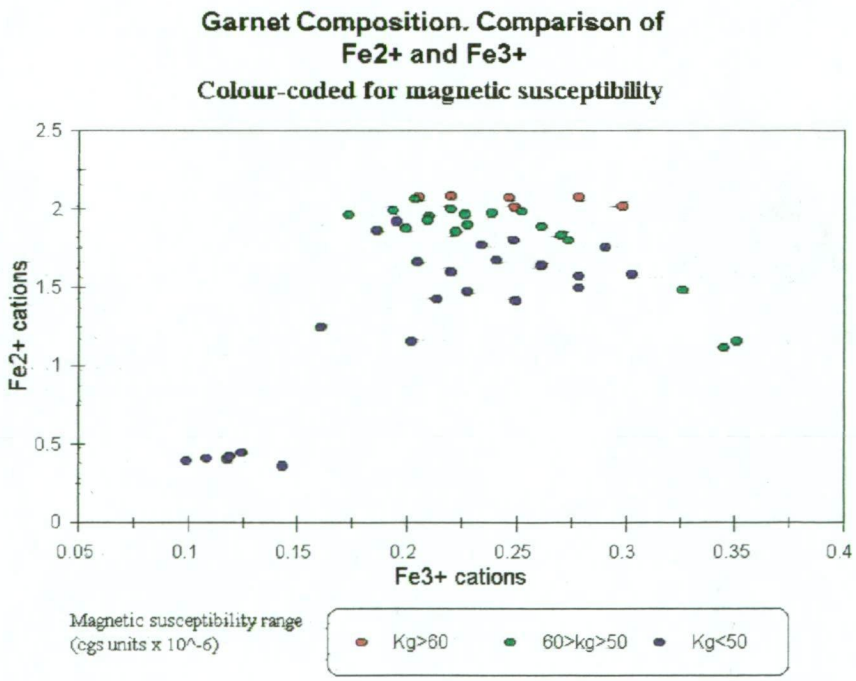

The six pyrope garnets show up as the low-Fe^{2+}-Fe^{3+} group in the lower left of figure 13.6, and as the high-Si-low-Fe^{2+} group in the upper left of figure 13.7. All six had low magnetic susceptibilities, below what could be estimated with the methods employed here.

Figure 13.7

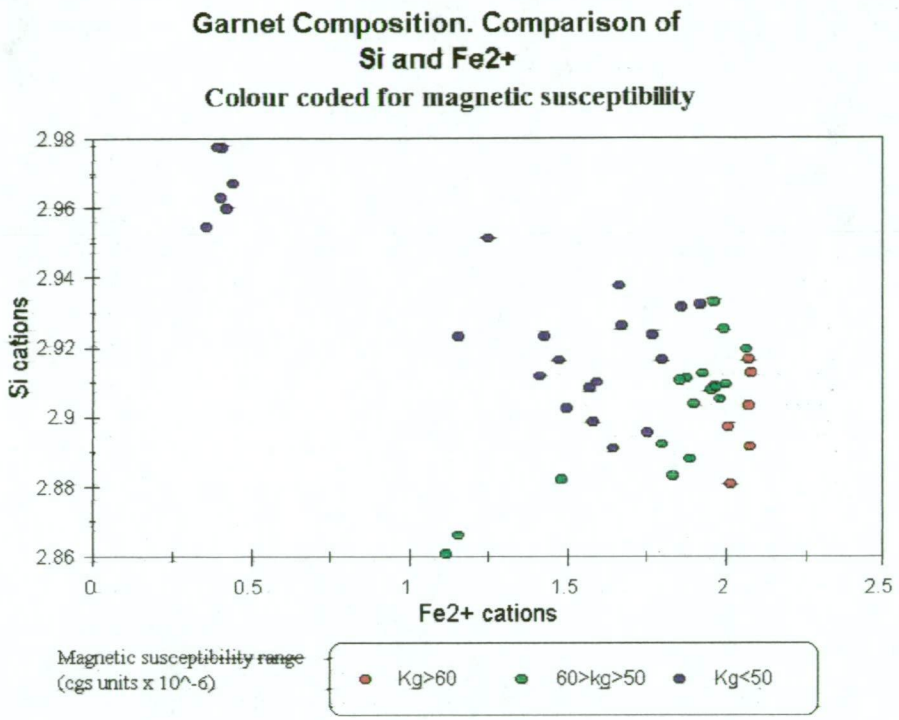

As expected, the magnetic susceptibilities are influenced by the Fe^{2+} content, and figure 13.6 indicates that magnetic susceptibility is also weakly influenced by the Fe^{3+} content, with higher Fe^{3+} tending to produce higher magnetic susceptibilities. As mentioned above, some Fe^{3+} has substituted in place of Si in some of the garnets, and this shows up in figure 13.7 where a lower Si content is associated with an increase in magnetic susceptibility.

Particle rotation parallel to the field rotation (ie. rotation axes parallel to each other)

Garnets used for rotation and susceptibility measurements (whose analyses are given above) were chosen for an absence of visible inclusions. Rotation parallel to the field rotation, as described for the ilmenites and chromites in the previous two chapters, occurred in very few of these garnets.

Three of the garnet particles that did rotate relatively strongly parallel to the field rotation were examined at the CSIRO rock magnetism laboratory in Sydney for the presence of ferromagnetic inclusions. The analysis data for the three particles discussed below are reproduced in Table 13.1. The data has been given here in terms of cation numbers in the unit formula, so as to allow easier comparison with the plotted analysis data given in figures 13.4 and 13.5.

The "drop-out" frequency is the approximate field rotation frequency at which particle rotation parallel to the field rotation ceased.

Table 13.1

Analysis data for the three particles examined for ferromagnetic inclusions.
(given in terms of cation numbers in the unit formula)

	CRAB-34	CRAB-33	CRAA-7	
Rotation drop-out frequency;-...	75 Hz	30 Hz	20 Hz	
Mg	1.00	0.64	0.71	cations
Al	1.98	1.96	1.96	"
Si	2.96	2.94	2.96	"
Ca	0.12	0.24	0.14	"
Ti	0.00	0.00	0.00	"
Cr	0.00	0.00	0.00	"
Mn	0.08	0.13	0.11	"
Zn	0.00	0.00	0.00	"
Fe^{2+}	1.77	1.94	2.00	"
Fe^{3+}	0.09	0.16	0.12	"

All three particles contained visible black and opaque inclusions, and one of these, in particle CRAB-34 (CRA Sample B, particle 34 in appendix F) analysed as $FeTiO_3$. The inclusions in the other two particles were not exposed by polishing and were not accessible to analysis.

The particles, contained inside the glass tubes used for the rotation observations, were magnetised to saturation in a magnetic field of 1 Tesla, and then progressively AF demagnetised. At each step of the demagnetisation the remanent magnetisation was measured. The intensity figures given for the particle magnetisation (Y axis) incorporate a correction component for the magnetisation of the glass tubes, and are in units of $\mu G.cm^3$ divided by 10.8. The latter unit is based on the volume of the rock samples usually measured by the equipment. The garnet particles had an approximate diameter of only about 0.8 mm.

Figures 13.8 to 13.10 are the computer print-outs of the demagnetisation results. In each of the figures, the demagnetisation can be approximated by two linear trends, as shown. The initial, steeper trend represents the demagnetisation of larger multi-domain ferromagnetic (or ferrimagnetic) centres, while the flatter trend represents the demagnetisation of the 'harder' single-domain centres.

Figure 13.8

Demagnetisation of particle CRAB-34.
(Note: 1 Oe = 79.6 A/m)

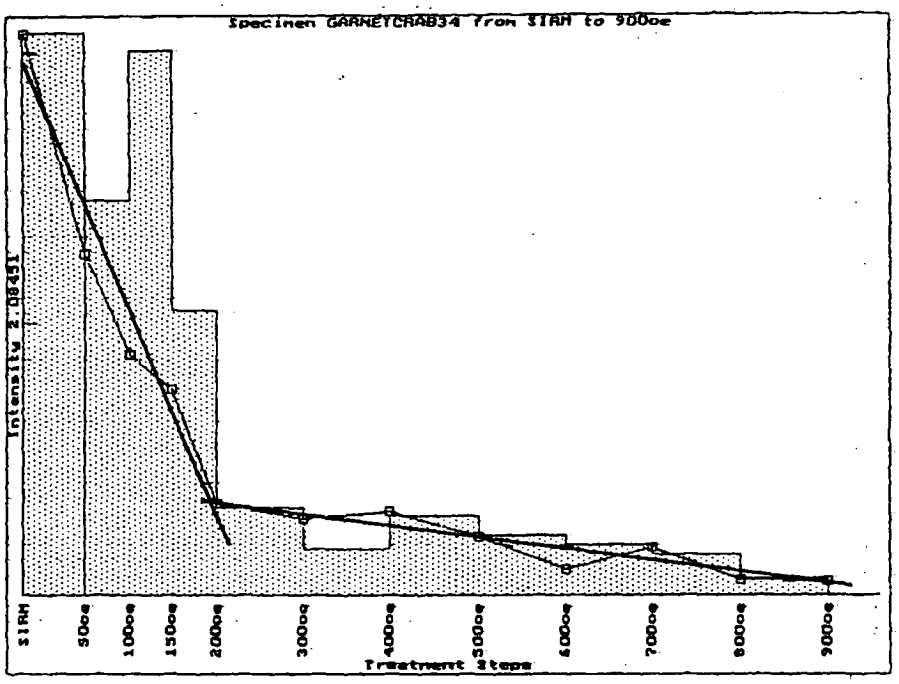

(Reprinted from original CSIRO print-out)

Figure 13.9

Demagnetisation of particle CRAB-33.
(Note: 1 Oe = 79.6 A/m)

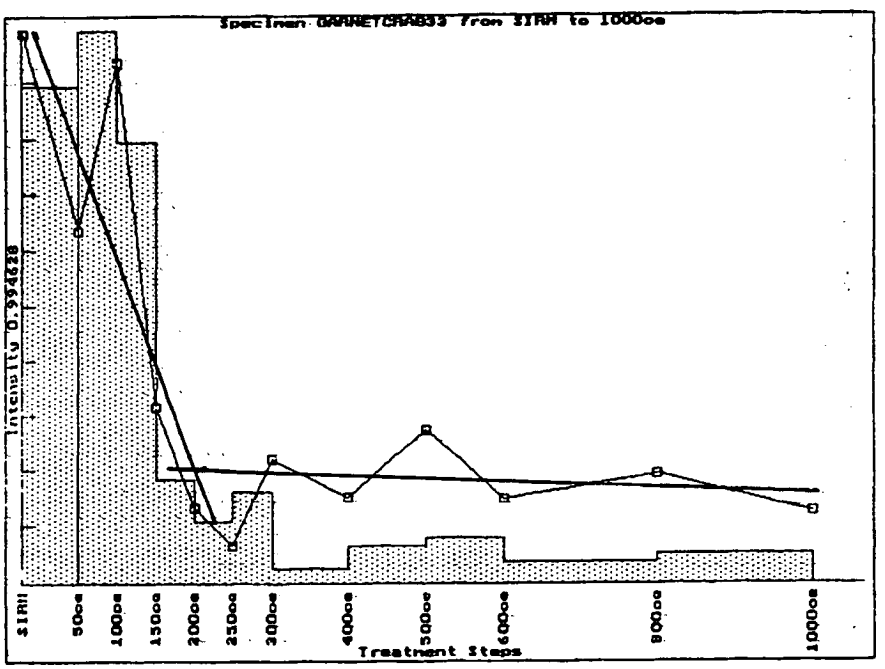

(Reprinted from original CSIRO print-out)

Figure 13.10
Demagnetisation of particle CRAA-7
(Note: 1 Oe = 79.6 A/m)

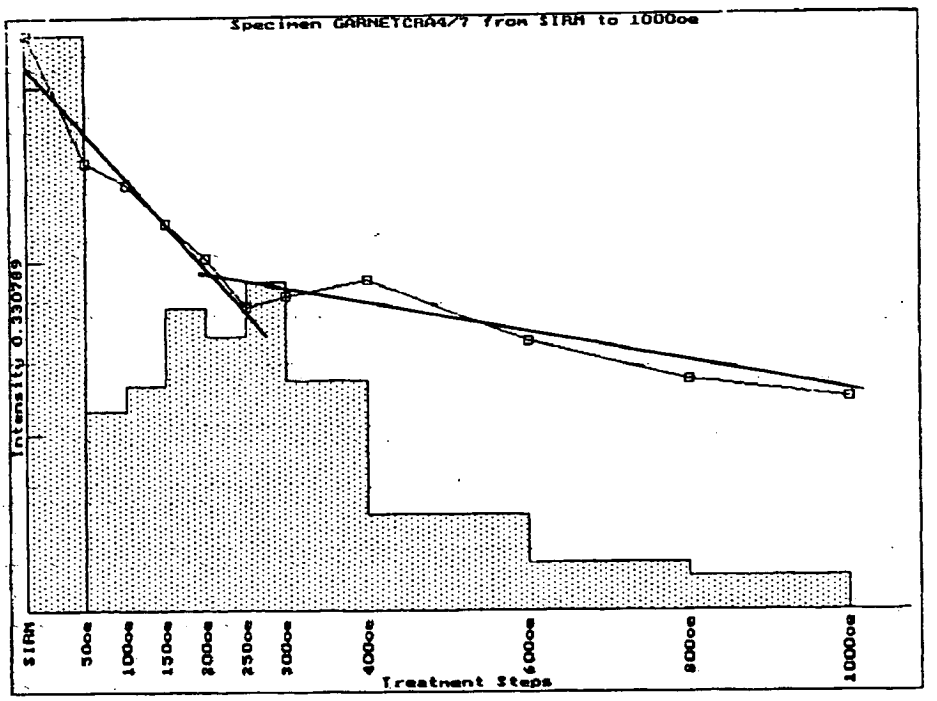

(Reprinted from original CSIRO print-out)

The relative saturation magnetic moments for the three particles are in the same order as the drop-out frequency for the particle rotation, and each of the particles is shown as containing some ferromagnetic or ferrimagnetic centres, with the only exposed inclusion analysing as ilmenite. Garnets with the compositions of these three particles should be paramagnetic at room temperatures. The implication is that any garnet particle rotations parallel to the external magnetic field rotations are due to the presence of ferromagnetic or ferrimagnetic inclusions.

Particle rotations perpendicular to the magnetic field rotations

The continuous rotation of a particle around an axis that is perpendicular to the magnetic field rotation axis is an unexpected and unusual sight. In magnetic fields rotating at between 20 and 60 Hz, this 'perpendicular' rotation is very slow, about 0.1 to 0.5 Hz, and appears to proceed in steps of between 45 and 90^0.

As can be seen from appendix G, there was quite a range in the observed characteristics and the apparent strength of this type of particle rotation, and the rotations could probably be classified according to more than one criterion (e.g. the field strength at which rotation commenced or the frequency range over which rotation occurred). Here an attempt has been made to grade the rotations in order of a perceived overall rotation strength (on a scale from 0 to 10), but there will be quite significant overlap between the four chosen rotation groups due to the subjective nature of the observations and the different rotation

characteristics. In spite of these difficulties a compositional trend can be observed in the results, and is best described in terms of the Fe^{2+} and Al composition of the garnets. Figure 13.11 illustrates that particle rotations perpendicular to the field rotations are associated with high Fe^{2+} and high Al compositions for the garnets.

Figure 13.11

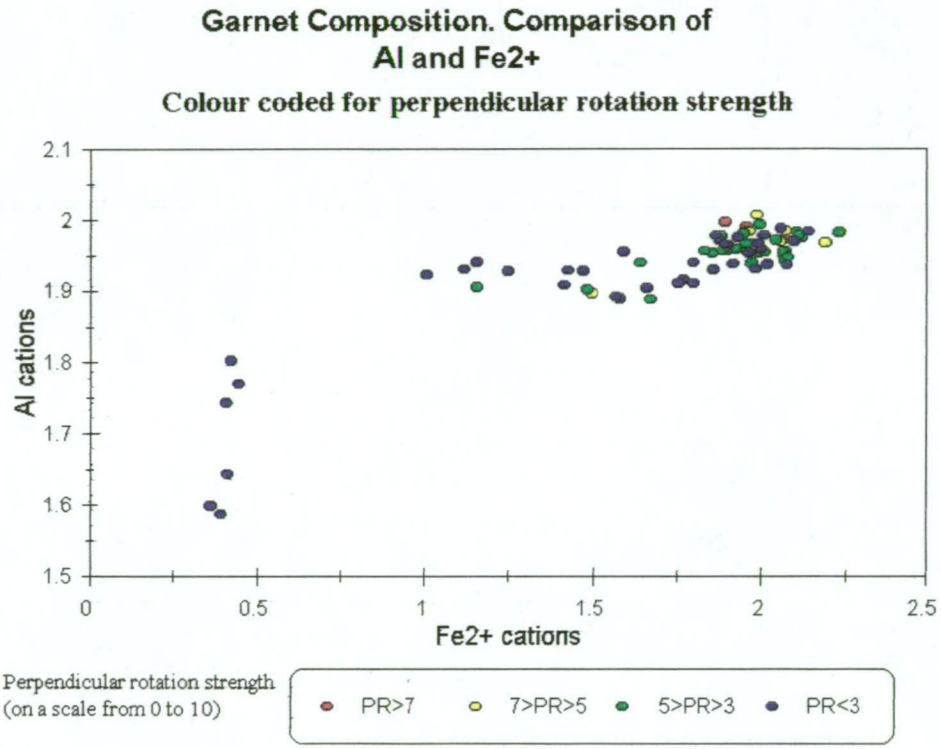

The scatter plot of figure 13.11 does indicate a trend towards higher Fe^{2+} and Al for particles with higher perpendicular rotation strengths.

For garnets with higher magnetic susceptibilities the Fe^{2+} content was the main determinant (figure 13.7). The trend for garnets with higher perpendicular rotation strengths is similar.

The implication is that those garnets that have magnetic ions in only the A sites are those which rotate perpendicular to the field rotations, and that the number of magnetic ions in the A sites determines the rotation strength. None of the pyrope garnets showed any tendency to perpendicular rotation.

Discussion

The strength of both parallel and perpendicular rotations correlate with higher Fe^{2+}. Where the parallel rotations are strong, ferromagnetic inclusions are indicated.

It was calculated in chapter 5 that, although the *magnitude* of the precessional torque should be enough (given a magnetic susceptibility of about 7.5×10^{-7} in SI units) to cause perpendicular particle rotations, the torque acts for far too short a time to actually cause such rotations. In fact the *average* torque is only 10^{-6} of that required to rotate the particles.

In spite of the theoretical problems mentioned above, some almandine garnet particles do show perpendicular rotations, and show them very convincingly. It was also noted in chapter 10 that there is some evidence for perpendicular rotations in magnetite. In fact, the particles are behaving as though the precessional torque described by Stephenson (1980) is acting continiously, instead of as 10^{-8} sec pulses. This implies continuous electron spin reversals, always around the same axis, and suggests some type of resonance. Such a process is difficult to reconcile with theory, and the whole problem of perpendicular particle rotations requires more detailed examination.

If precessional effects during electron spin reversals are in fact the cause of the perpendicular particle rotations, then such rotations should only occur in ferromagnetic materials (otherwise the Einstein de Haas effect should apply, and this is far too small). However ferromagnetic particles, and those with ferromagnetic inclusions, should also rotate parallel to the field rotations. This is found to be the case when garnet particles contain ferromagnetic inclusions. The problem here is that garnet particles which do not appear to be ferromagnetic, and which do not rotate parallel to the field rotations, are observed to rotate perpendicular to the field rotation. If any ferromagnetic (or ferrimagnetic) inclusions are present they would normally be expected to cause parallel rotations stronger than any perpendicular rotations. Therefore we have alamandine garnet particles, with no visible inclusions, which have to be ferromagnetic if the perpendicular rotations are real, but which also appear to be paramagnetic because they exhibit no parallel rotations.

The suggested dual paramagnetic and ferromagnetic nature of some almandine garnets can be accommodated if they contain superparamagnetic particles (see chapter 2). The required particle size, if the particles are magnetite, is less than 0.035 μm, which explains why no inclusions were observed. The observation of perpendicular rotations over only a limited field rotation frequency range can be explained by superparamagnetic relaxation times of the order of the field rotation period.

The identification of superparamagnetic particles within almandine garnets could help to solve the problem of the perpendicular rotations, but such observations require special methods and equipment not available for this investigation.

Section 4

Experimental Results for Particle Separation Trials

Chapter 14

Low-Entrapment Separation of Ferromagnetic and Ferrimagnetic Particles

Introduction

As mentioned in chapter 3, one of the problems with wet-drum low-intensity magnetic separators is the trapping of non-magnetic particles within magnetic flocs. This can either lose valuable non-magnetic material (such as gold) to the magnetic fraction, or pollute the magnetic fraction with unwanted non-magnetics (e.g. when producing magnetite for sale). This is generally overcome by using several stages of magnetic separation (as in figure 3.5), sometimes with demagnetisation stages between them.

Some attempt is made, within the design of wet-drum separators, to minimise the problem by periodically rotating the magnetic flocs as they pass through the separator. The rotation of the magnetic flocs, by reversing the magnetic field direction, is neither energetic nor frequent, and much non-magnetic material remains entrapped. Nevertheless the floc rotation does decrease entrapment, and indicates that enhanced rotation would improve the separation. Continuous magnetic particle rotation is needed, at rotation speeds fast enough to break down the magnetic flocs.

In the normal wet-drum separator, where the magnets are stationary and the particle (or floc) rotation is caused by the rotation of the outer drum past fixed magnetic poles (see chapter 3), it is not possible to significantly increase the speed of the outer drum rotations without dislodging many particles due to fluid drag. The solution to the problem lies in rotating the magnets while keeping the outer drum stationary. With this alternative arrangement the particles can be made to rotate at quite high frequencies (up to as high as 100 Hz) without being dislodged by fluid drag forces. The faster the particles rotate, the more the magnetic flocs are broken up, and the cleaner the magnetic product. The removal of the magnetic particles from the separator must now rely on the rotation of the particles. The particles must roll themselves out of the separator.

Another problem with conventional attractive magnetic separation occurs when ferromagnetic (such as grinding iron) or strong ferrimagnetic materials (such as magnetite) need to be removed from finely ground dry powders. Attractive forces between dry particles make it very dificult to isolate the magnetic particles. Each magnetic particle is very likely to take with it a clump of attached non-magnetic particles. Once again the solution lies in very energetically rotating the magnetic particles so as to dislodge the non-magnetic ones.

Chapter 8 described various experimental rotating field separators, and this chapter is concerned with trials on the designs shown in figures 8.3 to 8.9.

Rotating Field Separation of Magnetite and Iron

Experimental trials of wet separation of magnetite from sand.

An initial trial used the separator illustrated in figures 8.3 and 8.4. The magnet drum was fitted with ceramic magnets, which produced a magnetic field at the separation surface of about 0.1 Tesla. The width of the separator was 10 cm. The separation in this case was completely wet, with no pasage of the magnetics from water to air during separation (as in the later trials). A magnetic field rotation frequency of 30 Hz was used. The trial mixture for separation was made up of 1 kg of magnetite, from the Kara mine south of Burnie, mixed with 1 kg of quartz sand from Pioneer in north-east Tasmania (EL 11/96). Particle sizes were generally within the range 75 to 600 μm. The performance of the separator can be summarised by:

Drum diameter:	240 mm
Feed rate:	1.2 tonnes/hour.m (solids)
Separation rate:	0.6 tonnes/hour.m
Magnetite recovery:	99.8%
Entrapment of non-magnetics:	0.2% of non-magnetics weight

So far as actual recovery and entrapment figures are concerned, this model of the rotating field separator performed very well indeed. At a separation rate of 0.6 tonnes/hour.m it was obviously not being over-fed, and could probably separate magnetite at up to 1 tonne/hour.m. The main draw-back was that the magnetite separated along with large volumes of water, whereas most applications would require the magnetite to contain as little water as possible (such as it does from a conventional wet drum separator).

Another problem is that commercial wet-drum separators regularly separate magnetite at around 10 tonnes/hour.m. The separation rate for the rotating field separator could be approximately doubled by doubling the field rotation frequency, but this would still fall well short of commercially expected separation rates.

The second trial used the version of the rotating field separator shown in figures 8.5 and 8.6. This separator seeks to produce a drier magnetite product by using the particle rotations to roll the particles up out of the water and over the top of the separator, as described in chapter 8. The field strength at the separation surface was approximately 0.1 Tesla, and a magnetic field rotation frequency of 50 Hz was used. The test mixture for this trial was made up of 1.3 kg of sand-blasting sand (0.1 to 1.5 mm particle size) mixed with 1 kg of mixed magnetite from the Kara and Savage River mines (0.03 to 1 mm particle size). This was fed to the separator in slurry form. The maximum slurry density was 25% solids by weight, and the maximum feed rate was approximately 2 tonnes/hour.m. This was approximately twice the feed rate used in the first test above. A magnetic trap was used in the outlet line for the non-magnetics, to make sure no unseparated magnetite was lost.

After separation, the products were dried under infra-red lamps, and then repeatedly hand-separated to determine the non-magnetic entrapment and magnetite recovery. The separator performance can be summarised as follows;

Drum diameter:	240 mm
Maximum feed rate:	2 tonnes/hour.m
Maximum separation rate:	1 tonne/hour.m
Slurry composition:	maximum 25% solids by weight

Magnetite recovery;	99.5%
Entrapment of non-magnetics;	0.9% of non-magnetics weight

The difference in the entrapment figures for the two separator models needs to be explained. This is important because the main aim of the rotating field separation of ferromagnetics and strong ferrimagnetics is to lower the non-magnetic entrapment. As magnetic particles roll under the separator drum they do so as a thick mat of particles, with particles further from the magnet drum rolling on top of closer particles. This thick mat of rotating particles carries with it a layer of water. Although the non-magnetic particles may be sheared away from the magnetic particles, smaller non-magnetics become caught up and transported by the water flow along with the magnetics. The separator shown in figure 8.3 (initial trial) has an extra magnetics outlet, and is fitted with a splitter. When this separator is being set up for operation, the control water is adjusted so that the water flow either way over the top of the splitter is close to zero. The water flow that is carried with the separating particles is therefore prevented from passing the top of the splitter, and a region of mild turbulence is created. In addition the separating particles enter a region of clean water before leaving the separator, and this allows non-magnetic particles to drop away without being replaced by others. If the control water flow is reduced, non-magnetic entrapment does increase. If the control water flow is increased, then entrapment falls off even further, but magnetics recovery also decreases. The separator shown in figure 8.5 has no splitter, and there is little to prevent the "dirty" water flow being carried to the outlet with the moving mat of magnetics.

Practical tests on the separation of magnetite and pyrrhotite from gold concentrate

Osborne mines, about 300 km from Mt Isa in Queensland, need to remove magnetite and monoclinic pyrrhotite from their gold concentrate before the concentrate is processed across tables. At present they employ a small wet drum separator made by Eriez Magnetics, but report an unacceptable gold loss due to particle entrapment of between 8 and 10% (Pers. comm., Karen Hall, concentrator metallurgist, Osborne Mines).

The mine provided a 15 kg concentrate sample from their Knelson concentrator for test separation using the separator illustrated in figures 8.5 and 8.6.

Because of the problems discussed above, the separator was modified slightly before the separation. Instead of the "auxiliary water" entering as shown in figure 8.5, the entry was re-located 100 mm higher, so that there was a water flow down through the squeeze-pan gap, in the reverse direction to particle travel. The water level inside the separator was also raised to just below the top of the separator.

The separated fractions, obtained in a single pass, were returned to Osborne Mines for analysis and comparison with the magnetic fractions from their present wet drum separator. The analysis results were reported back as follows:

Fraction	Weight % of total sample	Distribution between fractions (wt %) Cu	Au	S	Fe
Magnetics	12.7	1.63	0.31	7.92	30.41
Non-magnetics	87.3	98.37	99.69	92.08	69.59

The gold entrapment has been reduced by a factor of approximately 30, over that achieved with their present conventional wet drum separator. The real gold entrapment may in fact have been even lower than given above, as some of the gold was later found to be magnetic due to the presence of inclusions. These inclusions were identified microscopically under reflected light as being magnetite and hematite.

Discussion of wet separation results

Rolling the particles out of water and over the top of the separator produces some extra problems. The passage from water to air involves some opposing forces from water surface tension, and the particles need to roll themselves up a "magnetic slope", away from the magnet drum, as they pass over the top of the separator. In this "wet-to-dryer" type of separation there is no water flow to assist the motion of the particles. At high separation rates, particles tend to congregate at the point where they must roll out of the water. For the separator shown in figure 8.5, with a field strength of 0.1 Tesla at the separation surface, and used in the second trial above, a maximum separation rate of just under 2 tonnes/hour/m was reached. Attempts to force a higher separation rate led to a build-up of magnetics at the water-exit point, and to eventual clogging of the separator at this point. Most of the problem appeared to be caused by the larger particles. If the field rotation frequency was dropped to 30 Hz then little difficulty was experienced with the larger particles. This particular problem was greatly decreased by raising the water level inside the separator, and the problem was not at a significant level during the Osborne mines separation. .

The rotation index, as measured in chapter 10, is not applicable for strongly ferromagnetic or ferrimagnetic particles such as iron and magnetite in an actual separation situation. The rotation indices for these particles were measured in very low external fields, where the field strength was of a similar magnitude to the coercive force. In an actual separation situation, such as has been used above, $H >> H_c$, and possibly $H > H_A$. Domain wall velocities may be expected to play no part in increasing the particle torque. The most probable explanation for the experienced difficulties with the separation of larger magnetite particles is given by equation 7.8. While the maximum "rollable" particle sizes predicted by equation 7.8 are above the particle sizes being separated here, equation 7.8 does not take into account the other retarding forces that act on the particles in the separation above. In particular it does not consider the effects of water tension, or the reverse torque applied to the particles by gravity as they climb up a near-vertical slope, or the retarding forces applied by collisions with other particles. The maximum separable particle size is therefore considerably smaller than that predicted by equation 7.8. Experience with the above separations suggests that it is uncomfortably close to 1 mm in the small experimental separator.

Increasing the magnetic field strength should improve separation, but as indicated by equation 7.8, this will only be by a small amount, limited to a decrease in the second term in the denominator of equation 7.8. The main factor involved is the value of the constant C (the drum calibration constant) in equation 7.8. Perhaps a reasonable operating field strength would be 0.12 to 0.15 Tesla for wet drum separation, but the main requirement would be to increase the depth of field. This has the potential to greatly increase separator performance. Magnet drums constructed for commercial rotating field separation will use larger magnets and larger drum diameters. This will considerably lower the value of the constant C, and should raise the maximum separable particle size considerably. While the particle size effect may be explained by the relationship given as equation 7.8, the better separation of the larger particles at a lower field rotation frequency is most probably due to particle inertia. If the

larger particles are at the point of ceasing rotation (due to the factors expressed in equation 7.8), then increasing the particle acceleration time, by decreasing the field rotation frequency, allows particle rotation to continue. This is the same phenomena as the frequency dependence of the rotation index discussed in chapters 4 and 10.

Increasing the depth of field (ie. decreasing the field gradient), and consequently decreasing the surface interaction and increasing the resultant torque applied to larger particles, should also allow another problem to be overcome. Water tension effects can become significant as the particles roll over the top of the separator and begin to climb the "magnetic hill" away from the magnet drum. If there is insufficient water on the separation surface, particle rotation can cease. This leads to the formation of vertical and parallel fans of particles. Particle movement ceases as the fans rapidly grow backwards towards the water surface, and the separator clogs up. The effect is similar to the magnetic "fanning" used to separate steel sheets in some mills and factories. The fans usually begin to form at the point where the separating surface moves more quickly away from the magnet drum. A spray of water on to the upper separation surface usually helps to prevent this fan formation (by decreasing water surface tension effects), but it is also obvious that an increased magnetic torque and a lower gradient to the magnetic "hill" decrease it as well.

The magnetic "hill" gradient required for the particles to roll over the slurry input point will obviously decrease with a larger magnet drum diameter. Most of the magnet drums in present attractive wet drum separators are 500 mm to 900 mm in diameter. If a magnet drum of these diameters is used, together with an increased magnetic field depth, this fanning should not occur, and separation rates should be considerably increased above 2 tonnes/hour.m.

Dry separation of grinding iron and magnetite from fine powders

This separation employed the separator shown in figure 8.9 (chapter 8), which was fitted with the rare-earth magnet drum described in chapter 7. The field strength at the separating surface was approximately 0.2 Tesla, and a field rotation frequency of 100 Hz was used for the tests. Attractive magnetic separation produces considerable entrapment of non-magnetic particles, and magnetic particles are too easily prevented from separation by overlying non-magnetics. Rotating field separation reduces entrapment, as described above, but the strong particle rotations also enable magnetic particles to more easily "dig themselves out" from under overlying non-magnetics.

The test material was silica flour provided for test separation by Index Mineral Processors, Tasmania. Particle sizes were less than 75 μm. The sample provided was stated to have an analysed Fe_2O_3 content of 31 to 32 ppm, and Index Minerals hoped to reduce this to a figure of 18 ppm in order to make the product acceptable for sale. It was thought that most of the analysed Fe could in fact be grinding iron. An initial examination using rare-earth hand magnets, followed by electron microprobe analysis of some grains, indicated that while some metallic iron was present, a good deal of the iron may be tied up in minerals such as almandine garnets and chromites which this separation method would not remove. Based on approximate particle-counts after the above hand separation, it was thought that the dry rotating field separation method may reduce the analysed Fe_2O_3 to between 22 and 27 ppm, assuming that only the grinding iron particles could be removed.

For such finely ground particles as were being separated here, no attempt was made to carry out any hand magnet examination of the separated products to check on particle entrapment or magnetic recovery. The monitoring of the separation was carried out by analysis of the separated silica, organised by Index Minerals. Two passes through the separator were made, with the separated silica flour being sampled after each pass.

For the separator shown in figure 8.9 the magnetic particles are attracted to the separator surface and rolled back up and over the top of the separator, in the opposite direction to the path followed by the non-magnetic particles.

After separation the separated products were returned to Index Minerals for analysis. The analysis results were reported in terms of ppm Fe_2O_3. This appears to be irrespective of which compounds or alloys contain the Fe. The separation results are summarised by;

Head analysis;		31.7 ppm Fe_2O_3
Fe_2O_3 content of silica;	after 1st pass;	26.7 ppm
	after 2nd pass;	26.6 ppm

Comments on the dry separation test

These separation results were, as was expected from the preliminary examination, not encouraging to Index Minerals. The fact that the second pass of the silica through the separator produced little improvement in the results, indicates that most of the grinding iron, and possibly all of it, was removed in the separation. The remaining 26.5 ppm of analysed Fe_2O_3 is probably accounted for by the garnet and chromite (plus other unobserved weakly-magnetic iron minerals) in the silica.

Unfortunately no conventional magnetic separation tests were reported as being attempted on this material, and no comparison with conventional separation was available.

Wet Rotating Field Separation of Monoclinic Pyrrhotite

Between 1989 and 1991 Renison Tin, near Rosebery on the west coast of Tasmania, was examining the possible improvements that could be made to the performance of the sulphide circuit of their treatment plant by the magnetic removal of pyrrhotite prior to using flotation to remove the remaining sulphides from the cassiterite. In 1989 separation tests were carried out using a wet drum separator, and the results of these tests were reported by Beros (1991). In 1990 Kerr-Smiley and Moore examined the possibility of using a WHIMS (see chapter 3) in the re-treatment of old tailings. The composition of the old tailings was very similar to the material used in the wet drum separation tests, and the purpose in both tests was to remove the pyrrhotite, plus any other magnetic sulphides.

The wet drum failed to remove most of the magnetic sulphides, while the WHIMS not only removed the unwanted sulphides, but most of the cassiterite as well. A good deal of the cassiterite removed by the WHIMS was removed by entrapment within the magnetics, but some had been removed as composite particles. Mineralogical examination had shown that some of the cassiterite existed as composite particles and inclusions within pyrrhotite and

quartz, and as composites with talc. Pyrrhotite inclusions within cassiterite were also common. Above about 75 μm particle size, composite particles dominated.

In 1994 samples of mill feed were provided by Renison for tests with rotating magnetic field separation (Allen, 1995). The mill feed samples had approximately the same mineralogical composition as the samples used for the wet drum and WHIMS tests. The rotating field separations were carried out to see if the cassiterite entrapment problem could be overcome, and the previous wet drum and WHIMS test results allowed a rare comparison between the three magnetic separation methods.

Comparison of separator magnetic characteristics

The wet drum separator (see chapter 3) used a magnet drum of 900 mm diameter, with a magnetic field at the separation surface of 0.1 Tesla. The outer drum was rotated at a rate of 13 rpm (Beros 1991). The WHIMS separator was a laboratory-sized test machine employing a coarse expanded mesh matrix. The magnetic field could be varied up to 1 Tesla, and the tests referred to here were repeated at various field strengths from 0.1 Tesla to 1 Tesla (Kerr-Smiley and Moore, 1990). The rotating field separator is illustrated in figures 8.7 and 8.8. The magnetic field strength at the separating surface was 0.22 Tesla, and a field rotation frequency of 50 Hz was used.

No data on feed rates was provided for either the WHIMS or wet drum separations, and none was determined for the rotating field separation.

Particle sizes used, and their effect on %Sn in the non-magnetic fraction

No details were given on the particle size used in the wet drum separation tests. Kerr-Smiley and Moore (1990) give the particle size for the WHIMS test as 93% passing 75μm. The material for the rotating field separation tests is given as approximately 80% passing 300 μm and 32% passing 75 μm (Allen, 1995).

The particle size used for the rotating field test was therefore larger than that used for the WHIMS tests. Because cassiterite existing as composite particles and inclusions becomes increasingly more dominant above 75 μm, the magnetic fractions from the rotating field separation test will inevitably show a higher % removal of Sn due to this cause. Kerr-Smiley and Moore (1990) found that grinding to 80% passing 35 μm was necessary to liberate most of the cassiterite, at which size the WHIMS was able to retain 63.5% of the Sn in the non-magnetics at 1 Tesla.

The WHIMS results quoted below are for the separation of material where 93% passed 75 μm.

Comparison of test results

The WHIMS results were originally given at magnetic field strengths of 0.1, 0.2, 0.4, 0.6, 0.8, and 1 Tesla. Because these field strengths extend well above those used for the rotating field separator (approximately 0.2 Tesla), the first three WHIMS separation steps (0.1, 0.2 and 0.4 Tesla) have been regarded as comparable to the three magnetic fractions produced by the rotating field separator (M1, M2 and M3).

For the wet drum separator the results were monitored only by analysing the products for Sn and S. For the WHIMS and rotating field separations the separation products were

analysed for Sn, S, Fe, and Mn. The Mn results were used by Renison as an indicator of the siderite separation. The analysis of the separation products for all three machines was carried out by XRF at Renison.

Feed to the rotating field separator was controlled by the feed cone arrangement shown in figure 8.16. Separated fractions were collected in buckets large enough to accommodate all the water used, so that no overflows occurred. The products were allowed to settle for several days before the water was removed and the products dried, weighed and sampled for analysis.

The results are given in terms of the percentage distribution of the analysed elements across the separation fractions.

Wet drum separation results

Fraction	Distribution%	
	Sn	S
Magnetics	6.4	31.7
Non-magnetics	93.6	68.3

WHIMS separation results

Fraction	Distribution%			
	Sn	Fe	S	Mn
0.1 Tesla	32.0	63.0	65.6	12.1
0.2 Tesla	11.2	16.9	16.7	33.2
0.4 Tesla	7.3	7.7	6.2	30.6
Non-magnetics	49.5	12.4	5.9	24.1

Rotating field separation results

Fraction	Distribution%			
	Sn	Fe	S	Mn
M1outlet (most magnetic)	24.4	65.6	76.8	5.7
M2 outlet	5.3	7.1	7.7	6.7
M3 outlet	11.5	10.8	6.5	49.6
Non-magnetics	59.0	16.5	9.1	37.9

Discussion of separation results

About 30% of the total feed material consisted of pyrrhotite, which made up about 60 to 70% of all sulphides present. Siderite made up about 5% of the feed material.

While the wet drum has retained most of the cassiterite in the non-magnetic fraction, it has obviously not removed very much of the pyrrhotite, let alone any other sulphides.

The WHIMS has obviously removed all the pyrrhotite, plus a good percentage of the remaining sulphides, but it retained less than half the cassiterite in the "non-magnetic" (>0.4 Tesla) fraction. A good deal of the cassiterite was removed with the strongest magnetics, but a significant amount was also removed with the second magnetic fraction. While most of the pyrrhotite and other sulphides have been removed in the first fraction, the second fraction also containd significant sulphide levels. The siderite (indicated by the Mn) is distributed over all the fractions.

The rotating field separator, in spite of using coarser material with more composite particles and inclusions, has retained considerably more cassiterite in the non-magnetics than the WHIMS. The retention of sulphides and siderite in the non-magnetics is more than for the WHIMS, but the analysis reflects a much more accurate split, across the magnetic fractions, between the different minerals present.

While less cassiterite now appears in the most magnetic fraction than for the WHIMS, the difference is even greater in the second magnetic fraction. These differences may be explained in terms of a considerably lowered entrapment in the rotating field separator. This lowered entrapment must be less than the results here indicate, because of the increased inclusions and composites expected with the larger particle size used for the rotating field separation. Cassiterite begins to increase again the M3 fraction, and this probably reflects small pyrrhotite inclusions within cassiterite.

For the WHIMS separation the sulphide and siderite separations overlapped considerably. The rotating field separation has confined most of the sulphide separation to the M1 fraction and most of the siderite separation to the M3 fraction. The rotating field separator, much more so than the WHIMS, has produced magnetic fractions which could be taken, if desired, as separate sulphide and siderite concentrates.

The rotating field separator, operating at about 0.2 Tesla shows up here as being almost equivalent to a WHIMS operating at twice that field strength. It has considerably lower particle entrapment and produces a more accurate split between minerals of different magnetic characteristics.

Summary and Conclusions

Wet low-intensity rotating magnetic field separation, using small magnet drums fitted with low-cost ceramic magnets, can reduce non-magnetic particle entrapment in magnetite separations to as low as 0.2% of the non-magnetics. Experimental separations so far indicate that magnetite separation rates to 4 tonnes/hour.m can probably be achieved, while still obtaining magnetite recovery rates above 99.5%, and particle entrapment below 0.5% of non-magnetics. The low particle entrapment of these separators makes them attractive for the separation of magnetics from gold concentrates, and for the production of very clean magnetite.

Dry rotating field magnetic separators, using magnet drums fitted with rare-earth magnets, and using field rotation frequencies of 100 Hz or more, are effective in removing grinding iron from finely ground powders, where particle sizes may be as small as 10 μm.

Wet rotating field separation, using magnet drums fitted with rare-earth magnets, is able to produce magnetic particle separations similar to those produced by a WHIMS operating at approximately twice the magnetic field strength. However these rotating field separations are more precise in their differentiation between minerals of different magnetic characteristics, and produce very little entrapment of lower-magnetism particles.

For ferrimagnetic particles such as magnetite there exists a relationship between the strength of the particle rotation, the size of the particle, and the frequency of the magnetic

field rotation. In general the strength of the particle rotation decreases with increasing particle size and increasing field rotation frequency. This relationship is of considerable importance for the design of rotating field magnetic separators, and is predicted by the existence of a maximum separable particle size (see chapter 7). In practice the maximum magnetite particle size that can be separated by a commercial wet rotating field separator is decreased below that predicted by equation 7.8, by water surface tension and particle interference effects, and may be as low as 1-2 mm. The frequency dependence of the separation for particles close to the maximum separable particle size is a similar phenomena to the frequency dependence of the rotation index (chapter 4), and may be explained by particle inertia effects.

Later Work

Since completion of the experimental work for this thesis, a new low-intensity magnet drum has been constructed. The new drum has a diameter of 670 mm and uses larger ceramic magnets than the small 240 mm drum used for the thesis. This larger drum has a higher field at the drum surface (0.186 Tesla, compared to 0.16 Tesla for the 240 mm drum used for the thesis work above), and has a greater depth of field (35.6 mm, compared to 17.2 mm for the 240 mm drum). These figures represent a significant improvement on the smaller drum, as is illustrated in figure 14.1. The new drum, set up for magnetite separation, is illustrated in figure 14.1.

Figure 14.1

The new magnet drum, at 670 mm diameter and 15 mm length, is really a short section of a practical commercial-sized separator. It will be used to develop practical launders and to carry out test separations on materials provided by mining companies.

Some tests have already been carried out for the Savage River Mine in western Tasmania. The Savage River mine produces magnetite, most of which is used for the manufacture of iron, but some is sold as heavy media for coal washing operations. After initial preparation (crushing and screening etc.) The ore goes through the "rougher" magnetic separators. These are 2.5 m long wet drum separators of the type discussed in chapter 3, and each "unit" is a three-stage wet drum separator. The magnetite is separated three times, to cut down on non-magnetic entrapment. After the "rougher" separation, the magnetite concentrate is re-ground before passing to the "finisher" separators. The "finisher" separators are also three-stage units.

Samples of both rougher and finisher feeds were provided by Savage River, for rotating field separation tests. The samples were separated only once, using the separator shown in figure 14.1. Three "finisher" feed samples were separated, but only one "rougher" feed sample. The separated samples were returned to the mine for analysis. The rotating field separations were carried out at a field rotation frequency of 50 Hz and at feed rates of approximately 10 tonnes/hour.m. The analysis results, in the form reported back by the mine, are given below. Unfortunately the results were reported back differently for the rougher and finisher separations.

(a) Rougher sample

Rougher feed	9.8%	Ferrous%
Plant rougher concentrate	17.2%	"
Plant non-mags.	1.7%	"
Rot. Field concentrate	18.2%	Ferrous%
Rot. Field non-mags.	1.1%	"

(b) Finisher samples

	Typical feed	Plant con. Range	Sample 1	Sample 2	Sample 3
Tot. Fe	59.96	67.55-68.03	67.09	67.08	67.16
Ni	0.039	0.034-0.05	0.036	0.035	0.034
TiO_2	0.97	0.62-0.97	0.75	0.75	0.76
MgO	5.09	1.53-1.99	1.83	1.99	2.03
Fe^{2+}	19.6	21.2	21.3	21.4	21.4

All four rotating field separation results are very close to the typical plant (wet drum) separation results. There is some indication that the single-stage rotating field separation has performed better than the normal 3-stage wet drum separation on the coarser "rougher" feed, but slightly worse than the 3-stage wet drum separation on the "finisher" feed. A single stage rotating field separation appears to be roughly equivalent to a three-stage conventional wet drum separation.

Chapter 15

Small-Sample Rotating-Field Magnetic Separation as an Exploration Tool

Introduction

The ilmenite and chromite rotation measurements in chapters 11 and 12 showed that chromites and Mg-ilmenites with low Fe^{3+} do not rotate readily in a rotating magnetic field. Even though some ilmenites and chromites of other compositions have also been found not to rotate, subjecting a sample of ilmenites and chromites to a rotating magnetic field separation should produce a concentrate in which the the above minerals could be more easily identified.

The purpose of this chapter is therefore to show that a specialised rotating field magnetic separation can be a useful mineralogical tool in mineral exploration.

An exploration application of rotating field separation was tested on a small mineral lease in NE Tasmania (EL 11/96), about 3 km NE of Pioneer. Fracture lines through the granite rocks contain multiple quartz veins flanked by zones of deep kaolinisation. In some cases the quartz veins are capped by small gossan zones just under the surface. There was a suspicion that these quartz veins and fracture lines may be associated with a basic or ultrabasic intrusion (now completely weathered) within the granite. One way to determine this is to identify mineral particles such as chromite and Mg-ilmenite associated with these zones. Geochemical analysis had already been conducted, but while it had indicated minor chemical changes over the fracture lines, the nature of these changes was inconsistent and confusing.

The idea was to use the rotating field mineral separation methods suggested by chapters 11 and 12 to examine panned heavy mineral concentrates from small 2 kg soil samples, for the presence of chromites and Mg-ilmenites. The concentrates obtained from the clay samples were generally considerably smaller than 0.1 g, and consisted of particles with an average size of about 50 μm. This meant that there may be up to 350,000 very small particles to sort through in a typical sample, which may contain fewer than 100 (maybe fewer than 10) of the desired particles.

While some of the separated ilmenites were measured for rotational characteristics, and are included in the data presented in chapter 11, most of the particles were too small for these measurements.

Separation Equipment and Methods

The cell designed for this trial, and its use, have been described in chapter 8 (see figures 8.10 and 8.11).

Samples of clay were obtained from small hand-dug sample pits, usually at a depth of about 80 cm. Each sample was only about 3 kg in weight. After the clay sample was broken down in water and the suspended clay particles washed out, the remaining sand was panned to a heavy mineral concentrate, and dried. The sample weight at this stage was usually less than 0.1 g. Iron particles (from shovel and crow-bar) were removed magnetically, with a rare-earth hand magnet at about 5 cm above the sample. The same rare-earth hand magnet was then used to lift out any particles that could be lifted when in contact with the magnet. This included any monazite, garnet and xenotime that happened to be present. The magnetic particles separated in this fashion then became the sample for the rotating field magnetic separation, which was carried out as described in chapter 8.

Particle identification was done with electron microprobe analysis. Up to 40 particles (or as many as could be obtained) from each non-rotating magnetic fraction were mounted for microprobe analysis. Particles from some of the rotating fractions were also mounted for analysis.

The rotating separation reduced the particle numbers by between 70 to 90%, with up to 2/3 of the non-rotating minerals being monazite. This reduction in particle numbers greatly assisted the visual recognition of *possible* chromites and Mg-ilmenites, and boosted the probability of identifying any of these minerals by microprobe analysis to approximately 5%.

Analysis results

The full analysis results for the EL 11/96 ilmenites are included in Appendix B. While some of the chromite analyses for EL 11/96 are given in Appendix C (those which were measured for rotation), the full chromite analysis results are given in Appendix H.

Ilmenite analyses

Figure 11.3 indicates that ilmenite tends to contain either Mn or Mg, but not significant amounts of both. Figures 11.4 and 11.5 show two distinct groups of Mg-ilmenites, only one of which (the Mg/Fe^{2+} substitution trend) includes the picro-ilmenites. Particles in the latter group do not usually rotate, while some of the particles in the other group (lower Mg but higher Fe^{3+}) are among the most strongly rotating ilmenites observed. The EL 11/96 Mg-ilmenites form a group at the lower-right of the Mg/Fe^{2+} trend in figure 11.4, and are shown separately in figure 15.1, where the particles are colour-coded according to whether they were found in the rotating or non-rotating fractions after separation. Only one of the EL 11/96 Mg-ilmenites falls into the high-Mg/low-Fe^{2+} group of picro-ilmenites shown in figure 11.4.

Figure 15.1

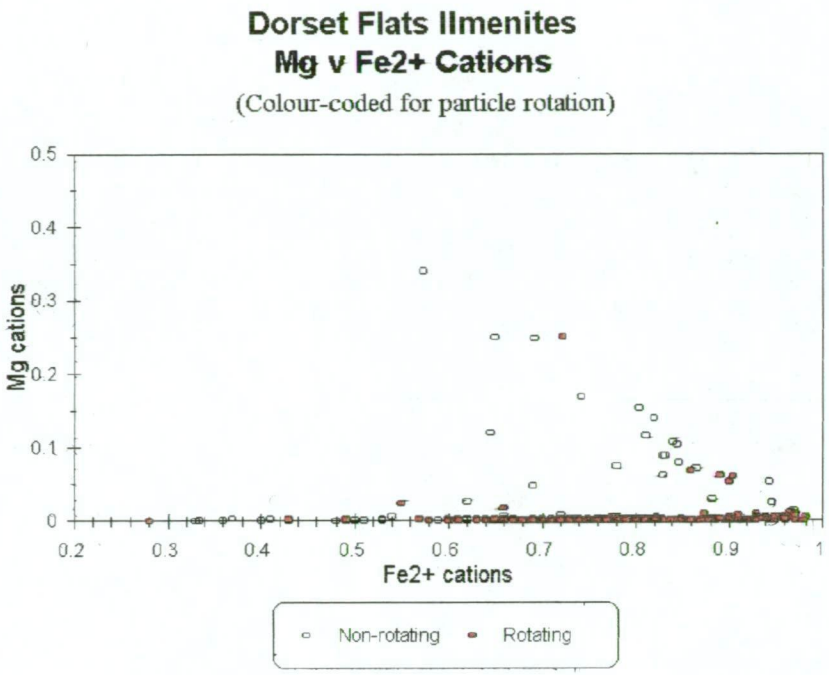

Chromite analyses

Figure 15.2 plots the EL 11/96 chromites in terms of their Fe and Cr ratios. All of them fall within the non-rotating area indicated in figure 12.7. Figure 15.3 illustrates the relationship between the Fe^{2+} and Fe^{3+} compositions for the chromites, which were determined according to the method by Finger (1972). They contain little Fe^{3+} (average of about 0.1 cations) and very little Si and Ti.

Figure 15.2

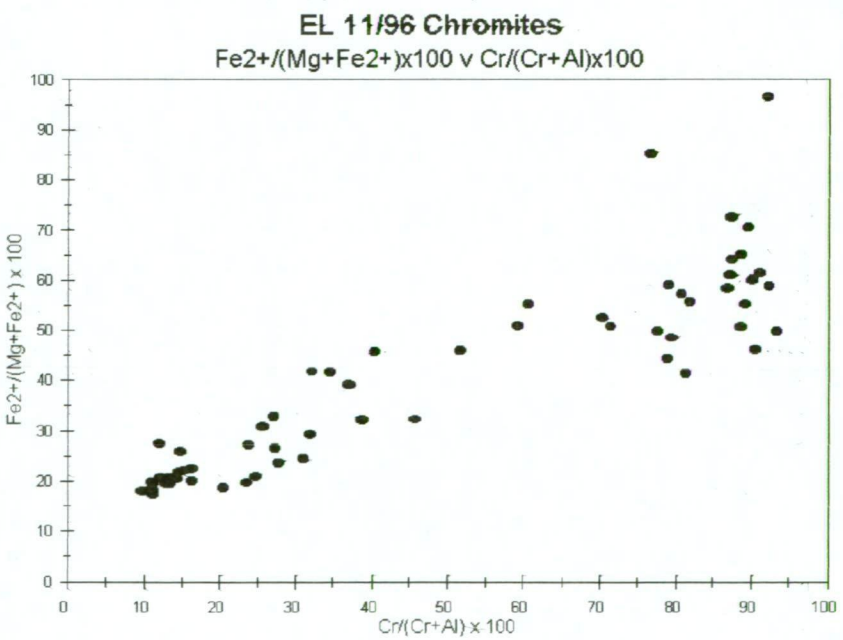

Figure 15.3

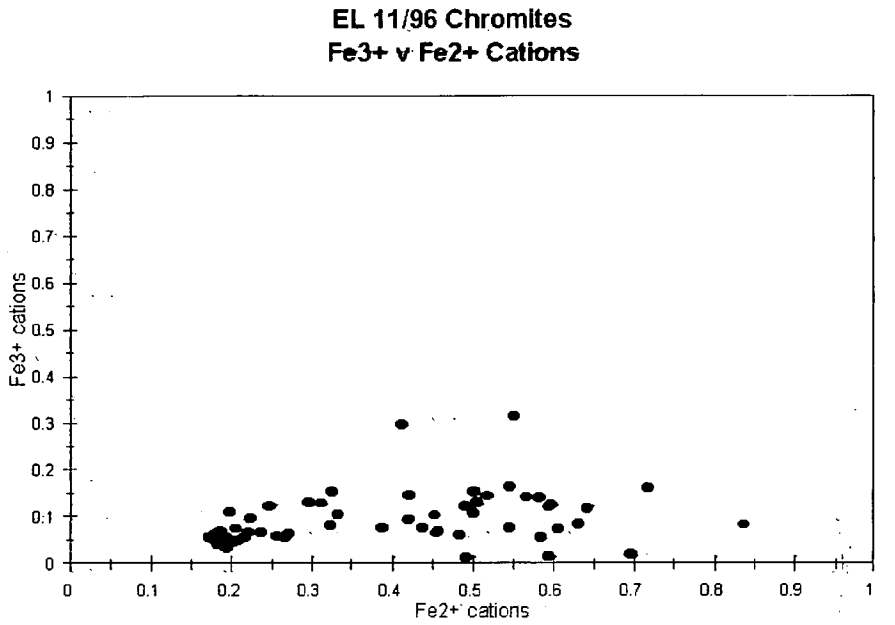

Most of the chromites discussed in chapter 12, which have an $Fe^{3+} < 0.2$ cations, do not show signifcant rotation. The lack of rotation in the EL/96 chromites and their low Fe^{3+} contents also fits this pattern. The fact that no chromites appear to have been separated in the rotating fraction reflects the restricted Fe^{2+}/Fe^{3+} composition of the particles.

Figure 15.4 plots the chromites according to the approximate magnetic ion occupancy of the A and B sites (refer to chapter 12, figures 12.4 and 12.9).

Figure 15.4

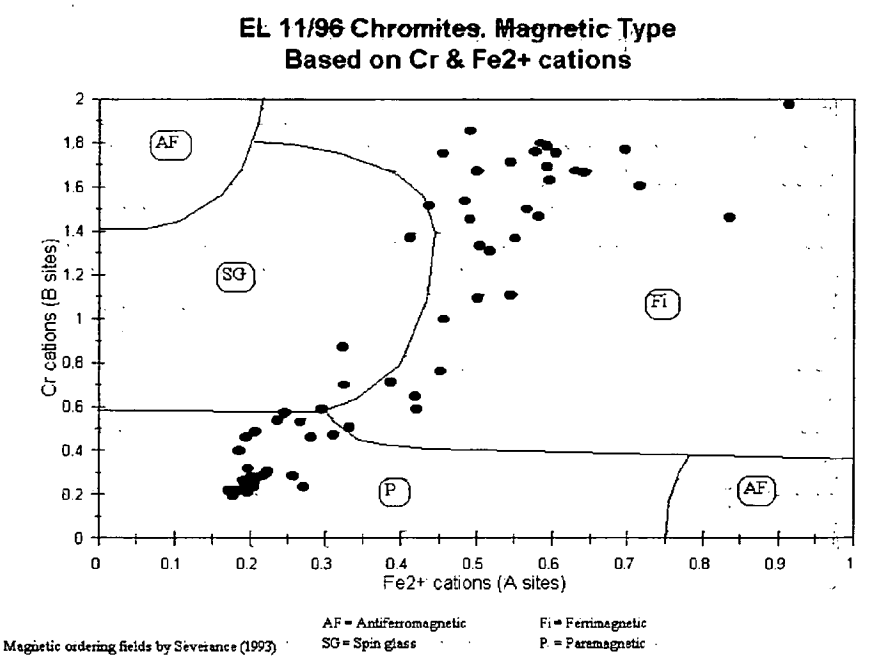

The distribution of magnetic types is very similar to that inferred for the kimberlitic chromites, except that the pattern has been shifted to the right (lower Mg), and away from the region of spin glasses (SG in figure 15.4).

The Surface Distribution of the Ilmenites and Chromites

Figure 15.5 shows the location of EL 11/96 in NE Tasmania. The location is approximately 3 km NE of Pioneer, on the E side of the Ringarooma River, with access via a 4-wheel-drive track from Tebrakunna Rd.

Figure 15.5
Location of EL 11/96

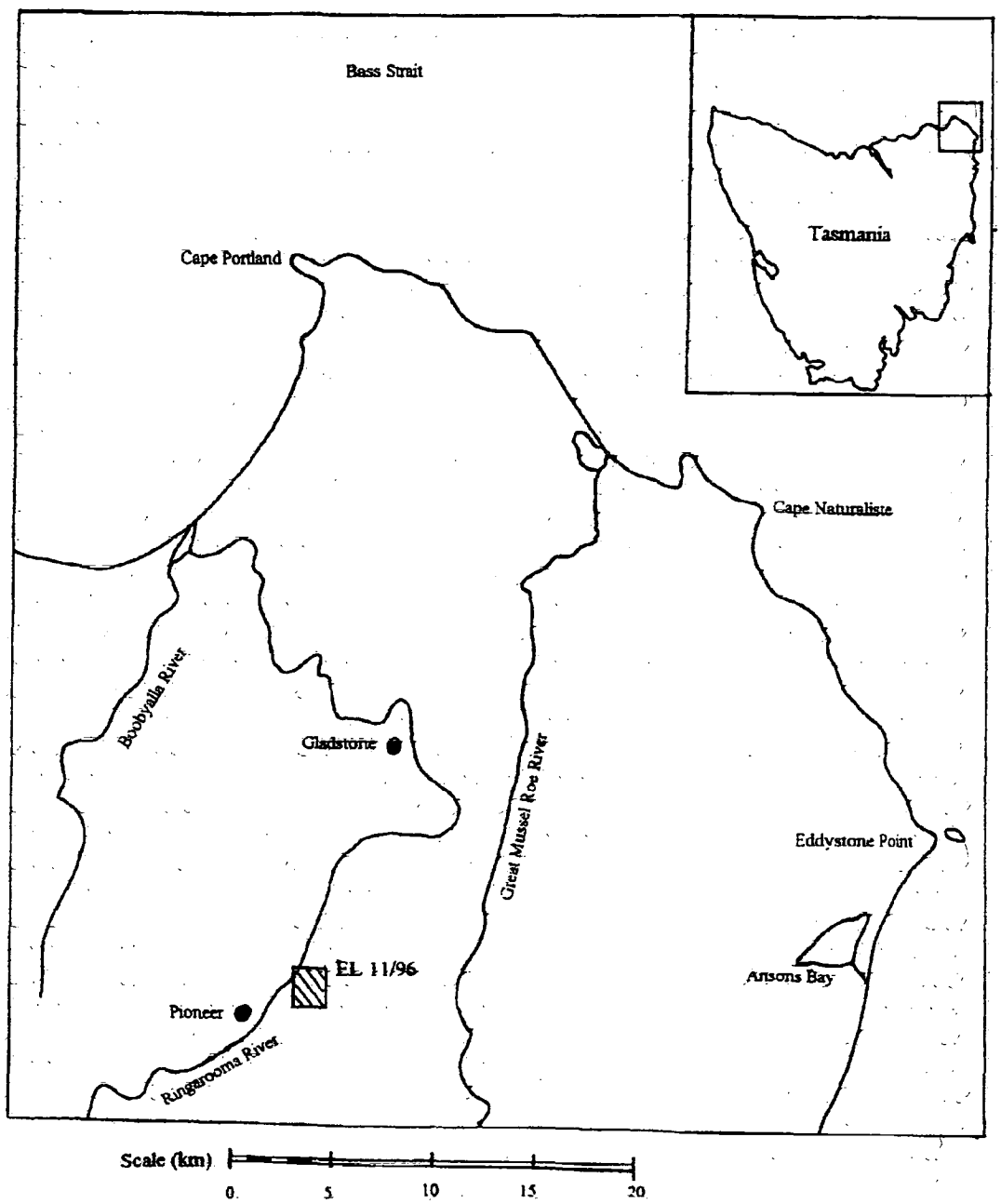

The only outcropping rock in the area is mapped as Devonian coarse-grained granite/adamellite. This granite, which outcrops over almost the entire area, except for the northernmost half km, is deeply kaolinised in the vicinity of parallel groups of quartz veins that trend at about 340^0 (M). Samples were taken at 25 m intervals along six E-W (M) lines across these quartz veins. Mg-ilmenites were found at locations indicated in figure 15.6, and chromites were found at locations shown in figure 15.7.

Figure 15.6

Mg-ilmenite distribution on EL 11/96

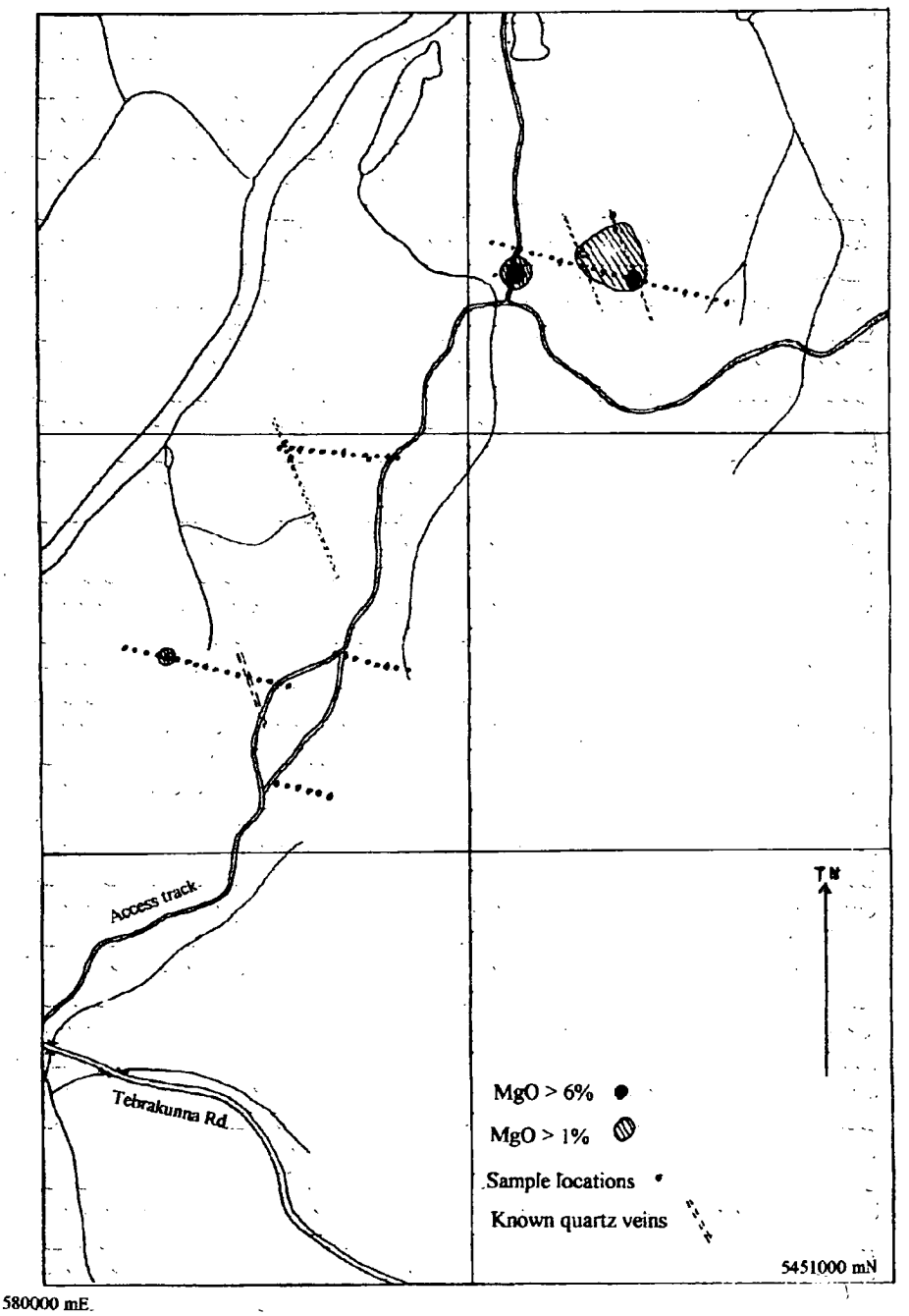

(Grid lines at 1 km intervals)

Figure 15.7
Chromite distribution on EL 11/96

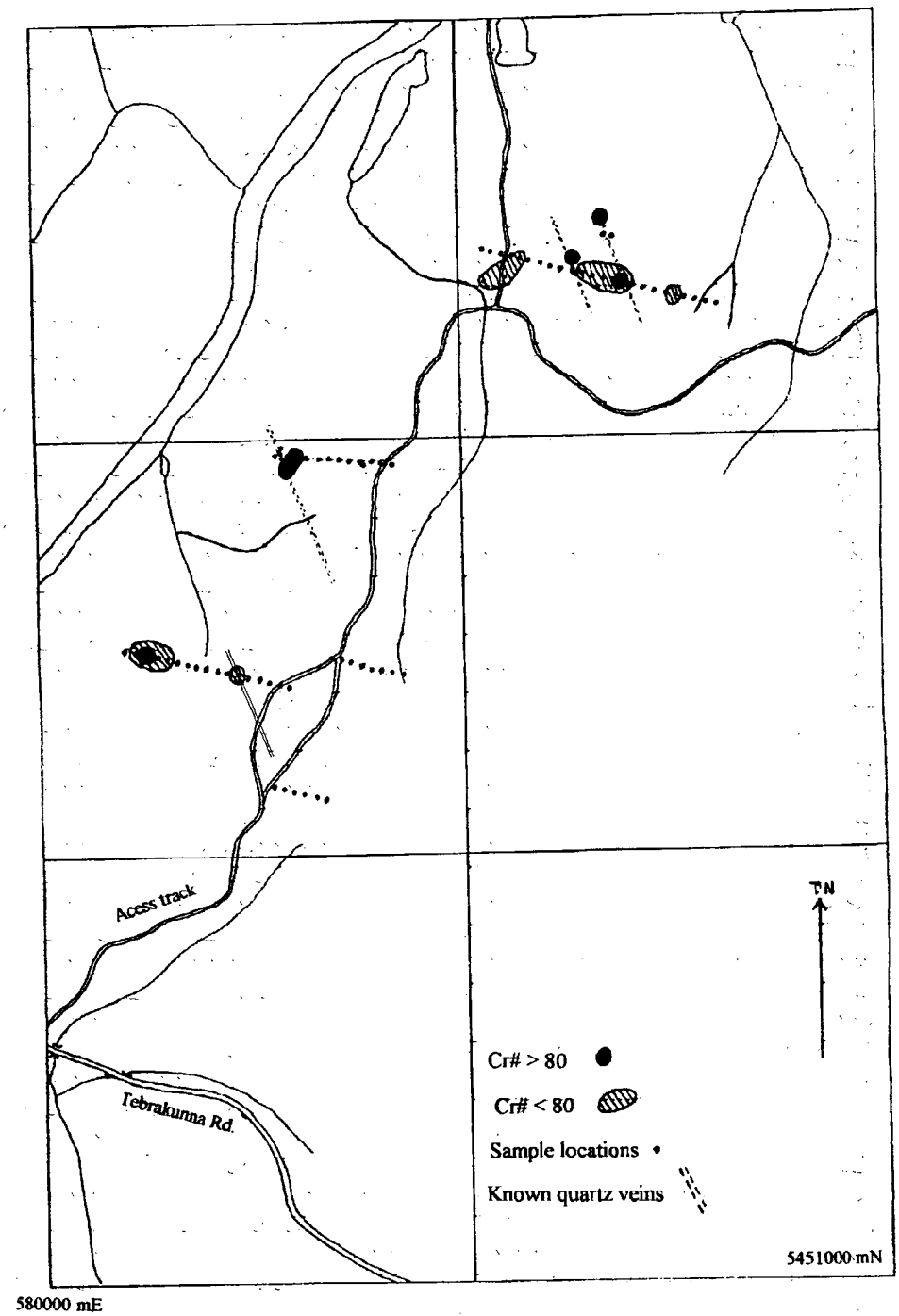

(Grid lines at 1 km intervals)

The quartz veins are fragmented, but still in place within the weathered rock. They appear to mark borders between clay of differing textures. The association with the known quartz veins is apparent for both the chromites and the Mg-ilmenites. It is noteworthy that Mg-ilmenites only appear at locations where chromites are also found. The few locations where no quartz veins are apparent are still in deeply greisenised regions, and show some

geophysical signals (self-potential and magnetic) as well as minor geochemical differences (Allen and McCormack, 1997).

Conclusions

The use of the small-sample separation cell illustrated in figures 8.11 and 8.12 has been able to remove sufficient numbers of the more magnetic and more "rotatable" ilmenite particles so as to allow the detection of the Mg-ilmenites and chromites by visual selection of particles, followed by routine microprobe analysis of sample sets of 15 to 40 particles from the non-rotating fraction.

Both the chromite and the Mg-ilmenites are not granite minerals, and are normally associated with ultramafic rocks.

The sample sites where these Mg-ilmenites and chromites are found form a meaningful and mutually supportive distribution pattern. The distribution pattern is able to provide geological information that would be difficult to obtain by other surface methods in this area. In the case of EL 11/96, employing the rotating field separation has made it possible to identify interesting sites that are not clearly indicated in the geochemical results, and which may be associated with ultramafic intrusions (date unknown) into the Devonian granite.

Note: Since the completion of the above work, a larger (approx. 200 kg) sample was obtained from further south on the southern-most quartz vein in figures 15.6 and 15.7, and gravity-concentrated to a heavy mineral concentrate. The concentrate was separated using a commercial version of the equipment shown in figures 8.13 and 8.14 (and discussed in chapter 16), and the non-rotating fraction was sent to Rio Tinto in Perth (Western Australia) for observation for any Mg-ilmenites. Three Mg-ilmenites were found, with MgO contents from 4 to 7%.

Chapter 16

The Large Sample Separation of Picro-Ilmenite and Kimberlitic Chromite

Introduction

Chapter 11 showed that the higher magnetic susceptibilities and rotation indices for most naturally occurring ilmenites could be used to both magnetically lift and roll these particles out of a sample, leaving behind a Mg-ilmenite (Mg/Fe^{2+} substitution trend) and picro-ilmenite concentrate. Although the picro-ilmenites may have had a higher magnetic susceptibility than some other ilmenites, they generally had very low to zero rotation indices.

This concept was tested in chapter 15, where a separation cell for small samples was used to concentrate Mg-ilmenites to a level where the chances of detecting any Mg-ilmenites in a group of 15 to 40 (tentatively) visually identified particles was sufficient to produce meaningful results from small (2 kg) samples taken during a routine geochemical soil-sampling survey. The particle sizes investigated in this survey were considerably smaller (at an average of 50 μm) than those normally used for visually identifying picro-ilmenites.

Chapter 12 showed that kimberlitic chromites, similar to the picro-ilmenites, also had low magnetic susceptibilities and rotation indices, and would therefore also be concentrated in any picro-ilmenite concentration. The survey described in chapter 15 was also used successfully to concentrate the chromites and to produce a surface map of chromite distribution.

Chapter 15 suggested that rotating field separation can be used to concentrate diamond indicator minerals on a very small sample and very small particle scale (<0.1g and <100μm), but the heavy-mineral sample size used in diamond exploration varies from several hundred grams to over 1 kg, with particle sizes generally between 200 to 400 μm. Such sample sizes can not, of course, be handled by the method employed for the separations in chapter 15. A continuous separation is required.

A continuous separation method presents some different problems to a small batch separation. The routine separations in chapter 15 were carried out by raising the separation cell slowly up towards the rotating magnet drum, as described in chapter 8. In this way the more magnetic particles were removed progressively. It is not possible to progressively remove the more magnetic particles in this way during a continuous separation. Either the separation must be repeated at decreasing distances below the magnet drum, or some other method of removing the more magnetic particles must be found. To attempt the complete separation at the closest distance to the magnet drum would simply clog the separator.

This chapter describes tests on a continuous separation cell, and combines this with a method for removing the more magnetic particles before they enter the separation cell.

Separation Results

Single-cell separation, at decreasing distances below the magnet drum

The separation cell described in figures 8.13 and 8.14, with a 1 cm wide separation platform, was used in this test. Separated magnetic fractions were collected in bottles, as shown in figure 8.15, and the feed rate to the cell was controlled by the particle feed cone in figure 8.16.

For this first test separation Rio Tinto Exploration (formerly CRA Exploration), Perth, W.A., provided 130 g of ilmenite that contained ten picro-ilmenites from a kimberlite called Skerring. The picro-ilmenites had been marked by laser, in a line across each particle.

Using a magnetic field rotation frequency of 30 Hz, 4 separations were carried out, with the separation platform at decreasing distances below the magnet drum. An average feed rate of 43g/hour was used.

(a)	At 27 mm below the magnet drum.	
	Rotating fraction	95.40 g
	Non-rotating fraction	35.65 g
(b)	At 13 mm below the magnet drum.	
	Rotating fraction	31.47 g
	Non-rotating fraction	4.18 g
(c)	At 11 mm below the magnet drum.	
	Rotating fraction	2.03 g
	Non-rotating fraction	2.17 g
(d)	At 10 mm below the magnet drum.	
	Rotating fraction	1.23 g
	Non-rotating fraction	0.92 g

All 10 picro-ilmenites were recovered from the last 0.92 g of concentrate (0.7% of the original ilmenite sample).

This series of separations represented a rather cautious trial of the method. In between the last two separations the non-rotating fraction was checked to ensure that laser-marked picro-ilmenites were still present. It was not until after the last separation that all 10 picro-ilmenites were finally identified within the last non-rotating fraction.

A two-stage single-pass separation for picro-ilmenites

The multi-stage separation above was necessary in order to accommodate those ilmenites that had a high magnetic susceptibility. This procedure was necessary in order to prevent the more magnetic ilmenites from lifting against the upper surface of the separation cell, and clogging the cell. These particles need to be removed from the main sample before the ilmenites enter the main separation cell. For this purpose the two-stage separation illustrated in figure 8.16 was constructed. The first stage is really a simplified version of the low-entrapment separator shown in figure 8.7, and up to the first splitter in figure 8.7 it works in the same way. The magnetic susceptibility of the particles removed at this stage depends on the distance between the 1st stage tube and the magnet drum, and this can be adjusted.

For this trial separation CRA Exploration provided a 180 g (approx) test sample of 400 to 500 μm ilmenites containing an unknown number of laser-marked picro-ilmenites of the same size. The actual number of picro-ilmenites was advised after the separation as twenty one. Separation was carried out with the separating platform of the second separation cell (figure 8.13) 9 mm below the magnet drum. A rotating field frequency of 30 Hz was used, with a feed rate of 350 g/hour. The results were:

Initial sample weight	177 g
Weight of final concentrate (non-rotating)	0.54 g (0.3% of original sample)
No. of picro-ilmenites recovered from concentrate	14

After being advised that seven picro-ilmenites had been missed, the separation was repeated at a feed rate of 150 g/hour, with the pre-separation cell about 2 mm further from the magnet drum, and with the final separation cell at 10 mm below the magnet drum. This second separation recovered a further 4 picro-ilmenites.

Rotation and susceptibility measurements were made on the four picro-ilmenites recovered in the second separation, and they were analysed by electron microprobe. This was done to determine if they were initially missed by chance or because they were more magnetic.

With Mg values between 0.33 and 0.44 and Fe^{2+} values between 0.51 and 0.56, these particles plotted right in the middle of the picro-ilmenite group in figure 11.5. Magnetic susceptibility measurements, at between 100 and 130 x 10^{-6} (cgs) also placed them well within the expected picro-ilmenite values. Measurements of particle rotation did reveal some differences. Most picro-ilmenites either did not rotate at all at the field strengths used here, or the rotation ceased above about 30 Hz field rotation frequency. The four picro-ilmenites missed in the first separation rotated, quite uncharacteristically, at all field rotation frequencies up to the maximum available of 57 Hz. It is possible that the different rotational characteristics for these picro-ilmenites reflects some inclusions, or different formation conditions. Unfortunately it is not known if all the laser-marked picro-ilmenites in this sample came from the same source.

The four unseparated picro-ilmenites therefore appear to have been missed because of their stronger rotations rather than by chance or by separator over-feeding. In order to accommodate these more 'rotatable' picro-ilmenites, it appears to be only necessary to lower the field strength slightly and to accept the resulting lower degree of concentration. The remaining three picro-ilmenites are assumed to be missed again in the second separation for the same reason.

Discussion and Conclusions

The separator used in the latter of the two trials above achieved a feed rate of 350 g/hour. This was achieved in spite of the narrow tube used for the preliminary separation, which allowed a separation width of less than 1 cm, and in spite of the short path-length through the main separator cell (only 5 cm magnet drum width), which severely restricted the time available for final particle separation. The feed rate should be able to be at least doubled (to at least 700 g/hour), and the separation made more precise if the magnet drum diameter were increased to about 250 to 300 mm and the drum length increased to about 100 mm. An increase in drum diameter allows more time for the preliminary separation, and reduces further

any possible particle entrapment (although the above trials did not present this as a problem). An increase in drum length allows a wider particle trace through the preliminary separation (say 5 cm instead of the 1 cm in the above trials), and a faster passage of particles through the final separation for the same separation time.

Kimberlitic chromites and pyrope garnets have lower magnetic susceptibilities and rotation indices than the picro-ilmenites, as was determined in chapters 12 and 13. These particles will also be retained in any rotating field picro-ilmenite separation. Any separation such as described above will therefore produce a concentrate containing all three of the main diamond indicator minerals.

Commercial Developments Since the Above Trials

Since the thesis work was completed, the separation of diamond indicator minerals has been further developed. The above suggested modifications to the separator were initially incorporated into the design of a larger prototype separator (shown in figure 16.1), built specifically for the development of indicator mineral separations. This separator used a 400 mm diameter magnet drum and a drum length of 100 mm. The maximum field strength available at a separation surface was 0.45 Tesla.

Figure 16.1

A Rotating Field Separator for Diamond Indicator Minerals

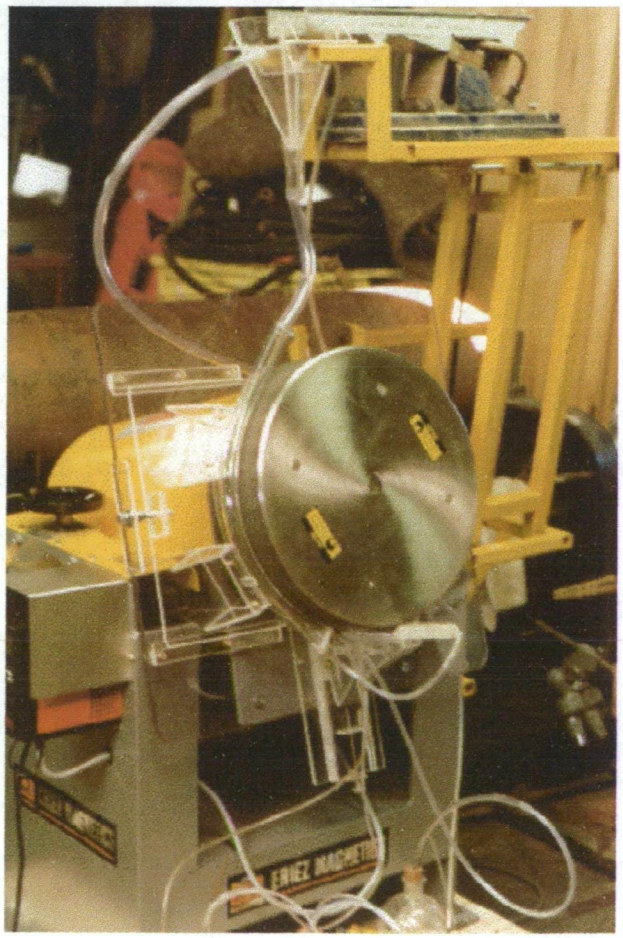

This is the same basic design as shown in figure 8.16. During the initial trials of the above machine, the remaining three missing laser-marked picro-ilmenites were recovered from the 177 g test sample mentioned above.

A total of 34 samples, from less than 50 g to more than 1.5 kg, were provided by Rio Tinto (Perth, W. A.) for machine evaluation. The samples included some of the more difficult ones where chemical etching (of ilmenites) had been unable to provide any advantage. The results of these trials were sufficiently encouraging for Rio Tinto to order the construction of the final version of the separator, which is illustrated in Figure 16.2.

Figure 16.2

The rotating field indicator mineral separator constructed for Rio Tinto Exploration

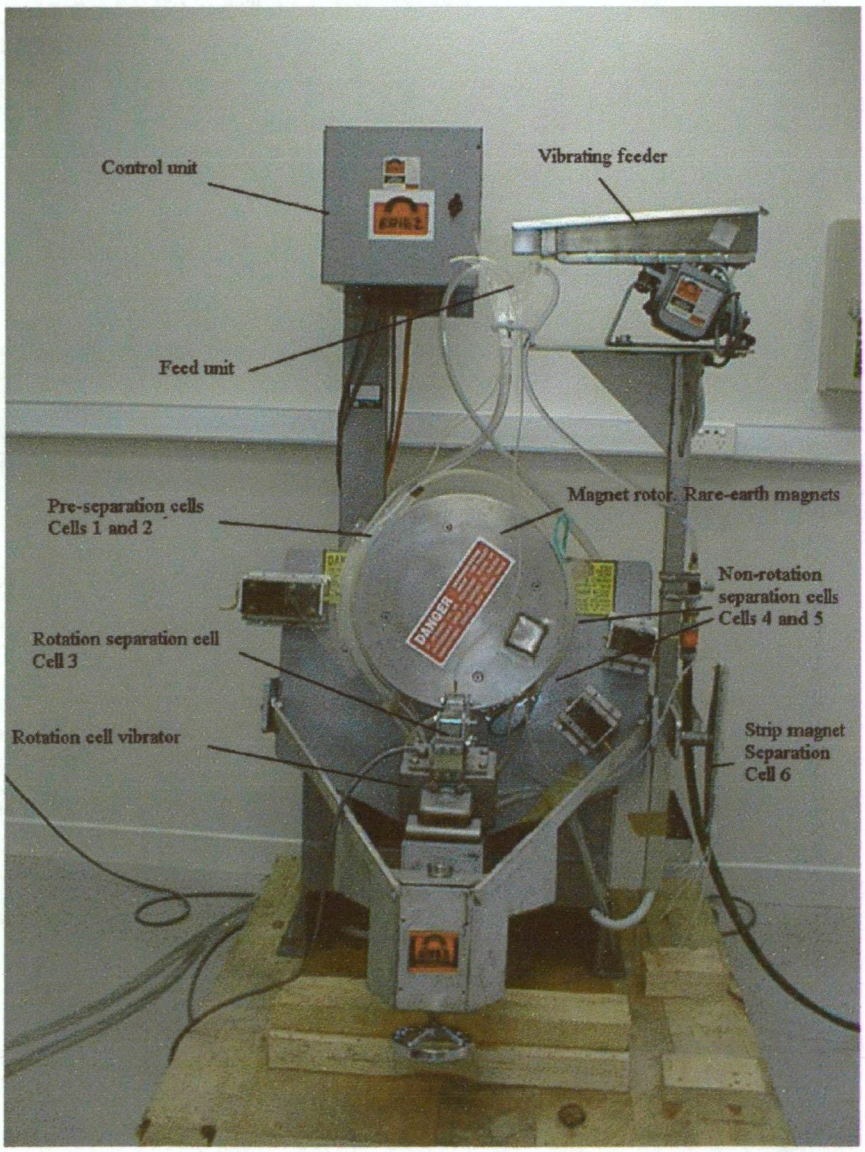

The separator illustrated in figure 16.2 is a multiple-stage separator, producing seven different magnetic fractions. The separation system is illustrated schematically in figure 16.3.

Figure 16.3

Separator stages and fractions

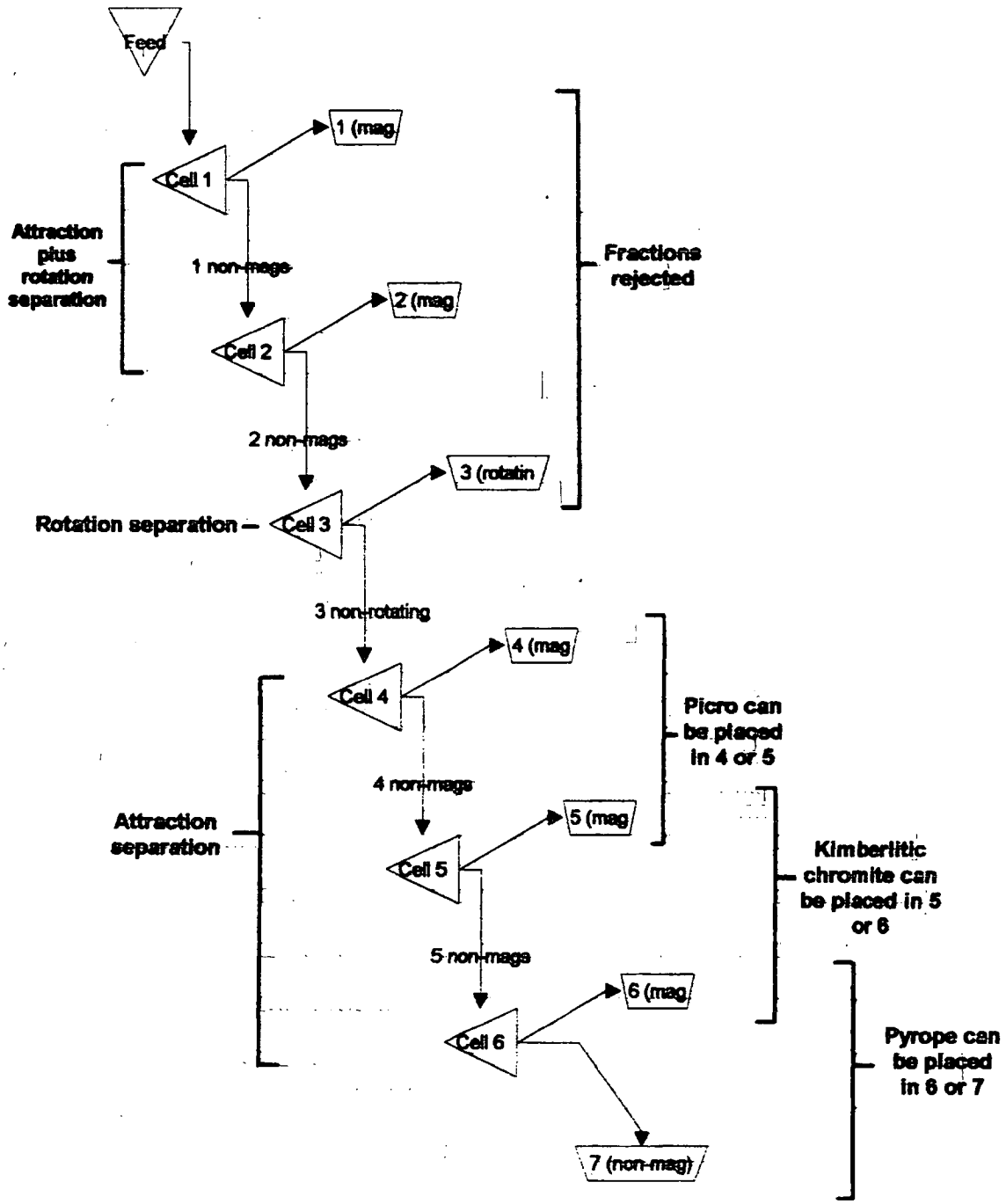

Locations of the various separation cells are shown in figure 16.2.

During commissioning of the separator (at Rio Tinto's laboratory, Perth, W.A.), field strength settings (i.e. cell distances from the magnet drum surface) were determined which allowed about 90% of the indicator minerals to be distributed as follows:

Picro ilmenites to fraction 4
Kimberlitic chromites to fraction 5
Pyrope garnets to fraction 6

However, by moving cells 4 and 5 to a slightly lower field strength, 90% of the picro ilmenite can be sent to fraction 5, and 90% of the kimberlitic chromite to fraction 6 if the particular sample contains large quantities of non-rotating particles slightly more magnetically susceptible than picro ilmenite. Particle transport through the separator is accomplished by particle rotation plus gravity (cells 1 and 2), vibration and particle rotation (cell 3), and water flow drag and gravity (cells 4, 5, and 6).

Depending on the distribution of particle magnetic properties, up to 2 kg per hour of concentrate can be separated. Particle sizes are generally restricted to between 200μm and 800 μm. Sample weights requiring observation (visual identification of indicators by trained "observers") are, *depending on sample characteristics*, reduced by between 95% and 30%. Most of the samples to be separated with this separator have already had the very magnetic and the very weakly magnetic material removed. Therefore fractions 1, 2, 6 and 7 usually contain very little material. Nearly all the pyrope garnets (and any diamonds) will have been removed. The pyrope garnets are separated elsewhere (in the process used by Rio Tinto) with a Magstream separator (see chapter 3).

Chapter 17

The Eddy Current Separation of Small Metallic Particles

Introduction

Chapter 6 developed an expression (equation 6.7) that calculated the minimum cubic-shaped particle size that could be rolled by eddy-current effects for a given combination of magnetic field strength and field rotation frequency. Figure 6.2 plots the relationship between rollable particle size and the required field rotation frequency for various different metals, given a field strength of 0.45 Tesla. This graph indicates that the eddy current rolling effect may be able to be used as a practical separation method for metallic particles considerably smaller than the present commercial separation particle size limit of about 1.5 mm.

The equipment available here, and which has been used for other mineral rotation tests, has a maximum useable field strength of about 0.26 Tesla, and a maximum available field rotation frequency of about 250 Hz. If figure 6.2 is re-drawn for a magnetic field strength of 0.26 Tesla, as in figure 17.1, it can be seen that the available field strength and rotation frequencies are adequate to test the model for all the metals shown, except lead.

Figure 17.1

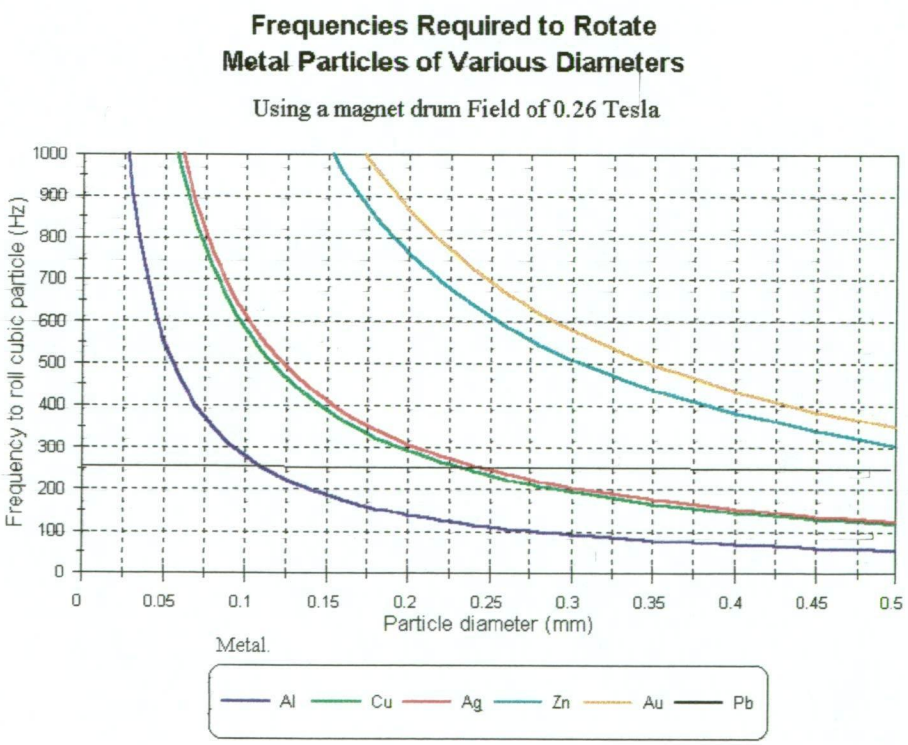

The aims of this chapter are to demonstrate that the theory of chapter 6 does predict the real behaviour of small metallic particles in a rotating magnetic field, and to trial a separation method which could be developed further for the practical eddy current separation of such small metallic particles as free gold.

A Comparison of Theoretical and Experimental Particle Rolling Frequencies

Small metallic cubes, on which the theoretical predictions have been based, are not easily manufactured. Short 5 mm lengths of copper wire were used instead. The lengths were cut with side-cutters, which tended to squash and distort the cut ends. If the cut at one end is at right angles to the cut at the other, this distortion can be used to make the wires roll roughly as if they have a square cross-section. Such shape approximations are certainly close enough for an initial test of the predicted magnetic field rolling frequencies.

Seven different copper wire gauges were used (0.15, 0.25, 0.3, 0.6, 1, 1.9, and 3.5mm), and ten 5 mm lengths were cut for each wire gauge. Each length was placed separately on a level plastic surface above the magnet drum. The rotation of the magnet drum was then increased gradually until the wire began to roll. Figure 17.2 plots the average field rotation frequencies at which each wire gauge began to roll, in a magnetic field strength of 0.24 Tesla. The calculated (theoretical) field rotation frequencies are also plotted.

Figure 17.2

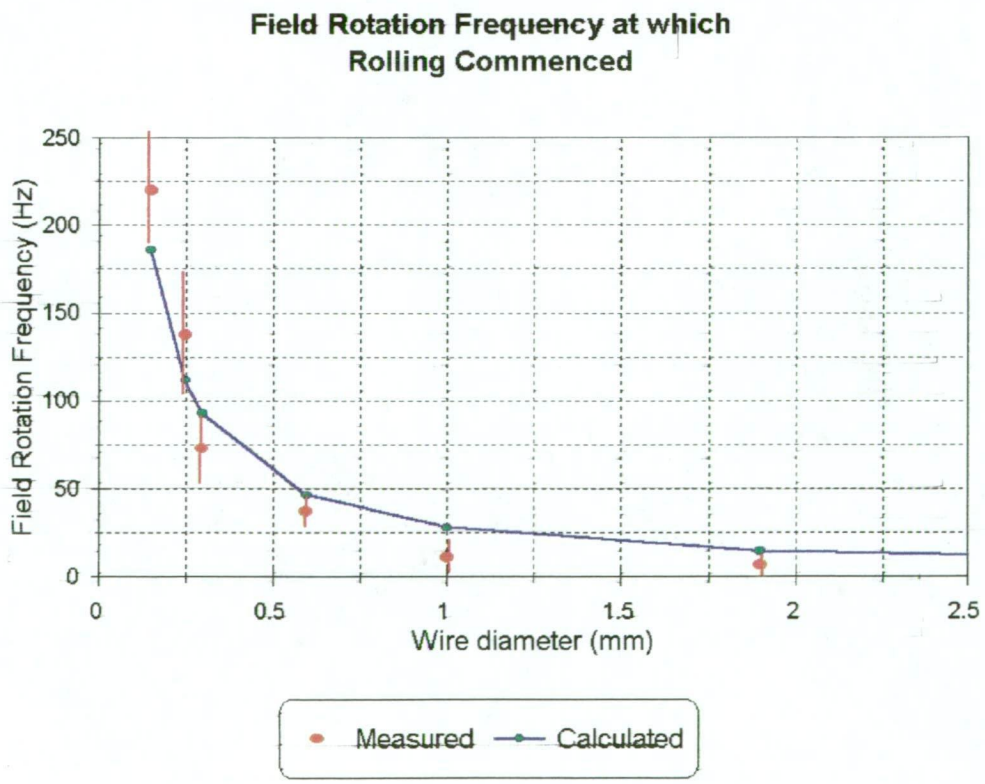

While the measured field rotation frequencies were usually a little lower than the predicted frequencies, it can be said that the theoretical predictions do approximate what can be achieved in practice. The above tests were repeated with the wires submerged in water, and gave almost identical results.

The use of short wires rather than small particles in this test should not, in theory, have affected the validity of the results. While the length may be increased, so have both the mass and the volume, in the same proportion. The torque required to roll the wire, with its squashed ends, remains in proportion to the length.

A Practical Eddy-Current Separation for Small Conductive Particles

The equipment illustrated in figures 8.19 and 8.20 was constructed to test a practical eddy-current separation method. In its basic layout it is very similar to the eddy current separators currently used for larger metallic particles, such as illustrated in figure 3.13. The main difference is that particle feed is now directly above the magnet drum and the belt now serves to transport the non-metallic particles away from the separation region, rather than to transport all particles to the separation region.

Tests on the equipment shown in figure 8.20 achieved only 73% recovery of copper particles, with most particles below about 100 μm remaining unseparated.

In a later test, a magnet drum specially built by Eriez Magnetics in Melbourne was used. This magnet drum had a diameter of 380 mm, a length of 100 mm, and a field strength at the separation surface of 0.48 Tesla. This drum is illustrated in figure 16.1 (where it is set up for diamond indicator mineral concentration). The separation arrangement remained the same as shown in figure 8.20. The field rotation frequency used was 300 Hz. The theory in chapter 6 predicts that such a field strength and rotation frequency should allow copper particles down to 45 μm and aluminium particles down to 23 μm to be rotated. An initial qualitative test, using only Al and Cu filings, showed that 100% of all available Cu and Al particles (down to about 30 μm) were able to be rolled, and that it did not matter if the particles were in water or dry.

Two separation trials were carried out. The feed material for the first trial consisted of (by weight):

90% zircon	75-150 μm
10% Al particles (filings)	30-1000 μm

The feed material for the second trial consisted of (by weight):

81% zircon	75-150 μm
19% Cu particles (filings)	30-500 μm

Feed rates for both trials were approximately 30 kg/hr/m, and the belt travel (outer drum travel) was approximately 3 cm/sec. With this feed arrangement the length of the magnet drum determines the actual feed rate, so that feed rates can be given per m length of magnet drum. The metallic particle shapes tended to be very irregular and usually elongated.

The first trial recovered 90% of the Al particles as 95% pure Al (by weight). Most particles below about 50 μm (in smaller diameter) did not separate. The second trial recovered 80% of the Cu particles as 80% pure Cu, with most particles below about 75 μm remaining unseparated.

Discussion and Conclusions

While the ability of a rotating magnetic field to roll an isolated cubic-shaped metallic particle is quite well predicted by the theory of chapter 6, the commencement of particle rolling may be significantly delayed by interference from non-metallic particles. Trial separations, such as the trials detailed above where a 5:1 or 10:1 metal:non-metal ratio was used, suggest that the numerator of equation 6.7 needs to be multiplied by a factor of about 2 for the equation to take into account the interference of non-metallic particles. Figure 17.3 shows the approximate field rotation frequencies required for practical separations.

Figure 17.3

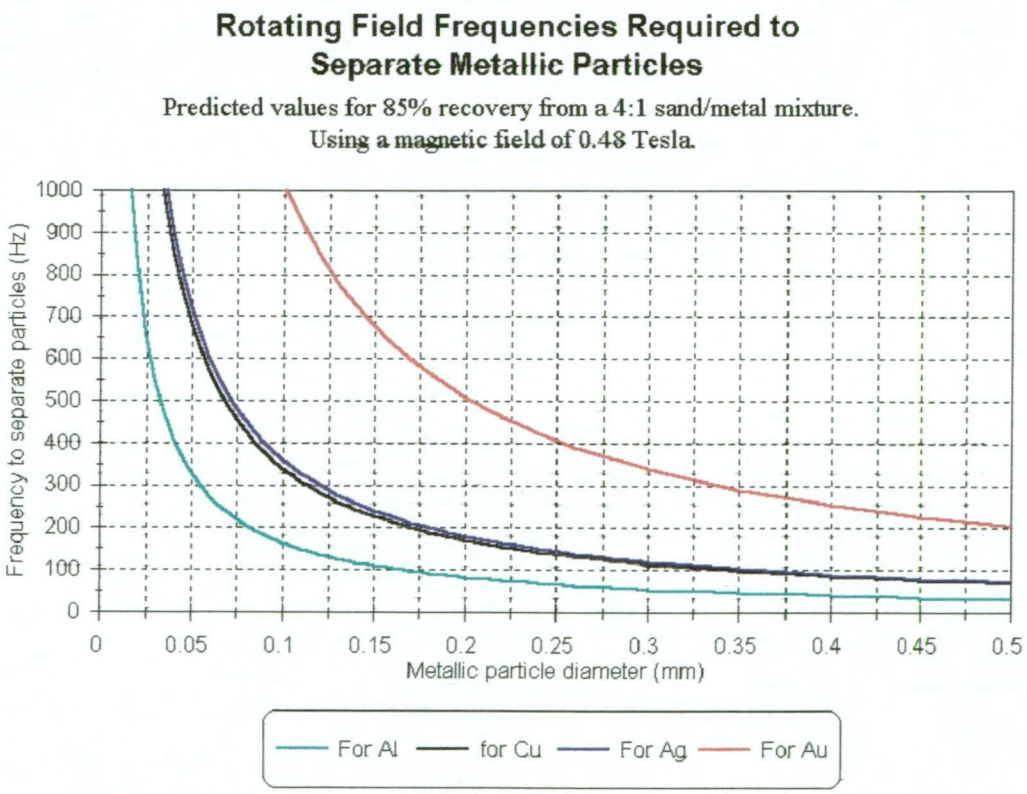

If it is supposed that for good separation the particles need to be only 1 particle deep on the transport belt, then some estimate of maximum separation rates for the method can be arrived at. For 100 μm particles the field rotation needs to be about 150 Hz to cause particle rotations. Therefore it is a reasonable estimate to assume that a field rotation of 300 Hz will

give a maximum rolling speed along a surface of about 4.7 cm/sec. For a belt travel of 4 cm/sec, with 100 μm particles and a field strength of 0.48 Tesla, the maximum feed rate should be about 130 kg/hr/m. The maximium feed rate should increase almost in proportion to the square of the particle diameter.

Rotating field eddy current separation can be used on a slurry as well as on dry material. In this respect the method has a substantial advantage over conventional eddy current separation, where the material must be dry. However the rotating field eddy current separation and the conventional repulsive eddy-current separation should be seen as complimentary. The conventional methods are applicable to particles above about 1.5 mm, while the rotating field method is more applicable for particles less than 1.5 mm.

Section 5

Summary and Conclusions

Chapter 18

Summary of Equipment Design, Rotating Field Theory and Experimental Results

Production of a Rotating Magnetic Field

Although a rotating magnetic field can be produced very simply, and much more accurately than the method employed here (eg. by rotating two opposing magnetic poles around a central point), the method used here has the advantage of producing a rotating field effect over a large enough area to make it of practical use for mineral separation. All measurements of particle rotational behaviour can then be made using the same equipment used for practical mineral separation.

The construction of the magnet drum was described in chapter 7 and illustrated in figures 7.1 to 7.4. The arrangement shown in figure 7.3 produced a field, at 10 mm above the magnet poles, that varied by about ! 0.005 T throughout a field rotation (see figure 7.5), and that rotated at a reasonably constant angular velocity (see figure 7.6).

The field and gradient at varying distances from the drum surface were found to be described by equations 18.1 and 18.2. These relationships are able to accurately describe the field above all five magnet drums constructed during the course of the thesis, requiring only the field at the drum surface (B_s) and a calibration constant (C) to be known.

$$B = \frac{B_s}{C^{(\frac{x}{x_0})}} \qquad \text{(T)} \qquad 18.1$$

Where: B_s is the field at the drum surface (T)
C is the calibration constant for the drum
x is the distance radially out from the drum surface (m)
$x_0 = 10^{-3}$ m

$$\frac{'B}{'x} = \frac{-B_s \ln(C)}{C^{(\frac{x}{x_0})}} \qquad \text{(T/m)} \qquad 18.2$$

Measurement of Magnetic Susceptibility, Magnetic Moment and Rotation Indices

All three of these values were calculated from two measurements of distance below the magnet drum surface. The method was described in detail in chapter 7 (figures 7.8 and 7.9). Distance measurements were made at the point where particles first commenced continuous rotation, and the point where they were lifted against the force of gravity. These measurements gave the fields and gradients at these points.

Once the field and gradient at which the particles lifted is determined, the magnetic susceptibility and mass magnetic moment can be calculated using the equations given in chapter 4 (equations 4.2 and 4.7).

$$k_g = \frac{\mu_0 a\left(1-\frac{D_f}{D_p}\right)}{4\pi B_l \frac{\partial B_l}{\partial x} \times 10^{-3}} \qquad \text{(cgs units)} \qquad 18.3$$

$$M_m = \frac{\mu_0 a}{\frac{\partial B_l}{\partial x}} \qquad \text{(Wb.m/kg)} \qquad 18.4$$

Where: k_g is the mass magnetic susceptibility (cgs units)
M_m is the mass magnetic moment (Wb.m/kg)
μ_0 equals $4\pi \times 10^{-7}$
a is the acceleration due to gravity (m/se^2)
D_f is the density of the immersion fluid (kg/m^3)
D_p is the density of the particle (kg/m^3)
B_l is the lifting field (T)

The rotation index was introduced in chapter 4 as a measure of how strongly a particle rotates compared to the rotation strength predicted by its magnetisation. Ideally it represents the sine of the angle between the external field and the particle magnetisation. In practice this may not be the case, due to uncertainties about the particle magnetisation at the field strength where it rotates (magnetistaion is inferred from the lifting field strength). Due to these difficulties, two rotation indices were introduced in chapter 4. The paramagnetic rotation index (R_p), which assumes the particle magnetisation is proportional to the external field, and the ferromagnetic rotation index (R_f), which assumes that the particle magnetisation is essentially the same at both lift and rotation.

$$R_p = \frac{d\left(\frac{\mu_0 a}{4\pi \times 10^{-3}}\left(1-\frac{D_f}{D_p}\right)-k_g B_r \frac{\partial B_r}{\partial x}\right)}{2k_g B_r^2} \qquad \text{(dimensionless)} \qquad 18.5$$

$$R_f = \frac{\mu_0 d\left(a\left(1-\frac{D_f}{D_p}\right)-\frac{M_m}{\mu_0}\frac{\partial B_r}{\partial x}\right)}{2M_m B_r} \qquad \text{(dimensionless)} \qquad 18.6$$

Where: d is the particle diameter (m)
B_r is the rotating field (T)

Factors Affecting Particle Rotation

Magnetocrystalline and shape anisotropy

For paramagnetic particles, particle rotation results from magnetocrystalline anisotropy. This anisotropies are discussed in chapter 2. In this case, after considering the affects of particle inertia, the rotation index will indicate the magnitude of the anisotropy. For ferromagnetic and ferrimagnetic particles, the rotation may also be affected by other factors such as domain wall velocities and the relationship between the rotating field and the critical field for domain wall motion. If no domain wall or critical field effects are involved, then the anisotropies may be related to the ideal rotation index (R_{fo} in equation 4.19) by the equations below, which assume a particle which has a prolate spheroid shape, and also assume that the shape and magnetocrystalline anisotropies are in the same direction

For a uniaxial crystalline anisotropy (see chapter 2):

$$\sin \vee = \frac{(K_1+K_s)\sin 2h}{MH}$$

and for a cubic anisotropy where field rotation is in a plane containing two easy magnetisation directions:

$$\sin \vee = \frac{\frac{K_1}{2}\sin 4h+K_s \sin 2h}{MH} \qquad 18.7$$

Where: K_1 is the first magnetocrystalline anisotropy constant
K_s is the shape anisotropy constant
ϕ is the angle between particle magnetisation (M) and external field (H)
θ is the angle between particle magnetisation direction and the easy magnetisation direction

The shape anisotropy constant (K_s) contains the factor (N_a - N_c), which is the difference between the demagnetising factors along the a and c axes. If the particle is spherical (or cubic, octahedral, etc.) in shape, N_a, N_b, and N_c are all equal and the K_s term in the above equations disappears. If the shape anisotropy is not along an easy axis of magnetisation, then the relationships are much more complex than is given above, and are not considered here.

Calculations of the magnitude of the angle θ (see chapter 4) indicate that for magnetite, in the fields needed for particle lift, the angle is about 15^0.

Coercive force effects (magnetically ordered particles)

Coercive force is a measure of the resistance of a magnetic domain structure to change, and is defined as the reverse field needed to reduce the magnetisation of a saturated material to zero. If a particle has a high coercive force, the external field may well rotate the particle without exceeding the coercive force. In this case the maximum torque is placed on the particle when the angle (ϕ) between the particle magnetisation and the external field is 90^0. In this case the ferromagnetic rotation index is predicted to be1.

As the external field (H) increases past the coercive force (H_c), domain wall motion commences when $H.sin(\phi)$ is greater than the coercive force. Domain wall motion becomes important when $H.sin(\phi)$ becomes greater than the coercivity of remanence (H_{cr}), or:

$$\sin \vee \mathrm{m} \frac{H_{cr}}{H} \qquad 18.8$$

Where H is the external field and H_{cr} is the coercivity of remanence (A/m)

If a particle is rotated at fields greater than but close to H_{cr}, the rotation index becomes less than 1. At higher fields domain rotation through an angle θ against the anisotropy field occurs, and increases with H. This leads to a decrease in the magnitude of the angle ϕ between the magnetisation and the external field. Therefore, as the field required to rotate a particle increases towards the anisotropy field, the rotation index decreases towards zero.

Rotating field mineral separation, at least for minerals such as magnetite, will normally be carried out at field strengths well above H_{cr}, and may even be carried out at field strengths greater than the anisotropy field (H_A).

As particle sizes become smaller, coercive force increases, and for some rotating field separations there will be a particle size where H becomes less than H_c.

Domain wall velocity effects (for magnetically ordered particles)

The relationship between domain wall velocity and the external field was given in chapter 2 (equation 2.9) as:

$$v = c(H - H_0) \qquad 18.9$$

Where: H_0 is the critical field for domain wall motion (approx. equals H_c)
c is a constant for the material, known as the wall mobility

Domain wall effects only become significant when H is close to H_0. If this is the case, they tend to increase the rotation index by retarding the ability of the particle magnetisation to change to a new direction of easy magnetisation as the external field rotates. The actual time to complete domain wall motion through a crystal depends on the number of domain walls moving through the crystal.

The rotation index may be written to include an approximation of the effects of domain wall velocity (assuming a single domain wall) as:

$$R_f = \sin\left(\gamma + \frac{360fd}{c(H-H_0)}\right) \qquad 18.10$$

Where: f is the field rotation frequency
d is the particle size (m)

Particle inertia effects

If a stationary particle is subjected to a torque as a result of external field rotation, the particle has only a finite time to respond to the torque and to accelerate to the field rotation frequency, before the field moves on to the next direction of easy magnetisation. Therefore, as the field rotation frequency increases, a higher torque is required to commence particle rotation. This implies a decrease in the measured rotation index as the field rotation frequency increases. The measured rotation index, for a ferromagnetic particle, may be expressed to include both domain wall velocity effects and particle inertia effects as:

$$R_f = \frac{\sin\left(\gamma + \frac{360fd}{c(H-H_0)}\right)}{1 + \frac{\rho d^2 f^2}{5AM_m H}} \qquad 18.11$$

Where M_m is the particle mass magnetic moment
A is a the fraction of a cycle available for particle angular acceleration

Eddy current effects

Eddy currents occur as a result of domain wall motion in magnetically ordered particles, and are one of the main factors controlling wall motion, but these effects are not considered here. The concern here is with eddy currents developed within electrically conducting particles. These eddy currents were examined in chapter 6, where the minimum particle size which could be rotated by eddy current effect alone was given as:

$$d = \frac{8aqD}{0B^2 f} \quad \text{(m)} \qquad 18.12$$

Where: ρ is the resistivity of the material (ohm.m)
D is the particle density (kg/m^3)

The minimum particle size is proportional to the resistivity, and this factor limits the use of eddy current as a rotating force to those materials thathave very low resistivity. Practical rotating field eddy current separation is limited to the metallic elements and alloys. For gold particles, using fields of about 0.4 Tesla and field rotation frequencies of only about 300 Hz, the expression predicts that particles down to about 200 μm should rotate, but the actual separable particle size, when particle rotation may be considerably hindered by other particles, is larger than this.

Maximum particle size for rotating field separations

Practical rotating field separations involve the magnetic rotation of particles while they are being held against a surface by magnetic attraction, gravity, or both. While the magnetic torque applied to a particle in a rotating magnetic field is proportional to the particle mass (or the particle volume), the opposing torques, caused by interaction with the surface, are proportional to both the particle mass and the particle diameter. The surface reaction forces therefore increase faster than the rotational torque, and a particle size is reached when the particle is not able to be magnetically rotated.

It was shown in chapter 7 (equation 7.8) that the maximum separable particle size for a cubic-shaped particle is given by:

$$d = \frac{2R_f}{\ln(C)\%10^3 ! \frac{!_0 a}{M_m B}} \quad \text{(m)} \qquad 18.13$$

The minus sign in the denominator applies to the separation when the particles are being held up under the magnet drum, and the plus sign applies to particles that are held down on the top surface above the magnet drum.

The maximum separable particle size depends partly on the particular material being separated (through R_f and M_m) and partly on the construction of the magnet drum itself (through C). The strength of the magnetic field only determines the size difference between under-drum and over-drum separations.

The value of the calibration constant (C) determines the field gradient of the magnet drum, and has a significant effect on the maximum separable particle sizes. For example, decreasing C from a value of 1.125 (for the drum in figure 7.4) to a value of 1.03 (for a proposed commercial separator drum) raises the maximum separable particle size over the top of the drum from 5.7 mm to 17 mm.

Particle Rotation Results

Iron Particle Rotations

Measurements of rotation indices for iron particles are given in chapter 10. The measured rotation indices (at 10 Hz field rotation frequency) averaged 0.15, with no rotation indices above 0.25. Modelling of the rotation index frequency response, using a simplified version of equation 18.11, indicated that no domain wall velocity effect was present, and that the variation of rotation index with frequency was due to particle inertia only. Because the coercive forces for soft iron are listed as well below the rotating field of 0.0017 Tesla, the rotation field for the iron was probably well above the critical field (or the coercive force), and no domain wall velocity effects would be expected.

The measured rotation indices are about half of the expected value, in spite of an expected increase due to shape anisotropy. The iron particles were filings, and most of them were flattened and elongated rather than cubic in shape. This would have led to an increased rotating field, and to an over-estimation of the particle magnetic moment (which is based on particle diameter for a cubic shaped particle). While the measured R_f would more accurately represent the rotational characteristics of these particles in a particle separation process, the measured R_f values could very easily indicate a $\sin\phi$ which would be 50% lower than it should be. For these flattened particles the true angle between the particle magnetisation and the external field (ϕ) would probably have been around 22.5^0.

There was some evidence for particle rotation at right angles to the field rotation, but this was not at a strength that seriously affected normal particle rotation measurements (which are in the same direction as the field rotations).

Magnetite Particle Rotations

Magnetite rotation characteristics are also discussed in chapter 10. Unlike the iron particles, the measured magnetite rotation indices show a very wide range, from less than 0.05 to greater than 2. This was in spite of a much lower expected measurement error for the more bulky magnetite particles. Most of the higher rotation indices were associated with the larger particles, and the rotation index generally decreased with decreasing particle size. In general the rotation index decreased with increasing field rotation frequency, as was found with the iron particles, but for larger particles there appeared to be a peak in rotation indices at a field rotation frequency of about 30 Hz for both 1 mm and 0.7 mm particle sizes. A simple modelling of the rotation index frequency variation indicated that domain wall velocity effects were significant, and were causing the observed peaks in the rotation indices for the larger particles. The magnetite rotation index frequency response was therefore due to a combination of particle inertia and domain wall velocity effects. The modelling indicated that the angle ϕ between particle magnetisation and external field (excluding lag angle due to domain wall velocity effects) was about 22^0.

The coercive forces for natural magnetite particles which are given in the literature (see chapter 2), are of the same order of magnitude as the field strengths actually needed to rotate the particles (see appendix A). The particles are therefore rotating in field strengths where coercive force effects (chapter 4, figure 4.3) and domain wall velocity effects (equation 4.17) may be expected to increase the measured rotation indices to as high as 1, with the remaining discrepancy (greater than 1 for some particles) being accounted for by particle shape factors and measurement error.

The modelling of the rotation index frequency response indicates that this approach may be able to be refined for the measurement of domain wall velocities in individual small particles.

The great variation in rotation indices probably occurs due to the presence of a varying numbers of domain walls in particles, and significant variations in coercive force. These are expected in natural particles due to varying grain size, crystal imperfections or polycrystalline particles, and should have the effect of reducing any domain wall velocity effects in proportion to the number of domain walls present.

Magnetite particles showed evidence of particle rotation at right angles to the external field rotations. The strength of this type of particle rotation generally increased with particle size, and peaked at a field rotation frequency of about 40 Hz and a field strength of about 12000 A/m. At lower external field strengths than those normally required to rotate the particles parallel to the field (when the particles are supported in a heavy liquid), the perpendicular rotation strength showed signs of becoming stronger than the parallel rotation strength.

As most practical magnetic separation of magnetite will take places in field strengths that are a factor 10^2 greater than the minimum particle rotation field strengths, coercive force and domain wall velocity effects should not have any effect on magnetite separation in rotating magnetic fields.

Ilmenite Particle Rotations

Ilmenite particle rotations are discussed in chapter 11. Rotation indices vary from very close to zero (i.e. undetectable with this equipment) to greater than 1. The probable existence of hematite-rich phases within many ilmenite particles makes the interpretation of the higher rotation indices considerably more complex than for the magnetite. The possible existence of such phases, in varying widths and lengths, implies that particle magnetisation characteristics could include a number of different coercive forces. At rotation the various components of the crystal could be subjected to rotating fields that range from well below the coercive force to well above the coercive force. Domain wall velocity effects may influence some components of the crystal but not others. In many cases the ferrimagnetic components of the crystal, which react to a rotating field, will be intergrown with an ilmenite composition that is paramagnetic at room temperature.

There are therefore sufficient explanations for rotation indices above the expected maximum value of 0.7.

In spite of the above, which may be expected to introduce an apparently random relationship between rotation indices and particle chemical composition (depending on where in the crystal the analysis was done), a general relationship was found between ilmenite particle rotation and chemical composition. This probably indicates that most of the measured particles did not contain significant hematite-rich phases.

The most significant relationship between particle rotation and chemical composition was illustrated in figure 11.9, where an Fe^{3+} cation content above about 0.25 is associated with particles of high magnetic susceptibility but low rotation indices. Fe^{3+} contents below about 0.1 cations are frequently associated with low magnetic susceptibilities but high rotation indices.

The picro-ilmenites, of interest as diamond indicator minerals, fall approximately between the above two groups. They have very low to zero rotation indices, but generally have higher mass magnetically susceptibilities (average about 100 x 10^{-6} cgs) than other ilmenites of such low rotation indices. These relationships were illustrated in figures 11.10 and 11.11.

The relationship between the Fe^{2+}/Fe^{3+} content of ilmenites and their "rollability" was also illustrated in figure 11.8, where the picro-ilmenites show up as a lower Fe^{3+} / low Fe^{2+} group. Much of the Fe^{2+} has been replaced by Mg ions, thereby decreasing the overall spin-orbit coupling basis for the magnetocrystalline anisotropy. At the same time, the Fe^{3+} content has maintained a significant magnetic susceptibility, but made little contribution to the magnetocrystalline anisotropy.

The magnetic concentration of the picro-ilmenites, desired within the diamond exploration field, can therefore be best accomplished by first removing the more magnetically susceptible particles in an attractive separation, then removing (by rotating field separation) those particles of similar susceptibility, but which have high rotation indices, and lastly by using another attractive separation to remove those particles of both low susceptibility and rotation index.

Although some perpendicular particle rotations may have been observed, these were not convincing, and were certainly not significant.

Chromite Particle Rotations

Chromite particle rotations were examined in chapter 12. Rotation indices varied in a very similar way to those of ilmenite, and for similar reasons. Some chromites contained phases of inversion or phases which would be intermediate between normal and inverse spinel (see figure 12.13). These tended to have both high rotation indices and susceptibilities.

Most of the chromite particles measured as paramagnetic, but two chemical composition groups showed significant rotation indices and susceptibilities. Those chromites that contained smaller inversion or intermediate phases (such as the one illustrated in figure 12.13) showed high rotation indices and high susceptibilities. Those chromites that appear to have a generally higher Fe^{3+} and Fe^{2+} content have lower rotation indices but higher susceptibilities (see figure 12.18). This is very similar to the ilmenite compositional control.

The kimberlitic chromites, of interest in diamond exploration, fall in the apparently paramagnetic group. Although the majority of chromites have macroscopic magnetic properties similar to the kimberlitic chromites, and magnetic separation does not promise the same concentration as for the picro-ilmenites, the more magnetic chromites can be removed by a combination of attractive separation (to remove the high-susceptibility chromites) and rotating field separation (to remove the high rotation index chromites). The application of a further stage of attractive separation, as proposed above for the picro-ilmenite separation, then leaves the less-susceptible kimberlitic chromites in the last separation fraction, separated from the picro-ilmenites.

No significant perpendicular rotations were observed.

Garnet Particle Rotations

Chapter 13 examined garnet particle rotations.

All the common naturally occurring garnets (eg. pyrope, spessartine, grossular, almandine) are paramagnetic at room temperature, and no particle rotations should occur. When particle rotation in the same direction as the field rotation ("parallel" rotation) does occur, it appears to be due to the presence of ferromagnetic inclusions within the particle (see figures 13.8 to 13.10). If garnet particles with no obvious inclusions are measured, they appear as magnetically isotropic and paramagnetic (no parallel rotation at all).

Many almandine garnet particles, which show no parallel rotation, can be made to rotate slowly around a horizontal axis which is at right angles to the field rotation axis (a "perpendicular" rotation). This appears to be associated with a directional bias in the external field, such that the external field is always stronger when in one orientation than in the opposite orientation.

The precessional effects from a *slowly rotating* electron spin system are about 6 orders of magnitude too small, and can not quantitatively account for the rotations. When Stephenson's ideas (1980) of *sudden* electron spin direction changes are considered (see chapter 5), the *magnitude* of the precessional torque is great enough to cause particle rotation, *but the torque would only be expected to act for short (10^{-8} sec) pulses.* The average torque should be the same as for the slowly rotating case. Precessional particle rotation effects would only be possible if the increased torque acted continuously. The "perpendicular" particle rotations, if they are caused by electron precession effects, imply that the spin reversals are not only sudden, but are also continiuous and always in the same direction. There is little theoretical support for such a phenomena.

If the "perpendicular" rotations were caused by electron precession effects, then they would normally be associated with magnetically ordered materials. If the material is magnetically ordered the particles should rotate parallel to the field rotation more readily than perpendicular to it. However this apparent conflict could be explained if the almandine garnet particles were host particles for an assembly of small superparamagnetic particles. The small size of the superparamagnetic particles (less than 0.035 μm, if they are magnetite) would make them undetectable to a light microscope and to the electron microprobe used for the analyses here. Superparamagnetic particles are in a size range where thermal energy (in this case at room temperatures) exceeds anisotropy energy. Whole particle magnetisation switches randomly between directions of easy magnetisation, due to thermal agitation, so that a superparamagnetic particle behaves like a paramagnetic unit. Very little parallel torque is

applied, by a rotating field, to an assembly of such randomly-oriented particles in a host particle.

The cause of the "perpendicular" particle rotations observed directly in almandine garnet, and indirectly in magnetite, requires more investigation than it was possible to give here.

The very low magnetic susceptibility of the pyrope garnets (which show no parallel *or* perpendicular rotations) indicates that, in any magnetic separation for diamond indicator minerals, they will be in the non-rotating, lowest-susceptibility, magnetic fraction.

Practical Separation Results

Low-Intensity, Low-Entrapment, Magnetic Separation of Magnetite and Pyrrhotite

In this type of magnetic separation, which was discussed in chapter 14, the magnetic particles are both attracted and rotated. The magnetic attraction holds the particles against a surface, while the field rotations are used to rotate them rapidly so that they energetically expell any entrapped non-magnetics as they roll themselves out of the separator. The separation can be carried out totally wet, dry, or "wet-to-dryer" (see figures 8.3 to 8.9).

An example of the reduction in non-magnetic entrapment that can be obtained by using the rotating field method was provided by the trial separation of magnetite and monoclinic pyrrhotite from a gold concentrate provided by Osborne Mines in Queensland (see chapter 14). In the first pass through the separator their present wet drum separator entraps between 8 and 10% of the total gold within the magnetic product, forcing them to use multiple passes through the separator to lower the gold entrapment. The rotating field separation, carried out on the experimental separator shown in figure 8.6, produced an apparent gold entrapment of 0.3% of the total gold, using only one pass through the separator. The actual gold entrapment may have been lower than this, as some of the gold particles were later found to be magnetic due to the presence of magnetite and hematite inclusions. In this trial the gold entrapment in magnetics has been reduced by a factor of about 30.

Rotating field magnetic separation is limited by a largest separable particle size, described by equation 7.8. In the experimental separator, with its relatively shallow depth of field, this may (in practice) have been uncomfortably close to 1 or 2 mm particle diameter, but in the larger proposed commercial separators a much greater depth of field is expected to raise this to a practical diameter of at least 5 mm.

The separation of diamond indicator minerals

The separation method illustrated in figure 8.16, suggested by the particle rotation and susceptibility measurements described above, was able to concentrate the picro-ilmenites into as little as 1% of the original ilmenite sample. This process involved the initial attractive separation of the more highly susceptible ilmenites, followed by a rotating field separation to remove those low-susceptibility ilmenites with significant rotation indices.

The method has since been further developed along the lines suggested by the particle rotation measurements above, using the newly-available equipment illustrated in figure 16.1. It

is currently employed on a routine basis to produce individual concentrates for picro-ilmenites, kimberlitic chromites and pyrope garnets.

A small-scale (single cell) rotating field separation (see chapter 15), was used to process very small heavy mineral, small particle concentrates, from routine geochemical soil samples. This was able to produce a distribution map of chromites and high-Mg ilmenites for an exploration lease in NE Tasmania (figures 15.6 and 15.7).

The eddy current separation of small non-magnetic metallic particles

Using the magnet drum illustrated in figure 16.1, set up similar to the arrangement illustrated in figure 8.20 (but with a conveyor belt instead of the outer rotating drum), it was possible to carry out practical separations (from zircon sand) on Al and Cu particles down to 50 and 75 μm respectively. While expected particle feed rates to such a separation are only about 100 kg/hr.m for 100 μm particles, for 500 μm particles the feed rate is expected to rise to more than 1 tonne/hr.m.

Except for the expected very low particle feed rates, and the need for higher fields and rotation frequencies, there appears to be no reason why separations could not be carried out on particles down to 20μm (for Al).

Chapter 19

Implications and Conclusions

The Measurement of Particle Rotation and Magnetisation Characteristics

Particle Magnetic Rotation Indices

In chapter 4 a method was developed for describing particle rotation characteristics, and this was subsequently developed into a measurement that could be made on individual small particles, and is referred to here as the particle rotation index.

The magnitude of the measurement depends primarily on the type and magnitude of the magnetic anisotropy, but also, in the case of ferromagnetic or ferrimagnetic materials, on such particle magnetic properties as the coercive force. It is therefore a characteristic of the particle. While the magnetic susceptibility of a particle describes its "attractability", the rotation index describes its "rotatability".

The basic concept of the rotation index is that it is a measure of the maximum angle which can be obtained between the particle magnetisation and the external field. In practice the measurement is made at the point where the particle is able to be rolled across a surface by a rotating magnetic field, and because the measurement is made in a *rotating* field, other factors, such as particle inertia and domain wall velocity, affect the measurement. If rotation index measurements are made at a number of field rotation frequencies, modelling of the frequency response allows these factors to be removed from the measurements so that the angle between magnetisation and external field is obtained, and this was indicated in chapter 4 and illustrated in chapter 10. This implies that rotating field measurements can be used to estimate anisotropy forces in small particles.

Domain wall velocity

Accurate measurements of material magnetisation characteristics, such as coercive force, anisotropy and domain wall mobilities, can already be made, but not always very easily or very cheaply, or on small individual particles.

On the other hand, the particle measurements made in this thesis were approximate, but easily made on a routine basis, on many hundreds of individual particles over a wide particle size range, using very simple and relatively cheap equipment. Although the measurements were made here in order to apply the average results to rotating field mineral particle separation (and consequently did not have to be very accurate), the simple measurements have revealed a surprising amount of detail about particle magnetisation processes such as coercive force and apparent domain wall velocity.

Equation 4.22 indicates that the measurement of apparent particle rotation indices over a range of field rotation frequencies could be developed to estimate apparent domain wall velocities in small ferromagnetic particles. The modelling of the measured rotation index frequency response for magnetite and iron particles in chapter 10, using a simplified version of equation 4.22, further illustrates this possibility. The equipment and the methods used here were not designed with accurate measurements in mind, and therefore the modelling results in chapter 10 all the more point out the possibility of further development of the method as a relatively quick and easy way to measure dynamic particle magnetisation factors. These factors may be of considerable importance in geophysics.

"Perpendicular" particle rotations

Particle rotation observations in rotating magnetic fields have revealed a particle rotation which has its axis perpendicular to the field rotation axis. It is tempting to explain such a particle rotation by the precessional effects of rotational magnetism discussed by Stephenson (1980). Calculations here indicate that these spin precession effects *should not* be of sufficient magnitude to cause particle "sideways" (or "perpendicular") rotations in particles of similar magnetisation to almandine garnets.

The observed phenomena of perpendicular particle rotation requires more examination than it was possible to give it here.

Mineral genesis and exploration studies

The examination of ilmenite and chromite rotational characteristics, and the relationship between these characteristics and the particle chemical composition (discussed in chapters 11 and 12), show that particle magnetic rotation characteristics are sensitive to chemical composition and cation ordering. Particle magnetic characteristics can therefore imply a great deal about the conditions (chemical environment, pressure, temperature) under which the particle formed.

The information which can be obtained by measurements in a rotating magnetic field includes information on particle anisotropy, coercive force, superparamagnetism, and dynamic magnetisation processes such as domain wall motion, and is considerably greater than can be obtained by magnetic susceptibility measurements alone. There is a case for the future refining of the particle rotation measurement method to allow its use as a fairly simple laboratory technique using relatively small and cheap equipment.

The same basic equipment used for the particle measurements can also be used to concentrate the particles for the measurements. Small-scale separation by rotating magnetic fields can be used as a routine part of an exploration programme, to concentrate (or search for) particles with magnetic characteristics that might indicate an environment of geological interest. The technique was used on an exploration lease in north-east Tasmania (chapter 15), where it was able to indicate probable regions of ultramafic intrusion. This investigation was carried out before the more detailed separation method illustrated in figure 16.1 was developed, making possible the separation of a more complex magnetic spectrum of minerals.

Low-Intensity Magnetic Separation

The recovery of small magnetic particles

In many low-intensity magnetic separation applications, particle entrapment is not a major concern. This is the case in the recovery of fine magnetite after coal-washing operations, where the main aim is to recover as much of the magnetite as possible. Most of the magnetite which is lost during recovery is the finer material, so that repeated magnetic separations lead to an increasingly coarse recovered magnetite. Conventional wet separation is more efficient in the recovery of the larger particles.

Rotating field separation, on the other hand, is very efficient in the lower particle sizes but the efficiency drops off as the particle size approaches the maximum seperable particle size. There are several reasons for this efficiency difference at small particle sizes. One reason is that, as the particle size decreases, the coercive force rises rapidly until at particle sizes of only a few microns (especially if the magnetite contains some Ti) it approaches the separating field strength. The particle rotation index then begins to increase, and the particles rotate more strongly. Another reason is that it is much easier for overlying non-magnetic particles to "sit on" a fairly weakly attracted small magnetite particle than to suppress an energetically-rotating small magnetite particle. The energetically-rotating particles have an increased ability to "dig themselves out" from overlying non-magnetics.

Low-intensity rotating field separation has applications in the magnetic separation of very small magnetite particles, where recovery percentages are economically important. However there is also a minimum seperable particle size, which is defined by an approach to superparamagnetism at very small particle sizes (below about 0.05 μm for magnetite). This is far below the particle sizes normally separated.

Low-entrapment separation

Entrapment of non-magnetic particles is a significant problem in applications such as the separation of magnetite (and monoclinic pyrrhotite) from gold concentrate, or the preparation of a magnetite product for sale. Often a three-stage series separation has to be employed to reduce entrapment losses, such as the unit illustrated in figure 3.5, where demagnetisation stages are required between each magnetic separation. In such cases the total capital cost is much more than three times the individual unit cost.

For the separation example (Osborne Mines) given in chapter 14, three conventional separation stages, as shown in figure 3.5, would be required to reduce the gold entrapment to the same level as was achieved in a single stage rotating field separation. The reason for the very low entrapment figures is that the continuous and energetic rotation of the magnetic particles rapidly expels any non-magnetics that may initially become entrapped.

In applications where low particle entrapment is required, low-entrapment rotating field separation would significantly reduce the capital costs of separation, and may also be expected to reduce maintenance costs and plant complexity.

The Separation of Diamond Indicator Minerals

Attractive magnetic separation is already used to prepare heavy mineral concentrates for observation for the three main diamond indicator minerals. This aims to remove those particles that are more magnetically susceptible than the picro-ilmenites. However, because the process does not have a very precise cut-of point for magnetic susceptibility, and the picro-ilmenites have a higher magnetic susceptibility than many other ilmenite particles, this still leaves very large samples for time-consuming observation under microscopes.

Removal of the remaining more highly magnetically ordered particles by rotating field separation can reduce observation times further, by up to 90%. If the rotating field separation is then followed by a precise attractive separation to remove particles of lower susceptibility than the picro-ilmenites, observation times may be cut even further. In fact, it has proved possible to include all the separation stages, except the initial coarse separation, on the one machine. This has been done with the separator shown in figure 16.1.

Although the rotating field separation method does not replace the highly-skilled observers, who must do the final visual identification of the diamond indicator minerals, it greatly reduces observation times. This either allows greater certainty by permitting larger samples to be processed, or greatly increases the area that can be explored in a given time scale or within a given exploration budget.

Eddy Current Separation

Eddy current separation has previously been restricted mainly to the recycling industry, and to the separation of metallic particles greater than about 5 mm. This means that it has not yet been economically feasible to routinely recover metallic copper and aluminium from finely chopped wire and cabling. This material is currently stock-piled in the hope of future improved methods. The main emphasis in eddy current separation has been on the use of bulk repulsive forces to throw particles off a conveyor belt, but as the particles become smaller there is less bulk repulsion and more particle rotation.

Chapter 6 examined the torque placed on a metallic particle by a rotating magnetic field, and showed that it could be used as the basis for extending eddy current separation to particle sizes down to a few tens of μm. Experimental work then showed that the use of rotating magnetic fields permits the eddy current rotation (and therefore separation) of particles down to less than 50μm. Separation rates above 1 tonne/hr.m are indicated for particle sizes down to 0.5 mm, decreasing rapidly below this particle size to about 100 kg/hr.m for 100 μm particles. One of the advantages of rotating field eddy current separation is that it can take place in water, where fluid drag would prevent the use of a bulk repulsive force method.

Rotating field eddy current separation therefore places eddy current separation within the particle size range normally dealt with in other magnetic mineral separation processes, and brings it into consideration as a separating method for larger free gold particles.

Future Directions

Both the theoretical and practical aspects discussed here have laid a basis for the further development of rotating field mineral separation.

There are four main areas for future (commercial) development:

1. Low intensity, low entrapment separation.
2. Medium intensity mineral sands processing.
3. Eddy current separation.
4. Diamond exploration.

1. Commercially, the most obvious application is in the area of low intensity magnetic separation (mainly magnetite and pyrrhotite). Low intensity magnetic separators are used somewhere in the processing circuits of most mines throughout the world, and in many of these cases particle entrapment is a significant problem. The market for low intensity, low entrapment, rotating field separators is very large indeed, and the development of these separators would probably be the most financially rewarding of the possible applications.

2. The magnetic separation of mineral sands is a subject that is currently receiving much attention. Rare earth magnetic separators, similar to low intensity wet drum separators, have appeared fairly recently and are being employed in this application. However one of the problems with these separators is that they can not discriminate between low-susceptibility (but still ferrimagnetic) ilmenite and chromite. A rotating field separator can distinguish between these two minerals. Although this thesis did not investigate possible designs for a high-feed ilmenite-chromite separator, the data does indicate that a rotating field separation could offer *qualitative* improvements over conventional attraction separation.

The possible market for medium intensity rotating field separators for mineral sands applications is growing quickly at present, and there is a need to investigate high-feed designs for these separators.

3. Because the ability to separate small metallic particles by eddy current methods does not yet exist, the current market for such separators is small. However the potential future market (in the recycling industry) for a practical small-particle eddy current separator is very large. This application needs to be further investigated and developed, but it would have to create its own market.

4. Although the diamond exploration application was one of the main motivations behind this thesis, the possible market for rotating field diamond indicator mineral separators is very specialised and quite small. Practical rotating field separators for this application are already well developed as a result of work for this thesis.

References

and Appendices

References

Allen, N. R. (1993): *Rotating magnetic field separation of minerals.* Hons. thesis. University of Tas. Geology Dept. Unpublished. 221 pages.

Allen, N. R. (1995): *A comparison of the rotating field magnetic separator with wet drum and WHIMS separators using material from Renison.* A report to Renison Ltd., Tasmania. Unpublished. 9 pages

Allen, N. R. and van Moort, J. C, (1997): *A new low-intensity magnetic separator which employs rotating magnetic fields to reduce particle entrapment.* In: Sixth Mill Operators Conference. The Australasian Institute of Mining and Metallurgy. Publication series 3/97: 171-175.

Anderson, J. C. (1968): Magnetism and Magnetic Materials. Chapman and Hall Ltd., London. 248 pages.

Anovitz, L. M., Essene, E. J., Metz, G. W., Bohlen, S. R., Westrum Jr., E. F. and Hemingway, B. S. (1993): *Heat capacity and phase equilibria of almandine,* $Fe_3Al_2Si_3O_{12}$. Geochimica et Cosmochimica Acta. 57: 4191-4202.

Banerjee, S. K. (1991): *Magnetic properties of Fe-Ti oxides.* Reviews in Mineralogy, 25: 107-128.

Batty, M. H. (1981): Mineralogy for Students. Second edition. Longman Scientific & Technical. Hong Kong. 355 pages.

Bean, C. P. and Jacobs, T. S. (1956) *Magnetic granulometry and superparamagnetism.* Journal of Applied Physics, 27/12: 1448-1452.

Beros, G.S., (1991): *Magnetic separation within Renison's sulphide circuit.* In: Fourth Mill Operators Conference. The Australian Institute of Mining and Metallurgy. 171-177.

Blakemore, J. S. (1985): Solid State Physics. Second edition. Cambridge University Press, Cambridge. 506 pages.

Calas, G. (1988): *Electron paramagnetic resonance.* in: Hawthorne, F. C. (Ed): Reviews in Mineralogy. Volume 18. Spectroscopic Methods in Mineralogy and Geology. 513-571.

Carey, R., and Isaac, E. D. (1966): Magnetic Domains, and Techniques for their Observation. The English Universities Press Ltd., London. 168 pages.

Carmichael, C. M. (1961): *The magnetic properties of ilmenite-haematite crystals.* Proc. Roy. Soc. A, 263. 509-530.

Carmichael, R. S. (1989): Magnetic Properties of Minerals and Rocks. CRC Press Inc.

Chikazumi, S., and Charap, H. (1978): Physics of Magnetism. Robert E Kreiger Publ. Co., N.Y. 554 pages.

Chikazumi, S. (1997): Physics of Ferromagnetism. International Series of Monographs in Physics. Oxford Science Publications. ISBN 0198517769.

Coey, J. M. D. and Ghose, S. (1988): *Magnetic phase transitions in silicate minerals.* in: Ghose S., Coey J. M. D., Salje E. (Ed): Structural and Magnetic Phase Transitions in Minerals. Springer-Verlag, New York. 244 pages.

Cullity, B. D. (1972): Introduction ot Magnetic Materials. Adison-Wesley, Massachusetts. 666 pages.

Dalmign, W. L., Voskuyl, W. P. H., and Roorda, H. J. (1979): *Low energy separation of nonferrous metals by eddy current techniques.* Paper presented at the CRE/MER Congress, Berlin, Oct. 1979.

Davis, J.J, and Lyman, G.J. (1983): *Magnetite recovery using a wet drum separator.* Proc. AusIMM, 287: 51-60.

Deer, W. A., Howie, R. A. and Zussman, J. (1965): Rock Forming Minerals. Vol. I. Ortho and Ring Silicates. Longmans, London. 333 pages.

Deer, W. A., Howie, R. A. and Zussman, J. (1982): Rock Forming Minerals. Vol. IA. Orthosilicates. Second edition. Longmans, London. 919 pages.

Dillon, Jr. J. F. (1963): *Domains and domain walls.* in: Magnetism. Volume 3. Ed. Rado, G. T. and Suhl, H. (1963). Academic Press, New York and London. 415-464.

Dorfman, Ya. G. (1965): Diamagnetism and the Chemical Bond. Edward Arnold Ltd, London. 182 pages.

Eisberg, R., Resnick, R. (1985): Quantum Physics of Atoms, Molecules, Solids, Nuclei, and Particles. Second edition. John Wiley & Sons. USA. 713 pages.

Finger, L. W. (1972): *The uncertainty of the calculated ferric iron content of a microprobe analysis.* Carneg. Inst. Wash. Year Book 71: 600-603.

Gordon, L., Nord, Jr., Charles, A., and Lawson. (1989): *Order-disorder transition-induced twin domains and magnetic properties in ilmenite-hematite.* American Mineralogist. 74: 160-176.

Hugh St., O'Neill, C., and Navrotsky, A. (1984): *Cation distributions and thermodynamic properties of binary spinel solid solutions.* American Mineralogist. 69: 733-753.

Jiles, D. (1991): Introduction to Magnetism and Magnetic Materials. Chapman & Hall, London. 440 pages.

Kerr-Smiley, N. and Moore, G. (1990): *Renison tailings retreatment.* Internal project report for Renison Ltd. Tasmania. Unpublished.

Knowles, J. E. (1961): *The estimation of domain wall velocity in a square-loop ferrite, and some observations on the reversal process.* Proc. Phys. Soc. LXXVIII, 2: 233-238.

Koizumi, I. (1926): Patent serial No. 8892/25. Patent Office, London

Krupicka, S., and Novak, P. (1982): in: Wohlfarth E. P. (Ed), Ferromagnetic Materials. Vol. 3. Chapter 4. Norh Holand Publishing Company.

Lucas, H., Muggeridge, M. T. & McConchie, D. M. (1989): *Iron in kimberlitic ilmenites and chromian spinels*: in Kimberlites and Related Rocks, Volume 1, Their Mantle/Crust Setting, Diamonds and Diamond Exploration. Geological Society of Australia Special Publication, 14: 311-320. Blackwell, Melbourne.

M°Carthy, J. B. (1922): Patent Serial No. 351,049. United States Patent Office.

Mathieu, G. I., Townsend, M. G., Wronski, Z. S. (1990): *Canmet technology leads to novel separator using FeNdB super magnets: Sorting of aluminium from spent potlining.* Canmet. Canada Centre for Mineral and Energy Technology. Division report MSL 90-6 (J). Project 30.21.02. 18 pages.

Maxwell, J. C. (1873): A Treatise on Electricity and Magnetism. Vol. I. Clarendon Press, Oxford. 425 pages.

Maxwell, J. C. (1873): A Treatise on Electricity and Magnetism. Vol. II. Clarendon Press, Oxford. 438 pages.

Moskowitz, L.R., (1976): Permanent Magnet Design and Application Handbook. Cahners Books International. 385 pages.

Nye, J. F., (1957): Physical Properties of Crystals. Oxford University Press, London. 322 pages.

Obertteuffer, J. A. (1974): *Magnetic separation: A review of principles, devices, and applications.* IEEE Transactions on Magnetics, Vol. Mag-10, No. 2, June 1974. 223-238.

O'Dell, T. H. (1981): Ferromagnetodynamics. MacMillan Press. 230 pages.

O'Reilly, W. (1984): Rock and Mineral Magnetism. Blackie, Glasgow and London. 220 pages.

Parry, L. G. (1965): *Magnetic properties of dispersed magnetite powders.* Pil. Mag. 11: 303.

Peng, Y., Shuyi, L., and Jin, C. (1993): *The separation performance of the pulsating high-gradient magnetic separator.* Magnetic and Electrical Separation. 4: 211-221.

Pilbrow, J. R. (1990): Transition Ion Electron Paramagnetic Resonance. Clarendon Press, Oxford. 717 pages.

Putnis, A. (1992): Introduction to Mineral Sciences. Cambridge University Press. 457 pages.

Rado, G. T., Suhl, H. (1963): Magnetism. Volume 3. Academic Press, New York and London. 623 pages.

Rayner, J. G., Holtham, P. N., and Napier-Munn, T. J. (1995): *The performance and on-line monitoring of dense medium wet drum magnetic separators.* Julius Kruttschnitt Minerals Research Centre, Indooroopilly, Qld. Development report. 19 pages.

Sack, R. O., and Ghiorso, M. S. (1991): *Chromian spinels as petrogenetic indicators: Thermodynamics and petrological applications.* American Mineralogist. Volume 76. pp 827-847.

Schloemann, E. (1980): *Application of ferrites to environmental problems- Recovery of non-ferrous metals from waste using barium-ferrite magnets.* in: Ferrites: Proceedings of the International Conference. Sept.-Oct. 1980, Japan. 867-873.

Schloemann, E. and Facinelli, D. (1981): *High-capacity nonferrous-metal separator using permanent magnets.* in: Procedings of 2nd Symposium on Materials and Energy from Refuse. Ed. A. Buekens. Oct. 20-22, Antwerp.

Schloemann, E. (1982): *Eddy-current techniques for segregating nonferrous metals from waste.* Conservation & Recycling. 5: 149-162.

Smit, J. and Wijn, H. P. J. (1959): Ferrites. Cleaver-Hume Press Ltd. London. 369 pages.

Standley, K. J. (1972): Oxide Magnetic Materials. Second edition. Clarendon Press Oxford. 254 pages.

Stacey, F. D. and Banerjee, S. K. (1974): The Physical Principals of Rock Magnetism. Elsevier Scientific Publishing Co., New York. 195 pages.

Stephenson, A. (1980): *Gyromagnetism and the remanence acquired by a rotating rock in an alternating field.* Nature. 284: 48-49.

Stephenson, A. (1980): *A gyroremanet magnetisation in anisotropic magnetic material.* Nature. 284: 49-51.

Stephenson, A. and Molyneux, L. (1991): *A versatile instrument for the production, removal, and measurement of magnetic remanence at different temperatures.* Meas. Sci. Technol. 2: 280-286.

Suwa, K., Enami, M., Hiraiwa, I., and Yang, T. (1987): *Zn-Mn ilmenite in the Kuiqi granite from Fuzhou, Fujian Province, east China.* Mineralogy and Petrology. 36: 111-120.

Talkington, W., Watkinson, D. H., Whittaker, P. J., and Jones, P. C. (1983): *Platinum-group-mineral inclusions in chromite from the Bird River Sill, Manitoba.* Mineralium Deposita. 18: 245-255.

Thompson, J. V. (1992): *Byproduct gold from construction aggregates.* Engineering & Mining Journal, June 1992. Reprint. 4 pages.

Turnbull, R. M. (1979): The Structure of Matter. Blackie, Glasgow and London. 266 pages.

Wagner, D. (1972): Introduction to the Theory of Magnetism. Translation by Ferdinand Cap. Pergammon Press. 278 pages.

Williams, D. E. G. (1966): The Magnetic Properties of Matter. Longmans, Green and Co Ltd. 225 pages.

Yarwood, J. (1973): Atomic and Nuclear Physics. University Tutorial Press Ltd., London. 608 pages.

Appendix A

Iron Rotation and Analysis Results

Sample source	Element weight %											Lifting field (T)						Rotation field (T)							Ferromagnetic rotation index				
	S	Cr	Mn	Fe	Ni	Cu	Zn	As	Sn	Sb	Pb	Bi	At 10 Hz	At 20Hz	At 30Hz	At 40Hz	At 50Hz	At 57Hz	At 10Hz	At 20Hz	At 30Hz	At 40Hz	At 50Hz	At 57Hz	10 Hz	20 Hz	30 Hz	40 Hz	50 Hz	57
Fe Filings	0.01	23.40	0.60	50.60	20.76	0.12	0.03	0.06	0.00	0.00	0.00	0.00	0.0275	0.0275	0.0275	0.0275	0.0275	0.0275	0.0080	0.0095	0.0095	0.0085	0.0095	0.0095	0.07	0.06	0.04	0.05	0.04	0.04
	0.01	0.02	0.46	98.01	0.06	0.04	0.00	0.13	0.00	0.00	0.06	0.24	0.0059	0.0059	0.0059	0.0059	0.0059	0.0059	0.0009	0.0009	0.0009	0.0010	0.0011	0.0011	0.16	0.16	0.16	0.14	0.13	0.12
	0.12	0.07	1.35	97.16	0.00	0.04	0.00	0.13	0.00	0.00	0.04	0.00	0.0095	0.0095	0.0095	0.0095	0.0095	0.0095	0.0026	0.0029	0.0037	0.0047	0.0047	0.0047	0.08	0.07	0.05	0.03	0.03	0.03
	0.03	0.09	1.04	97.55	0.09	0.02	0.00	0.17	0.00	0.00	0.00	0.00	0.0095	0.0095	0.0095	0.0095	0.0095	0.0095	0.0011	0.0013	0.0014	0.0016	0.0016	0.0018	0.22	0.19	0.16	0.14	0.14	0.12
	0.00	0.10	0.55	96.73	0.01	0.03	0.04	0.14	0.00	0.00	0.00	0.00	0.0107	0.0107	0.0107	0.0107	0.0107	0.0107	0.0021	0.0023	0.0029	0.0033	0.0037	0.0042	0.12	0.11	0.08	0.07	0.06	0.05
	0.00	0.07	0.36	96.15	0.04	0.10	0.05	0.19	0.00	0.00	0.00	0.01	0.0095	0.0095	0.0095	0.0095	0.0095	0.0095	0.0009	0.0010	0.0011	0.0016	0.0018	0.0018	0.28	0.25	0.22	0.14	0.12	0.12
	0.00	0.09	0.55	97.80	0.01	0.01	0.02	0.14	0.00	0.00	0.00	0.00	0.0107	0.0107	0.0107	0.0107	0.0107	0.0107	0.0018	0.0021	0.0026	0.0033	0.0037	0.0037	0.14	0.12	0.09	0.07	0.06	0.06
	0.21	0.02	0.22	97.18	0.12	0.07	0.01	0.12	0.00	0.02	0.23	0.50	0.0153	0.0153	0.0153	0.0153	0.0153	0.0153	0.0021	0.0023	0.0023	0.0023	0.0026	0.0033	0.19	0.16	0.16	0.16	0.14	0.11
	0.01	0.08	0.58	98.15	0.07	0.00	0.03	0.15	0.00	0.00	0.00	0.28	0.0107	0.0107	0.0107	0.0107	0.0107	0.0107	0.0023	0.0026	0.0033	0.0037	0.0042	0.0042	0.11	0.09	0.07	0.06	0.05	0.05
	0.00	0.13	0.54	97.69	0.03	0.03	0.00	0.12	0.00	0.00	0.30	0.00	0.0107	0.0107	0.0107	0.0107	0.0107	0.0107	0.0023	0.0026	0.0029	0.0033	0.0035	0.0035	0.11	0.09	0.08	0.07	0.06	0.06
	0.01	0.03	0.37	96.45	0.04	0.14	0.08	0.16	0.00	0.04	0.00	0.00	0.0107	0.0107	0.0107	0.0121	0.0121	0.0121	0.0023	0.0026	0.0033	0.0037	0.0037	0.0042	0.11	0.09	0.07	0.07	0.07	0.06
	0.01	0.08	0.62	97.70	0.06	0.01	0.00	0.12	0.00	0.00	0.00	0.18	0.0107	0.0107	0.0107	0.0107	0.0107	0.0107	0.0026	0.0033	0.0037	0.0042	0.0042	0.0042	0.09	0.07	0.06	0.05	0.05	0.05
Nail	0.05	0.05	0.42	96.73	0.00	0.01	0.05	0.15	0.00	0.00	0.05	0.00	0.0085	0.0085	0.0085	0.0085	0.0085	0.0085	0.0022	0.0026	0.0028	0.0029	0.0033	0.0033	0.08	0.07	0.06	0.06	0.05	0.05
	0.01	0.02	0.37	97.27	0.03	0.00	0.01	0.11	0.00	0.00	0.12	0.14	0.0053	0.0053	0.0053	0.0053	0.0050	0.0050	0.0016	0.0018	0.0021	0.0022	0.0026	0.0026	0.07	0.06	0.05	0.04	0.03	0.03
	0.03	0.04	0.31	97.36	0.06	0.00	0.03	0.14	0.00	0.00	0.02	0.13	0.0095	0.0095	0.0095	0.0095	0.0095	0.0095	0.0023	0.0026	0.0033	0.0037	0.0037	0.0037	0.09	0.08	0.06	0.05	0.05	0.05
	0.05	0.05	0.43	96.42	0.00	0.00	0.05	0.15	0.00	0.02	0.00	0.48	0.0067	0.0067	0.0067	0.0067	0.0067	0.0067	0.0014	0.0014	0.0016	0.0018	0.0021	0.0026	0.11	0.11	0.09	0.08	0.07	0.05
	0.02	0.03	0.39	96.61	0.01	0.00	0.05	0.14	0.00	0.01	0.34	0.21	0.0095	0.0095	0.0095	0.0095	0.0095	0.0095	0.0014	0.0018	0.0021	0.0022	0.0021	0.0022	0.16	0.12	0.11	0.10	0.11	0.10
	0.03	0.01	0.38	96.78	0.00	0.00	0.02	0.13	0.00	0.00	0.00	0.00	0.0085	0.0085	0.0085	0.0085	0.0085	0.0085	0.0018	0.0018	0.0019	0.0022	0.0023	0.0025	0.11	0.11	0.10	0.08	0.08	0.07
	0.00	0.02	0.36	97.00	0.01	0.05	0.00	0.16	0.00	0.00	0.00	0.00	0.0080	0.0080	0.0080	0.0080	0.0080	0.0080	0.0016	0.0018	0.0021	0.0023	0.0023	0.0026	0.11	0.10	0.08	0.07	0.07	0.06
Steel rod	0.00	0.05	1.21	96.52	0.00	0.03	0.03	0.18	0.00	0.00	0.00	0.01	0.0095	0.0101	0.0095	0.0095	0.0101	0.0101	0.0026	0.0029	0.0033	0.0035	0.0037	0.0037	0.08	0.07	0.06	0.05	0.05	0.05
	0.00	0.05	1.25	96.37	0.00	0.00	0.03	0.21	0.00	0.01	0.00	0.02	0.0085	0.0085	0.0085	0.0085	0.0085	0.0085	0.0018	0.0021	0.0023	0.0023	0.0025	0.0026	0.11	0.09	0.08	0.08	0.07	0.07
	0.02	0.00	1.20	97.24	0.07	0.03	0.00	0.16	0.00	0.00	0.00	0.00	0.0095	0.0095	0.0095	0.0095	0.0095	0.0095	0.0021	0.0022	0.0023	0.0026	0.0026	0.0028	0.11	0.10	0.09	0.08	0.08	0.07
	0.00	0.01	1.25	96.45	0.00	0.00	0.00	0.19	0.00	0.00	0.00	0.00	0.0090	0.0085	0.0090	0.0095	0.0095	0.0095	0.0026	0.0029	0.0029	0.0033	0.0037	0.0037	0.07	0.06	0.06	0.06	0.05	0.05
	0.00	0.04	1.30	96.64	0.01	0.00	0.03	0.14	0.00	0.00	0.00	0.28	0.0095	0.0090	0.0095	0.0090	0.0090	0.0090	0.0019	0.0019	0.0023	0.0026	0.0029	0.0033	0.11	0.11	0.09	0.07	0.06	0.05
	0.00	0.07	1.22	96.92	0.03	0.00	0.00	0.15	0.00	0.00	0.12	0.00	0.0095	0.0095	0.0095	0.0095	0.0095	0.0095	0.0018	0.0021	0.0025	0.0029	0.0033	0.0031	0.12	0.11	0.08	0.07	0.06	0.06
Stainless	0.63	16.86	2.11	67.64	8.59	0.30	0.06	0.13	0.00	0.02	0.00	0.03	0.0557	0.0557	0.0557	0.0557	0.0591	0.0591	0.0095	0.0121	0.0136	0.0136	0.0153	0.0153	0.14	0.11	0.09	0.09	0.08	0.08
steel pipe	0.22	17.82	1.55	69.34	8.07	0.22	0.00	0.09	0.00	0.00	0.00	0.00	0.0557	0.0557	0.0557	0.0557	0.0557	0.0557	0.0067	0.0067	0.0075	0.0085	0.0090	0.0095	0.22	0.22	0.19	0.16	0.15	0.14
	0.00	18.01	1.24	69.60	7.82	0.21	0.06	0.10	0.00	0.03	0.00	0.00	0.0391	0.0391	0.0391	0.0391	0.0391	0.0391	0.0047	0.0042	0.0053	0.0053	0.0059	0.0063	0.22	0.25	0.19	0.19	0.16	0.15
	0.89	17.40	2.52	67.41	7.77	0.24	0.00	0.06	0.00	0.00	0.07	0.00	0.0591	0.0591	0.0591	0.0627	0.0627	0.0627	0.0107	0.0121	0.0136	0.0153	0.0172	0.0172	0.13	0.11	0.10	0.09	0.08	0.08
	0.05	17.38	1.24	69.32	8.26	0.21	0.02	0.11	0.00	0.01	0.07	0.00	0.0495	0.0495	0.0495	0.0495	0.0495	0.0495	0.0136	0.0136	0.0153	0.0153	0.0182	0.0182	0.08	0.08	0.07	0.07	0.05	0.05
	0.02	17.64	1.23	69.45	7.94	0.25	0.00	0.09	0.00	0.05	0.00	0.07	0.0627	0.0627	0.0627	0.0627	0.0627	0.0591	0.0095	0.0095	0.0107	0.0121	0.0136	0.0136	0.16	0.16	0.14	0.12	0.11	0.10
	0.94	17.38	2.47	67.62	7.52	0.23	0.00	0.11	0.00	0.03	0.31	0.09	0.0495	0.0467	0.0495	0.0467	0.0467	0.0495	0.0121	0.0121	0.0128	0.0136	0.0136	0.0136	0.09	0.08	0.08	0.07	0.07	0.08
Averages	0.11	4.60	0.93	89.37	2.42	0.07	0.02	0.13	0.00	0.01	0.05	0.08	0.0195	0.0194	0.0195	0.0196	0.0197	0.0197	0.0038	0.0041	0.0046	0.0050	0.0054	0.0056	0.13	0.11	0.10	0.08	0.08	0.07

Appendix A

Magnetite Rotation and Analysis Results

Note: Total Fe given as FeO

Sample source	Element weight %									Lifting field (T)						Rotation field (T)						Ferromagnetic Rotation index				
	MgO	Al2O3	SiO2	TiO2	Cr2O3	MnO	FeO	NiO	ZnO	At 10Hz	At 20Hz	At 30Hz	At 40Hz	At 50Hz	At 57Hz	At 10Hz	At 20Hz	At 30Hz	At 40Hz	At 50Hz	At 57Hz	10 Hz	20 Hz	30 Hz	40 Hz	50 Hz	57
Kara	0.23	0.51	0.44	0.08	0.03	0.47	89.07	0.02	0.08	0.0095	0.0095	0.0095	0.0107	0.0107	0.0121	0.0007	0.0008	0.0011	0.0013	0.0014	0.0017	0.36	0.32	0.22	0.22	0.19	0.18
Magnetite	0.17	1.05	0.56	0.09	0.00	0.68	89.93	0.04	0.12	0.0107	0.0107	0.0107	0.0107	0.0107	0.0121	0.0029	0.0033	0.0044	0.0053	0.0053	0.0056	0. 08	0.07	0.04	0.03	0.03	0.03
	0.03	0.32	0.11	0.08	0.00	0.45	91.67	0.00	0.00	0.0107	0.0107	0.0107	0.0107	0.0107	0.0107	0.0021	0.0026	0.0029	0.0037	0.0042	0.0047	0.12	0.09	0.08	0.06	0.05	0.04
	0.06	0.83	0.06	0.17	0.01	0.43	90.42	0.00	0.10	0.0101	0.0107	0.0107	0.0107	0.0107	0.0107	0.0023	0.0023	0.0029	0.0035	0.0042	0.0047	0.10	0.11	0.08	0.06	0.05	0.04
	0.07	0.60	0.13	0.04	0.00	0.46	91.22	0.01	0.03	0.0095	0.0095	0.0095	0.0095	0.0095	0.0095	0.0021	0.0023	0.0029	0.0033	0.0037	0.0037	0.11	0.09	0.07	0.06	0.05	0.05
	0.13	1.37	0.06	0.19	0.02	0.69	88.48	0.00	0.14	0.0090	0.0090	0.0090	0.0090	0.0090	0.0090	0.0023	0.0026	0.0029	0.0035	0.0042	0.0047	0.08	0.07	0.06	0.05	0.03	0.03
	0.05	0.55	0.23	0.08	0.01	0.19	90.95	0.02	0.04	0.0095	0.0095	0.0095	0.0095	0.0095	0.0095	0.0026	0.0033	0.0039	0.0044	0.0044	0.0047	0.08	0.06	0.04	0.03	0.03	0.03
	0.02	0.24	0.12	0.08	0.04	0.54	91.34	0.00	0.03	0.0095	0.0095	0.0095	0.0095	0.0095	0.0095	0.0033	0.0037	0.0042	0.0047	0.0047	0.0047	0.06	0.05	0.04	0.03	0.03	0.03
	0.03	0.59	0.16	0.11	0.01	0.66	90.76	0.04	0.12	0.0230	0.0230	0.0230	0.0217	0.0217	0.0217	0.0006	0.0006	0.0006	0.0007	0.0007	0.0007	1.17	1.04	1.04	0.87	0.87	0.87
	0.05	0.36	0.22	0.07	0.04	0.54	88.29	0.00	0.00	0.0095	0.0095	0.0095	0.0095	0.0095	0.0095	0.0004	0.0004	0.0004	0.0004	0.0005	0.0006	0.68	0.68	0.60	0.60	0.53	0.47
	0.17	0.68	0.20	0.07	0.03	0.48	90.16	0.00	0.16	0.0095	0.0095	0.0095	0.0095	0.0095	0.0095	0.0004	0.0004	0.0004	0.0004	0.0005	0.0006	0.68	0.68	0.60	0.60	0.53	0.47
	0.09	1.28	0.08	0.20	0.02	0.54	89.93	0.01	0.00	0.0090	0.0090	0.0090	0.0090	0.0090	0.0090	0.0016	0.0018	0.0023	0.0026	0.0029	0.0031	0.13	0.11	0.08	0.07	0.06	0.06
	0.11	0.56	0.24	0.01	0.05	0.61	90.46	0.00	0.08	0.0095	0.0095	0.0095	0.0095	0.0090	0.0107	0.0018	0.0018	0.0021	0.0026	0.0033	0.0035	0.12	0.12	0.11	0.08	0.05	0.06
	0.19	0.73	0.35	0.05	0.01	0.52	90.41	0.03	0.06	0.0095	0.0095	0.0095	0.0095	0.0095	0.0095	0.0009	0.0009	0.0010	0.0014	0.0018	0.0019	0.28	0.28	0.25	0.16	0.12	0.11
Kara										0.0085	0.0085	0.0085	0.0085	0.0085	0.0085	0.0002	0.0002	0.0002	0.0003	0.0005	0.0006	1.25	1.25	1.25	0.87	0.47	0.41
Magnetite										0.0095	0.0095	0.0095	0.0095	0.0095	0.0095	0.0010	0.0011	0.0016	0.0021	0.0023	0.0026	0.25	0.22	0.14	0.11	0.09	0.08
										0.0095	0.0095	0.0095	0.0095	0.0090	0.0016	0.0018	0.0023	0.0033	0.0029	0.0033	0.14	0.12	0.09	0.06	0.07	0.05
										0.0136	0.0136	0.0136	0.0136	0.0136	0.0136	0.0008	0.0011	0.0013	0.0017	0.0018	0.0018	0.47	0.32	0.28	0.20	0.19	0.19
										0.0107	0.0107	0.0107	0.0107	0.0107	0.0107	0.0021	0.0026	0.0029	0.0033	0.0037	0.0039	0.12	0.09	0.08	0.07	0.06	0.05
										0.0121	0.0121	0.0121	0.0121	0.0121	0.0121	0.0006	0.0008	0.0010	0.0011	0.0014	0.0018	0.53	0.41	0.32	0.28	0.22	0.16
										0.0121	0.0121	0.0121	0.0121	0.0121	0.0121	0.0016	0.0018	0.0023	0.0029	0.0037	0.0044	0.19	0.16	0.12	0.09	0.07	0.05
										0.0095	0.0095	0.0095	0.0095	0.0095	0.0095	0.0007	0.0007	0.0009	0.0011	0.0016	0.0016	0.36	0.36	0.28	0.22	0.14	0.14
										0.0095	0.0095	0.0095	0.0095	0.0095	0.0090	0.0008	0.0008	0.0010	0.0013	0.0016	0.0016	0.32	0.32	0.25	0.19	0.14	0.13
										0.0144	0.0144	0.0144	0.0144	0.0144	0.0144	0.0004	0.0004	0.0005	0.0006	0.0006	0.0006	0.92	0.92	0.82	0.72	0.64	0.64
										0.0121	0.0121	0.0121	0.0121	0.0107	0.0107	0.0004	0.0004	0.0004	0.0006	0.0006	0.0007	0.87	0.87	0.77	0.60	0.47	0.41
										0.0095	0.0095	0.0095	0.0095	0.0095	0.0095	0.0008	0.0008	0.0010	0.0013	0.0016	0.0018	0.32	0.32	0.25	0.19	0.14	0.12
										0.0107	0.0107	0.0107	0.0107	0.0107	0.0121	0.0021	0.0021	0.0026	0.0033	0.0039	0.0042	0.12	0.12	0.09	0.07	0.05	0.06
										0.0107	0.0107	0.0107	0.0107	0.0107	0.0107	0.0002	0.0003	0.0003	0.0003	0.0004	0.0004	1.41	1.10	1.10	1.10	0.87	0.87
										0.0107	0.0107	0.0107	0.0107	0.0107	0.0107	0.0004	0.0004	0.0004	0.0006	0.0006	0.0007	0.87	0.87	0.68	0.53	0.47	0.41
										0.0136	0.0136	0.0136	0.0136	0.0136	0.0136	0.0018	0.0021	0.0026	0.0033	0.0037	0.0042	0.19	0.16	0.12	0.09	0.08	0.07
										0.0095	0.0095	0.0095	0.0095	0.0095	0.0095	0.0002	0.0002	0.0002	0.0002	0.0003	0.0003	1.79	1.79	1.41	1.25	0.98	0.98
										0.0101	0.0101	0.0095	0.0095	0.0095	0.0095	0.0021	0.0029	0.0033	0.0033	0.0033	0.0037	0.11	0.07	0.06	0.06	0.06	0.05
										0.0259	0.0259	0.0259	0.0259	0.0259	0.0259	0.0009	0.0009	0.0009	0.0010	0.0014	0.0014	0.82	0.87	0.82	0.72	0.50	0.50
										0.0090	0.0090	0.0090	0.0090	0.0090	0.0085	0.0009	0.0010	0.0023	0.0029	0.0033	0.0037	0.26	0.23	0.08	0.06	0.05	0.04
										0.0075	0.0075	0.0075	0.0067	0.0075	0.0067	0.0001	0.0001	0.0001	0.0001	0.0002	0.0002	1.59	2.01	1.79	2.27	1.41	0.98
										0.0075	0.0075	0.0075	0.0085	0.0095	0.0121	0.0004	0.0003	0.0002	0.0003	0.0003	0.0004	0.53	0.77	0.98	0.87	0.87	0.98
										0.0085	0.0085	0.0085	0.0095	0.0107	0.0095	0.0004	0.0004	0.0005	0.0006	0.0008	0.0009	0.53	0.53	0.47	0.41	0.36	0.28
										0.0085	0.0085	0.0085	0.0085	0.0085	0.0085	0.0009	0.0007	0.0007	0.0007	0.0007	0.0008	0.25	0.32	0.32	0.32	0.32	0.28
										0.0172	0.0172	0.0172	0.0172	0.0172	0.0193	0.0006	0.0008	0.0007	0.0008	0.0007	0.0008	0.87	0.60	0.68	0.60	0.68	0.68
										0.0172	0.0172	0.0172	0.0172	0.0172	0.0172	0.0004	0.0004	0.0004	0.0004	0.0004	0.0005	1.25	1.41	1.41	1.25	1.10	0.98
										0.0090	0.0090	0.0085	0.0085	0.0085	0.0095	0.0004	0.0002	0.0002	0.0002	0.0003	0.0003	0.72	1.04	1.10	1.10	0.87	0.98
										0.0095	0.0095	0.0095	0.0095	0.0085	0.0085	0.0004	0.0003	0.0004	0.0004	0.0004	0.0005	0.77	0.98	0.77	0.77	0.53	0.47
										0.0085	0.0085	0.0085	0.0085	0.0085	0.0085	0.0026	0.0026	0.0029	0.0037	0.0042	0.0047	0.07	0.07	0.06	0.04	0.03	0.02
										0.0090	0.0090	0.0095	0.0095	0.0095	0.0095	0.0023	0.0021	0.0021	0.0023	0.0029	0.0033	0.08	0.10	0.11	0.09	0.07	0.06
										0.0090	0.0090	0.0090	0.0090	0.0090	0.0085	0.0009	0.0008	0.0009	0.0010	0.0013	0.0014	0.26	0.30	0.26	0.23	0.18	0.14
										0.0090	0.0090	0.0090	0.0090	0.0090	0.0085	0.0029	0.0037	0.0037	0.0037	0.0042	0.0042	0.06	0.04	0.04	0.04	0.03	0.03
										0.0172	0.0172	0.0172	0.0172	0.0172	0.0172	0.0004	0.0004	0.0004	0.0004	0.0005	0.0006	1.25	1.25	1.25	1.10	0.98	0.87

Appendix A

Magnetite Rotation and Analysis Results

Note: Total Fe given as FeO

Sample source	Element weight %									Lifting field (T)						Rotation field (T)						Ferromagnetic Rotation index				
	MgO	Al2O3	SiO2	TiO2	Cr2O3	MnO	FeO	NiO	ZnO	At 10Hz	At 20Hz	At 30Hz	At 40Hz	At 50Hz	At 57Hz	At 10Hz	At 20Hz	At 30Hz	At 40Hz	At 50Hz	At 57Hz	10	20	30	40	50	57
										0.0095	0.0095	0.0095	0.0095	0.0095	0.0095	0.0004	0.0003	0.0004	0.0004	0.0004	0.0004	0.60	0.87	0.77	0.77	0.68	0.60
										0.0095	0.0095	0.0095	0.0095	0.0095	0.0095	0.0006	0.0006	0.0009	0.0010	0.0013	0.0013	0.47	0.41	0.28	0.25	0.19	0.19
										0.0085	0.0085	0.0085	0.0085	0.0085	0.0085	0.0008	0.0008	0.0009	0.0011	0.0013	0.0014	0.28	0.28	0.25	0.19	0.16	0.14
										0.0075	0.0075	0.0075	0.0075	0.0075	0.0075	0.0016	0.0023	0.0026	0.0023	0.0033	0.0033	0.11	0.07	0.06	0.07	0.04	0.04
										0.0095	0.0095	0.0095	0.0095	0.0095	0.0095	0.0023	0.0033	0.0035	0.0033	0.0037	0.0042	0.09	0.06	0.05	0.06	0.05	0.04
										0.0071	0.0071	0.0067	0.0067	0.0067	0.0067	0.0002	0.0002	0.0003	0.0004	0.0004	0.0004	0.92	0.82	0.68	0.53	0.47	0.41
										0.0095	0.0095	0.0095	0.0095	0.0095	0.0095	0.0006	0.0006	0.0006	0.0008	0.0009	0.0009	0.47	0.47	0.41	0.32	0.28	0.28
										0.0085	0.0085	0.0085	0.0085	0.0085	0.0085	0.0001	0.0001	0.0002	0.0002	0.0002	0.0002	1.79	2.01	1.59	1.41	1.10	1.10
										0.0063	0.0063	0.0063	0.0059	0.0059	0.0059	0.0002	0.0002	0.0002	0.0003	0.0004	0.0004	1.17	0.92	0.72	0.53	0.47	0.41
										0.0095	0.0095	0.0095	0.0095	0.0095	0.0095	0.0002	0.0002	0.0003	0.0003	0.0003	0.0004	1.41	1.10	0.98	0.98	0.87	0.68
										0.0090	0.0090	0.0090	0.0090	0.0090	0.0085	0.0013	0.0016	0.0021	0.0023	0.0026	0.0028	0.18	0.13	0.10	0.08	0.07	0.06
										0.0153	0.0153	0.0153	0.0153	0.0153	0.0153	0.0003	0.0003	0.0003	0.0004	0.0004	0.0005	1.59	1.59	1.41	1.25	1.10	0.87
Averages	0.10	0.69	0.21	0.09	0.02	0.52	90.22	0.01	0.07	0.01	0.01	0.01	0.01	0.01	0.01	0.001	0.001	0.001	0.002	0.002	0.002	0.55	0.55	0.49	0.44	0.36	0.33

Appendix A

Magnetite rotations according to particle size
Measured rotation & rolling distances

Sample source	Particle size (microns)	Lifting field (T) At 10Hz	At 20Hz	At 30Hz	At 40Hz	At 50Hz	At 57Hz	Rotation field (T) At 10Hz	At 20Hz	At 30Hz	At 40Hz	At 50Hz	At 57Hz	Ferromagnetic Rotation index 10 Hz	20 Hz	30 Hz	40 Hz	50 Hz	57 Hz
Kara magnetite	1000	0.0075	0.0075	0.0075	0.0075	0.0075	0.0075	0.0001	0.0001	0.0001	0.0001	0.0002	0.0002	3.23	4.09	3.63	5.17	2.87	2.27
	1000	0.0075	0.0075	0.0075	0.0085	0.0095	0.0121	0.0004	0.0003	0.0002	0.0003	0.0003	0.0004	1.12	1.59	2.02	1.79	1.79	2.02
	1000	0.0085	0.0085	0.0085	0.0095	0.0107	0.0095	0.0004	0.0004	0.0005	0.0006	0.0008	0.0009	1.12	1.12	0.99	0.88	0.79	0.62
	700	0.0085	0.0085	0.0085	0.0085	0.0085	0.0085	0.0009	0.0007	0.0007	0.0007	0.0007	0.0008	0.39	0.49	0.49	0.49	0.49	0.43
	700	0.0172	0.0172	0.0172	0.0172	0.0172	0.0193	0.0006	0.0008	0.0007	0.0008	0.0007	0.0008	1.25	0.88	0.99	0.88	0.99	0.99
	700	0.0172	0.0172	0.0172	0.0172	0.0172	0.0172	0.0004	0.0004	0.0004	0.0004	0.0004	0.0005	1.79	2.01	2.01	1.79	1.59	1.41
	700	0.0090	0.0090	0.0085	0.0085	0.0085	0.0095	0.0004	0.0002	0.0002	0.0002	0.0003	0.0003	1.05	1.50	1.59	1.59	1.25	1.41
	500	0.0095	0.0095	0.0095	0.0095	0.0085	0.0085	0.0004	0.0003	0.0004	0.0004	0.0004	0.0005	0.80	1.01	0.80	0.80	0.56	0.50
	500	0.0085	0.0085	0.0085	0.0085	0.0085	0.0085	0.0026	0.0026	0.0029	0.0037	0.0042	0.0047	0.10	0.10	0.08	0.07	0.06	0.05
	500	0.0090	0.0090	0.0095	0.0095	0.0095	0.0095	0.0023	0.0021	0.0021	0.0023	0.0029	0.0033	0.11	0.13	0.14	0.12	0.10	0.08
	500	0.0090	0.0090	0.0090	0.0090	0.0090	0.0085	0.0009	0.0008	0.0009	0.0010	0.0013	0.0014	0.29	0.33	0.29	0.26	0.21	0.17
	350	0.0090	0.0090	0.0090	0.0090	0.0090	0.0085	0.0029	0.0037	0.0037	0.0037	0.0042	0.0042	0.06	0.05	0.05	0.05	0.04	0.04
	350	0.0172	0.0172	0.0172	0.0172	0.0172	0.0172	0.0004	0.0004	0.0004	0.0004	0.0005	0.0006	0.89	0.89	0.89	0.79	0.71	0.63
	350	0.0090	0.0090	0.0090	0.0085	0.0085	0.0085	0.0003	0.0002	0.0002	0.0002	0.0002	0.0002	0.59	0.95	0.95	0.89	0.79	0.71
	350	0.0095	0.0095	0.0095	0.0095	0.0095	0.0095	0.0004	0.0003	0.0004	0.0004	0.0004	0.0004	0.44	0.63	0.56	0.56	0.50	0.44
	250	0.0095	0.0095	0.0095	0.0095	0.0095	0.0095	0.0006	0.0006	0.0009	0.0010	0.0013	0.0013	0.25	0.22	0.16	0.14	0.11	0.11
	250	0.0085	0.0085	0.0085	0.0085	0.0085	0.0085	0.0008	0.0008	0.0009	0.0011	0.0013	0.0014	0.16	0.16	0.14	0.11	0.10	0.09
	250	0.0075	0.0075	0.0075	0.0075	0.0075	0.0075	0.0016	0.0023	0.0026	0.0023	0.0033	0.0033	0.07	0.05	0.04	0.05	0.03	0.03
	250	0.0095	0.0095	0.0095	0.0095	0.0095	0.0095	0.0023	0.0033	0.0035	0.0033	0.0037	0.0042	0.06	0.04	0.04	0.04	0.04	0.03
	180	0.0071	0.0071	0.0067	0.0067	0.0067	0.0067	0.0002	0.0002	0.0003	0.0004	0.0004	0.0004	0.34	0.30	0.25	0.20	0.18	0.16
	180	0.0095	0.0095	0.0095	0.0095	0.0095	0.0095	0.0006	0.0006	0.0006	0.0008	0.0009	0.0009	0.18	0.18	0.16	0.13	0.11	0.11
	180	0.0085	0.0085	0.0085	0.0085	0.0085	0.0085	0.0001	0.0001	0.0002	0.0002	0.0002	0.0002	0.65	0.74	0.58	0.52	0.41	0.41
	180	0.0063	0.0063	0.0063	0.0059	0.0059	0.0059	0.0002	0.0002	0.0002	0.0003	0.0004	0.0004	0.43	0.34	0.27	0.20	0.18	0.16
	130	0.0095	0.0095	0.0095	0.0095	0.0095	0.0095	0.0002	0.0002	0.0003	0.0003	0.0003	0.0004	0.37	0.29	0.26	0.26	0.23	0.18
	130	0.0090	0.0090	0.0090	0.0090	0.0090	0.0085	0.0013	0.0016	0.0021	0.0023	0.0026	0.0028	0.05	0.04	0.03	0.03	0.03	0.02

Appendix B

Ilmenite rotation and lift measurements and analysis results

Sample Source	Oxide weight %									Lifting field (T)		Rotating field (T)		Mag. Suscept. (SI)		Paramag. rot. Index		Ferromag. rot. Index	
	MgO	Al2O3	SiO2	TiO2	Cr2O3	MnO	FeO	NiO	ZnO	At 10 Hz	At 57 Hz	At 10 Hz	At 57 Hz	At 10hz	At 57hz	at 10hz	At 57 Hz	At 10 Hz	At 57 Hz
CRA Sample 2 (500 microns)	0.00	0.00	0.00	50.40	0.02	5.73	42.70	0.06	0.13	0.09	0.09	0.01	0.03	9.8E-06	9.8E-06	1.007	0.141	0.10795	0.033
	0.02	0.00	0.00	50.61	0.03	5.36	42.86	0.03	0.24	0.10	0.12	0.04	0.04	8.7E-06	6.1E-06	0.094	0.108	0.02534	0.028
	0.02	0.00	0.00	49.32	0.00	4.47	44.99	0.03	0.04	0.10	0.12	0.03	0.04	8.7E-06	6.1E-06	0.160	0.141	0.03599	0.033
	0.08	0.66	0.38	54.93	0.01	3.24	36.73	0.02	0.00	0.10	0.15	0.01	0.03	7.7E-06	3.8E-06	1.279	0.384	0.12328	0.062
	0.02	0.00	0.02	49.19	0.00	4.36	45.40	0.01	0.06	0.13	0.18	0.02	0.05	4.8E-06	2.7E-06	0.433	0.206	0.06650	0.042
	0.02	0.00	0.01	50.93	0.01	5.20	42.99	0.00	0.06	0.09	0.11	0.02	0.03	9.8E-06	6.9E-06	0.339	0.160	0.05748	0.036
	0.01	0.00	0.00	49.99	0.02	5.97	42.90	0.01	0.03	0.12	0.15	0.03	0.04	6.1E-06	3.8E-06	0.234	0.160	0.04579	0.036
	0.05	0.00	0.00	50.11	0.03	8.46	41.37	0.00	0.00	0.09	0.10	0.01	0.03	9.8E-06	8.7E-06	0.793	0.160	0.09432	0.036
	0.04	0.00	0.00	49.13	0.00	4.11	46.16	0.02	0.00	0.13	0.15	0.03	0.05	4.8E-06	3.8E-06	0.206	0.108	0.04233	0.028
	0.03	0.00	0.00	50.42	0.05	6.19	43.25	0.02	0.08	0.15	0.15	0.05	0.07	3.8E-06	3.8E-06	0.108	0.046	0.02777	0.015
	0.05	0.00	0.00	49.48	0.03	4.55	44.34	0.00	0.12	0.17	0.18	0.06	0.07	3.0E-06	2.7E-06	0.108	0.071	0.02777	0.021
	0.02	0.00	0.01	51.63	0.00	6.58	41.79	0.06	0.10	0.12	0.13	0.05	0.05	5.4E-06	4.8E-06	0.094	0.094	0.02534	0.025
	0.03	0.00	0.00	49.90	0.00	4.57	44.75	0.04	0.04	0.15	0.17	0.05	0.05	3.8E-06	3.0E-06	0.123	0.123	0.03035	0.030
	0.02	0.00	0.03	49.78	0.00	5.34	44.54	0.00	0.15	0.15	0.15	0.06	0.07	3.8E-06	3.8E-06	0.062	0.046	0.01886	0.015
	0.03	0.00	0.01	49.87	0.01	5.39	44.33	0.00	0.02	0.20	0.21	0.17	0.12	2.1E-06	1.9E-06	0.006	0.028	0.00285	0.010
	0.01	0.00	0.01	49.76	0.04	5.06	44.28	0.00	0.00	0.14	0.15	0.02	0.04	4.3E-06	3.8E-06	0.703	0.160	0.08808	0.036
	0.02	0.00	0.00	49.81	0.00	4.01	45.47	0.00	0.06	0.12	0.13	0.01	0.04	5.4E-06	4.8E-06	1.279	0.141	0.12328	0.033
	0.04	0.00	0.21	50.45	0.01	5.32	42.86	0.00	0.12	0.15	0.15	0.03	0.05	3.8E-06	3.8E-06	0.489	0.108	0.07143	0.028
	0.00	0.00	0.02	48.74	0.01	4.44	45.01	0.00	0.08	0.22	0.22	0.14	0.20	1.7E-06	1.7E-06	0.023	0.004	0.00886	0.002
	0.03	0.00	0.02	49.95	0.00	4.33	43.73	0.03	0.04	0.19	0.21	0.09	0.08	2.4E-06	1.9E-06	0.046	0.094	0.01512	0.025
	0.03	0.00	0.00	50.20	0.05	5.65	43.19	0.00	0.11	0.20	0.22	0.13	0.17	2.1E-06	1.7E-06	0.019	0.012	0.00751	0.005
	0.02	0.00	0.01	48.58	0.00	5.59	44.94	0.01	0.06	0.21	0.21	0.15	0.14	1.9E-06	1.9E-06	0.015	0.019	0.00624	0.008
	0.01	0.00	0.00	48.94	0.02	5.77	44.19	0.00	0.00	0.21	0.21	0.15	0.18	1.9E-06	1.9E-06	0.015	0.006	0.00624	0.003
	0.05	0.00	0.00	48.52	0.00	4.11	46.45	0.00	0.00	0.19	0.19	0.03	0.04	2.4E-06	2.4E-06	0.793	0.300	0.09432	0.053
	0.03	0.07	0.51	64.92	0.00	0.95	18.41	0.05	0.08	0.27	0.27	0.21	0.22	1.2E-06	1.2E-06	0.009	0.006	0.00391	0.003
	0.04	0.12	0.21	62.47	0.06	3.36	24.50	0.00	0.08	0.27	0.24	0.03	0.05	1.2E-06	1.5E-06	1.622	0.384	0.14053	0.062
										0.29	0.30	0.24	0.30	9.7E-07	9.3E-07	0.008	0.000	0.00348	0.000
	0.00	0.00	0.12	57.82	0.04	3.24	32.70	0.01	0.00	0.27	0.25	0.15	0.22	1.2E-06	1.3E-06	0.033	0.004	0.01181	0.002
	0.02	0.13	0.96	57.81	0.02	4.55	30.56	0.02	0.00	0.28	0.28	0.28	0.28	1.0E-06	1.0E-06		0.000	0.00000	0.000
	0.03	0.00	0.50	63.20	0.01	3.79	26.02	0.00	0.11	0.28	0.28	0.13	0.16	1.0E-06	1.0E-06	0.053	0.033	0.01694	0.012
CRA sample 2 (second batch)	0.01	0.00	0.01	49.95	0.01	3.79	44.91	0.00	0.00	0.08	0.09	0.01	0.03	1.4E-05	9.8E-06	0.489	0.108	0.07143	0.028
	0.03	0.00	0.02	50.15	0.00	6.63	42.43	0.00	0.01	0.09	0.10	0.02	0.03	1.1E-05	8.7E-06	0.433	0.123	0.06650	0.030
	0.03	0.00	0.02	50.04	0.00	6.61	43.50	0.00	0.00	0.09	0.09	0.03	0.04	9.8E-06	9.8E-06	0.108	0.053	0.02777	0.017
	0.04	0.06	0.00	49.32	0.00	4.29	44.95	0.00	0.00	0.09	0.09	0.01	0.03	9.8E-06	9.8E-06	1.007	0.094	0.10795	0.025
	0.04	0.00	0.00	49.58	0.04	6.16	42.60	0.02	0.00	0.09	0.10	0.03	0.04	9.8E-06	7.7E-06	0.182	0.108	0.03906	0.028
	0.01	0.00	0.00	48.89	0.03	3.94	46.16	0.00	0.00	0.11	0.12	0.07	0.06	6.9E-06	6.1E-06	0.019	0.039	0.00751	0.013
	0.01	0.00	0.00	48.57	0.01	5.06	45.19	0.05	0.19	0.13	0.12	0.03	0.05	4.8E-06	5.4E-06	0.234	0.062	0.04579	0.019
	0.01	0.00	0.02	49.66	0.00	5.37	43.64	0.02	0.00	0.12	0.12	0.04	0.05	6.1E-06	5.4E-06	0.141	0.094	0.03309	0.025
	0.03	0.00	0.02	48.55	0.00	4.81	45.27	0.05	0.12	0.12	0.14	0.06	0.06	5.4E-06	4.3E-06	0.046	0.053	0.01512	0.017
	0.03	0.00	0.00	49.77	0.02	4.24	44.87	0.00	0.08	0.12	0.14	0.02	0.04	6.1E-06	4.3E-06	0.623	0.160	0.08220	0.036
	0.04	0.00	0.00	49.07	0.03	4.67	45.67	0.00	0.13	0.15	0.15	0.06	0.07	3.8E-06	3.8E-06	0.082	0.046	0.02305	0.015
	0.02	0.00	0.01	49.32	0.06	5.39	44.86	0.10	0.00	0.14	0.15	0.07	0.08	4.3E-06	3.8E-06	0.039	0.033	0.01342	0.012
	0.03	0.00	0.00	48.38	0.02	4.83	45.93	0.02	0.13	0.13	0.13	0.03	0.05	4.8E-06	4.8E-06	0.234	0.101	0.04579	0.027

Sample Source	Oxide weight %									Lifting field (T)		Rotating field (T)		Mag. Suscept. (SI)		Paramag. rot. Index		Ferromag. rot. Index	
	MgO	Al2O3	SiO2	TiO2	Cr2O3	MnO	FeO	NiO	ZnO	At 10 Hz	At 57 Hz	At 10 Hz	At 57 Hz	At 10hz	At 57hz	at 10hz	At 57 Hz	At 10 Hz	At 57 Hz
	0.03	0.00	0.00	47.41	0.00	5.07	46.00	0.00	0.00	0.16	0.17	0.07	0.10	3.2E-06	3.0E-06	0.058	0.028	0.01807	0.010
	0.03	0.00	0.02	48.46	0.00	5.44	44.94	0.00	0.06	0.17	0.18	0.14	0.13	3.0E-06	2.7E-06	0.006	0.012	0.00285	0.005
	0.02	0.00	0.02	46.78	0.02	5.03	46.86	0.02	0.00	0.18	0.18	0.07	0.12	2.7E-06	2.7E-06	0.071	0.019	0.02089	0.008
	0.01	0.00	0.01	47.64	0.00	6.11	44.53	0.00	0.15	0.20	0.21	0.13	0.16	2.1E-06	1.9E-06	0.019	0.012	0.00751	0.005
	0.03	0.00	0.00	49.27	0.00	5.03	44.97	0.07	0.07	0.21	0.21	0.11	0.17	1.9E-06	1.9E-06	0.039	0.009	0.01342	0.004
	0.04	0.00	0.00	49.88	0.00	4.35	44.19	0.00	0.13	0.20	0.20	0.17	0.19	2.1E-06	2.1E-06	0.006	0.002	0.00285	0.001
	0.05	0.00	0.00	49.44	0.00	4.90	44.79	0.11	0.13	0.22	0.22	0.12	0.21	1.7E-06	1.7E-06	0.039	0.002	0.01342	0.001
CRA picro-ilmenites	8.97	0.42	0.06	46.51	0.19	0.26	40.17	0.09	0.02	0.22	0.22	0.22	0.22	1.7E-06	1.7E-06		0.000	0.00000	0.000
	9.50	0.60	0.05	47.72	0.19	0.21	38.35	0.06	0.10	0.22	0.22	0.22	0.22	1.7E-06	1.7E-06		0.000	0.00000	0.000
	9.26	0.57	0.05	47.29	0.24	0.27	38.41	0.05	0.08	0.22	0.24	0.22	0.24	1.7E-06	1.5E-06		0.000	0.00000	0.000
	9.35	0.56	0.07	47.37	0.29	0.29	38.63	0.12	0.02	0.22	0.22	0.22	0.22	1.7E-06	1.7E-06		0.000	0.00000	0.000
	12.67	0.54	0.00	52.11	0.57	0.37	31.25	0.16	0.00	0.30	0.29	0.30	0.29	9.3E-07	9.7E-07		0.000	0.00000	0.000
	12.96	0.78	0.03	53.26	0.38	0.24	30.89	0.07	0.06	0.29	0.29	0.29	0.29	9.7E-07	9.7E-07		0.000	0.00000	0.000
	8.85	0.03	0.03	49.81	0.44	0.16	38.29	0.03	0.00	0.12	0.13	0.04	0.05	6.1E-06	4.8E-06	0.141	0.094	0.03309	0.025
	11.49	0.15	0.01	51.00	0.64	0.36	34.28	0.00	0.00	0.25	0.26	0.25	0.26	1.3E-06	1.2E-06		0.000	0.00000	0.000
	9.10	0.06	0.02	50.40	0.54	0.29	37.37	0.10	0.00	0.24	0.24	0.21	0.24	1.5E-06	1.4E-06	0.004	0.001	0.00184	0.000
NSW Mg-ilmenites	3.00	0.00	0.01	36.13	0.20	0.22	56.78	0.00	0.00	0.01	0.01	0.00	0.01	1.6E-03	1.2E-03	0.329	0.047	0.02305	0.020
	3.70	0.01	0.02	39.18	0.21	0.21	52.43	0.00	0.00	0.01	0.01	0.01	0.01	1.2E-03	1.0E-03	0.092	0.016	0.00886	0.007
										0.01	0.01	0.00	0.01	1.6E-03	1.3E-03	0.092	0.000	0.00886	0.000
	3.51	0.00	0.00	37.95	0.21	0.20	53.23	0.11	0.01	0.01	0.01	0.00	0.01	1.6E-03	9.1E-04	0.092	0.047	0.00886	0.020
	3.61	0.00	0.03	39.33	0.21	0.10	52.24	0.03	0.03	0.01	0.01	0.00	0.01	1.6E-03	1.0E-03	0.183	0.060	0.01512	0.025
	2.36	0.00	0.00	33.73	0.28	0.12	57.98	0.05	0.03	0.01	0.01	0.00	0.01	1.6E-03	1.0E-03	0.247	0.035	0.01886	0.016
	2.26	0.00	0.00	32.45	0.31	0.09	58.65	0.00	0.07	0.01	0.01	0.00	0.01	1.3E-03	8.1E-04	0.936	0.035	0.04579	0.016
	3.53	0.00	0.00	39.36	0.18	0.18	52.12	0.12	0.00	0.01	0.01	0.01	0.01	1.3E-03	8.1E-04	0.075	0.047	0.00751	0.020
										0.01	0.01	0.00	0.01	1.6E-03	1.2E-03	0.111	0.000	0.01029	0.000
	2.37	0.02	0.01	32.70	0.30	0.03	58.79	0.01	0.00	0.01	0.01	0.00	0.01	1.0E-03	7.2E-04	0.132	0.060	0.01181	0.025
	2.93	0.00	0.01	35.83	0.37	0.21	55.91	0.15	0.01	0.01	0.01	0.00	0.01	1.3E-03	8.1E-04	0.132	0.075	0.01181	0.030
	3.33	0.00	0.00	38.17	0.22	0.17	53.43	0.00	0.08	0.01	0.01	0.00	0.01	1.3E-03	1.0E-03	0.329	0.060	0.02305	0.025
	4.64	0.00	0.01	42.30	0.32	0.21	49.47	0.00	0.15	0.03	0.04	0.02	-	8.6E-05	6.1E-05	0.035	-	0.00391	-
	3.89	0.00	0.03	40.11	0.21	0.25	50.85	0.02	0.02	0.04	0.04	0.03	0.03	6.1E-05	6.1E-05	0.035	0.007	0.00391	0.004
	4.13	0.00	0.00	40.78	0.18	0.20	51.73	0.00	0.21	0.03	0.03	0.03	0.03	9.7E-05	7.7E-05	0.016	0.000	0.00184	0.000
	4.01	0.01	0.00	41.23	0.15	0.29	51.43	0.05	0.00	0.03	0.04	0.03	0.05	7.7E-05	6.1E-05	0.016	-0.030	0.00184	-0.018
	4.15	0.00	0.02	41.66	0.21	0.16	50.69	0.00	0.03	0.03	0.03	0.03	-	7.7E-05	6.8E-05	0.016	-	0.00184	-
	4.12	0.00	0.01	40.71	0.23	0.21	51.92	0.00	0.00	0.02	0.02	0.02	0.02	1.6E-04	1.6E-04	0.060	0.007	0.00624	0.004
	4.31	0.00	0.00	42.02	0.14	0.45	50.43	0.05	0.05	0.06	0.06	0.05	-	2.7E-05	2.4E-05	0.025	-	0.00285	-
	4.18	0.00	0.00	41.39	0.25	0.24	50.74	0.00	0.08	0.06	0.06	0.05	-	2.7E-05	2.4E-05	0.025	-	0.00285	-
	4.28	0.00	0.00	41.30	0.22	0.33	50.72	0.00	0.00	0.06	0.06	0.04	-	2.4E-05	2.1E-05	0.060	-	0.00624	-
	4.23	0.00	0.05	41.04	0.13	0.22	50.92	0.00	0.00	0.24	0.24	-	-	1.4E-06	1.4E-06		-	-	-
										0.05	0.06	0.04	0.07	3.0E-05	2.7E-05	0.035	-0.026	0.00391	-0.015
										0.04	0.05	0.02	0.06	4.3E-05	3.8E-05	0.156	-0.022	0.01342	-0.012
	4.60	0.00	0.03	42.68	0.18	0.33	49.32	0.04	0.00	0.07	0.08	0.07	-	1.7E-05	1.3E-05		-	0.00000	-
	4.73	0.00	0.02	43.29	0.13	0.20	49.13	0.00	0.03	0.09	0.09	0.08	-	1.0E-05	1.0E-05	0.007	-	0.00089	-
	4.76	0.00	0.01	43.21	0.25	0.15	49.26	0.05	0.10	0.07	0.07	0.07	-	1.7E-05	1.5E-05		-	0.00000	-
	4.54	0.00	0.00	42.57	0.17	0.27	49.58	0.05	0.01	0.07	0.07	0.06	-	1.9E-05	1.5E-05	0.016	-	0.00184	-
	4.95	0.02	0.03	42.67	0.12	0.16	49.01	0.06	0.00	0.07	0.07	0.07	-	1.7E-05	1.5E-05	0.007	-	0.00089	-
	4.43	0.00	0.02	43.20	0.20	0.22	49.46	0.00	0.00	0.07	0.07	0.07	-	1.7E-05	1.5E-05		-	0.00000	-
	9.93	0.54	0.00	50.81	0.25	0.19	36.94	0.07	0.00	0.22	0.22	-	-	1.8E-06	1.8E-06		-	-	-
	7.95	0.21	0.00	49.98	0.19	0.28	40.21	0.06	0.03	0.19	0.19	-	-	2.2E-06	2.2E-06		-	-	-
	8.79	0.85	0.05	48.47	0.21	0.29	39.46	0.00	0.00	0.11	0.13	0.11	-	6.5E-06	5.1E-06	0.007	-	0.00089	-
	4.83	0.00	0.01	43.47	0.18	0.45	48.53	0.01	0.05	0.09	0.10	0.08	-	9.2E-06	8.2E-06	0.016	-	0.00184	-

Sample Source	Oxide weight %									Lifting field (T)		Rotating field (T)		Mag. Suscept. (SI)		Paramag. rot. Index		Ferromag. rot. Index	
	MgO	Al2O3	SiO2	TiO2	Cr2O3	MnO	FeO	NiO	ZnO	At 10 Hz	At 57 Hz	At 10 Hz	At 57 Hz	At 10hz	At 57hz	at 10hz	At 57 Hz	At 10 Hz	At 57 Hz
	6.97	0.13	0.01	48.75	0.21	0.30	41.93	0.00	0.00	0.14	0.16	-	-	4.0E-06	3.2E-06		-	-	-
	8.36	0.34	0.05	49.80	0.25	0.20	39.14	0.12	0.03	0.18	0.18	-	-	2.5E-06	2.5E-06		-	-	-
EL 11/96	0.04	0.00	0.04	54.94	0.07	7.20	27.87	0.05	5.26	0.34	0.34	-	-	7.3E-07	7.3E-07		-	-	-
Combined ilmenite sample	0.03	0.00	0.03	51.82	0.04	8.06	39.39	0.00	0.11	0.25	0.27	0.24	0.34	1.3E-06	1.2E-06	0.002	-0.006	0.00089	-0.003
	0.05	0.00	0.04	52.60	0.02	5.72	38.42	0.00	0.15	0.26	0.27	0.25	0.34	1.2E-06	1.2E-06	0.001	-0.006	0.00053	-0.003
	0.06	0.00	0.03	53.18	0.06	5.60	37.29	0.00	0.31	0.26	0.27	0.25	0.34	1.2E-06	1.2E-06	0.001	-0.006	0.00053	-0.003
	0.01	0.00	0.01	52.02	0.01	5.64	42.41	0.00	0.03	0.25	0.27	0.22	0.34	1.3E-06	1.2E-06	0.004	-0.006	0.00184	-0.003
	0.04	0.00	0.00	51.17	0.00	7.16	41.01	0.00	0.00	0.23	0.24	0.22	0.22	1.6E-06	1.5E-06	0.001	0.002	0.00053	0.001
	0.05	0.00	0.00	51.46	0.01	7.17	40.29	0.00	0.13	0.23	0.24	0.23	0.34	1.6E-06	1.5E-06		-0.007	0.00000	-0.004
	0.05	0.00	0.03	51.40	0.03	5.88	42.67	0.00	0.00	0.22	0.22	0.12	0.21	1.8E-06	1.7E-06	0.031	0.002	0.01119	0.001
	0.03	0.00	0.03	51.91	0.02	7.33	39.86	0.00	0.05	0.23	0.24	0.22	0.24	1.6E-06	1.5E-06	0.001	0.000	0.00053	0.000
	0.02	0.00	0.01	51.73	0.01	3.52	44.17	0.02	0.00	0.23	0.24	0.22	0.24	1.6E-06	1.5E-06	0.001	0.000	0.00053	0.000
	0.05	0.00	0.03	51.96	0.05	2.42	45.06	0.03	0.00	0.23	0.24	0.22	0.24	1.6E-06	1.5E-06	0.001	0.000	0.00053	0.000
	0.05	0.00	0.00	56.02	0.02	4.32	33.88	0.00	0.07	0.27	0.29	0.24	0.34	1.2E-06	9.7E-07	0.003	-0.004	0.00127	-0.002
	0.04	0.00	0.03	52.00	0.00	8.11	39.84	0.00	0.25	0.24	0.25	0.22	0.34	1.5E-06	1.3E-06	0.002	-0.007	0.00089	-0.004
	0.05	0.00	0.00	51.64	0.01	7.96	39.55	0.00	0.30	0.24	0.25	0.22	0.34	1.5E-06	1.3E-06	0.002	-0.007	0.00089	-0.004
	0.07	0.00	0.00	51.07	0.00	7.22	41.80	0.10	0.07	0.24	0.24	0.21	0.34	1.5E-06	1.5E-06	0.004	-0.007	0.00184	-0.004
	0.05	0.00	0.02	51.68	0.00	4.22	43.80	0.08	0.10	0.22	0.23	0.21	0.24	1.7E-06	1.6E-06	0.002	-0.002	0.00089	-0.001
	0.08	0.00	0.02	51.25	0.06	9.23	39.61	0.00	0.03	0.16	0.17	0.01	0.02	3.2E-06	3.0E-06	11.552	1.622	0.39795	0.141
	0.03	0.00	0.02	52.10	0.02	8.00	38.95	0.00	0.12	0.21	0.22	0.10	0.12	1.9E-06	1.7E-06	0.046	0.039	0.01512	0.013
	0.05	0.00	0.02	51.14	0.00	7.37	41.29	0.00	0.04	0.19	0.19	0.04	0.09	2.3E-06	2.3E-06	0.403	0.057	0.06368	0.018
	0.01	0.00	0.05	51.85	0.05	6.83	41.50	0.11	0.07	0.13	0.14	0.02	0.05	4.6E-06	4.3E-06	0.654	0.082	0.08451	0.023
	0.00	0.00	0.00	52.25	0.02	8.54	38.34	0.00	0.12	0.23	0.24	0.19	0.34	1.6E-06	1.5E-06	0.008	-0.007	0.00348	-0.004
	0.04	0.09	0.15	57.63	0.04	2.55	33.82	0.00	0.00	0.19	0.19	0.05	0.09	2.4E-06	2.3E-06	0.160	0.049	0.03599	0.016
	0.06	0.00	0.00	51.23	0.00	5.41	42.53	0.05	0.12	0.21	0.21	0.14	0.15	1.9E-06	1.9E-06	0.019	0.015	0.00751	0.006
	0.04	0.00	0.00	51.75	0.03	7.57	40.50	0.00	0.10	0.13	0.13	0.03	0.05	4.8E-06	4.8E-06	0.206	0.108	0.04233	0.028
	0.05	0.00	0.03	53.04	0.01	6.10	38.88	0.00	0.00	0.10	0.10	0.00	0.00	8.7E-06	8.7E-06	49.818	6.714	0.84183	0.300
	0.06	0.00	0.06	49.25	0.05	2.51	45.45	0.00	0.03	0.12	0.12	0.10	0.06	6.1E-06	6.1E-06	0.004	0.046	0.00184	0.015
	0.04	0.00	0.00	48.39	0.06	2.21	47.54	0.00	0.00	0.13	0.13	0.05	0.06	4.8E-06	4.8E-06	0.082	0.066	0.02305	0.020
	0.06	0.35	0.25	63.94	0.00	4.44	25.61	0.05	0.10	0.12	0.12	0.01	0.02	6.1E-06	6.1E-06	3.719	0.489	0.21974	0.071
	0.03	0.00	0.00	51.77	0.01	8.96	38.64	0.07	0.00	0.12	0.12	0.00	0.01	6.1E-06	6.1E-06	56.047	6.714	0.89379	0.300
	0.01	0.00	0.01	52.44	0.01	7.93	40.60	0.00	0.12	0.27	0.27	0.24	-	1.2E-06	1.2E-06	0.004	-	0.00184	-
	0.08	0.00	0.00	52.82	0.06	7.42	39.97	0.04	0.14	0.24	0.25	0.24	-	1.5E-06	1.3E-06		-	0.00000	-
	0.04	0.00	0.00	52.11	0.00	6.34	40.94	0.07	0.47	0.24	0.24	0.21	-	1.5E-06	1.5E-06	0.004	-	0.00184	-
	0.04	0.00	0.00	52.93	0.01	8.76	39.09	0.00	0.13	0.25	0.26	0.22	-	1.3E-06	1.2E-06	0.004	-	0.00184	-
	0.02	0.00	0.00	53.94	0.00	7.65	38.85	0.00	0.09	0.25	0.27	0.24	-	1.3E-06	1.2E-06	0.002	-	0.00089	-
	0.06	0.00	0.02	52.49	0.03	8.14	39.93	0.06	0.09	0.25	0.26	0.23	-	1.3E-06	1.2E-06	0.003	-	0.00127	-
	0.06	0.00	0.01	52.03	0.00	9.34	39.19	0.04	0.00	0.28	0.28	0.27	-	1.0E-06	1.0E-06	0.002	-	0.00089	-
	0.04	0.00	0.02	52.25	0.03	10.22	38.52	0.03	0.15	0.30	0.30	0.30	-	9.3E-07	9.3E-07		-	0.00000	-
	0.06	0.00	0.03	56.24	0.01	5.71	35.28	0.00	0.06	0.28	0.29	0.28	-	1.0E-06	9.7E-07		-	0.00000	-
	0.02	0.00	0.05	54.13	0.00	8.09	36.17	0.01	0.00	0.30	0.32	0.30	-	9.3E-07	8.2E-07		-	0.00000	-
	0.01	0.00	0.02	53.66	0.02	9.03	36.71	0.08	0.18	0.32	0.33	-	-	8.2E-07	7.7E-07		-	-	-
	0.05	0.00	0.05	56.26	0.02	7.43	32.29	0.00	0.13	0.33	0.34	-	-	7.7E-07	7.3E-07		-	-	-
	0.05	0.00	0.04	54.32	0.01	8.63	36.54	0.04	0.00	0.30	0.31	-	-	9.3E-07	8.8E-07		-	-	-
	0.05	0.00	0.01	57.34	0.00	7.60	31.18	0.00	0.02	0.33	0.33	-	-	7.7E-07	7.7E-07		-	-	-
	0.02	0.00	0.01	53.17	0.04	9.34	37.57	0.00	0.00	0.30	0.31	0.29	-	9.3E-07	8.8E-07	0.001	-	0.00035	-
	0.07	0.00	0.01	53.18	0.00	6.56	40.68	0.05	0.27	0.07	0.07	0.00	0.00	1.6E-05	1.6E-05	27.639	10.763	0.62335	0.384
	0.05	0.00	0.01	48.03	0.02	1.77	51.30	0.01	0.08	0.11	0.11	0.02	0.03	6.9E-06	6.9E-06	0.384	0.141	0.06186	0.033
	0.11	0.09	0.06	60.41	0.04	5.74	28.56	0.02	0.12	0.15	0.15	0.01	0.01	3.8E-06	3.8E-06	9.566	2.936	0.36084	0.194
	0.04	0.00	0.00	52.63	0.00	9.20	38.37	0.03	0.04	0.17	0.17	0.02	0.05	3.0E-06	3.0E-06	1.622	0.182	0.14053	0.039
	0.00	0.04	0.05	60.81	0.00	5.65	27.95	0.00	0.00	0.19	0.20	0.01	0.03	2.4E-06	2.1E-06	3.304	0.703	0.20633	0.088

Sample Source	Oxide weight %									Lifting field (T)		Rotating field (T)		Mag. Suscept. (SI)		Paramag. rot. Index		Ferromag. rot. Index	
	MgO	Al2O3	SiO2	TiO2	Cr2O3	MnO	FeO	NiO	ZnO	At 10 Hz	At 57 Hz	At 10 Hz	At 57 Hz	At 10hz	At 57hz	at 10hz	At 57 Hz	At 10 Hz	At 57 Hz
	0.08	0.18	0.16	62.42	0.00	4.79	26.24	0.08	0.00	0.18	0.18	0.01	0.03	2.7E-06	2.7E-06	2.057	0.552	0.15994	0.077
	0.06	0.18	0.02	59.71	0.04	4.56	31.89	0.00	0.05	0.34	0.34	0.34	0.34	7.3E-07	7.3E-07		0.000	0.00000	0.000
	4.90	0.06	0.01	54.00	0.01	0.47	42.22	0.00	0.02	0.21	0.21	0.02	0.05	1.9E-06	1.9E-06	1.279	0.234	0.12328	0.046
	0.03	0.00	0.02	51.55	0.00	7.50	41.68	0.07	0.04	0.25	0.25	0.17	0.20	1.3E-06	1.3E-06	0.019	0.009	0.00751	0.004
	0.02	0.00	0.00	52.15	0.00	10.20	38.59	0.04	0.23	0.26	0.26	0.21	0.25	1.2E-06	1.2E-06	0.008	0.001	0.00348	0.001
	0.03	0.00	0.02	51.88	0.08	3.29	44.07	0.04	0.10	0.27	0.29	0.24	-	1.1E-06	9.7E-07	0.005	-	0.00244	-
	0.06	0.00	0.00	51.77	0.11	2.92	43.87	0.05	0.38	0.26	0.27	0.21	-	1.2E-06	1.1E-06	0.008	-	0.00348	-
	0.05	0.00	0.00	51.64	0.01	8.93	39.52	0.00	0.36	0.27	0.27	0.21	0.26	1.2E-06	1.2E-06	0.009	0.001	0.00391	0.000
	0.02	0.00	0.00	52.14	0.00	9.25	38.39	0.00	0.19	0.27	0.29	0.22	0.34	1.2E-06	9.7E-07	0.006	-0.004	0.00285	-0.002
	0.03	0.00	0.02	52.16	0.03	9.72	39.31	0.00	0.00	0.27	0.27	0.21	0.27	1.2E-06	1.1E-06	0.009	-0.000	0.00391	0.000
	0.03	0.00	0.00	52.01	0.04	7.69	40.69	0.02	0.00	0.27	0.27	0.21	0.27	1.2E-06	1.1E-06	0.008	-0.000	0.00348	0.000
	0.04	0.00	0.00	51.95	0.03	11.43	37.14	0.00	0.10	0.27	0.27	0.24	0.27	1.2E-06	1.1E-06	0.004	-0.000	0.00184	0.000
	0.03	0.00	0.00	52.39	0.02	9.73	38.56	0.00	0.04	0.27	0.27	0.21	0.26	1.2E-06	1.2E-06	0.009	0.001	0.00391	0.000
										0.34	0.34	0.34	0.34	7.3E-07	7.3E-07		0.000	0.00000	0.000
	0.06	0.00	0.00	52.47	0.01	8.83	39.03	0.00	0.00	0.26	0.27	0.21	-	1.2E-06	1.2E-06	0.008	-	0.00348	-
	0.00	0.00	0.00	51.91	0.01	7.12	41.28	0.00	0.12	0.27	0.27	0.24	-	1.2E-06	1.2E-06	0.004	-	0.00184	-
	0.02	0.00	0.02	52.44	0.00	11.25	37.37	0.04	0.10	0.27	0.27	0.22	0.27	1.2E-06	1.2E-06	0.006	0.000	0.00285	0.000
	0.06	0.00	0.02	52.02	0.05	9.07	39.52	0.00	0.17	0.27	0.27	0.26	-	1.2E-06	1.2E-06	0.001	-	0.00035	-
	0.01	0.00	0.01	53.29	0.00	11.24	36.85	0.01	0.05	0.27	0.27	0.24	-	1.2E-06	1.1E-06	0.004	-	0.00184	-
	0.03	0.00	0.05	52.48	0.03	7.81	40.45	0.05	0.17	0.27	0.27	0.24	0.27	1.2E-06	1.1E-06	0.004	0.001	0.00184	0.000
	0.03	0.00	0.00	52.47	0.02	9.00	38.97	0.06	0.09	0.26	0.26	0.17	0.22	1.2E-06	1.2E-06	0.021	0.005	0.00831	0.002
	0.03	0.00	0.00	53.08	0.00	10.29	36.70	0.01	0.10	0.27	0.29	0.27	-	1.1E-06	9.7E-07	0.001	-	0.00035	-
	0.03	0.00	0.00	53.43	0.00	11.58	34.76	0.00	0.16	0.27	0.29	0.27	-	1.2E-06	9.7E-07		-	0.00000	-
	0.02	0.00	0.02	52.79	0.05	3.30	42.31	0.00	0.25	0.31	0.33	0.31	-	8.8E-07	7.7E-07		-	0.00000	-
	0.05	0.00	0.04	52.08	0.05	6.29	41.26	0.00	0.00	0.27	0.27	0.21	0.26	1.2E-06	1.2E-06	0.009	0.001	0.00391	0.000
	0.02	0.00	0.00	51.63	0.06	6.15	41.86	0.00	0.07	0.27	0.27	0.25	0.27	1.2E-06	1.2E-06	0.002	0.000	0.00089	0.000
	0.09	0.00	0.00	52.56	0.01	10.43	36.39	0.02	0.11	0.28	0.29	0.27	-	1.0E-06	9.7E-07	0.002	-	0.00089	-
	0.04	0.00	0.03	54.44	0.00	8.57	34.30	0.03	0.00	0.30	0.32	0.30	-	9.3E-07	8.2E-07		-	0.00000	-
	0.04	0.00	0.02	53.99	0.00	9.30	34.38	0.00	0.01	0.30	0.30	0.27	0.30	9.3E-07	9.3E-07	0.004	0.000	0.00184	0.000
	0.04	0.00	0.00	53.46	0.00	9.80	36.47	0.07	0.11	0.30	0.31	0.27	-	9.3E-07	8.8E-07	0.004	-	0.00184	-
	0.06	0.00	0.03	51.87	0.00	10.66	37.86	0.06	0.05	0.31	0.32	0.28	-	8.8E-07	8.2E-07	0.003	-	0.00127	-
	0.07	0.00	0.00	52.10	0.00	9.66	38.26	0.00	0.06	0.29	0.28	0.29	-	9.7E-07	1.0E-06		-	0.00000	-
	0.06	0.00	0.01	52.36	0.03	9.38	38.58	0.00	0.04	0.28	0.29	0.28	-	1.0E-06	9.7E-07		-	0.00000	-
	0.06	0.00	0.00	53.11	0.04	9.34	37.16	0.00	0.01	0.28	0.30	0.28	-	1.0E-06	9.3E-07		-	0.00000	-
	0.04	0.00	0.01	52.00	0.00	9.79	38.38	0.00	0.01	0.27	0.29	0.27	-	1.1E-06	9.7E-07	0.001	-	0.00035	-
	0.06	0.00	0.03	54.47	0.04	6.43	35.90	0.00	0.05	0.30	0.30	0.30	-	9.3E-07	9.3E-07		-	0.00000	-
	0.05	0.00	0.01	51.84	0.00	9.81	37.70	0.00	0.08	0.30	0.30	0.30	-	9.3E-07	9.3E-07		-	0.00000	-
	0.05	0.00	0.00	51.99	0.00	7.81	40.07	0.00	0.35	0.26	0.26	0.19	0.25	1.2E-06	1.2E-06	0.014	0.001	0.00575	0.001
	0.04	0.00	0.00	51.38	0.06	3.54	44.49	0.03	0.07	0.24	0.26	0.24	0.26	1.5E-06	1.2E-06		0.000	0.00000	0.000
	0.05	0.00	0.00	50.82	0.07	3.28	44.84	0.02	0.33	0.24	0.24	0.22	0.24	1.5E-06	1.5E-06	0.002	0.000	0.00089	0.000
	0.06	0.74	0.08	57.72	0.02	7.09	30.48	0.00	0.00	0.06	0.06	0.00	0.00	2.5E-05	2.5E-05	89.786	3.304	1.13511	0.206
	0.06	0.00	0.02	51.65	0.02	8.71	39.28	0.00	0.27	0.21	0.24	0.21	0.24	1.9E-06	1.5E-06		0.000	0.00000	0.000
	0.02	0.00	0.00	52.15	0.01	6.32	41.64	0.00	0.00	0.21	0.21	0.09	0.11	1.9E-06	1.9E-06	0.062	0.039	0.01886	0.013
	0.09	0.07	0.03	54.46	0.00	10.29	33.02	0.00	0.00	0.33	0.33	0.33	-	7.7E-07	7.7E-07		-	0.00000	-
	0.05	0.00	0.02	51.23	0.00	10.05	39.18	0.00	0.00	0.28	0.27	0.26	0.27	1.0E-06	1.1E-06	0.003	-0.000	0.00127	0.000
	9.71	0.15	0.01	52.22	0.23	0.77	35.83	0.00	0.10	0.27	0.27	-	-	1.2E-06	1.2E-06		-	-	-
	0.06	0.00	0.03	52.26	0.01	7.12	40.20	0.00	0.13	0.28	0.29	0.24	-	1.0E-06	9.7E-07	0.005	-	0.00244	-
	0.06	0.00	0.00	51.85	0.03	7.38	38.53	0.04	0.13	0.25	0.27	0.24	-	1.3E-06	1.2E-06	0.002	-	0.00089	-
CRA 500 micron	12.43	0.00	0.04	53.58	0.75	0.31	30.83	0.06	0.00	0.24	0.24	0.23	0.24	1.5E-06	1.5E-06	0.001	0.000	0.00035	0.000
picro's from 180g	11.26	0.00	0.02	52.91	0.93	0.35	32.49	0.11	0.13	0.24	0.25	0.24	0.24	1.5E-06	1.4E-06		0.001	0.00000	0.000
test separation	9.04	0.39	0.03	49.10	0.13	0.34	37.93	0.01	0.07	0.21	0.21	0.20	0.21	1.9E-06	1.9E-06	0.001	0.000	0.00035	0.000

Sample Source	Oxide weight %									Lifting field (T)		Rotating field (T)		Mag. Suscept. (SI)		Paramag. rot. Index		Ferromag. rot. Index	
	MgO	Al2O3	SiO2	TiO2	Cr2O3	MnO	FeO	NiO	ZnO	At 10 Hz	At 57 Hz	At 10 Hz	At 57 Hz	At 10hz	At 57hz	at 10hz	At 57 Hz	At 10 Hz	At 57 Hz
Rio Tinto picro-ilmenites Analyses only.	12.70	0.21	0.06	55.20	0.71	0.25		0.00	0.00										
	10.10	0.26	0.09	56.10	0.41	0.33		0.16	0.00										
	4.41	0.00	0.12	48.70	0.09	0.32		0.21	0.00										
	9.67	0.07	0.27	50.40	1.23	0.23		0.05	0.07										
	11.30	0.92	0.16	52.90	1.16	0.19		0.17	0.24										
	9.00	0.64	0.15	50.90	1.61	0.22		0.13	0.12										
	4.70	0.00	0.26	48.10	0.21	0.41		0.09	0.08										
	5.70	0.00	0.29	50.20	0.00	0.44		0.10	0.00										
	6.26	0.07	0.33	50.00	1.26	0.32		0.11	0.15										
	10.00	0.82	0.25	51.30	1.41	0.29		0.16	0.10										
	6.49	0.00	0.20	47.80	1.51	0.25		0.05	0.11										
	8.74	0.22	0.22	52.60	0.86	1.19		0.07	0.09										
	5.93	0.13	0.23	49.30	1.08	0.23		0.14	0.17										
	6.32	0.00	0.11	48.40	2.68	0.21		0.00	0.00										
	8.55	0.00	0.13	50.10	0.32	0.25		0.00	0.02										
	13.40	0.27	0.22	57.20	0.62	0.33		0.00	0.14										
	9.30	0.00	0.20	53.50	1.98	0.29		0.17	0.03										
	6.67	0.01	0.29	47.90	1.37	0.31		0.04	0.00										
	10.80	0.28	0.20	55.20	0.11	0.29		0.08	0.15										
	9.09	0.15	0.23	51.50	1.41	0.37		0.00	0.15										
	5.81	0.13	0.27	50.10	0.14	0.55		0.07	0.07										
	10.90	0.02	0.05	54.70	0.38	0.23		0.21	0.08										
	8.05	0.09	0.22	51.80	0.91	0.40		0.09	0.10										
	10.40	0.00	0.17	56.00	0.24	0.47		0.08	0.00										
	8.71	0.00	0.29	49.20	1.29	0.43		0.07	0.04										
Rio Tinto Picro-ilmenites (no analysis)										0.25	0.25	0.25	-	1.3E-06	1.3E-06		-	0.00000	-
										0.29	0.29	-	-	9.8E-07	9.8E-07		-	-	-
										0.22	0.22	-	-	1.8E-06	1.8E-06		-	-	-
										0.14	0.14	0.14	0.14	4.3E-06	4.0E-06		0.000	0.00000	0.000
										0.19	0.19	-	-	2.4E-06	2.4E-06		-	-	-
										0.19	0.19	0.18	0.19	2.4E-06	2.4E-06	0.002	0.000	0.00089	0.000
										0.15	0.15	0.12	0.13	3.8E-06	3.8E-06	0.009	0.004	0.00391	0.002
										0.34	0.34	-	-	7.3E-07	7.3E-07	-	-	-	-
										0.34	0.34	-	-	7.3E-07	7.3E-07	-	-	-	-
										0.25	0.25	0.21	0.25	1.3E-06	1.3E-06	0.006	0.000	0.00285	0.000
										0.27	0.27	0.27	0.27	1.2E-06	1.2E-06		0.000	0.00000	0.000
										0.27	0.27	-	-	1.2E-06	1.2E-06	-	-	-	-
										0.19	0.19	0.15	0.16	2.4E-06	2.4E-06	0.009	0.006	0.00391	0.003
										0.14	0.14	0.14	0.14	4.0E-06	4.0E-06	0.001	0.001	0.00044	0.000
										0.27	0.27	0.27	-	1.2E-06	1.2E-06		-	0.00000	-
										0.24	0.24	0.24	0.24	1.5E-06	1.5E-06		0.000	0.00000	0.000
										0.24	0.24	0.24	0.24	1.5E-06	1.5E-06		0.000	0.00000	0.000
										0.24	0.24	0.24	0.24	1.5E-06	1.5E-06		0.000	0.00000	0.000
										0.09	0.09	0.06	0.07	1.1E-05	1.1E-05	0.015	0.006	0.00624	0.003
										0.25	0.25	0.23	0.24	1.3E-06	1.3E-06	0.003	0.002	0.00136	0.001
										0.21	0.21	0.20	0.20	1.9E-06	1.9E-06	0.002	0.002	0.00089	0.001
										0.21	0.21	0.19	0.20	1.9E-06	1.9E-06	0.004	0.002	0.00184	0.001
										0.24	0.24	0.24	0.24	1.5E-06	1.5E-06		0.000	0.00000	0.000

Sample Source	Oxide weight %									Lifting field (T)		Rotating field (T)		Mag. Suscept. (SI)		Paramag. rot. Index		Ferromag. rot. Index	
	MgO	Al2O3	SiO2	TiO2	Cr2O3	MnO	FeO	NiO	ZnO	At 10 Hz	At 57 Hz	At 10 Hz	At 57 Hz	At 10hz	At 57hz	at 10hz	At 57 Hz	At 10 Hz	At 57 Hz
										0.27	0.27	0.27	-	1.2E-06	1.2E-06		-	0.00000	-
										0.24	0.24	0.24	-	1.5E-06	1.5E-06		-	0.00000	-
										0.24	0.24	0.24	-	1.5E-06	1.5E-06		-	0.00000	-
										0.25	0.25	-	-	1.3E-06	1.3E-06		-	-	-
										0.18	0.18	0.18	-	2.7E-06	2.7E-06		-	0.00000	-
										0.21	0.21	0.21	0.21	1.9E-06	1.9E-06		0.000	0.00000	0.000
										0.22	0.22	0.22	-	1.7E-06	1.7E-06		-	0.00000	-
										0.19	0.19	0.18	0.19	2.4E-06	2.4E-06	0.002	0.000	0.00089	0.000
										0.24	0.24	0.24	-	1.4E-06	1.4E-06		-	0.00000	-
										0.16	0.16	0.16	0.16	3.4E-06	3.4E-06		0.000	0.00000	0.000
										0.27	0.27	-	-	1.2E-06	1.2E-06		-	-	-
										0.27	0.27	0.27	-	1.2E-06	1.2E-06		-	0.00000	-
										0.27	0.27	-	-	1.2E-06	1.2E-06		-	-	-
										0.25	0.25	-	-	1.3E-06	1.3E-06		-	-	-
EL 11/96	4.59	0.00	0.00	50.93	0.03	1.90	40.43	0.00	0.15										
Mg-Ilmenites	1.17	0.51	0.09	60.19	0.11	0.62	30.08	0.00	0.07										
	6.97	0.00	0.00	54.28	0.01	0.93	36.74	0.00	0.01										
	3.68	0.10	0.01	52.97	0.21	0.41	38.75	0.08	0.00										
	1.57	0.10	0.04	54.76	0.09	0.51	37.75	0.02	0.00										
	1.56	0.00	0.00	50.05	0.01	0.58	44.16	0.03	0.00										
	1.78	0.81	0.08	51.53	0.22	0.68	33.49	0.09	0.07										
	1.88	0.00	0.00	49.19	0.12	0.45	45.64	0.06	0.00										
	3.06	0.00	0.01	49.03	0.24	0.51	43.94	0.07	0.06										
	2.79	0.00	0.03	50.85	0.13	0.59	43.63	0.05	0.10										
	2.36	0.00	0.00	49.09	0.13	0.45	46.47	0.09	0.00										
	1.36	0.00	0.01	50.03	0.12	0.62	45.31	0.01	0.07										
	2.79	0.00	0.03	50.85	0.13	0.59	43.63	0.05	0.10										
	2.36	0.00	0.00	49.09	0.13	0.45	46.17	0.09	0.00										
	2.87	0.00	0.05	50.70	0.25	0.57	43.77	0.05	0.01										
	2.07	0.00	0.00	48.99	0.10	0.56	45.54	0.08	0.07										
	3.21	0.15	0.01	42.27	0.00	1.41	49.80	0.00	0.31										
	0.63	0.00	0.00	51.03	0.05	0.62	45.92	0.03	0.00										
	0.62	0.21	0.16	63.02	0.07	0.24	26.91	0.00	0.00										
	4.59	0.00	0.00	50.93	0.03	1.90	40.43	0.00	0.15										
	1.57	0.00	0.00	52.04	0.09	0.41	40.55	0.00	0.00										
	1.84	1.31	4.84	46.77	0.03	1.91	41.31	0.03	0.11										
	1.37	0.00	0.01	51.91	0.13	0.15	44.43	0.00	0.00										
	6.97	0.68	0.00	57.94	0.00	0.59	32.20	0.33	0.55										
	6.92	0.42	0.00	52.78	0.14	0.52	37.28	0.33	0.36										
	4.17	0.22	0.00	51.93	0.00	0.40	41.52	0.30	0.00										
EL 11/96	0.06	0.00	0.01	50.61	0.03	6.34	41.15	0.00	0.05	0.24	0.25	0.24	0.34	1.5E-06	1.3E-06		-0.007	0.00000	-0.004
Ilmenites	0.04	0.00	0.01	50.59	0.00	7.36	39.37	0.06	0.16	0.24	0.24	0.20	0.34	1.5E-06	1.5E-06	0.006	-0.007	0.00285	-0.004
	0.06	0.05	0.03	50.51	0.03	6.44	40.79	0.00	0.06	0.22	0.22	0.20	0.22	1.7E-06	1.7E-06	0.004	0.000	0.00184	0.000
	0.05	0.00	0.00	50.61	0.03	7.04	40.60	0.03	0.07	0.22	0.24	0.21	0.24	1.7E-06	1.5E-06	0.002	0.000	0.00089	0.000
	0.04	0.00	0.01	50.58	0.02	6.50	40.22	0.02	0.09	0.24	0.25	0.21	0.25	1.5E-06	1.3E-06	0.004	0.000	0.00184	0.000
	0.01	0.00	0.00	50.45	0.01	4.15	42.98	0.04	0.00	0.24	0.24	0.22	0.34	1.5E-06	1.5E-06	0.002	-0.007	0.00089	-0.004
	0.05	0.00	0.03	50.80	0.02	7.35	40.24	0.00	0.07	0.25	0.25	0.21	0.34	1.3E-06	1.3E-06	0.006	-0.007	0.00285	-0.004
	0.03	0.00	0.01	50.15	0.04	1.50	44.78	0.01	0.40	0.24	0.24	0.21	0.34	1.5E-06	1.5E-06	0.004	-0.007	0.00184	-0.004

Sample Source	Oxide weight %									Lifting field (T)		Rotating field (T)		Mag. Suscept. (SI)		Paramag. rot. Index		Ferromag. rot. Index	
	MgO	Al2O3	SiO2	TiO2	Cr2O3	MnO	FeO	NiO	ZnO	At 10 Hz	At 57 Hz	At 10 Hz	At 57 Hz	At 10hz	At 57hz	at 10hz	At 57 Hz	At 10 Hz	At 57 Hz
	0.04	0.00	0.00	50.17	0.13	2.10	45.02	0.00	0.07	0.24	0.24	0.24	0.24	1.5E-06	1.5E-06		0.000	0.00000	0.000
	0.05	0.00	0.00	50.51	0.01	6.58	40.66	0.00	0.11	0.24	0.24	0.21	0.24	1.5E-06	1.5E-06	0.004	0.000	0.00184	0.000
	0.01	0.00	0.00	50.67	0.00	7.71	39.80	0.02	0.07	0.24	0.24	0.19	0.24	1.5E-06	1.4E-06	0.009	0.000	0.00391	0.000
	0.04	0.00	0.00	50.43	0.02	1.86	45.37	0.04	0.09	0.24	0.24	0.21	0.34	1.5E-06	1.5E-06	0.004	-0.007	0.00184	-0.004
										0.34	0.34	0.34	0.34	7.3E-07	7.3E-07		0.000	0.00000	0.000
	0.05	0.00	0.02	50.62	0.06	4.88	41.71	0.00	0.19	0.24	0.24	0.24	0.34	1.5E-06	1.5E-06		-0.007	0.00000	-0.004
	0.05	0.00	0.00	50.55	0.00	7.03	40.43	0.00	0.01	0.24	0.24	0.21	0.24	1.4E-06	1.4E-06	0.005	0.000	0.00224	0.000
	0.04	0.00	0.01	50.56	0.00	7.29	40.01	0.06	0.06	0.24	0.24	0.21	0.24	1.5E-06	1.5E-06	0.004	0.000	0.00184	0.000
	0.03	0.00	0.03	50.38	0.00	7.60	39.70	0.04	0.09	0.24	0.24	0.21	0.24	1.5E-06	1.5E-06	0.004	0.000	0.00184	0.000
	0.03	0.00	0.00	50.29	0.03	6.38	39.65	0.02	0.00	0.13	0.13	0.01	0.02	4.8E-06	4.8E-06	4.186	1.007	0.23396	0.108
	0.05	0.00	0.00	50.39	0.00	5.81	41.36	0.01	0.17	0.24	0.24	0.21	0.34	1.5E-06	1.5E-06	0.004	-0.007	0.00184	-0.004
	0.01	0.00	0.00	50.32	0.00	7.46	39.89	0.01	0.04	0.24	0.24	0.22	0.24	1.5E-06	1.5E-06	0.002	0.000	0.00089	0.000
										0.36	0.36	0.34	0.34	6.5E-07	6.5E-07	0.002	0.002	0.00089	0.001
										0.34	0.34	0.34	0.34	7.3E-07	7.3E-07		0.000	0.00000	0.000
	0.03	0.00	0.00	50.64	0.00	7.60	37.53	0.06	0.36	0.19	0.19	0.01	0.02	2.4E-06	2.4E-06	5.302	1.622	0.26505	0.141
	0.04	0.00	0.00	51.11	0.01	8.35	38.66	0.00	0.08	0.25	0.25	0.06	0.12	1.3E-06	1.3E-06	0.265	0.053	0.04946	0.017
	0.01	0.00	0.02	51.34	0.00	7.73	39.46	0.05	0.21	0.24	0.24	0.22	0.23	1.5E-06	1.5E-06	0.002	0.001	0.00089	0.000
	0.06	0.00	0.00	51.52	0.06	5.02	40.76	0.00	0.33	0.14	0.13	0.01	0.03	4.3E-06	4.8E-06	1.827	0.300	0.14995	0.053
	0.04	0.00	0.00	50.79	0.00	6.77	40.87	0.00	0.04	0.25	0.25	0.21	0.25	1.3E-06	1.3E-06	0.006	0.000	0.00285	0.000
	0.02	0.00	0.00	50.63	0.00	7.20	41.01	0.00	0.08	0.24	0.24	0.07	0.08	1.5E-06	1.5E-06	0.141	0.108	0.03309	0.028
	0.05	0.00	0.03	51.26	0.00	6.00	39.99	0.01	0.06	0.24	0.24	0.08	0.12	1.5E-06	1.5E-06	0.108	0.046	0.02777	0.015
	0.06	0.00	0.00	51.15	0.02	7.79	39.24	0.02	0.00	0.21	0.21	0.02	0.05	1.9E-06	1.9E-06	1.622	0.234	0.14053	0.046
	0.04	0.00	0.01	51.34	0.03	7.16	39.02	0.00	0.22	0.19	0.18	0.04	0.04	2.4E-06	2.7E-06	0.384	0.265	0.06186	0.049
	0.04	0.00	0.05	50.56	0.00	6.76	40.92	0.03	0.05	0.16	0.16	0.01	0.03	3.4E-06	3.4E-06	3.719	0.552	0.21974	0.077
	0.06	0.56	0.11	59.82	0.00	5.98	26.47	0.01	0.14	0.19	0.18	0.01	0.01	2.4E-06	2.7E-06	13.626	2.936	0.43342	0.194
	0.05	0.00	0.00	50.76	0.01	7.65	39.71	0.00	0.19	0.15	0.15	0.09	0.17	3.8E-06	3.8E-06	0.023	-0.003	0.00886	-0.002
	0.05	0.00	0.01	50.43	0.02	7.01	40.38	0.03	0.10	0.24	0.24	0.03	0.06	1.5E-06	1.5E-06	1.279	0.234	0.12328	0.046
	0.03	0.00	0.00	50.20	0.02	5.79	41.42	0.03	0.23	0.25	0.25	0.17	0.18	1.3E-06	1.3E-06	0.019	0.015	0.00751	0.006
	0.06	0.00	0.00	50.24	0.01	3.56	42.91	0.00	0.00	0.22	0.24	0.03	0.06	1.7E-06	1.5E-06	0.894	0.182	0.10093	0.039
	0.07	0.00	0.03	48.47	0.00	4.16	45.01	0.00	0.06	0.19	0.19	0.04	0.06	2.4E-06	2.4E-06	0.384	0.123	0.06186	0.030
	0.06	0.00	0.00	49.78	0.10	5.18	42.60	0.01	0.00	0.25	0.27	0.20	0.22	1.3E-06	1.2E-06	0.009	0.006	0.00391	0.003
	0.03	0.00	0.02	52.88	0.00	7.63	36.89	0.02	0.25	0.19	0.19	0.01	0.02	2.4E-06	2.4E-06	12.110	2.057	0.40779	0.160
	0.04	0.00	0.00	50.96	0.00	7.19	39.55	0.01	0.09	0.24	0.24	0.19	0.24	1.5E-06	1.5E-06	0.009	0.000	0.00391	0.000
	0.06	0.00	0.00	50.64	0.13	4.46	42.56	0.00	0.06	0.24	0.24	0.10	0.17	1.5E-06	1.5E-06	0.062	0.015	0.01886	0.006
	0.07	0.00	0.01	55.70	0.00	6.42	32.11	0.01	0.04	0.34	0.34	0.34	0.34	7.3E-07	7.3E-07		0.000	0.00000	0.000
	0.04	0.00	0.01	51.25	0.00	6.57	39.51	0.06	0.00	0.34	0.34	0.34	0.34	7.3E-07	7.3E-07		0.000	0.00000	0.000
	0.07	0.00	0.00	50.88	0.00	6.40	40.16	0.00	0.91	0.25	0.25	0.21	0.34	1.3E-06	1.3E-06	0.006	-0.007	0.00285	-0.004
	0.05	0.00	0.02	51.09	0.00	5.90	41.55	0.00	0.03	0.17	0.15	0.01	0.01	3.0E-06	3.8E-06	8.501	1.622	0.33936	0.141
	0.01	0.00	0.00	51.36	0.01	5.39	41.23	0.03	0.08	0.24	0.24	0.21	0.24	1.5E-06	1.5E-06	0.004	0.000	0.00184	0.000
	0.04	0.00	0.00	51.43	0.00	5.76	40.83	0.00	0.07	0.25	0.25	0.22	0.34	1.3E-06	1.3E-06	0.004	-0.007	0.00184	-0.004
	0.02	0.00	0.00	50.85	0.00	4.25	42.38	0.00	0.34	0.25	0.25	0.24	0.34	1.3E-06	1.3E-06	0.002	-0.007	0.00089	-0.004
										0.28	0.28	0.25	0.28	1.0E-06	1.0E-06	0.004	0.000	0.00184	0.000
	0.03	0.00	0.04	51.48	0.02	5.52	41.58	0.01	0.09	0.27	0.28	0.24	0.34	1.2E-06	1.0E-06	0.004	-0.004	0.00184	-0.002
	0.03	0.00	0.04	51.48	0.02	5.52	41.58	0.01	0.09	0.25	0.25	0.22	0.34	1.3E-06	1.3E-06	0.004	-0.007	0.00184	-0.004
	0.06	0.10	0.02	58.00	0.00	4.88	28.76	0.00	0.03	0.36	0.36	0.34	0.34	6.5E-07	6.5E-07	0.002	0.002	0.00089	0.001
	0.04	0.03	0.01	57.86	0.01	4.88	29.25	0.00	0.15	0.36	0.36	0.34	0.34	6.5E-07	6.5E-07	0.002	0.002	0.00089	0.001
	0.05	0.06	0.05	58.66	0.02	4.73	28.59	0.03	0.12	0.36	0.36	0.34	0.34	6.5E-07	6.5E-07	0.002	0.002	0.00089	0.001

Sample Source	Oxide weight %									Lifting field (T)		Rotating field (T)		Mag. Suscept. (SI)		Paramag. rot. Index		Ferromag. rot. Index	
	MgO	Al2O3	SiO2	TiO2	Cr2O3	MnO	FeO	NiO	ZnO	At 10 Hz	At 57 Hz	At 10 Hz	At 57 Hz	At 10hz	At 57hz	at 10hz	At 57 Hz	At 10 Hz	At 57 Hz
	0.03	1.07	0.05	56.88	0.00	5.52	28.33	0.00	0.19	0.36	0.36	0.34	0.34	6.5E-07	6.5E-07	0.002	0.002	0.00089	0.001
	0.05	0.10	0.02	58.23	0.05	4.67	29.21	0.02	0.10	0.36	0.36	0.34	0.34	6.5E-07	6.5E-07	0.002	0.002	0.00089	0.001
	0.06	0.05	0.00	58.28	0.04	5.43	28.58	0.02	0.14	0.34	0.34	0.32	0.34	7.3E-07	7.3E-07	0.002	0.000	0.00089	0.000
	0.04	0.00	0.01	51.53	0.00	6.96	40.25	0.02	0.14	0.25	0.25	0.24	0.34	1.3E-06	1.3E-06	0.002	-0.007	0.00089	-0.004
	0.04	0.00	0.00	51.11	0.00	6.62	40.11	0.02	0.41	0.25	0.25	0.22	0.25	1.3E-06	1.3E-06	0.004	0.000	0.00184	0.000
	0.04	0.00	0.00	50.93	0.05	6.17	40.28	0.00	0.20	0.25	0.25	0.22	0.34	1.3E-06	1.3E-06	0.004	-0.007	0.00184	-0.004
	0.00	0.00	0.00	51.25	0.04	5.08	41.58	0.00	0.03	0.27	0.27	0.24	0.34	1.2E-06	1.2E-06	0.004	-0.006	0.00184	-0.003
	0.02	0.00	0.00	51.53	0.02	6.75	39.77	0.00	0.31	0.25	0.25	0.22	0.34	1.3E-06	1.3E-06	0.004	-0.007	0.00184	-0.004
	0.05	0.00	0.00	51.29	0.00	6.68	39.39	0.02	0.36	0.27	0.27	0.24	0.34	1.2E-06	1.2E-06	0.004	-0.006	0.00184	-0.003
	0.06	0.00	0.00	49.87	0.12	4.47	43.35	0.05	0.04	0.24	0.24	0.24	0.34	1.5E-06	1.4E-06		-0.007	0.00000	-0.004
	0.05	0.00	0.01	51.47	0.04	6.28	40.76	0.00	0.08	0.25	0.25	0.21	0.25	1.3E-06	1.3E-06	0.006	0.000	0.00285	0.000
	0.08	0.11	0.03	56.45	0.03	5.26	30.71	0.02	0.11	0.36	0.36	0.34	0.34	6.5E-07	6.5E-07	0.002	0.002	0.00089	0.001
	0.04	0.23	0.05	56.43	0.04	1.83	32.68	0.00	0.01	0.30	0.30	0.29	0.34	9.3E-07	9.3E-07	0.001	-0.003	0.00035	-0.002
	0.05	0.00	0.04	51.13	0.03	6.85	40.25	0.04	0.10	0.25	0.25	0.19	0.22	1.3E-06	1.3E-06	0.012	0.004	0.00504	0.002
	0.06	0.00	0.03	56.36	0.02	5.34	31.30	0.00	0.11	0.36	0.36	0.34	0.34	6.5E-07	6.5E-07	0.002	0.002	0.00089	0.001
										0.25	0.25	0.21	0.34	1.3E-06	1.3E-06	0.005	-0.007	0.00244	-0.004
										0.25	0.25	0.24	0.34	1.3E-06	1.3E-06	0.002	-0.007	0.00089	-0.004
										0.24	0.24	0.19	0.22	1.4E-06	1.4E-06	0.010	0.003	0.00435	0.001
										0.24	0.24	0.21	0.24	1.5E-06	1.5E-06	0.004	0.000	0.00184	0.000

Appendix C

Chromites. Rotation, lift and analysis results.

Sample	Oxide weight %									Lifting field (T)		Rotating field (T)		Mag. suscept. (SI)		Paramag. rot. Index		Ferromag. rot. index	
	MgO	Al2O3	SiO2	TiO2	Cr2O3	MnO	FeO	NiO	ZnO	At 10Hz	At 57Hz	At 10Hz	At 57Hz	At 10Hz	At 57Hz	At 10Hz	At 57Hz	At 10Hz	At 57Hz
CRA Kimb2	15.87	24.37	0.08	0.50	40.44	0.19	16.76	0.14	0.11	0.3092	0.3092	0.3092	0.3092	8.5E-07	8.5E-07	0.002	0.002	-0.005	-0.005
CRA Kimb2	10.46	10.10	0.00	0.89	53.38	0.43	22.86	0.15	0.19	0.2531	0.2591	0.2304	0.2591	1.3E-06	1.2E-06	0.006	-0.004	-0.004	-0.010
CRA Kimb2	12.01	6.10	0.04	0.11	63.49	0.26	15.97	0.08	0.06	0.3092	0.3092	0.3092	0.3092	8.5E-07	8.5E-07	0.002	0.002	-0.005	-0.005
CRA Kimb2	11.00	7.83	0.00	1.05	52.78	0.35	24.65	0.10	0.09	0.2250	0.3092	0.1820	0.3092	1.6E-06	8.5E-07	0.016	0.002	-0.001	-0.005
CRA Kimb2	14.74	22.85	0.00	0.03	47.64	0.22	13.35	0.09	0.20	0.3092	0.3092	0.3092	0.3092	8.5E-07	8.5E-07	0.002	0.002	-0.005	-0.005
CRA Kimb2	10.38	9.70	0.01	0.96	55.53	0.29	21.66	0.10	0.13	0.3092	0.3092	0.3092	0.3092	8.5E-07	8.5E-07	0.002	0.002	-0.005	-0.005
CRA Kimb2	16.93	28.58	0.11	0.28	35.51	0.09	16.50	0.19	0.06	0.3092	0.3092	0.3092	0.3092	8.5E-07	8.5E-07	0.002	0.002	-0.005	-0.005
CRA Kimb2	12.62	14.72	0.00	0.52	51.29	0.23	18.49	0.06	0.10	0.3092	0.3092	0.3092	0.3092	8.5E-07	8.5E-07	0.002	0.002	-0.005	-0.005
CRA Kimb2	9.24	5.43	0.01	0.44	58.37	0.40	23.54	0.10	0.13	0.3092	0.3092	0.3092	0.3092	8.5E-07	8.5E-07	0.002	0.002	-0.005	-0.005
CRA Kimb2	16.86	29.07	0.01	0.81	38.24	0.20	13.28	0.18	0.14	0.3092	0.3092	0.3092	0.3092	8.5E-07	8.5E-07	0.002	0.002	-0.005	-0.005
CRA Kimb2	12.43	13.24	0.00	0.79	51.94	0.35	19.58	0.13	0.18	0.3092	0.3092	0.3092	0.3092	8.5E-07	8.5E-07	0.002	0.002	-0.005	-0.005
CRA Kimb2	14.82	27.55	0.00	0.63	40.54	0.21	14.81	0.12	0.16	0.3092	0.3092	0.3092	0.3092	8.5E-07	8.5E-07	0.002	0.002	-0.005	-0.005
CRA Kimb2	9.56	6.56	0.04	3.44	44.24	0.36	32.63	0.22	0.11	0.2915	0.2915	0.2915	0.2915	9.6E-07	9.6E-07	0.000	0.000	-0.007	-0.007
CRA Kimb2	8.28	2.80	0.00	2.08	53.11	0.34	30.25	0.18	0.17	0.2915	0.2915	0.2915	0.2915	9.6E-07	9.6E-07	0.000	0.000	-0.007	-0.007
CRA Kimb2	15.35	20.48	0.04	0.37	46.51	0.18	15.32	0.11	0.00	0.3092	0.3092	0.3092	0.3092	8.5E-07	8.5E-07	0.002	0.002	-0.005	-0.005
CRA Kimb2	17.47	30.62	0.09	0.33	33.37	0.10	16.57	0.25	0.07	0.3092	0.3092	0.3092	0.3092	8.5E-07	8.5E-07	0.002	0.002	-0.005	-0.005
CRA Kimb2	10.10	9.04	0.03	0.35	56.77	0.29	21.71	0.03	0.09	0.3092	0.3092	0.3092	0.3092	8.5E-07	8.5E-07	0.002	0.002	-0.005	-0.005
CRA Kimb2	11.35	5.04	0.04	0.50	60.08	0.33	20.06	0.12	0.00	0.3092	0.3092	0.3092	0.3092	8.5E-07	8.5E-07	0.002	0.002	-0.005	-0.005
CRA Kimb2	10.77	9.67	0.01	0.63	55.29	0.30	21.30	0.16	0.18	0.2915	0.2915	0.2915	0.2915	9.6E-07	9.6E-07	0.000	0.000	-0.007	-0.007
CRA Kimb2	18.17	35.09	0.09	0.17	29.88	0.16	14.29	0.20	0.12	0.3092	0.3092	0.3092	0.3092	8.5E-07	8.5E-07	0.002	0.002	-0.005	-0.005
CRA Kimb2	12.84	10.80	0.03	0.48	54.17	0.11	19.25	0.14	0.00	0.3092	0.3092	0.3092	0.3092	8.5E-07	8.5E-07	0.002	0.002	-0.005	-0.005
CRA Kimb2	17.41	38.57	0.01	0.38	28.61	0.22	12.96	0.20	0.16	0.3092	0.3092	0.3092	0.3092	8.5E-07	8.5E-07	0.002	0.002	-0.005	-0.005
CRA Kimb2	10.36	8.97	0.04	0.91	47.68	0.19	29.10	0.17	0.11	0.3092	0.3092	0.3092	0.3092	8.5E-07	8.5E-07	0.002	0.002	-0.005	-0.005
CRA Kimb2	15.87	25.30	0.07	0.38	39.05	0.21	17.12	0.20	0.14	0.3092	0.3092	0.3092	0.3092	8.5E-07	8.5E-07	0.002	0.002	-0.005	-0.005
CRA Kimb2	9.39	4.72	0.00	1.66	54.17	0.34	27.19	0.12	0.15	0.2443	0.2443	0.2304	0.2443	1.4E-06	1.4E-06	0.004	-0.006	-0.005	-0.012
CRA Kimb2	11.97	5.29	0.06	0.40	63.55	0.37	16.66	0.08	0.01	0.3092	0.3092	0.3092	0.3092	8.5E-07	8.5E-07	0.002	0.002	-0.005	-0.005
CRA Kimb2	16.03	25.82	0.10	0.13	37.31	0.23	18.86	0.25	0.14	0.3092	0.3092	0.3092	0.3092	8.5E-07	8.5E-07	0.002	0.002	-0.005	-0.005
SP2B	9.49	7.73	0.00	0.41	50.74	0.53	28.77	0.05	0.27	0.1438	0.1356	0.0121	0.0330	3.9E-06	4.4E-06	4.115	0.468	0.242	0.065
SP2B	9.48	7.75	0.01	0.36	50.98	0.55	28.67	0.07	0.14	0.1278	0.1278	0.0067	0.0136	5.0E-06	5.0E-06	10.603	2.558	0.406	0.185
SP2B	9.67	7.37	0.01	0.42	51.55	0.56	28.20	0.11	0.01	0.1438	0.1438	0.0042	0.0096	3.9E-06	3.9E-06	34.499	6.609	0.755	0.314
SP2B	10.71	7.26	0.02	0.41	52.48	0.50	26.56	0.11	0.32	0.1356	0.1356	0.0114	0.0183	4.4E-06	4.4E-06	4.115	1.586	0.242	0.140
SP2B	9.65	7.84	0.01	0.37	51.24	0.66	28.29	0.03	0.00	0.1071	0.1136	0.0076	0.0145	7.1E-06	6.3E-06	5.871	1.788	0.295	0.150
SP2B	9.21	7.76	0.02	0.40	50.76	0.49	29.25	0.07	0.07	0.1438	0.1438	0.0246	0.0330	3.9E-06	3.9E-06	0.979	0.530	0.105	0.070
SP2B	9.99	7.67	0.02	0.38	51.51	0.41	27.57	0.09	0.00	0.1356	0.1278	0.0246	0.0261	4.4E-06	5.0E-06	0.867	0.679	0.097	0.083
SP2B	9.38	7.86	0.00	0.40	50.37	0.42	28.87	0.16	0.14	0.1438	0.1356	0.0261	0.0311	3.9E-06	4.4E-06	0.867	0.530	0.097	0.070
SP2B	9.53	7.73	0.00	0.37	50.70	0.51	28.07	0.06	0.09	0.1438	0.1525	0.0067	0.0206	3.9E-06	3.5E-06	13.428	1.586	0.460	0.140
SP2B	9.55	7.58	0.00	0.35	51.18	0.53	28.11	0.11	0.06	0.1356	0.1278	0.0136	0.0206	4.4E-06	5.0E-06	2.881	1.105	0.198	0.113
SP2B	10.79	7.51	0.00	0.38	52.24	0.52	26.09	0.12	0.00	0.1930	0.1886	0.0528	0.0898	2.2E-06	2.3E-06	0.364	0.100	0.054	0.019
SP2B	10.81	7.38	0.03	0.36	52.48	0.46	25.90	0.07	0.08	0.2250	0.2250	0.1438	0.2096	1.6E-06	1.6E-06	0.043	0.004	0.006	-0.005
SP2B	9.70	7.72	0.01	0.34	51.21	0.55	27.72	0.10	0.01	0.1820	0.1656	0.0394	0.0453	2.5E-06	3.0E-06	0.600	0.364	0.076	0.054
SP2B	10.98	7.58	0.05	0.37	52.24	0.39	26.25	0.11	0.00	0.1438	0.1438	0.0076	0.0194	3.9E-06	3.9E-06	10.603	1.586	0.406	0.140

Sample	Oxide weight %									Lifting field (T)		Rotating field (T)		Mag. suscept. (SI)		Paramag. rot. Index		Ferromag. rot. index	
	MgO	Al2O3	SiO2	TiO2	Cr2O3	MnO	FeO	NiO	ZnO	At 10Hz	At 57Hz	At 10Hz	At 57Hz	At 10Hz	At 57Hz	At 10Hz	At 57Hz	At 10Hz	At 57Hz
SP2B	10.84	7.56	0.04	0.35	51.94	0.38	26.29	0.12	0.07	0.2000	0.2000	0.0270	0.0276	2.0E-06	2.0E-06	1.586	1.511	0.140	0.136
SP2B	10.96	7.40	0.01	0.36	52.49	0.48	25.73	0.10	0.06	0.1656	0.1778	0.0183	0.0246	3.0E-06	2.6E-06	2.381	1.511	0.178	0.136
SP2B	9.40	7.51	0.00	0.39	51.43	0.53	28.75	0.04	0.16	0.1716	0.1820	0.0270	0.0384	2.8E-06	2.5E-06	1.160	0.630	0.116	0.079
SP2B	9.79	7.51	0.00	0.40	52.01	0.47	27.36	0.10	0.09	0.2250	0.2172	0.0418	0.0574	1.6E-06	1.7E-06	0.826	0.392	0.094	0.057
SP2B	9.38	7.69	0.02	0.41	50.93	0.60	28.14	0.02	0.08	0.1580	0.1618	0.0163	0.0418	3.3E-06	3.1E-06	2.747	0.413	0.193	0.059
SP2B	9.50	7.69	0.00	0.42	50.99	0.53	27.88	0.03	0.15	0.2358	0.2304	0.1438	0.2304	1.5E-06	1.5E-06	0.050	0.000	0.008	-0.007
SP2B	9.92	7.92	0.00	0.41	50.47	0.51	28.41	0.13	0.09	0.2358	0.2304	0.0898	0.1438	1.5E-06	1.5E-06	0.174	0.046	0.031	0.007
SP2B	11.29	7.67	0.00	0.35	52.26	0.54	25.42	0.18	0.09	0.2531	0.2531	0.1656	0.2443	1.3E-06	1.3E-06	0.039	0.002	0.006	-0.006
SP2B	10.84	7.41	0.00	0.39	52.45	0.54	26.30	0.09	0.00	0.2277	0.2304	0.0510	0.0631	1.6E-06	1.5E-06	0.557	0.364	0.073	0.054
SP2B	10.01	7.57	0.03	0.39	51.58	0.46	27.26	0.01	0.06	0.2443	0.2304	0.1405	0.1820	1.4E-06	1.5E-06	0.060	0.018	0.010	-0.000
SP5A	10.42	12.13	0.00	0.40	47.14	0.56	28.24	0.15	0.17	0.1930	0.2048	0.1356	0.2048	2.2E-06	1.9E-06	0.030	-0.012	0.003	-0.019
SP5A	11.33	10.23	0.00	0.31	51.40	0.24	25.20	0.11	0.00	0.3092	0.3092	0.3092	0.3092	8.5E-07	8.5E-07	0.002	0.002	-0.005	-0.005
SP5A	10.33	11.64	0.02	0.38	48.17	0.44	27.80	0.13	0.19	0.1820	0.1716	0.0498	0.1278	2.5E-06	2.8E-06	0.364	0.024	0.054	0.001
SP5A	10.14	12.14	0.04	0.39	47.36	0.53	28.46	0.13	0.10	0.1136	0.1136	0.0498	0.0594	6.3E-06	6.3E-06	0.124	0.078	0.023	0.014
SP5A	10.17	11.89	0.03	0.41	47.66	0.52	28.56	0.12	0.19	0.1438	0.1438	0.0898	0.1205	3.9E-06	3.9E-06	0.046	0.012	0.007	-0.002
SP5A	9.98	12.07	0.00	0.38	46.77	0.44	28.91	0.07	0.27	0.1438	0.1438	0.0276	0.0498	3.9E-06	3.9E-06	0.767	0.216	0.090	0.037
SP5A	10.15	12.01	0.00	0.40	47.48	0.53	28.70	0.06	0.22	0.2048	0.2048	0.1278	0.1618	1.9E-06	1.9E-06	0.046	0.018	0.007	-0.000
SP5A	10.29	12.07	0.00	0.40	47.55	0.47	27.75	0.10	0.03	0.1930	0.1930	0.0709	0.1618	2.2E-06	2.2E-06	0.189	0.012	0.033	-0.002
SP5A	9.86	12.20	0.00	0.43	47.34	0.46	28.58	0.12	0.24	0.1820	0.1820	0.0898	0.1278	2.5E-06	2.5E-06	0.092	0.030	0.017	0.003
SP5A	11.60	12.43	0.04	0.40	47.54	0.31	26.39	0.10	0.00	0.1820	0.1716	0.0798	0.1525	2.5E-06	2.8E-06	0.124	0.008	0.023	-0.004
SP5A	10.41	11.74	0.03	0.39	47.55	0.37	27.89	0.11	0.05	0.1010	0.0952	0.0246	0.0394	8.0E-06	9.0E-06	0.468	0.143	0.065	0.026
SP5A	10.36	11.62	0.02	0.42	47.96	0.66	27.98	0.06	0.15	0.1930	0.1863	0.1010	0.1278	2.2E-06	2.3E-06	0.078	0.033	0.014	0.004
SP5A	9.86	12.15	0.00	0.41	47.18	0.56	29.15	0.14	0.27	0.1249	0.1163	0.0709	0.0898	5.2E-06	6.0E-06	0.062	0.020	0.011	0.000
SP5A	10.78	12.17	0.01	0.36	48.16	0.43	26.73	0.07	0.12	0.1618	0.1618	0.0528	0.0752	3.1E-06	3.1E-06	0.247	0.107	0.041	0.020
SP5A	10.38	11.68	0.00	0.37	48.01	0.43	27.57	0.08	0.26	0.2749	0.2749	0.2591	0.2749	1.1E-06	1.1E-06	0.004	-0.002	-0.005	-0.008
SP5A	10.92	11.29	0.02	0.37	48.09	0.50	26.98	0.09	0.03	0.3092	0.3092	0.3092	0.3092	8.5E-07	8.5E-07	0.002	0.002	-0.005	-0.005
SP5A	11.56	12.15	0.00	0.40	48.29	0.33	25.98	0.12	0.01	0.3092	0.3092	0.2915	0.3092	8.5E-07	8.5E-07	0.004	0.002	-0.005	-0.005
SP5A	10.60	11.18	0.00	0.34	48.86	0.33	27.12	0.06	0.00	0.3092	0.3092	0.3092	0.3092	8.5E-07	8.5E-07	0.002	0.002	-0.005	-0.005
SP5A	10.83	11.49	0.00	0.34	49.36	0.40	27.02	0.13	0.13	0.2358	0.2304	0.2172	0.2048	1.5E-06	1.5E-06	0.005	0.008	-0.005	-0.004
SP5A	11.41	12.05	0.05	0.33	48.41	0.36	26.30	0.15	0.16	0.2749	0.2749	0.2749	0.2749	1.1E-06	1.1E-06	0.000	0.000	-0.007	-0.007
SP5A	11.28	11.33	0.01	0.38	49.43	0.49	26.11	0.08	0.05	0.3092	0.3092	0.3092	0.3092	8.5E-07	8.5E-07	0.002	0.002	-0.005	-0.005
SP5A	11.12	12.21	0.00	0.38	48.28	0.38	26.91	0.06	0.00	0.2749	0.2848	0.2304	0.2848	1.1E-06	1.0E-06	0.012	-0.001	-0.002	-0.007
SP5A	10.95	11.16	0.02	0.41	49.32	0.33	26.23	0.08	0.09	0.2749	0.2915	0.2749	0.2915	1.1E-06	9.6E-07	0.000	0.000	-0.007	-0.007
SP5A	11.40	11.52	0.02	0.38	48.67	0.43	26.77	0.08	0.10	0.3092	0.3092	0.3092	0.3092	8.5E-07	8.5E-07	0.002	0.002	-0.005	-0.005
SP5A	11.44	11.98	0.02	0.39	47.80	0.34	27.12	0.07	0.00	0.2915	0.3092	0.2915	0.3092	9.6E-07	8.5E-07	0.000	0.002	-0.007	-0.005
SP5A	11.12	12.18	0.00	0.36	48.40	0.59	26.47	0.11	0.00	0.2915	0.2915	0.2591	0.2915	9.6E-07	9.6E-07	0.008	0.000	-0.004	-0.007
SP5A	10.84	11.68	0.01	0.38	48.97	0.47	27.16	0.09	0.23	0.3092	0.3092	0.2848	0.3092	8.5E-07	8.5E-07	0.005	0.002	-0.005	-0.005
SP5A	11.27	10.97	0.00	0.37	49.50	0.36	26.21	0.07	0.09	0.3092	0.3092	0.3092	0.3092	8.5E-07	8.5E-07	0.002	0.002	-0.005	-0.005
SP5A	10.83	11.32	0.00	0.38	49.14	0.41	27.11	0.03	0.22	0.3092	0.3092	0.3092	0.3092	8.5E-07	8.5E-07	0.002	0.002	-0.005	-0.005
SP5A	10.78	11.10	0.00	0.36	49.36	0.37	26.77	0.00	0.08	0.2915	0.2915	0.2915	0.2915	9.6E-07	9.6E-07	0.000	0.000	-0.007	-0.007
SP5A	10.37	11.88	0.00	0.36	47.60	0.44	28.04	0.10	0.15	0.2531	0.2531	0.2304	0.2443	1.3E-06	1.3E-06	0.006	0.002	-0.004	-0.006
SP5A	12.04	12.23	0.00	0.36	48.43	0.27	25.02	0.07	0.04	0.3092	0.3092	0.3092	0.3092	8.5E-07	8.5E-07	0.002	0.002	-0.005	-0.005
SP5A	11.58	11.19	0.07	0.35	50.08	0.49	25.61	0.10	0.06	0.3092	0.3092	0.3092	0.3092	8.5E-07	8.5E-07	0.002	0.002	-0.005	-0.005
SP5A	11.42	11.69	0.00	0.32	48.91	0.47	25.80	0.14	0.05	0.3092	0.3092	0.3092	0.3092	8.5E-07	8.5E-07	0.002	0.002	-0.005	-0.005
SP5A	11.11	11.54	0.00	0.37	48.26	0.47	26.66	0.13	0.13	0.2915	0.3092	0.2653	0.3092	9.6E-07	8.5E-07	0.006	0.002	-0.004	-0.005

Sample	Oxide weight %									Lifting field (T)		Rotating field (T)		Mag. suscept. (SI)		Paramag. rot. Index		Ferromag. rot. index	
	MgO	Al2O3	SiO2	TiO2	Cr2O3	MnO	FeO	NiO	ZnO	At 10Hz	At 57Hz	At 10Hz	At 57Hz	At 10Hz	At 57Hz	At 10Hz	At 57Hz	At 10Hz	At 57Hz
SP5A	11.58	10.99	0.01	0.37	50.07	0.34	25.70	0.04	0.22	0.3092	0.3092	0.2915	0.3092	8.5E-07	8.5E-07	0.004	0.002	-0.005	-0.005
SP5A	11.10	11.41	0.01	0.28	48.39	0.46	26.99	0.10	0.12	0.3092	0.3092	0.3092	0.3092	8.5E-07	8.5E-07	0.002	0.002	-0.005	-0.005
SP5A	11.32	11.21	0.00	0.35	49.87	0.50	26.05	0.11	0.00	0.3092	0.3092	0.3092	0.3092	8.5E-07	8.5E-07	0.002	0.002	-0.005	-0.005
SP5A	11.64	11.60	0.00	0.34	48.79	0.43	26.27	0.08	0.16	0.3092	0.3092	0.3092	0.3092	8.5E-07	8.5E-07	0.002	0.002	-0.005	-0.005
SP5A	11.33	9.96	0.00	0.30	51.44	0.32	24.43	0.08	0.10	0.3092	0.3092	0.3092	0.3092	8.5E-07	8.5E-07	0.002	0.002	-0.005	-0.005
SP5A	10.95	11.37	0.00	0.34	49.01	0.57	26.89	0.12	0.00	0.3092	0.3092	0.3092	0.3092	8.5E-07	8.5E-07	0.002	0.002	-0.005	-0.005
SP5A	11.69	12.07	0.04	0.40	48.89	0.49	25.58	0.08	0.00	0.3092	0.3092	0.3092	0.3092	8.5E-07	8.5E-07	0.002	0.002	-0.005	-0.005
SP5A	11.57	11.61	0.04	0.35	48.93	0.38	25.57	0.08	0.00	0.3092	0.3092	0.3092	0.3092	8.5E-07	8.5E-07	0.002	0.002	-0.005	-0.005
SP5A	11.22	11.21	0.00	0.35	49.55	0.45	25.74	0.10	0.10	0.3092	0.3092	0.3092	0.3092	8.5E-07	8.5E-07	0.002	0.002	-0.005	-0.005
SP5A	11.17	11.34	0.00	0.35	48.35	0.43	26.84	0.01	0.11	0.3092	0.3092	0.3092	0.3092	8.5E-07	8.5E-07	0.002	0.002	-0.005	-0.005
SP5A	11.54	11.28	0.01	0.32	49.64	0.51	25.28	0.09	0.11	0.3092	0.3092	0.3092	0.3092	8.5E-07	8.5E-07	0.002	0.002	-0.005	-0.005
SP5A	11.37	11.06	0.01	0.34	49.42	0.47	25.82	0.01	0.00	0.3092	0.3092	0.3092	0.3092	8.5E-07	8.5E-07	0.002	0.002	-0.005	-0.005
SP5A	11.28	11.23	0.00	0.31	49.92	0.44	26.06	0.10	0.08	0.3092	0.3092	0.3092	0.3092	8.5E-07	8.5E-07	0.002	0.002	-0.005	-0.005
SP5A	11.23	11.43	0.00	0.34	48.63	0.47	26.39	0.12	0.00	0.3092	0.3092	0.3092	0.3092	8.5E-07	8.5E-07	0.002	0.002	-0.005	-0.005
SP5A	11.17	11.60	0.01	0.37	48.59	0.30	26.28	0.10	0.12	0.3092	0.3092	0.3092	0.3092	8.5E-07	8.5E-07	0.002	0.002	-0.005	-0.005
SP2	9.86	11.52	0.00	0.45	46.71	0.41	29.42	0.10	0.30	0.0631	0.0631	0.0047	0.0108	2.0E-05	2.0E-05	5.215	0.979	0.276	0.105
SP2	10.37	10.11	0.03	0.41	49.44	0.68	27.75	0.01	0.24	0.0206	0.0194	0.0004	0.0006	1.9E-04	2.2E-04	99.637	34.499	1.303	0.755
SP2	10.19	11.00	0.00	0.45	48.25	0.32	28.26	0.18	0.08	0.0846	0.0798	0.0076	0.0121	1.1E-05	1.3E-05	3.654	1.247	0.227	0.121
SP2	10.90	9.76	0.00	0.44	50.41	0.48	26.65	0.13	0.15	0.0311	0.0293	0.0013	0.0015	8.4E-05	9.5E-05	17.002	11.932	0.521	0.432
SP2	10.66	9.05	0.00	0.42	50.48	0.51	27.32	0.04	0.00	0.0240	0.0218	0.0004	0.0007	1.4E-04	1.7E-04	84.485	27.252	1.198	0.668
SP2	10.57	9.82	0.00	0.42	49.03	0.57	28.23	0.07	0.02	0.0194	0.0194	0.0005	0.0006	2.2E-04	2.2E-04	43.670	27.252	0.853	0.668
SP2	10.42	10.31	0.02	0.45	49.51	0.63	27.54	0.12	0.17	0.0470	0.0418	0.0037	0.0096	3.7E-05	4.7E-05	4.633	0.530	0.259	0.070
SP2	9.92	11.27	0.00	0.48	48.28	0.50	28.24	0.16	0.20	0.0350	0.0350	0.0011	0.0018	6.6E-05	6.6E-05	27.252	10.603	0.668	0.406
SP2	9.66	9.81	0.01	0.45	49.49	0.40	29.10	0.06	0.02	0.0560	0.0560	0.0023	0.0063	2.6E-05	2.6E-05	17.002	2.270	0.521	0.173
SP2	10.65	9.79	0.00	0.38	50.00	0.63	27.05	0.12	0.17	0.0121	0.0108	0.0003	0.0004	5.5E-04	7.0E-04	55.278	27.252	0.963	0.668
SP2	10.20	11.05	0.01	0.46	47.60	0.52	28.81	0.10	0.13	0.1930	0.1820	0.0498	0.0952	2.2E-06	2.5E-06	0.413	0.078	0.059	0.014
SP2	10.10	10.67	0.00	0.50	48.91	0.58	27.81	0.03	0.17	0.1656	0.1618	0.0311	0.0798	3.0E-06	3.1E-06	0.806	0.092	0.093	0.017
SP2	9.94	11.93	0.01	0.49	47.18	0.50	28.49	0.16	0.19	0.0798	0.0752	0.0311	0.0470	1.3E-05	1.4E-05	0.164	0.046	0.029	0.007
SP2	10.21	10.06	0.00	0.48	48.97	0.46	27.78	0.08	0.22	0.0898	0.0798	0.0060	0.0108	1.0E-05	1.3E-05	6.609	1.586	0.314	0.140
SP2	10.25	11.40	0.01	0.46	47.50	0.37	28.18	0.11	0.16	0.1278	0.1278	0.0194	0.0218	5.0E-06	5.0E-06	1.247	0.979	0.121	0.105
SP2	10.02	10.13	0.00	0.41	48.62	0.44	28.50	0.11	0.03	0.2048	0.2048	0.0276	0.0470	1.9E-06	1.9E-06	1.586	0.530	0.140	0.070
SP2	10.14	10.28	0.00	0.43	48.67	0.45	28.60	0.14	0.18	0.1930	0.1930	0.1438	0.1438	2.2E-06	2.2E-06	0.024	0.024	0.001	0.001
SP2	10.86	11.06	0.00	0.37	48.35	0.42	27.61	0.04	0.18	0.0709	0.0709	0.0045	0.0102	1.6E-05	1.6E-05	7.438	1.406	0.335	0.130
SP2	10.19	11.03	0.00	0.48	48.10	0.62	28.43	0.16	0.21	0.0898	0.0898	0.0085	0.0163	1.0E-05	1.0E-05	3.245	0.867	0.212	0.097
SP2	9.86	11.56	0.00	0.51	46.98	0.44	29.59	0.13	0.12	0.0898	0.0898	0.0096	0.0153	1.0E-05	1.0E-05	2.558	0.979	0.185	0.105
SP2	9.87	10.07	0.01	0.44	48.79	0.62	29.12	0.09	0.11	0.2096	0.2048	0.0846	0.1525	1.9E-06	1.9E-06	0.151	0.024	0.027	0.001
SP2	10.54	11.02	0.03	0.44	48.42	0.58	28.75	0.13	0.10	0.2172	0.2048	0.1071	0.1820	1.7E-06	1.9E-06	0.092	0.008	0.017	-0.004
SP2	10.95	10.71	0.09	0.41	48.88	0.47	27.14	0.12	0.00	0.2250	0.2172	0.0669	0.1438	1.6E-06	1.7E-06	0.304	0.038	0.048	0.005
SP2	10.49	10.07	0.00	0.42	49.59	0.49	27.78	0.10	0.23	0.2096	0.2048	0.0669	0.1278	1.9E-06	1.9E-06	0.260	0.046	0.042	0.007
SP2	10.63	10.07	0.01	0.42	49.99	0.39	27.25	0.15	0.10	0.2915	0.2915	0.2915	0.2915	9.6E-07	9.6E-07	0.000	0.000	-0.007	-0.007
CRA K	11.96	9.58	0.21	3.23	48.62	0.31	24.19	0.22	0.02	0.2172	0.2048	0.1071	0.1820	1.7E-06	1.9E-06	0.092	0.008	0.017	-0.004
CRA K	9.67	9.31	0.02	0.02	59.81	0.35	19.12	0.03	0.12	0.0846	0.0846	0.0096	0.0136	1.1E-05	1.1E-05	2.270	1.105	0.173	0.113
CRA K										0.1618	0.1618	0.0108	0.0194	3.1E-06	3.1E-06	6.609	2.015	0.314	0.161
CRA K	9.08	12.73	0.28	1.24	46.94	0.17	25.65	0.18	0.08	0.2915	0.2915	0.2915	0.2915	9.6E-07	9.6E-07	0.000	0.000	-0.007	-0.007
CRA K	12.12	16.27	0.26	1.29	38.80	0.30	28.89	0.25	0.08	0.2915	0.2915	0.2915	0.2915	9.6E-07	9.6E-07	0.000	0.000	-0.007	-0.007
CRA K	9.13	4.55	0.45	4.50	55.44	0.34	20.56	0.13	0.16	0.2915	0.2915	0.2915	0.2915	9.6E-07	9.6E-07	0.000	0.000	-0.007	-0.007
CRA K	9.66	15.87	0.29	0.62	41.87	0.26	26.93	0.21	0.09	0.2591	0.2591	0.2915	0.2591	1.2E-06	1.2E-06	-0.006	-0.004	-0.009	-0.010

Sample	Oxide weight %									Lifting field (T)		Rotating field (T)		Mag. suscept. (SI)		Paramag. rot. Index		Ferromag. rot. index	
	MgO	Al2O3	SiO2	TiO2	Cr2O3	MnO	FeO	NiO	ZnO	At 10Hz	At 57Hz	At 10Hz	At 57Hz	At 10Hz	At 57Hz	At 10Hz	At 57Hz	At 10Hz	At 57Hz
CRA K	10.11	3.45	0.54	4.82	54.02	0.44	21.29	0.19	0.14	0.2591	0.2591	0.2591	0.2591	1.2E-06	1.2E-06	-0.004	-0.004	-0.010	-0.010
CRA K	10.38	2.19	0.03	4.44	59.06	0.34	19.61	0.16	0.03	0.2749	0.2749	0.2749	0.2749	1.1E-06	1.1E-06	-0.002	-0.002	-0.008	-0.008
CRA K	11.41	13.94	0.19	1.00	43.45	0.24	26.70	0.22	0.03	0.3092	0.3092	0.3092	0.3092	8.5E-07	8.5E-07	0.002	0.002	-0.005	-0.005
CRA K	10.15	3.40	0.85	4.53	55.78	0.20	20.15	0.15	0.10	0.3092	0.3092	0.3092	0.3092	8.5E-07	8.5E-07	0.002	0.002	-0.005	-0.005
CRA K	11.02	15.15	0.25	1.19	41.22	0.18	26.21	0.25	0.04	0.3092	0.3092	0.3092	0.3092	8.5E-07	8.5E-07	0.002	0.002	-0.005	-0.005
CRA K	10.37	3.11	1.86	3.82	57.45	0.29	18.66	0.10	0.07	0.3092	0.3092	0.3092	0.3092	8.5E-07	8.5E-07	0.002	0.002	-0.005	-0.005
CRA K	8.29	7.71	0.18	1.21	55.20	0.27	23.20	0.21	0.04	0.2749	0.2749	0.2749	0.2749	1.1E-06	1.1E-06	0.000	0.000	-0.007	-0.007
CRA K	10.17	3.99	1.64	4.67	52.30	0.23	20.15	0.15	0.11	0.3092	0.3092	0.3092	0.3092	8.5E-07	8.5E-07	0.002	0.002	-0.005	-0.005
CRA K	11.37	14.80	0.25	0.81	42.48	0.29	26.44	0.17	0.12	0.2915	0.2915	0.2915	0.2915	9.6E-07	9.6E-07	0.000	0.000	-0.007	-0.007
CRA K	8.99	5.16	3.99	7.58	41.83	1.02	21.09	0.16	0.16	0.2915	0.2915	0.2172	0.2915	9.6E-07	9.6E-07	0.024	0.000	0.001	-0.007
CRA K	9.19	3.93	2.06	3.81	55.96	0.31	18.16	0.12	0.10	0.3092	0.3092	0.3092	0.3092	8.5E-07	8.5E-07	0.002	0.002	-0.005	-0.005
CRA K	9.93	3.26	1.84	4.00	55.80	0.25	18.34	0.14	0.02	0.3092	0.3092	0.3092	0.3092	8.5E-07	8.5E-07	0.002	0.002	-0.005	-0.005
CRA K	11.91	4.04	1.20	4.86	52.60	0.32	20.55	0.16	0.05	0.3092	0.3092	0.3092	0.3092	8.5E-07	8.5E-07	0.002	0.002	-0.005	-0.005
CRA K										0.2915	0.2915	0.0898	0.1820	9.6E-07	9.6E-07	0.281	0.046	0.045	0.007
CRA K	11.05	13.24	0.24	1.00	44.13	0.22	27.68	0.16	0.00	0.3092	0.3092	0.3092	0.3092	8.5E-07	8.5E-07	0.002	0.002	-0.005	-0.005
CRA K	10.72	3.41	1.04	4.37	54.33	0.32	19.60	0.18	0.15	0.3092	0.3092	0.3092	0.3092	8.5E-07	8.5E-07	0.002	0.002	-0.005	-0.005
CRA K										0.3092	0.3092	0.2591	0.2915	8.5E-07	8.5E-07	0.012	0.004	-0.002	-0.005
CRA K										0.3092	0.3092	0.3092	0.3092	8.5E-07	8.5E-07	0.002	0.002	-0.005	-0.005
CRA K										0.3092	0.3092	0.3092	0.3092	8.5E-07	8.5E-07	0.002	0.002	-0.005	-0.005
CRA K	10.76	7.30	0.08	0.30	64.57	0.25	13.95	0.10	0.10	0.3092	0.3092	0.3092	0.3092	8.5E-07	8.5E-07	0.002	0.002	-0.005	-0.005
CRA K	9.89	2.84	3.31	4.66	48.38	0.27	19.54	0.08	0.06	0.3092	0.3092	0.3092	0.3092	8.5E-07	8.5E-07	0.002	0.002	-0.005	-0.005
CRA K										0.3092	0.3092	0.3092	0.3092	8.5E-07	8.5E-07	0.002	0.002	-0.005	-0.005
CRA K										0.3092	0.3092	0.3092	0.3092	8.5E-07	8.5E-07	0.002	0.002	-0.005	-0.005
CRA K	10.39	14.11	0.29	1.03	44.44	0.26	26.02	0.12	0.04	0.3092	0.3092	0.3092	0.3092	8.5E-07	8.5E-07	0.002	0.002	-0.005	-0.005
CRA K										0.3092	0.3092	0.3092	0.3092	8.5E-07	8.5E-07	0.002	0.002	-0.005	-0.005
CRA K	10.31	3.23	0.72	3.80	56.83	0.36	19.43	0.10	0.14	0.3092	0.3092	0.3092	0.3092	8.5E-07	8.5E-07	0.002	0.002	-0.005	-0.005
CRA K	10.78	2.97	8.78	4.84	38.63	0.38	19.65	0.14	0.13	0.3092	0.3092	0.3092	0.3092	8.5E-07	8.5E-07	0.002	0.002	-0.005	-0.005
CRA K	11.03	13.11	0.22	1.01	44.46	0.27	27.69	0.18	0.00	0.3092	0.3092	0.3092	0.3092	8.5E-07	8.5E-07	0.002	0.002	-0.005	-0.005
CRA K	13.98	25.60	0.05	0.16	45.06	0.21	12.55	0.11	0.09	0.3092	0.3092	0.3092	0.3092	8.5E-07	8.5E-07	0.002	0.002	-0.005	-0.005
CRA K	10.92	12.84	0.22	2.36	46.03	0.28	22.74	0.14	0.00	0.3092	0.3092	0.3092	0.3092	8.5E-07	8.5E-07	0.002	0.002	-0.005	-0.005
CRA K	12.98	3.04	0.06	5.19	55.22	0.28	21.00	0.17	0.07	0.3092	0.3092	0.3092	0.3092	8.5E-07	8.5E-07	0.002	0.002	-0.005	-0.005
CRA K										0.3092	0.3092	0.3092	0.3092	8.5E-07	8.5E-07	0.002	0.002	-0.005	-0.005
CRA K										0.3092	0.3092	0.3092	0.3092	8.5E-07	8.5E-07	0.002	0.002	-0.005	-0.005
CRA K	9.54	6.73	3.12	4.25	48.87	0.37	18.85	0.13	0.08	0.3092	0.3092	0.3092	0.3092	8.5E-07	8.5E-07	0.002	0.002	-0.005	-0.005
CRA K	11.07	13.00	0.22	0.98	43.69	0.20	27.55	0.14	0.00	0.3092	0.3092	0.3092	0.3092	8.5E-07	8.5E-07	0.002	0.002	-0.005	-0.005
CRA K	10.73	2.46	9.01	4.93	39.77	0.36	20.86	0.11	0.10	0.3092	0.3092	0.3092	0.3092	8.5E-07	8.5E-07	0.002	0.002	-0.005	-0.005
CRA K	11.40	6.05	0.09	0.39	63.74	0.27	16.04	0.13	0.06	0.3092	0.3092	0.3092	0.3092	8.5E-07	8.5E-07	0.002	0.002	-0.005	-0.005
CRA K	10.99	13.08	0.21	1.06	44.17	0.30	27.67	0.18	0.05	0.3092	0.3092	0.3092	0.3092	8.5E-07	8.5E-07	0.002	0.002	-0.005	-0.005
CRA K	9.69	2.87	3.24	4.23	50.04	0.41	18.46	0.12	0.03	0.3092	0.3092	0.3092	0.3092	8.5E-07	8.5E-07	0.002	0.002	-0.005	-0.005
CRA K	9.33	3.28	4.24	4.13	47.87	0.36	18.37	0.10	0.10	0.3092	0.3092	0.3092	0.3092	8.5E-07	8.5E-07	0.002	0.002	-0.005	-0.005
CRA K	9.05	3.04	3.37	4.00	51.34	0.30	18.42	0.12	0.06	0.3092	0.3092	0.3092	0.3092	8.5E-07	8.5E-07	0.002	0.002	-0.005	-0.005
CRA K	11.25	3.44	1.06	4.41	54.06	0.33	19.81	0.12	0.06	0.3092	0.3092	0.3092	0.3092	8.5E-07	8.5E-07	0.002	0.002	-0.005	-0.005
CRA K										0.3092	0.3092	0.3092	0.3092	8.5E-07	8.5E-07	0.002	0.002	-0.005	-0.005
CRA K										0.3092	0.3092	0.3092	0.3092	8.5E-07	8.5E-07	0.002	0.002	-0.005	-0.005
CRA K	10.04	3.44	0.32	3.61	59.53	0.35	18.31	0.09	0.05	0.3092	0.3092	0.3092	0.3092	8.5E-07	8.5E-07	0.002	0.002	-0.005	-0.005
EGV-1	8.95	4.67	0.00	0.00	63.81	0.31	21.09	0.01	0.14	0.3092	0.3092	0.3092	0.3092	8.5E-07	8.5E-07	0.000	0.000	-0.007	-0.007
EGV-1	8.11	7.48	0.02	0.12	60.29	0.24	21.06	0.03	0.16	0.3092	0.3092	0.3092	0.3092	8.5E-07	8.5E-07	0.000	0.000	-0.007	-0.007

Sample	Oxide weight %									Lifting field (T)		Rotating field (T)		Mag. suscept. (SI)		Paramag. rot. Index		Ferromag. rot. index	
	MgO	Al2O3	SiO2	TiO2	Cr2O3	MnO	FeO	NiO	ZnO	At 10Hz	At 57Hz	At 10Hz	At 57Hz	At 10Hz	At 57Hz	At 10Hz	At 57Hz	At 10Hz	At 57Hz
EGV-1	8.34	4.91	0.00	0.04	62.02	0.34	22.59	0.00	0.10	0.3092	0.3092	0.3092	0.3092	8.5E-07	8.5E-07	0.000	0.000	-0.007	-0.007
EGV-1	7.20	6.48	0.00	0.03	61.00	0.48	23.13	0.03	0.21	0.3092	0.3092	0.3092	0.3092	8.5E-07	8.5E-07	0.000	0.000	-0.007	-0.007
EGV-1	6.92	5.51	0.02	0.03	59.83	0.42	25.03	0.02	0.00	0.3092	0.3092	0.3092	0.3092	8.5E-07	8.5E-07	0.000	0.000	-0.007	-0.007
EGV-1	8.92	5.74	0.00	0.03	61.07	0.36	22.10	0.00	0.13	0.3092	0.3092	0.3092	0.3092	8.5E-07	8.5E-07	0.000	0.000	-0.007	-0.007
EGV-1	6.90	6.64	0.04	0.08	55.61	0.38	27.64	0.00	0.24	0.3092	0.3092	0.3092	0.3092	8.5E-07	8.5E-07	0.000	0.000	-0.007	-0.007
EGV-1	8.09	4.28	0.01	0.05	62.28	0.44	23.00	0.04	0.15	0.3092	0.3092	0.3092	0.3092	8.5E-07	8.5E-07	0.000	0.000	-0.007	-0.007
EGV-1	7.89	5.89	0.04	0.02	59.51	0.40	24.22	0.02	0.22	0.3092	0.3092	0.3092	0.3092	8.5E-07	8.5E-07	0.000	0.000	-0.007	-0.007
EGV-1	6.84	6.10	0.00	0.05	57.89	0.48	26.11	0.06	0.21	0.3092	0.3092	0.3092	0.3092	8.5E-07	8.5E-07	0.000	0.000	-0.007	-0.007
EGV-1	6.08	5.16	0.00	0.05	62.28	0.19	21.27	0.13	0.26	0.3092	0.3092	0.3092	0.3092	8.5E-07	8.5E-07	0.000	0.000	-0.007	-0.007
EGV-1	11.26	19.64	0.04	0.17	44.13	0.28	22.53	0.00	0.00	0.3092	0.3092	0.3092	0.3092	8.5E-07	8.5E-07	0.000	0.000	-0.007	-0.007
EGV-1	7.97	5.89	0.00	0.05	59.60	0.52	23.28	0.02	0.13	0.3092	0.3092	0.3092	0.3092	8.5E-07	8.5E-07	0.000	0.000	-0.007	-0.007
EGV-1	9.19	19.48	0.00	0.13	42.54	0.45	26.81	0.07	0.19	0.3092	0.3092	0.3092	0.3092	8.5E-07	8.5E-07	0.000	0.000	-0.007	-0.007
EGV-1	8.65	4.41	0.04	0.04	63.76	0.30	20.30	0.00	0.02	0.3092	0.3092	0.3092	0.3092	8.5E-07	8.5E-07	0.000	0.000	-0.007	-0.007
EGV-1	8.30	4.37	0.00	0.03	62.32	0.46	22.63	0.00	0.09	0.3092	0.3092	0.3092	0.3092	8.5E-07	8.5E-07	0.000	0.000	-0.007	-0.007
EGV-1	9.09	4.87	0.00	0.04	62.53	0.45	20.68	0.02	0.00	0.3092	0.3092	0.3092	0.3092	8.5E-07	8.5E-07	0.000	0.000	-0.007	-0.007
EGV-1	6.98	7.91	0.00	0.06	57.71	0.58	23.04	0.00	0.19	0.3092	0.3092	0.3092	0.3092	8.5E-07	8.5E-07	0.000	0.000	-0.007	-0.007
EGV-1	7.99	4.44	0.01	0.01	62.03	0.33	22.48	0.01	0.22	0.3092	0.3092	0.3092	0.3092	8.5E-07	8.5E-07	0.000	0.000	-0.007	-0.007
EGV-1	10.56	20.35	0.00	0.14	41.96	0.30	24.40	0.07	0.20	0.3092	0.3092	0.3092	0.3092	8.5E-07	8.5E-07	0.000	0.000	-0.007	-0.007
EGV-1	7.30	5.13	0.01	0.04	61.51	0.35	22.20	0.07	0.09	0.3092	0.3092	0.3092	0.3092	8.5E-07	8.5E-07	0.000	0.000	-0.007	-0.007
13246	4.67	9.32	0.00	0.15	31.94	0.40	50.25	0.33	0.28	0.0121	0.0121	0.0037	0.0053	5.5E-04	5.5E-04	0.281	0.124	0.045	0.023
13246	4.72	10.53	0.01	0.24	22.97	0.29	57.14	0.51	0.09	0.0085	0.0096	0.0004	0.0004	1.1E-03	8.9E-04	10.603	13.428	0.406	0.460
13246	6.27	15.85	0.00	0.17	30.13	0.31	44.23	0.26	0.37	0.0246	0.0246	0.0121	0.0173	1.3E-04	1.3E-04	0.092	0.030	0.017	0.003
13246	5.35	12.73	0.08	0.38	32.26	0.31	45.39	0.35	0.10	0.0136	0.0136	0.0042	0.0060	4.4E-04	4.4E-04	0.281	0.124	0.045	0.023
13246	4.96	14.62	0.00	0.17	32.03	0.43	45.32	0.36	0.11	0.0206	0.0206	0.0016	0.0047	1.9E-04	1.9E-04	4.633	0.530	0.259	0.070
13246	3.83	1.23	0.02	0.37	30.88	0.35	49.82	0.31	0.15	0.0153	0.0153	0.0047	0.0085	3.5E-04	3.5E-04	0.281	0.066	0.045	0.012
13246	2.50	7.69	0.04	0.18	31.10	0.44	55.11	0.28	0.20	0.0102	0.0102	0.0026	0.0037	7.9E-04	7.9E-04	0.413	0.189	0.059	0.033
13246	4.28	12.26	0.01	0.26	30.27	0.34	47.10	0.38	0.34	0.0194	0.0194	0.0102	0.0121	2.2E-04	2.2E-04	0.078	0.046	0.014	0.007
13246	4.45	13.18	0.00	0.24	30.02	0.30	48.09	0.43	0.05	0.0246	0.0246	0.0183	0.0206	1.3E-04	1.3E-04	0.024	0.012	0.001	-0.002
13246	5.16	12.18	0.00	0.22	30.11	0.31	48.50	0.23	0.27	0.0194	0.0206	0.0096	0.0153	2.2E-04	1.9E-04	0.092	0.024	0.017	0.001
13246	8.23	11.08	0.25	0.12	53.16	0.47	25.92	0.10	0.17	0.0394	0.0394	0.0015	0.0060	5.2E-05	5.2E-05	21.526	1.247	0.590	0.121
13246	6.29	16.51	0.00	0.11	29.53	0.32	44.03	0.30	0.18	0.0218	0.0218	0.0067	0.0108	1.7E-04	1.7E-04	0.281	0.092	0.045	0.017
13246	1.83	2.82	0.15	0.19	52.65	1.13	38.85	0.00	0.57	0.0330	0.0350	0.0013	0.0063	7.5E-05	6.6E-05	19.131	0.867	0.555	0.097
13246	5.88	12.26	0.02	0.24	32.67	0.22	45.03	0.29	0.00	0.0330	0.0330	0.0173	0.0183	7.5E-05	7.5E-05	0.078	0.066	0.014	0.012
13246	10.01	12.18	0.01	0.08	57.35	0.33	19.46	0.00	0.08	0.1071	0.1071	0.0194	0.0218	7.1E-06	7.1E-06	0.867	0.679	0.097	0.083
13246	8.81	16.63	0.02	0.06	44.16	0.45	28.22	0.12	0.13	0.0631	0.0709	0.0060	0.0173	2.0E-05	1.6E-05	3.245	0.468	0.212	0.065
13246	11.02	18.99	0.04	0.08	45.72	0.36	22.35	0.12	0.19	0.0528	0.0528	0.0076	0.0108	2.9E-05	2.9E-05	1.406	0.679	0.130	0.083
13246	9.66	9.20	0.01	0.01	60.62	0.44	19.14	0.08	0.15	0.0798	0.0752	0.0102	0.0173	1.3E-05	1.4E-05	1.788	0.530	0.150	0.070
13246	9.63	19.56	0.00	0.10	44.69	0.30	24.50	0.08	0.06	0.0752	0.0752	0.0042	0.0121	1.4E-05	1.4E-05	9.422	1.105	0.381	0.113
13246	11.15	19.62	0.00	0.12	45.51	0.29	22.29	0.11	0.26	0.0952	0.0952	0.0121	0.0218	9.0E-06	9.0E-06	1.788	0.530	0.150	0.070
13246	1.81	2.63	0.01	0.20	53.70	0.69	39.14	0.03	0.21	0.0594	0.0594	0.0047	0.0153	2.3E-05	2.3E-05	4.633	0.413	0.259	0.059
13246	10.23	17.99	0.03	0.20	44.86	0.22	24.97	0.10	0.27	0.0798	0.0798	0.0136	0.0173	1.3E-05	1.3E-05	0.979	0.600	0.105	0.076
13246	8.72	19.47	0.05	0.09	41.92	0.50	27.02	0.17	0.32	0.0669	0.0669	0.0153	0.0183	1.8E-05	1.8E-05	0.530	0.364	0.070	0.054
13246	4.50	5.29	1.91	0.23	49.35	0.75	38.18	0.05	0.19	0.1071	0.1071	0.0096	0.0232	7.1E-06	7.1E-06	3.654	0.600	0.227	0.076
13246	8.17	11.52	0.01	0.01	55.37	0.34	23.14	0.04	0.29	0.0752	0.0798	0.0153	0.0194	1.4E-05	1.3E-05	0.679	0.468	0.083	0.065
13246	9.56	12.91	0.03	0.03	54.72	0.30	21.72	0.03	0.19	0.1438	0.1438	0.0232	0.0311	3.9E-06	3.9E-06	1.105	0.600	0.113	0.076
13246	8.61	20.74	0.01	0.06	39.75	0.37	28.80	0.12	0.30	0.1356	0.1278	0.0418	0.0528	4.4E-06	5.0E-06	0.281	0.143	0.045	0.026
13246	6.28	17.05	0.02	0.12	35.63	0.28	37.91	0.22	0.21	0.0952	0.0952	0.0246	0.0350	9.0E-06	9.0E-06	0.413	0.189	0.059	0.033
13246	8.46	13.19	0.00	0.07	46.03	0.39	30.03	0.13	0.21	0.1618	0.1618	0.0276	0.0330	3.1E-06	3.1E-06	0.979	0.679	0.105	0.083

Sample	Oxide weight %									Lifting field (T)		Rotating field (T)		Mag. suscept. (SI)		Paramag. rot. Index		Ferromag. rot. index	
	MgO	Al2O3	SiO2	TiO2	Cr2O3	MnO	FeO	NiO	ZnO	At 10Hz	At 57Hz	At 10Hz	At 57Hz	At 10Hz	At 57Hz	At 10Hz	At 57Hz	At 10Hz	At 57Hz
13246	11.03	19.84	0.01	0.08	46.61	0.34	20.50	0.07	0.15	0.1356	0.1278	0.0063	0.0153	4.4E-06	5.0E-06	13.428	2.015	0.460	0.161
13246	11.83	20.05	0.00	0.08	44.89	0.29	21.54	0.17	0.21	0.1205	0.1136	0.0330	0.0418	5.6E-06	6.3E-06	0.364	0.189	0.054	0.033
13246	8.89	9.23	0.04	0.05	58.83	0.40	21.80	0.00	0.25	0.1010	0.0952	0.0194	0.0218	8.0E-06	9.0E-06	0.767	0.530	0.090	0.070
13246	7.35	15.82	0.00	0.07	47.80	0.42	27.60	0.05	0.16	0.1438	0.1356	0.0096	0.0246	3.9E-06	4.4E-06	6.609	0.867	0.314	0.097
13246	8.47	5.22	0.00	0.02	61.24	0.56	23.19	0.10	0.15	0.1278	0.1278	0.0173	0.0246	5.0E-06	5.0E-06	1.586	0.767	0.140	0.090
13246	7.96	14.50	0.04	0.07	49.27	0.37	26.30	0.02	0.03	0.0952	0.0952	0.0183	0.0194	9.0E-06	9.0E-06	0.767	0.679	0.090	0.083
13246	8.62	18.55	0.02	0.08	42.80	0.36	27.63	0.11	0.24	0.2915	0.2915	0.2848	0.2915	9.6E-07	9.6E-07	0.001	0.000	-0.006	-0.007
13246	10.66	16.87	0.00	0.07	46.43	0.32	24.14	0.15	0.12	0.2915	0.2915	0.1820	0.2172	9.6E-07	9.6E-07	0.046	0.024	0.007	0.001
13246	10.11	19.91	0.01	0.02	41.82	0.34	26.02	0.13	0.05	0.2304	0.2304	0.0218	0.0594	1.5E-06	1.5E-06	3.245	0.413	0.212	0.059
13246	9.36	6.07	0.01	0.02	64.41	0.40	18.91	0.05	0.03	0.3092	0.3092	0.3092	0.3092	8.5E-07	8.5E-07	0.002	0.002	-0.005	-0.005
13246	8.56	10.53	0.01	0.09	57.31	0.46	22.52	0.04	0.18	0.2591	0.2591	0.0752	0.0898	1.2E-06	1.2E-06	0.320	0.216	0.049	0.037
13246	8.87	11.37	0.02	0.11	55.77	0.35	22.37	0.00	0.14	0.2915	0.2848	0.1278	0.1618	9.6E-07	1.0E-06	0.124	0.062	0.023	0.011
13246	8.20	12.91	0.00	0.11	52.02	0.43	25.62	0.07	0.33	0.2443	0.2304	0.0952	0.1278	1.4E-06	1.5E-06	0.164	0.066	0.029	0.012
13246	8.49	17.22	0.00	0.12	46.91	0.36	25.28	0.01	0.16	0.3092	0.3092	0.3092	0.3092	8.5E-07	8.5E-07	0.002	0.002	-0.005	-0.005
13246	9.84	13.95	0.02	0.06	53.31	0.19	21.33	0.02	0.08	0.2915	0.2915	0.1618	0.1618	9.6E-07	9.6E-07	0.066	0.066	0.012	0.012
13246	7.58	4.52	0.00	0.06	63.87	0.52	23.26	0.02	0.19	0.3092	0.3092	0.3092	0.3092	8.5E-07	8.5E-07	0.002	0.002	-0.005	-0.005
13246	7.46	4.62	0.00	0.04	65.38	0.40	21.07	0.03	0.24	0.3092	0.3092	0.3092	0.3092	8.5E-07	8.5E-07	0.002	0.002	-0.005	-0.005
13246	8.71	10.10	0.04	0.07	58.08	0.42	21.85	0.08	0.19	0.3092	0.3092	0.3092	0.3092	8.5E-07	8.5E-07	0.002	0.002	-0.005	-0.005
13246	9.45	13.22	0.06	0.04	53.89	0.27	22.02	0.05	0.11	0.3092	0.3092	0.3092	0.3092	8.5E-07	8.5E-07	0.002	0.002	-0.005	-0.005
13246	8.10	11.02	0.02	0.07	51.20	0.38	27.77	0.04	0.23	0.3092	0.3092	0.3092	0.3092	8.5E-07	8.5E-07	0.002	0.002	-0.005	-0.005
13246	8.84	4.43	0.00	0.04	66.33	0.40	19.62	0.00	0.00	0.3092	0.3092	0.3092	0.3092	8.5E-07	8.5E-07	0.002	0.002	-0.005	-0.005
13246	9.32	3.29	0.03	0.00	68.18	0.42	17.81	0.04	0.07	0.3092	0.3092	0.3092	0.3092	8.5E-07	8.5E-07	0.002	0.002	-0.005	-0.005
13246	13.39	31.56	0.00	0.10	33.87	0.31	19.04	0.09	0.13	0.3092	0.3092	0.3092	0.3092	8.5E-07	8.5E-07	0.002	0.002	-0.005	-0.005
13246	11.32	16.02	0.00	0.05	50.35	0.22	20.67	0.12	0.23	0.3092	0.3092	0.3092	0.3092	8.5E-07	8.5E-07	0.002	0.002	-0.005	-0.005
13246	12.12	15.79	0.00	0.08	54.55	0.47	15.91	0.00	0.07	0.3092	0.3092	0.3092	0.3092	8.5E-07	8.5E-07	0.002	0.002	-0.005	-0.005
13246	20.44	54.33	0.05	0.12	11.00	0.10	10.90	0.41	0.16	0.3092	0.3092	0.3092	0.3092	8.5E-07	8.5E-07	0.002	0.002	-0.005	-0.005
13246	11.31	22.92	0.00	0.06	43.88	0.39	21.04	0.05	0.14	0.3092	0.3092	0.3092	0.3092	8.5E-07	8.5E-07	0.002	0.002	-0.005	-0.005
13246	20.22	54.62	0.05	0.08	10.79	0.16	11.77	0.41	0.09	0.3092	0.3092	0.3092	0.3092	8.5E-07	8.5E-07	0.002	0.002	-0.005	-0.005
13246	8.86	11.75	0.02	0.08	55.82	0.43	22.19	0.00	0.07	0.3092	0.3092	0.3092	0.3092	8.5E-07	8.5E-07	0.002	0.002	-0.005	-0.005
13246	20.46	55.07	0.04	0.12	10.86	0.17	10.62	0.40	0.00	0.3092	0.3092	0.3092	0.3092	8.5E-07	8.5E-07	0.002	0.002	-0.005	-0.005
DF	6.74	5.28	0.00	0.07	61.69	0.38	26.54	0.03	0.19	0.3092	0.3092	0.3092	0.3092	8.5E-07	8.5E-07	0.002	0.002	-0.005	-0.005
DF	2.90	11.24	0.07	0.10	55.00	0.44	32.67	0.12	0.30	0.2304	0.2304	0.1525	0.1820	1.5E-06	1.5E-06	0.038	0.018	0.005	-0.000
DF	7.73	4.65	0.00	0.00	63.14	0.37	25.19	0.13	0.07	0.3092	0.3092	0.3092	0.3092	8.5E-07	8.5E-07	0.002	0.002	-0.005	-0.005
DF	10.76	10.54	0.03	0.08	60.72	0.18	20.41	0.01	0.03	0.2915	0.2915	0.2443	0.2915	9.6E-07	9.6E-07	0.012	0.000	-0.002	-0.007
DF	5.61	5.09	0.02	0.04	64.70	0.22	24.75	0.06	0.30	0.2915	0.2915	0.2915	0.2915	9.6E-07	9.6E-07	0.000	0.000	-0.007	-0.007
DF	10.00	14.82	0.00	0.05	52.60	0.30	25.20	0.05	0.29	0.2591	0.2591	0.0798	0.1618	1.2E-06	1.2E-06	0.281	0.046	0.045	0.007
DF	7.71	6.10	0.01	0.05	62.17	0.51	26.01	0.16	0.17	0.3092	0.3092	0.3092	0.3092	8.5E-07	8.5E-07	0.002	0.002	-0.005	-0.005
DF	11.61	10.82	0.02	0.05	60.28	0.28	19.30	0.08	0.23	0.3092	0.3092	0.3092	0.3092	8.5E-07	8.5E-07	0.002	0.002	-0.005	-0.005
DF	15.68	30.12	0.00	0.45	38.04	0.21	16.70	0.19	0.08	0.3092	0.3092	0.3092	0.3092	8.5E-07	8.5E-07	0.002	0.002	-0.005	-0.005
DF	8.66	9.20	0.04	0.00	57.91	0.35	25.85	0.00	0.10	0.3092	0.3092	0.3092	0.3092	8.5E-07	8.5E-07	0.002	0.002	-0.005	-0.005
DF	7.97	4.98	0.03	0.08	67.55	0.27	21.80	0.06	0.14	0.3092	0.3092	0.3092	0.3092	8.5E-07	8.5E-07	0.002	0.002	-0.005	-0.005
DF	13.68	36.36	0.08	0.67	25.86	0.22	23.59	0.21	0.06	0.3092	0.3092	0.3092	0.3092	8.5E-07	8.5E-07	0.002	0.002	-0.005	-0.005
DF	8.33	10.13	0.01	0.06	57.06	0.31	26.58	0.13	0.16	0.3092	0.3092	0.3092	0.3092	8.5E-07	8.5E-07	0.002	0.002	-0.005	-0.005
DF	10.38	20.28	0.00	0.10	44.12	0.36	24.95	0.00	0.30	0.3092	0.3092	0.3092	0.3092	8.5E-07	8.5E-07	0.002	0.002	-0.005	-0.005

Appendix D

SP5A and SP2 Chromite line analysis results

(Points are numbered from the left of grain, with grains oriented as for figures 12.10 to 12.12)

Sample source	Grain number	Point number	Oxide weight % MgO	Al2O3	SiO2	TiO2	Cr2O3	MnO	FeO	NiO	ZnO	Pt Wt %
SP5A	1	1	9.93	11.84	0.04	0.37	45.23	0.39	28.42	0.10	0.12	0.000
		2	10.00	11.83	0.07	0.40	45.32	0.42	27.78	0.08	0.16	0.000
		3	10.07	11.88	0.00	0.40	45.38	0.51	29.25	0.14	0.00	0.000
		4	10.16	11.86	0.00	0.36	45.58	0.43	27.75	0.06	0.14	0.000
		5	10.19	11.89	0.02	0.41	45.43	0.47	27.36	0.09	0.18	0.000
		6	10.17	11.94	0.04	0.39	45.44	0.49	27.47	0.16	0.05	0.000
		7	10.14	11.96	0.04	0.36	45.18	0.53	27.47	0.08	0.10	0.000
		8	10.04	11.96	0.00	0.39	45.21	0.41	27.65	0.12	0.22	0.000
		9	9.98	11.96	0.01	0.34	45.61	0.37	27.88	0.09	0.01	0.000
		10	9.97	12.00	0.02	0.38	45.74	0.44	27.58	0.11	0.04	0.000
SP5A	2	1	11.28	9.97	0.03	0.33	49.42	0.42	25.05	0.07	0.04	0.000
		2	11.27	10.10	0.00	0.39	49.28	0.56	24.96	0.16	0.03	0.000
		3	11.12	10.16	0.00	0.34	49.49	0.55	24.93	0.02	0.03	0.000
		4	11.22	10.19	0.00	0.36	49.55	0.44	24.84	0.16	0.00	0.000
		5	11.17	10.10	0.00	0.36	49.07	0.45	24.91	0.04	0.06	0.000
		6	11.10	10.29	0.00	0.35	49.17	0.42	24.86	0.11	0.16	0.000
		7	11.06	10.19	0.00	0.34	48.96	0.21	25.20	0.07	0.03	0.000
		8	11.11	10.15	0.00	0.36	48.75	0.35	25.26	0.06	0.11	0.000
		9	11.03	10.26	0.01	0.31	48.70	0.42	25.03	0.11	0.02	0.021
		10	11.12	10.20	0.00	0.32	48.82	0.51	24.65	0.06	0.00	0.000
SP5A	3	1	10.32	11.37	0.00	0.35	46.23	0.53	27.26	0.06	0.11	0.000
		2	10.32	11.52	0.02	0.41	46.33	0.39	27.56	0.10	0.04	0.000
		3	10.24	11.33	0.00	0.40	46.14	0.53	27.79	0.06	0.09	0.000
		4	10.23	11.42	0.01	0.41	46.58	0.40	27.52	0.08	0.04	0.009
		5	10.17	11.24	0.00	0.34	46.60	0.51	27.15	0.07	0.16	0.006
		6	10.21	11.55	0.00	0.36	46.06	0.40	27.62	0.13	0.23	0.000
		7	10.21	11.54	0.02	0.39	46.47	0.32	27.39	0.04	0.15	0.000
		8	10.32	11.41	0.00	0.38	46.60	0.39	27.34	0.10	0.07	0.000
		9	10.24	11.15	0.00	0.37	46.49	0.44	26.83	0.08	0.01	0.000
		10	10.20	11.18	0.00	0.37	46.72	0.37	27.47	0.06	0.00	0.000
SP5A	4	1	9.79	11.94	0.00	0.38	45.44	0.43	28.68	0.08	0.17	0.000
		2	9.91	11.91	0.02	0.04	46.06	0.35	28.15	0.12	0.06	0.000
		3	9.97	11.88	0.02	0.39	45.89	0.60	28.13	0.08	0.10	0.000
		4	9.95	11.67	0.02	0.40	46.02	0.53	28.02	0.09	0.08	0.000
		5	9.98	11.70	0.00	0.38	46.02	0.53	27.99	0.07	0.23	0.000
		6	10.10	11.57	0.00	0.36	45.87	0.37	27.72	0.13	0.07	0.000
		7	10.06	11.59	0.02	0.36	46.18	0.46	27.48	0.07	0.06	0.000
		8	9.97	11.75	0.00	0.35	46.41	0.47	27.93	0.14	0.01	0.000
		9	10.03	11.57	0.00	0.39	46.09	0.46	27.62	0.05	0.03	0.000
		10	10.08	11.50	0.02	0.41	46.37	0.47	27.21	0.12	0.00	0.000
SP5A	5	1	9.83	11.89	0.00	0.42	45.46	0.53	28.49	0.06	0.06	0.000
		2	9.92	11.67	0.00	0.40	45.71	0.31	28.33	0.02	0.00	0.000
		3	9.97	11.68	0.00	0.40	45.91	0.43	27.67	0.08	0.25	0.000
		4	10.05	11.38	0.00	0.37	46.11	0.35	28.01	0.07	0.22	0.000
		5	10.04	11.49	0.02	0.38	46.19	0.53	27.81	0.02	0.13	0.000
		6	9.99	11.52	0.03	0.34	46.43	0.45	27.86	0.08	0.18	0.000
		7	10.03	11.61	0.00	0.35	46.03	0.51	28.09	0.02	0.01	0.000
		8	10.00	11.57	0.00	0.38	46.37	0.44	27.92	0.06	0.00	0.002
		9	9.83	11.51	0.03	0.34	46.03	0.44	28.19	0.10	0.15	0.000
		10	9.89	11.54	0.02	0.39	46.16	0.48	27.81	0.07	0.18	0.000
SP5A	6	1	9.76	11.94	0.02	0.43	45.16	0.37	28.27	0.13	0.10	0.000
		2	9.84	11.89	0.00	0.42	45.69	0.46	28.05	0.04	0.18	0.000
		3	9.84	11.79	0.01	0.37	45.21	0.39	28.11	0.10	0.15	0.000
		4	9.81	11.65	0.04	0.39	45.63	0.39	28.31	0.08	0.05	0.000
		5	9.90	11.49	0.02	0.39	45.12	0.47	28.44	0.01	0.16	0.000
		6	9.68	11.70	0.02	0.39	45.34	0.42	28.51	0.12	0.07	0.000
		7	9.76	11.56	0.01	0.41	45.67	0.23	28.36	0.08	0.15	0.000
		8	9.76	11.66	0.00	0.41	45.29	0.51	28.38	0.08	0.20	0.000
		9	9.75	11.63	0.00	0.39	45.58	0.40	28.27	0.08	0.22	0.017
		10	9.86	11.70	0.00	0.42	45.53	0.51	28.03	0.05	0.21	0.000

Appendix D

SP5A and SP2 Chromite line analysis results

(Points are numbered from the left of grain, with grains oriented as for figures 12.10 to 12.12)

Sample source	Grain number	Point number	Oxide weight % MgO	Al2O3	SiO2	TiO2	Cr2O3	MnO	FeO	NiO	ZnO	Pt %
SP5A	7	1	9.55	11.87	0.01	0.37	45.30	0.56	28.70	0.05	0.10	0.000
		2	9.54	11.71	0.00	0.35	45.90	0.53	28.65	0.08	0.19	0.000
		3	9.63	11.66	0.04	0.40	45.53	0.56	28.36	0.13	0.09	0.000
		4	9.72	11.73	0.00	0.35	46.02	0.44	28.47	0.02	0.15	0.000
		5	9.77	11.67	0.01	0.38	45.54	0.46	28.14	0.06	0.18	0.000
		6	9.76	11.82	0.00	0.40	46.03	0.35	28.24	0.16	0.12	0.000
		7	9.85	11.63	0.04	0.38	46.07	0.39	28.14	0.10	0.12	0.000
		8	9.72	11.52	0.05	0.40	45.85	0.45	28.28	0.13	0.16	0.000
		9	9.96	11.66	0.00	0.36	45.86	0.26	28.04	0.07	0.00	0.000
		10	9.59	11.65	0.00	0.41	46.10	0.34	28.02	0.11	0.14	0.000
SP5A	8	1	9.68	12.05	0.02	0.42	45.46	0.55	28.00	0.10	0.28	0.000
		2	9.98	11.87	0.00	0.40	45.38	0.32	27.33	0.01	0.24	0.000
		3	10.05	11.65	0.00	0.35	45.52	0.39	27.39	0.14	0.18	0.000
		4	10.02	11.80	0.04	0.40	45.74	0.42	27.40	0.10	0.00	0.000
		5	10.14	11.72	0.00	0.42	45.79	0.42	27.37	0.15	0.17	0.001
		6	10.15	11.84	0.02	0.41	46.03	0.66	27.34	0.11	0.04	0.000
		7	10.00	11.71	0.00	0.39	45.63	0.53	27.75	0.07	0.03	0.000
		8	9.98	11.66	0.00	0.43	45.97	0.43	27.20	0.11	0.11	0.014
		9	10.05	11.58	0.00	0.40	46.01	0.37	27.14	0.12	0.27	0.000
		10	10.08	11.84	0.01	0.41	46.01	0.50	27.33	0.06	0.09	0.000
SP5A	41	1	10.66	12.03	0.00	0.41	48.02	0.33	28.12	0.17	0.12	
		2	10.37	11.78	0.00	0.37	48.49	0.37	27.50	0.06	0.07	
		3	10.45	11.55	0.03	0.38	48.70	0.33	27.73	0.10	0.09	
		4	10.50	11.48	0.02	0.48	49.02	0.32	27.17	0.08	0.09	
		5	10.52	11.50	0.00	0.38	46.07	0.40	27.31	0.07	0.06	
		6	10.46	11.34	0.02	0.37	49.11	0.41	27.17	0.09	0.06	
		7	10.57	11.38	0.01	0.39	49.06	0.47	27.29	0.08	0.08	
		8	10.59	11.32	0.00	0.34	49.03	0.34	26.83	0.06	0.09	
		9	10.59	11.38	0.00	0.37	49.10	0.25	26.48	0.11	0.11	
		10	10.64	11.16	0.00	0.37	49.16	0.35	26.89	0.07	0.08	
SP5A	42	1	11.42	12.03	0.00	0.36	48.86	0.32	25.84	0.11	0.13	
		2	11.52	11.95	0.00	0.37	48.69	0.32	25.42	0.01	0.05	
		3	11.50	12.01	0.00	0.42	48.89	0.40	25.27	0.09	0.13	
		4	11.50	12.01	0.00	0.38	49.02	0.33	25.38	0.10	0.08	
		5	11.43	11.87	0.03	0.36	48.72	0.43	25.27	0.11	0.06	
		6	11.54	11.92	0.00	0.40	49.11	0.35	25.09	0.08	0.08	
		7	11.53	11.84	0.00	0.38	49.02	0.40	25.11	0.11	0.12	
		8	11.50	11.95	0.02	0.38	48.70	0.40	25.23	0.12	0.09	
		9	11.27	11.86	0.01	0.39	49.19	0.44	25.00	0.08	0.08	
		10	11.31	12.02	0.00	0.37	48.72	0.29	25.31	0.14	0.12	
SP5A	43	1	11.46	11.60	0.00	0.35	49.11	0.39	25.50	0.08	0.07	
		2	11.43	11.69	0.01	0.39	49.12	0.31	25.16	0.08	0.01	
		3	11.37	11.68	0.00	0.36	48.75	0.28	25.42	0.06	0.03	
		4	11.41	11.44	0.00	0.36	48.95	0.38	25.35	0.11	0.07	
		5	11.14	11.41	0.21	0.39	49.00	0.33	24.99	0.08	0.06	
		6	11.22	11.41	0.01	0.35	49.34	0.32	25.11	0.08	0.15	
		7	11.26	11.37	0.00	0.33	49.49	0.33	25.48	0.11	0.07	
		8	11.22	11.46	0.00	0.36	49.83	0.28	25.24	0.12	0.06	
		9	11.11	11.32	0.02	0.37	49.86	0.38	25.07	0.05	0.09	
		10	11.11	11.30	0.02	0.33	49.60	0.38	25.13	0.08	0.12	
SP5A	44	1	11.74	12.13	0.01	0.32	48.98	0.38	25.62	0.07	0.11	
		2	11.55	11.77	0.08	0.39	49.26	0.33	25.81	0.08	0.11	
		3	11.46	11.70	0.05	0.36	49.44	0.39	25.72	0.12	0.14	
		4	11.50	11.64	0.06	0.33	49.87	0.35	25.29	0.09	0.10	
		5	11.30	11.63	0.03	0.39	49.25	0.31	25.87	0.06	0.14	
		6	11.17	11.41	0.02	0.34	49.62	0.34	25.94	0.10	0.14	
		7	11.17	11.45	0.03	0.37	49.64	0.35	26.05	0.10	0.02	
		8	11.15	11.31	0.04	0.34	49.75	0.37	25.48	0.04	0.07	
		9	11.21	11.27	0.05	0.35	49.83	0.37	25.71	0.07	0.07	
		10	10.94	11.11	0.00	0.35	49.95	0.31	25.69	0.14	0.11	

Appendix D

SP5A and SP2 Chromite line analysis results

(Points are numbered from the left of grain, with grains oriented as for figures 12.10 to 12.12)

Sample source	Grain number	Point number	Oxide weight % MgO	Al2O3	SiO2	TiO2	Cr2O3	MnO	FeO	NiO	ZnO	Pt %
SP5A	45	1	11.09	11.15	0.00	0.38	49.29	0.34	26.51	0.09	0.13	
		2	11.07	11.21	0.00	0.36	49.58	0.34	26.19	0.09	0.06	
		3	11.08	11.05	0.00	0.40	49.06	0.33	26.42	0.04	0.12	
		4	10.98	11.13	0.00	0.37	49.13	0.28	26.37	0.07	0.13	
		5	11.03	11.19	0.00	0.38	49.35	0.35	26.37	0.09	0.09	
		6	10.99	11.20	0.00	0.34	49.29	0.35	26.29	0.10	0.07	
		7										
		8										
		9										
		10										
SP2	51	1	9.50	11.52	0.42	0.47	43.74	0.38	29.49	0.03	0.14	0.000
		2	9.52	11.17	0.00	0.49	44.79	0.41	29.07	0.06	0.11	0.000
		3	9.24	11.21	0.00	0.43	44.64	0.53	29.42	0.06	0.11	0.000
		4										0.000
		5	8.21	9.24	0.53	0.45	45.59	0.54	30.28	0.14	0.24	0.000
		6	8.49	10.86	0.87	0.43	42.08	0.65	31.72	0.12	0.19	0.000
		7	9.69	11.10	0.00	0.47	44.58	0.44	28.87	0.10	0.10	0.000
		8	9.72	11.24	0.00	0.49	44.67	0.49	28.98	0.12	0.07	0.000
		9	9.60	11.09	0.00	0.47	44.98	0.51	28.78	0.12	0.18	0.000
		10										0.000
SP2	52	1	8.38	9.71	0.01	0.43	45.69	0.63	30.76	0.11	0.20	0.000
		2	9.65	9.86	0.00	0.47	46.66	0.59	28.70	0.04	0.28	0.000
		3	8.79	9.80	0.01	0.42	46.10	0.71	30.06	0.11	0.08	0.000
		4	7.12	9.48	0.01	0.39	45.65	0.96	31.05	0.11	0.11	0.000
		5	8.72	7.85	0.91	0.38	38.25	0.58	38.19	0.20	0.13	0.000
		6	9.94	10.09	0.04	0.48	47.47	0.62	27.42	0.16	0.06	0.000
		7	8.86	9.21	0.08	0.46	44.05	0.61	32.29	0.09	0.20	0.002
		8	10.13	9.78	0.00	0.45	47.41	0.43	27.02	0.15	0.18	0.000
		9	10.01	9.60	0.01	0.40	47.27	0.45	27.16	0.08	0.27	0.000
		10	8.03	6.94	1.58	0.35	36.07	0.55	40.10	0.19	0.17	0.000
SP2	53	1	9.84	11.22	0.00	0.46	47.84	0.49	28.59	0.11	0.12	
		2	9.91	11.13	0.06	0.49	47.97	0.34	28.54	0.11	0.23	
		3	9.96	11.00	0.02	0.46	47.89	0.42	28.49	0.09	0.16	
		4	10.05	10.83	0.03	0.47	48.17	0.45	28.85	0.09	0.13	
		5	9.93	10.89	0.00	0.50	48.44	0.37	28.33	0.12	0.22	
		6	9.99	10.89	0.02	0.46	48.26	0.44	28.23	0.07	0.19	
		7	9.90	10.79	0.01	0.42	48.28	0.40	28.35	0.08	0.11	
		8	9.87	10.81	0.00	0.53	48.00	0.41	28.25	0.08	0.12	
		9	9.79	10.84	0.04	0.50	47.83	0.45	28.36	0.12	0.23	
		10	9.61	10.81	0.01	0.48	48.16	0.42	28.83	0.09	0.16	
SP2	54	1	10.63	9.71	0.00	0.46	50.45	0.41	27.05	0.07	0.18	
		2	9.91	10.48	4.05	0.55	46.07	0.43	25.36	0.00	0.09	
		3	10.61	9.54	0.00	0.42	50.47	0.45	26.37	0.09	0.12	
		4	10.33	9.52	0.00	0.40	50.43	0.43	27.20	0.06	0.04	
		5	10.41	9.54	0.00	0.40	50.60	0.44	27.30	0.11	0.19	
		6	9.92	9.51	0.36	0.39	49.24	0.43	27.61	0.11	0.13	
		7	9.84	9.42	0.00	0.41	50.29	0.52	27.57	0.15	0.15	
		8	9.88	9.29	0.10	0.40	49.52	0.45	27.39	0.13	0.11	
		9	10.38	9.41	0.35	0.40	49.89	0.45	27.66	0.15	0.06	
		10	10.35	9.39	0.03	0.45	50.42	0.33	25.86	0.08	0.14	
SP2	56	1	7.81	7.89	0.51	0.36	41.86	0.63	37.59	0.11	0.23	
		2	9.89	9.56	0.20	0.44	45.59	0.51	28.57	0.10	0.12	
		3	9.30	9.29	0.08	0.38	48.98	0.62	29.92	0.11	0.21	
		4	8.49	8.78	0.21	0.36	47.83	0.70	31.84	0.11	0.24	
		5	9.99	9.41	0.06	0.42	49.75	0.45	28.36	0.12	0.09	
		6	9.06	9.04	0.12	0.41	47.89	0.59	30.68	0.07	0.14	
		7	8.79	9.14	0.11	0.38	49.44	0.67	29.52	0.05	0.18	
		8	8.77	8.57	0.13	0.38	46.79	0.54	32.30	0.14	0.17	
		9	8.60	8.26	0.52	0.37	44.41	0.44	33.87	0.14	0.16	
		10	9.62	8.91	0.71	0.44	47.04	0.48	29.88	0.11	0.11	

Appendix D

SP5A and SP2 Chromite line analysis results

(Points are numbered from the left of grain, with grains oriented as for figures 12.10 to 12.12)

Sample source	Grain number	Point number	Oxide weight % MgO	Al2O3	SiO2	TiO2	Cr2O3	MnO	FeO	NiO	ZnO	Pt %
SP2	57	1	10.49	10.22	0.02	0.44	49.85	0.44	27.35	0.10	0.10	
		2	10.45	10.15	0.02	0.44	49.67	0.41	27.75	0.10	0.18	
		3	10.14	10.24	0.00	0.42	50.05	0.44	27.73	0.05	0.10	
		4	10.15	10.18	0.05	0.50	49.40	0.45	27.60	0.08	0.13	
		5	10.10	10.26	0.01	0.43	49.13	0.37	27.76	0.11	0.12	
		6	9.92	10.08	0.00	0.46	49.36	0.37	27.78	0.13	0.07	
		7	9.69	10.13	0.02	0.47	49.31	0.47	27.98	0.08	0.14	
		8	9.70	10.23	0.02	0.44	48.99	0.37	28.58	0.06	0.18	
		9	9.18	10.30	0.02	0.48	48.69	0.44	28.64	0.13	0.14	
		10	8.81	10.17	0.00	0.49	47.68	0.43	29.54	0.01	0.15	
SP2	58	1	9.58	11.30	0.01	0.50	48.12	0.49	28.42	0.09	0.12	
		2	9.61	11.18	0.00	0.46	48.07	0.45	28.77	0.09	0.17	
		3	9.57	10.88	0.05	0.47	48.26	0.44	28.71	0.13	0.21	
		4	9.84	11.13	0.00	0.50	48.58	0.50	28.35	0.09	0.16	
		5	9.70	10.71	0.42	0.48	47.33	0.47	28.60	0.13	0.22	
		6	9.97	10.85	0.25	0.48	47.92	0.41	27.70	0.09	0.09	
		7	9.62	10.77	0.00	0.49	48.42	0.43	28.87	0.08	0.20	
		8	9.76	10.99	0.00	0.44	48.55	0.47	28.14	0.04	0.26	
		9	9.40	10.58	0.08	0.47	47.65	0.37	29.47	0.08	0.15	
		10	9.55	10.85	0.00	0.43	48.52	0.48	28.81	0.09	0.28	
SP2	59	1	9.05	9.76	0.00	0.45	48.73	0.53	29.97	0.09	0.08	
		2	9.71	9.70	0.20	0.43	49.47	0.45	28.44	0.10	0.14	
		3	9.70	9.80	0.00	0.43	49.86	0.51	28.43	0.14	0.09	
		4	9.65	9.91	0.00	0.47	49.32	0.41	27.81	0.09	0.13	
		5	9.83	9.88	0.00	0.42	49.75	0.40	28.44	0.10	0.11	
		6	9.56	9.77	0.04	0.45	49.45	0.50	28.85	0.07	0.16	
		7	9.44	9.75	0.05	0.43	49.13	0.58	28.91	0.09	0.14	
		8	9.05	9.46	0.15	0.39	47.12	0.42	31.34	0.09	0.11	
		9	9.52	9.72	0.04	0.48	49.23	0.40	29.33	0.09	0.07	
		10	9.87	9.80	0.03	0.49	48.43	0.41	28.08	0.10	0.17	
SP2	60	1	10.30	9.65	0.11	0.42	49.61	0.50	27.24	0.06	0.15	
		2	10.35	9.81	0.03	0.41	50.52	0.38	27.01	0.11	0.12	
		3	5.72	5.49	0.88	0.30	24.68	0.83	47.85	0.21	0.32	
		4	8.76	7.53	1.60	0.35	40.57	0.51	37.66	0.14	0.23	
		5	7.13	7.33	0.49	0.29	40.20	0.78	40.47	0.21	0.21	
		6	6.74	6.57	0.88	0.24	38.12	0.70	43.02	0.18	0.18	
		7	6.29	6.54	0.65	0.27	38.52	0.85	43.58	0.17	0.28	
		8	7.80	6.78	1.90	0.33	38.93	0.82	39.90	0.19	0.21	
		9	10.42	9.82	0.00	0.42	50.26	0.36	26.59	0.06	0.04	
		10	10.45	9.82	0.00	0.45	49.88	0.35	27.45	0.08	0.12	
SP2	61	1	10.16	11.07	0.00	0.46	45.54	0.42	28.25	0.17	0.22	0.000
		2	10.11	10.95	0.09	0.49	45.84	0.43	27.88	0.17	0.21	0.000
		3	10.04	10.97	0.02	0.45	45.68	0.29	28.28	0.12	0.00	0.000
		4	10.09	10.94	0.02	0.46	46.29	0.46	27.90	0.08	0.30	0.006
		5	10.09	11.04	0.00	0.48	45.87	0.43	28.66	0.10	0.06	0.000
		6	10.08	10.95	0.01	0.47	45.88	0.42	28.49	0.08	0.00	0.000
		7	10.13	10.74	0.02	0.47	45.22	0.43	28.31	0.11	0.14	0.000
		8	9.94	10.81	0.01	0.41	45.09	0.46	28.33	0.17	0.07	0.000
		9	9.87	10.69	0.00	0.45	44.85	0.48	28.34	0.06	0.08	0.000
		10	9.86	10.91	0.00	0.46	45.21	0.62	28.50	0.11	0.00	0.010
SP2	62	1	9.56	10.69	0.00	0.45	45.53	0.47	28.17	0.03	0.15	0.000
		2	9.70	10.62	0.00	0.55	46.86	0.31	28.10	0.12	0.18	0.000
		3	9.76	10.56	0.00	0.43	45.81	0.52	27.48	0.08	0.05	0.000
		4	9.85	10.54	0.02	0.50	46.47	0.42	27.88	0.16	0.19	0.000
		5	9.82	10.32	0.00	0.49	46.47	0.33	27.74	0.06	0.18	0.000
		6	9.84	10.25	0.02	0.45	46.86	0.44	27.78	0.12	0.29	0.000
		7	9.86	10.36	0.03	0.46	46.41	0.65	27.37	0.12	0.37	0.000
		8	9.98	10.25	0.00	0.46	46.15	0.43	27.09	0.07	0.25	0.000
		9	9.87	10.32	0.00	0.42	46.41	0.44	27.64	0.09	0.15	0.000
		10	10.03	10.12	0.00	0.50	46.53	0.58	27.37	0.16	0.22	0.000

Appendix D

SP5A and SP2 Chromite line analysis results

(Points are numbered from the left of grain, with grains oriented as for figures 12.10 to 12.12)

Sample source	Grain number	Point number	Oxide weight % MgO	Al2O3	SiO2	TiO2	Cr2O3	MnO	FeO	NiO	ZnO	Pt %
SP2	63	1	9.28	11.85	0.00	0.53	44.02	0.56	29.07	0.10	0.21	0.000
		2	9.60	11.78	0.00	0.46	45.13	0.54	28.67	0.14	0.30	0.000
		3	9.71	11.53	0.00	0.50	45.04	0.49	28.40	0.11	0.20	0.000
		4	9.82	11.55	0.02	0.45	45.46	0.56	28.00	0.15	0.19	0.000
		5	9.81	11.57	0.00	0.45	45.60	0.50	28.25	0.04	0.04	0.000
		6	9.81	11.65	0.00	0.50	45.45	0.47	28.05	0.10	0.27	0.000
		7	9.85	11.67	0.01	0.46	45.34	0.66	28.04	0.05	0.10	0.000
		8	9.87	11.73	0.00	0.48	45.48	0.56	27.94	0.00	0.10	0.000
		9	9.72	11.62	0.00	0.45	45.32	0.55	27.88	0.07	0.16	0.000
		10	9.66	11.69	0.01	0.48	45.16	0.51	28.20	0.15	0.16	0.000
SP2	64	1	9.25	9.50	0.03	0.42	45.41	0.47	30.90	0.11	0.16	0.004
		2	9.17	9.33	0.04	0.45	45.06	0.58	31.24	0.08	0.00	0.000
		3	9.27	9.32	0.02	0.40	45.74	0.46	30.68	0.13	0.00	0.000
		4	9.96	9.88	0.02	0.43	47.08	0.50	28.31	0.14	0.10	0.000
		5	10.16	9.81	0.00	0.46	47.19	0.55	27.95	0.11	0.18	0.000
		6	10.02	9.64	0.03	0.40	47.10	0.46	27.39	0.07	0.13	0.000
		7	10.06	9.80	0.01	0.45	46.88	0.62	27.79	0.15	0.13	0.000
		8	9.96	9.75	0.00	0.50	46.98	0.43	27.74	0.12	0.16	0.000
		9	10.02	9.85	0.00	0.47	47.24	0.44	27.79	0.04	0.16	0.000
		10	9.98	9.86	0.00	0.45	47.18	0.38	27.74	0.15	0.00	0.000
SP2	65	1	9.55	11.83	0.00	0.49	44.58	0.55	29.46	0.04	0.08	0.000
		2	9.56	11.36	0.02	0.46	44.06	0.58	29.76	0.02	0.15	0.000
		3	9.89	11.22	0.01	0.48	45.03	0.45	28.55	0.11	0.10	0.000
		4	10.03	11.20	0.02	0.46	45.43	0.48	28.06	0.07	0.29	0.000
		5	10.11	11.04	0.01	0.43	44.93	0.53	28.23	0.07	0.14	0.000
		6	10.33	11.11	0.00	0.49	45.23	0.66	28.01	0.07	0.20	0.000
		7	10.16	11.01	0.02	0.46	45.02	0.52	27.87	0.07	0.12	0.000
		8	10.21	11.05	0.01	0.42	45.37	0.42	27.83	0.08	0.15	0.000
		9	10.23	11.01	0.00	0.45	45.50	0.46	27.27	0.13	0.01	0.000
		10	10.27	10.92	0.02	0.43	45.94	0.50	27.69	0.06	0.12	0.000
SP2	66	1	10.27	10.11	0.05	0.50	47.18	0.35	27.41	0.05	0.16	0.000
		2	10.16	10.02	0.02	0.49	47.14	0.52	27.45	0.10	0.10	0.000
		3	10.29	10.11	0.00	0.49	47.40	0.47	27.01	0.13	0.21	0.000
		4	9.92	9.91	0.03	0.45	46.93	0.56	26.85	0.09	0.16	0.000
		5	10.37	10.06	0.01	0.46	47.42	0.48	27.17	0.07	0.12	0.000
		6	10.17	10.11	0.01	0.45	47.61	0.50	27.41	0.00	0.32	0.000
		7	10.02	9.88	0.00	0.41	47.34	0.43	27.06	0.07	0.04	0.000
		8	10.12	9.91	0.02	0.44	47.55	0.48	26.97	0.00	0.26	0.000
		9	10.10	9.75	0.00	0.49	47.35	0.48	27.04	0.08	0.16	0.000
		10	10.02	9.94	0.00	0.42	47.77	0.41	27.42	0.07	0.00	0.004
SP2	67	1	9.55	10.42	0.00	0.44	45.99	0.57	29.04	0.10	0.20	0.000
		2	9.78	10.20	0.00	0.43	46.49	0.41	28.00	0.03	0.08	0.000
		3	9.95	10.25	0.00	0.43	46.33	0.55	27.75	0.09	0.10	0.000
		4	9.87	10.04	0.02	0.46	46.35	0.56	27.57	0.08	0.12	0.000
		5	10.03	10.01	0.00	0.46	46.41	0.46	27.51	0.07	0.06	0.000
		6	9.98	10.18	0.03	0.44	46.46	0.48	27.55	0.07	0.23	0.000
		7	9.89	10.15	0.02	0.40	46.59	0.41	27.51	0.12	0.13	0.000
		8	9.91	10.25	0.01	0.47	46.67	0.41	27.89	0.05	0.18	0.000
		9	9.93	10.04	0.01	0.46	46.73	0.40	27.72	0.15	0.12	0.000
		10	9.91	10.13	0.03	0.41	46.70	0.47	27.43	0.03	0.10	0.000
SP2	68	1	10.98	11.42	0.00	0.39	45.61	0.42	26.85	0.12	0.04	0.000
		2	9.45	10.72	0.08	0.38	44.14	0.54	30.22	0.10	0.11	0.000
		3	10.67	11.17	0.02	0.45	45.81	0.47	26.74	0.07	0.08	0.000
		4	10.05	10.53	0.05	0.39	45.08	0.39	28.50	0.13	0.00	0.000
		5	10.57	10.82	0.00	0.44	46.22	0.44	26.85	0.12	0.00	0.000
		6	10.56	10.96	0.00	0.46	46.27	0.47	26.40	0.12	0.11	0.000
		7	10.30	10.62	0.09	0.41	45.41	0.44	28.00	0.12	0.01	0.000
		8	10.50	10.83	0.00	0.40	45.85	0.53	26.54	0.15	0.10	0.000
		9	10.51	10.82	0.00	0.45	46.08	0.47	26.44	0.13	0.07	0.000
		10	10.54	10.79	0.00	0.45	46.26	0.48	26.47	0.17	0.18	0.000

Appendix D

SP5A and SP2 Chromite line analysis results

(Points are numbered from the left of grain, with grains oriented as for figures 12.10 to 12.12)

Sample source	Grain number	Point number	Oxide weight % MgO	Al2O3	SiO2	TiO2	Cr2O3	MnO	FeO	NiO	ZnO	Pt %
SP2	69	1	10.58	11.14	0.01	0.40	45.57	0.40	27.71	0.12	0.18	0.031
		2	10.40	11.03	0.00	0.44	45.83	0.55	27.51	0.05	0.14	0.000
		3	10.51	10.84	0.00	0.45	45.83	0.50	27.68	0.15	0.11	0.000
		4	10.37	10.90	0.23	0.42	45.82	0.53	27.11	0.15	0.21	0.000
		5	10.38	10.90	0.01	0.40	45.81	0.49	27.43	0.10	0.27	0.000
		6	10.19	10.56	0.00	0.39	45.73	0.46	27.69	0.19	0.14	0.000
		7	10.20	10.89	0.00	0.41	46.02	0.38	27.74	0.15	0.10	
		8	8.64	9.95	0.05	0.42	43.76	0.54	31.88	0.12	0.20	
		9	10.10	10.80	0.02	0.43	45.87	0.30	27.68	0.17	0.15	
		10	9.92	10.69	0.00	0.42	45.69	0.45	27.78	0.11	0.10	
SP2	70	1	9.38	11.28	0.01	0.48	44.51	0.34	29.23	0.07	0.11	0.000
		2	9.01	11.39	0.04	0.44	44.08	0.61	28.50	0.12	0.19	0.000
		3	8.10	10.21	0.01	0.49	44.88	0.52	29.34	0.00	0.16	0.000
		4	9.51	11.18	0.02	0.47	44.76	0.47	28.69	0.07	0.14	0.000
		5	9.64	11.23	0.00	0.47	44.69	0.52	29.02	0.12	0.16	0.000
		6	9.50	11.09	0.00	0.49	44.47	0.46	29.16	0.15	0.24	0.000
		7	8.82	10.52	0.04	0.44	43.60	0.51	30.79	0.10	0.13	0.000
		8	9.56	11.11	0.08	0.46	44.37	0.39	28.73	0.08	0.18	0.000
		9	9.40	11.25	0.02	0.46	44.62	0.52	28.75	0.09	0.10	0.000
		10	9.11	10.89	0.01	0.46	44.78	0.68	29.48	0.04	0.15	0.000
SP2	71	1	9.85	10.01	0.00	0.47	47.32	0.58	28.09	0.05	0.16	0.000
		2	9.95	10.21	0.01	0.47	46.96	0.31	27.62	0.11	0.13	0.001
		3	10.04	10.35	0.02	0.42	47.39	0.63	27.87	0.09	0.20	0.000
		4	9.80	10.15	0.00	0.45	47.47	0.46	27.81	0.08	0.03	0.000
		5	10.06	10.10	0.00	0.41	46.63	0.46	27.26	0.20	0.10	0.000
		6	10.03	9.92	0.00	0.47	46.86	0.49	27.71	0.14	0.14	0.000
		7	9.93	9.83	0.01	0.45	46.89	0.47	27.99	0.05	0.19	0.000
		8	10.03	9.92	0.00	0.52	47.07	0.48	27.66	0.08	0.06	0.001
		9	9.81	9.86	0.00	0.44	47.15	0.44	27.61	0.10	0.14	0.000
		10	9.80	9.91	0.01	0.47	47.00	0.60	27.98	0.18	0.00	0.000
SP2	72	1	10.33	11.09	0.02	0.43	45.60	0.66	27.97	0.19	0.24	0.000
		2	10.40	10.98	0.00	0.48	45.79	0.53	28.19	0.12	0.30	0.007
		3	10.34	11.08	0.00	0.47	46.38	0.33	28.03	0.20	0.01	0.000
		4	10.33	10.88	0.00	0.47	45.96	0.56	28.08	0.16	0.03	0.000
		5	10.38	10.73	0.00	0.42	46.41	0.50	27.98	0.17	0.15	0.000
		6	10.15	10.83	0.01	0.44	46.04	0.42	27.76	0.08	0.00	0.000
		7	10.26	10.69	0.00	0.43	45.95	0.54	27.50	0.14	0.11	0.000
		8	10.31	10.76	0.00	0.45	46.53	0.43	27.70	0.19	0.07	0.000
		9	10.40	10.74	0.00	0.40	46.46	0.45	27.68	0.08	0.17	0.000
		10	10.35	10.73	0.01	0.43	45.81	0.47	27.69	0.10	0.14	0.005
SP2	73	1	11.16	10.72	0.00	0.40	45.94	0.47	26.73	0.02	0.08	0.002
		2	10.86	10.61	0.04	0.40	46.09	0.37	26.44	0.17	0.06	0.000
		3	10.90	10.77	0.01	0.40	46.35	0.56	26.29	0.09	0.00	0.000
		4	10.81	10.61	0.00	0.40	46.41	0.58	26.48	0.16	0.00	0.000
		5	10.78	10.55	0.01	0.39	46.20	0.40	26.79	0.08	0.09	0.016
		6	10.79	10.56	0.00	0.41	46.60	0.46	26.28	0.13	0.03	0.001
		7	10.80	10.52	0.00	0.39	46.68	0.54	26.57	0.10	0.19	0.000
		8	10.71	10.44	0.00	0.42	46.76	0.44	26.91	0.13	0.29	0.000
		9	10.78	10.55	0.00	0.44	46.24	0.43	26.24	0.14	0.11	0.000
		10	10.72	10.37	0.04	0.40	46.83	0.40	26.59	0.14	0.02	0.000
SP2	74	1	10.37	10.11	0.02	0.47	46.77	0.30	27.60	0.04	0.02	0.000
		2	10.34	10.03	0.00	0.43	47.24	0.39	27.29	0.09	0.16	0.000
		3	10.40	10.04	0.04	0.46	47.68	0.42	27.05	0.13	0.17	0.000
		4	10.33	10.02	0.02	0.42	46.94	0.43	27.01	0.16	0.30	0.000
		5	10.24	9.79	0.04	0.37	47.30	0.46	26.70	0.12	0.32	0.000
		6	10.38	9.85	0.00	0.44	46.97	0.60	27.25	0.03	0.07	0.000
		7	10.27	9.75	0.01	0.42	47.31	0.57	27.00	0.10	0.07	0.000
		8	10.19	9.83	0.00	0.47	47.52	0.51	27.23	0.10	0.06	0.008
		9	10.15	9.82	0.02	0.43	47.35	0.30	26.98	0.03	0.12	0.279
		10	10.35	9.86	0.00	0.43	48.12	0.46	27.62	0.11	0.07	0.000

Appendix D

SP5A and SP2 Chromite line analysis results

(Points are numbered from the left of grain, with grains oriented as for figures 12.10 to 12.12)

Sample source	Grain number	Point number	Oxide weight % MgO	Al2O3	SiO2	TiO2	Cr2O3	MnO	FeO	NiO	ZnO	Pt %
SP2	75	1	10.82	9.86	0.00	0.38	48.68	0.57	26.19	0.11	0.17	0.001
		2	10.81	9.74	0.01	0.39	48.30	0.45	26.48	0.07	0.19	0.002
		3	10.79	9.73	0.04	0.41	48.39	0.31	26.30	0.04	0.22	0.000
		4	10.61	9.62	0.01	0.41	48.39	0.32	26.72	0.06	0.28	0.000
		5	10.59	9.63	0.00	0.43	48.32	0.40	25.98	0.14	0.09	0.000
		6	10.39	9.74	0.00	0.42	48.46	0.35	26.17	0.13	0.00	0.000
		7	10.52	9.88	0.00	0.39	48.50	0.50	26.39	0.10	0.12	0.000
		8	10.41	9.69	0.00	0.40	47.96	0.44	26.41	0.11	0.00	0.000
		9	10.46	9.69	0.00	0.44	48.17	0.53	26.46	0.07	0.11	0.000
		10	10.27	9.69	0.01	0.40	48.03	0.47	26.81	0.10	0.24	0.005

Appendix E

Mapping of SP2 Chromite grain No. 74

(In figures 12.10 to 12.12, lines are numbered from the top, and points are numbered from the left)

Line Number	Point Number	Oxide weight % MgO	Al2O3	SiO2	TiO2	Cr2O3	MnO	FeO	NiO	ZnO
1	1	10.93	10.74	0.00	0.49	48.58	0.34	27.93	0.11	0.05
	2	10.74	10.54	0.10	0.46	48.65	0.41	27.78	0.08	0.09
	3	10.62	10.51	0.02	0.44	48.68	0.43	27.46	0.10	0.22
	4	10.74	10.54	0.00	0.43	48.42	0.50	27.94	0.14	0.12
	5	10.57	10.48	0.01	0.47	48.70	0.41	27.78	0.06	0.16
	6	10.37	10.47	0.00	0.45	48.64	0.36	27.43	0.07	0.10
	7	10.44	10.43	0.05	0.39	48.77	0.38	27.64	0.09	0.00
	8	10.49	10.27	0.01	0.43	48.69	0.36	27.63	0.10	0.25
	9	10.41	10.41	0.00	0.45	48.74	0.42	27.73	0.11	0.08
	10	10.05	10.26	0.02	0.47	48.72	0.42	28.04	0.07	0.13
	11	10.16	10.44	0.02	0.49	48.86	0.46	27.69	0.04	0.07
2	1	10.89	10.63	0.03	0.47	49.17	0.44	27.63	0.10	0.18
	2	10.82	10.61	0.02	0.47	48.97	0.37	26.95	0.07	0.11
	3	10.76	10.65	0.00	0.45	48.75	0.45	27.23	0.09	0.16
	4	10.57	10.44	0.04	0.43	48.64	0.34	27.24	0.08	0.09
	5	10.45	10.38	0.00	0.42	49.12	0.38	27.43	0.09	0.18
	6	10.47	10.39	0.03	0.46	49.23	0.48	27.28	0.10	0.09
	7	10.44	10.26	0.00	0.47	48.80	0.39	27.84	0.12	0.07
	8	10.50	10.26	0.00	0.45	49.43	0.40	27.25	0.15	0.14
	9	10.43	10.39	0.00	0.46	49.06	0.38	27.00	0.12	0.09
	10	10.41	10.31	0.00	0.43	48.99	0.40	27.20	0.07	0.06
	11	10.26	10.09	0.01	0.46	48.88	0.39	28.34	0.10	0.08
3	1	10.73	10.62	0.03	0.46	49.13	0.41	27.69	0.11	0.06
	2	10.58	10.36	0.09	0.46	48.58	0.36	26.90	0.11	0.15
	3	10.40	10.44	0.01	0.42	48.90	0.41	27.35	0.08	0.16
	4	10.62	10.37	0.14	0.45	48.89	0.35	27.01	0.07	0.12
	5	10.70	10.38	0.07	0.44	49.12	0.37	27.07	0.13	0.11
	6	10.51	10.28	0.00	0.49	49.21	0.39	27.09	0.10	0.14
	7	10.61	10.27	0.02	0.44	49.49	0.39	26.87	0.07	0.15
	8	10.48	10.43	0.02	0.44	49.09	0.39	27.18	0.07	0.19
	9	10.47	10.20	0.00	0.42	48.98	0.41	27.19	0.12	0.10
	10	10.49	10.26	0.01	0.45	48.80	0.39	27.68	0.08	0.10
	11	10.02	10.17	0.03	0.45	48.52	0.42	28.27	0.07	0.18
4	1	10.88	10.54	0.02	0.46	49.46	0.39	27.41	0.14	0.16
	2	10.81	10.59	0.00	0.46	49.06	0.34	27.21	0.07	0.07
	3	10.77	10.43	0.01	0.48	48.91	0.33	27.41	0.07	0.05
	4	10.52	10.43	0.03	0.50	49.11	0.40	26.60	0.12	0.11
	5	10.70	10.32	0.01	0.45	49.00	0.37	26.96	0.08	0.18
	6	10.61	10.18	0.00	0.45	49.15	0.44	26.82	0.14	0.09
	7	10.51	10.40	0.00	0.43	49.21	0.38	26.75	0.11	0.18
	8	10.52	10.30	0.03	0.44	49.56	0.36	27.01	0.13	0.28
	9	10.66	10.37	0.02	0.43	48.79	0.46	27.24	0.12	0.04
	10	10.49	10.24	0.06	0.45	49.13	0.37	26.81	0.13	0.14
	11	10.38	10.10	0.01	0.44	48.80	0.37	27.75	0.11	0.12
5	1	10.73	10.50	0.03	0.41	48.80	0.31	27.31	0.11	0.18
	2	10.71	10.52	0.01	0.45	48.73	0.43	27.14	0.08	0.17
	3	10.61	10.36	0.00	0.42	48.80	0.35	26.87	0.14	0.16
	4	10.77	10.41	0.00	0.44	49.17	0.40	27.09	0.12	0.14
	5	10.69	10.38	0.03	0.40	49.35	0.39	27.08	0.05	0.23
	6	10.60	10.28	0.03	0.41	49.14	0.37	26.83	0.13	0.03
	7	10.41	10.43	0.00	0.44	49.19	0.38	27.13	0.07	0.14
	8					49.33				
	9					49.38				
	10					49.34				
	11					48.51				

Appendix E

Mapping of SP2 Chromite grain No. 74

(In figures 12.10 to 12.12, lines are numbered from the top, and points are numbered from the left)

Line Number	Point Number	Oxide weight % MgO	Al2O3	SiO2	TiO2	Cr2O3	MnO	FeO	NiO	ZnO
6	1	10.54	10.19	0.02	0.49	48.93	0.35	26.93	0.09	0.27
	2	10.48	10.26	0.03	0.44	48.88	0.39	26.69	0.06	0.13
	3	10.57	10.12	0.08	0.40	48.83	0.36	26.99	0.05	0.16
	4	10.41	10.10	0.02	0.45	48.71	0.33	26.80	0.04	0.14
	5	10.51	10.04	0.00	0.43	48.53	0.43	26.42	0.10	0.10
	6	10.54	10.04	0.01	0.45	48.52	0.42	26.73	0.12	0.11
	7	10.52	9.91	0.01	0.44	48.86	0.38	26.64	0.11	0.14
	8	10.41	9.89	0.01	0.47	48.52	0.42	26.77	0.07	0.17
	9	10.28	9.94	0.02	0.49	48.85	0.44	26.71	0.11	0.09
	10	10.39	9.97	0.02	0.40	48.54	0.36	26.43	0.07	0.12
	11	10.09	9.82	0.00	0.40	48.53	0.33	27.50	0.05	0.11
7	1	10.59	10.30	0.02	0.42	48.71	0.35	26.51	0.08	0.09
	2	10.50	10.18	0.02	0.44	49.06	0.32	27.13	0.11	0.17
	3	10.53	10.14	0.02	0.44	49.32	0.38	27.11	0.09	0.20
	4	10.35	10.13	0.02	0.39	49.23	0.48	27.05	0.04	0.10
	5	10.36	10.08	0.01	0.39	48.64	0.50	26.66	0.09	0.11
	6	10.42	10.04	0.02	0.45	49.20	0.47	26.68	0.12	0.15
	7	10.46	10.06	0.05	0.45	49.27	0.40	26.67	0.08	0.18
	8	10.26	10.06	0.00	0.43	48.73	0.43	26.82	0.10	0.09
	9	10.02	9.87	0.03	0.46	48.67	0.45	26.95	0.11	0.18
	10	10.26	9.88	0.04	0.44	48.74	0.37	27.23	0.07	0.10
	11	10.20	9.98	0.03	0.45	49.14	0.35	27.10	0.09	0.15
8	1	10.19	10.22	0.00	0.43	48.60	0.38	27.52	0.05	0.22
	2	10.31	10.16	0.03	0.44	48.39	0.39	27.39	0.05	0.10
	3	10.71	10.04	0.37	0.45	47.98	0.42	27.12	0.07	0.11
	4	10.24	9.99	0.12	0.42	48.51	0.41	27.08	0.09	0.14
	5	10.39	9.98	0.01	0.43	48.71	0.43	27.27	0.09	0.04
	6	10.40	9.97	0.01	0.40	49.07	0.29	26.68	0.09	0.14
	7	10.40	9.95	0.02	0.44	48.77	0.32	26.95	0.12	0.07
	8	10.29	10.09	0.04	0.45	48.84	0.33	26.70	0.13	0.10
	9	10.39	9.99	0.04	0.47	48.88	0.43	26.67	0.11	0.10
	10	10.34	9.93	0.02	0.43	48.91	0.39	26.89	0.11	0.09
	11	10.43	9.95	0.02	0.44	48.69	0.35	26.19	0.06	0.11
9	1					48.14				
	2					48.80				
	3					49.19				
	4					49.25				
	5					49.55				
	6					49.82				
	7					49.44				
	8					48.81				
	9					49.56				
	10					49.47				
	11					49.47				
10	1					48.25				
	2					48.40				
	3					49.26				
	4					48.95				
	5					48.56				
	6					48.71				
	7					49.52				
	8					49.58				
	9					49.42				
	10					49.62				

Appendix E

Compositional Mapping of SP2 chromite grain 60

(in figures 12.10 to 12.12, lines are numbered from the top and points are numbered from the left)

Line Number	Point Number	Oxide weight % MgO	Al2O3	SiO2	TiO2	Cr2O3	MnO	FeO	NiO	ZnO
1	1	10.65	9.69	0.47	0.44	48.00	0.45	27.14	0.01	0.22
	2	10.74	10.01	0.00	0.42	48.93	0.36	26.59	0.06	0.13
	3	10.10	9.71	0.00	0.42	48.33	0.46	27.28	0.10	0.04
	4	5.47	5.57	0.94	0.27	35.68	0.95	45.29	0.20	0.32
	5	8.15	7.62	0.62	0.31	40.99	0.65	37.19	0.08	0.12
	6	5.80	6.14	0.91	0.29	37.74	0.69	41.54	0.13	0.31
	7	6.81	7.06	1.01	0.30	39.40	0.81	38.62	0.17	0.28
	8	7.87	7.47	1.03	0.29	39.37	0.76	38.14	0.10	0.30
	9	6.54	6.02	1.58	0.25	34.36	0.71	44.19	0.13	0.24
	10	5.39	6.45	0.23	0.30	38.55	1.01	42.86	0.20	0.21
	11	8.81	8.73	0.36	0.32	45.38	0.58	31.96	0.16	0.23
2	1	11.07	10.07	0.01	0.47	49.21	0.43	25.74	0.07	0.20
	2	10.99	10.14	0.01	0.38	49.46	0.30	26.00	0.08	0.02
	3	10.79	9.75	0.00	0.46	49.25	0.32	26.15	0.10	0.13
	4	6.52	6.80	0.86	0.28	38.31	0.89	40.52	0.16	0.32
	5	10.05	9.54	0.03	0.41	48.38	0.44	27.55	0.08	0.13
	6	9.67	7.54	2.95	0.31	36.86	0.64	36.35	0.14	0.16
	7	6.50	6.65	0.52	0.30	38.71	0.71	41.26	0.18	0.25
	8	7.87	7.92	0.43	0.35	41.43	0.62	36.63	0.19	0.15
	9	7.53	8.63	0.13	0.41	44.61	0.77	34.17	0.16	0.20
	10	6.04	6.37	0.46	0.29	37.76	0.63	41.97	0.14	0.21
	11	7.22	8.17	0.10	0.34	43.71	0.78	35.54	0.04	0.26
3	1	10.44	9.91	0.36	0.39	48.49	0.51	27.38	0.10	0.12
	2	10.93	10.05	0.00	0.44	49.62	0.37	25.82	0.01	0.05
	3	10.54	9.60	0.30	0.43	48.52	0.38	26.59	0.08	0.06
	4	7.61	7.38	0.79	0.34	40.54	0.76	38.06	0.14	0.21
	5	10.24	8.15	2.03	0.30	41.07	0.50	32.25	0.18	0.14
	6	7.91	7.20	0.83	0.33	39.77	0.64	37.50	0.07	0.18
	7	7.90	6.59	1.63	0.32	35.81	0.61	41.41	0.11	0.13
	8	8.15	8.00	0.95	0.30	42.25	0.81	35.30	0.11	0.23
	9	5.71	6.79	0.54	0.27	39.74	1.09	40.77	0.22	0.32
	10	6.74	7.17	0.16	0.34	41.10	0.74	39.59	0.17	0.17
	11	4.94	6.51	0.12	0.30	38.93	1.01	43.02	0.17	0.31
4	1	10.10	9.49	0.34	0.38	46.79	0.51	29.10	0.14	0.12
	2	9.50	9.29	0.18	0.37	46.96	0.56	29.88	0.09	0.09
	3	9.49	9.46	0.35	0.39	47.72	0.53	28.12	0.10	0.00
	4	8.98	8.43	0.51	0.34	44.32	0.51	32.22	0.12	0.15
	5	8.15	7.55	0.39	0.28	40.24	0.57	37.91	0.20	0.09
	6	7.07	7.50	0.35	0.29	40.70	0.83	38.33	0.14	0.21
	7	10.82	7.81	2.90	0.32	39.65	0.51	33.44	0.08	0.15
	8	6.37	6.96	0.28	0.30	39.33	0.84	40.77	0.14	0.20
	9	6.45	6.44	1.16	0.26	36.80	0.80	42.28	0.18	0.21
	10	7.30	7.19	0.89	0.35	41.18	0.80	37.65	0.13	0.19
	11	6.75	6.76	0.32	0.26	39.84	0.84	40.46	0.13	0.32
5	1	9.88	9.29	0.68	0.36	46.32	0.56	29.07	0.12	0.18
	2	8.23	8.55	0.24	0.35	44.63	0.74	33.17	0.13	0.15
	3	10.76	9.90	0.03	0.46	49.21	0.39	25.97	0.08	0.11
	4	10.72	9.93	0.00	0.42	49.15	0.39	26.01	0.08	0.15
	5	5.85	5.49	1.25	0.27	33.65	0.77	46.31	0.19	0.13
	6	8.60	7.28	1.74	0.29	38.02	0.59	38.01	0.20	0.21
	7	7.05	7.23	0.63	0.26	39.09	0.68	40.02	0.21	0.26
	8	8.09	6.96	1.50	0.29	38.35	0.66	38.62	0.15	0.24
	9	5.43	6.32	0.27	0.30	37.80	0.90	43.79	0.18	0.32
	10	7.61	8.34	0.36	0.37	43.60	0.76	34.83	0.20	0.20
	11	9.96	9.20	0.17	0.39	46.62	0.54	29.28	0.12	0.23

Appendix E

Mapping of SP2 chromite grain 60

(in figures 12.10 to 12.12, lines are numbered from the top and points are numbered from the left)

Line Number	Point Number	Oxide weight % MgO	Al2O3	SiO2	TiO2	Cr2O3	MnO	FeO	NiO	ZnO
6	1	10.33	9.53	0.08	0.40	47.56	0.51	28.50	0.15	0.11
	2	10.48	9.67	0.07	0.40	47.98	0.39	27.61	0.04	0.09
	3	10.39	9.41	0.63	0.34	47.35	0.48	27.65	0.14	0.17
	4	10.43	9.83	0.03	0.40	48.47	0.46	26.71	0.07	0.11
	5	8.67	8.33	0.49	0.34	43.26	0.53	34.39	0.14	0.15
	6	5.82	5.83	0.81	0.26	36.67	0.85	43.29	0.22	0.21
	7	5.29	6.04	0.41	0.27	36.13	0.86	45.17	0.15	0.45
	8	6.04	6.88	0.18	0.30	39.73	0.92	41.83	0.17	0.27
	9	6.08	7.09	0.13	0.32	40.97	0.96	39.64	0.13	0.16
	10	8.53	7.65	1.52	0.29	40.13	0.66	36.35	0.18	0.22
	11	8.84	8.46	0.06	0.37	44.79	0.62	33.04	0.09	0.19
7	1	8.40	8.27	0.67	0.31	42.64	0.72	34.63	0.14	0.26
	2	8.84	8.73	0.41	0.37	45.76	0.62	31.53	0.09	0.26
	3	10.65	9.51	0.55	0.42	47.78	0.46	27.36	0.11	0.21
	4	9.22	8.17	0.99	0.39	43.10	0.60	32.65	0.11	0.24
	5	7.68	7.21	0.68	0.32	39.49	0.58	39.20	0.11	0.09
	6	6.34	7.29	0.27	0.34	40.93	0.76	38.66	0.13	0.31
	7	6.35	7.13	0.11	0.32	41.21	0.87	39.21	0.17	0.31
	8	6.75	6.33	1.49	0.26	36.81	0.84	41.17	0.15	0.28
	9	6.86	7.27	0.05	0.29	41.08	0.72	39.04	0.14	0.25
	10	10.94	8.52	2.35	0.33	42.48	0.45	29.47	0.19	0.06
	11	6.87	7.33	0.27	0.37	40.44	0.75	39.06	0.09	0.20
8	1	11.01	10.13	0.01	0.44	48.95	0.37	26.14	0.08	0.12
	2	10.18	9.69	0.14	0.41	47.98	0.44	27.78	0.08	0.00
	3	10.27	9.68	0.35	0.39	48.17	0.45	27.57	0.06	0.10
	4	6.04	6.53	0.46	0.28	38.25	0.70	41.91	0.16	0.33
	5	7.42	7.91	0.16	0.36	42.20	0.79	36.28	0.19	0.19
	6	10.30	9.69	0.01	0.41	48.51	0.43	27.13	0.09	0.13
	7	6.03	6.46	0.32	0.31	38.01	0.72	43.35	0.21	0.23
	8	6.98	7.53	0.34	0.35	41.98	0.81	37.31	0.17	0.31
	9	6.38	6.16	1.05	0.22	36.23	0.93	43.54	0.13	0.29
	10	6.87	6.64	1.08	0.33	37.27	0.72	40.92	0.28	0.16
	11	6.42	7.01	0.23	0.29	40.72	0.81	39.86	0.19	0.21
9	1	10.58	9.71	0.08	0.41	47.80	0.41	27.66	0.16	0.11
	2	9.37	9.32	0.26	0.37	46.93	0.49	29.68	0.09	0.15
	3	8.81	8.44	0.36	0.40	43.37	0.53	33.55	0.13	0.19
	4	8.19	7.10	1.63	0.32	38.84	0.75	37.96	0.16	0.25
	5	8.62	6.54	2.71	0.29	35.56	0.70	39.21	0.14	0.07
	6	10.28	7.36	3.09	0.29	37.86	0.71	35.80	0.12	0.27
	7	5.91	6.31	0.69	0.30	38.16	0.90	42.10	0.17	0.40
	8	6.89	7.10	0.48	0.26	39.73	0.76	39.51	0.10	0.31
	9	7.99	6.51	2.06	0.30	35.76	0.67	40.84	0.16	0.11
	10	7.39	7.38	0.92	0.29	40.90	0.77	37.25	0.09	0.35
	11	4.81	6.12	0.09	0.31	39.11	1.03	43.51	0.18	0.28

Appendix F

Qualitative observations of garnet rotations

Garnet particle number	Particle size (um)	Type of rotation: with field	Type of rotation: perp. field	Comment
CRA4-1	400-500			no rotation
CRA4-2	400-500			no rotatio
CRA4-3	400-500			no rotation. At 22 hz particle vibrates up & down tube
CRA4-4	400-500			No continuous rotation. Only 180 degree nodding at 22 & 72 hz.
CRA4-5	400-500			No rotation
CRA4-6	400-500			No rotation
CRA4-7	400-500	yes (20 hz)		Rotation becomes too weak to continue above about 20 hz.
CRA4-8	400-500			No rotation. Particle adopts different orientation at different frequencies
CRA4-9	400-500			No rotation
CRA4-10	400-500	yes (5 hz)		Below 5 hz (hand rotation of drum), particle rotates with field.
CRA4-11	400-500			no rotation
CRA4-12	400-500			No rotation
CRA4-13	400-500			No rotation. Some tendency shown when particle rising or falling.
CRA4-14	400-500			No rotation
CRA4-15	400-500			No rotation
CRA4-16	400-500	yes (30 hz)		Rotation becomes too weak to continue above about 30 hz.
CRA4-17	400-500			No rotation
CRA4-18	400-500	yes (30 hz)		Rotation becomes too weak to continue above about 30 hz.
CRA4-19	400-500			No rotation
CRA4-20	400-500			No rotation
CRA4-21	400-500			No rotation
CRA4-22	400-500	yes (10 hz)		Rotation becomes too weak to continue above about 10 hz
CRA4-23	400-500			No rotation
CRA4-24	400-500			No rotation
CRA4-25	400-500			No rotation
CRA4-26	400-500			No rotation
CRA4-27	400-500			No rotation
CRA4-28	400-500			No rotation
CRA4-29	400-500			No rotation
CRA4-30	400-500			No rotation
Alm-1	800-1000		yes (25 hz)	Continuous rotation strength and direction seem to depend on off-vertical field gradient. Rotation ceases above about 25 Hz
Alm-2	800-1000		yes (25 hz)	Continuous rotation strength seems to depend on off-vertical field gradient. Rotation ceases above about 25 Hz.
CRAB-31	1000-1200			No rotation
CRAB-32	1000-1200		yes (25 hz)	Easier to get rotation with off-vertical field gradient. Rotation ceases above about 25 Hz
CRAB-33	1000-1200	yes (30 hz)		Rotation becomes too weak to continue above about 30 hz.
CRAB-34	1000-1200	yes (75hz)		Roation becomes too weak to continue above 75 hz.
CRAB-35	1000-1200			No rotation
CRAB-36	1000-1200	yes (75 & >100 hz)		Rotation at field frequency drops out at 75 hz & replaced by slower rotation.
CRAA-37	600-800		yes (25 hz)	Weak rotation for off-vertical gradient. Only nodding for vertical gradient. Rotation ceases above about 25 Hz.
CRAA-38	600-800			No rotation
CRAA-39	600-800			No rotation. Particle was composite pink & orange.
CRAA-40	600-800			No rotation
CRAA-41	600-800			No rotation
CRAA-42	600-800		yes (24 hz)	Very weak rotation & difficult to get going. No difference for off-vertical gradient. Roation ceases above about 24 Hz.
UTG-A1				No rotation
UTG-A2		yes (8 hz & 25 hz)		Rotation at field frequency below 8 hz. Rotation slows above 8 hz & drops out at 25 hz.
UTG-B1				No rotation
UTG-B2				No rotation
CRAC-A1	300-425		yes	Rotation perpendicular to field very weak. Cessation frequency too indeterminant to estimate.
CRA4-A1	400-500			No rotation
CRAC-A2	300-425			No rotation
CRA4-A2	400-500			No rotation
CRA4-A3	400-500		yes	Very weak rotation. Uncertain cessation frequency.
BHG-A1	212-300			No rotation
BHG-A2	212-300			No rotation
BHG-A3	212-300			No rotation

Appendix G

Garnet rotation observations & lift fields, and analysis results

Sample source	Grain number	Perpendicular rotation comment	Oxide weight %									Lifting field (T)		Rotation field (T)		Mag. Susceptibility (SI)		Paramagnetic rotation index	
			MgO	Al2O3	SiO2	CaO	TiO2	Cr2O3	MnO	FeO	ZnO	10Hz	57Hz	10Hz	57Hz	10Hz	57Hz	10Hz	57Hz
CRA Sample B	1	weak perp. 25-35 Hz	6.68	21.16	36.74	1.86	0.00	0.06	2.07	31.69	0.00	0.3195	0.3195	-	-	6.9E-07	6.9E-07	-	-
	2	Weak perp. 25-35 Hz	6.49	20.93	36.92	0.93	0.00	0.00	1.57	32.70	0.03	0.3195	0.3195	-	-	6.9E-07	6.9E-07	-	-
	3	Weak perp. 25-30 Hz	6.70	21.09	36.74	1.07	0.03	0.04	1.39	32.43	0.00	0.3195	0.3195	-	-	6.9E-07	6.9E-07	-	-
	4	Weak perp. 25-30 Hz	4.47	20.48	36.06	2.19	0.01	0.03	1.85	34.09	0.05	0.3012	0.3012	-	-	7.8E-07	7.8E-07	-	-
	5	None	3.97	20.70	36.26	2.41	0.00	0.00	3.22	34.41	0.02	0.3012	0.3012	-	-	7.8E-07	7.8E-07	-	-
	6	Weak perp. 35-40 Hz	5.29	20.65	36.60	4.74	0.03	0.09	10.87	22.65	0.00	0.3158	0.3195	-	-	7.1E-07	6.9E-07	-	-
	7	Weak perp. 29-45 Hz	6.67	21.07	36.90	1.40	0.00	0.07	1.51	32.06	0.03	0.3310	0.3310	-	-	6.5E-07	6.5E-07	-	-
	8	Par. & Weak perp. 10-40 Hz	5.38	20.84	36.62	1.36	0.01	0.04	1.55	33.94	0.05	0.3012	0.3012	0.2942	-	7.8E-07	7.8E-07	0.001	-
	9	Weak perp. 10-30 and 35-60	6.29	20.74	36.67	1.41	0.03	0.00	1.43	32.97	0.03	0.3195	0.3195	-	-	6.9E-07	6.9E-07	-	-
	10	Weak perp. at 50 Hz	8.32	21.31	37.39	3.09	0.03	0.00	1.66	27.62	0.03	0.3389	0.3389	-	-	6.2E-07	6.2E-07	-	-
	11	None	6.90	20.83	36.58	1.17	0.00	0.00	3.04	31.01	0.00	0.3121	0.3195	-	-	7.3E-07	6.9E-07	-	-
	12	Weak perp. 25-35 Hz	6.55	20.90	36.95	1.21	0.03	0.00	1.63	31.93	0.03	0.3121	0.3195	-	-	7.3E-07	6.9E-07	-	-
	13	Weak perp. 25-30 Hz	7.28	21.06	36.97	1.64	0.01	0.00	1.22	31.28	0.00	0.3195	0.3195	-	-	6.9E-07	6.9E-07	-	-
	14	Weak perp. 30-50 Hz	3.87	20.32	35.87	2.58	0.05	0.00	2.61	33.06	0.01	0.3084	0.3084	-	-	7.4E-07	7.4E-07	-	-
	15	Weak perp. 30-40 Hz	6.70	20.97	36.46	1.49	0.01	0.04	1.59	32.10	0.00	0.3084	0.3158	-	-	7.4E-07	7.1E-07	-	-
	16	Nodding only, below 40	5.48	20.57	36.47	1.80	0.03	0.03	2.14	33.18	0.00	0.3158	0.3158	-	-	7.1E-07	7.1E-07	-	-
	17	Weak perp. 20-40 Hz	6.20	20.75	36.28	2.00	0.04	0.03	1.71	31.46	0.00	0.3233	0.3233	-	-	6.8E-07	6.8E-07	-	-
	18	Weak perp. 25-45 Hz	4.23	20.61	36.32	1.62	0.03	0.01	3.08	34.01	0.00	0.3012	0.3012	-	-	7.8E-07	7.8E-07	-	-
	19	Only a hint of perp. at 30 Hz	6.16	20.91	36.70	1.44	0.00	0.00	1.70	32.76	0.00	0.3195	0.3195	-	-	6.9E-07	6.9E-07	-	-
	20	Weak perp. 35-40 &> 50 Hz	6.05	21.00	36.66	3.18	0.00	0.00	12.06	22.06	0.01	0.3158	0.3195	-	-	7.1E-07	6.9E-07	-	-
	21	Some nodding 25-40	5.52	20.84	36.47	1.21	0.00	0.00	2.53	32.95	0.00	0.3121	0.3121	-	-	7.3E-07	7.3E-07	-	-
	22	Some nodding 40-50	6.72	21.19	36.87	1.96	0.03	0.03	1.43	31.20	0.00	0.3195	0.3195	-	-	6.9E-07	6.9E-07	-	-
	23	Weak perp. 35-60 Hz	5.26	20.70	36.16	1.29	0.00	0.00	2.57	33.34	0.00	0.3012	0.3048	-	-	7.8E-07	7.6E-07	-	-
	24	None	3.59	20.37	35.84	1.48	0.00	0.00	4.14	34.49	0.00	0.3012	0.3012	-	-	7.8E-07	7.8E-07	-	-
	25	None	Not	Analysed								0.3389	0.3389	-	-	6.2E-07	6.2E-07	-	-
	26	None	7.13	20.69	37.21	7.21	0.12	0.04	1.30	25.12	0.03	0.3389	0.3389	-	-	6.2E-07	6.2E-07	-	-
	27	None	10.97	21.52	38.19	6.00	0.07	0.00	0.63	21.01	0.00	0.3389	0.3389	-	-	6.2E-07	6.2E-07	-	-
	28	Weak perp. 20-30 Hz	4.30	20.32	36.28	6.12	0.02	0.05	5.89	26.86	0.00	0.3271	0.3233	-	-	6.6E-07	6.8E-07	-	-
	29	None	6.23	20.40	36.69	3.53	0.00	0.10	1.43	30.51	0.03	0.3349	0.3349	-	-	6.3E-07	6.3E-07	-	-
	30	None	10.01	21.44	38.67	6.37	0.00	0.10	0.80	21.95	0.01	0.3389	0.3389	-	-	6.2E-07	6.2E-07	-	-
	31	None	5.27	20.75	37.04	10.02	0.07	0.00	0.72	24.63	0.02	0.3389	0.3389	-	-	6.2E-07	6.2E-07	-	-
	32	Some nodding 35-50	4.98	20.43	36.74	5.34	0.00	0.02	1.88	29.81	0.00	0.3389	0.3389	-	-	6.2E-07	6.2E-07	-	-
	33	Some nodding 20-50	5.46	20.09	36.33	6.42	0.08	0.00	2.17	27.91	0.00	0.3389	0.3389	-	-	6.2E-07	6.2E-07	-	-
	34	Some nodding >20	5.24	20.14	36.77	7.09	0.10	0.07	0.74	28.45	0.04	0.3389	0.3389	-	-	6.2E-07	6.2E-07	-	-
	35	Weak perp. >30 Hz	4.37	20.81	36.54	6.55	0.00	0.22	2.92	28.45	0.06	0.3389	0.3389	-	-	6.2E-07	6.2E-07	-	-
	36	None	4.23	20.44	36.49	6.74	0.05	0.00	1.42	30.43	0.00	0.3389	0.3389	-	-	6.2E-07	6.2E-07	-	-
	37	None	5.98	20.50	36.69	3.17	0.07	0.16	1.54	30.42	0.03	0.3389	0.3389	-	-	6.2E-07	6.2E-07	-	-
	38	none	3.39	20.55	36.63	11.60	0.08	0.00	1.08	25.27	0.01	0.3389	0.3389	-	-	6.2E-07	6.2E-07	-	-
	39	Good perp. 16-60 Hz	Not	Analysed								0.3389	0.3389	-	-	6.2E-07	6.2E-07	-	-
	40	Good perp. 20-50 Hz	5.61	20.67	37.27	8.63	0.10	0.10	0.87	26.97	0.02	0.3389	0.3389	-	-	6.2E-07	6.2E-07	-	-
	41	None	7.13	20.76	37.00	1.43	0.00	0.00	0.98	31.64	0.01	0.3389	0.3389	-	-	6.2E-07	6.2E-07	-	-
	42	Some nodding >30 Hz	5.89	20.22	36.61	6.76	0.06	0.04	1.33	27.50	0.01	0.3389	0.3389	-	-	6.2E-07	6.2E-07	-	-
	43	None	5.53	20.30	36.91	6.85	0.10	0.05	0.84	27.81	0.00	0.3389	0.3389	-	-	6.2E-07	6.2E-07	-	-
	58	None	18.95	20.42	40.34	5.36	0.06	2.79	0.45	9.21	0.00	0.3389	0.3389	-	-	6.2E-07	6.2E-07	-	-
	59	None	19.73	20.96	40.55	4.50	0.02	2.67	0.66	8.83	0.02	0.3389	0.3389	-	-	6.2E-07	6.2E-07	-	-

Sample source	Grain number	Perpendicular rotation comment	Oxide weight %									Lifting field (T)		Rotation field (T)		Mag. Susceptibility (SI)		Paramagnetic rotation index	
			MgO	Al2O3	SiO2	CaO	TiO2	Cr2O3	MnO	FeO	ZnO	10Hz	57Hz	10Hz	57Hz	10Hz	57Hz	10Hz	57Hz
CRA	59	None	19.73	20.96	40.55	4.50	0.02	2.67	0.66	8.83	0.02	0.3389	0.3389	-	-	6.2E-07	6.2E-07	-	-
Sample B	60	None	19.42	18.21	40.25	5.82	0.74	4.69	0.42	7.92	0.00	0.3389	0.3389	-	-	6.2E-07	6.2E-07	-	-
	61	None	19.16	20.21	40.46	5.54	0.07	3.49	0.58	8.51	0.05	0.3389	0.3389	-	-	6.2E-07	6.2E-07	-	-
	62	None	19.91	18.50	40.29	5.49	0.70	4.65	0.47	8.14	0.01	0.3389	0.3389	-	-	6.2E-07	6.2E-07	-	-
	63	None	19.72	19.09	40.75	5.60	0.70	3.70	0.40	8.42	0.01	0.3389	0.3389	-	-	6.2E-07	6.2E-07	-	-
CRA	1		5.08	21.23	36.81	1.60	0.04	0.06	2.74	33.06	0.01								
Sample A	2		4.87	21.43	37.14	1.72	0.00	0.00	2.19	34.05	0.00								
	3		5.46	21.35	37.50	2.22	0.00	0.00	0.98	33.77	0.00								
	4		5.16	21.41	37.62	2.66	0.02	0.03	3.35	31.61	0.04								
	5		4.62	21.56	37.06	2.24	0.00	0.00	3.03	33.07	0.00								
	6		4.83	21.38	37.49	0.97	0.04	0.07	3.01	34.31	0.02								
	7		5.02	21.23	37.46	1.48	0.02	0.05	2.59	34.10	0.00								
	9		6.17	21.48	37.50	1.55	0.02	0.04	2.41	31.90	0.04								
	11		5.46	21.51	37.26	2.51	0.00	0.02	2.02	31.88	0.00								
	12		5.41	21.75	37.15	1.80	0.00	0.00	2.34	32.75	0.00								
	13		3.48	21.06	37.32	2.61	0.00	0.00	3.82	33.70	0.03			No rotation measurements					
	14		5.34	21.45	37.46	2.45	0.00	0.03	2.32	31.84	0.00								
	15		5.15	21.53	37.97	2.26	0.04	0.02	1.16	33.31	0.03								
	16		5.55	21.63	37.47	2.32	0.04	0.00	2.22	32.63	0.00								
	17		3.79	21.13	36.73	1.14	0.02	0.01	2.39	35.78	0.03								
	18		4.40	21.41	37.41	4.64	0.00	0.00	2.40	30.92	0.00								
	19		5.43	21.42	37.59	1.51	0.00	0.05	1.21	34.07	0.00								
	20		3.49	21.04	36.69	2.40	0.01	0.04	4.75	32.91	0.05								
	21		5.64	21.65	37.97	2.46	0.04	0.00	1.49	32.68	0.00								
	22		4.13	21.20	37.12	2.46	0.00	0.01	3.07	33.27	0.01								
	23		3.92	21.20	37.03	1.54	0.02	0.01	2.30	35.91	0.04								
	24		4.46	21.54	37.21	1.97	0.01	0.01	5.58	31.74	0.00								
	25		3.36	21.30	36.87	1.85	0.03	0.00	3.75	35.20	0.00								
	26		5.46	21.75	37.53	3.90	0.00	0.00	1.24	31.20	0.06								
	27		2.89	21.32	37.65	11.94	0.04	0.03	9.03	20.18	0.02								
	28		4.69	21.44	37.40	2.06	0.00	0.00	2.54	33.06	0.00								
	29		4.27	21.28	37.27	2.55	0.00	0.05	3.73	32.63	0.02								
	30		4.94	21.32	37.39	2.12	0.00	0.00	1.97	33.54	0.01								
	31		4.34	21.17	36.92	2.12	0.02	0.00	2.62	33.81	0.00								
	32		5.57	21.44	37.80	2.76	0.00	0.03	2.75	31.25	0.00								
	33		4.26	21.34	37.18	2.20	0.01	0.00	1.77	34.48	0.00								
CRA4-1		none	5.78	21.34	37.41	1.59	0.00	0.03	1.44	33.08	0.00								
CRA4-2		none	5.20	21.36	37.55	4.10	0.00	0.09	2.43	30.55	0.05								
CRA4-3		?	4.93	21.32	37.30	2.01	0.02	0.02	1.57	33.45	0.04								
CRA4-4		?	7.00	21.50	37.82	1.43	0.01	0.00	2.08	31.13	0.01								
CRA4-5		none	7.96	21.69	38.21	3.09	0.01	0.08	1.19	28.85	0.00								
CRA4-6		none	5.71	21.26	37.87	1.96	0.00	0.00	1.58	32.90	0.01								
CRA4-7		Parallel (drop out 20 Hz)	6.13	21.27	37.87	1.73	0.01	0.00	1.64	32.35	0.04								
CRA4-8		?	6.04	21.74	37.62	1.84	0.02	0.00	1.94	32.62	0.06								
CRA4-9		none	6.56	21.50	38.18	3.64	0.04	0.00	2.22	28.56	0.00								
CRA4-10		Parallel (drop out 5 Hz)	6.53	21.43	37.60	2.39	0.04	0.01	1.66	31.39	0.00								
CRA4-11		none	6.84	21.46	38.06	2.40	0.03	0.04	1.82	30.26	0.01								
CRA4-12		none	6.38	21.43	37.82	2.13	0.00	0.01	3.03	30.19	0.00								
CRA4-13		?	5.05	21.21	37.13	3.40	0.02	0.02	2.55	31.54	0.02								
CRA4-14		none	5.97	21.28	37.78	2.01	0.00	0.05	1.67	31.78	0.00								

Sample source	Grain number	Perpendicular rotation comment	Oxide weight %									Lifting field (T)		Rotation field (T)		Mag. Susceptibility (SI)		Paramagnetic rotation index	
			MgO	Al2O3	SiO2	CaO	TiO2	Cr2O3	MnO	FeO	ZnO	10Hz	57Hz	10Hz	57Hz	10Hz	57Hz	10Hz	57Hz
CRA4-15		none	5.31	21.59	37.69	3.80	0.00	0.05	4.30	29.89	0.00								
CRA4-16		Parallel (drop out 30 Hz)	7.40	21.40	38.03	3.01	0.00	0.04	1.51	29.54	0.00								
CRA4-17		none	5.61	21.25	37.80	3.87	0.02	0.00	2.12	31.17	0.00								
CRA4-18		Parallel (drop out 30 Hz)	4.85	21.47	37.44	2.26	0.00	0.00	3.04	32.49	0.00								
CRA4-19		none	5.90	21.33	37.64	2.26	0.02	0.07	2.00	31.02	0.01								
CRA4-20		none	5.93	21.45	37.86	5.58	0.06	0.00	8.19	22.88	0.01								
CRA4-21		none	6.09	21.33	37.60	1.50	0.00	0.02	2.38	32.00	0.05								
CRA4-22		Parallel (drop out 10 Hz)	5.96	21.40	37.84	2.48	0.06	0.00	2.24	31.58	0.00								
CRA4-23		none	7.23	21.59	37.94	1.67	0.00	0.00	1.75	30.57	0.00			No rotation measurements (only observations)					
CRA4-24		none	5.00	21.55	37.22	2.63	0.03	0.01	1.88	32.61	0.01								
CRA4-25		none	4.94	21.48	37.57	4.13	0.01	0.00	2.76	30.70	0.00								
CRA4-26		none	8.34	21.55	38.31	2.62	0.00	0.03	1.19	29.12	0.02								
CRA4-27		none	5.24	21.18	37.58	2.56	0.02	0.06	1.52	33.09	0.00								
CRA4-28		none	6.00	21.43	37.58	1.62	0.02	0.02	2.21	32.29	0.01								
CRA4-29		none	5.15	21.18	37.72	3.61	0.00	0.00	1.93	31.17	0.00								
CRA4-30		none	5.79	21.26	37.66	1.98	0.00	0.00	1.61	33.15	0.02								
CRAB-31		none	5.16	21.23	37.42	2.27	0.00	0.04	2.34	33.60	0.02								
CRAB-32		Good perp. (peak at 25 Hz)	7.05	21.61	37.79	1.20	0.00	0.04	1.14	31.53	0.00								
CRAB-33		Parallel (drop out 30 Hz)	5.53	21.34	37.73	2.82	0.00	0.02	1.98	32.12	0.00								
CRAB-34		Parallel (drop out 75 Hz)	8.78	22.08	38.90	1.52	0.03	0.01	1.29	28.98	0.02								
CRAB-35		none	5.83	21.40	37.65	0.87	0.00	0.07	1.94	32.93	0.00								
CRAB-36		Parallel (drops out at 75 Hz)	6.33	21.15	37.80	1.83	0.00	0.07	2.22	31.91	0.00								
CRAA-37		Good perp (peak at 25 Hz)	5.96	21.36	37.53	2.01	0.00	0.01	1.37	31.94	0.04								
CRAA-38		none	4.04	21.05	36.89	1.50	0.03	0.02	1.55	35.83	0.02								
CRAA39		none	6.33	21.73	38.02	1.64	0.01	0.00	1.79	32.16	0.00								
CRAA-40		none	2.60	21.15	37.50	10.81	0.04	0.02	4.57	24.72	0.00								
CRAA-41		none	6.26	21.43	37.49	1.36	0.00	0.05	1.99	32.22	0.01								
CRAA-42		Good perp. (peak at 25 Hz)	4.93	21.27	37.52	1.97	0.04	0.00	2.11	33.94	0.00								
UTG-A1		none	0.39	20.40	36.31	3.93	0.10	0.00	34.59	12.10	0.02								
UTG-A2		Parallel (drop out 25 Hz)	0.43	20.16	36.33	3.99	0.08	0.03	33.86	11.81	0.06								
UTG-B1		none	0.44	20.10	36.32	4.14	0.07	0.03	34.24	12.22	0.00								
UTG-B2		none	0.39	20.21	36.16	4.06	0.08	0.04	34.14	11.42	0.00								
CRAC-A1		perp (v. weak)	5.76	21.22	37.49	1.09	0.03	0.08	1.45	33.43	0.00								
CRA4-A1		none	7.51	21.53	38.16	1.25	0.02	0.00	1.90	30.91	0.01								
CRAC-A2		none	5.72	21.29	37.44	1.07	0.00	0.05	1.16	34.07	0.00								
CRA4-A2		none	5.03	21.24	37.44	5.47	0.01	0.04	2.64	28.79	0.00								
CRA4-A3		perp (v. weak)	5.28	21.03	37.50	3.56	0.00	0.00	2.40	30.89	0.00								
BHG-A1		none	0.20	20.75	36.38	8.41	0.09	0.02	28.36	11.77	0.03								
BHG-A2		none	0.19	20.75	36.65	8.22	0.10	0.00	28.49	11.46	0.06								
BHG-A3		none	0.22	20.56	36.35	8.33	0.10	0.05	29.15	11.91	0.00								

Appendix H

EL 11/96 Chromites

(All chromites found in the rotating magnetic field separation "non-rotating" fraction)

			Oxide weight %					
MgO	Al2O3	SiO2	TiO2	Cr2O3	MnO	FeO tot.	NiO	ZnO
19.24	51.04	0.00	0.23	13.77	0.10	12.66	0.25	0.06
13.66	34.51	0.00	0.22	30.39	0.21	18.81	0.17	0.35
17.92	53.74	0.04	0.05	10.99	0.22	14.88	0.32	0.24
13.23	34.51	0.09	0.93	27.26	0.29	20.63	0.21	0.22
21.24	56.24	0.08	0.07	10.70	0.22	10.44	0.33	0.05
9.89	13.57	0.00	0.17	50.88	0.23	22.90	0.13	0.07
15.64	31.75	0.14	0.78	29.97	0.14	19.37	0.24	0.00
11.50	25.23	0.01	0.11	40.27	0.23	20.07	0.08	0.12
4.96	5.36	0.00	0.04	55.38	0.33	28.60	0.09	0.01
16.73	36.69	0.12	0.82	25.81	0.18	17.75	0.23	0.08
21.06	56.42	0.02	0.06	10.31	0.18	10.67	0.34	0.05
19.92	53.42	0.02	0.04	13.36	0.09	11.11	0.38	0.12
19.98	54.11	0.04	0.12	11.26	0.20	12.67	0.45	0.06
20.16	53.61	0.05	0.09	9.99	0.21	13.86	0.32	0.00
20.95	56.53	0.07	0.16	10.29	0.08	10.19	0.30	0.12
20.34	54.39	0.03	0.06	12.71	0.13	10.96	0.41	0.24
16.64	41.01	0.11	0.80	21.21	0.21	18.73	0.21	0.17
9.55	5.37	0.02	0.04	61.84	0.35	21.23	0.11	0.06
10.30	4.51	0.00	0.03	64.29	0.43	18.05	0.07	0.11
6.87	5.90	0.00	0.05	61.53	0.49	24.86	0.00	0.13
7.24	4.14	0.00	0.02	63.35	0.33	23.14	0.02	0.25
8.64	7.45	0.00	0.39	50.83	0.65	30.52	0.04	0.05
11.71	7.93	0.04	0.41	52.09	0.56	25.50	0.08	0.08
8.57	5.12	0.02	0.01	62.78	0.44	21.47	0.00	0.07
18.13	38.60	0.14	0.51	25.89	0.36	15.71	0.14	0.06
9.94	10.65	0.00	0.07	54.79	0.48	21.84	0.00	0.02
20.09	54.31	0.00	0.05	12.56	0.08	11.56	0.34	0.00
19.69	53.26	0.00	0.07	13.64	0.14	12.38	0.43	0.06
7.90	6.38	0.03	0.06	63.51	0.30	18.81	0.06	0.12
18.25	51.67	0.05	0.05	13.38	0.07	13.92	0.36	0.10
20.23	55.83	0.03	0.10	10.52	0.12	10.19	0.35	0.15
20.04	53.60	0.01	0.03	11.90	0.10	11.06	0.32	0.06
20.62	54.56	0.08	0.18	10.22	0.10	10.98	0.36	0.03
15.71	39.70	0.08	0.70	22.11	0.13	18.02	0.23	0.05
20.66	55.26	0.07	0.15	10.40	0.12	10.66	0.35	0.12
9.57	3.17	0.05	0.00	67.52	0.34	17.36	0.03	0.12
9.21	18.86	0.01	0.19	43.46	0.38	26.26	0.13	0.14
20.09	54.10	0.00	0.04	12.17	0.08	10.84	0.34	0.20
12.04	31.79	0.02	0.17	32.05	0.32	22.14	0.09	0.17
20.40	53.00	0.00	0.10	15.40	0.10	11.10	0.30	0.20
19.80	46.50	0.00	0.10	21.50	0.00	11.00	0.40	0.10
20.30	48.30	0.00	0.20	18.70	0.10	11.40	0.30	0.00
19.50	45.80	0.00	0.10	22.60	0.10	11.30	0.20	0.10
19.40	50.30	0.00	0.30	14.60	0.10	14.30	0.40	0.10
18.30	42.20	0.00	0.20	24.20	0.10	12.90	0.20	0.00
20.70	56.40	0.00	0.10	9.20	0.10	10.40	0.50	0.00
18.80	46.40	1.50	0.20	21.70	0.00	11.40	0.30	0.20
17.90	43.40	0.00	0.10	24.30	0.00	14.00	0.10	0.00
0.60	3.90	0.00	0.00	68.30	0.50	25.30	0.00	1.40
8.10	3.70	0.00	0.00	67.10	0.20	22.60	0.00	0.00
6.74	5.28	0.00	0.07	61.69	0.38	26.54	0.03	0.19
2.90	11.24	0.07	0.10	55.00	0.44	32.67	0.12	0.30
7.73	4.65	0.00	0.00	63.14	0.37	25.19	0.13	0.07
10.76	10.54	0.03	0.08	60.72	0.18	20.41	0.01	0.03
5.61	5.09	0.02	0.04	64.70	0.22	24.75	0.06	0.30
10.00	14.82	0.00	0.05	52.60	0.30	25.20	0.05	0.29
7.71	6.10	0.01	0.05	62.17	0.51	26.01	0.16	0.17
11.61	10.82	0.02	0.05	60.28	0.28	19.30	0.08	0.23
15.68	30.12	0.00	0.45	38.04	0.21	16.70	0.19	0.08
8.66	9.20	0.04	0.00	57.91	0.35	25.85	0.00	0.10
7.97	4.98	0.03	0.08	67.55	0.27	21.80	0.06	0.14
13.68	36.36	0.08	0.67	25.85	0.22	23.59	0.21	0.06
8.33	10.13	0.01	0.06	57.06	0.31	26.58	0.13	0.16
10.38	20.28	0.00	0.10	44.12	0.36	24.95	0.00	0.30